The Late Paleozoic tectonic evolution of Central Asian orogenic belt in Central-Eastern inner Mongolia

Pan Zhao

ÉCOLE DOCTORALE SCIENCES DE LA TERRE ET DE L'UNIVERS

Institut des Sciences de la Terre d'Orleans
School of Earth and Space Sciences, PekingUniversity

THÈSE EN COTUTELLE INTERNATIONALE

présentée par :

Pan ZHAO

soutenue le : 17 Octobre 2014

pour obtenir le grade de :
Docteur de l'université d'Orléans
et de l'Université de Pékin

Discipline : Sciences de la Terre et de l'Univers

L'évolution tectonique du Paléozoïque supérieur de la Ceinture Orogénique de l'Asie Centrale du Centre-Oriental de la Mongolie intérieure

THÈSE dirigée par :

CHEN Yan	Professeur, Université d'Orléans
XU Bei	Professeur, Université de Pékin

RAPPORTEURS :

ZHANG Shihong	Professeur, Chinese University of Geosciences (Beijing)
LIN Wei	Professeur, Institute of Geology and Geophysics, CAS

JURY (indiquez tous les membres du jury – y compris directeur(s) thèse et rapporteurs) :

CHEN Yan	Professeur, Université d'Orléans
FAURE Michel	Professeur, Université d'Orléans
LIN Wei	Professeur, Institute of Geology and Geophysics, CAS
LIU Junlai	Professeur, China University of Geosciences (Beijing)
SCAILLET Bruno	Professeur, Université d'Orléans
WANG Tao	Professeur, Chinese Academy of Geological Sciences
XU Bei	Professeur, Peking University
ZHANG Shihong	Professeur, China University of Geosciences (Beijing)

Pan ZHAO

L'évolution tectonique du Paléozoïque supérieur de la Ceinture Orogénique de l'Asie Centrale du Centre-Oriental de la Mongolie intérieure

Le Centre-Est de la Mongolie intérieure, faisant la partie sud-est de la Ceinture Orogénique de l'Asie Centrale (CAOB), est une zonede clé pour étudier l'histoire de l'accrétion-collision entre la Chine du Nord (NCC) et les blocs continentaux du Nord. Les contraintes du cadre tectonique et de la connaissance de l'évolution tectonique sont importantes pour comprendre l'accrétion de la CAOB car il n'y a pas de consensus sur le mode et la période de l'accrétion entre NCC et les blocs du Nord. Par conséquent, des études pluridisciplinaires ont été effectuées sur les roches sédimentaires et magmatiques du Paléozoïque supérieur dans le centre-oriental de la Mongolie Intérieure. Surla base de nosétudes sédimentologiques, géochronologiques, géochimiques et paléomagnétiques, etcompte tenu des résultatsprécédentsen pétrographie, géochimie et paléontologie, l'évolution sédimentaire et tectonique du Paléozoïque supérieur duCentre-Oriental de la Mongolie Intérieure a été bien établie.Les études détaillées en sédimentologie et géochimie montrent une transition entre les dépôts molassiques du Dévonien à la dénudation du Carbonifère inférieur et les sédiments marins du Carbonifère supérieure vers les dépôts de bassin d'extension au Permien. D'après nos analyses détaillées des faciès sédimentaires, descaractéristiques géochimiques des roches magmatiques et nos données paléomagnétiques, nous proposons un modèle géodynamique de subduction-collision-extension post-orogénique pour le Paléozoïque au Centre-Oriental de la Mongolie Intérieure.

Mots-clés: Ceinture Orogénique de l'Asie Centrale (CAOB), Centre-Oriental de la Mongolie intérieure, Paléozoïquesupérieure, sédimentologie, paléomagnétisme

The Late Paleozoic tectonic evolution of Central Asian Orogenic Belt in Central-Eastern Inner Mongolia

Central-eastern Inner Mongolia, located in the southeastern part of the Central Asian Orogenic Belt (CAOB), is a key area to study the collisional-accretionary history between the North China Craton (NCC) and the northern continental blocks. The establishment of precise constraints of this tectonic framework and evolutional history are importantto understand the accretion of CAOB. However, no any consensus has been achieved about the way and the timing of the accretion between NCC and the northern blocks. Therefore, multidisciplinary studies have been carried out on the Late Paleozoic strata and magmatic rocks in central-eastern Inner Mongolia. Based on our sedimentological analyses, detrital zircon geochronological constraints, geochemical studies and paleomagnetic investigations, integrating the previous results in petrology, geochemistry and paleontology, the Late Paleozoic sedimentary-tectonic evolution of the central-eastern Inner Mongolia has been established. Detailed sedimentological and geochemical studies show atransition from the Devonian molassic deposits to the Early Carboniferous denudation and from the Late Carboniferous inland-sea sediments to the Permian extensional basin deposits. According to the comprehensive analyses on sedimentary facies, geochemical characteristics and paleomagnetic data, we propose a Paleozoic subduction-collision- post-orogenic extension tectonic model for central-eastern Inner Mongolia.

Key words: Central Asian Orogenic Belt, Central-East Inner Mongolia, Late Paleozoic, sedimentology, paleomagnetism

Institut des Sciences de la Terre d'Orléans, 45067 Orléans, France

Institut des Sciences de laTerre et Espace de l'Universite de Pékin, 100871, Pékin, Chine

Acknowledgements

At this last station of my voyage of Ph. D degree pursuit, I want to express my gratitude to all people who have helped me in this wonderful and fruitful journey.

I would like to express my gratitude to Prof. Bei XU for his guidance and many positive suggestions during my research, especially for his confidence in allowing me sufficient freedom to eoplore my thinking. I would also like to thank Prof. Bei Xu for sending me to France to learn professional knowledge, which expands my view a lot.

I would also like to express my gratitude to Prof. Yan CHEN who offered me great support and help during my one and a half years study in France. As a supervisor, he provided me everything I could image to make my living and study smooth in France, from professional paleognetism to life attitude. His prodound knowledge of geology, active minds and hardwork attitude bring me deep effect.

A special tribute is to be paid to Prof. Michel FAURE, who taught me how to abserve rock deformation in the field and how to combine these deformation together to discuss a tectonic problem. These methods will play profound influence in my future career.

Many of my fellow graduate students have helped me a lot. I want to express my appreciation to Wang Yu, Wei Wei, Pang Xuyong, Shi Guanzhong, Tong Qinlong, Fang Junqin, Li Ruibiao, Cheng Shengdong, Luo Zhiwen, Zhang Chenhao, Wang Yanyang and Liao Wen from Peking University. In addition, many thanks want to express to the generous help of Nicolas Charles, Flavien Choulet, Nour Harbat, Gao Qiang, Liu Qianghui, Li Hao and Ji Wenbin from Université d'Orléans.

A special word of thanks must be extended to Dr. Shufang Wang, who accompanied and supported me during my six years doctoral study and will stay with and supported me in the future.

Finally, I would like to express my gratitude to my parents for supporting me in many ways during my twenty-year study. Their love and care is the best impetus for me and the very first I want to return.

The Late Paleozoic tectonic evolution of Central Asian Orogenic Belt in Central-Eastern Inner Mongolia

Abstract:

Central-eastern Inner Mongolia, located in the southeastern part of the Central Asian Orogenic Belt (CAOB), is a key area to study the collisional-accretionary history between the North China Craton (NCC) and the northern continental blocks. The constraints to its tectonic framework and evolutional history are important to understand the tectonics of CAOB. Meanwhile, no consensus has been achieved about the way and the timing of the accretion between NCC and its northern blocks. Therefore, multidisciplinary studies have been carried out on the Late Paleozoic strata and magmatic rocks in central-eastern Inner Mongolia. Based on our sedimentological analyses, detrital zircon geochronological constraints, geochemical studies and paleomagnetic comparison, together with the previous petrological, geochemistry, and paleontological studies, the Late Paleozoic sedimentary-tectonic evolution of the central-eastern Inner Mongolia has been established.

The Late Silurian-Early Devonian and Late Devonian red sandstone molassic deposits unconformably covered the ophiolitic melanges along the South Orogen and North Orogen, respectively, postdating the two orogens. Detrital zircon dating displays unimodal age peak at 462 Ma, indicating the single provenance from the nearby magmatic arcs. During the Devonian, the Airgin Sum-Xilinhot-Xing'an Block (AXXB, the China-Mongolia tract) was dominated by shallow marine sediments, representing intracontinental basin deposits within the welded Erguna-Xing'an Block. Detrital zircon geochronological data present bimodal age peaks at 510 Ma and 440 Ma, suggesting bidirectional provenances from both the northern Erguna-Xing'an Block and the southern Baolidao Arc.

The central-eastern Inner Mongolia came into subaerial denudation stage in the Early Carboniferous, with littoral facies and neritic facies sediments only deposited in southern Sunidzuoqi and northern Aohanqi areas. During the Late Carboniferous, the central-eastern Inner Mongolia was dominated by clastic-carbonate deposits, which

unconformably covered the underlying Precambrian basement, Early Paleozoic Arcs, ophiolitic mélanges, pre-Carboniferous strata and intrusions, indicating a regional transgression. The Late Carboniferous strata can be correlated by rock assemblages and fossils, presenting similar sedimentary type and environment. Detrital zircon dating revealed two main age peaks at 440 Ma and 310 Ma, and abundant Neoproterozoic grains, indicating that the provenances are mainly local magmatic rocks and metamorphic basement. The Late Carboniferous inland-sea deposits covered the three blocks and two orogenic belts, representing the first stable sedimentary cover after the amalgamation of these blocks. The Upper Carboniferous Baoligaomiao Formation with terrestrial deposits and volcanic rocks developed near the China-Mongolia border. Detrital zircon geochronological data present the same bimodal age peaks at 440 Ma and 310 Ma, indicating that provenances are from the local sedimentary and magmatic rocks. These terrestrial deposits can be considered as the northern margin of the Late Carboniferous inland sea in central-eastern Inner Mongolia. The age peak of 440 Ma, representing the Early Paleozoic Arc magmatism, was identified from all three blocks separated by two suture zones, indicating that this provenance has strided the suture zones during the Carboniferous, which is an important evidence for the pre-Carboniferous amalgamation of these blocks.

During the Permian, extensional basin clastic-volcanic rocks deposited above the Late Carboniferous carbonate deposits, represented by the Early Permian volcanic rocks, the Middle Permian shallow marine fauna bearing clastic-carbonate sediments and the Late Permian fluvial-lacustrine facies deposits.The geochemical study of the Early Permian volcanic rocks display bimodal characteristics, implying an intraplate crustal thinningsetting. While the Late Permian terrestrial basin deposits marked the termination of the marine environment in central-eastern Inner Mongolia. Along the Southern Orogen, a Middle Permian alkaline magmatic belt represented by syenite, quartz syenite and syenitic granite,was recognized. The Permian strata developed above the Late Carboniferous inland-sea carbonate, representing a wide rift above the post-orogenic cover.

Late Devonian and Permian paleomagnetic poles were obtained for the

Songliao-Hunshandake Block at λ=46.8°N, φ=349.1°E, dp=14.6°, dm=27.3° with N=3 and λ=48.7°N, φ=3.7°E, dp=5.2°, dm=9.1° with N=6, respectively. The comparison of our new paleomagnetic poles with available data from North China Craton, Mongolia Block and Siberia Block indicates that (1) the Paleo-Asian Ocean has been closed at least before the Late Devonian, and NCC, Songliao-Hunshandake Block (SHB) and Mongolia Block have been welded into a single block since then; (2) the newly formed unified block is not a rigid one, with strike-slip movements occurring within and at the boundary of these blocks, producing relative rotations among them.

Detailed sedimentological and geochemical studies show the transition from the Devonian molassic deposits to the Early Carboniferous denudation and from the Late Carboniferous inland-sea sediments to the Permian extensional basin deposits. According to the comprehensive analysis of sedimentary facies, geochemical characteristics and paleomagnetic data, we proposed a Paleozoic subduction - collision - post-orogenic extension tectonic model for central-eastern Inner Mongolia. The Early Paleozoic bidirectional subduction of the Paleo-Asian Ocean produced Bainaimiao Arc at the northern margin of NCC, and Baolidao Arc at the southern margin of AXXB. At the Late Silurian-Late Devonian, the collision and agglomeration of NCC, SHB and AXXB occurred by two subparallel orogenic belts, the ophiolitic mélanges of which were unconformably covered by molassic deposits. During the Late Carboniferous, the first stable post-orogenic sedimentary cover developed, characterized by widespread carbonate deposits, which unconformably overlaid the underlying strata and intrusions, indicating an inland-sea basin deposits. Early-Middle Permian, extensional rift developed in the central-eastern Inner Mongolia, characterized by widespread magmatic rocks and shallow marine deposits. In the Late Permian the central-eastern Inner Mongolia came into continental environment setting.

Keywords：*Central Asian Orogenic Belt, Central-Eastern Inner Mongolia, Late Paleozoic, sedimentology, paleomagnetism*

L'évolution tectonique du Paléozoïque supérieur de l'Asie centrale ceinture orogénique en Centre-Est de la Mongolie intérieure

Résumé:

Le Centre-Orientalde la Mongolie intérieure, situé auSud-Est de la Ceinture Orogénique de l'Asie Centrale (CAOB), est une zone de clé pour étudier l'histoire de l'accrétion-collision entre la Chine du Nord (NCC) et les blocs continentaux du Nord. Les contraintes de son cadre tectonique et de son évolution sont importantes pour comprendre l'accrétion de CAOB car il n'existe aucun consensus sur le mode et la période d'accrétion entre NCC et les blocs du Nord. Par conséquent, les études pluridisciplinaires ont été effectuées sur les roches sedimentaires et magmatiques du Paléozoïque supérieur du Centre-Orientalde la Mongolie intérieure. Sur la base de nos études sédimentologiques, géochronologiques, géochimiques et paléomagnétiques, compte tenu des études pétrologiques, géochimiques et paléontologiques précédentes, l'évolution sédimentaire et tectonique du Paléozoïque supérieur du Centre-est de la Mongolie intérieure a été établie.

Les dépôts molassiques du Dévonien inférieur et du Dévonien supérieurre couvrent en discordance les mélanges ophiolitiques des orogènes du Sud et du Nord, respectivement. Le pic d'âge des zircons détritiques est à 462 Ma, indiquant une provenance unique depuis des arcs magmatiques proches. Pendant le Dévonien inférieur, la sédimentation sur le bloc d'Airgin sum-Xilinhot-Xing'an (AXXB, situé sur la frontière entre la Chine et la Mongolie), a été dominée par les sédiments marins, qui sont similaires aux dépôts des bassins intracontinentaux dans le bloc Erguna-Xing'an. Les analyses des âges de zircons détritiques montrent deux pics d'âge à 510 Ma et 440 Ma, suggérant une double provenance depuis le bloc Erguna-Xing'an et de l'arc Baolidao.

Le Centre-Orientalde la Mongolie intérieure était en phase de dénudation subaérienne au Carbonifère inférieur, avec des dépôts marins dans le Sud de Sunidzuoqi et le Nord d'Aohanqi. Au cours du Carbonifère supérieur, la sédimentation du Centre-Orientalde la Mongolie intérieure était dominée par les

dépôts clastiques-carbonatés, qui couvraient en discordanceles roches précambriennes, les arcs paléozoïques, les mélanges ophiolitiques et les strates pré-carbonifères et les intrusions, indiquant une transgression régionale. Les strates du Carbonifère supérieur peuvent se corréler par les assemblages de facièset de fossiles qui présentent le même type d'assemblage biostratigraphiques et d'environnement sédimentaire. Les données deszircons détritiques révèlent deux pics d'âge à 440 Ma et 310 Ma avec des grains hérités néoprotérozoïques, ce qui indique que les provenances sont principalement des roches magmatiques paléozoïques et métamorphiques précambriennes locales. Les dépôts du Carbonifère supérieurcouvrent trois blocs et deux ceintures orogéniques, représentant la première couverture sédimentaire stable après l'agglomération de ces blocs. Les dépôts continentaux de la Formation de Baoligaomiao d'âge Carbonifère supérieur se sont développé sàla frontière Chine-Mongolie. Les données de zircons détritiques présentent les mêmes deux pics à 440 Ma et 310 Ma, ce qui indique que les provenances sont des roches magmatiques et sédimentaires locales. Ces dépôts continentaux peuvent être considérés comme la marge du Nord de la mer épicontinentaleau Carbonifère dans le Centre-Orientalde la Mongolie intérieure. Le pic d'âge à440 Ma, représentant le magmatisme d'arc du Paléozoïque, a été identifié sur lestrois blocs séparés par deux zones du sutures, ce qui indique que les dépôts de cette provenance onttraverséles zones de sutures au Carbonifère. Ceci présente une preuve importantepour l'agglomération pré-carbonifère de ces blocs.

Au cours du Permien, les formations sont représentées par des roches volcaniques du Permien inférieur, des sédiments clastiques-carbonatés marins du Permien Moyen et des dépôts de faciès fluvio-lacustre du Permien supérieur, ce qui indique des dépôts de bassin extensifau-dessus dedépôts du Carbonifère supérieure. Les roches volcaniques du Permien présentent des caractéristiques géochimiques bimodales, ce qui implique une amincissement intraplaque (rift ou pull-apart). Alors les dépôts des faciès fluvio-lacustres du Permien supérieur marquent la fin de l'environnement marin au Centre-Orienal de la Mongolie intérieure. Une ceinture alcaline magmatique du Permien moyen a été reconnue le long de l'Orogène du Sud, représentée par syénite, syénite à quartz et granite syénitique. Les strates

permiennesse sont développées au-dessus des dépôts carbonifères, représentant un rift large au-dessus de la couverture post-orogénique.

Deux pôles paléomagnétiques d'âges dévonien supérieur et permien ont été obtenus pour le bloc Songliao-Hunshandake (SHB) à λ=46.8°N, φ=349.1°E, dp=14.6°, dm=27.3° avec N=3 et λ=48.7°N, φ=3.7°E, dp=5.2°, dm=9.1° avec N=6, respectivement. La comparaison de nos nouveaux pôles paléomagnétiques avecceux de Chine du Nord, de Mongolie et de Sibérie indique que (1) l'océan paléo-asiatique a été fermé au moins avant le Dévonien supérieur, et que les blocs NCC, SHB et Mongolie ont été soudés enun seul bloc avant le Dévonien; (2) cependant ce nouveau bloc unifié n'est pas rigide, les mouvements de décrochement accommodés par des rotations relatives se sont produits à l'intérieur et à la limite de ce bloc.

Les études détaillées de sédimentologie et de géochimie montrent une transition entre les dépôts molassiques du Dévonien à la dénudation au Carbonifère inférieur et des sédiments marins continentaux du Carbonifère supérieur vers les dépôts de bassin d'extension au Permien. D'après les analyses détaillées des faciès sédimentaires, les caractéristiques géochimiques et les données paléomagnétiques, nous proposons un modèle tectonique de subduction - collision -extension post-orogénique pour le Paléozoïque du Centre-Orientalde la Mongolie intérieure. La subduction bidirectionnelle au Paléozoïque inférieur de l'océan paléo-asiatique produit l'arc de Bainaimiao à la marge du Nord de NCC, et l'arc de Baolidao à la marge du Sud d'AXXB. Au Silurien supérieur-Dévonien supérieur, la collision et l'agglomération de NCC, SHB et AXXB ont eu lieu surles deux ceintures orogéniques subparallèles. Les mélanges ophiolitiques ont été recouverts en discordance par desdépôts molassiques. Au cours du Carbonifère supérieur, la première couverture sédimentaire stable post-orogénique s'est développée, caractérisée par des dépôts de carbonates répandus qui ont couvert ensuite en discordanceles strates sous-jacentes et les intrusions, indiquant un dépôt de bassin marin-continental. Pendant le Permien inférieur et moyen, une zone à croûte amincie s'est développée au Centre-Orientalde la Mongolie intérieure, caractérisée par des roches magmatiques alcalines et les dépôts marins peu profonds. À la fin du Permien le Centre-Orientalde la Mongolie intérieure est en

phase d'évolution continentale.

Mots-clés: Ceinture Orogéniquede l’Asie Centrale (CAOB), Centre-Orientalde la Mongolie intérieure, Paléozoïquesupérieur, sédimentologie, paleomagnétisme

摘　要

内蒙古中东部地区位于中亚造山带东南缘，是研究华北板块与其北部陆块碰撞拼贴历史的关键区域，对其构造格局及演化历史的限定对整个中亚造山带具有重要意义。同时，前人对于华北板块与其北部各陆块的碰撞拼贴时限和方式具有很大争议。针对该争议，本文通过沉积学分析、碎屑锆石年代学限定、地球化学研究和古地磁对比，结合前人岩石学、地球化学和古生物学研究，对内蒙古中东部晚古生代沉积－构造演化进行限定。

内蒙古中东部沿南北两条造山带分别发育晚志留-早泥盆世和晚泥盆世磨拉斯建造，不整合覆盖于两条蛇绿混杂带之上，限定双冲造山最终完成于晚泥盆世。碎屑锆石年代学得到 462Ma 的单一年龄峰，显示来自岛弧的单一物源。泥盆纪艾里格庙-锡林浩特-兴安地块西段（中蒙边境一带）发育浅海相沉积，代表艾里格庙-锡林浩特-兴安地块与额尔古纳地块早古生代碰撞拼合后的陆内海相盆地沉积。碎屑锆石测试显示其两个主要年龄峰值为 510Ma 和 440Ma，说明其物源来自额尔古纳-兴安地块本身及南部宝力道岛弧岩浆岩。

早石炭世，内蒙古中东部进入剥蚀阶段，仅苏尼特左旗南部及敖汉旗北部发育滨浅海相沉积。晚石炭世内蒙古中东部地区发育陆表海碎屑－碳酸盐岩沉积岩系，底部不整合覆盖于前寒武纪基底、早古生代岛弧岩浆岩、蛇绿混杂带、前石炭纪地层及石炭纪侵入岩之上，代表由海侵导致的区域超覆不整合。区域内晚石炭世地层可通过岩石组合和化石进行对比，表明相同的沉积类型和沉积环境。碎屑锆石年代学显示 440Ma 和 310Ma 两个主要年龄峰值及大量新元古代锆石，说明晚石炭世物源主要为本地岩浆岩和变质基底，代表原地剥蚀和近源沉积的特征。晚石炭世陆表海沉积覆盖于整个内蒙古中东部地区，横跨南北三个板块（艾里格庙－锡林浩特－兴安地块、松辽－浑善达克地块和华北克拉通）和两个造山带（北造山带和南造山带），代表陆块拼合后的第一个稳定盖层沉积。晚石炭世中蒙边境发育宝力高庙组陆相碎屑-火山沉积岩系。碎屑锆石年代学研究显示 310 Ma 和 440 Ma 两个主要年龄峰，显示其物源主要来自于额尔古纳－兴安地块原地岩浆岩及南部宝力道岛弧。该陆相沉积可作为内蒙古中东部陆表海沉积的北部边缘。作为代表早古生代岛弧岩浆事件的 440Ma 年龄峰，其出现于由南北两条缝合带分隔的三个陆块之上，说明石炭纪沉积时，作为物源的早古生代岛弧岩浆

岩已经跨越缝合带进行沉积，同样说明三个陆块在石炭纪之前已经碰撞拼合。

二叠纪内蒙古中东部地区发育陆内伸展盆地碎屑-火山沉积岩系，由早二叠世双峰式火山岩、中二叠世富含动物化石浅海相碎屑-碳酸盐岩和晚二叠世含植物化石陆相沉积组成。早二叠世双峰式火山岩地球化学特征，显示其喷发于陆内裂谷环境。晚二叠世陆相地层的普遍出现标志着内蒙古中东部已结束海相沉积演化。在内蒙古中东部沿镶黄旗-克什克腾旗识别出一条中二叠世碱性岩带，代表该时期的一条陆内伸展裂谷带。二叠纪地层沉积于晚石炭世陆表海碳酸盐岩之上，代表造山后稳定盖层之上的裂谷伸展作用。

古地磁研究得到松辽-浑善达克地块晚泥盆世和二叠纪两个古地磁极，分别为 λ=46.8°N, φ=349.1°E, dp=14.6°, dm=27.3°, N=3 和 λ=48.7°N, φ=3.7°E, dp=5.2°, dm=9.1°, N=6。通过与周围块体进行古地磁极对比得出：（1）古亚洲洋至少于晚泥盆世已经闭合，华北克拉通、松辽-浑善达克地块和蒙古地块已经碰撞拼合；（2）华北克拉通、浑善达克地块和蒙古地块完成拼合后并非形成一个刚体，板块内部及板块边缘的走滑运动导致板块之间的相对旋转。

详细的沉积学和地球化学研究展示了内蒙古中东部由泥盆纪磨拉斯不整合，到早石炭世造山后剥蚀，以及晚石炭世陆表海向二叠纪伸展盆地的演化过程。在综合分析沉积组合、碎屑锆石年龄、地球化学特征和古地磁数据基础上，提出古生代内蒙古中东部地区完整的俯冲-造山-造山后伸展的构造演化模式：早古生代古亚洲洋双向俯冲，于华北克拉通北缘产生白乃庙岛弧，并于艾里格庙－锡林浩特－兴安地块北缘产生宝力道岛弧。晚志留世-晚泥盆世，通过南北两个造山带完成华北克拉通、松辽-浑善达克地块和艾里格庙-锡林浩特-兴安地块的碰撞拼合。晚石炭世，内蒙古中东部出现造山后第一个稳定的沉积盖层，以遍布全区的碳酸盐岩沉积为特征，并不整合覆盖于下伏地层和岩浆岩之上，代表造山后陆表海沉积。早-中二叠世，内蒙古中东部地区发育裂谷伸展作用，以面状分布的火山岩和基性-酸性侵入岩为特征。晚二叠世内蒙古中东部进入陆相演化阶段。

关键词：中亚造山带，内蒙古中东部，晚古生代，沉积学，古地磁学

Content

Chapter 1 Introduction

1.1 Basic information of the Central Asian Orogenic Belt

1.1.1 Accretionary Orogenic Belt

作为板块运动的重要产物，造山带纪录了板块相向运动最终阶段的岩石圈变形、地壳增厚及火山－沉积作用。虽然造山带最初被认为是威尔逊旋回晚期板块碰撞的产物（Wilson, 1966），但是地球上一些造山带并没有发生板块间碰撞，例如美洲的科迪勒拉造山带、西太平洋造山带及横跨欧亚大陆的中亚造山带（Cawood et al., 2009）。因此，前人通过对造山带不同特征的研究，将其分为碰撞造山带、增生型造山带和陆内造山带（图 1-1; Cawood et al., 2009）。碰撞造山带以两个板块碰撞产生，增生型造山带则纪录了大陆及大洋地壳物质不断拼贴增生的过程，而陆内造山带产生于距离板块边缘较远（一般大于 1000 公里）的大陆内部（Guy, 2012）。本文研究对象中亚造山带属于增生型造山带，因此对增生型造山带的特征进行总结。

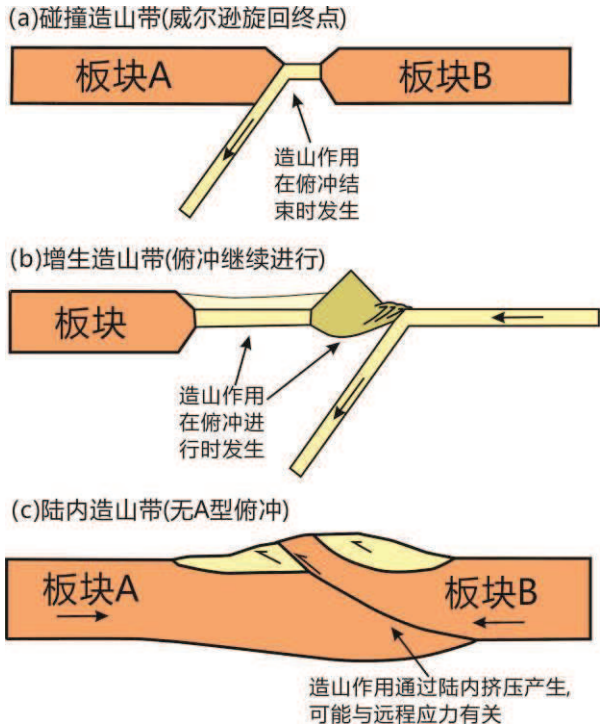

图 1-1 碰撞、增生和陆内三种造山示意性剖面图（据 Cawood et al., 2009）

Figure 1-1 Schematic cross-sections through (a) collisional, (b) accretionary and (c) intracratonic orogens

增生型造山带形成于大洋地壳的俯冲位置，以显著的地壳横向和垂向生长为特征，其组成包括增生楔、岛弧、弧后物质、蛇绿岩、大洋高原、古老陆块、增生后花岗质岩石、最高至麻粒岩相的变质产物、高压－超高压变质岩以及碎屑沉积岩（Windley et al., 2007; Cawood et al., 2009）。增生型造山带一个重要的特征是形成大量的新生地壳物质，并作为全球地壳增生的重要部分（Maruyama and Parkinson, 2000; Jahn et al., 2000; 2004）。增生型造山带在演化过程中多伴随金属成矿作用，常形成大型、超大型各类矿床（Yakubchuk, 2005; Groves and Bierlein 2007, Seltmann et al., 2014; Goldfarb et al., 2014）。

增生型造山带一般都会经历很长的演化历史（数百个百万年）。增生型造山带始于洋壳向陆壳的俯冲。在俯冲过程中形成由原地的俯冲板片物质和上覆板块物质，以及外来的岛弧、弧后盆地、大洋高原、海山、古老陆块等形成的增生楔（Windley et al., 2007）。增生停止后，通常伴随有增生后花岗岩的侵位、高压－超高压变质岩的剥蚀和伸展碎屑沉积盆地的发育（Cawood et al., 2009）。增生型造山带最终在洋壳闭合和板块俯冲停止时都会经历一个碰撞阶段，并导致增生物质强烈的构造变形。在此阶段，会产生与碰撞造山带相似的逆冲和强烈的地壳缩短（Cawood et al., 2009）。因此，近来有学者提出增生型造山带并非一个完全独立的造山带类型，而是碰撞造山带的初始阶段（Schulmann and Paterson, 2011）。

1.1.2 Previous studies of the Central Asian Orogenic Belt

中亚造山带（Central Asian Orogenic Belt, CAOB）又称阿尔泰造山带（Altaids），自其提出便受到国内外地质学家的广泛关注，已成为目前地质学研究的热点领域（Sengör et al., 1993; Jahn, 2004; Windley et al., 2007; Kröner et al., 2007; Yarmolyuk et al., 2008; Xiao et al., 2010; Wilhem et al., 2012; Xu et al., 2013; Xiao and Santosh, 2014; Kröner et al., 2014; Safonova and Santosh, 2014）。Suess 最初识别出亚洲地壳在古生代沿着西伯利亚板块周缘生长，并将所产生的造山带命名为 Altaids。自此，在 Altaids 内部识别出多个构造单元及不同的次级造山带，例如哈萨克斯坦微陆块、图瓦－蒙古微陆块、乌拉尔造山带、天山造山带、北山造山带等（Sengör et al., 1993）。Sengör 等人在 1993 年对 Altaids 进行总结，将其中各个构造单元和造山带进行划分，并将其作为欧亚大陆古生代地壳生长的重要区域（Sengör et al., 1993）。Altaids 在后续的研究中又被多数学者命名为中亚造

山带（Windley et al., 2007; Kröner et al., 2007）。作为世界最大的显生宙增生型造山带之一，中亚造山带也是全球显生宙大陆地壳生长最为显著的地区（Han et al., 1997; Jahn et al., 2000; 2004）。中亚造山带具有以下三个主要特征：

第一，广阔的范围（图 1-1）。中亚造山带横跨欧亚大陆，东西长约 5000 公里，南北宽约 3000 公里，西起俄罗斯乌拉尔地区，经过乌兹别克斯坦、塔吉克斯坦、吉尔吉斯斯坦、哈萨克斯坦、中国西北地区、蒙古、中国东北地区，一直延伸至俄罗斯远东地区（图 1-1）（Sengör et al., 1993; Jahn, 2004; Windley et al., 2007）。

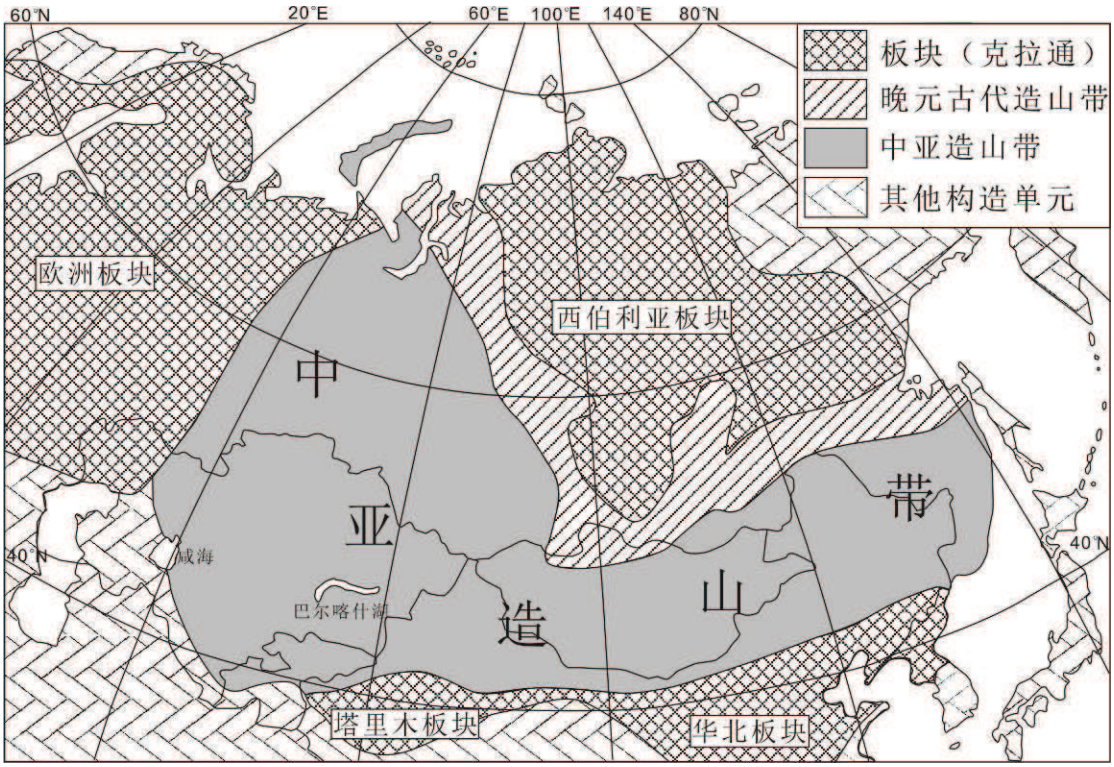

图 1-2 中亚造山带构造位置图（据 Sengör et al., 1993 和 Han et al., 2010）

Figure 1-2 Tectonic position of the Central Asian Orogenic Belt (from Sengör et al., 1993 and Han et al., 2010)

第二，复杂的构成。中亚造山带纪录了东欧克拉通、西伯利亚克拉通、塔里木克拉通和华北克拉通之间的碰撞拼贴过程（图 1-1; Sengör et al., 1993）。四个克拉通之间存在众多微陆块、海山和岛弧等，这些组分不断增生到克拉通边缘，并最终导致克拉通之间洋壳消失（图 1-2; Sengör and Natal'in, 1996; Windley et al., 2007）。

第三，长期演化过程。对于中亚造山带演化的开始，普遍认为其起源于中元

古代末期。以西伯利亚板块南缘 Eastern Sayan,地区的 Dunzhugur 蛇绿岩为标志，其锆石 U-Pb 年龄在 1020 Ma 左右，为中亚造山带内部发现的最古老蛇绿岩(Khain et al., 2002)。对于中亚造山带演化的结束，虽然不同地区造山时限不同，但普遍认为其最终结束于晚古生代末期（Kröner et al., 2010; Wilhem et al., 2012）。

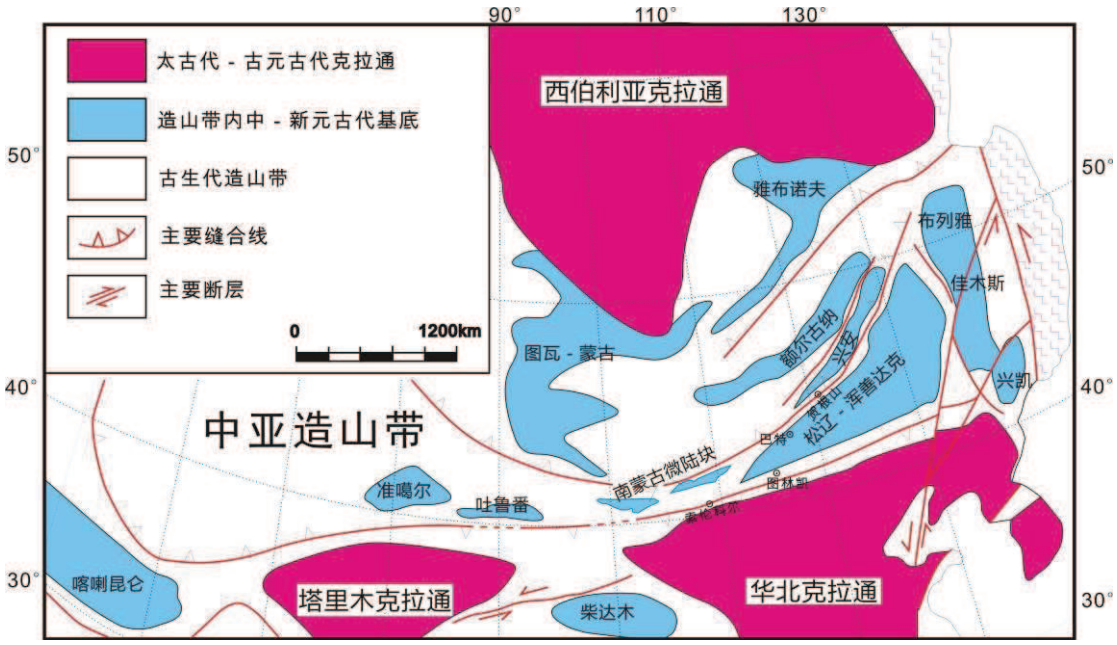

图 1-3 中亚造山带构造略图（修改自 Zhou et al., 2009）

Figure 1-3 Tectonic frameworks of the Central Asian Orogenic Belt (modified from Zhou et al., 2009)

1.1.3 Tectonic models of the Central Asian Orogenic Belt

对于中亚造山带的演化模式，目前主要有两种：

第一种模式认为存在一条初始马蹄形 Kipchak-Tuva-Mongol 岛弧，倾斜的俯冲导致平行于该岛弧产生右行剪切运动。西伯利亚克拉通顺时针的旋转，以及华北克拉通和塔里木克拉通向北的移动导致该岛弧的马蹄形弯曲。岛弧两侧存在的双俯冲导致大量新生地壳的增生，并通过岛弧的不断弯曲重复拼贴于克拉通边缘，形成中亚造山带的现今面貌（Sengör et al., 1993; Sengör and Natal'in, 1996）。

第二种模式认为在北部西伯利亚克拉通和南部华北克拉通和塔里木克拉通之间存在类似当今西南太平洋的多个独立地体（微陆块、大洋高原等）和多条俯冲带（图 1-3）。这些独立块体随着俯冲的不断进行拼贴于克拉通边缘，并最终导致洋壳消失和陆块碰撞（Windley et al., 2007; Xiao et al., 2010; Kröner et al., 2010;

Wilhem et al., 2012）。在此过程中可能伴随着多次小洋盆的打开和关闭（Kröner et al., 2010）。

最近有学者通过对蒙古南部的研究，提出中亚造山带经历了两阶段演化，第一阶段为泥盆纪－石炭纪的增生过程，第二阶段为二叠纪－侏罗纪的南北向碰撞挤压，并导致南北向的缩短（Lehmann et al., 2010; Schulmann and Paterson, 2011）。

1.2 Studies of Xing-Meng Orogenic Belt

1.2.1 Tectonic frameworks of Xing-Meng Orogenic Belt

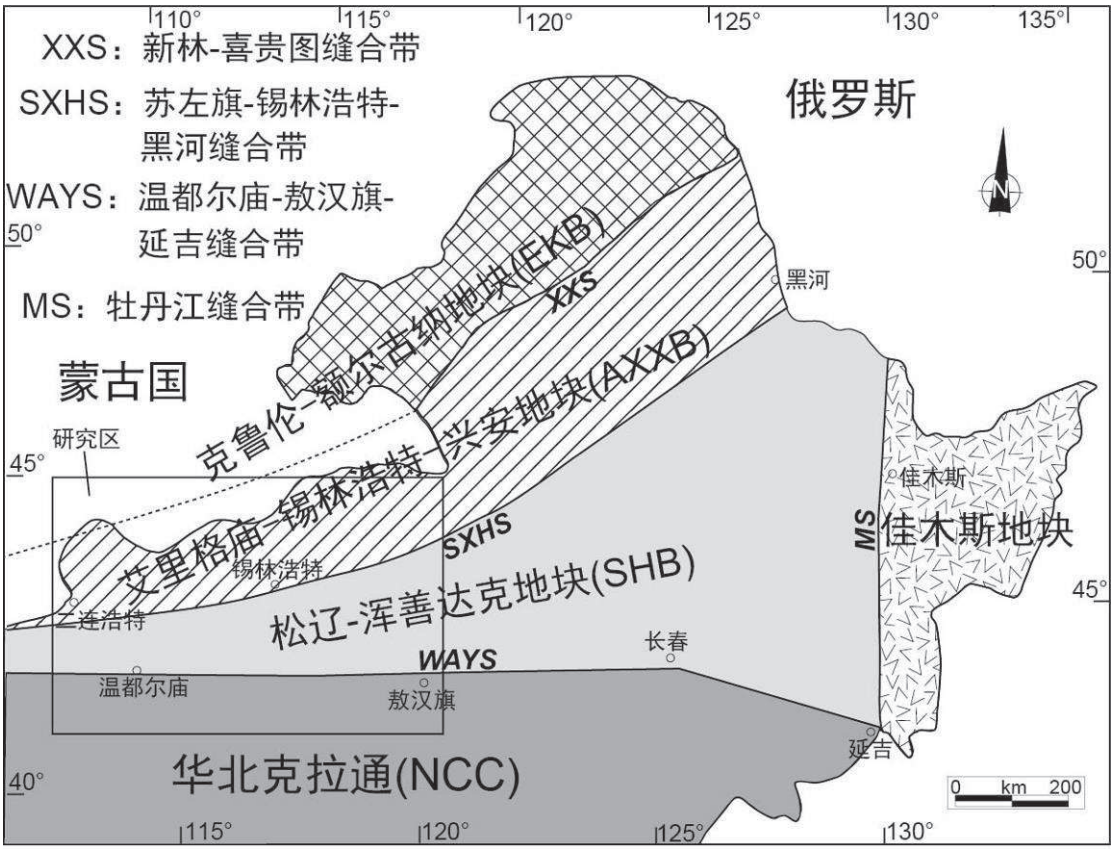

图 1-4 兴蒙造山带构造单元划分（修改自徐备等，2014）

Figure 1-4 Tectonic units of the Xing-Meng Orogenic Belt (modified from Xu et al., 2014)

中亚造山带东南部覆盖中国内蒙古自治区和东北地区，传统上将其称为兴蒙造山带，也成为满洲里造山带（Hsu et al., 1991）。该区北临蒙古-鄂霍茨克构造带，向西与蒙古各构造单元相连，东临太平洋构造带，南部连接华北板块，是研究中亚造山带东南缘构造演化的重要场所。其构造演化特征对恢复整个中亚造山

带的演化具有重要意义。

兴蒙造山带主要由以下几个陆块拼贴而成，由北至南依次为克鲁伦-额尔古纳地块，艾里格庙-锡林浩特-兴安地块，松辽-混善达克地块，佳木斯地块和华北克拉通（图 1-4; 徐备等, 2014）。这些地块分别由新林-喜贵图缝合带，苏左旗-锡林浩特-黑河缝合带，温都尔庙-西拉沐沦-长春缝合带和牡丹江缝合带分隔（图 1-4; 徐备等, 2014）。

华北克拉通以 2.5Ga 和 1.8Ga 岩浆事件为特征性基底。其北部四个块体的基底特征均表现为古元古代（1.8Ga）和新元古代（700-900Ma）岩浆岩为主，并出现少量中元古代岩浆岩（Wu et al., 2011; 张兴洲等, 2012; 孙立新等, 2012; Tang et al., 2013; 徐备等, 2014）。

新林-喜桂图缝合带分隔克鲁伦-额尔古纳地块和艾里格庙-锡林浩特-兴安地块（图 1-4）。西段喜桂图地区的头道桥蓝片岩早有报道（张兆忠等，1986）。最近周建波得到蓝片岩中锆石加权平均年龄为 500-490Ma（未发表资料），限定了缝合带形成的下限。北东段新林蛇绿岩自下而上主要由变质橄榄岩、层状堆晶岩、辉绿岩席和变玄武岩等组成（李瑞山，1991）。张丽等（2013）发现太平林场花岗片麻岩中变质锆石年龄为 494±10 Ma，可能代表与俯冲造山相关的变质事件。近年来有学者据新资料将额尔古纳与兴安地块的边界置于此缝合带，而不再采用德尔布干断裂带作为两者的分界线（Zhou and Wilde, 2013）。

苏左旗-锡林浩特-黑河缝合带分隔北部的艾里格庙-锡林浩特-兴安地块和南部的松辽-浑善达克地块，经西部艾力格庙、苏尼特左旗南、锡林浩特南和大石寨地区到黑河一线（图 1-4），以沿线分布的的早古生代岩浆岩、混杂岩和磨拉斯盆地为识别标志（徐备等, 2014）。缝合线时代由不整合覆盖在蛇绿混杂带之上的上泥盆统陆相磨拉斯沉积限定（Xu and Chen, 1997; Xu et al., 2013）。向东两板块缝合时代逐渐变新，由岩浆岩限定于早石炭世（张兴洲等, 2012）。

温都尔庙-敖汉旗-延吉缝合带作为松辽-浑善达克地块与华北克拉通之间的界限，从西向东沿图古日格-温都尔庙-正镶白旗-敖汉旗-吉中-延吉一线分布（图 1-4）。以发育早古生代岩浆岩、混杂岩、蓝片岩和磨拉斯盆地为标志（徐备等, 2014）。沿缝合线发育上志留-下泥盆统西别河组砂砾岩，不整合覆盖于奥陶纪地层或岩浆岩之上（Tang, 1990; 张允平等，2010; Xu et al., 2013），代表早古生代

造山带的前陆盆地沉积，并限定缝合时代在晚志留世之前。然而，根据华北板块北缘石炭纪-二叠纪的侵入岩研究，有学者认为缝合时代在晚二叠世甚至早三叠世（Xiao et al., 2003; Li, 2006; Zhang et al., 2009a; Cao et al., 2013; Yu et al., 2014）。

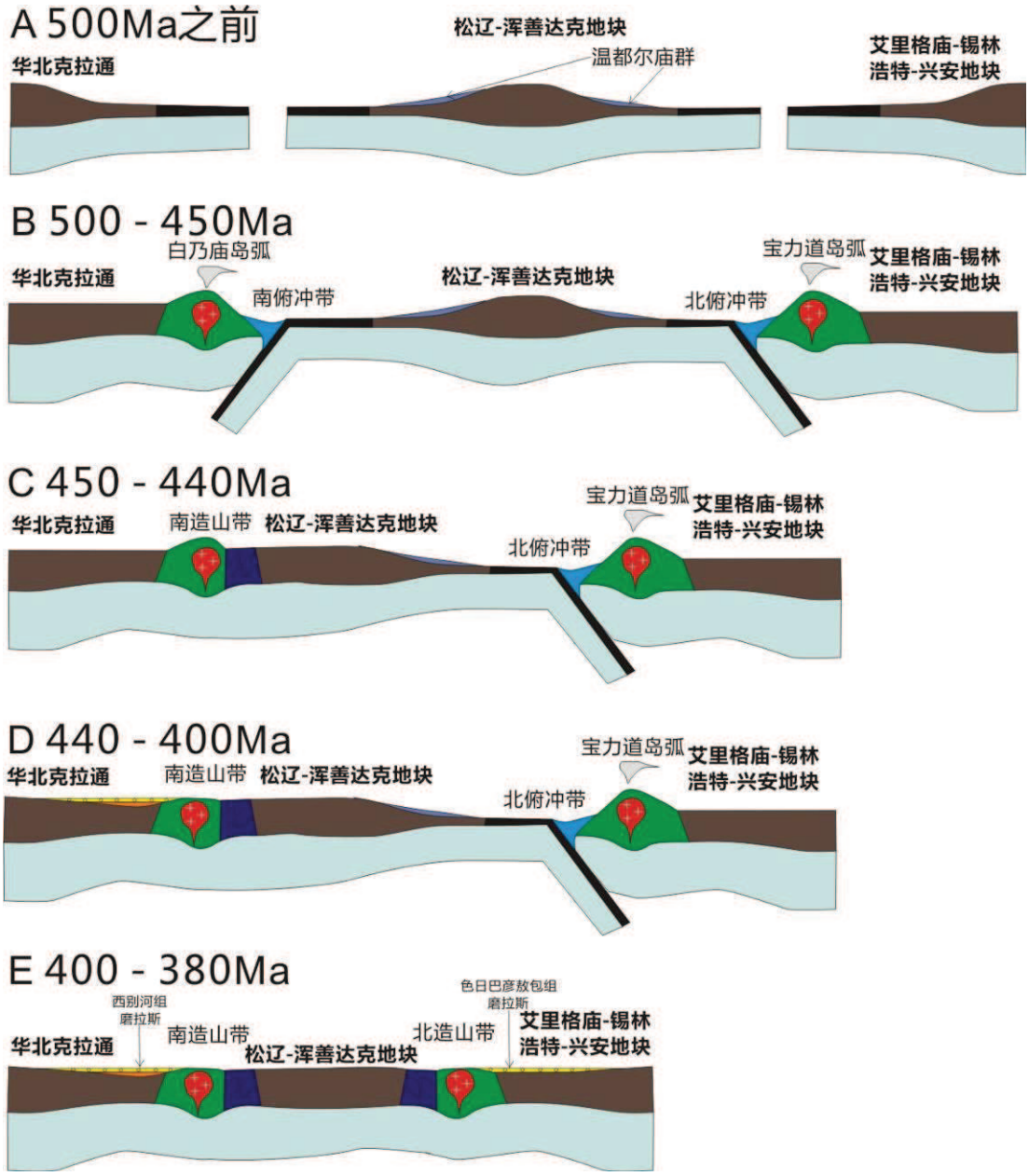

图 1-5 内蒙古中东部古生代构造演化模式图（据 Xu et al., 2013）

Figure 1-5 The Paleozoic tectonic evolutional model of eastern Inner Mongolia (from Xu et al., 2013)

牡丹江缝合带位于松辽-浑善达克地块与佳木斯地块之间，目前尚缺乏与碰撞有关的直接证据，但一些学者从岩浆作用和沉积作用两方面研究了其形成背景和演化过程。许文良等（2012）指出沿松嫩-张广才岭东缘存在南北向展布的早

古生代花岗岩，有 485Ma、450Ma 和 425Ma 等三个峰期。Wang et al.（2012）识别出缝合带以西存在晚奥陶闪长岩（443-451Ma）、英云闪长岩、流纹岩和中志留世二长花岗岩（424-430Ma），并据此提出它们可能代表早古生代佳木斯地块向西的俯冲。魏连喜等（2013）报道了晨明地区花岗闪长岩（433±1 Ma）和二长花岗岩（432±2 Ma），认为其产生于陆壳加厚环境，与俯冲后的地壳加厚有关。Meng 等（2010）对松嫩-张广才岭地块汤原地区和佳木斯地块宝清地区下泥盆统碎屑岩的研究也表明，两个地块在 413Ma（早泥盆世）之前已经拼合。

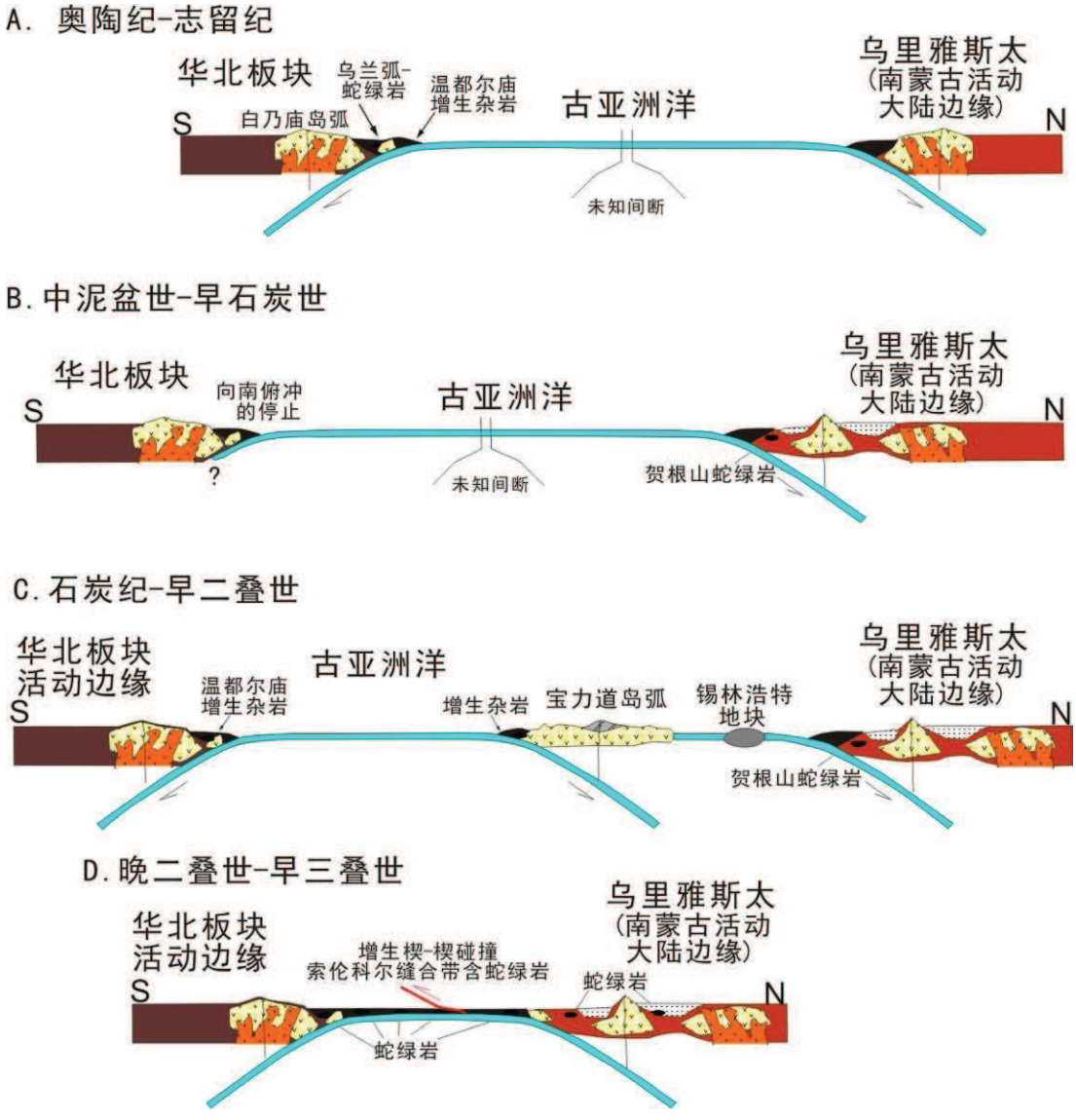

图 1-6 内蒙古中东部古生代构造演化模式图（据 Xiao et al., 2003）

Figure 1-6 The Paleozoic tectonic evolutional model of central-eastern Inner Mongolia (from Xiao et al., 2003)

1.2.2 Tectonic models of western Xing-Meng Orogenic Belt

本文研究区位于兴蒙造山带西段，地理位置属于内蒙古中东部地区（图 1-4）。目前对于该区构造演化仍存在很大争议，特别是对于古亚洲洋闭合的位置和时限。前人通过构造分析、沉积学、地球化学、年代学等方面的研究，对该区域构造演化提出两种主要模式：

第一种模式的提出主要基于造山带结构分析、地层不整合关系和构造变形角度（Tang, 1990; Xu et al., 2013；徐备等, 2014）。认为古亚洲洋由浑善达克地块（松辽-浑善达克地块西段）分隔成两支，并分别向南俯冲至华北板块之下形成白乃庙岛弧，向北俯冲至艾里格庙-锡林浩特-兴安地块之下形成宝力道岛弧（图 1-5）。浑善达克地块与华北克拉通于晚志留世发生碰撞，碰撞形成的蛇绿混杂带被上志留-下泥盆统西别河组砾岩不整合覆盖。浑善达克地块与北部艾里格庙-锡林浩特-兴安地块于晚泥盆纪发生碰撞，蛇绿混杂带被上泥盆统色日巴彦敖包组陆相磨拉斯砾岩不整合覆盖。自此，内蒙古中部地区已无广泛大洋存在，石炭纪－二叠纪本区进入陆表海-伸展盆地演化阶段（徐备等, 2014）。

第二种模式的提出主要基于对蛇绿岩和石炭纪－二叠纪侵入岩类的年代学和地球化学研究以及二叠纪碎屑锆石研究（Chen et al., 2000; Xiao et al., 2003; Zhang et al., 2009a; Eizenhofer et al., 2014）。认为华北板块与南蒙古大陆边缘（图 1-4 中艾里格庙-锡林浩特-兴安地块）之间并无显著陆块存在，古亚洲洋的南北双向俯冲在华北板块边缘形成白乃庙岛弧，在艾里格庙-锡林浩特-兴安地块边缘形成宝力道岛弧。古亚洲洋的俯冲从奥陶纪一直持续到二叠纪，直到晚二叠世－早三叠世华北板块与南蒙古板块最终沿着索伦科尔缝合带碰撞（图 1-6）。

1.3 Overwiew of the Study

1.3.1 Research purpose

对比以上两种演化模式，二者最主要的矛盾在于古亚洲洋最终闭合的时限，这一矛盾已困扰地质学家几十年。因此，本文将这一本区最大争议作为拟解决的科学问题进行论文选题。古亚洲洋闭合时限的争议主要集中于泥盆纪-二叠纪，因此泥盆纪－二叠纪各类岩石是解决这一争议的最佳目标。本文将该区泥盆纪－二叠纪沉积岩及火山岩作为研究对象，通过多学科研究来对古亚洲洋最终闭合时

限进行限定。

前人对该区的研究主要集中于造山带构造分析、岩浆岩岩石学、地球化学、地质年代学等方面，而对于地层学及地层对比、沉积物源分析和古地磁方面的研究则较为缺乏。因此，针对这三个较为薄弱的方面，本文将主要对晚古生代地层进行沉积学、物源分析和古地磁方面的研究。另外，结合对地层中火山岩和碱性侵入岩的年代学和地球化学讨论，来综合分析该区晚古生代构造演化特征，从而对古亚洲洋在内蒙古中东部闭合时限的问题提供新证据。

1.3.2 Research contents

本文具体研究内容包括以下几方面：

1) 泥盆纪－二叠纪沉积岩的沉积学研究。选取内蒙古中东部几个关键地区的泥盆纪－二叠纪地层剖面进行野外测量和观察，探讨其沉积特征并划分沉积相。通过区域对比讨论整个内蒙古中东部地区在各个时代的不同沉积环境。

2) 泥盆纪－二叠纪沉积岩的物源分析。在沉积学研究的基础上，选取地层剖面中的碎屑岩进行碎屑锆石 U-Pb 年代学实验，以此来探讨沉积地层物源。通过不同地区碎屑锆石结果的对比，讨论物源区的差别，从而追朔当时的盆地分布。

3) 泥盆纪－二叠纪地层古地磁研究。在野外剖面测量的基础上，选取适合进行古地磁实验的地层进行古地磁采样。通过实验室测量得到不同时代地层的古地磁方向，从而计算其古地磁极和古纬度，用于同华北克拉通、西伯利亚克拉通以及两者之间的各个块体进行对比，从而得到古板块不同时期的相对位置。

4) 火山岩年代学和地球化学研究。石炭纪和二叠纪地层中包含多个火山岩夹层（例如上石炭-下二叠统宝力高庙组、下二叠统大石寨组和下二叠统清凤山组）。通过对其进行精确的年代学测定，限定地层沉积的具体时代；通过地球化学研究反演火山喷发时的大地构造背景，从而为讨论区域大地构造提供依据。

5) 碱性岩年代学和地球化学研究。内蒙古中东部分布两条碱性岩带：北部中蒙边境早二叠世碱性岩带和中部中二叠世碱性岩带。北部早二叠世碱性岩带研究程度较高，本研究针对中部中二叠世碱性岩带进行年代学和地球化学研究，并讨论其大地构造背景。

1.3.3 Research Design and Methodology

针对以上研究内容，本论文将采用如下研究方法：

野外地质考察：以内蒙古中东部各 1:25 万和 1:20 万区域地质图为基础进行野外地质考察。选取出露较好的晚古生代地层进行剖面测量和野外观察。对地层之间接触关系和与侵入岩的关系进行野外识别。

沉积相划分和对比：通过对出露较好的地层进行野外测量和观察，绘制剖面图和柱状图。通过野外沉积构造观察，岩性和粒度变化，化石识别和采集等方面分析沉积相和沉积环境，进而通过区域对比反应整体构造环境。

年代学研究：包括对沉积岩的碎屑锆石研究和对岩浆岩的定年研究。在野外剖面测量过程中采集碎屑岩样品，对其进行碎屑锆石测年，结合镜下观察，对沉积物源进行分析。对岩浆岩的定年用来准确限定火山岩和侵入岩时代。锆石 LA-ICP-MS U-Pb 定年在中国地质大学（北京）和北京大学的 LA-ICP-MS 实验室完成。测试设备为激光剥蚀进样系统（UP193SS）和 Agilent 7500a 型四级杆等离子体质谱仪联合构成的激光等离子质谱仪。锆石 U/Pb 及年龄校准选用标准锆石 91500；元素含量以国际标样 NIST610 为外标，Si 为内标计算，NIST612 和 NIST614 做监控盲样。普通铅根据实测 ^{204}Pb 校正，方法同 Andersen（2002）。年龄值选用 $^{206}Pb/^{238}U$ 年龄，单个数据点误差均为 1σ。每个锆石测试点的同位素比值、U-Pb 表面年龄和元素含量计算采用澳大利亚 Glitter 4.4 程序，加权平均年龄计算及谐和图的绘制采用 Isoplot 软件 (Ludwig，2003)。样品测试过程中选择不谐和度值<10%的数值进行统计分析。

地球化学研究：在野外考察基础上采集火山岩和侵入岩样品进行地球化学研究，并结合年代学研究探讨不同时代岩浆岩的侵入环境，从而探讨该时代区域构造特征。样品的主量元素分析在北京大学造山带和地壳演化教育部重点实验室的 ARL ADVANTXP+ 扫描型波长色散顺序 X 射线荧光光谱仪上完成。微量元素分析在核工业地质研究所和加拿大 Acme 公司完成。微量元素在 Elan 6100DRC ICP-MS 上分析测定。

古地磁研究：在野外剖面测量过程中，选取合适地层进行古地磁采样。通过实验室剩磁测量得到不同时代地层的剩磁方向，从而计算板块的古纬度并比较不同板块之间的相对位置。古地磁研究在法国奥尔良大学磁学实验室完成。首先对

样品进行居里温度 (Curie) 和等温剩磁 (IRM)测量，获得岩石主要载磁矿物。然后对样品进行磁清洗，采用交变磁场退磁和加热退磁两种方法逐步退磁，并在退磁过程中进行剩磁测量，测定样品的剩磁矢量的强度和方向，直至把原生剩磁分离出来为止。加热退磁使用马氏炉进行，交变磁场退磁使用捷克制 Agico LDA-3 自动交变退磁仪和 2G-755R 交变退磁仪系统。剩磁测量使用捷克制 AGICO JR-5A 旋转磁力仪和 2G-760 超导磁力仪进行。最后进行数据处理，在计算机平台上使用 PMGSC software packages V4.2 对测试结果进行分析，具体分析手段如下：对于一个采样点来说，使用 Kirschvink 开发的主向量分析技术（Principal component analysis method; Kirschvink, 1980）对每个样品的测试结果进行分析，得出一个原生剩磁方向。然后对每个采样点（Site）所得到的原生剩磁方向进行 Fisher 统计（Fisher spherical statistics; Fisher, 1953），若干个较为集中的测试结果可以求得一个较为集中的特征剩磁方向。通过对每个层位的所有采样点再次进行 Fisher 统计，可以求出一个特定地层的较为集中的原生剩磁方向，通过该原生剩磁方向即可计算该地层形成时代的特征剩磁方向。获得地层的特征剩磁方向之后就可以利用该方向计算古地磁极，恢复古地理位置，进行古地理重建。古地理重建在普通微型计算机平台上使用 Cogné 开发的 Paleomag 软件完成（Cogné, 2003）。

Chapter 2 Geological Settings of western Xing-Meng Orogenic Belt

2.1 Tectonic frameworks of central-eastern Inner Mongolia

研究区横跨三个地块，由北向南依次为艾里格庙-锡林浩特-兴安地块、松辽-浑善达克地块和华北板块。三个板块由两条中古生代造山带分隔，分别命名为北造山带和南造山带（图 2-1; 徐备等, 2014）。

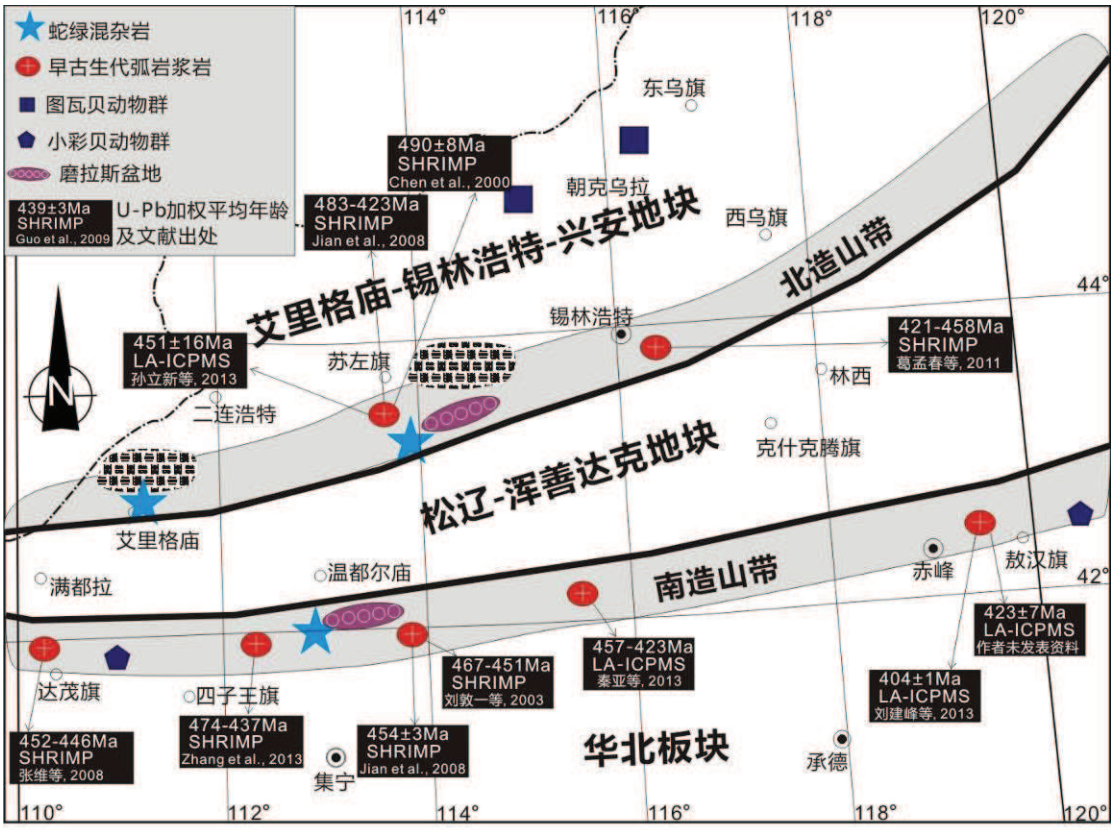

图 2-1 内蒙古中东部构造纲要图

Figure 2-1 Tectonic units of central-eastern Inner Mongolia

2.1.1 Airgin Sum-Xilinhot-Xing'an Block

该地块从艾力格庙向东到苏尼特左旗和锡林浩特地区，向西与蒙古境内的 Hutag Uul 地块相连（Bardarch, et al., 2002），向北东与兴安地块相连。Yarmolyuk et al.（2005）在蒙古境内的 Totoshan 地区得到片麻状花岗岩中锆石的上交点年龄为 952±8Ma，代表原岩形成时代。Wang et al.（2001）在中蒙边境雅干地区得到

片麻状花岗岩的锆石谐和年龄为916±16Ma。艾力格庙地区出露的艾力格庙群由石英岩、片麻岩和花岗片麻岩等组成，从石英岩中获得最年轻的碎屑锆石年龄为1151±41Ma（徐备未发表数据）。孙立新等（2013）在苏尼特左旗东部报道了年龄为1516±31Ma和1390±17Ma的花岗片麻岩，代表该区存在中元古代变质基底。对于该地块中一个重要的基底组成单元，基于Sm-Nd，Rb-Sr等时线法，锡林郭勒杂岩在上世纪八九十年代被认为是早－中元古代变质基底（徐备等，1996; 郝旭和徐备, 1997）。但随着锆石U-Pb的应用，早古生代碎屑锆石的厘定使得不少学者认为锡林郭勒杂岩属于早古生代沉积岩系（施光海等, 2003；薛怀民等, 2009；Chen et al., 2009；陈斌等, 2012）。然而，最近葛梦春等（2011）报道了锡林浩特地区锡林郭勒杂岩中的表壳岩，并从中获得 1005-1026Ma 的锆石变质核年龄，认为锡林郭勒杂岩属于中元古代基底，并在早古生代发生岩浆侵入和混合岩化，导致测试中出现早古生代碎屑锆石。上述古老岩石代表的前寒武纪地块构成一个重要构造单元。

2.1.2 Songliao-Hunshandake Block

该地块东部被松辽盆地、西部被浑善达克沙地所覆盖，呈东宽西窄的三角形，由于覆盖严重，基底物质出露较少，仅出露于地块边缘地区。松辽盆地东缘的云母片岩显示757±9Ma、843±10Ma的最小年龄峰值，说明其可能沉积于新元古代（Wang et al., 2014; 权京玉等，2013）。松辽盆地南部，裴福萍等（2006）从钻孔岩心中得到的火山角砾岩和变质辉长岩年龄分别为 1808±21Ma 和1873±13Ma。王颖等（2006）也在附近报道了1839±7Ma的变质闪长岩SHRIMP锆石年龄。这些数据表明松辽地块应存在早前寒武纪基底。在地块西部浑善达克沙地北缘（苏尼特左旗南）和南缘（温都尔庙地区），温都尔庙群绢云石英片岩的碎屑锆石图谱均出现大量5-22亿年的数据（徐备未发表数据；李承东, 2012），提供了地块西部可能存在前寒武纪基底的信息。

2.1.3 North China Craton

华北板块主要由新太古代－古元古代变质基底组成，以2.5 Ga和1.8 Ga两个主要的年龄峰为显著特征（Zhai and Santosh, 2011）。内蒙古中东部的华北北缘地区出露古元古代宝音图群白云母片岩、石英岩、角闪石片岩和大理岩等，时代

均为 2.5 Ga（张玉清和苏宏伟, 2002）。

2.1.4 Northern Orogen

北造山带沿艾里格庙－苏尼特左旗－锡林浩特－西乌旗一线延伸，分隔艾里格庙-锡林浩特-兴安地块与松辽-浑善达克地块（图 2-1）。沿线分布早古生代岩浆岩、蛇绿混杂岩和磨拉斯盆地（Xu et al., 2013; 徐备等, 2014）。缝合线北侧发育早古生代宝力道岛弧岩浆岩带，发育时间为 498-423 Ma（Chen et al., 2000; 石玉若等, 2004; Jian, et al., 2008）。石玉若等（2005）在苏左旗南部厘定出 425-423 Ma 的高钾富碱花岗岩，认为其标志着俯冲的结束。苏尼特左旗南部和艾里格庙地区分布着由早古生代绿片岩为基质，蛇绿岩、大理岩、灰岩、蓝片岩和含铁石英岩等为杂块的蛇绿混杂岩带（Xu and Chen, 1997; Xu et al., 2013）。对基质绿片岩的碎屑锆石显示 576-735 Ma 和 911-1044 Ma 两个主要的年龄群，而最小锆石年龄 488 Ma 限定了其原岩沉积晚于寒武纪末期（Xu et al., 2013）。在苏尼特左旗南和艾里格庙地区的蛇绿混杂带中均发现高压变质蓝片岩（徐备等, 2001; 李瑞彪等, 2014）。对苏尼特左旗南部蓝片岩的 ^{39}Ar-^{40}Ar 测年得到 383±13 Ma 的变质年龄（徐备等, 2001）。该蛇绿混杂带被上泥盆统色日巴彦敖包组陆相磨拉斯建造不整合覆盖，代表造山带内的磨拉斯盆地，从而限定了造山带发生早于晚泥盆世（Xu et al., 2013）。同时，这条造山带也是重要的生物群界线，其北以分布图瓦贝（*Tuvaella*）动物群为特色，见于东乌珠穆沁旗和朝克乌拉等地（图 2-1; 内蒙古自治区地质矿产局，1991）。

2.1.5 Southern Orogen

南造山带分隔松辽-浑善达克地块和华北板块，从西向东沿图古日格-达茂旗-温都尔庙-正镶白旗-敖汉旗-吉中-延吉一线分布。与北造山带一致，沿线分布早古生代岩浆岩、蛇绿混杂岩和磨拉斯盆地（Xu et al., 2013; 徐备等, 2014）。研究区覆盖其达茂旗至敖汉旗段。缝合线南侧发育早古生代白乃庙岛弧岩浆岩带，发育时间为 497-415 Ma（刘敦一等, 2003; 张维和简平, 2008; Jian, et al., 2008; Zhang et al., 2013; 秦亚等, 2013; 刘建峰等, 2013）。平行于白乃庙岛弧分布蛇绿混杂岩带，其中以温都尔庙地区乌兰沟和达茂旗地区红旗牧场为代表地区（唐克东，1992；胡骁等，1990；邵济安，1991；Xu et al., 2013; Shi et al., 2013）。混杂带中

高压蓝片岩得到蓝闪石和多硅白云母 ^{39}Ar-^{40}Ar 年龄为 445.6 ± 15 Ma, 453.2 ± 1.8 Ma 和 449.4 ± 1.8 Ma（Tang and Yan, 1993; De Jong et al., 2006）。该蛇绿混杂带被上志留统-下泥盆统西别河组陆相磨拉斯建造不整合覆盖，代表造山带内的磨拉斯盆地，从而限定了造山带发生早于晚志留世（张允平等，2010; Xu et al., 2013）。另外在白乃庙地区，年龄为 411±8Ma 的未变形伟晶岩脉切穿早古生代变形杂岩体，标志着碰撞造山带早于早泥盆世完成（Zhang et al., 2013）。

南北两个造山带演化结束之后，上述三个板块拼贴在一起，内蒙古中东部地区进入造山后陆内演化阶段（Tang, 1990）。

2.2 Devonian-Permian sedimentation

中-晚泥盆世之后，内蒙古中东部地区完成了从古亚洲洋到兴蒙造山带的构造格局转变。早泥盆世地层沿南造山带和中蒙边境分布。晚泥盆世地层仅局限于北造山带的苏尼特左旗和阿巴嘎旗地区，以含植物化石的陆相及海陆交互相沉积为特征。石炭纪则广泛分布陆相及滨浅海相碎屑岩和碳酸盐岩建造，同时发育辉长岩、花岗岩及双峰式火山岩等，构成多条不同类型的岩浆岩带。二叠纪则发生从早中二叠世浅海相碎屑岩－碳酸盐岩向晚二叠世陆相砾岩及泥岩的转变，并于早二叠世发育大规模火山作用（内蒙古自治区地质矿产局，1991）。研究区主要地区晚古生代地层列于表 2-1 中。

2.2.1 Devonian

早泥盆世沉积分布于研究区南部达茂旗、温都尔庙和敖汉旗地区，及北部中蒙边境地区（表 2-1；图 2-2）。达茂旗和温都尔庙地区下泥盆统西别河组（又称那清组），其底部可至志留纪顶部（张允平等, 2010）。西别河组角度不整合在蛇绿混杂岩、岛弧火山岩、加里东期花岗岩和弧后盆地复理石沉积之上，为一套由下部底砾岩、粗砂岩夹灰岩、中部红色砂岩和灰岩、上部石英砂岩和灰岩组成的陆相－海相磨拉斯建造（张允平等, 2010）。敖汉旗地区下石碑组以岩屑砂岩为主，最初被认为志留系沉积，最新碎屑锆石研究显示其沉积于早泥盆世（程胜东等，2014）。中蒙边境地区广泛分布下－中泥盆统泥鳅河组，地层沿北东东向展布（图 2-2）。除二连浩特北部查干敖包剖面底部为一套陆相红色砾岩－粗砂岩组合外，该剖面上部层位及东部各剖面均为含丰富浅海相动物化石的碎屑岩夹灰岩地层。

晚泥盆世沉积仅出现在北造山带苏尼特左旗南部和阿巴嘎旗南部，以色日巴彦敖包组为代表（图 2-2; Xu et al., 2013）。色日巴彦敖包组角度不整合覆盖在蛇绿混杂岩和温都尔庙群之上，为一套底部红色砾岩，向上渐变为砾岩与粗砂岩互层组成的陆相磨拉斯建造，并含植物化石 *Leptophloeum rhombicum*。顶部为约 50cm 厚的生物碎屑灰岩（邵济安, 1991; Xu et al., 2013）。

表 2-1 内蒙古中东部主要地区晚古生代地层表

Table 2-1 Comparison of the Late Paleozoic stratigraphic sequences in central Inner Mongolia

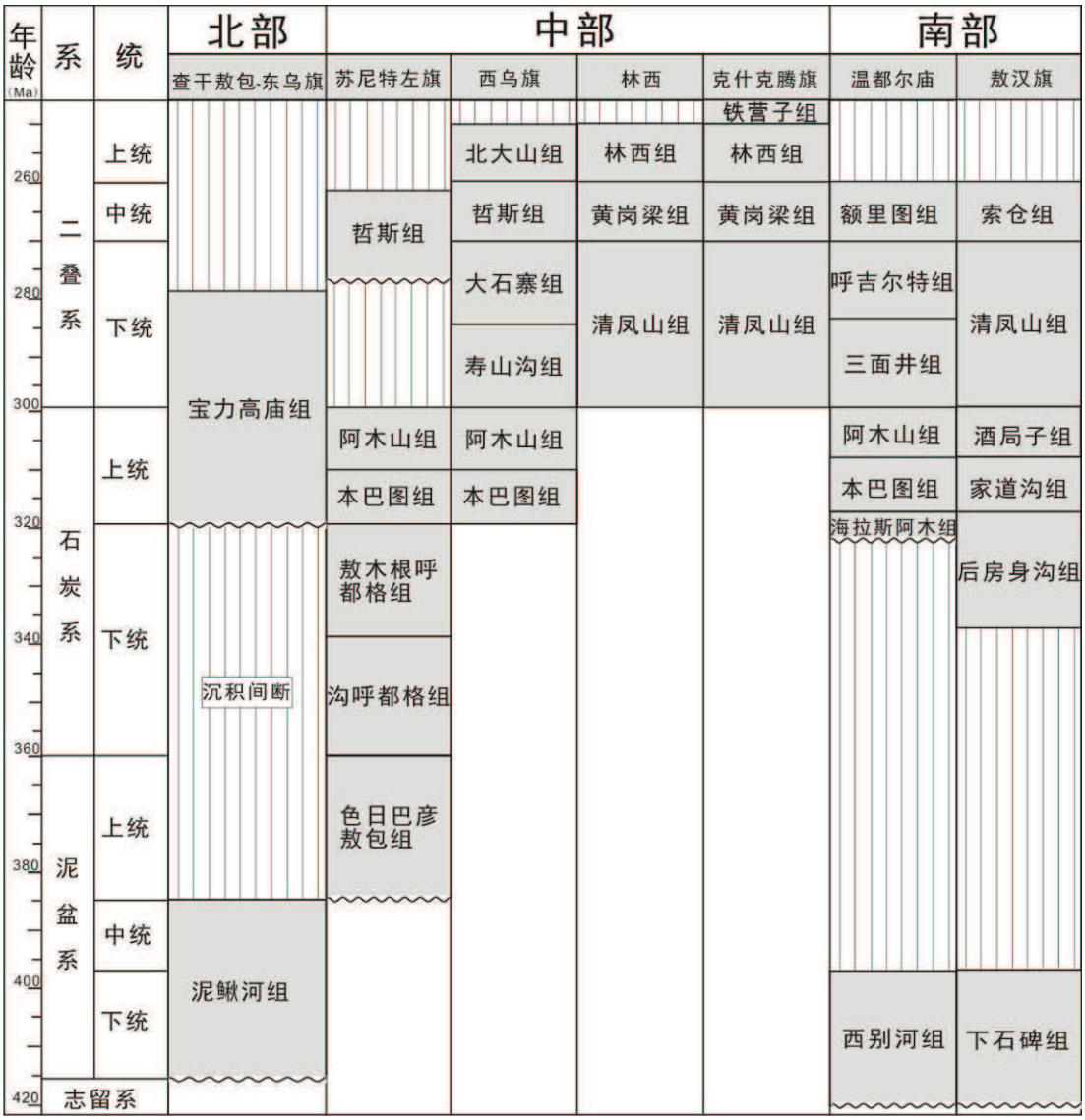

2.2.2 Carboniferous

早石炭世内蒙古大部分地区处于剥蚀状态，仅在苏左旗南部和敖汉旗北部发育下石炭统沉积（表 2-1；内蒙古地质矿产局, 1991）。苏尼特左旗南部下石炭统

为一套磨拉斯盆地沉积之上的潮坪相碎屑岩沉积（Xu and Chen, 1997; Xu et al., 2013）。敖汉旗北部下石炭统为一套巨厚层碳酸盐岩台地沉积，含大量腕足和珊瑚类化石，未见与下伏地层接触关系（内蒙古地质矿产局，1991）。

晚石炭世研究区北部（中蒙边境一带）发育陆相沉积盆地，分布于查干敖包－白音乌拉－东乌珠穆沁旗一线，以宝力高庙组陆相沉积－火山岩系为代表，向东北延伸至额尔古纳右旗及黑龙江省大部，以类磨拉斯建造不整合超覆在前寒武纪变质基底、早古生代沉积地层及蛇绿岩之上（内蒙古地质矿产局, 1991；鲍庆中等，2006），并出现华夏植物群与安加拉植物群的混生现象（辛后田等, 2011）。中部则发育陆表海盆地沉积，沉积建造以浅海相碳酸盐岩和碎屑岩为主（如本巴图组和阿木山组），分布范围覆盖整个内蒙古地区，从乌拉特中旗经苏尼特右旗、西乌旗、乌兰浩特等地，向东可延伸到吉林省北部。晚石炭世末，在造山带西南缘满都拉地区和东南缘敖汉旗地区，发育海陆交互相或陆相盆地，局部出现含煤岩系（如敖汉旗酒局子组），并出现华夏植物群化石 *Calamites*（内蒙古地质矿产局, 1991；1:25 万满都拉幅）。

晚石炭世碎屑沉积多夹火山岩，且分布广泛（图 2-3）。如曾维顺等（2011）获得大石寨地区大石寨组火山岩年龄为 314±1 Ma，据此提出晚石炭世应为裂陷盆地；辛后田等（2011）将东乌珠穆沁旗宝力高庙组厘定为 320-303Ma 的陆相火山-碎屑岩建造；汤文豪等（2011）在苏尼特右旗本巴图组中识别了 313-308Ma 的双峰式火山岩，并认为研究区应处于裂谷构造环境。

综上所述，石炭纪地层发育于广阔的陆相-海陆交互相-滨海相沉积盆地（内蒙古自治区地质矿产局，1991；邵济安, 1991），这类盆地不整合于早古生代造山带之上，属上叠型沉积古地理单元（徐备等, 2014）。

2.2.3 Permian

早二叠世初期，内蒙古中部地区继承了晚石炭世沉积特征，为一套海陆交互相碎屑岩组合，局部可见底部砾岩－粗砂岩组合。以寿山沟组、清凤山组下段和三面井组为代表（表 2-1）。早二叠世晚期区内普遍发育裂谷火山岩，以北部宝力高庙组火山岩段、中部大石寨组和南部清凤山组火山岩段为代表。北部宝力高庙组包含陆相碎屑沉积和双峰式火山岩组合，锆石 U-Pb 年代学所获其喷发年龄

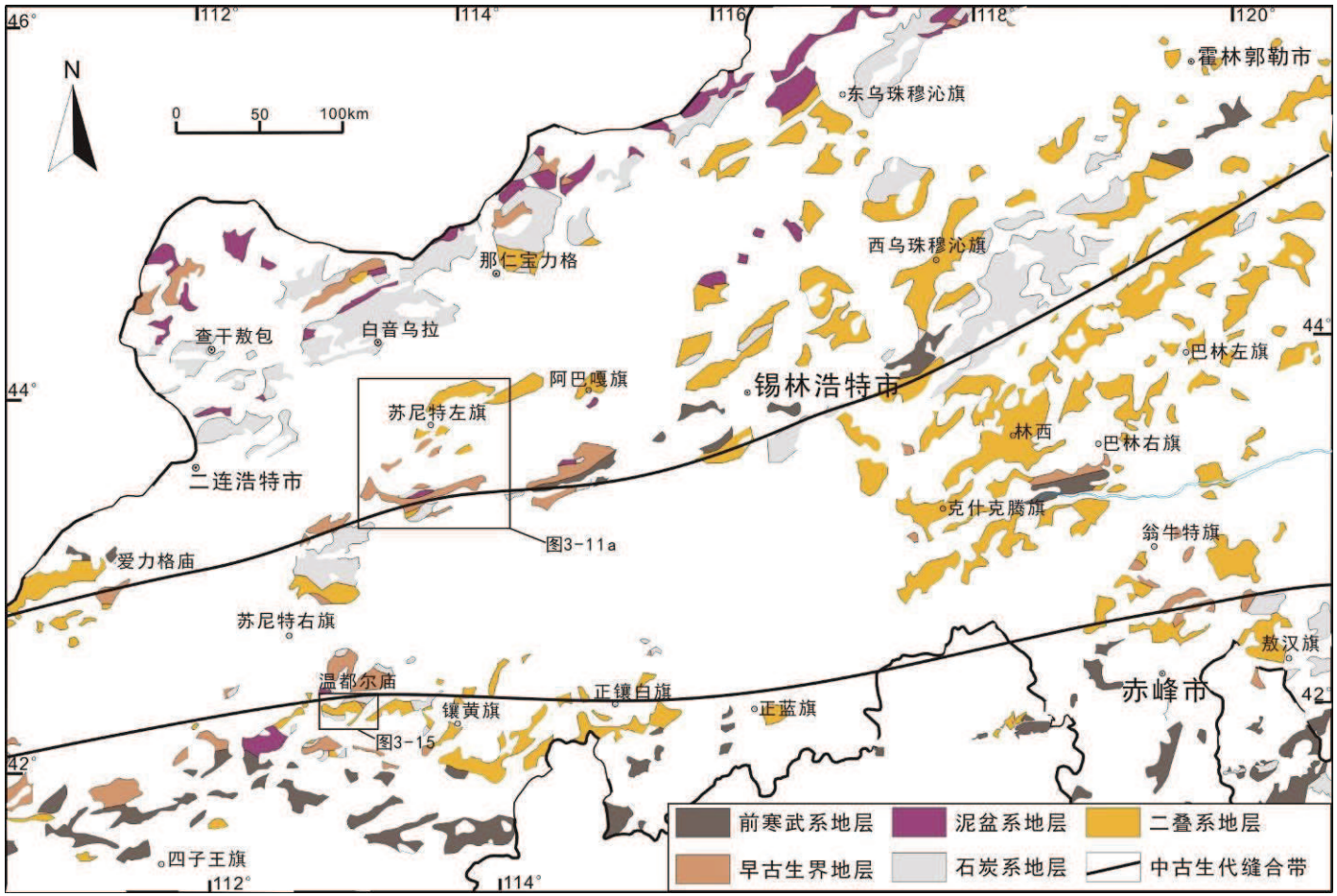

图 2-2 内蒙古中东部古生代地层分布图（内蒙古自治区地质矿产局，1991）

Figure 2-3 Distribution of the Devonian-Permian strata in central Inner Mongolia (IMBGMR, 1991)

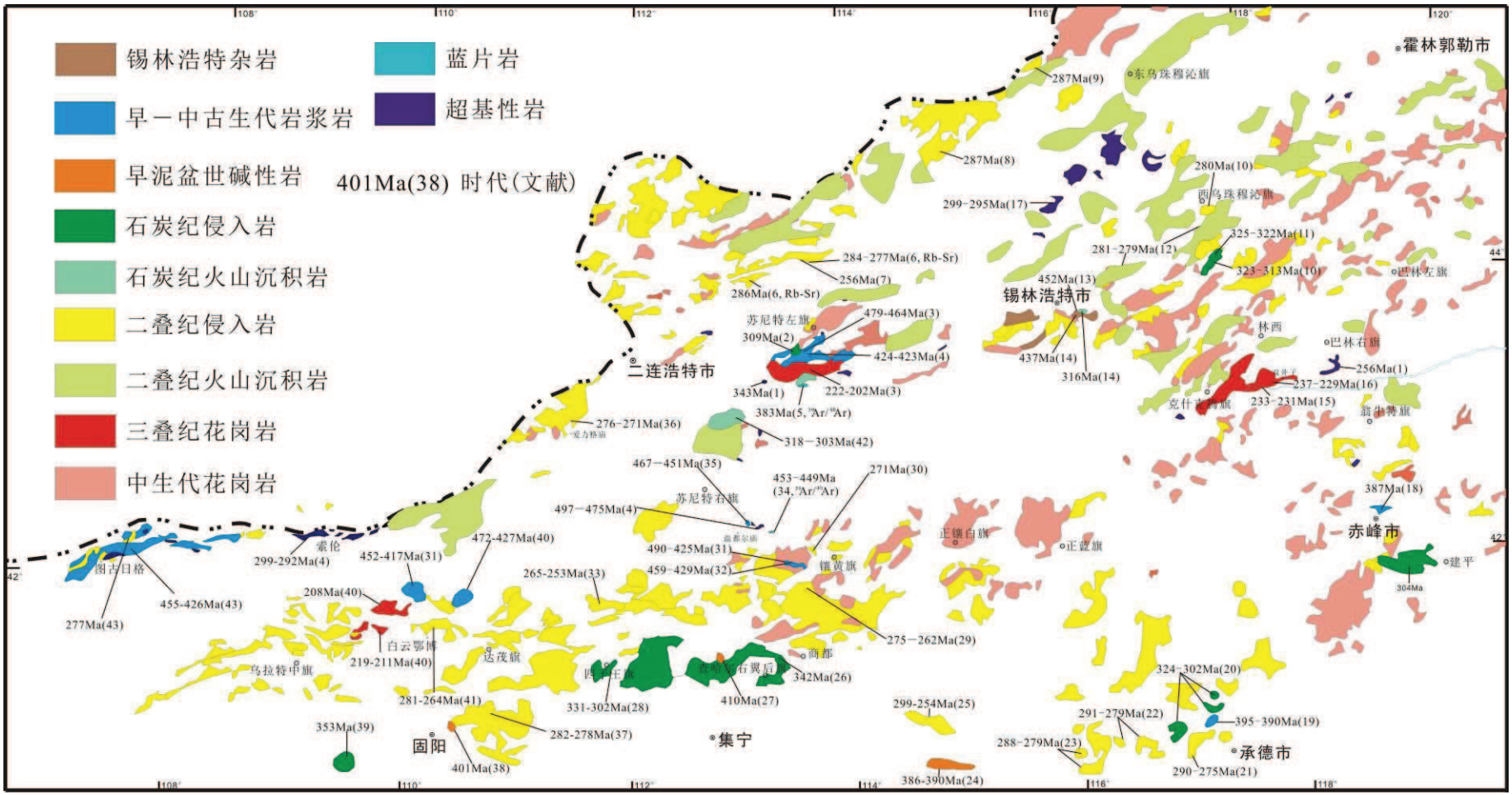

图 2-3 内蒙古中部泥盆纪－二叠纪岩浆岩分布图

Figure 2-3 Distribution of the Devonian-Permian magmatic rocks in central Inner Mongolia

在 290 Ma 左右（Zhang et al., 2011）。中部大石寨组双峰式火山岩的锆石 U-Pb 年代学所获其喷发年龄在 280 Ma 左右（Zhang et al., 2008）。

中二叠世内蒙古北部为隆起剥蚀区，仅在少数地区出现陆相沉积，例如东乌旗东部满都胡宝拉格地区新厘定出的早－中二叠纪碎屑岩，以出现华夏植物群化石为特征（周志广等, 2010）。中部沉积以哲斯组为代表的碎屑－碳酸盐岩，含丰富的浅海相动物化石，称之为哲斯生物群（Wang et al., 2004; 方俊钦等, 2014）。林西－克什克腾旗地区则发育黄岗梁组海陆交互相沉积。南部温都尔庙地区发育额里图组火山岩，而敖汉旗地区则发育索仓组海陆交互相碎屑岩（内蒙古地质矿产局，1991）。

晚二叠世内蒙古中部沉积仅分布于西乌旗－克什克腾旗一线，以北大山组和林西组陆相（主体为湖相）巨厚层黑色泥岩为特征，含丰富植物化石（内蒙古地质矿产局，1991）。克什克腾旗南部可见晚二叠世末期的铁营子组陆相磨拉斯沉积，底部以巨厚砾岩不整合覆盖在林西组和中二叠世侵入岩之上。

2.3 Devonian-Permian magmatism

2.3.1 Devonian

泥盆纪岩浆岩仅发育于华北板块北缘（图 2-3），以碱性岩和碱性花岗岩为主。锆石 U-Pb 年代学研究表明其侵位于 410-390 Ma（罗镇宽等, 2001; Jiang, 2005; Zhang et al., 2009b; 张晓晖和翟明国, 2010），可能代表南造山带形成之后华北北缘的伸展事件。

2.3.2 Carboniferous

石炭系岩浆岩主要分布于北部查干敖包和东乌旗地区，中部苏尼特左旗－锡林浩特－西乌旗一线，以及南部四子王旗－商都和承德－建平地区（图 2-3）。岩性以花岗岩、花岗闪长岩和辉长岩为主。已报道的石炭纪岩浆岩包括北部查干敖包地区的碱性花岗岩（317-308Ma，许立权等，2012）和东乌旗东部花岗岩（319Ma，梁玉伟，2013）。中部苏尼特左旗白音宝力道石英闪长岩（309±8 Ma，Chen et al., 2000），锡林浩特地区侵入锡林浩特杂岩中的石榴石花岗岩（316±3 Ma，施光海等，2003），西乌旗南部白音高勒石英闪长岩（323-300Ma，鲍庆中等，2007；

刘建峰等，2009；薛怀民等，2010）。南部四子王旗辉长岩（331±4 Ma，周志广等，2009）和花岗岩（320-317Ma，Zhang et al., 2012），承德地区花岗闪长岩（324-302Ma，Zhang et al., 2007; 2009a）等。对于石炭纪岩浆岩所代表的构造环境，存在俯冲和张性构造两种截然不同的观点。

2.3.3 Permian

二叠纪岩浆岩整体呈面状广泛分布于整个内蒙古中东部地区（图 2-3），包括花岗岩、碱性花岗岩、花岗闪长岩、辉长岩等(张晓晖和翟明国，2010；徐备等，2014)。

已有研究表明，兴蒙造山带内发育南、北两条二叠纪碱性岩带（徐备等，2014）。北带从沿中蒙边界由二连浩特北部向东延伸至东乌旗，由大量早二叠世碱性花岗岩（洪大卫等，1994; Wu et al., 2002）和双峰式火山岩（Zhang et al., 2011）组成。该带向西延至蒙古国南部，与 Yarmolyuk 等（2008）所划分的裂谷岩浆岩带连通。南带位于达茂旗-温都尔庙-镶黄旗一线，已报道达茂旗北部花岗岩时代为 270-257Ma（范宏瑞等, 2009）；镶黄旗南部毕力赫钾长花岗岩时代为 264Ma（路严明等, 2012）；克什克腾旗南部碱性岩时代为 264-263Ma（江小均等, 2011）。另外该带包含大量中二叠世花岗岩、花岗闪长岩及辉长－辉绿岩，共同组成兴蒙造山带南部中二叠世岩浆岩带（图 2-4; Liu et al., 2010; 章永梅等, 2009；王子进等, 2013; Cao et al., 2013）。

Chapter 3 Devonian sedimentology features and detrital zircon geochronology

泥盆纪沉积仅出现于北部中蒙边境地区，北造山带的苏左旗－阿巴嘎旗以及南造山带的达茂旗－温都尔庙地区。

3.1 China-Mongolia border areas

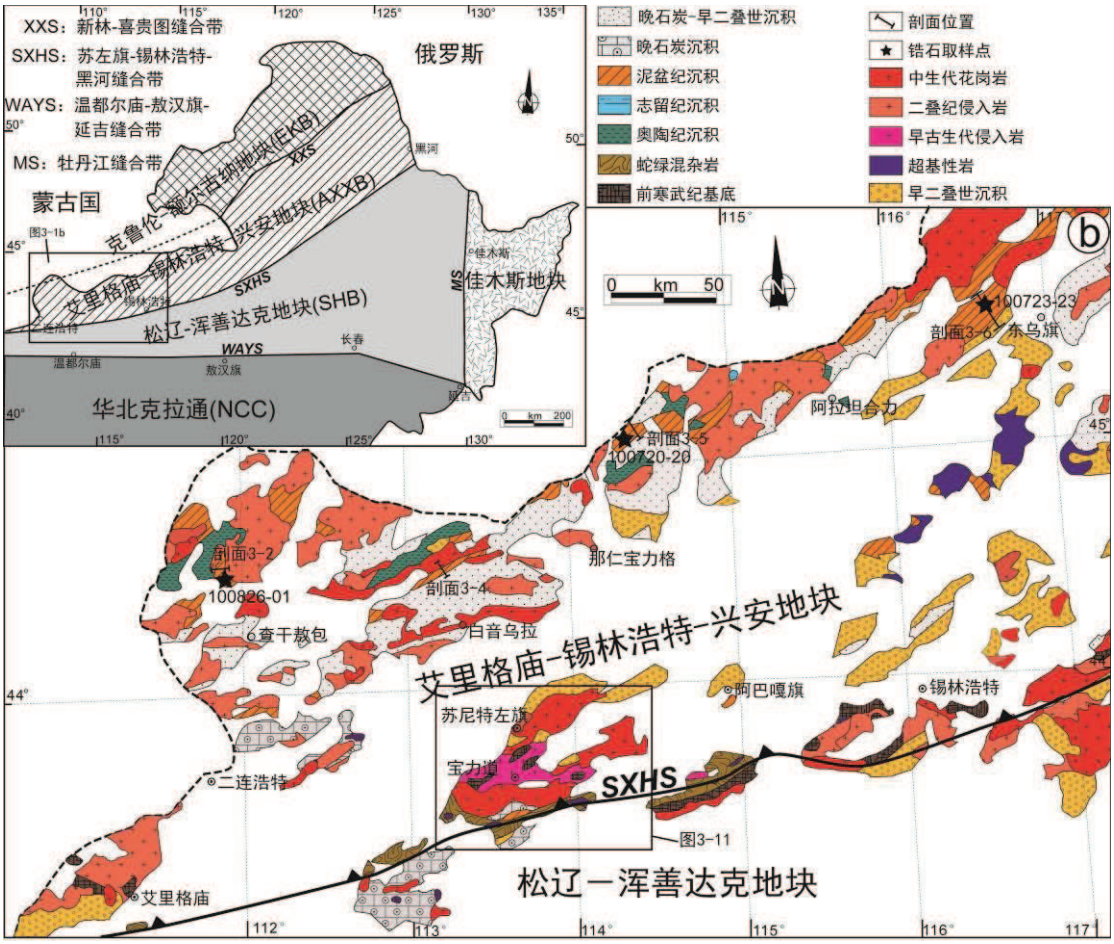

图3-1 内蒙古北部中蒙边境地区地质图及工作剖面位置（据内蒙古地质矿产局, 1991）。缝合带位置据 Xu et al., 2013

Figure 3-1 Geological map of China-Mongolia border area (from IMBGMR, 1991). The location of the suture zone is from Xu et al., 2013

中蒙边境地区位于艾里格庙-锡林浩特-兴安地块内部（图 3-1），该区泥盆纪沉积以下－中泥盆统泥鳅河组为代表（图 2-2），分布于查干敖包－白音乌拉－那仁宝力格－东乌旗一线（图 3-1）。与下伏奥陶纪－志留纪沉积接触关系不明。为

了探明其沉积环境和物源，本次分别在查干敖包、白音乌拉、那仁宝力格、东乌旗四个地区进行了野外剖面测量、沉积相分析及相应碎屑锆石测年工作。

3.1.1 Sedimentological studies and facies analyses

3.1.1.1 Chaganaobao area（剖面起点 GPS：44°30′57″N，111°54′51″）

查干敖包地区泥鳅河组分为两段，一段为红色底砾岩和红色粗砂岩；二段下部为红色细砾岩与砂岩，向上转变为灰岩，含丰富双壳类化石；二段上部为粉砂岩与凝灰岩-火山岩互层（图 3-2）。详细剖面测量描述如下：

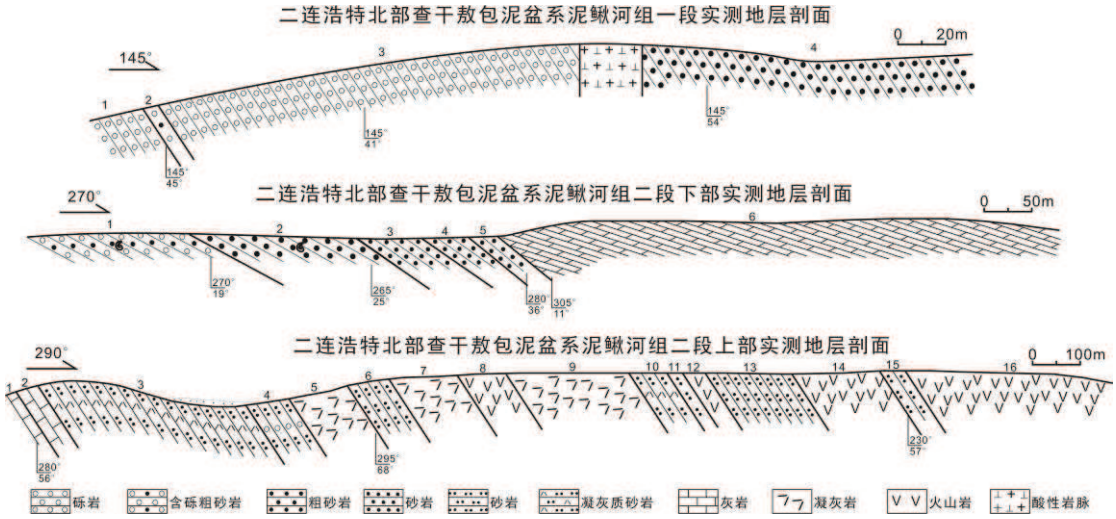

图 3-2 二连浩特北部查干敖包地区下—中泥盆统泥鳅河组实测地层剖面

Figure 3-2 Stratigraphic section of the Lower-Middle Devonian Niqiuhe Formation in Chaganaobao area, north of Erenhot

泥鳅河组二段上部实测地层剖面：

-----未见顶-----

16. 灰黄色含石英斑晶火山岩 287.7m

15. 浅灰绿色中-厚层状硅质粉砂岩 68.8m

14. 深灰绿色火山岩，含少量短柱状长石斑晶 149.2m

13. 灰绿色薄层状粉砂岩 140.9m

12. 含石英砾石火山岩 37.3m

11. 薄层状紫红色粉砂岩与砂岩互层 21.6m

10. 深灰黑色薄层状凝灰质粉砂岩 48.9m

9. 黄褐色凝灰岩，局部发育流纹构造 189.1m

图 3-3 查干敖包泥鳅河组剖面的野外照片：a，底砾岩; b，砾岩上部发育平行层理的红色粗砂岩; c，红色砂岩中的椭球形火山岩砾石; d，红色砂岩中的递变层理; e，红色砂岩中的双壳类化石; f，灰岩中的腕足类化石

Figure 3-3 Photograhps of the Niqiuhe Formation in Chaganaobao area: a, conglomerate at the bottom; b, red coarse-grained sandstone with parallel beddings on the top of conglomerate; c, ellipsoidal volcanic pebbles within red sandstone; d, red sandstone with graded beddings; e, bivalve within red sandstone; f, Brachiopoda within limestone

8. 灰绿色火山岩，含大量短柱状长石斑晶 82.9m

7. 流纹质凝灰岩，下部为灰黄色，上部为浅紫红色，发育流纹构造 114.4m

6. 灰黑色薄-中层状粉砂岩 76.3m

5. 黄绿色火山岩 24.9m

4. 灰黄色厚层状含石英砾石石英粉砂岩 49.7m

3. 薄层状凝灰质粉砂岩 247.1m

2. 灰白色厚层状亮晶灰岩，几乎不含生物碎屑 34.8

1. 紫红色薄层状亮晶灰岩，含化石碎片 20.7m

-----侏罗纪玄武岩覆盖-----

泥鳅河组二段下部实测地层剖面：

-----第四系覆盖-----

6. 灰白色厚层状灰岩，含大量腕足类和海百合茎化石 172.1m

5. 紫红色中-薄层状石英粗砂岩，发育递变层理，含大量腕足类和双壳类化石 22.3m

4. 土黄色中-薄层状钙质砂岩，含大量生物化石，以腕足类和海百合茎为主 25.2m

3. 黄绿色中-薄层状砂岩，发育长条形泥质孔，可能为生物成因 50.5m

2. 紫红色细砾岩 102.1m

1. 紫红色含火山砾石粗砂岩，砾石呈椭球形，磨圆较好 91.3m

-----第四系覆盖-----

泥鳅河组一段实测地层剖面：

-----第四系覆盖-----

4. 紫红色厚层状长石石英粗砂岩，发育平行层理 118.1m

3. 杂色砾岩 142.4m

2. 红褐色厚层状长石粗砂岩，见大量长石颗粒 4.9m

1. 紫红色砾岩，砾石粒径约 5-20cm，磨圆度高，分选较差 165.8m

-----第四系覆盖-----

一段底部砾岩层厚约 300m，砾石粒径约 5-20cm，磨圆度高，分选较差，成分主要为火山岩、石英岩、砂岩（图 3-3a）。向上粒度变细，转变为发育水平层理的红色石英粗砂岩（图 3-3b），表明动荡的沉积环境。二段下部红色砂岩发育大量火山岩砾石，砾石多呈椭球形，大小在 1cm 左右，杂乱分布于砂岩中（图 3-3c），说明动荡的沉积环境以及较近的物源。砂岩中发育多个递变层理（图 3-3d），并含有丰富动物化石，以双壳类为主（图 3-3e）。红色砂岩被厚层灰岩覆盖，灰岩中含有大量腕足类和海百合茎化石（图 3-3f），代表浅海相沉积环境。二段上部以粉砂岩和火山凝灰岩为主，显示区域内可能在该时期发生强烈的火山

作用。

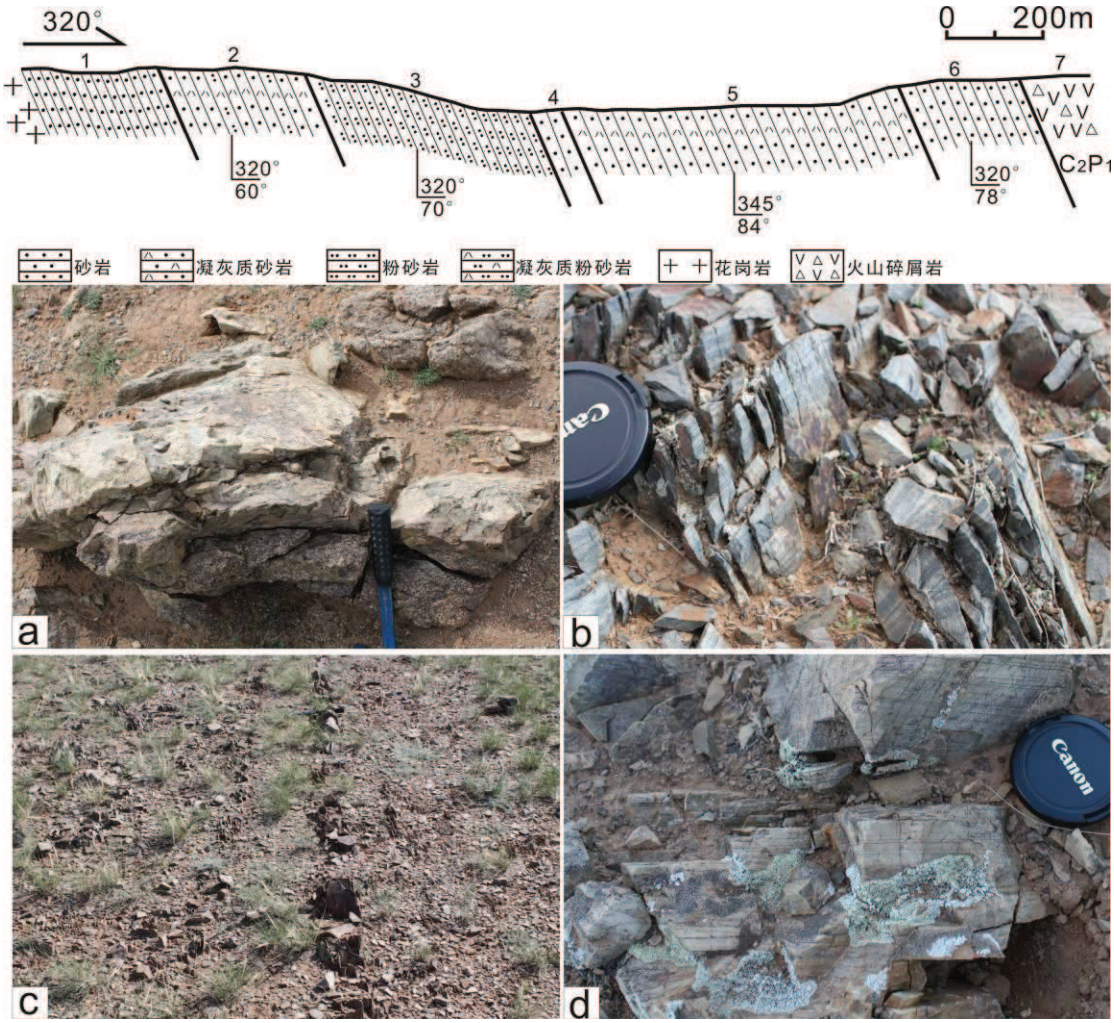

图 3-4 白音乌拉地区下－中泥盆统泥鳅河组实测地层剖面：a，地层底部被二叠纪花岗岩侵入; b，地层底部粉砂岩中发育的水平层理; c，砂岩和泥岩互层，显示良好的成层性; d，地层上部粉砂岩中发育的水平层理

Figure 3-4 Stratigraphic section of the Lower-Middle Devonian Niqiuhe Formation in Baiyinwula area: a, the strata was intruded by Permian granite; b, horizontal bedding within lower siltstone; c, interbedded sandstone and mudstone; d, horizontal bedding within upper siltstone

3.1.1.2 Baiyinwula area（剖面起点 GPS：44°32′04″N，113°10′30″）

白音乌拉泥鳅河组剖面为 GPS 测量，具体剖面描述如下：

------与晚石炭-早二叠世火山岩断层接触------

6. 灰白色厚层状石英砂岩

5. 凝灰质砂岩

4. 灰色片理化细砂岩

3. 劈理化灰黑色中-薄层粉砂岩

2. 凝灰质砂岩夹钙质粉砂岩

1. 深灰色含绢云母变质砂岩，发育水平层理

-----二叠纪花岗岩侵入-----

白音乌拉地区泥鳅河组以薄层状粉砂岩为主。野外未见其与下伏地层的接触关系，底部被二叠纪花岗岩所侵入（图 3-4a）。地层从底至顶均发育水平层理（图 3-4b，d），显示较为稳定的沉积环境。砂岩夹粉砂岩成层性好，侧向延伸较远（图 3-4c），可能代表开阔台地相的产物。上部层位发育凝灰质粉砂岩，说明沉积过程中伴随着区域火山作用。地层中含有丰富的浅海相动物化石，包括腕足类、双壳类、三叶虫和腹足类（1:25 万地质图白音乌拉幅）。综合以上沉积构造和化石特征，白音乌拉地区泥鳅河组主要为一套滨海－浅海环境下的碎屑沉积组合。

3.1.1.3 Narenbaolige area（剖面起点 GPS：45°11′40″N，114°38′38″）

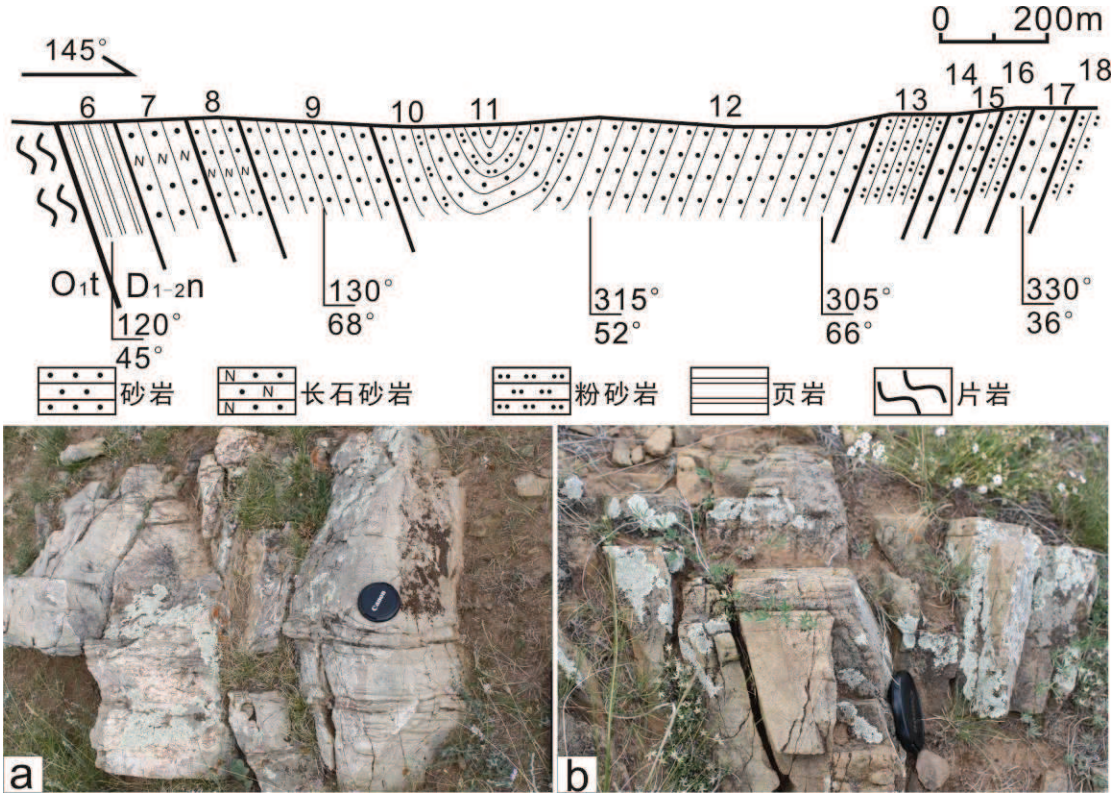

图 3-5 那仁宝力格地区泥鳅河组实测地层剖面：a，石英砂岩中发育的波状层理; b，砂岩中发育的平行层理

Figure 3-5 Stratigraphic section of the Lower-Middle Devonian Niqiuhe Formation in Narenbaolige area: a, wavy beddings within sandstone; b, parallel beddings within sandstone

那仁宝力格地区泥鳅河组剖面为 GPS 测量，具体剖面描述如下：

-----第四系覆盖-----

18. 黄绿色规制粉砂岩，表面风化为浅紫红色

17. 土黄色石英粗砂岩

16. 浅紫红色长石石英砂岩

15. 深灰色粉砂岩

14. 浅紫红色含砾粗砂岩，砾石以石英为主，并含少量深灰色泥质砾石，粒径 3-5mm，磨圆较差，向上砾石粒径变小

13. 深灰黑色中-厚层状粉砂岩

12. 土黄色中-厚层状细砂岩，层理不发育

11. 灰黑色中-厚层状砂岩夹粉砂岩，发育平行层理

10. 灰黑色中-厚层状粉砂岩，发育平行层理

9. 浅紫红色厚层状石英砂岩，向上颜色变为灰绿色

8. 灰白色中-厚层状长石石英细砂岩

7. 浅紫红色长石石英砂岩

6. 灰绿色粉砂质页岩，发育水平层理

-----与下-中奥陶统铜山组片岩断层接触-----

那仁宝力格地区泥鳅河组与底部下奥陶统铜山组呈断层接触（图 3-5）。整个泥鳅河组剖面组成一个大型向斜褶皱（图 3-5）。该剖面以正常沉积的细碎屑岩为主，剖面上下无明显粒度变化。地层中水平层理、波状层理、槽状交错层理等沉积构造广泛发育（图 3-5a，b），表明沉积环境属于水体不稳定的滨海潮汐环境。地层局部发育灰岩夹层，并含大量腕足类化石（1:25 万地质图阿巴嘎旗幅）。

3.1.1.4 East-Ujimqin area（剖面起点 GPS：45°36′23″N，116°44′24″）

东乌珠穆沁旗地区泥鳅河组剖面为 GPS 测量，具体剖面描述如下：

-----第四系覆盖-----

7. 灰黄色中-薄层状粉砂岩夹薄层生物碎屑灰岩，含大量腕足类和双壳类化石

6. 灰黑色生物碎屑灰岩，含大量腕足类、珊瑚和海百合茎化石

5. 黄绿色中-薄层状粉砂岩，含少量灰岩透镜体

4. 灰黑色生物碎屑灰岩，含大量珊瑚化石，厚约 8m

3. 灰白色薄-中层状粉砂岩

2. 灰黄色中层状石英砂岩

1. 灰黄色中-厚层状粉砂岩，含大量腕足类和三叶虫化石

------第四系覆盖------

与那仁宝力格地区泥鳅河组沉积类似，东乌旗地区泥鳅河组以黄色细砂岩为主，含大量三叶虫、腕足类、双壳类和珊瑚等化石（图 3-6）。细砂岩为薄层状，厚约 10cm，夹由大量珊瑚化石组成的生物礁灰岩（图 3-6b，d）。地层中沉积构造不发育。从岩石组合和化石组合反映出，泥鳅河组属于稳定的浅海相沉积。

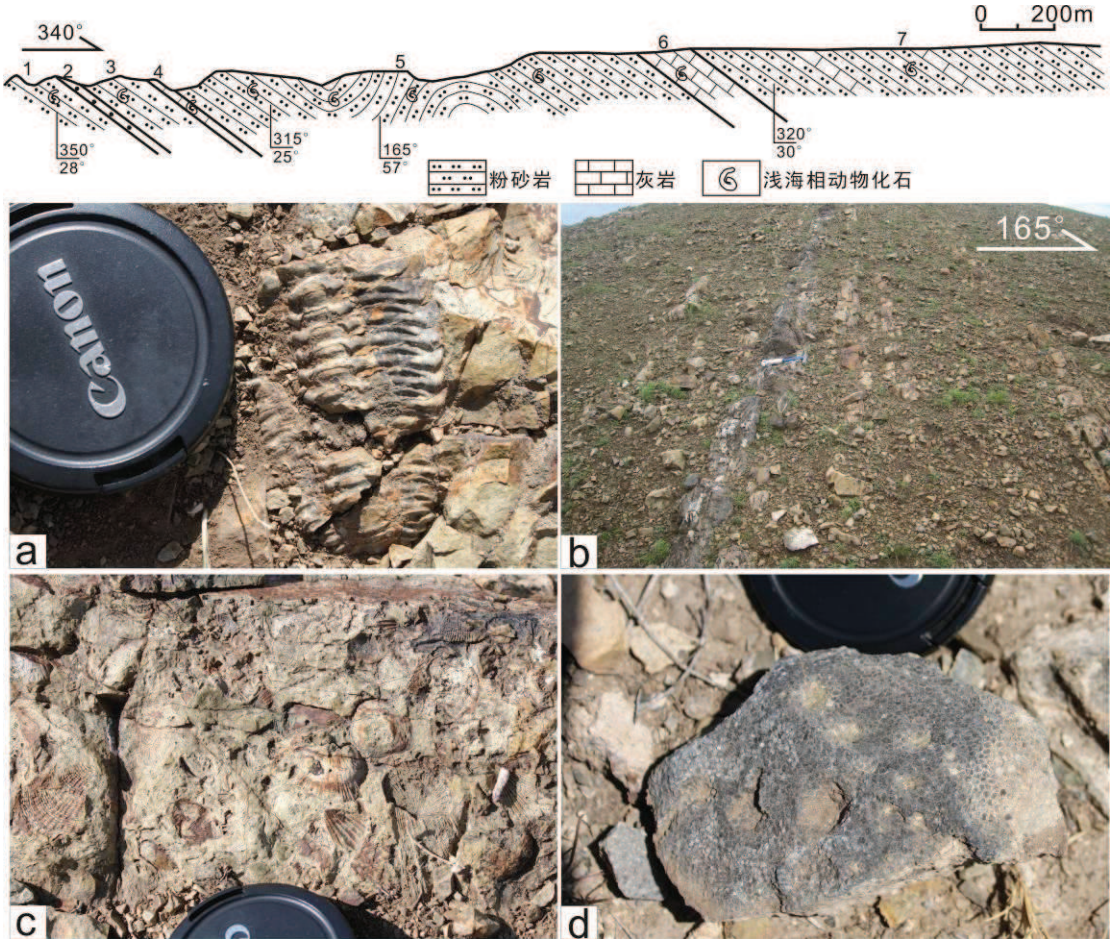

图 3-6 东乌旗地区泥鳅河组实测地层剖面：a，细砂岩中的三叶虫化石; b，薄层细砂岩夹灰岩; c，细砂岩中的腕足类化石; d，灰岩夹层中的珊瑚化石

Figure 3-6 Stratigraphic section of the Lower-Middle Devonian Niqiuhe Formation in East-Ujimqin area: a, Trilobita fossils; b, limestone interlayer within siltstone; c, Brachiopoda fossils; d, corals fossils

3.1.1.5 Summary of Sedimentological studies

对以上四个地区的沉积相分析显示，除查干敖包地区泥鳅河组底部类磨拉斯

沉积以外，中蒙边境地区下－中泥盆统泥鳅河组为一套滨海－浅海相沉积，以含丰富的浅海相动物化石为特征。查干敖包－那仁宝力格一带，泥鳅河组沉积之后整个区域进入剥蚀阶段，无晚泥盆世沉积。那仁宝力格－东乌旗一带，泥鳅河组被中－上泥盆统塔尔巴格特组和上泥盆统安格尔音乌拉组所覆盖。塔尔巴格特组为滨浅海相碎屑岩沉积，而安格尔音乌拉为一套含植物化石的海陆交互相地层，含植物化石 Lepidodendropsis sp.(拟鳞木)（1:25 万地质图东乌珠穆沁旗幅），整体表现为向上变浅的海退序列。安格尔音乌拉组之后，该区进入剥蚀阶段，无早石炭世沉积。

3.1.2 Detrital zircon geochronological study

In order to decipher the provenance of Devonian deposits in this region, three samples from Chaganaobao, Narenbaolige and East-Ujimqin were selected for detrital zircon dating, the sample position can be found in figure 3-1.

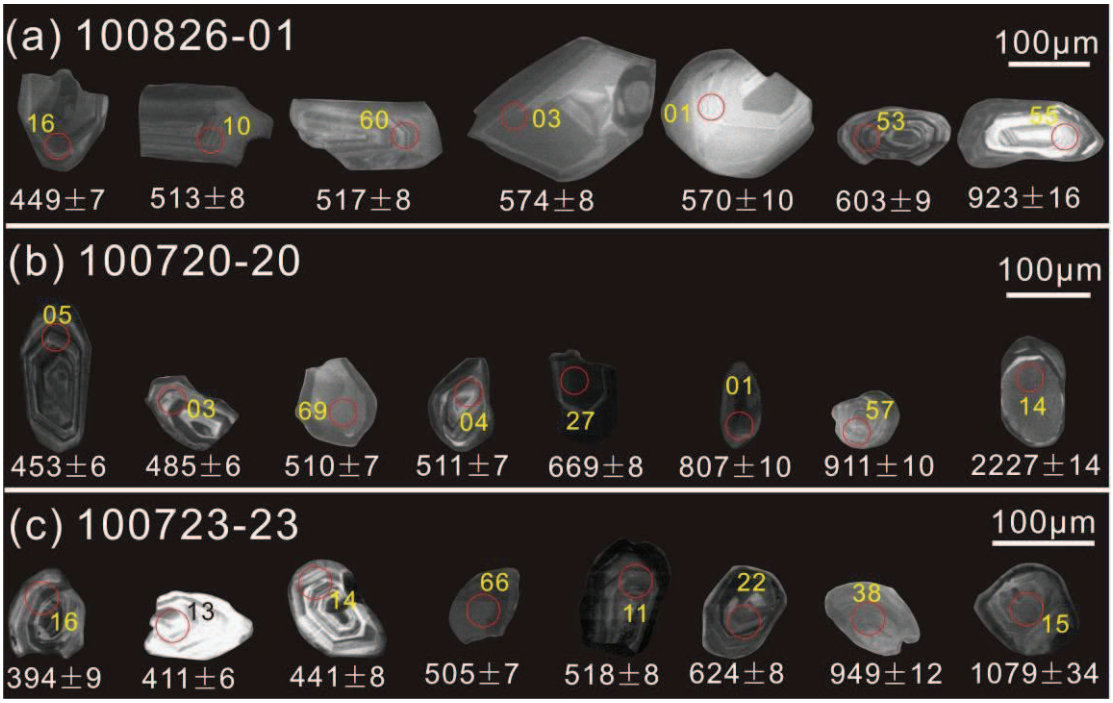

图 3-7 中蒙边境地区三个泥鳅河组砂岩样品锆石阴极发光(CL)图像

Figure 3-7 Cathodoluminescence (CL) images of samples from the Niqiuhe Formation in China-Mongolia border area

3.1.2.1 Chaganaobao area

The sandstone sample was selected from the parallel beddings bearing red

sandstone (Fig. 3-3b). The zircon grains are euhedral to subhedral, ranging from 50-150 μm in width and 100 to 250 μm in length with well-developed oscillatory growth zoning (Fig. 3-7a). The majority of zircons display high Th/U ratios ranging from 0.24 to 1.06, indicative of magmatic origin. However, seven grains show Th/U ratios less than 0.1 (0.08-0.09), which may indicate their metamorphic origin (Rubatto, 2002). All of 75 analyses are concordant, ranging from 449±7 to 923±16 Ma. Two main age populations are defined at 487-527 Ma (n=40) with a peak at 508 Ma, and

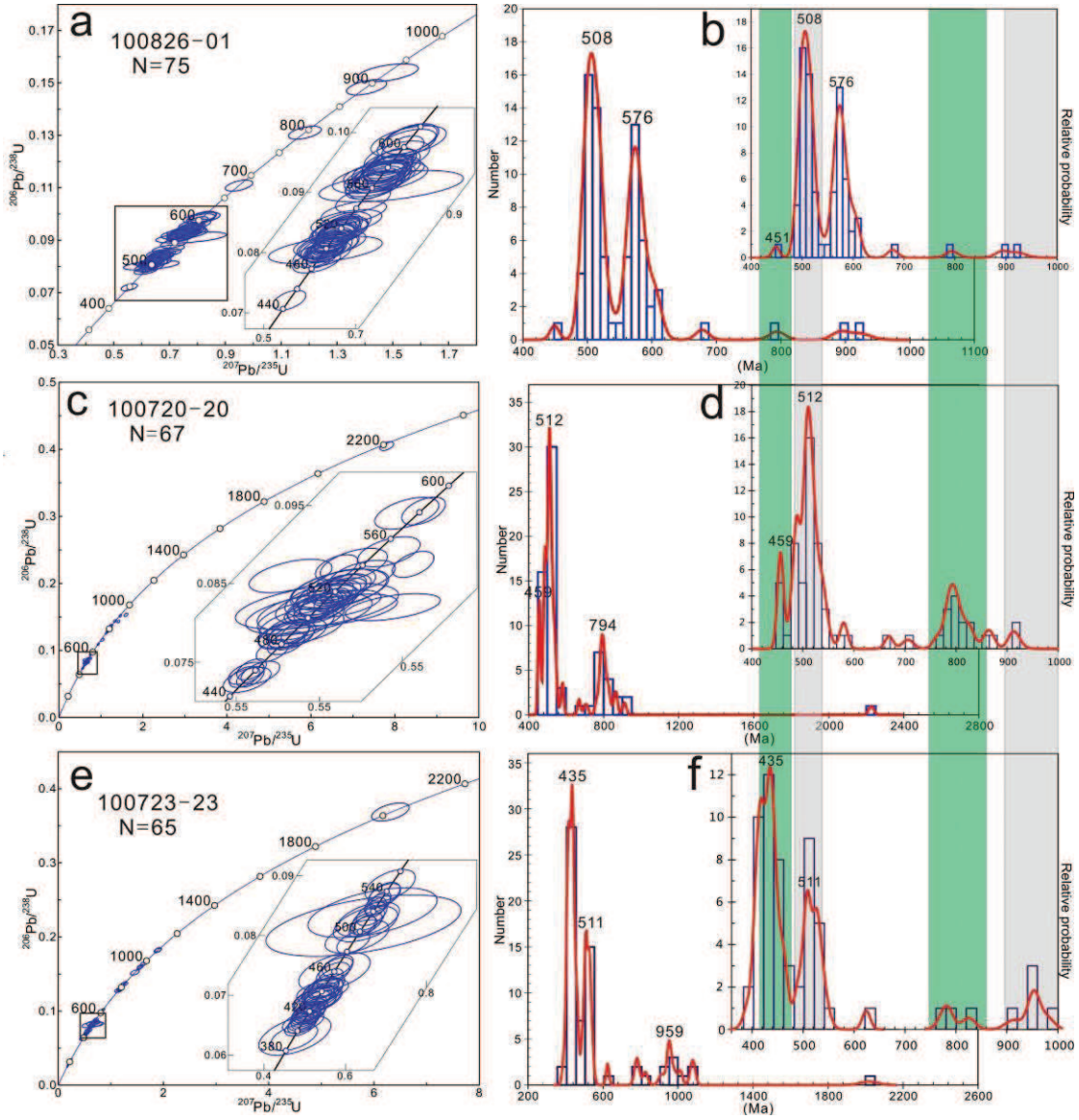

图 3-8 中蒙边境地区三个泥鳅河组砂岩样品碎屑锆石谐和线图及频率曲线图

Figure 3-8 U–Pb concordia and probability diagrams of zircon ages from the Niqiuhe Formation. The inset figures within each U–Pb Concordia diagram show zircon grains with ages of 400–600 Ma

536-608 Ma (n=30) with a peak at 576 Ma (Figs. 3-8a and b). Meanwhile, five zircons yielded ungrouped ages of 449, 678, 794, 892 and 923 Ma (Figs. 3-8a and b).

3.1.2.2 Narenbaolige area

The sample was selected from wavy beddings bearing sandstone (Fig. 3-5a). Most of zircon grains are subhedral to subrounded, ranging from 40 to 80 μm in width and 50-200 μm in length (Fig. 3-7b). Most zircon grains display oscillatory growth zoning, while a small proportion shows inherited cores and rims (Fig. 3-7b). Except two grains with Th/U ratio less than 0.1, all other zircons show high Th/U ratios from 0.11 to 1.09, indicating magmatic origin. Among a total of 75 U-Pb analyses, 67 of them are concordant and yielded ages ranging from 453±6 Ma to 2227±14 Ma (Figs. 3-8c and d). These grains fall into two main age populations at 453-581 Ma (n=49) with two peaks at 459 Ma and 512 Ma, and 669-917 Ma (n=17) with peak at 794 Ma (Figs. 3-8c and d). In addition, one grain yielded ages of 2227±14 Ma.

3.1.2.3 East-Ujimqin area

The sample was selected from fossils-bearing yellow sandstone (Fig. 3-6a). The zircon grains are euhedral to subhedral, ranging from 50-100 μm in width and 80 to 150 μm in length with oscillatory growth zoning (Fig. 3-7c). Except one grain showing Th/U ratio of 0.04, all other zircons show high Th/U ratios from 0.13 to 0.91, indicating magmatic origin. Among a total of 74 analyses, eight analyses were discarded because of high discordance, and one grain (#2325-20 with age of 214±3) was also discarded. The 65 concordant analyses yielded ages ranging from 394±6 Ma to 2018±45 Ma (Figs. 3-8e and f). Broadly, the grains fall into three age populations at 394-495 Ma (n=37) with a peak at 435 Ma, 505-546 Ma (n=15) with peak at 511 Ma, and 778-1078 Ma (n=11) with a small peak at 959 Ma, respectively (Figs. 3-8e and f). Meanwhile, two zircons yielded ages of 624 and 2018 Ma (Figs. 3-8e and f).

3.1.3 Provenance analyses

The detrital-zircon dating results presented above give us new clues to trace the provenance of these sediments and decipher the tectonic evolution. All these three Devonian samples display similar distributions in zircon-age probability diagrams,

characterized by predominant Early Paleozoic groups at ~440 Ma and ~510 Ma, and subordinate Neoproterozoic groups at ~570 Ma, ~800 Ma and ~950 Ma, respectively, with only few pre-1.0 Ga grains (Figs. 3-8 and 3-9a). It indicates relatively stable provenance for this belt during the Devonian.

The most striking feature of zircon-age distribution for this study is the predominant peak age at ~510 Ma (Fig. 3-9a). This significant age group was well documented from the EKB (Wu et al., 2005; 2012) and AXXB (Figs. 3-9b and 3-9c; Li et al., 2011; Han et al., 2011) by geochronological studies of granitoids and clastic rocks, which was considered as the orogenic related magmatic event due to the collision between the EKB and AXXB (Wu et al., 2005). Furthermore, this age group has also been revealed by zircon studies of igneous rocks from northwestern-central Mongolia (Fig. 3-9d; Rojas-Agramonte et al., 2011), central Mongolia (Demoux et al., 2009a), and southern Mongolia (Demoux et al., 2009b), and by detrital-zircon studies from northwestern Mongolia (Kelty et al., 2008) and central Mongolia (Bussien et al., 2011). Most of the ~510 Ma zircons display Th/U ratios higher than 0.1, implying that these zircon grains probably came from the Cambrian magmatic rocks exposed on the EKB, AXXB or/and the Mongolian blocks. Moreover, it was noticed that four zircons from Sample 100826-01 and one zircon from Sample 100723-23 present Th/U ratios less than 0.1 and U-Pb age of 497-517 Ma, showing the same feature with zircons from Pan-African events in the northeastern margin of the EKB and AXXB (Zhou et al., 2011a,b; Zhou and Wilde, 2013).

The age peak of ~440 Ma may represent the regional Early Paleozoic magmatic event. Two Early Paleozoic magmatic events have been documented from nearby blocks. After the amalgamation of the EKB and AXXB at the Cambrian, the Early Paleozoic post-collisional magmatic intrusions from ~490 to ~ 440 Ma were taken place on the newly formed EXB (Wu et al., 2005; Ge et al., 2005; Sorokin et al., 2011; Ren et al., 2012; Guo et al., 2013). To the south, the Early Paleozoic Baolidao arc magmatism at the southern margin of the AXXB was dated at 498-415 Ma (Jian et al., 2008; Xu et al., 2013). These two kinds of magmatic rocks can both be considered as

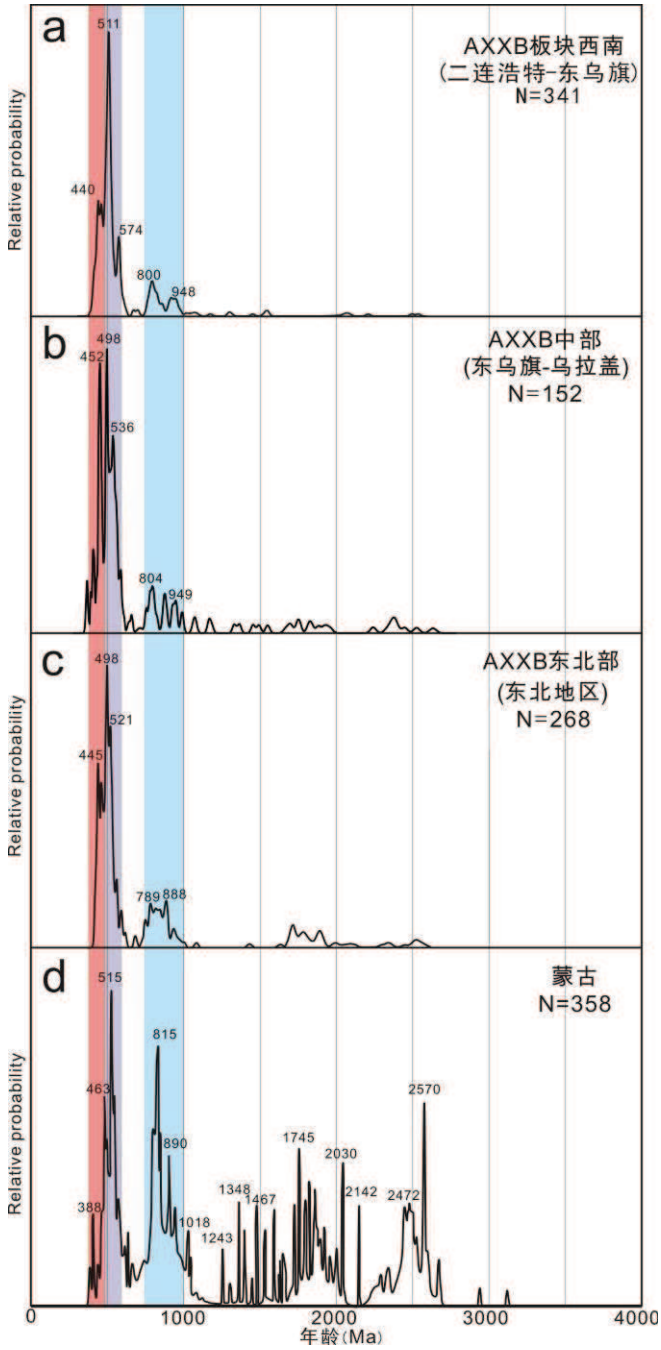

图 3-9 艾里格庙-锡林浩特-兴安地块（AXXB）西南部、中部和东北部，以及蒙古地区碎屑锆石图谱对比图：a, AXXB 西南部，数据来自本研究及该区奥陶纪数据（Zhao et al., 2014）; b, AXXB 中部，数据来自 Li et al., 2011; c, AXXB 东北部，数据来自 Han et al., 2011; c, 蒙古地区，数据来自 Rojas-Agramonte et al., 2011

Figure 3-9 Comparison of probability plots for the data from the western Airgin Sum-Xilinhot-Xing'an Block (a this study), middle Airgin Sum-Xilinhot-Xing'an Block (b; Li et al., 2011), northeastern Airgin Sum-Xilinhot-Xing'an Block (c; Han et al., 2011) and Mongolia (d; Rojas-Agranonte et al., 2011).

provenance regions for this zircon group. Notably, only one zircon from the western Chaganaobao Devonian sample (100826-01) presents an age around this age peak, with the main age group at 508 Ma (Fig. 3-8a), indicating that the main provenance for the Devonian strata therein could be the EXB. However, the percentage of the Early Paleozoic zircon grains increases eastwards (Figs. 3-8b, 3-8d and 3-8f). The easternmost Devonian sample from West Ujimqin (100723-23) presents the main age peak at 435 Ma, which is most likely from the southern Baolidao magmatic arc. This eastward tendency indicates that the contribution of the Baolidao arc to the provenance of Devonian strata increases from west to east.

The Neoproterozoic peaks (800-1000 Ma) are subordinate in our results (Fig. 3-8), and they cannot be used as an effective provenance indicator because this peak age represents the universal basement of nearly all blocks between NCC and Siberia Block (SIB). Neoproterozoic alkaline plutons have been identified from the EKB with the age of 950-737 Ma (Wu et al., 2011; Tang et al., 2013), which represent an extensive environment (Tang et al., 2013). For the eastern Jiamusi Block, gneisses and granitoids with the age of 913-777 Ma were reported at its western margin (Xie et al., 2008). This Neoproterozoic basement was also identified from the SHB by detrital-zircon dating of Late Neoproterozoic-Cambrian metasedimentary rocks (Xu et al., 2013; Wang et al., 2013). For the AXXB, ca. 900 Ma gneisses were reported along the China-Mongolia border (Wang et al., 2001; Y.Z. Zhou et al., 2013). The ca. 950 Ma magmatic events were also recorded in the central and southern Mongolia (Kröner et al., 2007; Demoux et al., 2009b). To the northern Tuva-Mongolia Block, a magmatism of the same age was also reported along the southern margin of SIB (Kuzmichev et al., 2001; Gladkochub et al., 2007). These universal Neoproterozoic magmatic rocks in these blocks correspond to an important global magmatic event, which may be related to the assemblage and break-up of Rodinia supercontinent (Li et al., 2008).

In summary, the results presented above indicate bidirectional provenances from the EXB to the north and the Early Paleozoic Baolidao arc to the south for the Ordovician-Devonian deposition. It provides new evidence to decipher the tectonic

evolution of this region.

3.2 Northern Orogen

北造山带地区发育上泥盆统色日巴彦敖包组，分布于苏尼特左旗南部和阿巴嘎旗南部（内蒙古地质矿产局, 1991）。色日巴彦敖包组为一套磨拉斯建造，不整合覆盖于蛇绿混杂带之上，限定了北造山带的完成时限（Xu et al., 2013）。

3.2.1 Sedimentological studies and facies analyses

本次对苏尼特左旗南部色日巴彦敖包组剖面（剖面位置见图 3-10b）进行了详细的剖面测量和沉积相分析，并对阿巴嘎旗南部色日巴彦敖包组进行了野外勘察。苏尼特左旗南部剖面描述如下：

-----被下石炭统沟呼都格组整合覆盖-----

12. 浅灰色中厚层状灰岩，底部夹一层灰色砂质灰岩。泥晶结构，块状构造，主要成分为方解石，含黑色燧石团块；下部砂质灰岩具黑色铁质结核。50.55m

11. 灰黄色细粒石英岩屑砂岩。砂状结构，块状构造，胶结物为泥质和硅质。 51.14m

10. 灰褐色薄层状细粒石英岩屑砂岩。细粒砂状结构，块状构造，主要成分为石英 85%，胶结物为硅质和泥质，层内微细平行层理发育，中下部发育灰岩透镜体。 82.67m

9. 灰黄色细粒石英岩屑砂岩。胶结物为硅质、泥质。 26.95m

8. 紫红色薄层细砂岩与绿色粉砂质页岩互层。细砂岩石英含量 60%，长石 25%。 91.52m

7. 深灰色中厚层状灰岩。泥晶结构，块状构造，主要成分为方解石，少量白云石。中部夹一层厚 1.5m 的粉砂岩。40.91m

6. 灰绿色中厚层状砂岩与泥质粉砂岩呈不等厚互层。灰绿色砂岩，中粒砂状结构，块状构造，主要成分为长石 50%，石英 25%和岩屑 25%胶结物为硅质和铁质。泥质粉砂岩灰绿色，粉砂状结构，块状构造，主要成分为岩屑，含钙质。具沉积韵律，韵律底部为含砾砂岩，向上渐变为粉砂岩，韵律厚度 0.5-1m。111.91m

5. 浅紫红色中厚层状粗粒石英岩屑砂岩夹薄层细砾岩。细砾岩为灰褐色，砾状结构，块状构造，砾石成分复杂，砾石含量 65%，胶结物为硅质和泥质。（上部为 85m 宽的第四系河床沉积）182.0m

2-4. 紫红色厚层砾岩夹长石砂岩，向上变细转变为薄层状泥质粉砂岩 7.52m

-----不整合关系-----

1. 绢云石英片岩

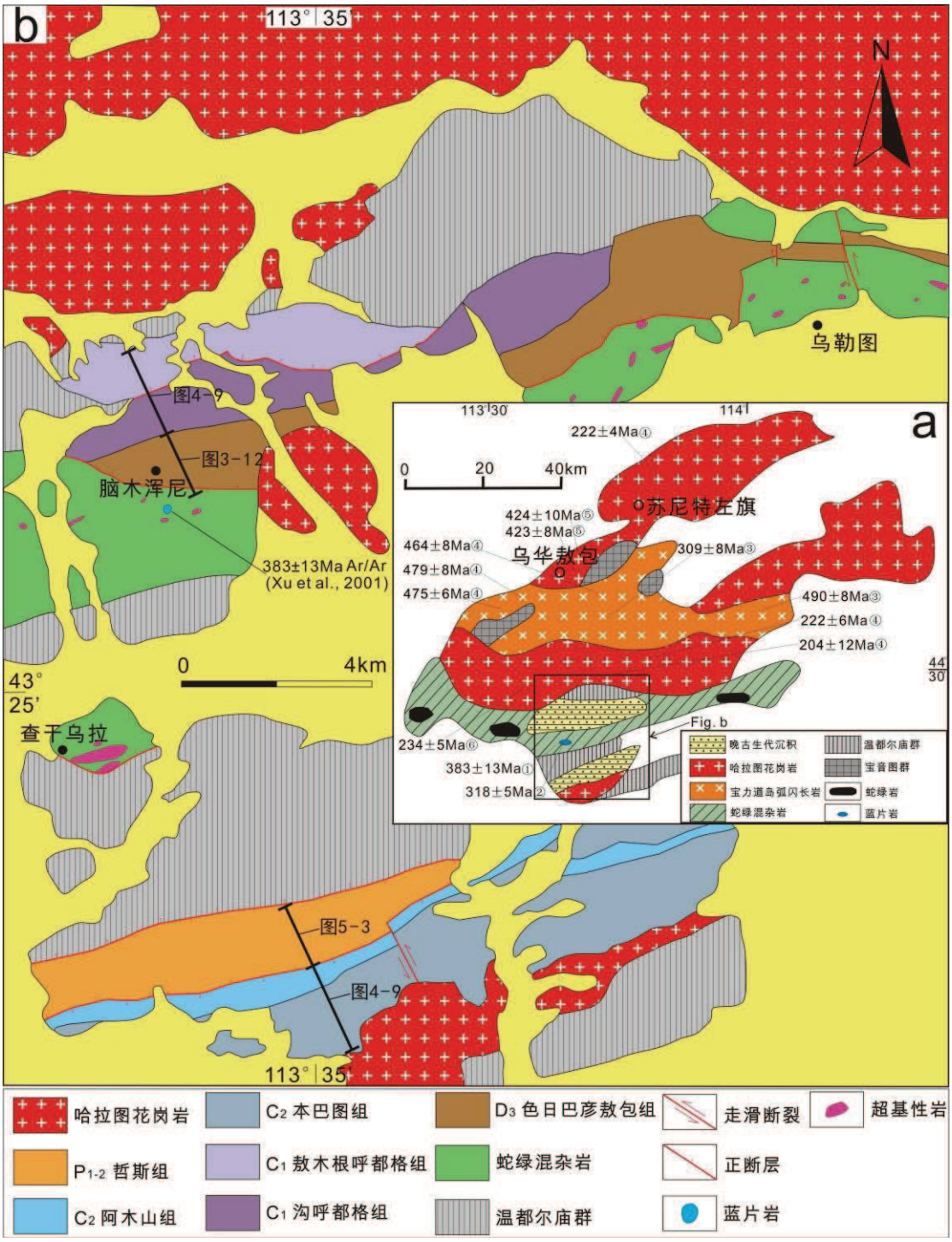

图 3-10 a，苏尼特左旗地区构造纲要图; b，苏尼特左旗南脑木浑尼地区地质图；色日巴彦敖包组剖面位置标于图中

Figure 3-10 a, Sketch geological map of Sunidzuoqi area; b, Geological map of Naomuhuni area, south of Sunidzuoqi County

苏尼特左旗南部色日巴彦敖包组不整合于蛇绿混杂带之上（图 3-11; 图 3-12a），下部由红色砾岩组成，上部为砾岩夹长石岩屑砂岩，中部和顶部各夹一层生物碎屑灰岩（图 3-11）。底部砾岩为紫红色，砾石大小在 1-15cm，砾石磨圆较好，分选较差（图 3-12b）。砾石成分复杂，包含火山岩、石英岩、片岩砂岩等。镜下照片显示，砾岩层和砂岩层中均含有大量的片岩岩屑（图 3-12c，d），来自于底部蛇绿混杂岩和温都尔庙群片岩。砾岩层中发现植物化石 Leptophloeum rhombicum（邵济安, 1991）。中部灰岩夹层厚约 40m，为泥质灰岩（图 3-13e），含有丰富的动物化石，例如 Nalivkinella profunda 和 Cyrtospirifer sulcifer（内蒙古地质矿产局, 1991；Xu et al., 2013）。上部以成熟度较低的长石岩屑砂岩和粉砂岩为主（图 3-11），顶部为厚 50m 的生物碎屑灰岩，可见大量生物碎屑物质（图 3-12f）。整个沉积序列可分为几个向上变细的沉积旋回，整体显示向上变细的海进序列，代表从陆相磨拉斯沉积向海相磨拉斯沉积的转变过程。

阿巴嘎旗南部色日巴彦敖包组由于出露较差，未作详细的剖面测量。

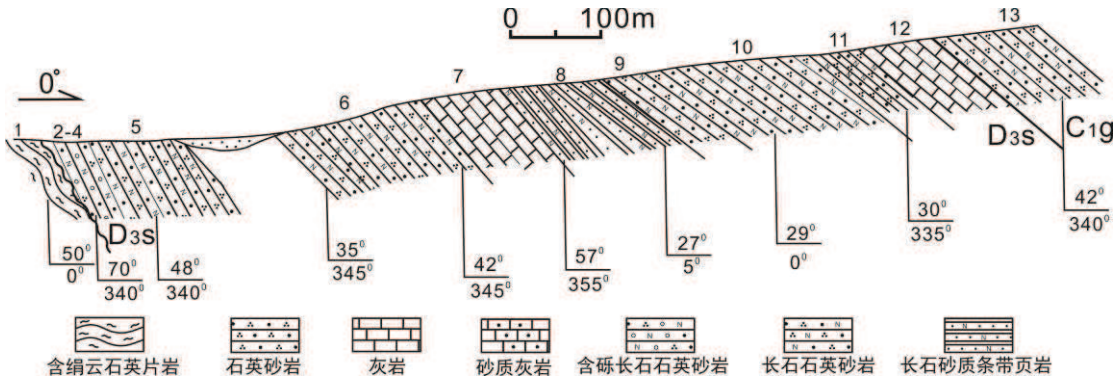

图 3-11 苏尼特左旗南部上泥盆统色日巴彦敖包组实测地层剖面

Figure 3-11 Stratigraphic section of the Upper Devonian Seribayanaobao Formation in the south of Sunidzuoqi County

3.2.2 Detrital zircon geochronological study

选取苏尼特左旗南部色日巴彦敖包组底部含砾粗砂岩（样品编号 090711-08）进行碎屑锆石年代学和 Hf 同位素研究，以期探讨其物源信息。徐备等（1994）在对该地区进行 1:50000 地质填图时，通过对剖面内斜层理的测量，认为物源来自于北部地区。

锆石颗粒为自形－半自形，长 60-150 μm，宽 40-80 μm，并发育良好的岩浆震荡环带（图 3-14）。总共选取 75 颗碎屑锆石进行 U-Pb LA-ICP-MS 年代学测试，

锆石的 Th/U 比为 0.27-1.64，显示岩浆成因锆石的特征。75 颗锆石的测试结果均

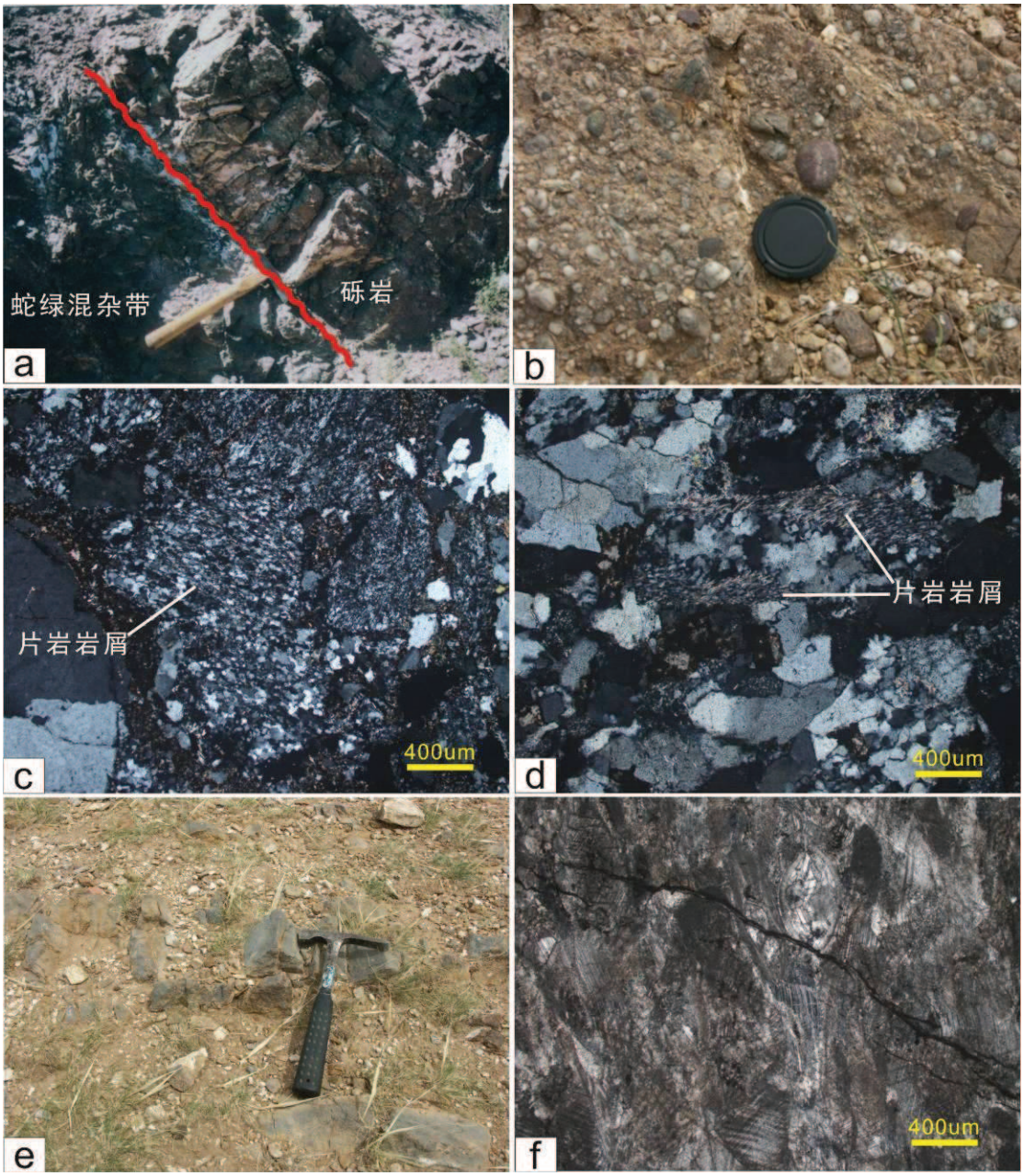

图 3-12 苏尼特左旗南部上泥盆统色日巴彦敖包组野外照片：a，底砾岩与蛇绿混杂带的不整合接触; b，下部砾岩层; c，砾岩层的镜下照片，显示丰富的片岩岩屑; d，下部砂岩层的镜下照片，显示丰富的片岩岩屑; e，中部泥质灰岩层; f，顶部生物碎屑灰岩镜下照片

Figure 3-12 Photographs of the Upper Devonian Seribayanaobao Formation in south of Sunidzuoqi County: a, unconformity between basal conglomerate and ophiolitic mélange; b, the basal conglomerate; c, photomicrograph of conglomerate with schist clastics; d, photomicrograph of sandstone with schist clastics; e, limestone interlayer; f, photomicrograph of the bioclastic limestone

位于谐和线上。锆石年龄范围在 442±6Ma 到 2729±24 Ma，仅出现一个主要的年龄群，为 442-525 Ma（N=66），峰值年龄在 463Ma（图 3-14）。另外还有八颗中－新元古代锆石，年龄在 906-1594 Ma；和一颗晚太古代锆石，年龄为 2729±24。

对于~460 Ma 的年龄峰，早古生代古亚洲洋向北的俯冲，沿着艾里格庙-苏尼特左旗南一带形成宝力道岛弧岩浆岩带，年龄在 498-415Ma（图 3-10a; Jian et al., 2008; Xu et al.,2013）。而中－新元古代和晚太古代锆石可能来自该区基底（Xu et al., 2013）。前以述及，根据斜层理数据得到色日巴彦敖包物源主要来自北部，本次碎屑锆石研究显示物源主要为北部宝力道岛弧岩浆岩（图 3-10a）。另外，对锆石的 Hf 同位素研究显示，早古生代碎屑锆石的 ε(Hf)值均为正值（图 3-13），说明岛弧形成过程中新生物质的出现，这与整个中亚造山带古生代新生物质的不断产生一致。

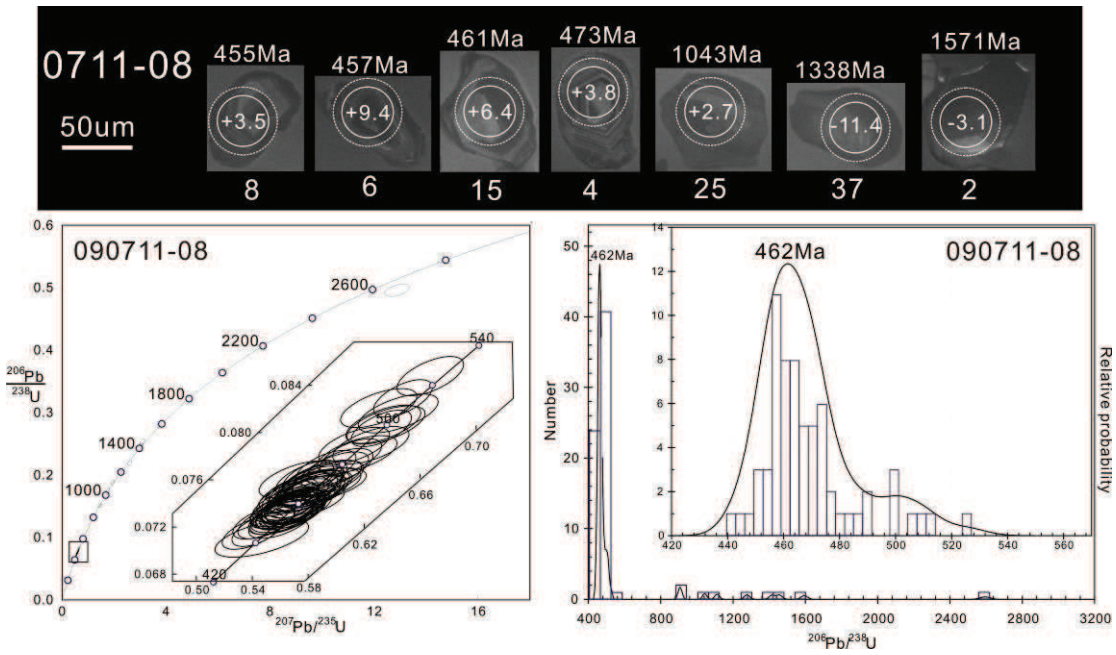

图 3-13 苏尼特左旗南部色日巴彦敖包组碎屑锆石 CL 图、年龄谐和线图及频率曲线图

Figure 3-13 Cathodoluminescence (CL) images, Concordia diagram and probability plot diagram of zircons from the Seribayanaobao Formation in south of Sunidzuoqi County

3.3 Southern Orogen

南造山带地区发育下泥盆统西别河组（温都尔庙地区称为那清组），分布于达茂旗－温都尔庙一线（内蒙古地质矿产局, 1991）。西别河组为一套磨拉斯建造，不整合覆盖于蛇绿混杂带之上，限定了南造山带的完成时限（张允平等, 2010）。

关于西别河组的时代归属，1:20 万地质图中多将其置于上志留统；1991 年内蒙古地质矿产局进行地层综合对比时将其置于下泥盆统；张允平等（2010）认为其沉积时代可能从晚志留世持续到早泥盆世。

3.3.1 Sedimentological studies and facies analyses

张允平等（2010）对达茂旗区域内的西别河组进行了详细的地层学研究。因此本次仅对温都尔庙地区西别河组（那清组）进行了剖面测量和沉积相分析，剖面未知见图 3-14。温都尔庙地区那清组剖面厚约 600m。底部为第四系覆盖，未见与下伏地层接触关系，顶部被下石炭统海拉斯阿木组不整合覆盖（图 3-14）。该剖面未见底部砾岩，该剖面下部为长石石英粗砂岩－砂岩组合（图 3-15a），上部为黄色粉砂岩/页岩夹灰岩透镜体（图 3-15b）。整个剖面组成一个粒度向上变细的序列，代表一个海进过程。上部粉砂岩－页岩中含有灰岩透镜体，透镜体中含有丰富的珊瑚、腕足、苔藓虫等海相生物化石，说明剖面上部为海相沉积。与张允平等（2010）在达茂旗附近西别河组进行横向对比，温都尔庙地区那清组相当于西别河组上部浅海相沉积部分，为磨拉斯盆地上部沉积。

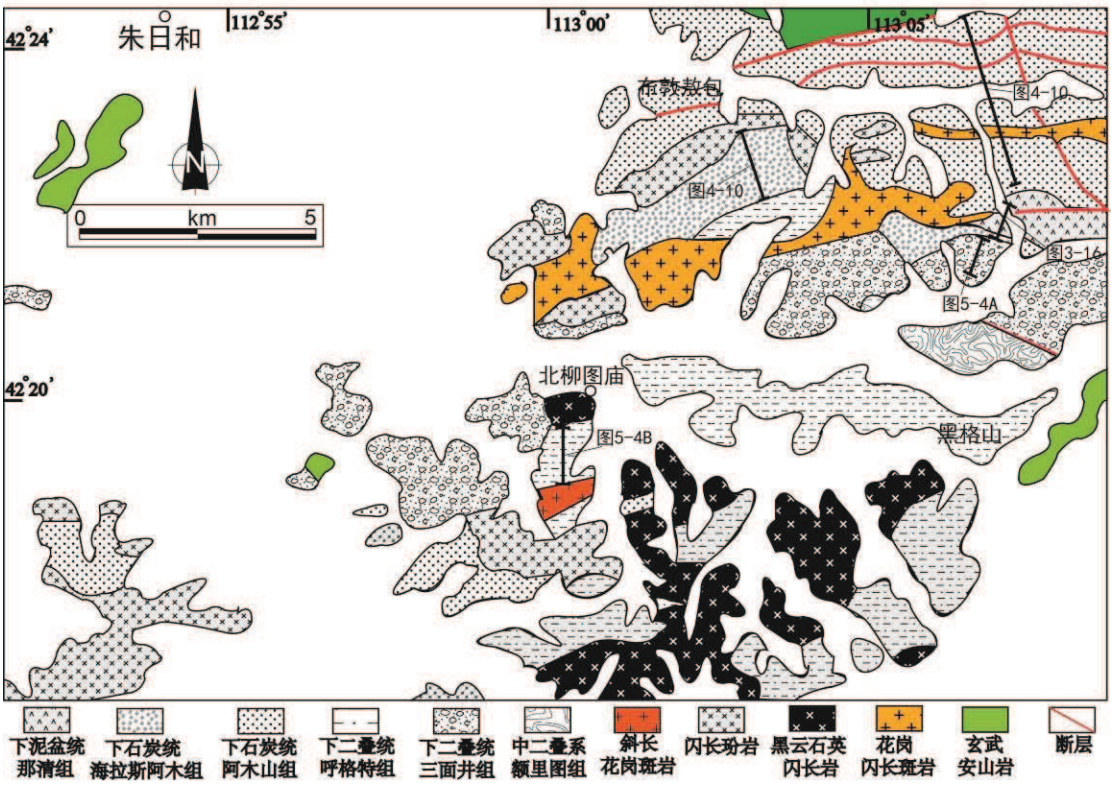

图 3-14 温都尔庙地区地质图

Figure 3-14 Geological map in Ondor Sum area

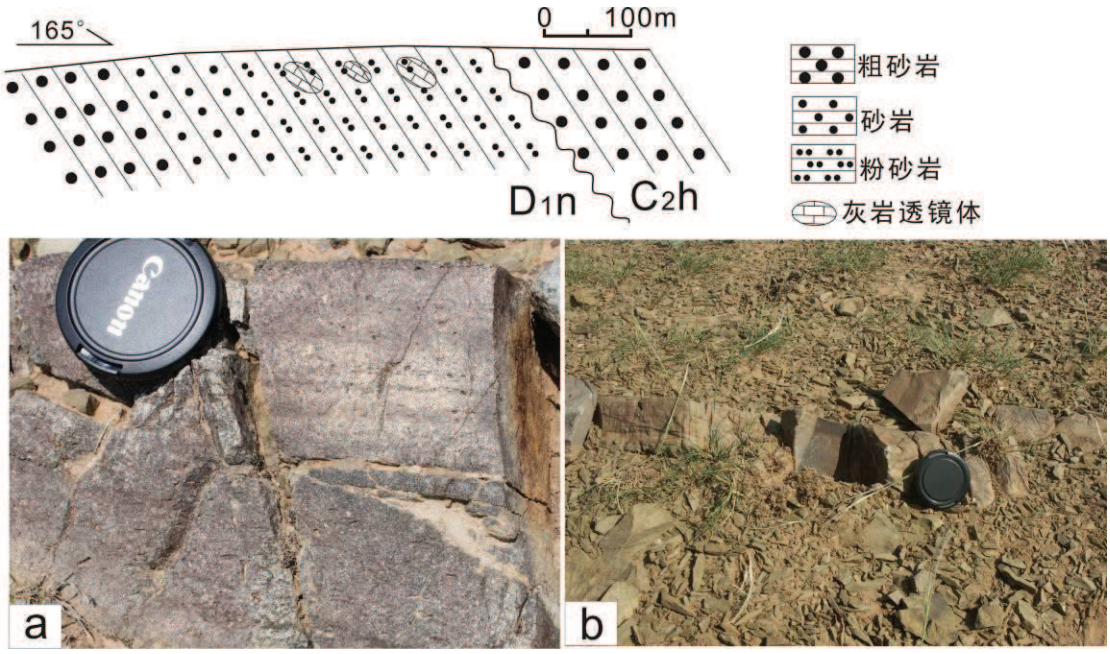

图 3-15 温都尔庙地区下泥盆统那清组实测地层剖面：a，下部砂岩; b，上部黄色粉砂岩夹灰岩透镜体

Figure 3-15 Stratigraphic section of the Lower Devonian Naqing Formation in Ondor Sum area: a, sandstone in the lower part; b, siltstone in the upper part with limestone lens

3.4 Summary of this chapter

根据沉积相分析和对比，以及碎屑锆石研究，内蒙古中东部泥盆纪地层可分为两类，即中蒙边境早－中泥盆世陆内盆地沉积和与造山带相关的磨拉斯盆地沉积。中蒙边境泥盆纪沉积以浅海相沉积为主，含丰富的腕足类、三叶虫、珊瑚等浅海相动物化石，代表额尔古纳－兴安地块形成后的陆内伸展盆地沉积，其物源主要来自于额尔古纳－兴安地块本身，并可能存在板块南缘宝力道岛弧物质的加入。南北两个造山带沿线的泥盆纪磨拉斯盆地沉积限定了两个造山带的形成时限分别为早泥盆世和晚泥盆世。泥盆纪沉积属于碰撞后的第一个盖层沉积。南造山带沿线，下泥盆统西别河组沉积之后进入剥蚀阶段，直到晚石炭世接受沉积。北造山带沿线，上泥盆统色日巴彦敖包组被下石炭统沟呼都格组整合覆盖，代表磨拉斯盆地上部沉积。

Chapter 4 Carboniferous sedimentology features and detrital zircon geochronology

早石炭世沉积在内蒙古中东部地区分布比较局限，仅出现于苏尼特左旗南及敖汉旗地区（图 4-1）。不同于早石炭世，晚石炭世沉积在内蒙古地区广泛分布（图

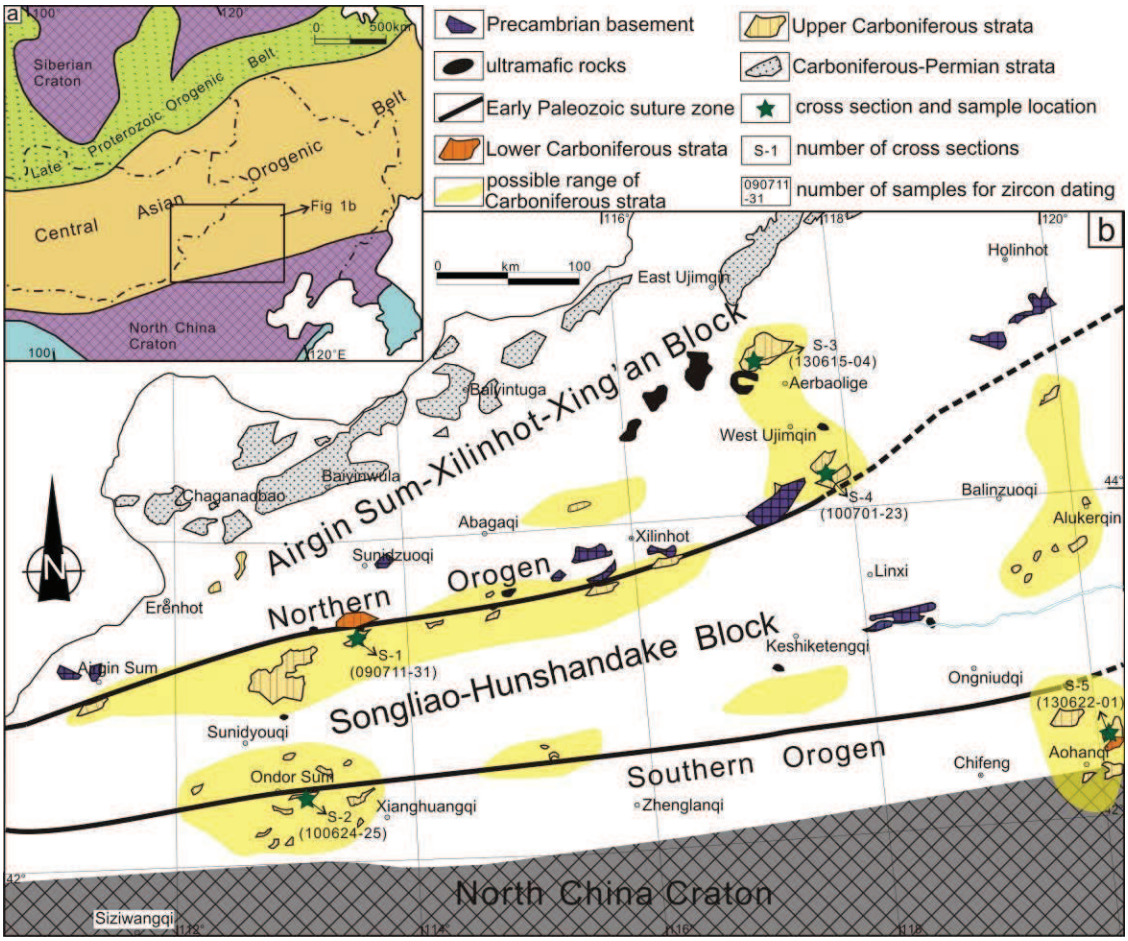

图 4-1 a，内蒙古中部地区在中亚造山带的位置（据 Sengör et al., 1993; Windley et al., 2007）；b，内蒙古中部地区石炭纪沉积分布图（据内蒙古地质矿产局, 1991）

Figure 4-1 (a) Location of the Altaid /Central Asian Orogenic Belt (CAOB) (compiled from Sengör et al., 1993; Windley et al., 2007). (b) Sketch geological map of central Inner Mongolia showing the main tectonic units: three blocks (North China Craton, Songliao-Hunshandake Block and Airgin Sum-Xilinhot-Xing'an Block) and two Early Paleozoic orogenic belts (Southern Orogen and Northern Orogen) (compiled from Jian et al., 2008; Xu et al., 2013). The Carboniferous strata, highlighted in this map, are compiled from IMBGMR, (1991). Note that they cover on the three blocks.

4-1），并在大部分区域以超覆不整合于下伏变质基底、早古生代岩浆岩和前石炭纪沉积地层之上（内蒙古地质矿产局, 1991）。中蒙边境地区石炭纪沉积以陆相碎屑-火山岩为主，而内蒙古中南部地区则以浅海相碎屑-碳酸盐岩沉积为主。本章将分对两区域内石炭纪沉积进行描述和讨论。

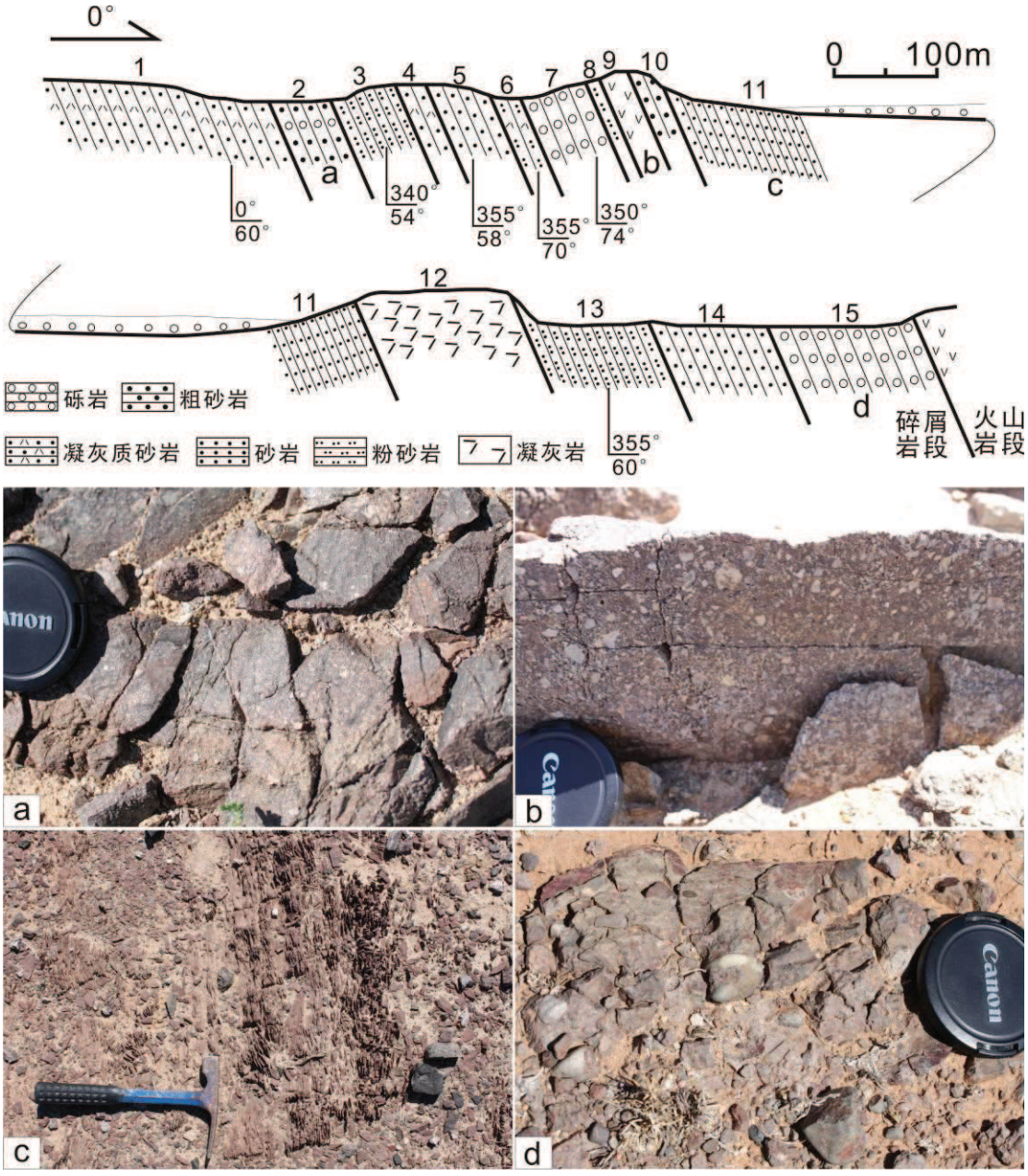

图 4-2 查干敖包地区上石炭统－下二叠统宝力高庙组碎屑岩段实测地层剖面：a，下部含砾粗砂岩; b，火山角砾岩夹层; c，红色粉砂岩，风化为薄片状; d，上部砾岩

Figure 4-2 Stratigraphic section of the Upper Carboniferous-Lower Permian Baoligaomiao Formation in Chaganaobao area: a, pebbly coarse-grained sandstone; b, volcanic breccias interlayer; c, red siltstone; d, the top conglomerate

4.1 China-Mongolia border area-terrestrial deposits

在中蒙边境地区，沿着宝力高庙－白音乌拉－白音图嘎－东乌旗一线分布上石炭统－下二叠统宝力高庙组沉积。为一套北东向展布碎屑岩和火山岩组成的陆相沉积－火山岩系，含丰富安加拉植物化石，例如 *Angaropteridium cardiopteroides*，*Noeggerathiopsis lotifolia*（内蒙古地质矿产局，1991）。与下伏泥盆纪沉积为角度不整合接触关系。

4.1.1 Sedimentological studies and facies analyses

4.1.1.1 宝力高庙地区（图 4-1 中剖面 B-1，剖面起点 GPS：44°17′35″N，112°01′02″）

宝力高庙地区上石炭－下二叠统宝力高庙组可分为下碎屑岩段和上火山岩段，本次研究对其下碎屑岩段进行了详细的剖面测量（图 4-2），具体剖面描述如下：

-----宝力高庙组火山岩段-----

15. 灰黑色砾岩，砾石以粉砂岩和泥岩为主，含少量石英砾石。砾石粒径 2-10cm，磨圆较好，分选较差

14. 黄褐色薄层状细砂岩

13. 灰白色中层状粉砂岩

12. 紫红色凝灰岩

11. 紫红色细砂岩，风化为薄片状

10. 黄褐色薄层状粗砂岩

9. 浅绿色火山岩

8. 紫红色薄层状粉砂岩，风化为薄片状

7. 灰绿色细粒岩，砾石成分以石英和粉砂岩为主，粒径 2-10mm，磨圆中等

6. 灰绿色凝灰质粉砂岩

5. 灰黄-灰绿色砂岩

4. 灰黄色中-薄层状凝灰质砂岩

3. 灰黄色-紫红色薄层状粉砂岩，夹少量薄层状细砂岩，风化为薄片状

2. 紫红色薄-中层含砾粗砂岩，砾石以石英颗粒为主，含少量泥岩砾石，磨圆较好，粒径集

中于 2-3mm，少数可达 1cm 以上

1. 灰绿色薄-中层状凝灰质砂岩

------第四系覆盖------

剖面底部为第四纪覆盖，不见其与下伏地层的接触关系，但最新的 1:25 万填图显示在该区，宝力高庙组与下伏泥鳅河组为不整合关系（1:25 万地质图洪格尔幅）。剖面下部为凝灰质砂岩和含砾粗砂岩（图 4-2a）。中部为红色粉砂岩夹少量火山岩（图 4-2b）。红色粉砂岩被风化为薄片状，显示良好的成层性（图 4-2c）。红色粉砂岩中发现安哥拉植物化石，如带匙叶 *Noederzarinii* Neuburg。红色粉砂岩总厚度约 500m，代表炎热环境下的陆相稳定沉积。剖面顶部为一套巨厚层砾岩，砾石磨圆很好，分选较好，粒径在 2-5cm，砾石成分复杂（图 4-2d），代表

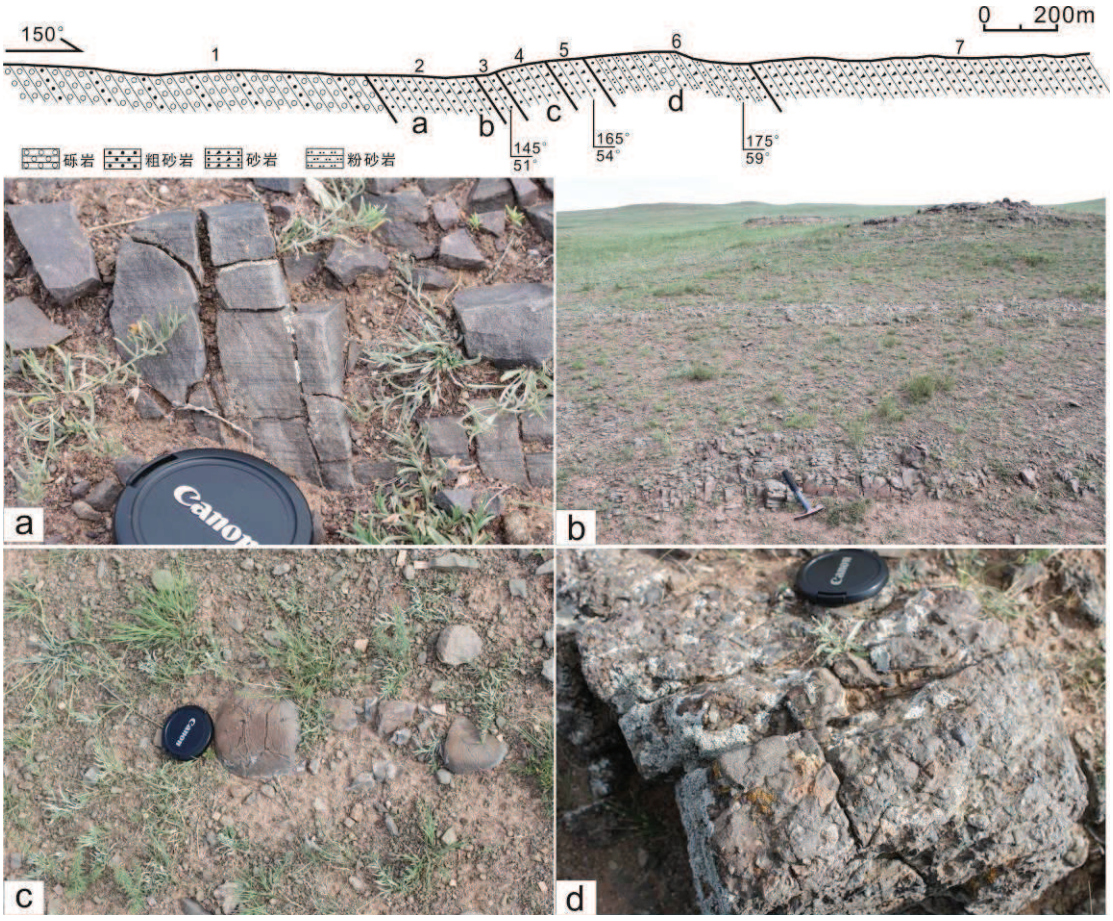

图 4-3 白音图嘎地区上石炭－下二叠统宝力高庙组实测地层剖面：a，红色砂岩中的水平层理; b，野外露头宏观照片; c，砂岩中的灰岩透镜体; d，砾岩夹层

Figure 4-3 Stratigraphic section of the Upper Carboniferous-Lower Permian Baoligaomiao Formation in Baiyintuga area: a, horizontal beddings in red sandstone; b, red sandstone; c, limestone lens within sandstone; d, conglomerate interlayer

河流相沉积。砾岩之上为该组上部火山岩段，由多个爆发相－溢流相火山岩组成，岩性以火山角砾岩、流纹岩和玄武质安山岩为主。巨厚的块状火山岩及爆发角砾岩显示了其陆相喷发的特征。

4.1.1.2 白音图嘎地区（图 4-1 中剖面 B-2，剖面起点 GPS：44°50′12″N，114°53′32″）

白音图嘎地区上石炭－下二叠统宝力高庙组可分为下碎屑岩段和上火山岩段，本次研究对其下碎屑岩段进行了详细的剖面测量（图 4-3），具体剖面描述如下：

-----宝力高庙组火山岩段-----

7. 灰绿色石英岩屑砂岩，发育水平层理

6. 灰绿色薄-中层状石英岩屑砂岩与灰绿色薄层状粉砂岩互层，夹灰黑色砾岩，砾石成分主要为泥岩，粒径 2mm-2cm，分选较差

5. 灰绿色薄-中层状石英岩屑砂岩与灰绿色薄层状粉砂岩互层，粉砂岩发育水平层理，并含少量灰岩透镜体

4. 紫红色薄-中层状长石石英岩屑砂岩，发育水平层理，少数层位含红色泥岩砾石

3. 灰绿色中层状石英岩屑砂岩，向上粒度变细

2. 灰紫色长石石英岩屑砂岩，发育水平层理

1. 紫红色厚层状细粒岩

-----第四系覆盖-----

剖面下部为红色细砾岩夹粗砂岩，向上转变为发育水平层理的红色砂岩（图 4-3a）。中部为发育水平层理灰绿色砂岩，地层层厚稳定，水平延伸较远，代表稳定沉积环境。灰绿色砂岩中偶见灰岩透镜体，大小在 20-30 cm 长，10 cm 宽（图 4-3c）。同时，灰绿色砂岩中夹砾岩夹层，砾石以砂岩和灰岩为主（图 4-3d）。上部为巨厚薄层砂岩，发育水平层理。白音图嘎地区，宝力高庙组底部砾岩不整合于中奥陶统裸河组和下泥盆统泥鳅河组之上（1:25 万地质图阿巴嘎旗幅）。上部砂岩和火山岩段发现大量安哥拉植物化石，例如辛匙叶（*Neoggerathiopsis* sp.）和带匙叶（Neo derzarinii）。宝力高庙组整体表现为向上变细的沉积序列，代表从陆相类磨拉斯向稳定湖相沉积的转变，局部夹河流相沉积。

4.1.1.3 东乌旗地区（图 4-1 中剖面 B-3，剖面起点 GPS：45°24′57″N，116°55′16″）

东乌旗地区上石炭－下二叠统格根敖包组可分为下碎屑岩段和上火山岩段（图 4-4）。本次研究对其下碎屑岩段进行了详细的剖面测量（图 4-3），具体剖面描述如下：

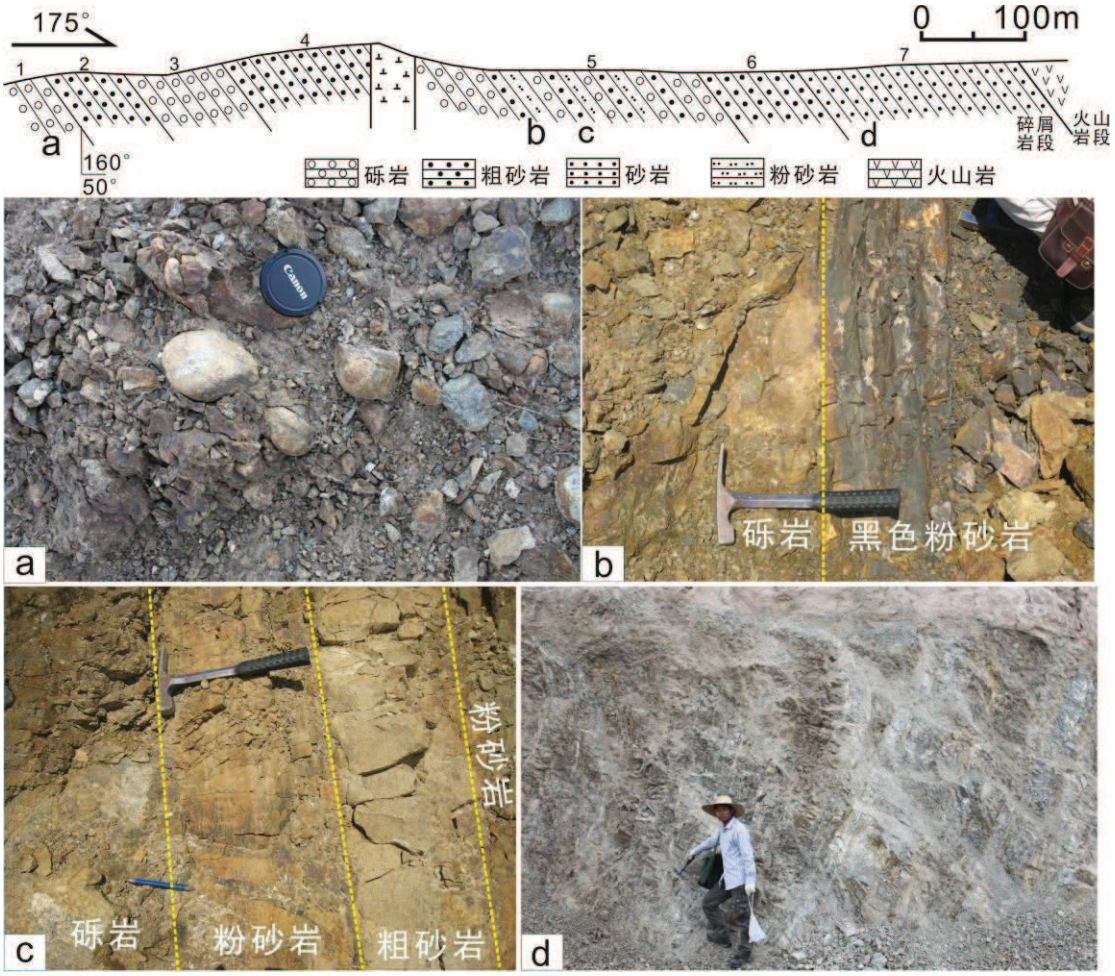

图 4-4 东乌旗上石炭－下二叠统格根敖包组实测地层剖面：a，底部砾岩; b，砾岩与黑色粉砂岩互层; c，砾岩、粉砂岩、粗砂岩互层关系; d，上部砂岩

Figure 4-4 Stratigraphic section of the Upper Carboniferous-Lower Permian Gegenaobao Formation in East-Ujimqin area: a, the bottom conglomerate; b, conglomerate interbedded with black siltstone; c, conglomerate, siltstone and coarse-grained sandstone interbedded; d, the upper sandstone

-----格根敖包组火山岩段-----

7. 黄褐色薄-中层状砂岩

6. 黄褐色中层状粗砂岩

5. 黄褐色砾岩、粗砂岩和泥岩互层。泥岩包含黑色泥岩和黄褐色泥岩

4. 黄绿色石英岩屑粗砂岩

3. 灰绿色砾岩，砾石大小 0.5-20cm，砾石成分以闪长岩、火山岩和石英为主，砾石磨圆较好，分选较差。砾岩中夹厚度为 5m 的细砂岩

2. 灰绿色岩屑石英粗砂岩

1. 灰绿色砾岩，砾石成分以闪长岩和火山岩为主，并含少量泥岩砾石。砾石磨圆较好，粒径 1-40cm

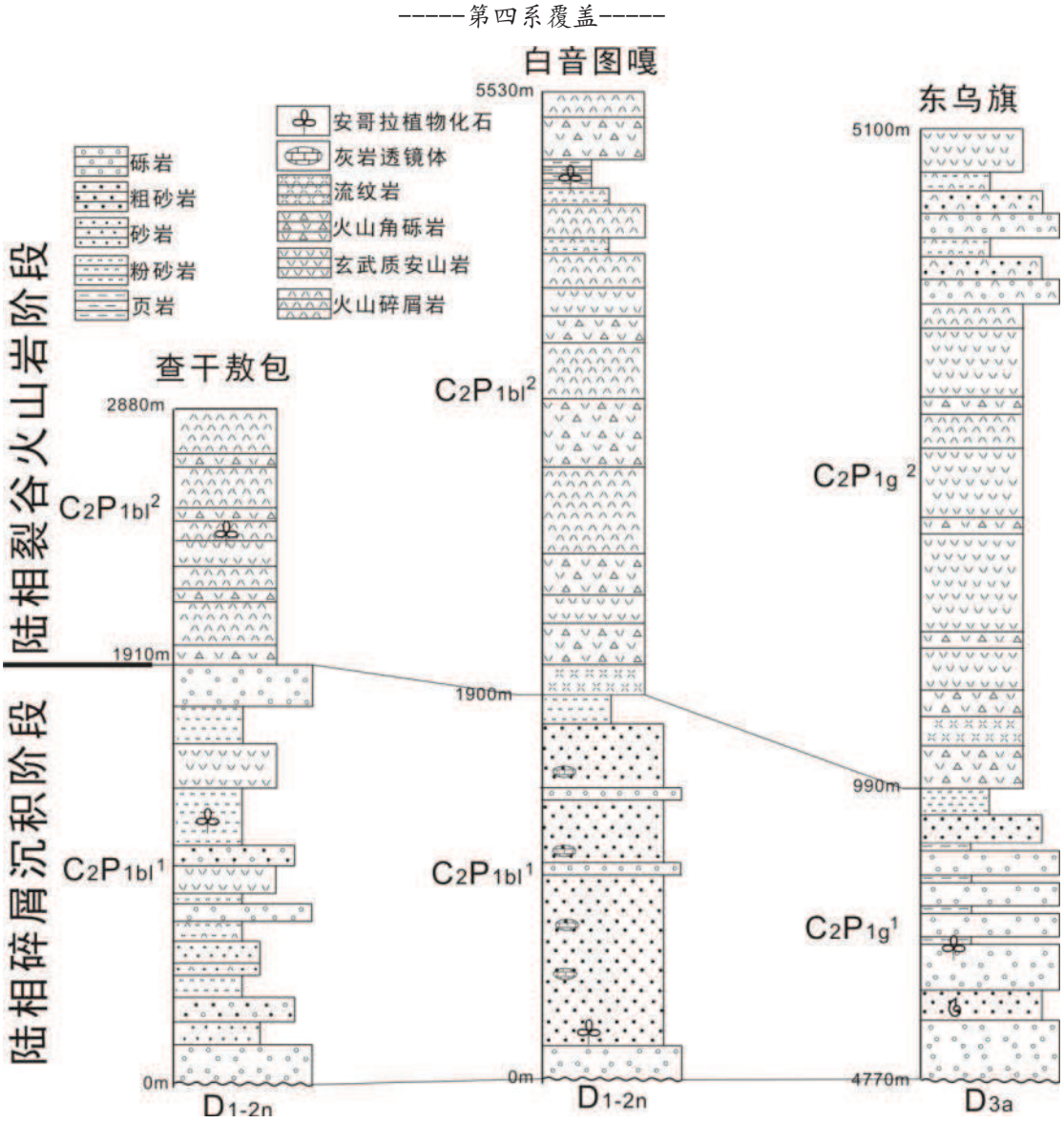

图 4-5 中蒙边境地区上石炭－下二叠统剖面柱状对比图

Figure 4-5 Comparison of the Late Carboniferous-Early Permian strata in China-Mongolia border area

实测地层剖面显示，格根敖包组下部为巨厚层砾岩，砾石大小 2-40 cm，分选较差，砾石磨圆中等（图 4-4a）。砾石成分以火山岩为主，并含少量砂岩、超

基性岩和硅质岩砾石，代表与下伏火山岩和超基性岩的不整合接触关系。中部为砾岩－粉砂岩或砾岩－粗砂岩－粉砂岩的互层（图 4-4b，c）。其中砾岩层厚较大，为 0.5-1.5 m，粉砂岩和粗砂岩层厚均在 20-40 cm，并且粉砂岩顶部常发育明显的冲刷构造。中部砾岩－粗砂岩－粉砂岩的组合代表典型的河漫滩沉积，粉砂岩中发现安哥拉植物化石，如匙叶 *Noeggerathiopsis* sp.（1:25 万地质图东乌珠穆沁旗幅）。剖面上部为薄层砂岩（图 4-4d），其顶部被该组火山岩段覆盖。

4.1.1.4 小结

综合以上三个地区上石炭－下二叠统沉积的描述，中蒙边境地区宝力高庙组/格根敖包组为一套正常的陆相碎屑岩－中酸性火山岩建造。其下部碎底砾岩不整合于下伏地层及超基性岩之上，以大量的安哥拉植物化石为特征，代表陆相碎屑岩沉积阶段（图 4-5）。其上部火山岩段以中酸性火山岩和火山碎屑岩为主，地球化学特征显示其具有板内裂谷火山岩的特征（Zhang et al., 2011），代表陆相沉积过程中的裂谷盆地发育阶段（图 4-5）。

4.1.2 Detrital zircon geochronological study

为探讨该区晚石炭世沉积的物源区，分别于查干敖包、白音图嘎和东乌旗三个宝力高庙组/格根敖包组剖面中选取砂岩样品进行碎屑锆石测年，具体采样位置见图 4-1。

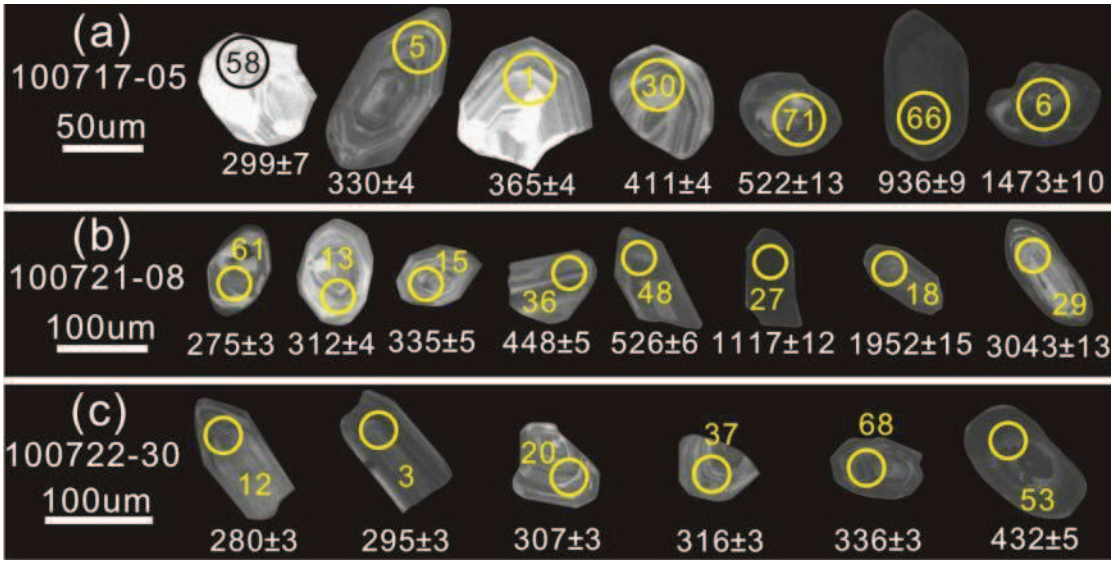

图 4-6 中蒙边境地区三个上石炭－下二叠统砂岩样品锆石阴极发光(CL)图像

Figure 4-6 Cathodoluminescence (CL) images of selected detrital zircons

4.1.2.1 查干敖包地区

砂岩样品（样品号 100717-05）采自中部已风化为薄片状红色砂岩（图 4-2c）。锆石颗粒为自形－半自形，长 60-150 μm，宽 40-80 μm，发育良好岩浆震荡环带（图 4-6a）。锆石的 Th/U 比为 0.14-1.08，显示岩浆成因锆石特征。共选取 75 颗锆石进行 U-Pb 年代学测试，其中 65 颗锆石的测试结果位于谐和线上，年龄范围在 299±7 Ma 到 1473±10 Ma。所有锆石仅表现为一个主要的年龄组，在 299-565 Ma（N=60），峰值年龄为 328 Ma（图 4-7a, b）。另外，含有四颗新元古代锆石

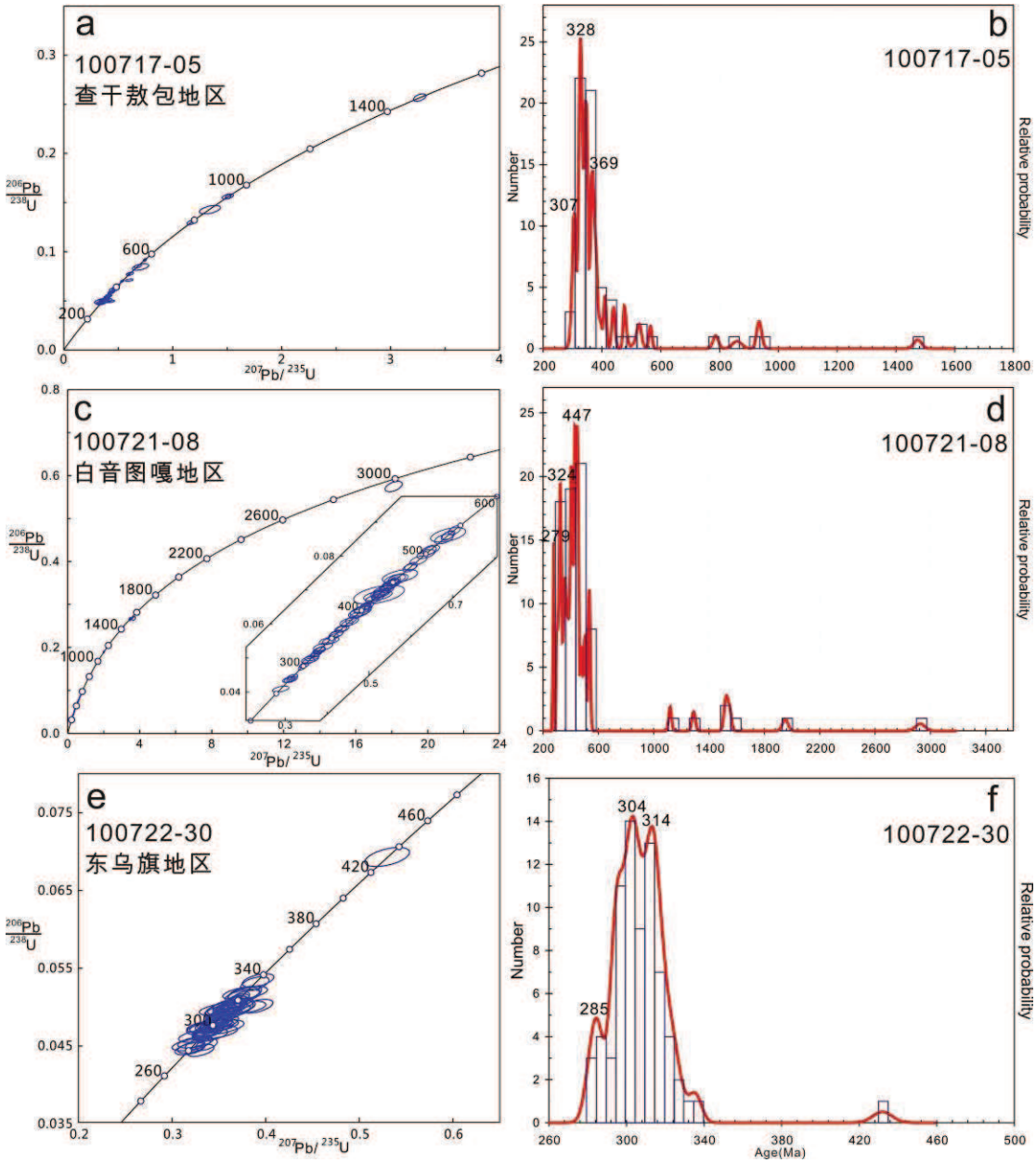

图 4-7 中蒙边境地区三个上石炭－下二叠统砂岩样品碎屑锆石谐和线图及频率曲线图

Figure 4-7 U–Pb concordia and probability diagrams of zircon ages of the five sandstones in this study

和一颗中元古代锆石。

4.1.2.2 白音图嘎地区

砂岩样品（样品号 100721-08）采自中部发育水平层理的红色砂岩（图 4-3a）。锆石颗粒自形－半自形，长 80-150 μm，宽 50-100 μm，并发育良好岩浆震荡环带（图 4-6b）。76 颗锆石的 Th/U 比为 0.13-1.79，显示典型岩浆锆石特征。共选取 76 颗锆石进行 U-Pb 年代学测试，其中 73 颗锆石测试结果位于谐和线上，年龄范围在 275±3 Ma 到 3043±13 Ma。所有锆石仅表现为一个主要年龄组，在 275-542 Ma（N=66），显示三个峰值年龄：279 Ma、324 Ma 和 447 Ma（图 4-7c, d）。另外，含有六颗古－中元古代锆石和一颗新太古代锆石。4.1.2.3 东乌旗地区

砂岩样品（样品号 100722-30）采自中部细砾岩（图 4-4b）。锆石颗粒为自形－半自形，长 80-200 μm，宽 50-100 μm，并发育良好岩浆震荡环带（图 4-6c）。75 颗锆石的 Th/U 比为 0.35-1.10，显示典型的岩浆锆石特征。共选取 75 颗锆石进行 U-Pb 年代学测试，其中 74 颗锆石的测试结果位于谐和线上，年龄范围在 280±3 Ma 到 432±5 Ma。所有锆石仅表现为一个主要年龄组，在 280-336Ma（N=73），峰值年龄为 304 Ma（图 4-7e, f）。另有一颗早古生代锆石，年龄为 432±5 Ma。

4.1.3 Provenance analyses

上述碎屑锆石研究显示相似的年龄分布特征，以 300-330Ma 为主要年龄峰值，两个次级年龄峰分别为 280 Ma 和 447 Ma，及少量元古代碎屑锆石（图 4-7）。

中蒙边境地区晚石炭世岩浆岩广泛分布，如查干敖包北部报道了 317-308 Ma 的碱性花岗岩（许立权等，2012）。东乌旗东部发现与成矿相关的 320Ma 的中粗粒花岗岩（梁玉伟等，2013）。另外，沿中蒙边境向西延伸至蒙古南部，晚石炭世－早二叠世花岗岩、碱性花岗岩和火山岩广泛分布，构成两条该期裂谷岩浆岩带（Yarmolyuk et al., 2008）。这些晚石炭世岩浆岩为 300-330 Ma 的碎屑锆石提供的原地物源。虽然该带南侧沿北造山带分布大量晚石炭世花岗岩类（汤文豪等，2011；施光海等，2003；刘建峰等，2009；鲍庆中等，2007；薛怀民等，2010），但由于北造山带一线晚石炭世为浅海相沉积盆地，这些晚石炭世岩浆岩很难作为该区上石炭－下二叠统陆相沉积的物源。盆地结构及物源特征将于 4.2 节详细叙述。

该区作为早二叠世中亚造山带几条重要的裂谷带之一（Jahn et al., 2009），发育大量裂谷相关双峰式火山岩和碱性花岗岩，年龄在 270-290 Ma（洪大卫等，1996; Zhang et al., 2011）。这些原地岩浆岩为中蒙边境陆相碎屑岩沉积提供了丰富的物源，导致碎屑锆石中 280 Ma 年龄峰的出现。

上述 3.1 节讨论该区泥盆纪沉积物源时，将早古生代年龄峰的物源归因于本地早古生代造山后花岗岩和南部宝力道岛弧岩浆岩。由于宝力高庙组不整合覆盖在泥盆纪沉积岩之上，因此，下伏泥盆纪碎屑的再次循环和原地的早古生代花岗岩均可以作为 447 Ma 年龄峰的物源。

综合以上碎屑锆石信息，以及宝力高庙组/格根敖包组与下伏奥陶纪－泥盆纪地层和早古生代岩浆岩的不整合关系，上石炭-下二叠统碎屑沉积主要以原地沉积岩和岩浆岩作为物源。

4.2 South of Inner Mongolia area-inland sea deposits

The Carboniferous strata, especially the Late Carboniferous ones, are widespread in central Inner Mongolia and crop out in the three blocks of this region (Fig. 4-1b). Along the Northen Orogen, they conformably covered the Late Devonian molassic deposits (Xu et al., 2013). While, they unconformably covered the Late Silurian-Early Devonian molassic deposits along the Southern Orogen (IMBGMR, 1991). We selected five typical sections for sedimentological studies. The positions of these five sections are marked in Fig. 4-1b. The stratigraphic framework in central Inner Mongolia has been constrained by several geological mapping projects, and paleontological studies (Li et al., 1996 and references therein), which provide a control on the timing and duration of the Carboniferous sedimentation. The relative chronostratigraphic framework for each locality is illustrated in Fig. 4-8. The Early Carboniferous deposits can only be identified in Sunidzuoqi and Aohanqi (Fig. 4-8). However, the Late Carboniferous strata, represented by Benbatu and Amushan formations, or Jiadaogou and Jiujuzi formations, are widespread in central Inner Mongolia (Fig. 4-8). Their detailed lithofacies and sedimentary environment will be discussed below.

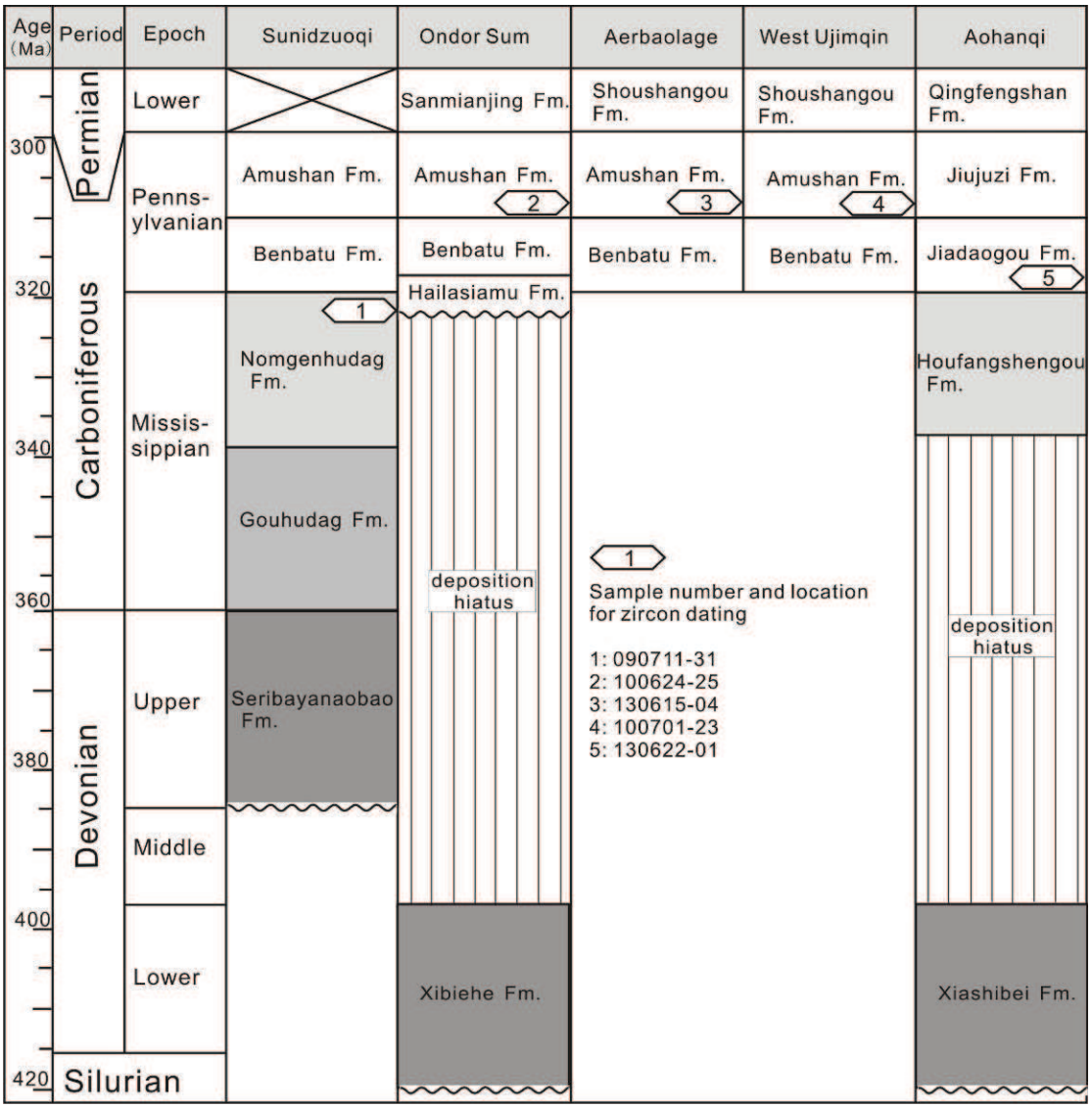

Figure 4-8 Comparison of stratigraphic sequences of the five locations in central Inner Mongolia, with sandstone samples for detrital zircon dating illustrated.

4.2.1 Sedimentological studies and facies analyses

4.2.1.1 Sunidzuoqi section

The Sunidzuoqi section (S-1 in Fig. 4-1b), located along the Northern Orogen (Fig. 1b), and developed above the Late Devonian molassic conglomerate-sandstone, which unconformably overlay the ophiolitic mélange (Xu and Chen, 1997; Xu et al., 2013). The Sunidzuoqi section is composed of, from bottom to top, Lower Carboniferous Gouhudag and Nomgenhudag formations, and Upper Carboniferous Benbatu and Amushan formations (Fig. 4-8).

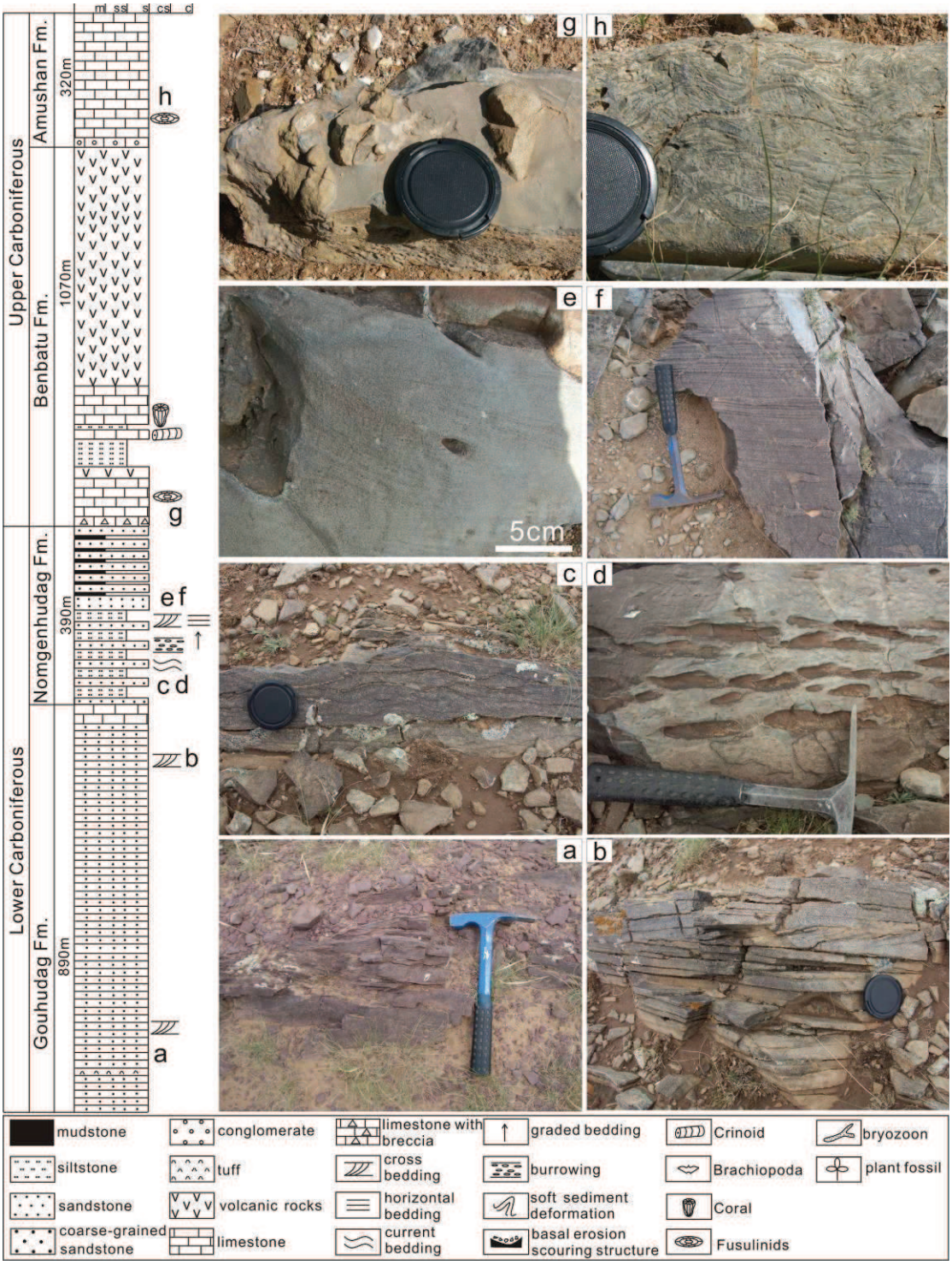

Figure 4-9 Stratigraphic sequence and photographs of the Carboniferous strata in Sunidzuoqi (S-1 in Fig. 1b). The position of each photograph is marked besides the column. a: purple lithic sandstone; b: inclined bedding; c: wavy bedding; d: bedding-parallel mud nodules; e: inclined bedding; f: flat bedding; g: limestone with sandstone breccias; h: bioclastic limestone. The legend is used for Figure 3 to figure 7.

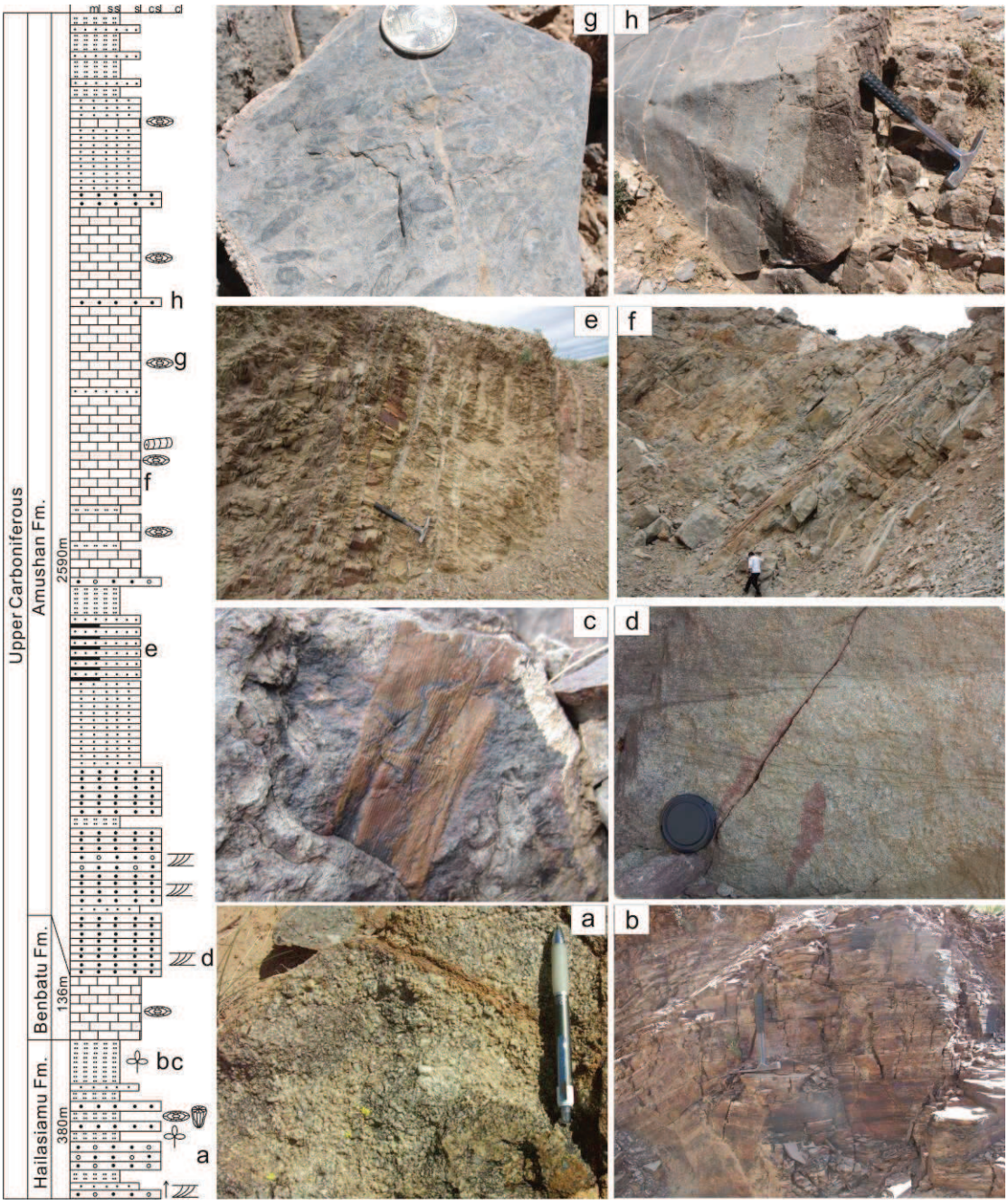

Figure 4-10 Stratigraphic sequence and photographs of the Carboniferous strata in Ondor Sum (S-2 in Fig. 1b). The position of each photograph is marked besides the column. a: quartz-rich coarse sandstone; b: thin-layered black siltstone; c: plant fossils within black siltstone; d: large-scale cross bedding; e: sandstone interbedded with mudstone; f: massive sparite and bioclastic limestone; g: fusulinids within limestone; h: pebbly sandstone layers within limestone sequence.

The 886 m-thick Gouhudag Formation is composed of purple lithic sandstone at

the lower part (Fig. 4-9a), yellowish sandstone at the upper part (Fig. 4-9b), and 40 m-thick limestone on the top. Inclined beddings can be observed in the sandstone part (Fig. 4-9b). The clastic materials, especially for the lower lithic sandstone, are mainly composed of polycrystalline lithic fragments, which originated from magmatic rocks, implying a possible provenance from nearby orogenic belt. The overlying Nomgenhudag Formation, with a thickness of 391 m, is characterized by sandstone interbedded with siltstone in the lower part, and laminated mudstone in the upper part (Fig. 4-9). This formation yields abundant sedimentary structures, such as wavy bedding (Fig. 4-9c), bedding-parallel mud nodules (Fig. 4-9d), inclined bedding (Fig. 4-9e) in sandstone, and flat bedding (Fig. 4-9f) and lamina in siltstone and mudstone. All these sedimentary structures indicate an alternation of turbulent and stable hydrodynamism.

Different from the Lower Carboniferous terrigenous sediments, the Upper Carboniferous Benbatu and Amushan formations are mainly composed of marine limestone with a few siltstone interlayers (Fig. 4-9). The base of Benbatu Formation is marked by the brecciated limestone with sandstone breccias of 2-10 cm in length (Fig. 4-9g), indicating an erosional basal contact. Following that, 0.2-1 m-thick beds of sparite and 0.1-0.5 m-thick beds of bioclastic limestone (Fig. 4-9h) are interbedded, with fossils of corals, fusulinids and crinoids. The upper part of the Benbatu Formation comprises 762 m-thick of rhyolite, dacite, basalt and tuff, with bimodal geochemical features consistent with an extensional setting (Tang et al., 2011). Following the volcanic rocks, the basal limestone of Amushan Formation contains pebbles of underlying volcanic rocks, also indicating an erosional contact, followed by interbedded sandy limestone, bioclastic limestone and sparite with fusulinids and crinoids (Fig. 4-9). These two limestone-dominated strata represent carbonate platform deposition.

4.2.1.2 Ondor Sum area

The Ondor Sum section (S-2 in Fig. 4-1b), located along the Southern Orogen (Fig. 4-1b), is composed of Upper Carboniferous Hailasiamu, Benbatu and Amushan formations, which unconformbly covered the Lower Devonian Xibiehe Formation

(Fig. 4-8).

The 380 m-thick Hailasiamu Formation is composed of quartz pebble bearing quartz sandstone interbedded with black siltstone in the lower part (Fig. 4-10a), and black siltstone in the upper part (Fig. 4-10b). Abundant plant fossils can be found in several black siltstone layers (Fig. 4-10c). The whole sequence represents a transition from fluvial to lacustrine facies deposition. The Benbatu Formation is not well developed in this area with only 136 m-thick fusulinids-bearing limestone (Fig. 4-10), representing carbonate platform deposition.

The 2590 m-thick Amushan Formation can be divided into three continuous sequences according to rock types. The lower clastic sequence is composed of massive coarse sandstone with large cross bedding in the lower part (Fig. 4-10d), followed by sandstone interbedded with mudstone in the upper part (Fig. 4-10e), representing an upward fining sequence from tidal flat with high water energy to littoral sea. The middle carbonate sequence consists mainly of massive sparite and bioclastic limestone, with abundant of fusulinids (Figs. 4-10f and 4-10g), indicating a platform deposition. Several sandstone and pebbly sandstone layers, which represent the input of terrigenous materials, can be found within the limestone sequence (Fig. 4h). The upper clastic sequence is composed of quartz sandstone, siltstone and limestone, with important lateral variations.

4.2.1.3 Aerbaolage area

The Aerbaolage section (S-3 in Fig. 4-1b), located to the north of the Northern Orogen (Fig. 4-1b), is composed of Upper Carboniferous Benbatu and Amushan formations (Fig. 4-8).

The Benbatu Formation starts with a 45 m-thick basal conglomerate, but the underlying formation is unknown. The gravels are rounded to sub-rounded, poorly sorted of 2-20 cm in diameter, with solo composition of felsic volcanic rocks (Fig. 4-11a). These features indicate an alluvial facies proximal rapid accumulation, which can be considered as molassic deposition. Following that, the 72 m-thick lithic coarse sandstone consists of mainly low mature fragments, such as lithic and feldspar, also indicating a proximal deposition. The 765 m-thick limestone is thick bedded, in which

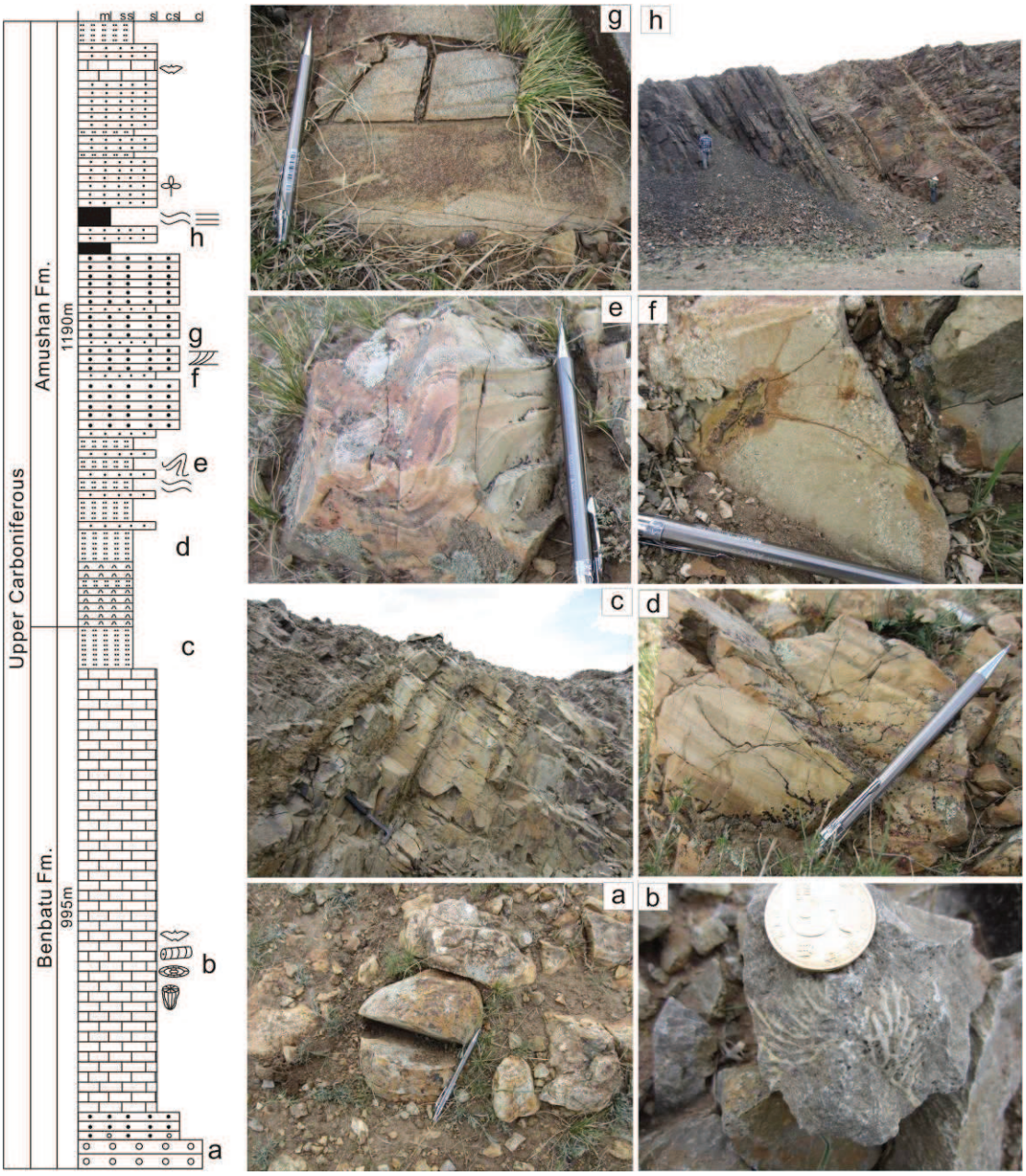

Figure 4-11 Stratigraphic sequence and photographs of the Carboniferous strata in Aerbaolage (S-3 in Fig. 1b). The position of each photograph is marked besides the column. a: conglomerate at the bottom of Benbatu Formation; b: corals within limestone layers; c: yellow siltstone at the top of Bentabu Fromation; d: horizontal bedding; e: soft sediment deformation; f: coarse sandstone interbedded with sandstone; g: cross bedding; h: the contact between black siltstone and massive sandstone.

shallow marine fossils, e.g., corals (Fig. 4-11b), brachiopods and crinoids have been found. These fossils well assign the strata to the Upper Carboniferous (IMBGMR, 1991). Then the limestone is covered by yellow siltstone (Fig. 4-11c). The whole

Benbatu Formation represents a fining upward sequence from basal conglomerate to littoral carbonate and clastic deposition.

Following the Benbatu Formation, the lower part of the Amushan Formation is composed of tuff and siltstone with horizontal beddings (Fig. 4-11d), which are interbedded with quartz sandstone. Wave beddings and soft sediment deformation can be observed (Fig. 4-11e), indicating turbulent environment. The middle part consists of mainly massive coarse sandstone interbedded with sandstone (Fig. 4-11f), with cross beddings (Fig. 4-11g), representing a near shore strongly turbulent environment with sufficient terrigenous material input. The upper part of this formation is composed of thick layered (1-3 m) sandstone interbedded with thin-medium layered (5-30 cm) black siltstone-mudstone (Fig. 4-11h), which may represent periodic sea level change. Wave beddings and horizontal beddings in siltstone and mudstone represent transgression and relative low water energy. While thick layered sandstone and plant debris indicate regression and turbulent water environment. Within the top limestone, abundant shallow marine fossils, e.g. brachiopods, corals and lamellibranches, have been observed (IMBGMR, 1991).

4.2.1.4 West-Ujimqin area

The West-Ujimqin section (S-4 in Fig. 4-1b), located along the Northern Orogen (Fig. 4-1b), consists of the Upper Carboniferous Benbatu and Amushan formations (Fig. 4-8).

The 490 m-thick Benbatu Formation is composed of conglomerate at the bottom, several fining upward cycles in the lower part and limestone in the upper part. The basal conglomerate represents a regional unconformity, which covered the underlying metamorphic basement (Bao et al., 2006). The fining upward cycles contain conglomerate-coarse sandstone-sandstone at the bottom and sandstone-siltstone-mudstone at the top, representing a fining upward sequence (Fig. 4-12a), which indicate a gradual transgression (Bao et al., 2006). Inclined beddings can be found within the coarse quartz-sandstone layers (Fig. 4-12b), showing turbulent environment. The blue thin-layered limestone contains numerous brecciated intraclasts (Fig. 4-12c) and fossil debris with soft sediment structures, also indicating

high water energy.

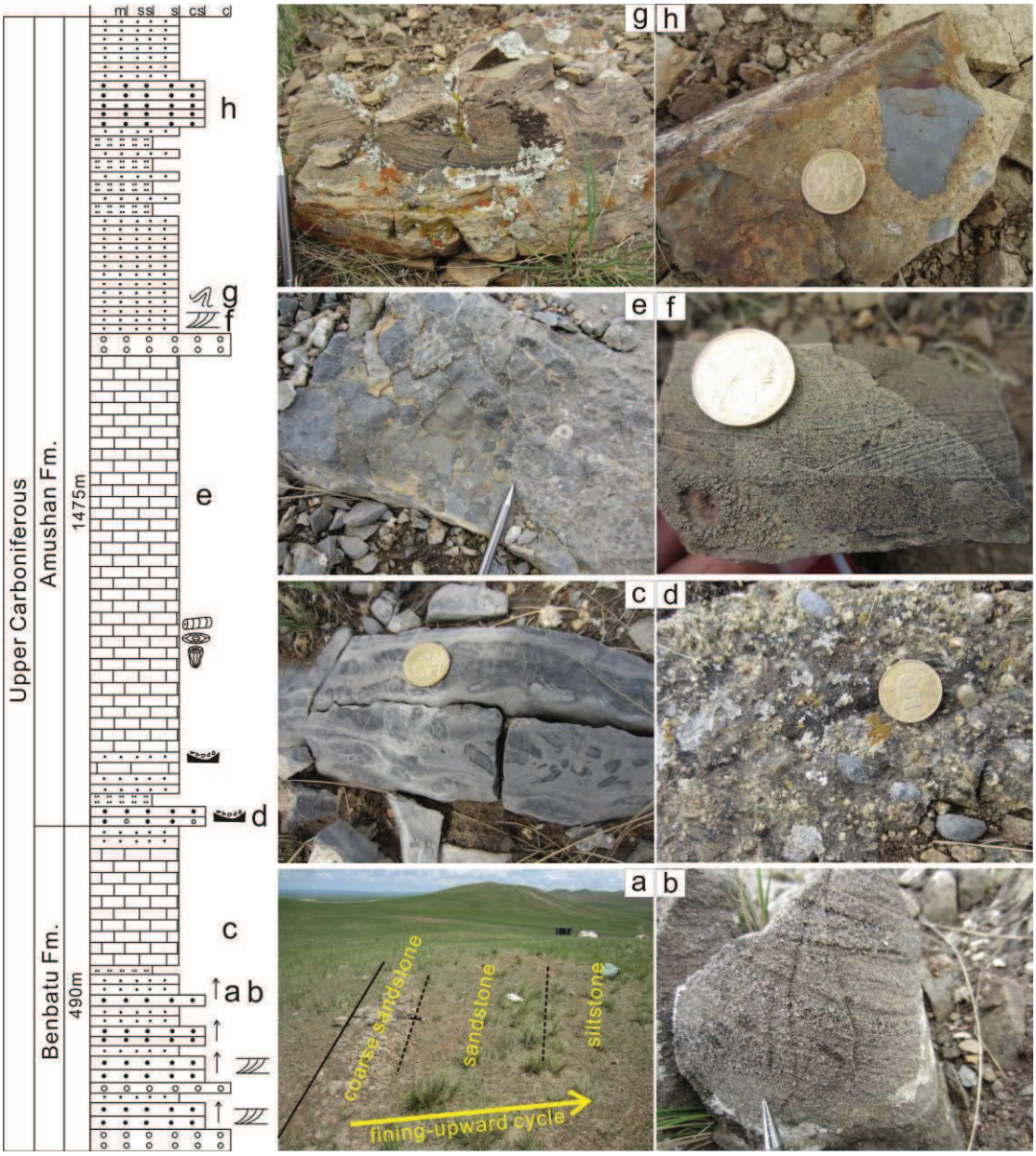

Figure 4-12 Stratigraphic sequence and photographs of the Carboniferous strata in West-Ujimqin (S-4 in Fig. 1b). The position of each photograph is marked besides the column. a: fining upward sequence at the bottom of Benbatu Fromation; b: inclined bedding in coarse sandstone; c: brecciated intraclasts in limestone; d: basal conglomerate at the bottom of the Amushan Formation; e: intraclast limestone and Crinoidea therein; f: inclined bedding in sandstone; g: soft sediment deformation; h: coarse sandstone with mud breccias.

Following the Benbatu Formation, the Amushan Formation starts with a basal conglomerate with pebbles of the underlying sandstone and limestone (Fig. 4-12d),

indicating an erosional contact, which may represent a regional regression. After 70 m-thick interbedded sandstone and limestone, carbonate deposits dominate the lower sequence with shallow marine fossils, e.g., corals, fusulinids and crinoids, representing a stable platform deposition. The upper part of this carbonate sequence is composed of intraclast limestone and sandy intraclast limestone (Fig. 4-12e), which indicate high energy mid-ramp deposits (Burchette and Wright, 1992). The upper clastic sequence is composed of conglomerate at the bottom, followed by sandstone and siltstone. Inclined beddings and soft sediment deformation are pervasive in the sandstone layers (Figs. 4-12f and 4-12g), indicating near shore deposition, which is also indicated by plant fossil debris found within the sandstone. Then, mud breccias are found within the low maturity yellow coarse feldspar-quartz sandstone (Fig. 4-12h), indicating a near shore deposition environment, possibly affected by storms.

4.2.1.5 Aohanqi area

The Aohanqi section (S-5 in Fig. 4-1b), located to the south of the Southern Orogen (Fig. 4-1b), is composed of the Lower Carboniferous Houfangshengou Formation and Upper Carboniferous Jiadaogou and Jiujuzi formations (Fig. 4-8).

The 1230 m-thick Houfangshengou Formation is composed of blue-grey thick-bedded limestone (0.3-1.5 m, Fig. 4-13a) with thin layers of siltstone interstratified in the upper part (Fig. 4-13b). The striking feature of this sequence is the abundant of shallow marine fossils, such as coral, crinoids, fusulinids and brachiopoda (Fig. 4-13c). The massive stratified beds and abundant corals represent reef limestone deposited on a carbonate platform (e.g. Coniglio and Dix, 1992). On the top of this formation, nodular limestone shows sea level fall, and significant energy fluctuations.

The 1054 m-thick Jiadaogou Formation is composed of 10-20 cm-thick bedded limestone interbeded with sandstone and siltstone (Figs. 4-13d and 4-13e). The most important difference from the underlying Houfangshengou Formation is the significant increase of siliciclastic materials. Meanwhile, brachiopodas, instead of corals, became the main fossils in this formation.

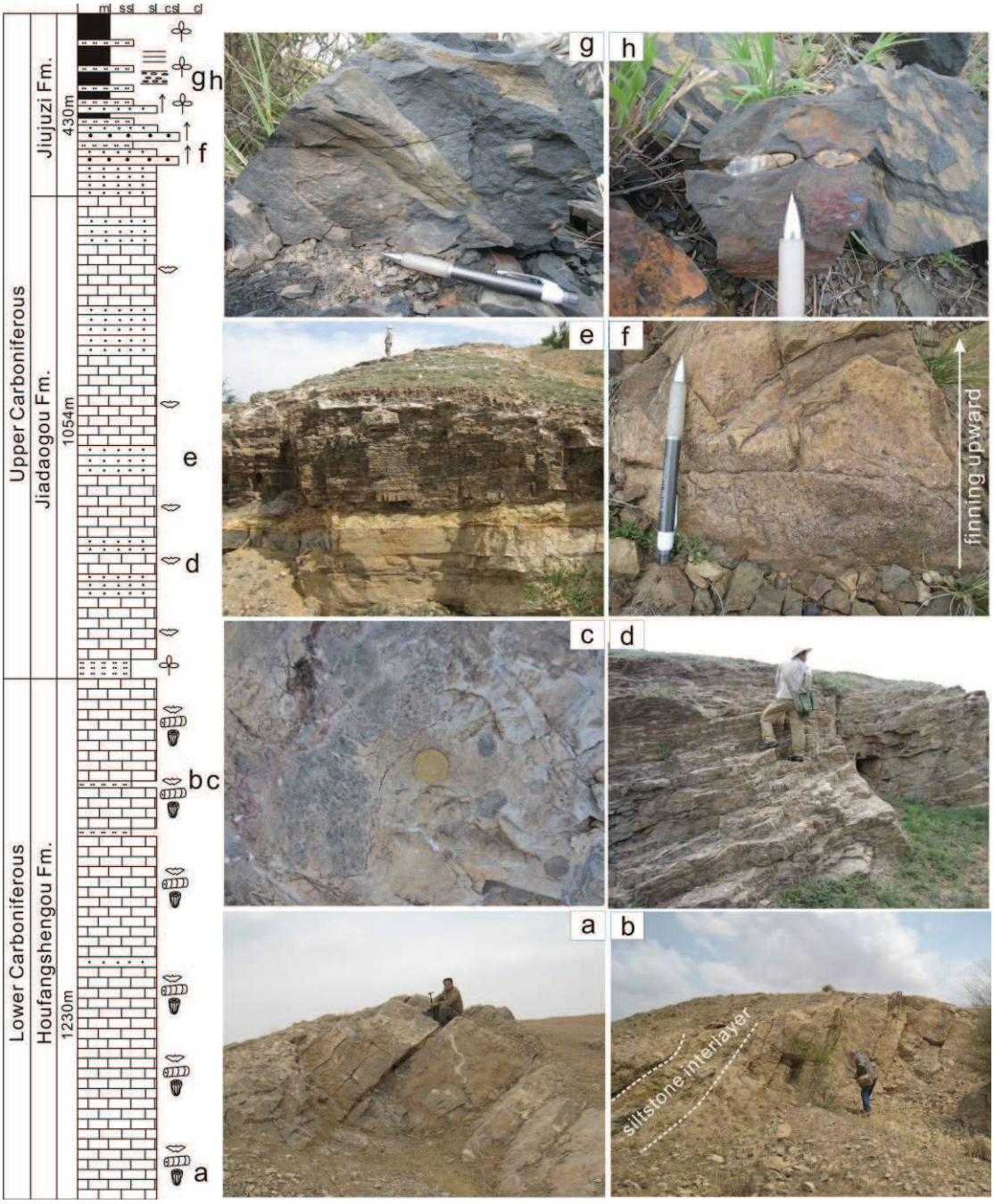

Figure 4-13 Stratigraphic sequence and photographs of the Carboniferous strata in Aohanqi (S-5 in Fig. 1b). The position of each photograph is marked besides the column. a: massive limestone; b: siltstone interlayer within limestone; c: corals in limestone; d: thin-bedded bioclastic limestone; e: limestone interbedded with siltstone; f: fining upward sequence of the Jiujuzi Formation sandstone; g: plant fossils in black shale; h: burrows in black shale.

The Jiujuzi Formation is 700 m thick with quartz sandstone interbedded with plant fossil-bearing black mudstone (Fig. 4-13). From bottom to top, the thickness of

black laminated mudstone increases from centimeter to meter scale, showing a thinning upward sequence. The quartz sandstone is medium- to thick-bedded with graded bedding (Fig. 4-13f). The angular to subangular quartz grains are of 2-5 mm in diameter and from grain supported at the bottom to matrix supported on the top (Fig. 4-13f). The black shale is laminated or homogeneous with abundant burrows and plant fossils (Figs. 4-13g and 4-13h). The basal contact with quartz sandstone is sharp whereas the upper contact is mainly erosive which shows a high energy environment when the coarse sandstone deposited. The quartz sandstone-shale sequence of Jiujuzi Formation is interpreted to represent the meandering fluvial deposits, characterized by thinning upward quartz sandstone-shale sequence, abundance of borrows and wood fossils (Hendrix et al., 1996; Prothero and Schwab, 2003). The quartz sandstone deposited in the flood period. The high energy streams bring coarse grains, cutting the former black shales, and forming an erosive contact. As the flood weakened, the amount of fine-grain material increased, developing graded beddings in the sandstone beds. After the flood, black shale deposited on the floodplain with mollusk burrows and plant grown.

4.2.2 Detrital zircon geochronological study

In order to determine the age and provenance of these Carboniferous strata, detrital zircon U-Pb dating was carried out on sandstone samples from each locality (Fig. 4-1b). The detailed information and location of each sample are given in Table 1, and Fig. 4-1b, respectively.

Table 4-1 Summary of sandstone sample for detrital zircon dating

Number	Location	GPS	Formation	Tectonic division
090711-31	Sunidzuoqi	43°28′58″N; 113°32′17″N	Nomgenhudag Fm.	between NOB and SOB
100624-25	Ondor Sum	42°22′13″N; 113°08′05″N	Amushan Fm.	South of SOB
130615-04	Aerbaolage	44°58′43″N; 117°10′15″N	Bentabu Fm.	North of NOB
100701-23	West-Ujimqin	44°15′29″N; 117°49′59″N	Amushan Fm.	North of NOB
130622-01	Aohanqi	42°34′26″N; 119°49′21″N	Jiadaogou Fm.	South of SOB

4.2.2.1 Lower Carboniferous sandstone from Sunidzuoqi (#090711-31)

This sample was collected from the upper part of the Lower Carboniferous

Nomgenhudag Formation. The zircon grains are euhedral to subhedral in shape, with 30-70 μm in width and 50-90 μm in length. Most grains show oscillatory zoning and some old grains show bright to grey cores with weak oscillatory growth zoning (Fig. 4-14a). Totally, 75 grains were analyzed with 69 concordant results (<10% discordance and most <5%). The Th/U ratios range from 0.23 to 1.35, characteristic of an igneous origin. The 69 concordant analyses yielded apparent ages ranging from 328±4 Ma to 2894±27 Ma and fell into two main age populations: 328-503 Ma (n=53) with main peak at 430 Ma and secondary peak at 348 Ma; 705-1313 Ma (n=13) without peak age (Fig. 4-15a, b). In addition, one Archean and two Paleoproterozoic grains yielded $^{207}Pb/^{206}Pb$ ages of 2894±27 Ma, 1631±31 Ma and 1581±106Ma, respectively.

4.2.2.2 Upper Carboniferous sandstone from Ondor Sum (#100624-25)

The sample was collected from the lower part of the Upper Carboniferous Amushan Formation. The zircon grains are euhedral to subhedral, ranging from 40-60

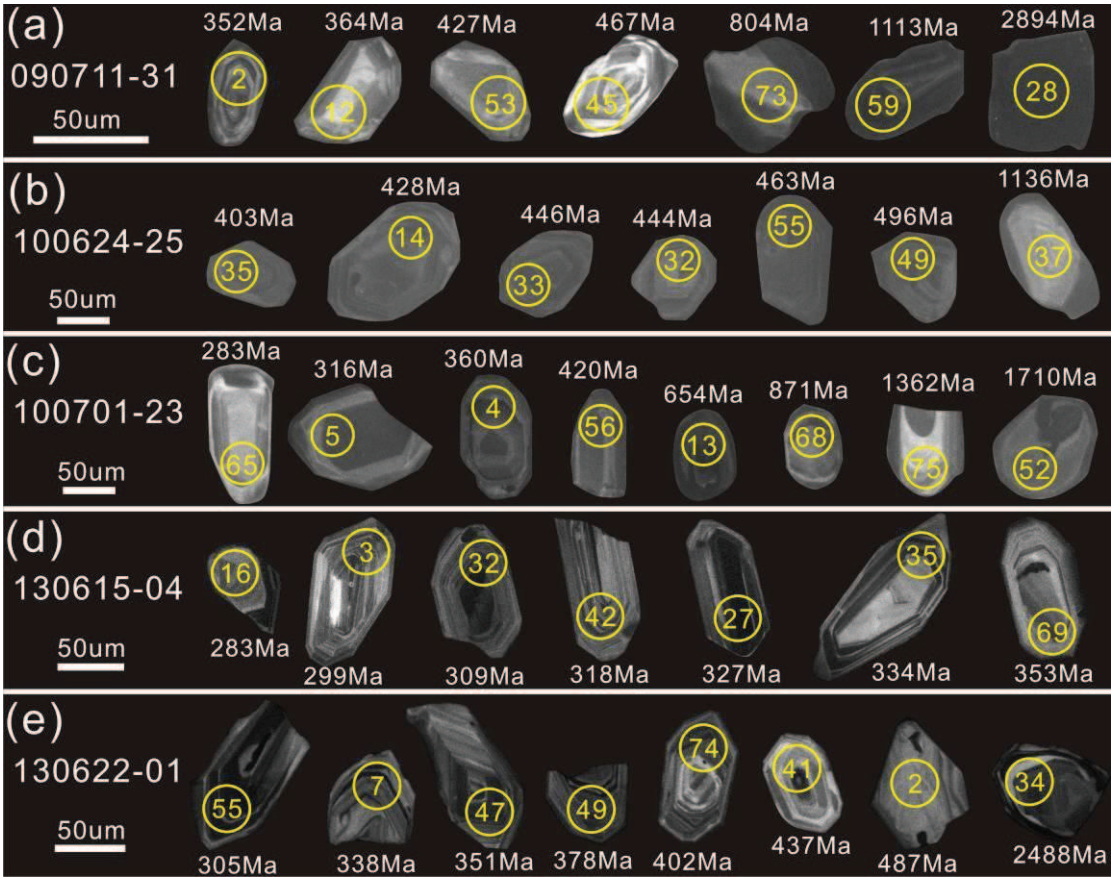

Figure 4-14 Cathodoluminescence (CL) images of selected detrital zircons from each sample. The circles represent U–Pb analytical sites with numbers in the circles and ages presented below.

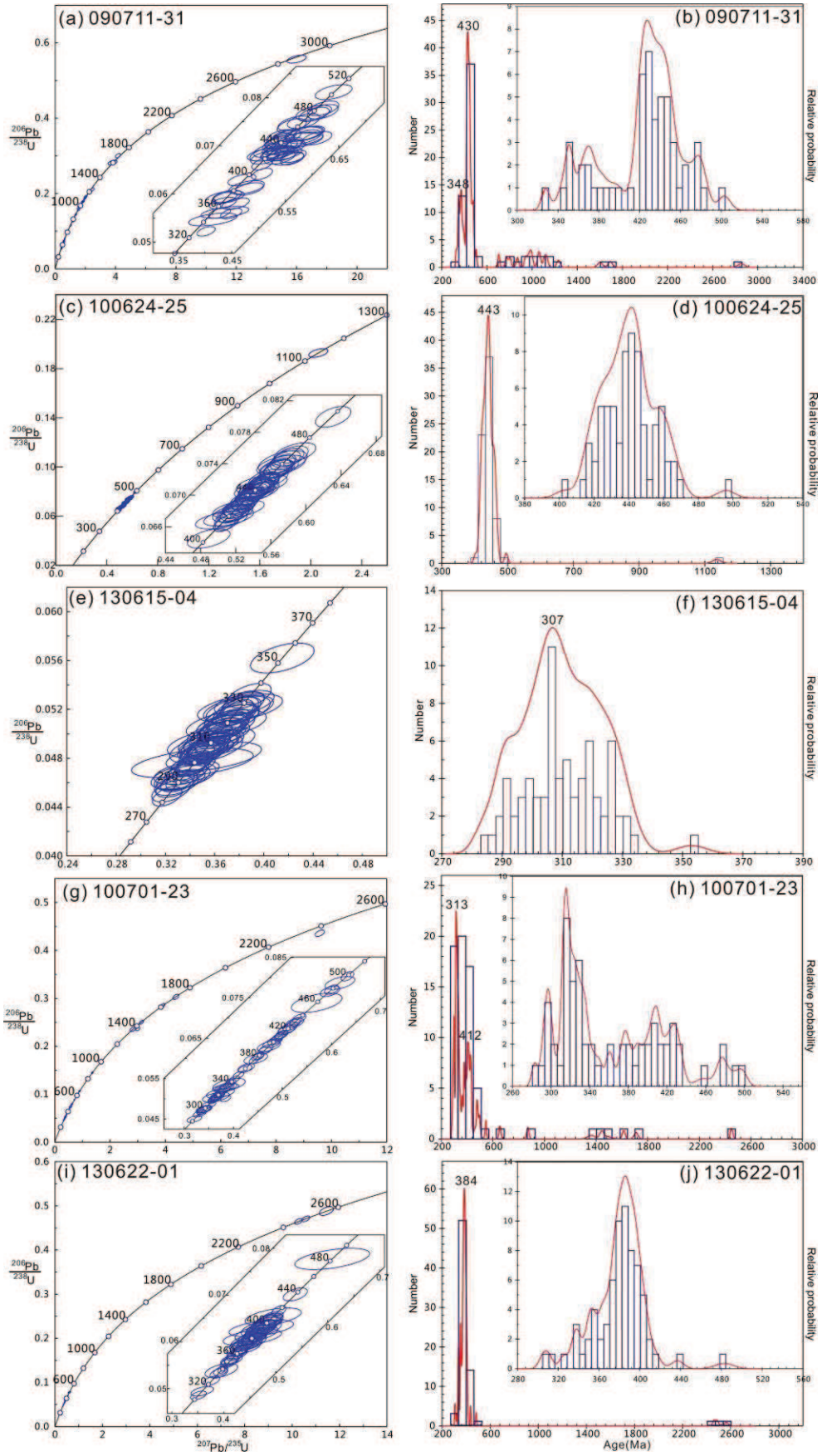

Figure 4-15 U–Pb concordia and probability diagrams of zircon ages of the five sandstone. The inset figures within each U-Pb Concordia diagram show zircon grains with ages of 250-500 Ma.

μm in width and 50-100 μm in length with oscillatory growth zoning (Fig. 4-14b). A total of 75 zircons were analyzed and 71 of them were concordant. The Th/U ratios range from 0.37 to 1.99, indicating a magmatic origin. Among the 71 concordant analyses, 70 of them yielded apparent ages ranging from 403±5 Ma to 496±5 Ma, with a peak age of 443 Ma (Fig. 4-15c, d). Only one grain yielded an age of 1136±29 Ma.

4.2.2.3 Upper Carboniferous sandstone from Aerbaolage (#130615-04)

The sample was collected from the lower part of the Upper Carboniferous Benbatu Formation. The zircon grains are euhedral, ranging from 40-60 μm in width and 80-200 μm in length with well developed oscillatory growth zoning (Fig. 4-14c). Seventy-three of the total 75 analyzed zircons were concordant. The Th/U ratios range from 0.34 to 1.34, indicating magmatic origin. The 73 concordant analyses fell into only one age population, ranging from 283±3 Ma to 353±5 Ma, with a peak age of 307 Ma (Fig. 4-15e, f).

4.2.2.4 Upper Carboniferous sandstone from West-Ujimqin (#100701-23)

The sample was collected from the lower part of the Upper Carboniferous Amushan Formation. The zircon grains are euhedral to subhedral, ranging from 40-60 μm in width and 50-150 μm in length with fine-scale oscillatory growth zoning (Fig. 4-14). Seventy of the total 75 analyzed zircons were concordant, with the Th/U ratios ranging from 0.15 to 1.41, indicating a magmatic origin. The 70 concordant analyses yielded apparent ages ranging from 283±3 Ma to 2450±9 Ma and fell into one main age population of 283-498 Ma (n=61), with age peaks of 313 Ma and 412 Ma (Fig. 4-15g, h). In addition, 9 Precambrian grains yielded ages from 545±5 Ma to 2450±9 Ma without peak age (Fig. 4-15g, h).

4.2.2.5 Upper Carboniferous sandstone from Aohanqi (#130622-01)

The sample was collected from the lower part of the Upper Carboniferous Jiadaogou Formation. The zircon grains are euhedral to subhedral, ranging from 40-80 μm in width and 50-150 μm in length with well-developed oscillatory growth zoning (Fig. 4-14e). Totally, 73 of 75 analyzed grains gave valid results, all of which were concordant. The Th/U ratios range from 0.15 to 1.72, indicating magmatic origin.

The concordant zircons yielded apparent ages ranging from 305±4 Ma to 2559±17 Ma and fell into one main age population of 305-483 Ma (n=70), with age peaks of 384 Ma (Fig. 4-15i, j). In addition, 3 Precambrian grains yielded ages at 2458±10 Ma, 2488±10 Ma and 2559±17 Ma (Fig. 4-15i, j).

4.2.3 Sedimentological comparison and correlation

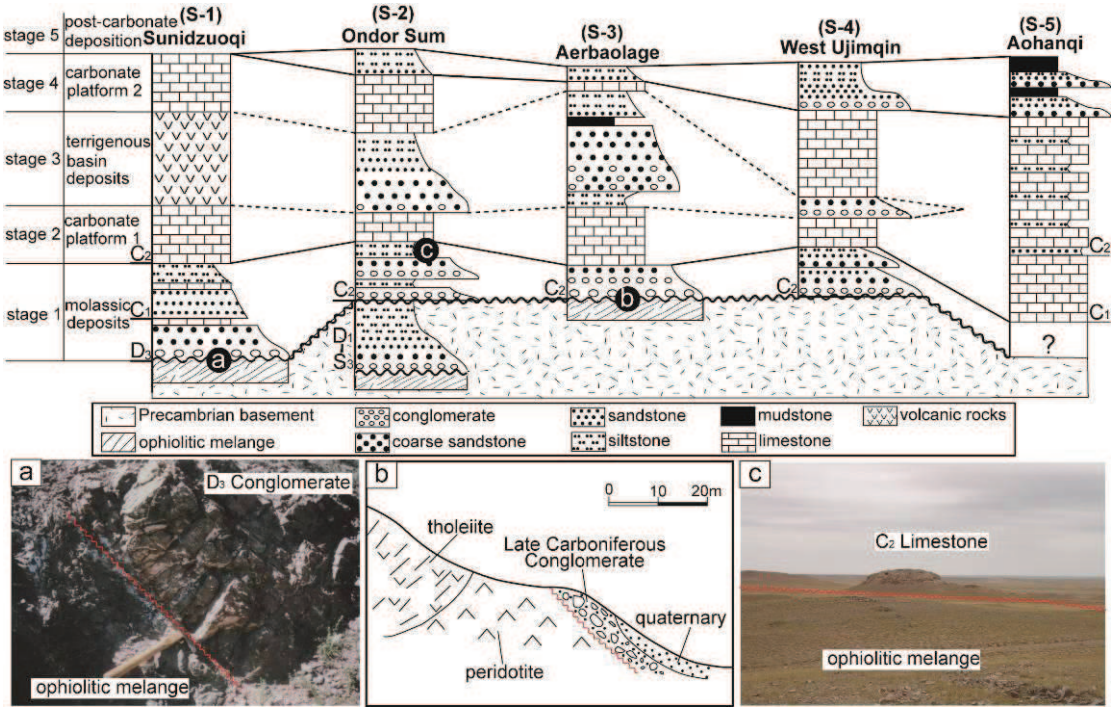

Figure 4-16 Tentative correlation diagram for the five sections analyzed in this study. See Figure 1b for locations of each section. Correlations were established by tracing similar beds in the field. Five sedimentary stages were distinguished according to different rock assemblages and sedimentary facies. a: Unconformity between Upper Devonian conglomerate and ophiolitic mélange in Sunidzuoqi (from Xu et al., 2013); b: Unconformity between Upper Carboniferous conglomerate and ophiolite in Aerbaolage (from Zhang et al., 2012); c: Unconformity between Upper Carboniferous limestone and ophiolitic mélange in Ondor Sum.

The sedimentological analyses demonstrate a basal contact of most of the Late Carboniferous strata with the underlying Precambrian basement and Early Paleozoic arc magmatic rocks. A tentative composite lithostratigraphic correlation of the Carboniferous strata in central Inner Mongolia based on the similarities in lithologic

assemblages, fossils and detrital zircon U-Pb dating results is illustrated in Fig. 4-16. Five main sedimentary stages are distinguished.

4.2.3.1 Basal molassic deposition

Two unconformities have been identified along both the southern and northern orogens, which postdated these two orogenic events before the Late Silurian and Late Devonian, respectively (Tang, 1990; Xu et al., 2013). Along the Southern Orogen, the Late Silurian- Early Devonian molassic sediments of Xibiehe Formation covered the metamorphic basement and ophiolitic mélange unconformbly (Tang, 1990; Li et al., 1996; Zhang et al., 2010). After that, the whole region along the Southern Orogen became a subaerial environment without sediments until the Late Carboniferous. For the Northern Orogen, the ophiolitic mélange was unconformably covered by the Late Devonian conglomerate of Seribayanaobao Formation, identified from the Sunidzuoqi area (Fig. 4-16a; Xu et al., 2013). Started with the Late Devonian terrestrial molassic conglomerate, the sequence became fining upward into the Early Carboniferous littoral terrigenous lithic sandstone and siltstone (Figs. 4-9 and 4-16).

At the beginning of the Late Carboniferous, an extensive transgression occurred after the Silurian-Devonian orogenic events (IMBGMR, 1991), producing the molassic-like deposition at the bottom of Late Carboniferous strata in several localities of central Inner Mongolia, e.g. Ondor Sum, Aerbaolag and West-Ujimqin (Fig. 4-16). In the Ondor Sum area, the lowermost Hailasiamu Formation, which unconformably covered the Xibiehe Formation (IMBGR, 1976), is mainly composed of fluvial coarse quartz-sandstone and plant fossils bearing lacustrine black siltstone, indicating a terrestrial deposition (Fig. 4-16). In the Aerbaolage area, although no direct unconformity was observed, the basal conglomerate of the Benbatu Formation can be considered as molassic deposition, with abundant volcanic boulders and pebbles (Fig. 4-11a). Meanwhile, the unconformity between the Late Carboniferous basal conglomerate and ophiolite was identified in the Aerbaolage area (Fig. 4-16b; Zhang et al., 2012). In the West-Ujimqin area, the basal conglomerate of Benbatu Formation unconformably covered the Precambrian Xilinhot metamorphic complex (Bao et al., 2006), also showing a molassic-like feature. However, for the Aohanqi

area, the Early Carboniferous started from carbonate deposits and the basal sediment is unclear, as no pre-Carboniferous sediment was identified here.

4.2.3.2 First stage of carbonate platform deposits

After the fining upward molassic deposition, the entire region came into a carbonate platform environment, represented by the Benbatu Formation limestone, which is characterized by abundant shallow marine fossils, e.g. fusulinids, corals, brachiopods (Fig. 4-16). The Benbatu Formation from the Sunidzuoqi, Ondor Sum, Aerbaolage and West-Ujimqin areas can be correlated by fusulinid combination. The *Profusulinella-Pseudostaffella* and *Fusulina-Fusulinella* zones characterize the lower and upper parts of the Benbatu Formation (IMBGMR, 1991; Li et al., 1996). Meanwhile, the Benbatu Formation can also be identified from the Siziwangqi and Alukerqin areas, which are located on both sides of the Southern Orogen (Fig. 4-1b), indicating that the transgression occurred in the whole central Inner Mongolia. Furthermore, a direct unconformity between the Late Carboniferous limestone and ophiolitic mélange was identified in the Ondor Sum area (Fig. 4-16c), indicating a transgressive overlap. During this stage, the whole area became into an extensive inland sea, producing widespread carbonate deposits with similar shallow marine fossils.

4.2.3.3 Terrigenous deposits and local volcanism within the carbonate platform

After the Benbatu Formation carbonate deposition, terrigenous clastic sediments dominated this region with locally volcanic occurrence (Fig. 4-16). In the Aerbaolage and Ondor Sum areas, thick-bedded coarse sandstone with large inclined beddings and cross beddings (Figs. 4-10d and 4-11g) is situated at the bottom of the Amushan Formation (Fig. 4-16). Furthermore, the high proportion of lithic and feldspar fragments, combining with conglomerate interlayers, indicate their low maturity, which might be deposited in an inland sea close to the provenance. In the West-Ujimqin area, the limestone pebbles within the basal conglomerate of the Amushan Formation indicate erosion of underlying carbonate deposition. In the Sunidzuoqi-Sunidyouqi area, the Chagannur volcanic rocks are situated above the Benbatu Formation limestone (Fig. 4-16). The geochemical features of the basalt and

rhyolite indicate an extensional setting (Tang et al., 2011). During this stage, the regional tectonics caused uplift and erosion of the underlying strata, producing clastic deposits in the nearby basins.

4.2.3.4 Second stage of carbonate platform deposits

Represented by the Amushan Formation limestone, a new stage of carbonate deposits overlay the terrigenous sediments (Fig. 4-16). Like the Benbatu Formation, the Amushan Formation can also be correlated by fusulinid fossils, e.g., *Triticites* and *Pseudoschwagerina* throughout the entire area (IMBGMR, 1991; Li et al., 1996; Shen et al., 2006). The distribution of the Amushan Formation carbonate deposits is more widespread than that of the Benbatu Formation, indicating the expansion of this inland sea.

4.2.3.5 Post-carbonate terrigenous clastic deposition

Following the Amushan Formation carbonate deposition, diverse depositional patterns occurred in central Inner Mongolia (Fig. 4-16). To the south of Sunidzuoqi, a subaerial environment followed the Amushan limestone without deposition until the Middle-Late Permian terrestrial conglomerate (Xu and Chen, 1997). In Ondor Sum, Aerbaolage and West Ujimqin areas, shallow marine or littoral facies clastic deposits overlay the Amushan limestone, and in turn were covered by the Early Permian shallow marine facies deposits (Bao et al., 2006; Gong et al., 2013). In Aohanqi area, the Upper Carboniferous carbonate-clastic sediments were followed by the Upper Carboniferous Jiujuzi Formation terrestrial facies deposits, with Cathaysian flora and coal seams therein (IMBGMR, 1991; Figs. 4-16 and 4-13h).

4.2.4 Carbonifeous provenance analyses

Detrital zircon age spectra of the five sandstone samples from the Carboniferous rocks are dominated by Phanerozoic grains that exhibit two main age clusters with peaks at 400-440 Ma and 310 Ma, and subordinate peaks at 340 Ma (Fig. 4-15). The Early Paleozoic peak at 400-440 Ma was identified from samples near the northern and southern suture zones, in Sunidzuoqi, Ondor Sum and West-Ujimqin (Fig. 4-1b),

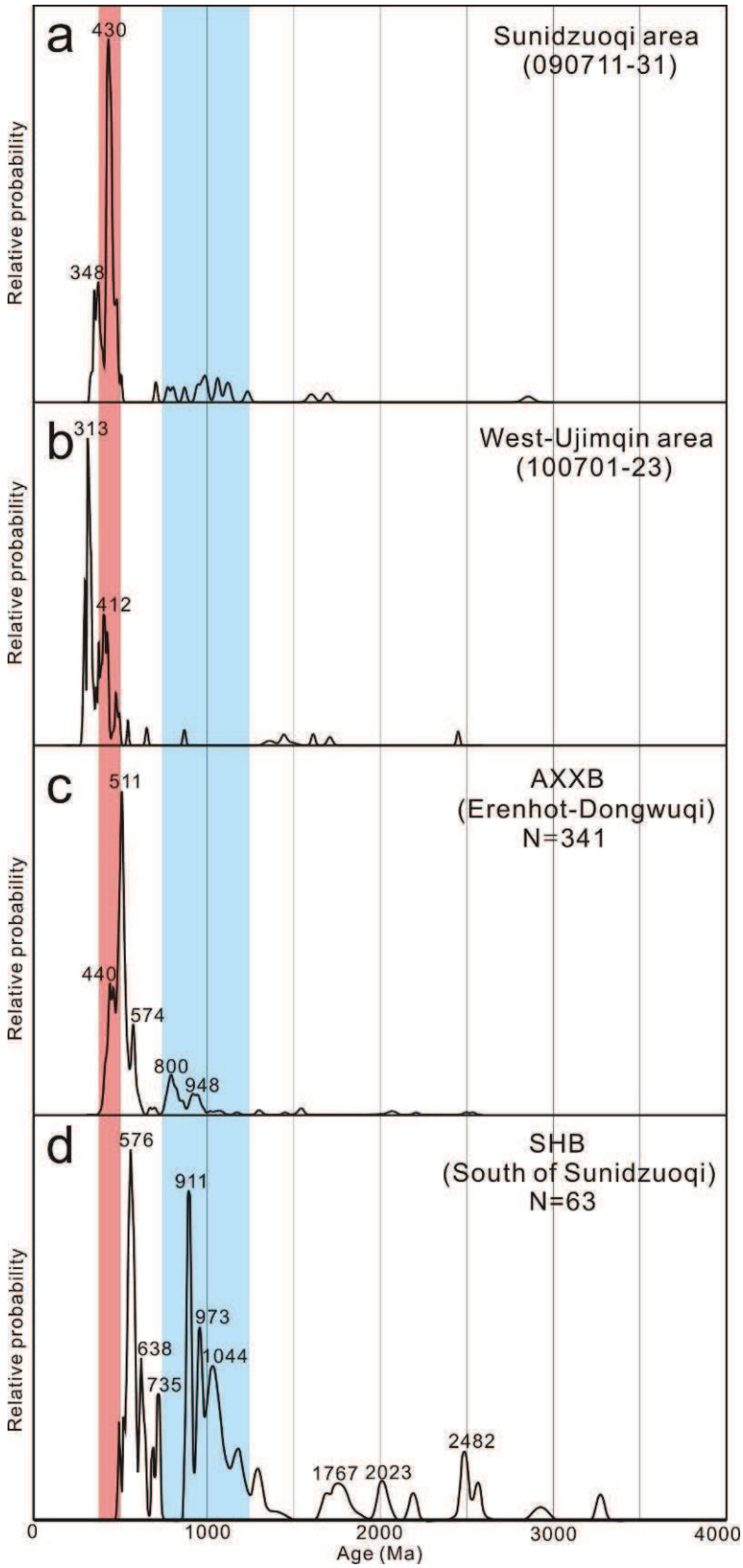

Figure 4-17. Comparison of probability plots for our Carboniferous data from Sunidzuoqi (a) and West-Ujimqin (b) with the Early Paleozoic data from Airgin Sum-Xilinhot-Xing'an Block (AXXB) (c; Zhao et al., 2014) and Songliao-Hunshandake Block (SHB) (d; Xu et al., 2013).

where the Early Paleozoic arc magmatic rocks are widespread (Jian et al., 2008; Xu et al., 2013; Zhang et al., 2013). This peak can also be traced from detrital zircon results of the Early Paleozoic sediments in AXXB and SHB (Fig. 4-17). The 310 Ma age peak was identified from the West-Ujimqin and Aerbaolag areas, where the Late Carboniferous magmatic rocks were well exposed (Bao et al., 2007; Liu et al., 2009; Xue et al., 2010), indicating that the local magmatic rocks were the main provenance for these zircons. Furthermore, the age peak at 384 Ma is only presented by the sample from Aohanqi, where the same age peak has been displayed from the Devonian strata (Cheng et al., 2014). This unique age cluster may be related to the Devonian syenitic complexes and mafic intrusions at the northern margin of the NCC (Luo et al., 2001; Jiang, 2005; Zhang et al., 2010; Zhang and Zhai, 2010).

Precambrian zircon grains can be traced from four samples and statistically a rigorous comparison is impossible because of the small number of grains (Fig. 4-15). However, the predominant Meso- to Neo-proterozoic grains are most likely supplied from the underlying AXXB and SHB, where such a Meso- to Neo-proterozoic basement is well documented (Fig. 4-17; Zhang et al., 2012; Xu et al., 2013; Wang et al., 2013; Zhao et al., 2014).

In summary, the detrital zircon dating results indicate that the provenances for these Late Carboniferous strata were mainly local magmatic rocks with subordinate input of basement clastics, indicating local erosion and proximal provenances. This kind of detrital zircon distribution pattern indicates that the Carboniferous strata deposited above the Precambrian basement of these three blocks and two Early Paleozoic orogenic belts. Therefore, the Carboniferous strata are most likely deposited in an inland sea above the welded block, but not in a wide ocean.

4.3 Summary of this chapter

根据上述沉积相分析和碎屑锆石研究，内蒙古中东部早石炭世大部分为剥蚀区，沉积仅发育于局部地区；晚石炭世沉积类型可分为两类，即中蒙边境晚石炭世陆相碎屑－火山沉积和内蒙古中南部陆表海碎屑－碳酸盐岩沉积。

中蒙边境晚石炭世发育陆相碎屑－火山沉积。碎屑锆石年代学研究显示其物

源主要来自于额尔古纳－兴安地块本身，以原地沉积岩和岩浆岩作为物源。该陆相沉积可以作为内蒙古中南部广泛陆表海沉积的北部边缘。

内蒙古中南部地区发育陆表海碎屑－碳酸盐岩沉积岩系，底部不整合覆盖在前寒武纪基底、早古生代岛弧岩浆岩、蛇绿混杂带、前石炭纪地层及石炭纪侵入岩之上，代表由海侵导致的区域超覆不整合。区域内晚石炭世地层可通过沉积类型和化石组合进行对比，表明其相同的沉积类型和沉积环境。晚石炭世陆表海沉积覆盖于整个内蒙古中南部地区，并横跨南北三个板块（艾里格庙－锡林浩特－兴安地块、松辽－浑善达克地块和华北克拉通）和两个造山带（北造山带和南造山带），代表陆块拼合后的第一个稳定沉积盖层，限定三个板块的拼合发生于石炭纪之前。另外，作为代表早古生代岛弧岩浆事件的 440Ma 年龄峰，其出现于由南北两条缝合带分隔的三个陆块之上，说明石炭纪沉积时，作为物源的早古生代岛弧岩浆岩已经跨越缝合带进行沉积，同样说明三个陆块在石炭纪之前已经碰撞拼合。

Chapter 5 Permian sedimentology features, geochemistry and geochronology studies of magmatic rocks

二叠纪沉积在内蒙古中东部分布广泛（图 5-1），且沉积类型复杂。早二叠世中蒙边境一带为陆相火山岩沉积，以宝力高庙组火山岩段为代表，之后该区域进入陆相剥蚀阶段，仅局部发育陆相地层（内蒙古地质矿产局，1991；周志广等，2010）。中蒙边境以南地区，早二叠世沉积比较复杂，且横向差异较大。研究区西部苏尼特左旗地区缺失早二叠世沉积，温都尔庙地区则为浅海相碎屑沉积（图 5-2）。研究区东部早二叠世早期发育浅海相和海陆交互相碎屑岩沉积，前者以西乌珠穆沁旗寿山沟组为代表，后者以克什克腾旗－敖汉旗一线清凤山组碎屑岩段为代表（图 5-2）。早二叠世晚期则发育火山岩沉积，以大石寨组和清凤山组上火山岩段为代表（图 5-2）。中二叠世沉积以浅海相－海陆交互相－陆相碎屑岩沉积为主，夹少量碳酸盐岩沉积，以哲斯组、黄岗梁组和索仓组为代表（图 5-2）。晚二叠世沉积仅集中于西乌珠穆沁旗－林西一带，以林西组和北大山组湖相巨厚层

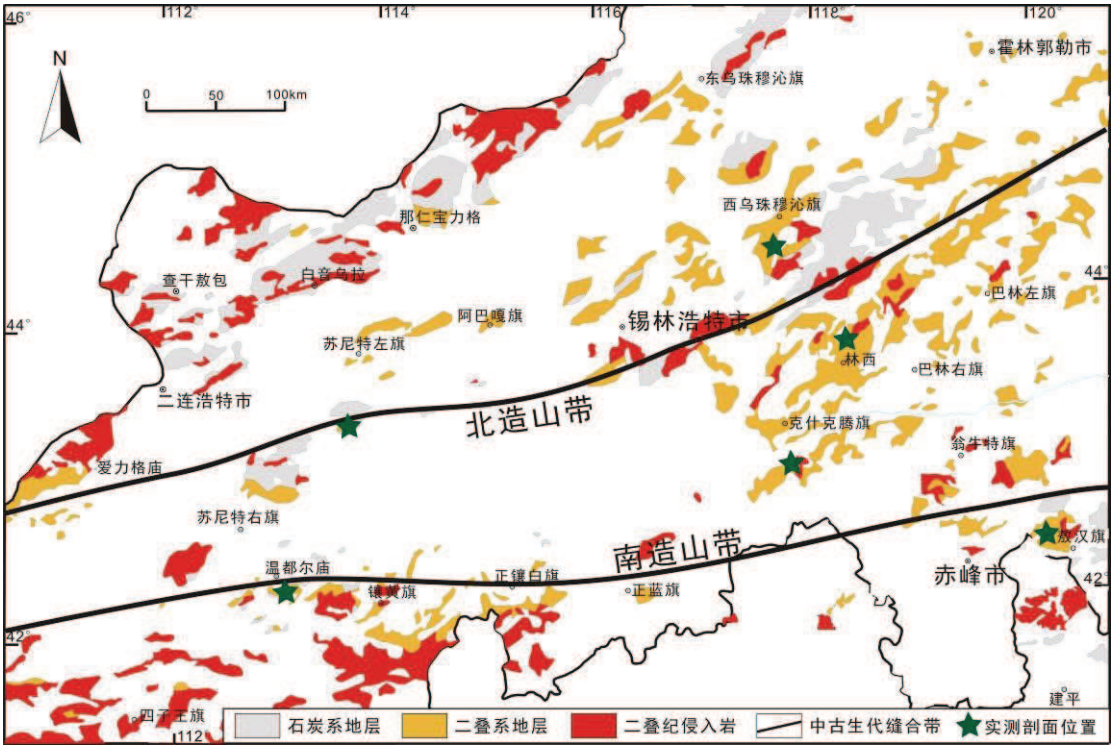

图 5-1 内蒙古中东部二叠纪地层与侵入岩分布图（据内蒙古地质矿产局，1991）

Figure 5-1 Distribution of Permian strata and intrusive rocks in central-eastern Inner Mongolia (from IMBGMR, 1991)

黑色粉砂岩－板岩为代表（图 5-2）。

二叠纪内蒙古中东部地区发育大量侵入岩，岩性包括辉长岩、闪长岩、花岗闪长岩、花岗岩和碱性岩（张晓晖和翟明国，2010；童英等，2010）。中蒙边境一带沿二连浩特至东乌珠穆沁旗发育碱性岩和碱性花岗岩，与蒙古南部构成早二叠世伸展相关碱性岩带（洪大卫等，1994；Jahn et al., 2009）。而该带以南二叠纪侵入岩的侵位环境仍无定论，存在俯冲岛弧与陆内伸展两种截然不同的观点。

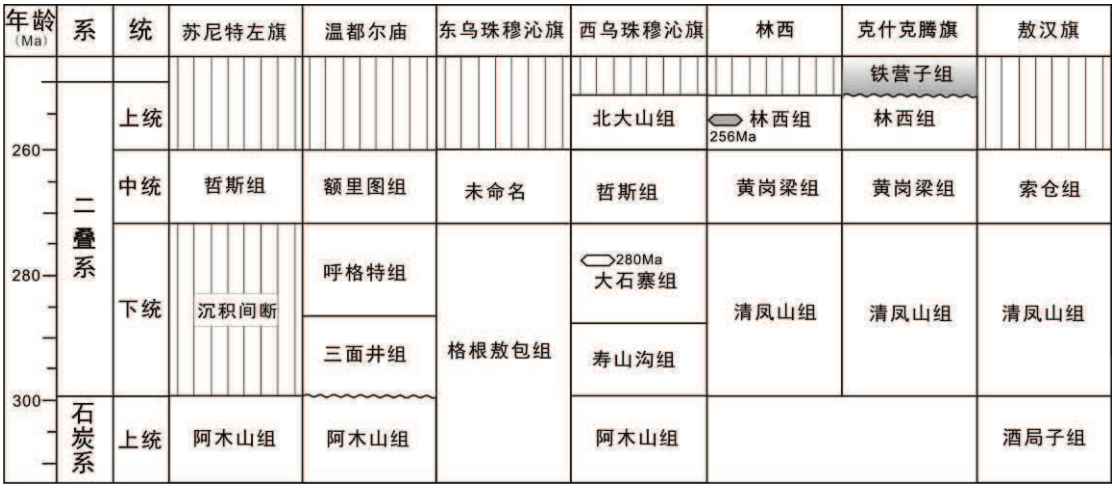

图 5-2 内蒙古中东部地区典型地区二叠纪地层对比图

Figure 5-2 Comparison of stratigraphic sequences of Permian strata in central-eastern Inner Mongolia

5.1 Sedimentological studies and facies analyses

选取内蒙古中东部六个地区进行野外剖面测量和沉积相分析，剖面位置及出露地层分别图示于图 5-1 和 5-2 中。根据地层出露情况和区域对比需要，在研究区西部选取苏尼特左旗和温都尔庙两个典型地区，研究区东部选取西乌珠穆沁旗、林西、克什克腾旗和敖汉旗四个地区（图 5-1）。

5.1.1 Sunidzuoqi area

该地区晚石炭世之后进入剥蚀阶段，缺失早二叠世沉积。仅出露中二叠统哲斯组，分布于苏尼特左旗东北部和南部（图 5-2），以陆相粗碎屑沉积为主。蒋干清等（1995a; b）对苏尼特左旗东北部哲斯组剖面进行了详细描述和沉积相分析，认为哲斯组下段主要为冲积扇－辫状河沉积以及泻湖－水下扇重力流沉积；上段主要为滨岸潮坪沉积、泻湖－水下重力流沉积及浅海沉积。哲斯组整体表现为陆

相粗碎屑岩向上转变为海陆交互相中细粒碎屑沉积向上变细的海侵序列(图 5-3；蒋干清等，1995a; b)。苏尼特左旗南部哲斯组底部为厚层底砾岩，并不整合覆盖在上石炭统阿木山组之上。随后红色薄层粉砂岩和页岩构成哲斯组下段主体，代表陆相细碎屑沉积阶段。哲斯组上段与苏尼特左旗东北部哲斯组类似，下部为巨厚层砾岩所代表的冲积扇－辫状河沉积，向上粒度逐渐变细，转变为滨岸潮坪沉积，并发现植物化石碎片。哲斯组沉积之后，该区再一次进入剥蚀阶段，缺失晚二叠世至晚三叠世沉积。

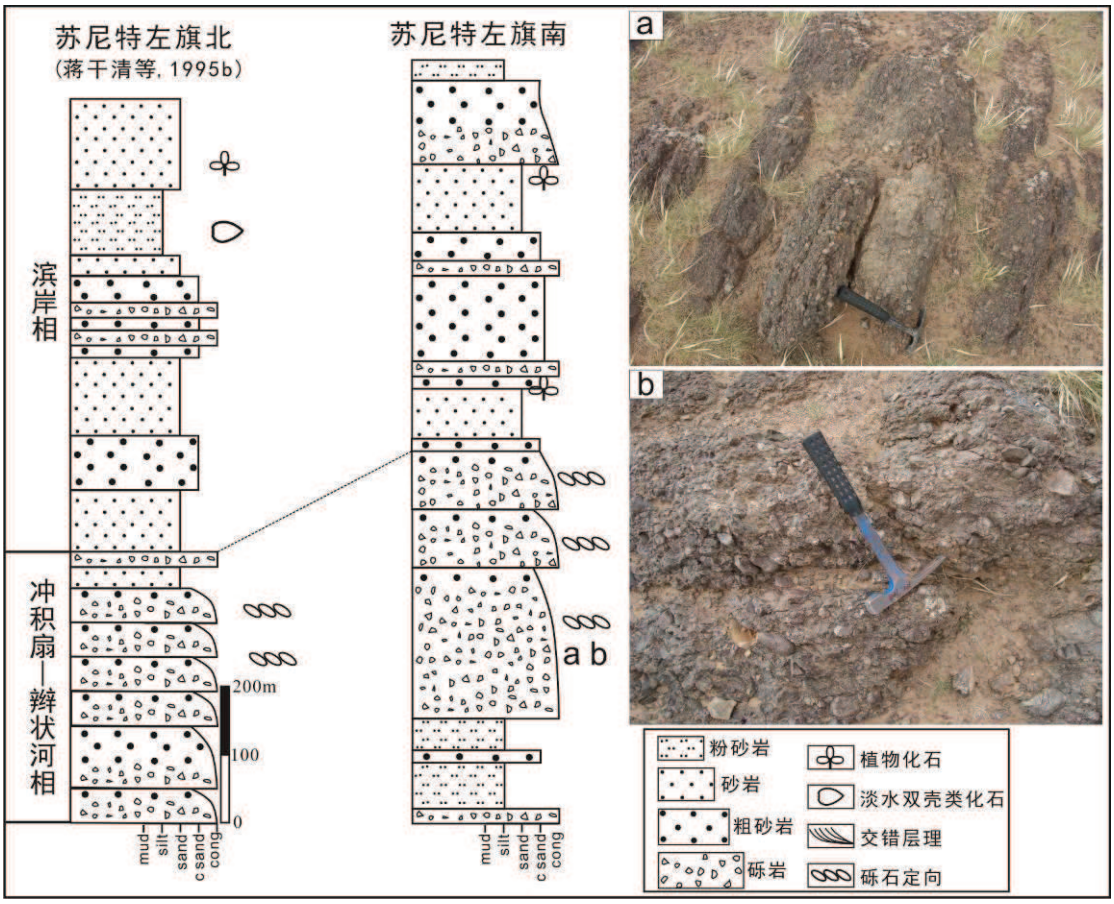

图 5-3 苏尼特左旗哲斯组地层柱状图：a 和 b，哲斯组底部砾岩

Figure 5-3 Stratigraphic sequence of the Zhesi Formation in Sunidzuoqi: a and b, the bottom conglomerate of Zhesi Formation

5.1.2 Ondor Sum area

该地区发育下二叠统三面井组和呼格特组，及中二叠统额里图组（图 5-2）。

5.1.2.1 下二叠统三面井组

本次研究对三面井组进行了详细的剖面测量（图 5-4A；剖面起点 GPS:

42°21′37″N，113°07′13″），具体剖面描述如下：

-----第四系覆盖-----

10. 灰黄色粉砂岩

9. 灰黄色中层状砂岩

8. 灰黄色粉砂岩

7. 灰黄色砂岩与粉砂岩互层

6. 黄绿色粉砂岩

5. 灰色厚层状灰岩，含大量蜓化石

4. 砾岩-粗砂岩-砂岩组成的向上变细的旋回

3. 巨厚层砂岩，砂岩中含大量灰岩团块，灰岩团块可达 10*50m 大小

2. 灰黄色中层状粗砂岩与中层状灰岩的互层

1. 砾岩，砾石棱角状，以灰岩砾石为主，粒径 1-20cm，分选较差

-----上石炭统海拉斯阿木组断层接触-----

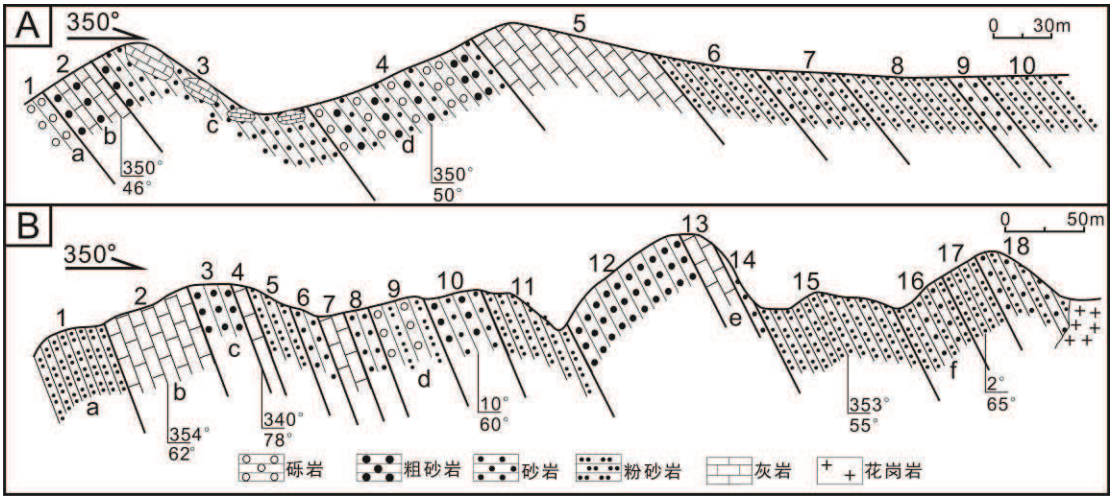

图 5-4　A，温都尔庙地区下二叠统三面井组实测地层剖面（a-d 为图 5-5 中照片位置）；B，温都尔庙地区下二叠统呼格特组实测地层剖面（a-f 为图 5-6 中照片位置）；剖面位置见图 3-15

Figure 5-4 A: Stratigraphic section of the Lower Permian Sanmianjing Formation in Ondor Sum (the position of each photo in figure 5-5 are marked by a-d);　B: Stratigraphic section of the Lower Permian Sanmianjing (A) Formation in Ondor Sum (the position of each photo in figure 5-6 are marked by a-f)

三面井组底部以底砾岩不整合覆盖在该区泥盆纪－石炭纪地层之上，底砾岩中含大量灰岩砾石（图 5-5a），并且在灰岩砾石中发现大量阿木山组典型蜓类化

石，因此砾石主要来自于下伏阿木山组灰岩。底砾岩之上为粗砂岩和灰岩互层（图5-5b），灰岩中见珊瑚和海百合茎等浅海相动物化石，代表浅海相与海陆交互相的交替。互层之上为厚层砂岩，砂岩中含大量灰岩团块，团块大小从几十米到几十厘米不等（图 5-5c）。砂岩之上发育多个砾岩－粗砂岩－砂岩旋回（图 5-5d），底部砾岩中砾石磨圆较好，分选较差；粗砂岩为块状，偶见斜层理发育。该段整体表现为滨岸相粗碎屑岩沉积，并出现由于海水进退导致的粒度旋回变化，整体表现为向上变细的海进序列。旋回之上为灰岩地层，灰岩中含大量蜓类化石，代表浅海相碳酸盐岩沉积。该组上部为厚层粉砂岩（图 5-4A），代表浅海相稳定细碎屑沉积。

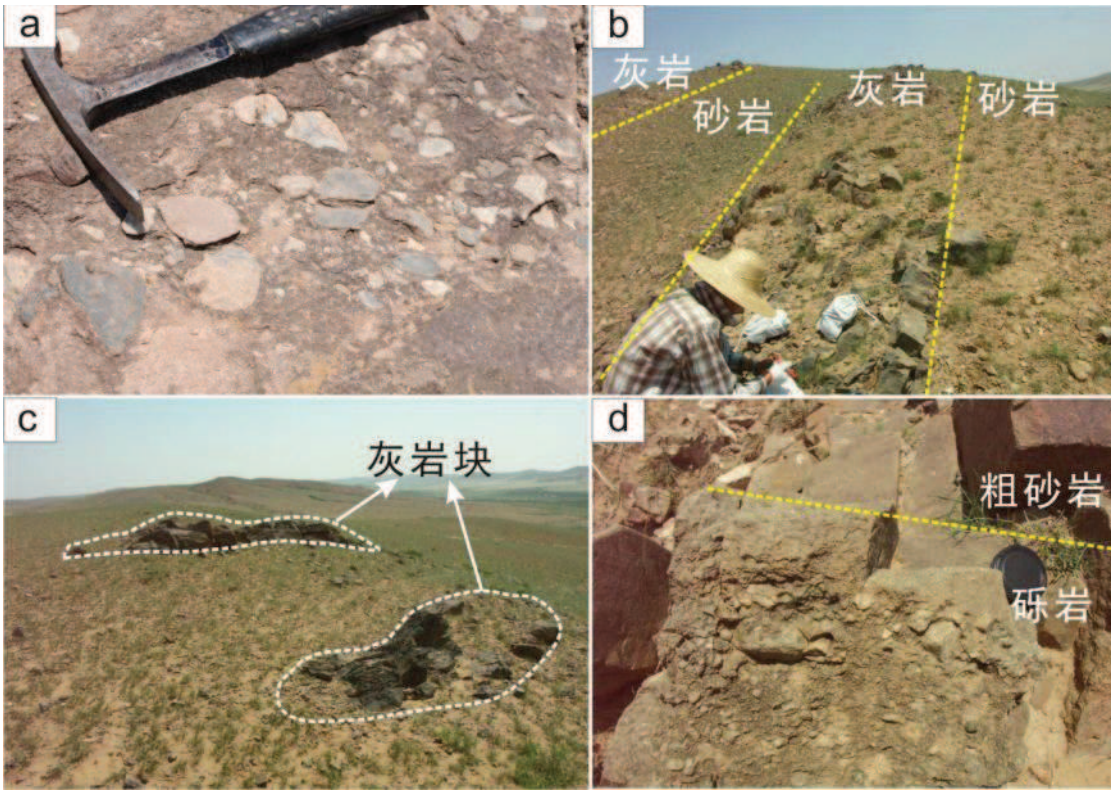

图5-5 温都尔庙地区下二叠统三面井组野外照片a，底砾岩中灰岩砾石; b，砂岩与灰岩互层; c，砂岩中灰岩团块; d，砾岩-粗砂岩旋回

Figure 5-5 Phtotgraphs of the Lower Permian Sanmianjing Formation in Ondor Sum area: a, the limestone pebbles within basal conglomerate; b, sandstone interbedded with limestone; c, limestone blocks within sandstone; d, conglomerate - coarse-grained sandstone sequence

5.1.2.2 下二叠统呼格特组

本次研究对三面井组进行了详细的剖面测量（图 5-4B；剖面起点 GPS:

42°18′43″N，112°59′47″），具体剖面描述如下：

-----花岗岩侵入-----

18. 灰白色砂岩与灰黑色粉砂岩互层

17. 灰黑色粉砂岩

16. 灰色砂岩与灰黑色粉砂岩互层

15. 灰黑色片理化粉砂岩

14. 粉砂岩、泥岩和砂岩的互层，泥岩片理化强烈，向上砂岩层逐渐增多并且层厚增厚，泥岩比例减少，反映海退序列。粉砂岩中发育水平层理

13. 灰黑色亮晶灰岩，局部含动物化石，以海百合茎为主

12. 灰黄色巨厚层粗砂岩/含砾粗砂岩，以石英颗粒为主

11. 灰黑色粉砂岩，含动物化石，弱变质，含绢云母，发育水平层理，夹层厚为 10cm 的灰岩

10. 浅紫红色厚层状粗砂岩与灰绿色砂岩互层

9. 浅紫红色厚层状砾岩与粉砂岩互层

8. 细粒岩，含大量生物化石及其碎片，砾石以石英为主，粒径 2-5mm，并含少量灰岩砾石

7. 生物碎屑灰岩，厚度约 3m

6. 厚度为 2m 的石英粗砂岩

5. 灰黑色薄层状粉砂岩

4. 生物碎屑灰岩

3. 黄色含砾粗砂岩，发育斜层理。向上逐渐变为细粒岩，砾石主要为石英，砾石磨圆较好，粒径 2-6mm

2. 灰黑色薄层状生物碎屑灰岩

1. 灰色粉砂岩和泥岩，夹少量砂岩层，发育水平层理。类似鲍马序列，为稳定环境下得沉积

-----花岗岩侵入-----

呼格特组剖面未见与下伏地层的接触关系，其岩性纵向变化较大，代表多变的沉积环境。剖面底部为发育水平层理的灰黑色粉砂岩（图 5-6a），显示稳定的沉积环境。之上为薄层状砂质灰岩（图 5-6b），代表碎屑物质供应充足的碳酸盐岩沉积。灰岩之上该剖面中部发育多个碎屑岩夹灰岩地层，代表海平面升降带来

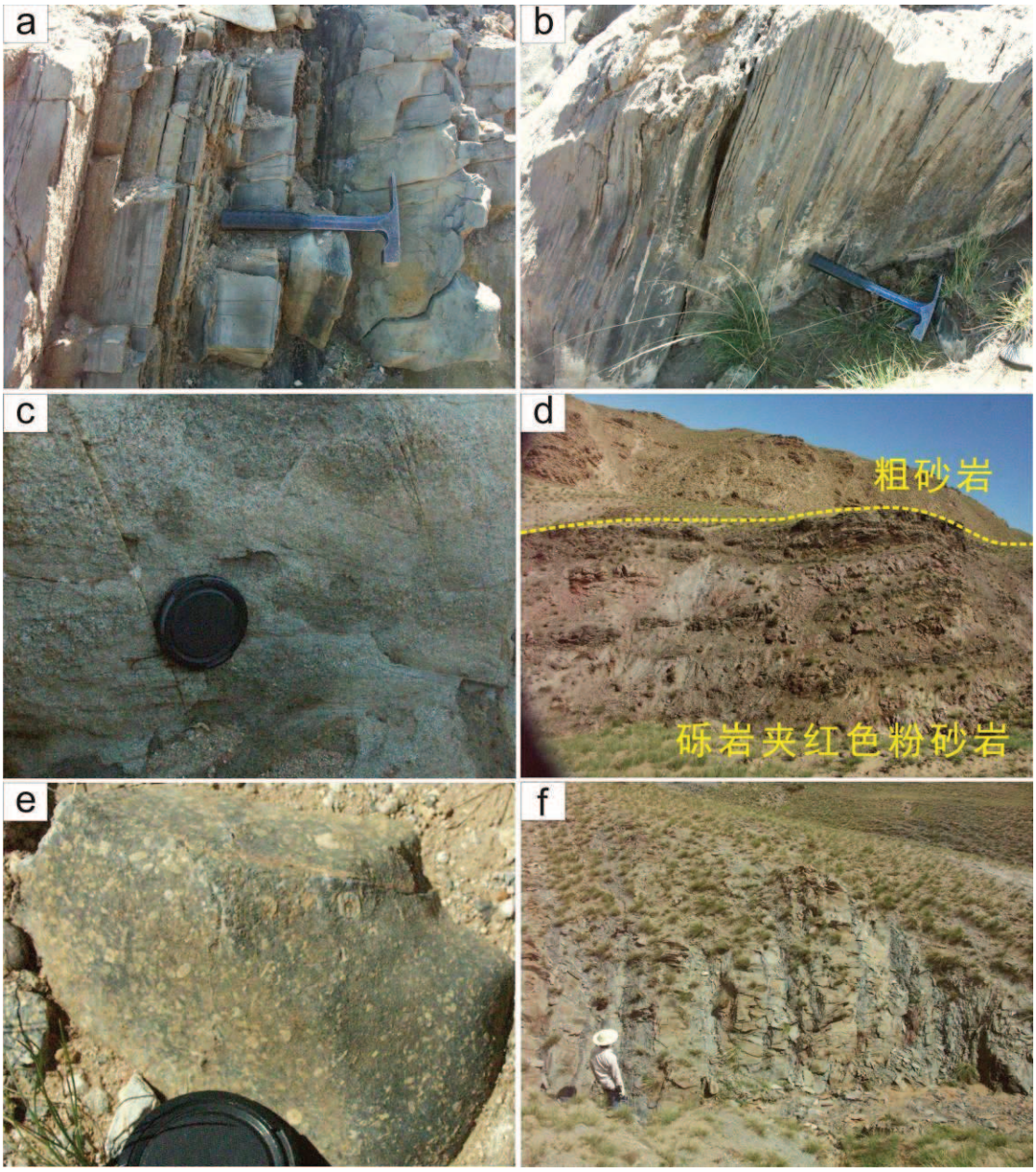

图 5-6 温都尔庙地区下二叠统呼格特组野外照片 a，下部发育水平层理薄层粉砂岩; b，薄层砂质灰岩; c，含砾粗砂岩中的斜层理; d，砾岩夹红色粉砂岩与上部粗砂岩接触; e，灰岩中的蜓类化石; f，剖面上部砂岩与黑色粉砂岩互层

Figure 5-6Phtotgraphs of the Lower Permian Hugete Formation in Ondor Sum area: a, the horizontal beddings bearing siltstone; b, thin-bedded sandy limestone; c,coarse-grained sandstone with cross beddings; d, conglomerate interbedded with red siltstone; e, fusulinids within limestone; f, sandstone interbedded with black siltstone on the upper part

的快速沉积相变化。发育斜层理的含砾粗砂岩（图 5-6c），砾石以石英为主，代

表海退之后的滨岸相沉积。砾岩与红色粉砂岩的互层则显示陆上滨岸环境（图5-6d）。灰岩夹层中富含蝬类和海百合茎化石（图 5-6e），代表海平面上升阶段的碳酸盐岩沉积。剖面上部为厚达 400 米的细碎屑沉积，主要为薄－中层状砂岩夹灰黑色薄层粉砂岩（图 5-6f），代表稳定的浅海相碎屑沉积。呼格特组整体表现为滨岸－滨海沉积环境向浅海相沉积转变的过程，中部由于海平面升降产生了沉积相快速转变，上部转变为稳定浅海相沉积，并沉积巨厚细碎屑沉积。

5.1.3 West-Ujimqin area

本区发育完整的二叠系沉积，下二叠统为寿山沟组碎屑岩和大石寨组火山岩，中二叠统发育哲斯组碎屑－碳酸盐岩沉积，上二叠统以北大山组黑色泥页岩为主（图 5-2；内蒙古地质矿产局，1991）。

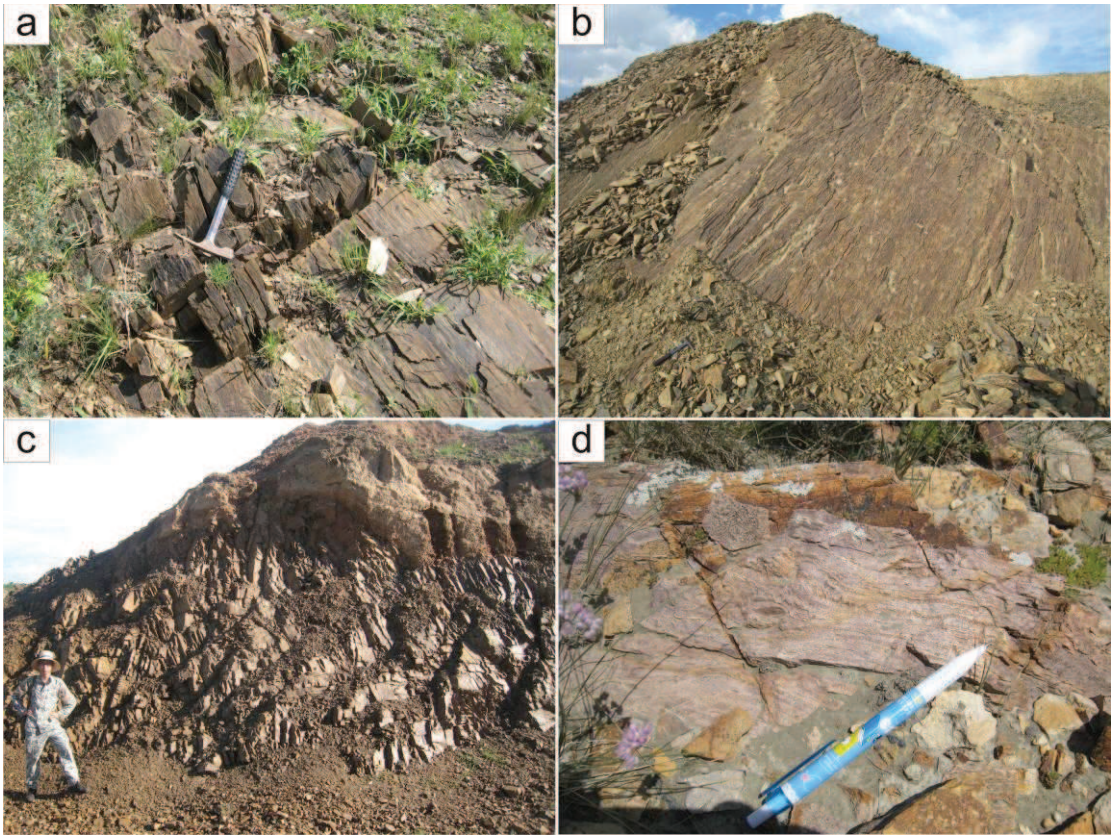

图 5-7 a,b 西乌珠穆沁旗下二叠统寿山沟组黄色粉砂岩; c，西乌珠穆沁旗下二叠统大石寨区块状玄武岩; d，西乌珠穆沁旗下二叠统大石寨组粉红色流纹岩

Figure 5-7 a and b Lower Permian Shoushangou Formation yellow siltstone in West-Ujimqin area; c and d Lower Permian Dashizhai Formation massive basalt and pink rhyolite

5.1.3.1 下二叠统寿山沟组

寿山沟组分布于西乌珠穆沁旗东北部，以灰黄色劈理化粉砂岩为主（图5-7a,b），夹少量灰岩夹层和砾岩，超覆不整合于下伏地层之上（鲍庆中等，2005）。最新的1:25万地质图西乌珠穆沁旗幅（鲍庆中等，2005; 2006）将其分为两段，下段粗碎屑沉积为灰黄色砾岩、含砾砂岩、粉砂岩夹薄层灰岩，灰岩中产腕足类和苔藓虫化石；上段细碎屑沉积为灰黑色泥质粉砂岩、粉砂质板岩、变质泥岩夹薄层砂岩和灰岩，产腕足类和卢木类化石。寿山沟组下部粗碎屑岩为海陆交互相沉积，向上转变为正常浅海细碎屑沉积，表现为海进序列。其碎屑锆石研究显示，除 8 颗锆石（9%）具有元古宙和早古生代的年龄信息（2490~502Ma）外，其余样品年龄大致可分成3 组：第1 组3 颗（3%），年龄为383±3Ma；第2 组6颗（7%），年龄为365±4Ma；第3组73 颗(81%)，年龄介于280～337 Ma之间，并出现289 Ma、300 Ma、309 Ma和325 Ma 四个年龄峰值，说明砂岩具有多时代物源混合的特征（郑月娟等，2013）。其主要年龄组锆石可能来源于西乌珠穆沁旗地区大量的晚石炭世－早二叠世侵入岩（鲍庆中等，2007a, b; 刘建峰等，2009; 薛怀民等，2010）。

5.1.3.2 下二叠统大石寨组

大石寨组为由绿色细碧岩、辉绿岩、玄武岩和粉红色流纹岩组成的双峰式火山岩组合。玄武岩呈块状，未见枕状构造等水下喷发特征（图5-7c）。粉红色流纹岩为块状，流纹构造发育（图5-7d）。整体表现为陆上喷发的特征。年代学研究得到其U-Pb锆石年龄为281-279 Ma，地球化学显示双峰式火山岩的特征，其中流纹岩具有A型花岗岩的地球化学特征（Zhang et al., 2008）。根据地球化学结果，大石寨组双峰式火山岩形成于碰撞后伸展环境（Zhang et al., 2008）。

5.1.3.3 中二叠统哲斯组

本次研究对哲斯组进行了详细的剖面测量（图4-3），具体剖面描述如下：

-----侏罗纪不整合覆盖-----

10. 灰黄色砾岩与粗砂岩组成的沉积旋回，单个旋回以砾岩为主，层厚 0.5-5m，旋回顶部发育 3-20cm 厚粗砂岩。未见顶，可见厚度 342m。

9. 灰黄色厚层细砂岩，含生物礁灰岩透镜体。细砂岩层厚 0.3-1m，含大量腕足类生物化石。生物礁灰岩透镜体直径 20-70cm，化石以腕足类和双壳类为主。厚 154m。

8. 灰白色中－薄层细砂岩与黑色薄层泥岩互层，发育软沉积变形。细砂岩层厚 10-20cm，

底部具有平行排列的泥岩砾石。厚 105m。

7. 灰色中一厚层细砂岩。与层 7 岩性相同，但不具有黑色泥岩互层。含大量腕足类生物化石。厚 101m。

6. 灰白色薄层生物碎屑灰岩，含大量海百合茎化石。厚 20m。

5. 灰白一浅红色中一厚层泥灰质粉砂岩。以大量苔藓虫化石为特征，并含少量双壳类化石。厚 155m。

4. 灰黄色薄层粉砂岩,单层厚度 2-10cm,发育水平层理。含大量腕足类和珊瑚化石。厚 137m。

3. 蓝灰色厚层状亮晶灰岩，单层厚 2-6m，基本不含化石。厚 210m。

2. 灰黄色薄层粉砂岩与粉砂质泥岩互层。厚 72m

1. 灰黄色薄层粉砂岩。未见底，可见厚度 54m。

-----大石寨组流纹岩断层接触-----

哲斯组主要分布于西乌珠穆沁旗南部约 10km，地层近直立，走向近东西，整体呈 NEE 向展布，横向延伸较远。岩性为一套以灰黄色粉砂岩、砂岩、蓝灰色灰岩和砾岩为主，夹黑色泥岩和生物碎屑灰岩，含大量腕足、珊瑚、双壳和苔藓虫等浅海相化石。哲斯组底部和中部发育浅海相碎屑沉积 (图 3)，整体表现为稳定的细碎屑沉积，以发育薄层水平层理的粉砂岩为主，显示稳定且充足的碎屑物质供给。底部 (第 1 层至第 2 层，总厚度 126 m) 以薄层状粉砂岩与泥岩互层为主，含大量海百合茎和腕足类化石。中部 (第 4 层至第 9 层，总厚度 672 m) 发育薄层状粉砂岩、泥灰质粉砂岩和厚层状细砂岩，部分层位夹有黑色泥岩。根据岩性特征和化石可将其划分为四段。一段为黄色薄层状粉砂岩，单层厚度在 1-5 cm。碎屑颗粒以石英为主，磨圆中等，多呈次圆－次棱角状。整体成分成熟度和结构成熟度均较高。粉砂岩层中含有大量保存完好的腕足类和珊瑚化石(图 5-9C)；二段为灰白－灰红色中－薄层状泥灰质粉砂岩，单层厚度在 5-15 cm。泥灰质粉砂岩以含大量苔藓虫化石区别于其他三段，并含少量双壳类化石(图 5-9D)。三段以灰白色粉砂岩与黑色泥岩互层为特征，粉砂岩层厚 10-30 cm，泥岩层厚 2-5 cm。单层粉砂岩底部可见大量黑色泥岩砾，泥岩砾呈扁平透镜状，扁平面平行层面排列(图 5-9F)，局部可见砂岩同沉积变形(图 5-9E)，表明较快的沉积物供给。四段以黄色厚层细砂岩为主，局部层位含有生物礁灰岩透镜体(图 5-9G)，均含大量腕足类生物化石。上述地层组合、沉积构造和古生物特征反映

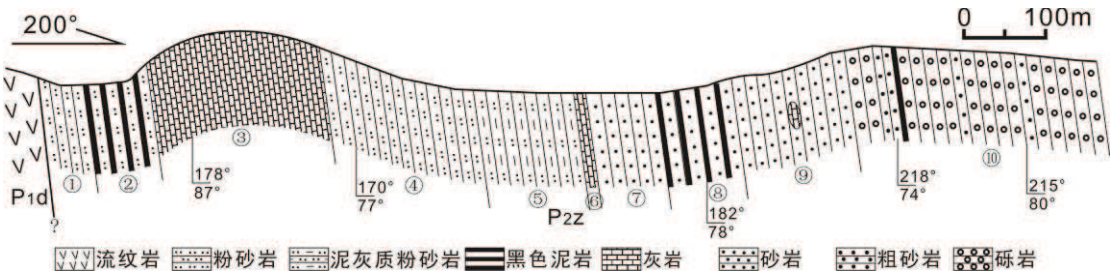

图 5-8 西乌珠穆沁旗南部中二叠统哲斯组实测地层剖面

Figure 5-8 Cross section of middle Permian Zhesi Formation in the south of West Ujimqin

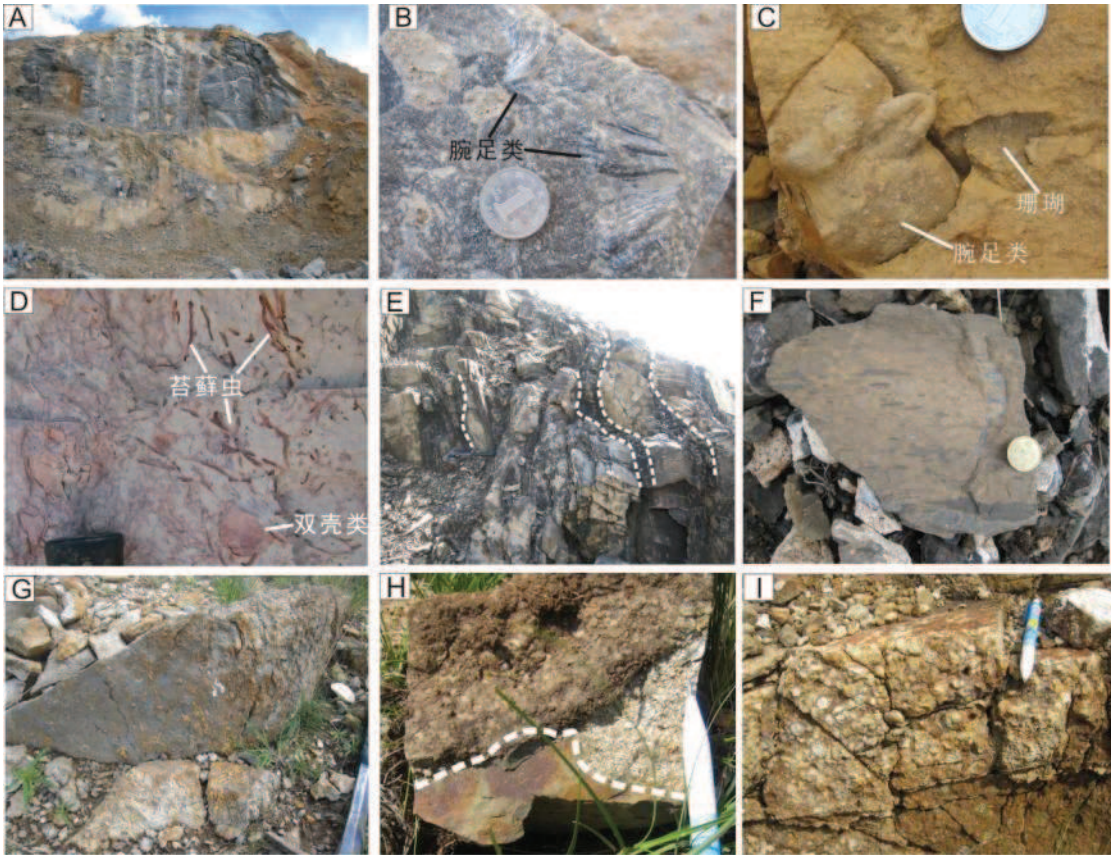

图 5-9 哲斯组野外沉积特征照片：A-厚层状亮晶灰岩; B-亮晶灰岩中腕足类化石; C-薄层粉砂岩中的腕足类和珊瑚化石; D-灰红色泥灰质粉砂岩中的苔藓虫和双壳类化石; E-细砂岩与黑色泥岩互层，细砂岩层发育软沉积变形; F-细砂岩层中水平排列的黑色泥岩砾石; G-细砂岩中的生物礁灰岩团块; H-砾岩与下部泥岩之间的冲刷构造; I-砾岩

Figure 5-9 Photographs of sedimentary characteristics in Zhesi Formation. A-thick bedded sparite; B-grey bioclastic limestone; C-Brachiopoda and coral in thin bedded siltstone; D-bryozoon and bivalve in argillo-calcareous siltstone; E-siltstone interbedded with black mudstone, with soft deformation; F-the parallel black mudstone lens in the fine-grained sandstone; G- biohermal limestone lens in the fine-grained sandstone; H-basal erosion scouring structure; I-conglomerate

沉积环境应是具有良好的透光性、生物活动密集和物源丰富的滨浅海区。

哲斯组地层中下部 (第 3 层，厚度 201 m)发育巨厚层台地相碳酸盐岩沉积，以亮晶灰岩为主，夹少量生物碎屑灰岩和砂质碎屑灰岩。亮晶灰岩呈深灰蓝色，单层厚度 2-6 m (图 5-9A)，含大量腕足类化石 (图 5-9B)。

剖面顶部第 10 层砾岩为冲积扇相沉积，可见厚度 342 m，由下部滨浅海相细砂岩直接突变为冲积扇相砾岩。发育多个砾岩－粗砂岩互层，单个互层厚度 5-30 m，以砾岩为主，仅在砾岩顶部发育 3-20 cm 厚的粗砂岩，砾岩层具有向上逐渐增厚的特征。最底部为砾岩－粗砂岩－砂岩－灰黑色泥岩旋回，泥岩层厚 2 m，与上层砾岩突变接触，界面发育明显冲刷构造(图 5-9H)。砾石大小均匀，粒径 2-5 cm，分选中等，磨圆较差，多呈棱角－次棱角状(图 5-9I)；砾石成分几乎全部为酸性火山岩，其物源可能来自于哲斯组底部下二叠统大石寨组火山岩，显示极低的结构成熟度和成分成熟度。粗砂岩以石英为主要碎屑物质，颗粒支撑，松散胶结。砾岩为主体的沉积特征，结合极低的结构和成分成熟度，表明砾岩层由原地火山岩遭受剥蚀并快速堆积形成。整体表现出向上砾岩层逐渐变厚，砂岩层变薄粒度变粗，泥岩层消失的特征，说明整体环境朝陆地演变。

综上所述，哲斯组下部和中部的沉积环境为浅海陆架或台地，缺乏代表大陆斜坡和深水盆地环境的沉积岩相特征；而上部为近岸环境，以快速堆积砾岩为特征，代表中二叠统海退过程。

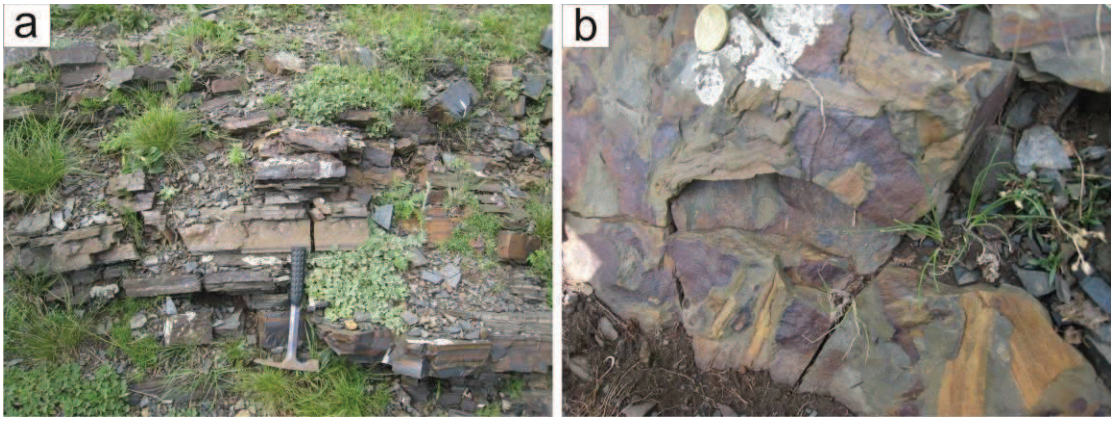

图 5-10 a，北大山组薄层黑色粉砂岩; b，黑色粉砂岩中的植物化石

Figure 5-10 the Upper Permian Beidashan Formation black siltstone (a) and the plant fossils (b)

5.1.3.4 上二叠统北大山组

北大山组分布于西乌珠穆沁旗南部，以黑色薄层粉砂岩和板岩为主（图 5-10a），夹少量砂岩和砾岩，厚度达 3700 米，含丰富植物化石（图 5-10b），为

一套稳定湖相细碎屑沉积。

5.1.4 Linxi area

图 5-11 林西地区林西组柱状图：a，粉砂岩中斜层理; b，黑色薄层泥岩; c，粉砂岩中波状层理; d，粉砂岩中波痕; e，黑色泥岩中双壳类化石; f，黑色泥岩中植物化石

Figure 5-11 Stratigraphic sequence and photographs of the Linxi Formation in Linxi area: a, inclined beddings within siltstone; b, black mudstone; c, wavy beddings within siltstone; d, wave ripple within siltstone; e, bivalve within black mudstone; f, plant fossils with black mudstone

林西地区发育下二叠统清凤山组，中二叠统黄岗梁组和上二叠统林西组（图5-2）。下二叠统清凤山组在该区仅发育火山岩段，主要为一套蚀变中基性熔岩、熔结角砾岩和凝灰岩，夹少量凝灰质粉砂岩、凝灰质砂岩。中二叠统黄岗梁组下

部为一层紫色砾岩，上部为灰紫色凝灰质砂岩夹少量含砾粗砂岩，顶部为黄绿色粉砂质板岩。

作为林西地区最具代表性地层，上二叠统林西组广泛分布，以林西北部关地剖面最为典型。为一套厚达 4000 m 的砂泥质沉积，含丰富植物化石和淡水双壳类化石，代表稳定湖相沉积。底部可见一层砾岩，为河流相砾岩沉积（图 5-11; Mueller et al., 1991）。砾岩之上为厚度巨大的黑色泥质岩夹粉砂岩。黑色泥岩呈块状或薄层状（图 5-11a），部分风化为薄片状。块状泥岩中发育小型斜层理和水平层理组合（图 5-11b），类似鲍马序列，可能代表深湖相沉积。粉砂岩层中可见波状层理和波痕（图 5-11c，d），代表水动力较强的浅湖沉积。 黑色泥岩中可见淡水双壳类化石和植物化石（图 5-11e，f），显示陆相淡水湖沉积的生物特征。林西组下部河流相砾岩和上部湖相沉积说明晚二叠世该区进入稳定陆内沉积环境，随着湖盆不断扩大沉积了巨厚泥砂质沉积。

5.1.5 Keshiketengqi area

克什克腾旗地区发育完整的二叠系沉积，包含下二叠统清凤山组，中二叠统黄岗梁组、上二叠统林西组以及上二叠统铁营子组（图 5-2）。

5.1.5.1 下二叠统清凤山组

下二叠统清凤山组分下碎屑岩段和上火山岩段（图 5-12）。下碎屑岩段由砾岩、砂岩和粉砂岩组成。碎屑岩段下部以砾岩为主，1:20 万地质图克什克腾旗幅将其作为滨海相磨拉斯建造，代表与下伏地层可能存在不整合接触关系。在柯单山附近下碎屑岩剖面中见砂岩中存在大量灰岩块，灰岩块大小不等，从几十厘米到十几米（图 5-12a,b），可能来自于下伏晚石炭世灰岩地层。这种沉积特征类似滑塌堆积（Festa et al., 2010; 2012）的以下典型特征：1. 滑塌岩块为次圆－次棱角状，直径从十厘米到几十米，并随机堆积于细粒碎屑岩基质中；2. 滑塌岩块岩性主要为灰岩，可能来自于下伏晚石炭世地层；3. 滑塌岩块与基质的接触关系表现出重力滑动的特征，如岩块滑动和碎屑崩落（Festa et al., 2010; 2012）。碎屑岩段中部为砾岩和粉砂岩互层，上部为砾岩和砂岩。清凤山组碎屑岩段反映海退－海进两个沉积旋回。

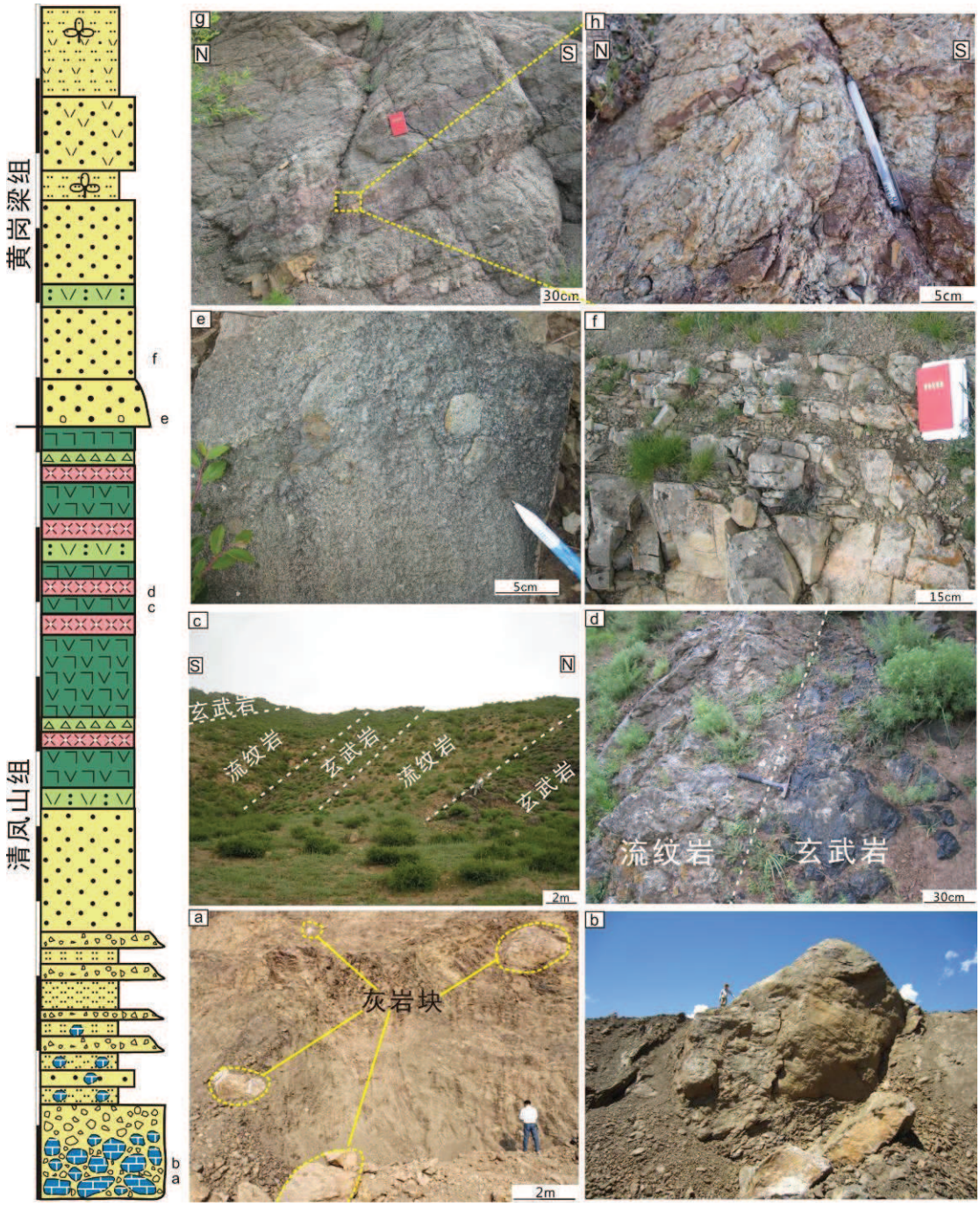

图 5-12 克什克腾旗地区清凤山组和黄岗梁组柱状图：a,b 清凤山组砂岩中灰岩块; c,d 清凤山组流纹岩和玄武岩互层; e, 黄岗梁组下部含砾凝灰质粗砂岩; f, 黄岗梁组薄－中层凝灰质砂岩; g,h 黄岗梁组河流相砾岩

Figure 5-12 Stratigraphic sequence and photographs of the Qingfengshan and Huanggangliang formations in Keshiketengqi area: a and b, limestone blocks within sandstone; c and d, basalt interbedded with rhyolite; e, tuffceous coarse-grained sandstone at the lower part of Huanggangliang Formation; f, tuffceous sandstone; g and h, alluvial conglomerate of Huanggangliang Formation

火山岩段以克什克腾旗南部广兴源剖面为代表，主要由玄武安山岩、流纹岩和凝灰岩组成，剖面可见流纹岩与玄武岩的互层产出（图 5-12c,d）。玄武安山岩呈巨厚层块状，未见枕状构造。流纹岩为灰白色，流纹构造不发育。对其年代学和地球化学研究将于本章第三节详细叙述。

5.1.5.2 中二叠统黄岗梁组

黄岗梁组代表剖面位于克什克腾旗南部广兴源，并整合覆盖于下二叠统清凤山组之上。下部为含砾凝灰质粗砂岩，含大量火山岩砾石（图 5-12e），说明沉积物源来源于下伏清凤山组。向上粒度变细，转变为薄－中层状凝灰质砂岩（图 5-12f）。上部为灰黄色砂岩和粉砂岩，并含大量华夏植物群化石，如于家楔叶（*Sphenophyllum yujiaense* Dong）、栉羊齿（*Pecopteris orientalis*）、卢木（*Calamites* sp.）等（1:20 万地质图克什克腾旗幅）。另外，在未含植物化石砂岩中发育腕足类和瓣鳃类动物化石，代表陆相和浅海相交互沉积。在克什克腾西山剖面发育河流相砾岩沉积，砾石呈扁平状，扁平面指向 NW300°-NW340°（图 5-12g,h），说明物源（水流）来自西北方向。

黄岗梁组整体表现为海陆交互相和陆相沉积，由下至上反映海退式沉积，发育大量华夏植物群化石。

5.1.5.3 上二叠统林西组

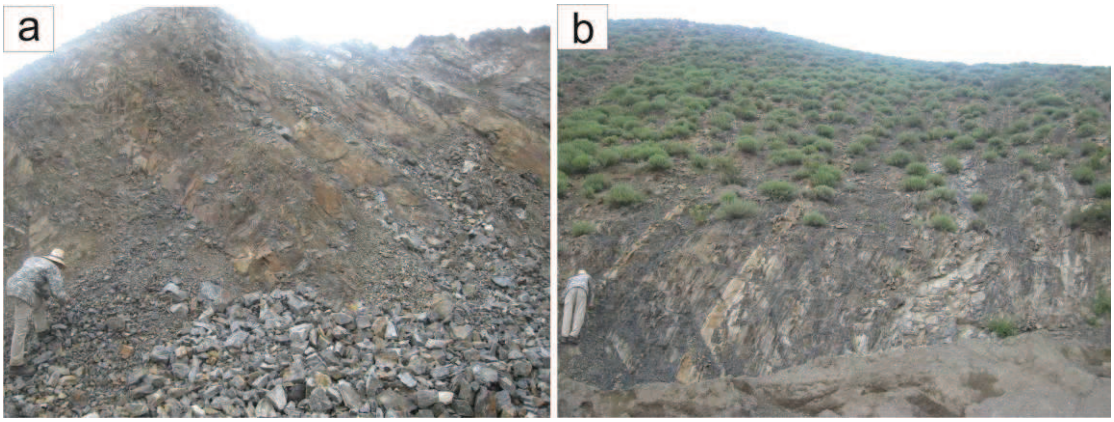

图 5-13 克什克腾旗地区林西组野外照片：a, 中层状砂岩与薄层黑色泥岩互层; b 薄层黑色泥岩

Figure 5-13 Photographs of Upper Permian Linxi Formation in Keshiketengqi: a, Sandstone interbedded with black mudstone; b, thin-bedded black mudstone

上二叠统林西组在该区分布较少，但与林西地区林西组一致，岩性由黑色泥岩和砂岩为主（图 5-13）。克什克腾旗地区林西组分布局限且厚度较小，说明代

表晚二叠世陆相湖盆的南部边缘沉积。

5.1.5.4 上二叠统铁营子组

铁营子组仅出现于克什克腾旗地区，厚 1700 m，主要由砾岩、粗砂岩和粉砂岩组成。底部砾岩厚达 300 m，不整合覆盖于下二叠统清凤山组和中二叠世碱性花岗岩之上，代表一次区域不整合事件。底砾岩中砾石磨圆和分选均较差，粒径 2-40 cm，杂乱堆积，成分以碱性花岗岩为主（图 5-14a），并含少量玄武岩和砂岩砾石，代表冲积扇相沉积（Chamyal et al., 1997; Kuhlemann and Kempf, 2002）。砾岩中夹含砾粗砂岩，砾石磨圆较好，分选较差，砾石大多呈扁平状，并指向同一方向（图 5-14b），为河流相沉积的典型特征。中部为砾岩与粗砂岩的互层，反映多次冲积扇沉积组合（图 5-14c）。上部变为中层状砂岩和薄层状红色粉砂岩（图 5-14d），红色粉砂岩中发现植物化石，如卢木（*Calamites* sp.）、栉羊齿（Pecopteris sp.）、带羊齿（*Taeniopteris* sp.）和楔叶（*Sphenophyllum* sp.）等（1:20 万地质图克什克腾旗幅），代表陆相盆地稳定细碎屑沉积。

铁营子组整体表现为由粗变细的沉积序列，反映由冲积扇相向陆相湖盆沉积

图 5-14 克什克腾旗地区铁营子组柱状图：a，底部灰紫色砾岩; b 含砾粗砂岩; c，砾岩与粗砂岩互层; d，上部中层状砂岩

Figure 5-14 Stratigraphic sequence and photographs of the Tieyingzi Formation in Keshiketengqi area: a, the basal conglomerate; b, pebbly coarse-grained sandstone; c, conglomerate interbedded with coarse-grained sandstone; d, sandstone at the upper part

转变的过程。铁营子组仅在克什克腾旗南部发现，底部不整合覆盖在下伏地层和侵入岩之上，可能代表局部山间盆地剥蚀沉积事件。

5.1.6 Aohanqi area

敖汉旗地区发育下二叠统清凤山组和中二叠统索仓组（图 5-2）。

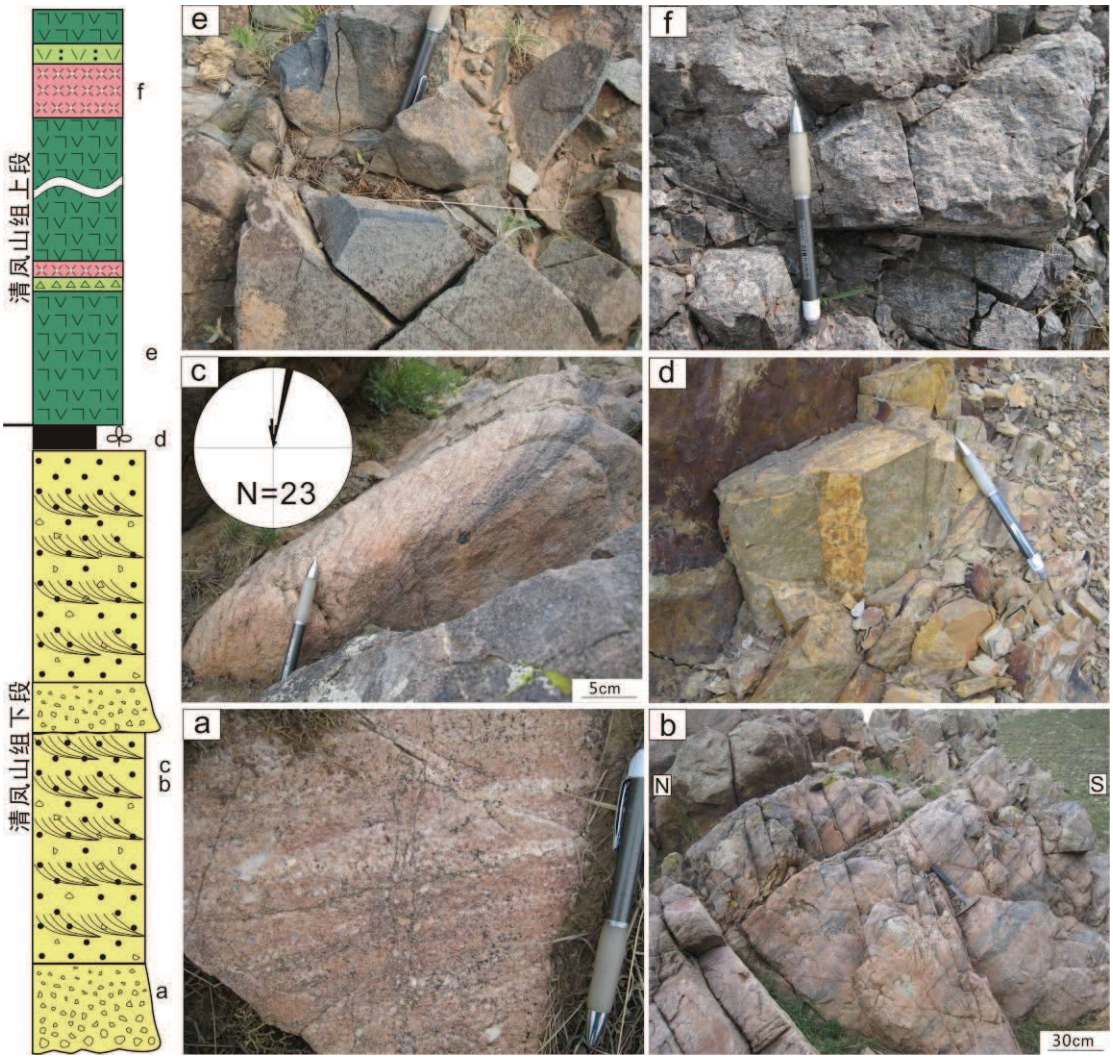

图 5-15 敖汉旗地区下二叠统清凤山组柱状图：a，碎屑岩段下部细砾岩; b 和 c，石英粗砂岩中大型槽状斜层理，插图为由斜层理计算的古流向; d，碎屑岩段顶部黄色泥岩; e，火山岩段下部块状玄武岩; f，火山岩段灰白色流纹岩，流纹构造发育

Figure 5-15 Stratigraphic sequence and photographs of the Qingfengshan Formation in Aohanqi area: a, fine-grained conglomerate; b and c, large cross beddings; d, yellow mudstone on th top of clastic sequence; e,basalt at the lower part of the volcanic sequence; f, grey rhyolite of the volcanic sequence, with rhyotaxitic structure

5.1.6.1 下二叠统清凤山组

清凤山组可分为下碎屑岩段和上火山岩段。下碎屑岩段厚 680m，主要由厚层石英粗砂岩和砾岩组成，顶部为厚 20 m 的黄色泥岩（图 5-15）。下部为石英细砾岩和含砾石英粗砂岩，碎屑颗粒中石英占 95%，石英砾石次圆－次棱角状（图 5-15a）。中部厚层状石英粗砂岩发育大量大型槽状斜层理，斜层理大小在 0.3-1 m（图 5-15b,c）。通过对斜层理进行测量和计算，得到水流方向为从南向北（图 5-15c），代表其物源来自该区南部。顶部石英粗砂岩突变为黄色泥岩（图 5-15d），含华夏植物群化石，如 *Calamites* sp.（内蒙古地质矿产局，1991）。清凤山组下碎屑岩段主体为发育大型斜层理石英粗砂岩，向上相变为泥岩，显示辫状河相沉积的特征（Ramos et al., 1986; Prothero and Schwab, 2003）。中火山岩段为玄武岩夹流纹岩和火山碎屑岩。玄武岩呈块状，厚度巨大，未见枕状构造（图 5-15e）。火山碎屑岩为显示中酸性的特征，含少量爆发角砾岩。流纹岩为灰白色，流纹构造明显，为厚层块状（图 5-15f）。与克什克腾旗清凤山组火山岩段类似，该剖面火山岩同样表现出双峰式火山岩的特征。

5.1.6.2 中二叠统索仓组

索仓组整合于下伏清凤山组之上，根据岩性不同可分为上下两段。下段为碳酸盐岩－碎屑岩段，上段为碎屑岩段。

下段厚 1000 m，下部为灰绿色粗砂岩和砂岩，发育平行层理（图 5-16a）。中部为厚层状泥质灰岩，含大量平行层理分布的泥质碎屑（图 5-16b），代表灰岩沉积时大量碎屑物质供给。同时泥质灰岩中可见砂岩团块，并显示重力滑动的特征（图 5-16c）。泥质灰岩这些特征反映其沉积于受波浪作用影响的内缓坡带。上部逐渐转变为砂岩和砾岩，代表一个向上变粗的海退序列。下碎屑岩段整体表现为滨海相沉积向滨岸沉积转变的过程。

上碎屑岩段厚 900 m，底部为砾岩，砾石次棱角状，分选较差。向上粒度逐渐变细，构成多个由粗到细的沉积旋回。下部旋回由砾岩－粗砂岩－砂岩－泥岩构成，厚达几十米；上部旋回由砂岩－粉砂岩－泥岩组成，厚度不足十米；各个旋回整体构成一个向上变细的沉积序列，粗碎屑岩减少，细碎屑岩厚度增加（图 5-16e）。旋回底部砾岩/粗砂岩直接覆盖于下伏泥岩之上，并表现出底蚀接触关系，代表粗碎屑岩沉积时较强的水动力条件。泥岩和粉砂岩为纹层状，并发育大量华

夏植物群化石（图 5-16f）。索仓组上段由多个由粗到细的沉积旋回构成，植物化石发育，代表曲流河相沉积（Prothero and Schwab, 2003）。

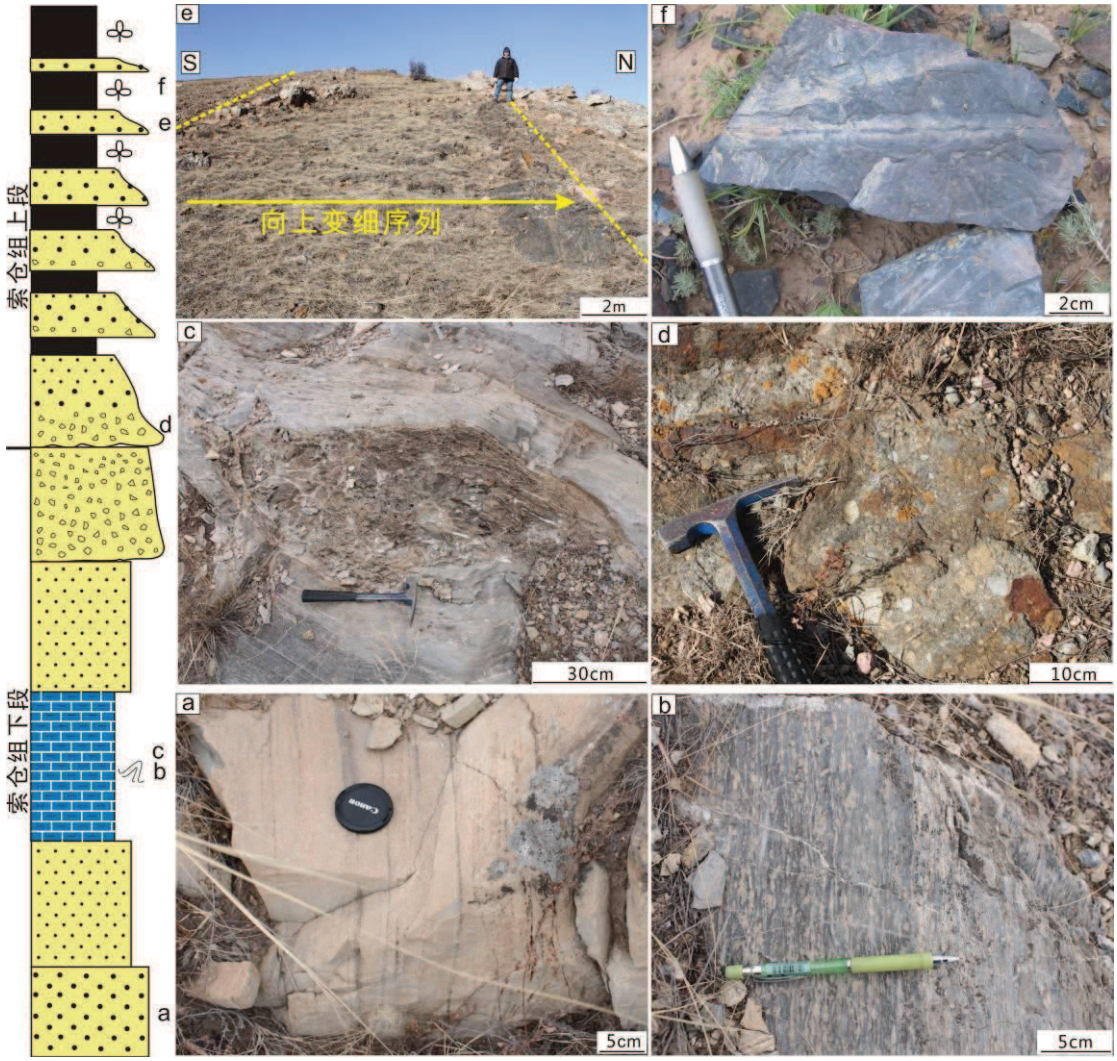

图 5-16 敖汉旗地区中二叠统索仓组柱状图：a，下部发育平行层理粗砂岩; b，泥质灰岩; c，泥质灰岩中砂岩透镜体; d，砾岩; e，索仓组上段由粗变细的沉积序列; f，泥岩中的植物化石

Figure 5-16 Stratigraphic sequence and photographs of the Middle Permian Suocang Formation in Aohanqi area: a, coarse-grained sandstone with parallel beddings; b, mudy limestone; c, sandstone lens within mudy limestone; d,conglomerate; e,fining upward sequence at the upper part of Suocang Formation; f, plant fossils within black mudstone

5.2 Geochemistry and geochronology studies of magmatic rocks

5.2.1 Early Permian volcanic rocks

前已述及，内蒙古中东部早二叠世发育大量火山岩，以北部宝力高庙组、中

部大石寨组和南部清凤山组火山岩为代表。Zhang et al. (2008)曾对中部大石寨组双峰式火山岩进行年代学和地球化学研究，得到其喷发年龄为 280 Ma，地球化学特征表明其喷发于伸展环境。本次研究对北部宝力高庙组流纹斑岩和南部清凤山组双峰式火山岩进行年代学和地球化学研究，并探讨其喷发环境。

5.2.1.1 北部宝力高庙组流纹斑岩

宝力高庙组火山岩采自白音乌拉北部（图 5-17），岩性以粉红色流纹斑岩（图 5-18a）为主，发育典型流纹构造（图 5-18b）。为准确限定火山岩喷发时代，对流纹斑岩(样品号 100718-55)进行 LA-ICP-MS U-Pb 定年。锆石颗粒自形，Th/U 为 0.57-2.04，发育宽缓岩浆环带，表现出岩浆成因锆石特征（图 5-19）。22 颗锆石计算的谐和年龄为 298.3±3.2Ma，为早二叠世（图 5-19）。

地球化学研究表明，白音乌拉北部宝力高庙组流纹斑岩 SiO_2 含量较高，在 76.84%-78.28%。Al_2O_3 含量较低，在 12.06%-12.72%。K_2O 含量较高，在 4.17%-4.69%。TiO_2 含量低，为 0.171%-0.194%。TFe_2O_3、CaO 和 MgO 含量较低，

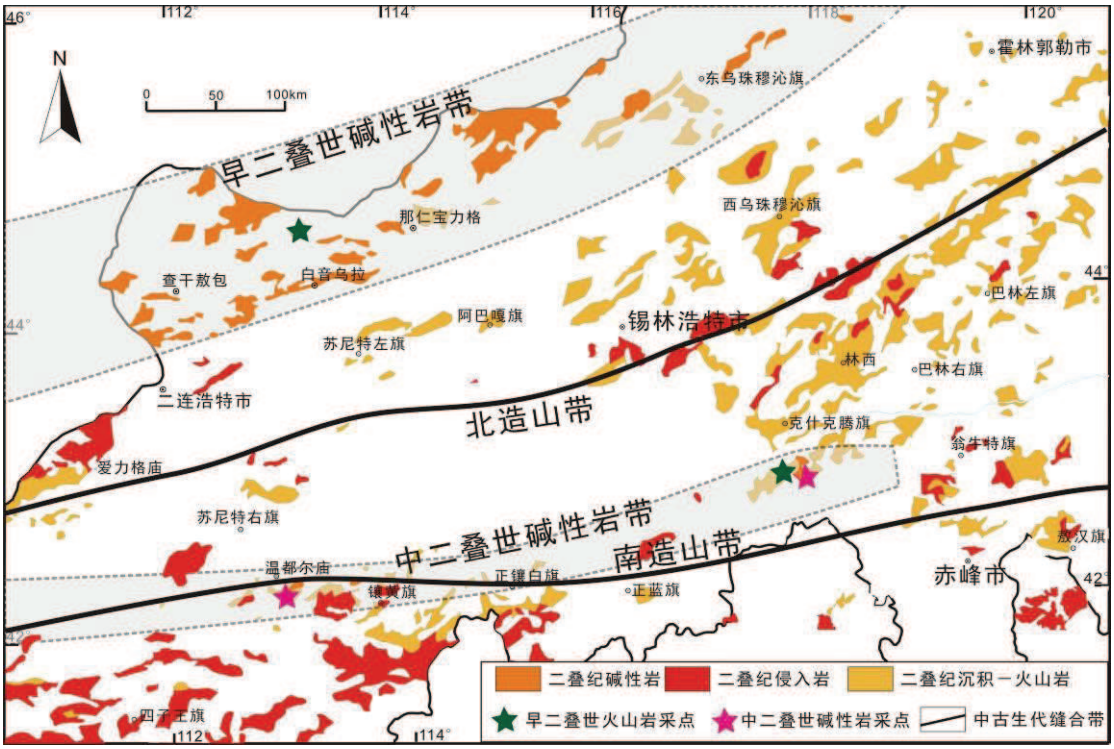

图 5-17 内蒙古中东部二叠纪地层与侵入岩分布图，显示北部早二叠世碱性岩带和南部中二叠世碱性岩带

Figure 5-17 Distribution of Permian volcanic strata and intrusions in central-eastern Inner Mongolia, showing two alkaline magmatic belt: the northern Early Permian alkaline magmatic belt and the southern Middle Permian alkaline magmatic belt

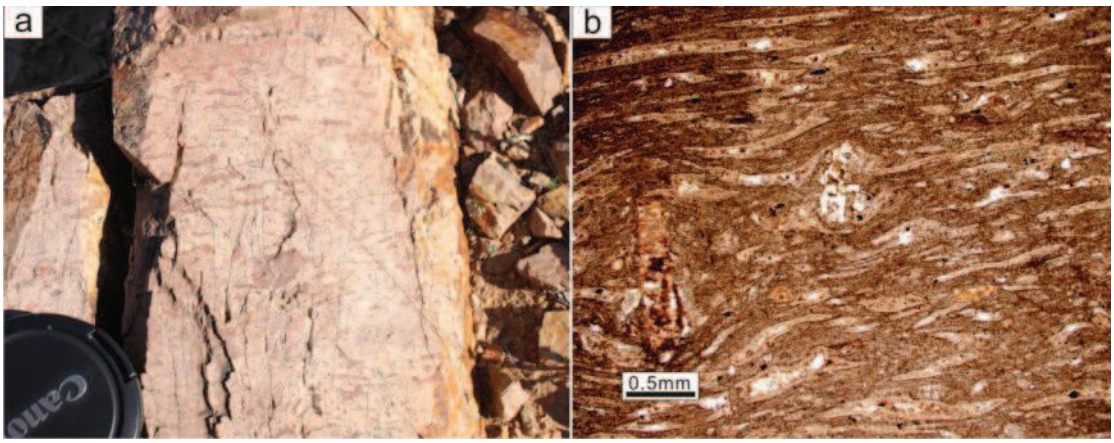

图 5-18 a，白音乌拉北部宝力高庙组流纹斑岩野外照片; b，流纹斑岩镜下照片显示流纹构造

Figure 5-18 Photograph (a) and photomicrograph (b) of Baoligaomiao Formation rhyolite in Baiyinwula area

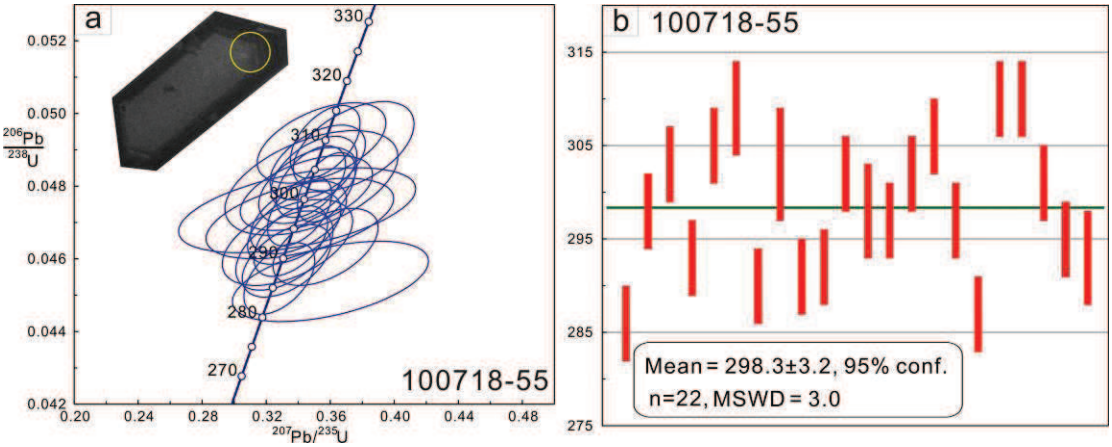

图 5-19 白音乌拉北部宝力高庙组流纹斑岩锆石年龄

Figure 5-19 U-Pb zircon geochronology results of Baoligaomiao Formation rhyolite in Baiyinwula area

分别为 0.79%-0.97%，0.07%-0.16%和 0.02%-0.13%。在 K_2O-SiO_2 图解中，投影到高钾钙碱性系列。

流纹斑岩的稀土元素总量变化范围为 110.7-208.1 ppm，LREE 含量在 77.08-169.5 ppm 之间，HREE 总含量在 30.79-45.97 ppm 之间，LREE/HREE=2.30-4.39，$(La/Yb)_N$=1.77-3.40，轻重稀土分异较明显，富集轻稀土元素。球粒陨石标准化 REE 分配曲线（图 5-20b）表现为稍向右倾的轻稀土和平坦的重稀土配分曲线，出现明显 Eu 负异常（图 5-20b），δEu 范围为 0.31-0.36。该稀土配分模式曲线与该地区早二叠世 A 型花岗岩类似（图 5-20b；Zhang et al.,

2014）。原始地幔标准化蛛网图上（图 5-20c），Rb、Th、和 K 等大离子亲石元素（LILE）较富集，相对亏损 Ba、P、Sr 和 Ti。构造判别图上，宝力高庙组流纹斑岩均落入板内岩浆岩（图 5-20d 和 e），代表其喷发于裂谷伸展环境，与该区早二叠世 A 型花岗岩反映相同构造环境。

5.2.1.2 南部清凤山组双峰式火山岩

清凤山组双峰式火山岩采自克什克腾旗南部（图 5-17），岩性以深绿色玄武安山岩和灰白色流纹岩互层为主（图 5-12c, d），块状结构。镜下显示玄武安山岩以辉石为斑晶，微晶斜长石为基质（5-21a）；流纹岩以微晶斜长石为主，含少量石英颗粒（图 5-21b）。为准确限定火山岩喷发时代，对玄武安山岩（样品号 110503-11）和流纹岩（样品号 101124-02）进行 LA-ICP-MS U-Pb 定年。玄武安山岩样品锆石颗粒自形，Th/U 为 0.40-0.96，发育基性岩特征的宽缓叶片状环带（图 5-22a）。23 颗锆石计算出的谐和年龄为 294.6±1.6Ma，位于早二叠世（图 5-22a 和 b）。流纹岩样品锆石颗粒自形，Th/U 为 0.38-1.00，发育典型酸性岩岩浆震荡环带（图 5-22c）。23 颗锆石计算出的谐和年龄为 288.7±4.7Ma，为早二叠世（图 5-22c 和 d）。

地球化学研究表明，克什克腾旗南部清凤山组火山岩落入玄武安山岩-安山岩和流纹岩（图 5-23a）。玄武安山岩 SiO_2 含量在 60.60%-61.85%。Al_2O_3 含量较高，在 15.31%-15.73%。K_2O 含量较低，在 0.77%-1.62%。TiO_2 含量高，为 1.022%-1.152%。TFe_2O_3、CaO 和 MgO 含量较高，分别为 8.56%-9.01%，1.97%-2.55%和 1.56%-1.85%。在 K_2O-SiO_2 图解中，投影到钙碱性系列。流纹岩 SiO_2 含量较高，在 77.26%-77.75%。Al_2O_3 含量较低，在 12.74%-13.07%。K_2O 含量较高，在 2.77%-3.26%。TiO_2 含量低，为 0.341%-0.369%。TFe_2O_3、CaO 和 MgO 含量较低，分别为 0.56%-0.68%，0.39%-0.46%和 0.21%-0.32%。在 K_2O-SiO_2 图解中，投影到高钾钙碱性系列。玄武安山岩的稀土元素总量变化范围为 113.2-121.3 ppm，LREE 含量在 91.75-100.1 ppm 之间，HREE 总含量在 19.79-21.23 ppm 之间，LREE/HREE=4.64-4.83，$(La/Yb)_N$=4.23-5.09，轻重稀土分异明显，富集轻稀土元素。流纹岩的稀土元素总量变化范围为 108.5-136.3 ppm，LREE 含量在 89.3-115.4

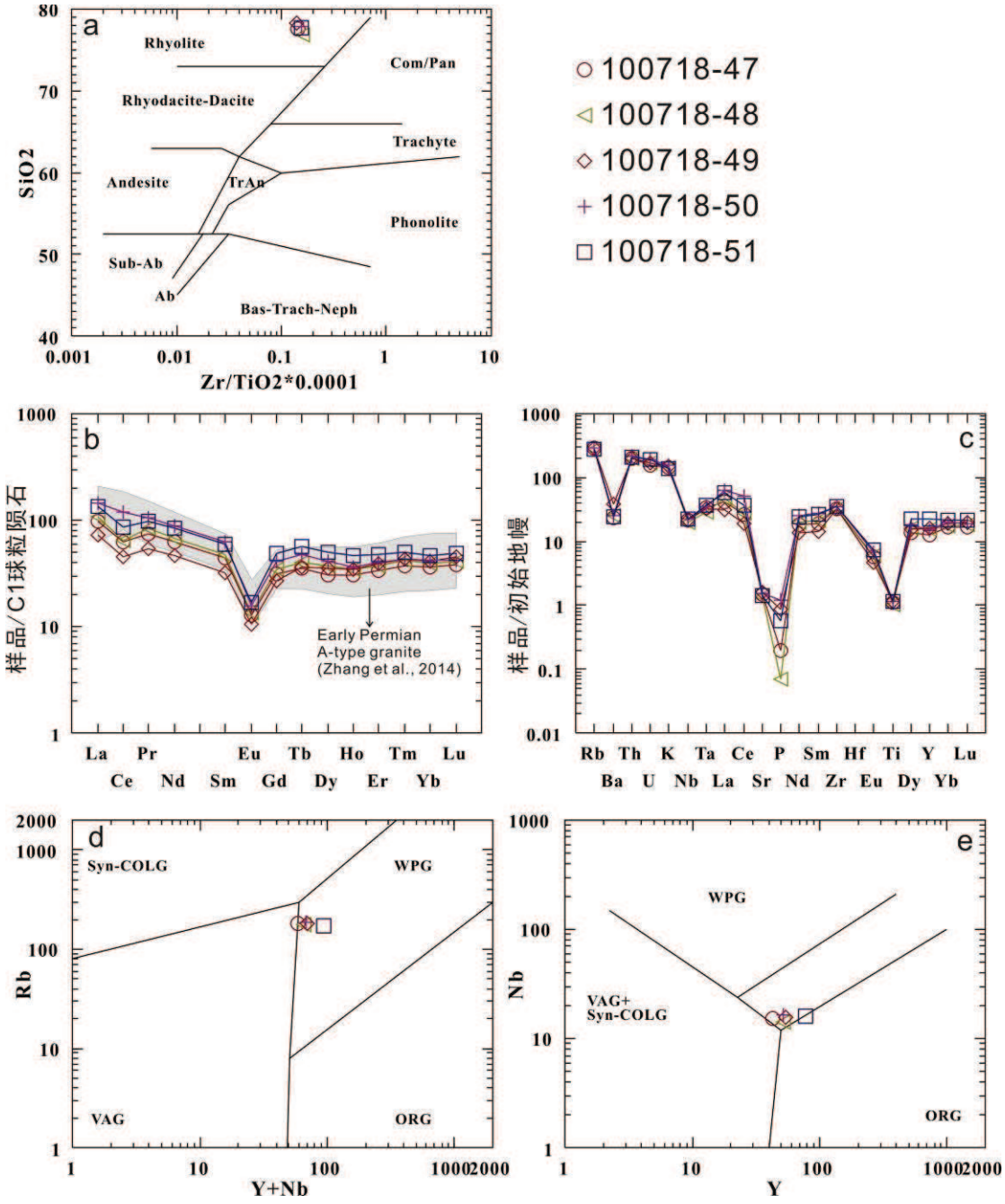

图 5-20 白音乌拉北部宝力高庙组流纹斑岩地球化学图解：a，岩性判别图; b, REE 分配图; c, 微量元素蛛网图; d 和 e，流纹斑岩构造判别图

Figure 5-20 Geochemistry diagrams of the Baoligaomiao Formation rhyolite in Baiyinwula area: a, rock classification diagram; b, Chondrite-normalized REE patterns; c, primitive mantle-normalized trace element spidergrams; d and e, Rb vs Y + Nb and Nb vs Y tectonic discrimination diagrams of Pearce et al. (1984) and Pearce (1996). VAG, volcanic arc granites; WPG, within-plate granites; COLG, collisional granites; ORG, oceanic ridge granites.

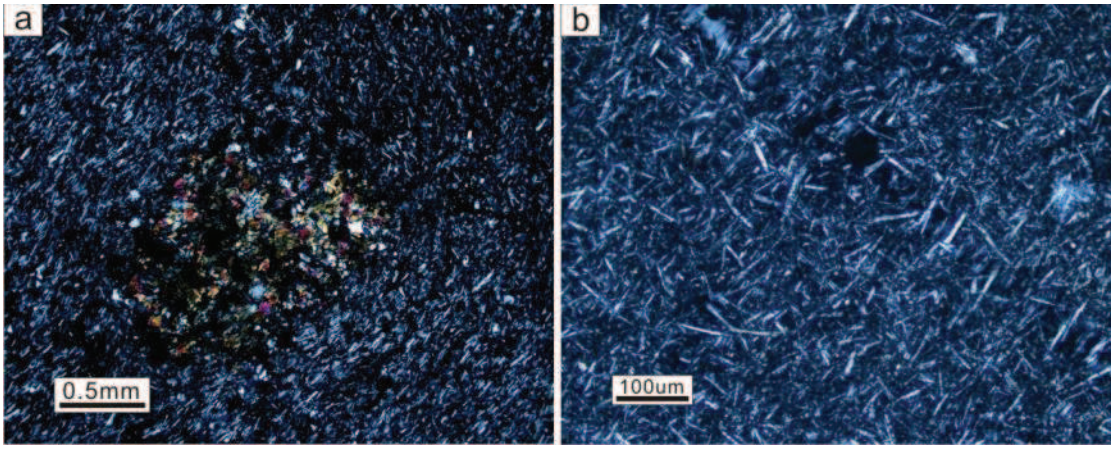

图 5-21 克什克腾旗南清凤山组玄武安山岩（a）和流纹岩（b）镜下照片

Figure 5-24 Photograph and photomicrograph of basaltic andesite (a) and rhyolite (b) in Keshiketengqi

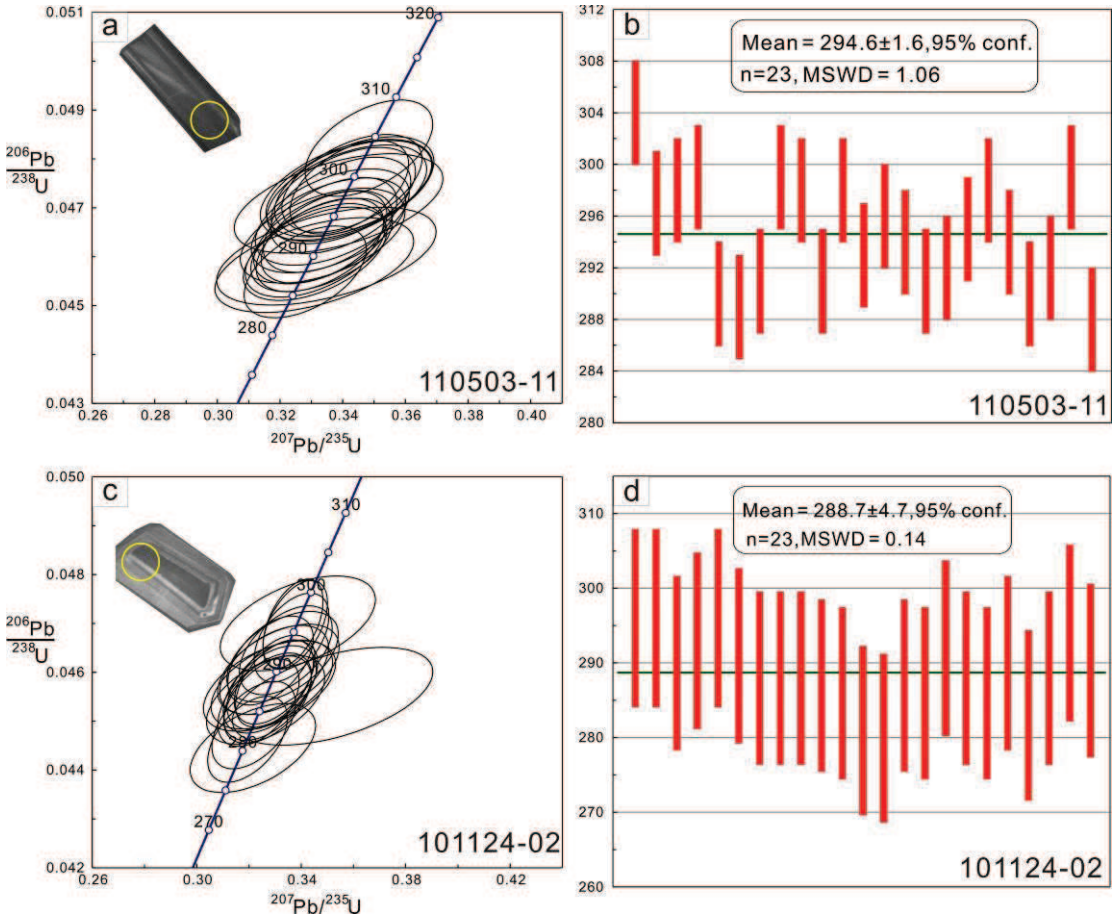

图 5-22 克什克腾旗南清凤山组双峰式火山岩年龄：a 和 b，玄武安山岩; c 和 d，流纹岩

Figure 5-22 U-Pb zircon geochronology results of Qingfengshan Formation bimodal volcanic rocks in Keshiketengqi area: a and b, basaltic andesite; c and d, rhyolite

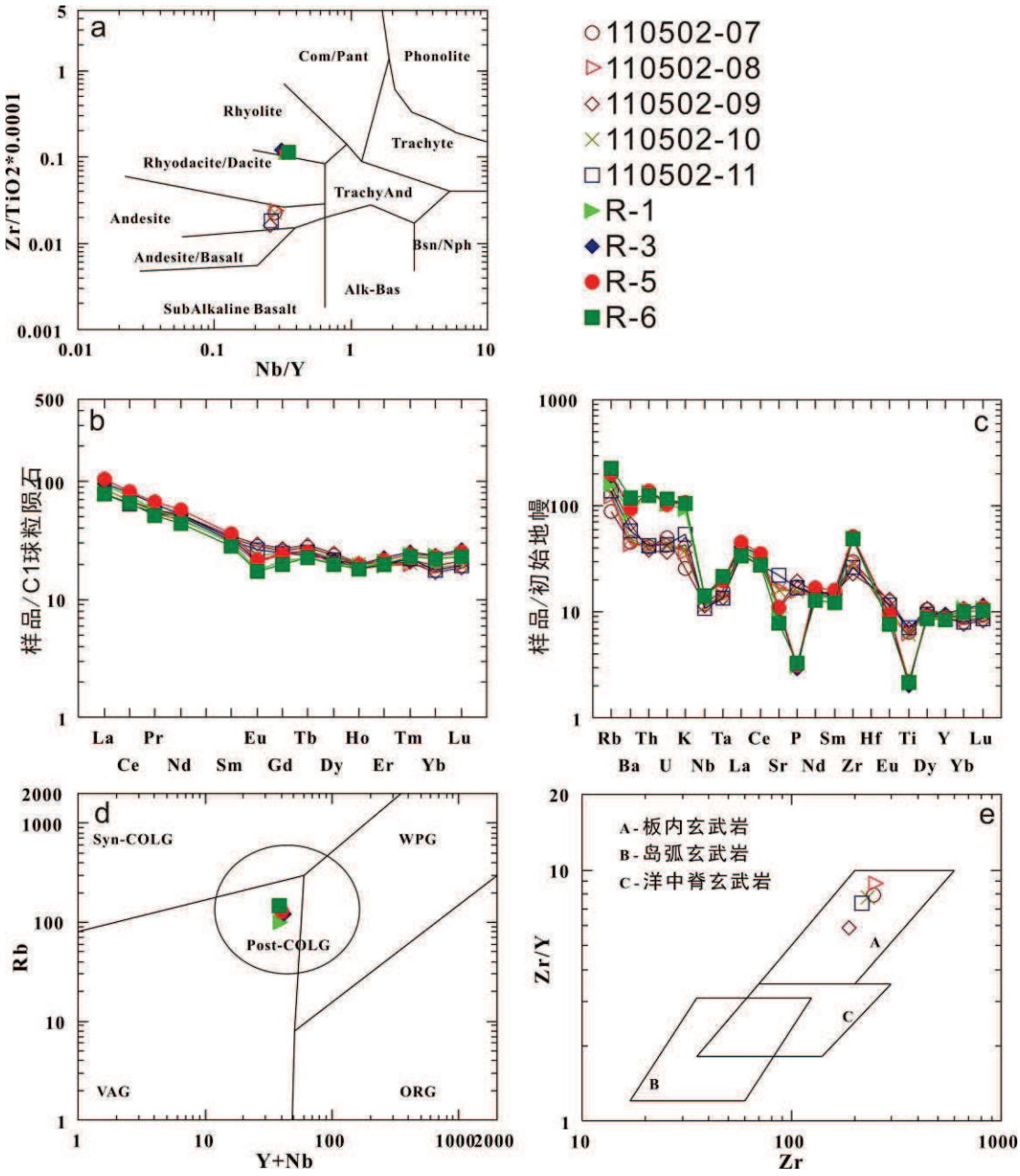

图 5-23 克什克腾旗南部清风山组玄武安山岩和流纹岩地球化学图解：a，岩性判别图; b, REE 分配图; c，微量元素蛛网图; d，流纹斑岩构造判别图; e，玄武安山岩构造判别图

Figure 5-23 Geochemistry diagrams of the Qingfengshan Formation basaltic andesite and rhyolite in Keshiketengqi area: a, rock classification diagram; b, Chondrite-normalized REE patterns; c, primitive mantle-normalized trace element spidergrams; d, Rb vs Y + Nb tectonic discrimination diagram of Pearce et al. (1984) and Pearce (1996). VAG, volcanic arc granites; WPG, within-plate granites; COLG, collisional granites; ORG, oceanic ridge granites; e, Zr vs Zr/Y (Pearce & Norry, 1979) plots for the basaltic andesite. A, within plate basalts; B, Island arc basalts; C, mid-ocean ridges basalts

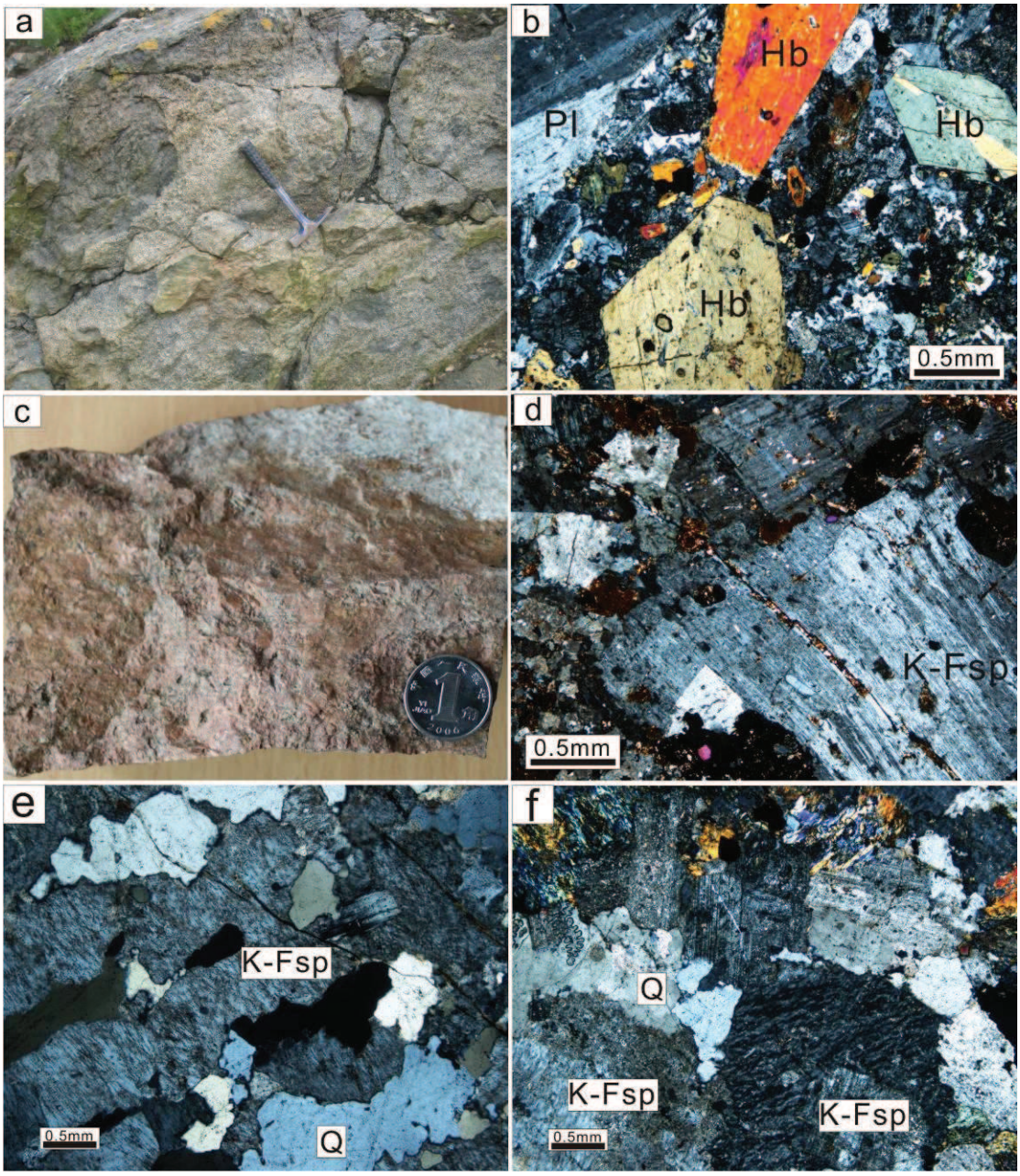

图 5-24 克什克腾旗南部含基性包体花岗闪长岩（a 和 b）、正长岩（c 和 d）和钾长花岗岩（e 和 f）野外和镜下照片

Figure 5-24 Photograph and photomicrograph of granodiorite (a and b), syenite (c and d) and alkaline granite (e and f) in Keshiketengqi area

ppm 之间，HREE 总含量在 19.20-21.67 ppm 之间，LREE/HREE=4.65-5.51，$(La/Yb)_N$=3.56-4.60，轻重稀土分异明显，富集轻稀土元素。玄武安山岩和流纹岩具有相似的球粒陨石标准化 REE 分配曲线（图 5-23b 和 c），表现为右倾的稀土配分曲线，轻稀土和重稀土的分异现象明显。Eu 负异常不明显（图 5-23b），玄武安山岩和流纹岩的 δEu 范围分别为 0.75-0.96 和 0.70-0.74。原始地幔标准化蛛

网图上（图 5-23c），玄武安山岩较流纹岩，Rb、Ba、Th、U、K 和 Zr 等 LILE 更富集，P、Sr 和 Ti 更亏损。玄武安山岩和流纹岩均亏损 Nb 和 Ta。构造判别图上，清凤山组流纹岩落入造山后岩浆岩内（图 5-23d），代表其喷发于伸展环境。玄武安山岩落入板内玄武岩内（图 5-23e），同样说明喷发于伸展环境。

5.2.2 Middle Permian alkaline intrusions

5.2.2.1 克什克腾旗南部碱性杂岩体

克什克腾旗南部发育碱性杂岩体，由含基性包体花岗闪长岩、正长岩和钾长花岗岩组成。花岗闪长岩为粗粒状，含基性包体，包体大小 5cm 至 1m（图 5-24a）。矿物以石英、长石和角闪石为主，矿物均为自形（图 5-24b）。正长岩为肉红色，矿物基本为钾长石（图 5-24c 和 d）。钾长花岗岩为粉红色，典型花岗结构，矿物以钾长石和石英为主，含少量角闪石，部分绿泥石化（图 5-24e 和 f）。

为准确限定碱性杂岩侵位时代，对花岗闪长岩（样品号 110718-13）、正长岩（样品号 110718-07）和钾长花岗岩（样品号 130619-10）进行 LA-ICP-MS U-Pb 定年。花岗闪长岩样品锆石颗粒自形，Th/U 为 0.52-1.22，发育岩浆震荡环带（图 5-25a）。25 颗锆石计算出的谐和年龄为 266.9±1.4Ma，为中二叠世（图 5-25a 和 b）。正长岩样品锆石颗粒自形，Th/U 为 0.61-1.04，发育宽缓岩浆环带（图 5-25c）。24 颗锆石计算出的谐和年龄为 265.3±1.6Ma，位于中二叠世（图 5-25c 和 d）。钾长花岗岩样品锆石颗粒自形，Th/U 为 0.43-1.51，无明显岩浆环带（图 5-25e）。22 颗锆石计算出的谐和年龄为 267.3±2.6Ma，为中二叠世（图 5-25e 和 f）。

为探讨该碱性杂岩侵入环境，对杂岩体中含基性包体花岗闪长岩和正长岩进行地球化学研究。数据显示，克什克腾旗南部花岗闪长岩落入石英闪长岩中，而正长岩除一个样品落入正长岩和花岗岩之间外，其余均落入霞石正长岩中（图 5-26a）。石英闪长岩 SiO_2 含量在 63.36%-64.13%。Al_2O_3 含量较高，在 16.02%-16.79%。K_2O 含量较低，在 1.73%-2.01%。TiO_2 含量为 0.625%-0.653%。TFe_2O_3、CaO 和 MgO 含量较高，分别为 6.00%-6.15%，4.89%-5.69% 和 0.24%-0.25%。在 K_2O-SiO_2 图解中，投影到钙碱性系列。霞石正长岩 SiO_2 含量为 57.87%-59.89%。Al_2O_3 含量较高，在 15.76%-17.42%。K_2O 含量高，在 4.81%-7.79%，Na_2O 含量高，为 4.16%-7.86%，显示高的总碱含量。TiO_2 含量为 0.515%-0.662%。TFe_2O_3、CaO 和 MgO 含量较低，分别为 2.96%-4.56%，0.87%-4.6%

和 0.01%-0.03%。

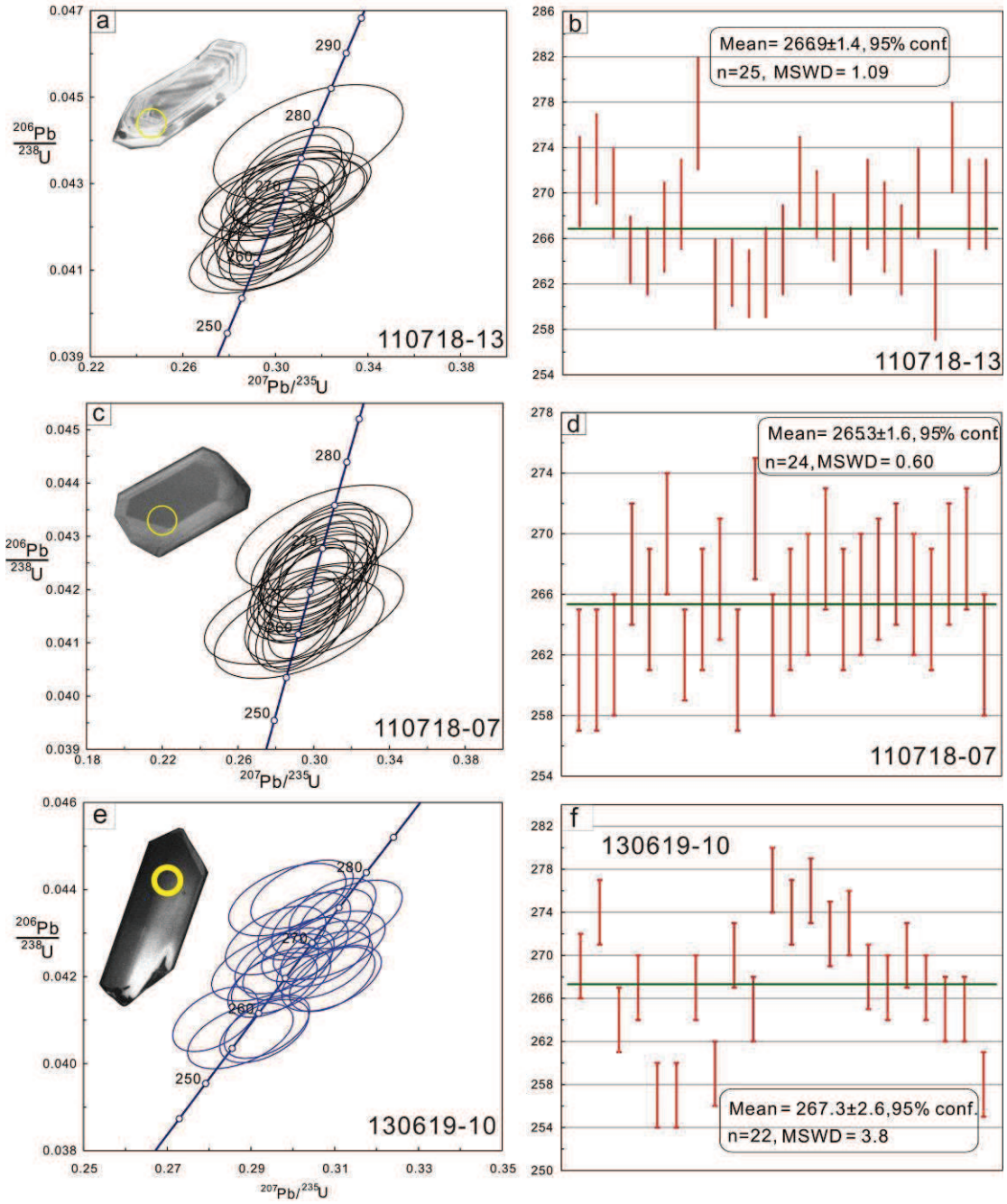

图 5-25 克什克腾旗南部含基性包体花岗闪长岩（a 和 b）、正长岩（c 和 d）和钾长花岗岩（e 和 f）锆石 U-Pb 年龄

Figure 5-25 Condordia diagrams of U-Pb data for zircons from granodiorite (a and b), syenite (c and d) and alkaline granite (e and f)

石英闪长岩的稀土元素总量变化范围为 75.48-79.97 ppm，LREE 含量在 64.67-68.98 ppm 之间，HREE 总含量在 10.52-11.19 ppm 之间，

LREE/HREE=5.98-6.56，$(La/Yb)_N$=5.90-6.65，轻重稀土分异明显，富集轻稀土元

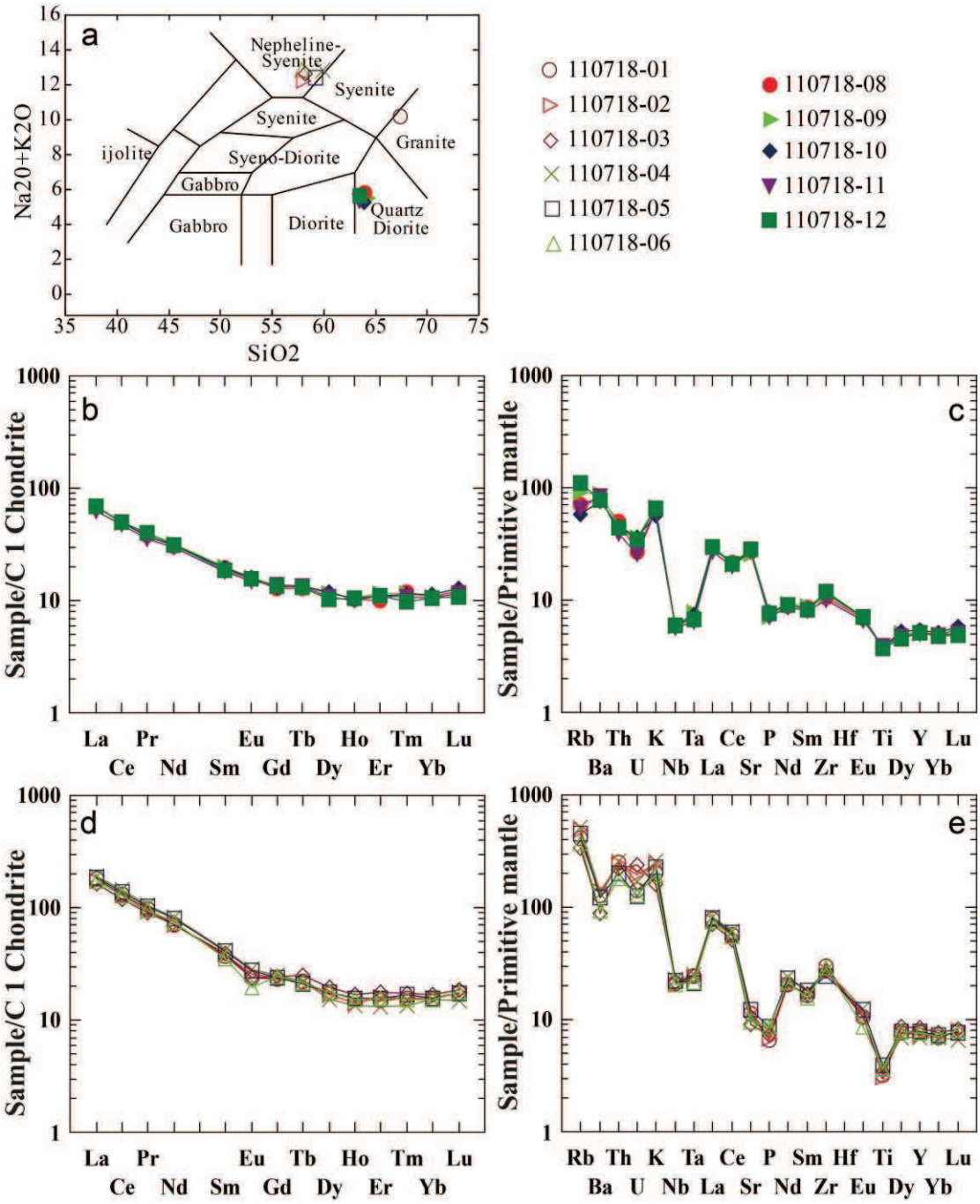

图 5-26 克什克腾旗南部中二叠世含基性包体花岗闪长岩和正长岩地球化学图解：a，岩性判别图; b 和c，含基性包体花岗闪长岩的REE 分配图和微量元素蛛网图; d 和e，正长岩的REE 分配图和微量元素蛛网图

Figure 5-26 Geochemistry diagrams of the granodiorite and syenite in Keshiketengqi area: a, rock classification diagram; b and d, Chondrite-normalized REE patterns for granodiorite (b) and syenite (d); c and e, primitive mantle-normalized trace element spidergrams for granodiorite (c) and syenite (e)

素。霞石正长岩的稀土元素总量变化范围为 180.2-205.8 ppm，LREE 含量在 161.6-189.6 ppm 之间，HREE 总含量在 16.17-18.58 ppm 之间，LREE/HREE=8.70-11.73，$(La/Yb)_N$=9.91-12.43，轻重稀土分异明显，富集轻稀土元素。石英闪长岩和霞石正长岩的球粒陨石标准化 REE 分配曲线均表现为右倾的稀土配分曲线，轻稀土和重稀土的分异现象明显（图 5-26b 和 d）。霞石正长岩相对石英闪长岩更加富集 LERR。二者 Eu 负异常均不明显（图 5-26b 和 d），δEu 范围分别为 0.941-0.998 和 0.67-0.88。原始地幔标准化蛛网图上（图 5-26c 和 e），石英闪长岩和霞石正长岩同样富集 Rb、Th、U、K 和 Zr 等 LILE，亏损 Nb、Ta、P 和 Ti。石英闪长岩较霞石正长岩，富集 Ba，和 Sr。

5.2.2.2 镶黄旗碱性岩

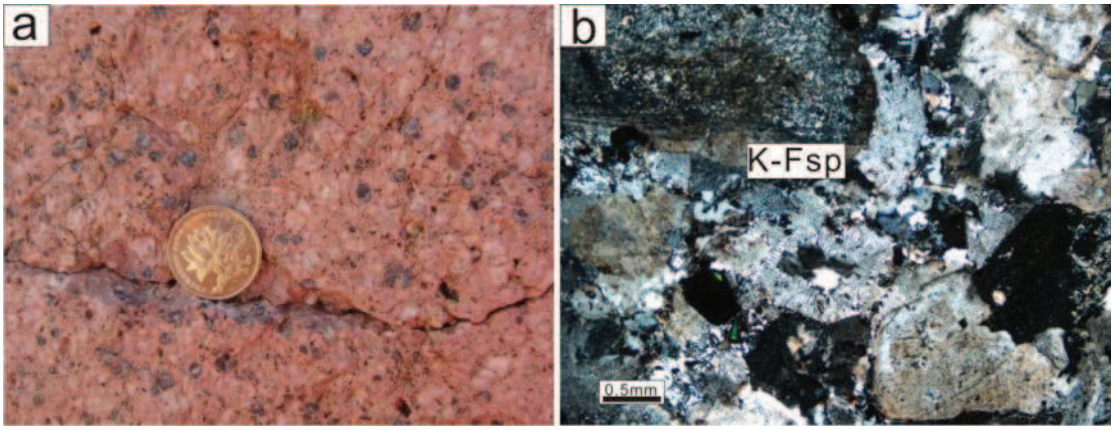

图 5-27 镶黄旗地区石英正长岩野外（a）和镜下照片（b）

Figure 5-27 Photograph (a) and photomicrograph (b) of quartz synite in Xianghuangqi

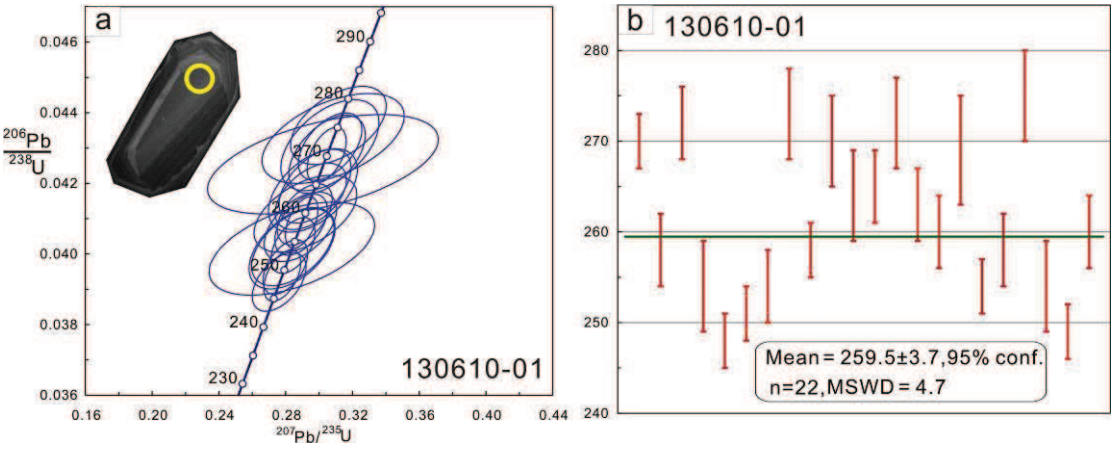

图 5-28 镶黄旗石英正长岩锆石 U-Pb 年龄

Figure 5-28 U–Pb Concordia diagram of quartz synite in Xianghuangqi

镶黄旗地区发育正长岩和石英正长岩，为肉红色，矿物以石英和碱性长石为主（图 5-27a 和 b）。为准确限定正长岩侵位时代，对石英正长岩（样品号 130610-01）进行 LA-ICP-MS U-Pb 定年。石英正长岩样品锆石颗粒自形，Th/U 为 0.49-0.93，发育宽缓岩浆震荡环带（图 5-28a）。22 颗锆石计算出的谐和年龄为 259.5±3.7Ma，位于中二叠世末（图 5-28a 和 b）。

5.3 Regional sedimentological comparison

对上述六个地区二叠纪地层的沉积学分析表明，内蒙古中东部地区二叠纪地层纵向相变较大，横向差别较小。因此，基于岩石组合、岩相、化石和碎屑锆石年龄等方面，我们对东部五个地区（由北向南分别为东乌珠穆沁旗、西乌珠穆沁旗、林西、克什克腾旗、敖汉旗）二叠纪地层进行了岩石地层对比，并将二叠纪地层划分为两个主要沉积阶段：早－中二叠世陆内伸展盆地沉积阶段和晚二叠世陆内盆地陆相沉积阶段（图 5-29）。并进一步将第一阶段分为早二叠世海陆交互相沉积、早二叠世裂谷火山岩沉积和中二叠世浅海相-海陆交互相沉积（图 5-29）。早早二叠世沉积发育于晚石炭世陆表海相碳酸盐岩之上，整合或不整合于下伏地层之上（图 5-29）。

5.3.1 The Early Permian shallow marine and marine-terrigenous facies deposits

该阶段以沟呼都格组碎屑岩段、寿山沟组、清凤山组碎屑岩段和酒局子组为代表。其中最北端东乌珠穆沁旗沟呼都格组碎屑岩段为冲积扇相和曲流河相沉积（图 5-29）。最南端敖汉旗地区酒局子组为曲流河相沉积，清凤山组下碎屑岩段为辫状河相沉积（图 5-29）。两处沉积均表现为陆相沉积的特征，代表晚石炭世陆表海沉积的南北两个边缘。西乌珠穆沁旗寿山沟组为以粉砂岩为主的浅海相沉积，厚度巨大，可能代表早二叠世一个海相盆地沉积中心（图 5-29）。克什克腾旗地区清凤山组碎屑岩段底部为类混杂堆积，向上转变为砂岩和粗砂岩/砾岩的互层，并发育大量浅海相动物化石，为浅海相沉积，可能代表早二叠世另一个海相盆地沉积中心（图 5-29）。中部林西地区不发育早二叠世碎屑沉积地层，说明该区早二叠世位于海平面以上，处于剥蚀阶段。

上述沉积特征显示，研究区南北两侧在早二叠世早期均为陆相沉积，南北两条蛇绿混杂带附近出现厚度巨大的浅海相细碎屑沉积，并于南部克什克腾旗地区

出现滑塌堆积，而中部林西地区则缺乏该期沉积。该沉积分布特征说明南北两条蛇绿混杂带附近可能是伸展盆地最初伸展的位置。而该伸展盆地的形成可能与先前构造带（蛇绿混杂带）活化形成的正断层有关（Ring, 1994; Gawthorpe and Leeder, 2000; Corti et al., 2007）。虽然正断层无法直接观测到，但沉积厚度分布，滑塌堆积位置及北部伸展岩浆岩分布指示正断层位于两条蛇绿混杂带附近（Leeder and Gawthorpe, 1987; Gawthorpe and Hurst, 1993; Turner, 2010）。沿着北部蛇绿混杂带分布大量晚石炭世双峰式火山岩和花岗岩，其中花岗岩侵入晚石炭世地层中，并作为晚石炭世末沿北缝合带的伸展作用（施光海等，2003; 鲍庆中等，2007a,b; 薛怀民等，2010; 汤文豪等，2011）。滑塌堆积一般与活动正断层相伴（Festa et al., 2010），克什克腾旗地区发现的滑塌堆积含大量下伏晚石炭世灰岩岩块，说明伸展断层切穿下伏灰岩地层，并造成大量巨型灰岩岩块“漂浮”于早二叠世砂岩中。

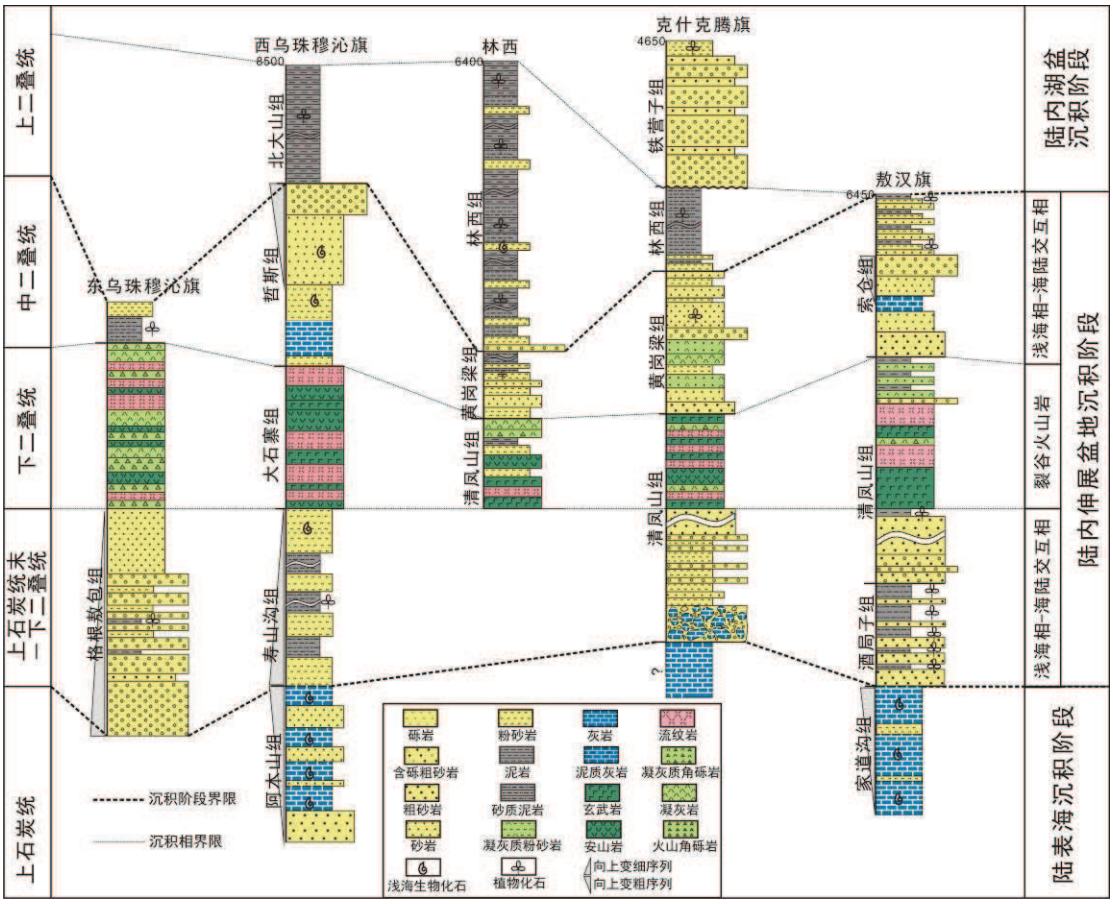

图 5-29 内蒙古东部五个二叠系剖面连井柱状图

Figure 5-29 A synthesis on Carboniferous-Permian sedimentary sequences of central-eastern Inner Mongolia showing five deposition stages and corresponding sedimentary model

5.3.2 The Early Permian rift-related volcanism

早二叠世晚期，内蒙古东部岩浆作用强烈，广泛发育火山岩地层：东乌珠穆沁旗发育格根敖包组火山岩，西乌珠穆沁旗发育大石寨组火山岩，林西、克什克腾旗和敖汉旗发育清凤山组火山岩（图 5-29）。随着伸展盆地的不断变宽和加深，触发了岩浆岩的侵入和喷发（Ebinger et al., 1993; Pascal et al., 2002, 2004）。在此阶段，火山岩同时出现并纵向跨越整个内蒙古东部地区（图 5-29）。本文对北部宝力高庙组和南部清凤山组火山岩地球化学研究，及前人对中部大石寨组火山岩地球化学研究（Zhang et al., 2008; 2011; Chen et al., 2012）均显示，火山岩为双峰式，以玄武岩、玄武安山岩和流纹岩为主，地球化学特征显示其侵位于碰撞后伸展环境（Zhang et al., 2008; Chen et al., 2012）。另外，内蒙古中东部发育大量与火山岩同期的花岗岩侵入体，地球化学显示其具有 A 型花岗岩的特征，被解释为与造山后伸展相关（施光海等，2004; 鲍庆中等，2007a,b; 罗红玲等，2009）。

5.3.3 The Middle Permian shallow marine and marine-terrigenous facies deposits

随着伸展进入高潮阶段，火山作用减弱，浅海相碎屑－碳酸盐岩沉积占据主导地位，填充于伸展盆地中（图 5-29；Prosser, 1993; Leppard and Gawthorpe, 2006; Turner, 2010）。由于盆地沉积中心不同的深度，哲斯组块状亮晶灰岩和厚层砂岩沉积于深的沉积中心（西乌珠穆沁旗）；而索仓组泥质灰岩和薄层砂岩沉积于浅的沉积中心（敖汉旗）（图 5-29）。软沉积变形存在于灰岩和砂岩层中，为伸展进入高潮阶段的标志（Prosser, 1993; Graham et al., 2001）。林西和克什克腾旗地区黄岗梁组沉积海陆交互相地层，代表伸展盆地中水深较浅的位置。

中二叠世沉积上部均表现为粒度逐渐变粗的海退序列，并在顶部发育含植物化石的陆相地层，例如林西和克什克腾地区黄岗梁组顶部和敖汉旗地区索仓组上段（图 5-29），表明随着不断海退，陆内伸展盆地演化结束，内蒙古中东部于中二叠世晚期进入陆相盆地沉积阶段。

5.3.4 The Late Permian fluvial-lacustrine facies deposits

晚二叠世陆相盆地沉积仅发育于西乌旗南部、林西和克什克腾旗地区，以北

大山组和林西组巨厚层黑色泥质岩代表（图 5-29），含大量植物化石，反映稳定的深湖相沉积。湖相沉积盆地的沉积中心位于西乌旗南部－林西一带，沉积厚度达 4000 m。晚二叠世，内蒙古中西部地区已进入剥蚀阶段，不存在此阶段沉积（内蒙古地质矿产局，1991）。巨厚的深湖相沉积之后，内蒙古中东部基本进入剥蚀阶段，仅在克什克腾旗南部发育铁营子组冲积扇－河流相沉积，可能代表局部山间盆地（图 5-29）。

Chapter 6 Paleomagnetic constrains to the Late Paleozoic tectonic evolution

Paleomagnetism is an efficient tool to study plate movements and to propose paleogeographic reconstructions. It could provide key arguments to solve the aforementioned controversy on Paleo-Asian Ocean. The paleomagnetism has been used to study the evolution of the Central Asian Orogenic Belt, especially for the western part (Levashova et al., 2003; 2007; 2009; Van der Voo et al., 2006; Wang et al., 2007; Gilder et al., 2008; Choulet et al., 2011; 2013; Bazhenov et al., 2012). For the eastern part, previous paleomagnetic studies have been concentrated on the study of the Mongol-Okhotsk Ocean between MOB and SIB (Kravchinsky et al., 2002a, 2002b; Cogné et al., 2005). Conversely, paleomagnetic constraints for the Paleo-Asian Ocean remain rare and they were mostly carried out from regions to the northern part of MOB, such as Trans-Baikal and upper Amur (Pruner, 1992; Xu et al., 1997; Kravchinsky et al., 2002a). Zhao et al (1990) have reported the first and only paleomagnetic study on Paleozoic rocks from Inner Mongolia, however, however, their results of the Late Permian (11 samples) and Carboniferous (29 samples) are clearly remagnetized with a negative fold test, Therefore no any reliable or utilizable Paleozoic paleomagnetic data are available up to now for Inner Mongolia area. For these reasons, a paleomagnetic study has been carried out on several sedimentary and volcanic rocks from Paleozoic formations in central-eastern Inner Mongolia.

6.1 Stratigraphy of sampled strata

The sampled strata range from Late Silurian to Late Permian, which are the key stages for studying the evolution of the eastern part of CAOB. In the following part, we describe the sampling localities using the tectonic division presented in the geological outline.

6.1.1 North margin of NCB

In the northern margin of NCB, two localities were sampled, namely Damaoqi in the west and Aohanqi in the east (localities a and b in Fig. 6-1b, respectively).

Late Silurian rocks are scarce in central-eastern Inner Mongolia, but are well defined as the Xibiehe Formation (S_3x) near Damaoqi County (Zhang et al., 2010). This Late Silurian formation is composed of sandstone with basal conglomerate grading upward into sandstone-limestone, containing corals and brachiopods, such as *Kyphophyllum, Progressum, syringopora*, etc (IMBGMR, 1991; 2002). In Damaoqi, 6 sites of yellow sandstone with variable beddings were collected over a 500 m-thick section (Fig. 6-2a and Table 6-1). The Xibiehe Formation underlies the Lower Devonian Chaganhabu Formation (D_1c) with an unconformable contact. The Early Devonian assignment is based on the abundant corals, brachiopods and bryozoans, such as *Favosites* sp. *Atrypa* sp. *Leptotrypafragilis* (IMBGMR, 2002). In the north of Damaoqi, the Chaganhabu Formation exposes a thick sequence of red sandstone, and 8 sites of red sandstone were collected from this ～800 m thick, gently folded section (Fig. 6-2b and Table 6-1). It is worth noting that a dextral strike-slip fault showing mylonitic deformation has been identified three kilometers to the east of the sampling sites during our field work.

To the north of Aohanqi County, 7 sites were selected from the Lower Carboniferous Houfangshengou Formation (C_1h), which consists of thick-bedded (0.2-1 m) black limestone (Fig. 6-2c and Table 6-1). This formation, more than 1200 m thick, attests for a stable platform carbonate setting. The well-preserved corals and brachiopods (*Gigantoproductus- Dibunophyllum*) constrain its Early Carboniferous age (IMBGMR, 1991). Open fold without cleavage can be observed in this formation.

6.1.2 Inner Mongolia Block (IMB, also called SHB in the previsou chapters)

Paleomagnetic samples were collected from 5 localities in IMB. From west to east, they are Sunidzuoqi, Abagaqi, Keshiketengqi, Linxi and West Ujimqin (localities c, d, e, f and g, relatively, in Fig 6-1b).

Near Sunidzuoqi and Abagaqi counties, 5 sites of red coarse sandstone (Fig. 6-2d)

and 6 sites of yellow siltstone (Fig. 6-2e) of the Upper Devonian Seribayanaobao Formation (D_3s) were collected, respectively (Table 6-1). The Upper Devonian Seribayanaobao Formation represents continental molasse deposits, which overlie

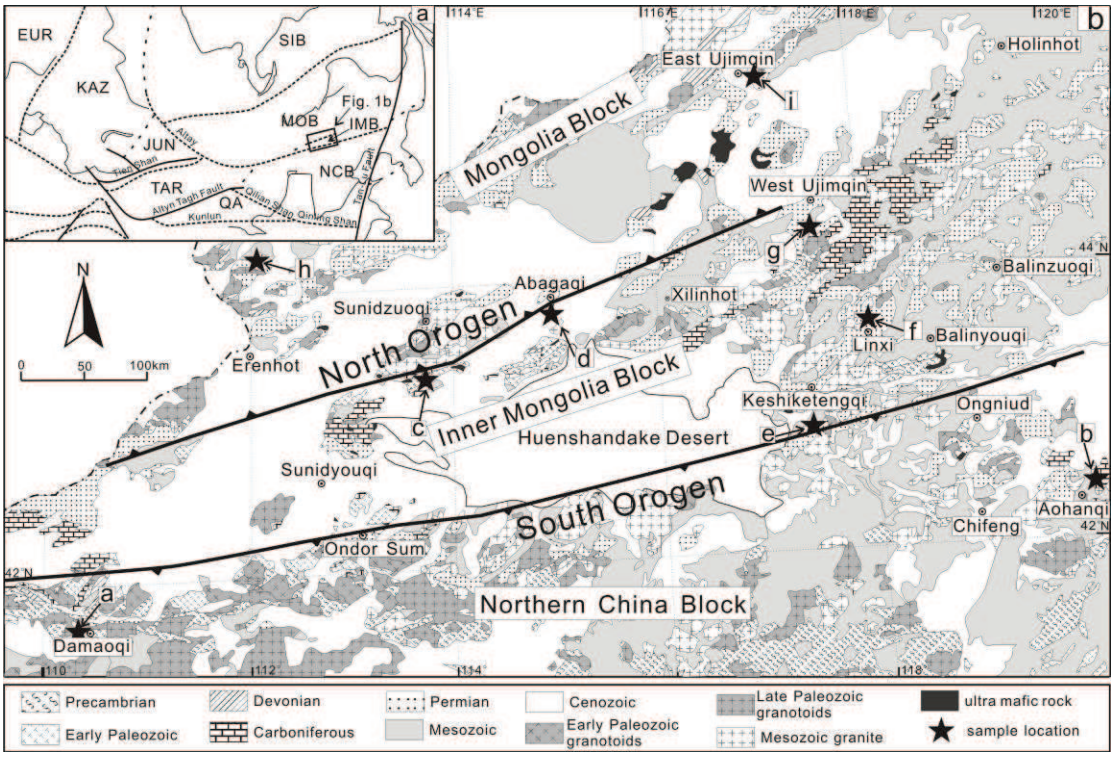

Figure 1. a. Sketch tectonic map of Northeast Asia showing the main blocks and boundaries (modified after Enkin et al., 1992). Block: EUR=Eurasia main plate; KAZ=Kazakhstan block; JUN=Junggar block; TAR=Tarim block; QA=Qaidam block; SIB=Siberia Block; MOB=Mongolia Block; NCB=North China Block; b. Geological map of eastern Inner Mongolia emphasizing the two orogenic belts (North Orogen and South Orogen), Late Paleozoic strata and intrusions (modified after IMBGMR, 1991; Xu et al., 2013). Sampling localities: a, Damaoqi; b, Aohanqi; c, Sunidzuoqi; d, Abagaqi; e, Keshiketengqi; f, Linxi; g, West Ujimqin; h, Erenhot; i, East Ujimqin.

unconformably the ophiolite mélange (Xu and Chen, 1997; Xu et al., 2013). Strata mainly consist of red conglomerate, red-yellow sandstone and yellow siltstone, with a top layer of argillaceous limestone. The plant fossils, such as *Leptophloeum rhombicum* in the sandstone and *Nalivkinella profunda, Cyrtospirifer sulcifer* in the limestone, attest to the Late Devonian age (Xu et al., 2013). Near Sunidzuoqi, 5 sites of red sandstone of the Lower Carboniferous Gouhuduge Formation (C_1g) were also collected from both limbs of a fold (Table 6-1). Sandstone of the Gouhuduge

Formation forms a 900m-thick series, which conformably overlies the Upper Devonian strata. Red lithic sandstone was deposited at site of transition from the molasse basin to a shallow sea (Xu and Chen, 1997). Open fold has been observed from Lower Carboniferous strata in the Sunidzuoqi; and the Upper Devonian strata in Abagaqi are highly tilted (Table 6-1).

To the south of Keshiketengqi County, 6 sites of coarse sandstone of the Upper Permian Tieyingzi Formation (P_3t) were collected from a section with very gentile bedding (Fig. 6-2f and Table 6-1). The Tieyingzi Formation contains rocks of continental alluvial-fluvial-lacustrine facies, which consist of conglomerate at the bottom, coarse-grained to conglomeratic sandstone in the middle, and red and green siltstone on the top. The Tieyingzi Formation unconformably overlies the Early-Middle Permian granite and volcanic strata, and the Upper Permian black siltstone, with pebbles of all aforementioned rocks at the bottom. The enriched Late Permian plant fossils, such as *Pecopteris* sp. *Calamites* sp. *Nephropsis* sp, and the occurrence of the unconformity as well, assign the Tieyingzi Formation to the Late Permian.

To the north of Linxi County, 3 sites of tuff and basalt of the Lower Permian Dashizhai Formation (P_1d) and 3 sites of sandstone of the Upper Permian Linxi Formation (P_3l) were collected (Fig. 6-2g and Table 6-1). The Dashizhai Formation is composed of volcanic rocks erupted between 285 and 270Ma, which belong to the major Late Paleozoic magmatic event widespread in Inner Mongolia (Zhang et al., 2008; Liu et al., 2009; Chen et al., 2012). The Linxi Formation is composed of fluvial conglomerate at the bottom with pebbles of volcanic rocks of Dashizhai Formation, covered by ca. 4000 m-thick black mudstone and dark yellowish siltstone/sandstone of fluvial-lacustrine facies (Mueller et al., 1991). The plant fossils and fresh water bivalves, such as *Brachythyris* sp. and *Rhombotrypella* sp., and the minimum age of detrital zircons (256±2Ma) (Han et al., 2011) well constrain its Late Permian age.

To the south of West Ujimqin County, 8 sites of limestone and 3 sites of grey fine-grained sandstone were sampled from the Upper Carboniferous Amushan Formation (C_2a; Fig. 6-2h). As a very common feature of the Late Carboniferous

deposits in Inner Mongolia, the Amushan Formation is composed of shallow marine facies carbonate and subordinate terrigeneous deposits with a well-defined age owing to enriched neritic fauna, such as *Pseudoschwagerina* and *Triticites*. All 8 sites were sampled in monoclinal limestone strata. To the north of West-Ujimqin, 5 sites of yellow sandstone of the uppermost part of the Upper Carboniferous-Lower Permian Gegenaobao Formation (C_2-P_{1g}) were sampled from both limbs of an open fold. The uppermost part of Gegenaobao Formation, directly overlies volcanic rocks and especially rhyolite that has yielded a zircon concordant U-Pb age at 266±2Ma (Zhao unpublished data). Therefore, the collected sandstone is mid-Permian in age and we further use P_{2g} to represent the age for these 5 sites. To the south of West Ujimqin, 6 sites of dark blue thick-bedded limestone were collected from the middle Permian Zhesi Formation (P_2z; Fig. 6-2i). The age determination of Zhesi Formation is based on the well-known Middle Permian Zhesi Fauna (Wang et al., 2004). The bedding attitude for the Zhesi Formation is nearly vertical, with very slight variations.

6.1.3 Southern margin of MOB (also called AXXB in previous chapters)

In the southern margin of MOB, two localities were chosen for paleomagnetic sampling. From west to east, they are Chaganaobao to the north of Erenhot (locality h in Fig. 6-1b) and East-Ujimqin (locality i in Fig. 6-1b).

To the north of Chaganaobao village, 7 sites of red coarse sandstone (Fig. 6-2j) and 1 site of conglomerate of the Lower-Middle Devonian Niqiuhe Formation ($D_{1\text{-}2}n$) were sampled on both limbs of the folded 4 km-long profile (Table 6-1). The Niqiuhe Formation is composed of red conglomerate in the lower part, red coarse sandstone and limestone in the middle part and tuffecous sandstone/siltstone in the upper part. Corals and brachiopods fossils of Early-Middle Devonian age, such as *Leptaenopyxis bouei, Derbina* and *Coelospira,* are described in this formation (IMBGMR, 1991). These strata were further intruded by Late Jurassic-Early Cretaceous granite and covered by contemporary volcanic rocks.

Near East Ujimqin County, 6 sites of volcaniclastic rocks were collected from the upper part of the Upper Carboniferous-Lower Permian Gegenaobao Formation

(C_2-P_1g; Fig. 6-2k and Table 6-1). The Gegenaobao Formation displays conglomerate and sandstone in the lower part and volcanic breccias-andesite-rhyolite-volcanoclastic rocks in the upper part, with a nearly vertical bedding attitude. Volcaniclastic rocks unconformably overlie the Late Devonian strata and granodiorite. The age was determined by brachiopods fossils in the clastic part, such as *Kochiproductus* sp., *Rhynchopora* sp., *Spirifer* sp.. Several meters apart from the sampling sites, a W-E trending dextral strike-slip shear zone was identified (Fig. 6-2l).

Figure 6-2 Photographs of sampled strata

For each site, six to eight cores were drilled using a portable gasoline drill. Cores were orientated by both magnetic and, if possible, solar compasses. The average difference between these two azimuths ranges between 1.5°±0.5° and 8.0°±1.4°.

Table 6-1. Paleomagnetic Sampling and measurement results from Inner Mongolia

Site	coordinate	Rock	Age	Strike/dip	n'/n	N/R	Dg	Ig	Ds	Is	k	α_{95}	Comments and poles
				North China Block (NCB)									
Damaoqi													
1[a]	41°55'N,109°56E	red sandstone	D_1c	343.6/51.5	6/6	6/0	0.7	70.8	53.1	27.4	131.0	6.7	
2[b]	41°55'N,109°56E	red sandstone	D_1c	258.5/14	8/8	5/3	124.7	2.6	123.5	12.7	36.8	9.2	λ=24.1° φ=354.2° dp=4.6° dm=9.2°
3	41°55'N,109°56E	red sandstone	D_1c	210/29	6/8	6/0	29.5	55.5	354.5	45.9	49.0	9.7	
4[b]	41°55'N,109°56E	red sandstone	D_1c	221/40	8/9	0/8	314.5	-17.2	317.1	-57.1	17.0	15.1	λ=24.4° φ=340.7° dp=8.1° dm=15.6°
5	41°55'N,109°56E	red sandstone	D_1c	176/35	0/4	-	-	-	-	-	-	-	dispersed
6[b]	41°55'N,109°56E	red sandstone	D_1c	220.5/24	4/5	0/4	107.5	-3.6	106.0	18.5	42.0	15.1	λ=14.2° φ=9.4° dp=7.6° dm=15.1°
7[b]	41°55'N,109°56E	red sandstone	D_1c	179.7/42	4/6	0/4	211.7	-16.3	195.3	-35.3	594.0	4.0	λ=46.3° φ=241.1° dp=2.1° dm=4.1°
8[b]	41°55'N,109°56E	red sandstone	D_1c	190/51	3/4	0/3	235.3	-12.1	211.7	-42.2	90.0	7.1	λ=29.5° φ=220.0° dp=3.7° dm=7.2°
9[a]	42°00'N,110°10'E	coarse sandstone	S_3x	289/20	6/6	2/4	6.1	63.8	11.1	44.0	94.0	6.9	
10[a]	42°00'N,110°10'E	coarse sandstone	S_3x	283.5/30	8/8	5/3	4.2	70.9	6.7	38.0	114.0	5.7	
12	42°00'N,110°10'E	coarse sandstone	S_3x	337/48	0/8	-	-	-	-	-	-	-	weak NRM, viscous
13[a]	42°00'N,110°10'E	greywacke	S_3x	338/49.5	7/9	4/3	5.8	66.0	44.2	26.7	21.2	13.4	
14	42°00'N,110°10'E	greywacke	S_3x	328/56	0/2	-	-	-	-	-	-	-	weak NRM, viscous
15	42°00'N,110°10'E	greywacke	S_3x	304/57	7/9	0/7	337.5	-9.5	314.5	-33.1	53.0	8.4	
			mean[a] (site 1, 9, 10,13)		4S/4S		3.3	67.1			653.0	3.6	λ=81.9° φ=125.4° dp=5.0° dm=6.0°
									31.1	36.0	23.1	16.8	
Aohanqi													
N01[a]	42°33'N,119°47'E	limestone	C_1h	246/26	8/8	8/0	10.5	64.0	355.1	40.5	59.0	7.3	
N02[a]	42°33'N,119°47'E	limestone	C_1h	248.7/36.3	7/8	7/0	9.0	62.5	354.3	28.8	23.8	12.6	
N03[a]	42°33'N,119°47'E	limestone	C_1h	252/32.3	11/11	10/1	5.4	67.5	352.8	36.2	71.5	5.4	
N04[a]	42°33'N,119°47'E	limestone	C_1h	239/41	8/8	4/4	44.9	76.6	347.3	44.2	32.0	9.9	

N05[a]	42°33'N,119°47'E	limestone	C_1h	238.7/38.3	6/8	6/0	7.2	69.0	346.3	33.4	66.3	8.3	
N06[a]	42°33'N,119°47'E	limestone	C_1h	310/18	5/6	4/1	354.3	57.6	8.2	43.4	19.2	17.9	
N07[a]	42°33'N,119°47'E	limestone	C_1h	312.5/18.5	8/8	7/1	20.0	66.1	29.9	49.2	56.0	7.5	
			mean[a]		7S/7S		9.6	66.6			110.0	5.8	λ=80.6° φ=161.9° dp=7.9° dm=9.6°
									357.8	40.0	37.8	9.9	
				Inner Mongolia Block (IMB)									
Sunidzuoqi													
O16	43°28'N,113°32'E	red coarse sandstone	D_3s	245/20	4/7	4/0	173.4	14.8	177.4	32.8	40.0	14.6	
O17	**43°28'N,113°32'E**	**red coarse sandstone**	**D_3s**	**245/20**	**6/10**	**0/6**	**164.3**	**-34.6**	**162.8**	**-15.0**	**50.0**	**11.0**	
O23	43°28'N,113°32'E	red coarse sandstone	D_3s	237/38	0/5	-	-	-	-	-	-	-	weak NRM, viscous
O24	**43°28'N,113°32'E**	**red coarse sandstone**	**D_3s**	**250/28**	**5/6**	**0/5**	**118.7**	**-55.6**	**131.7**	**-30.8**	**54.0**	**16.7**	
O25	**43°28'N,113°32'E**	**red coarse sandstone**	**D_3s**	**250/28**	**6/6**	**1/5**	**138.6**	**-52.8**	**143.6**	**-25.4**	**54.0**	**9.2**	
			mean		**3S/5S**		**143.6**	**-49.3**			**18.0**	**29.9**	
									144.6	**-24.3**	**24.3**	**25.5**	**λ=46.8° φ=349.1° dp=14.6° dm=27.2°**
					17s/17s		**134.1**	**-49.9**			**13.0**	**10.3**	
									139.9	**-25.9**	**14.9**	**9.6**	**λ=43.6° φ=356.9° dp=5.6° dm=10.4°**
O18	43°29'N,113°32'E	sandstone	C_1g	58/40	0/6	-	-	-	-	-	-	-	weak NRM, dispersed
O19	43°29'N,113°32'E	sandstone	C_1g	58/45	0/2	-	-	-	-	-	-	-	weak NRM, dispersed
O20	43°29'N,113°32'E	sandstone	C_1g	80/8	0/3	-	-	-	-	-	-	-	weak NRM, dispersed
O21	43°29'N,113°32'E	sandstone	C_1g	220/20	0/7	-	-	-	-	-	-	-	weak NRM, dispersed
O22	43°29'N,113°32'E	sandstone	C_1g	195/27	0/6	-	-	-	-	-	-	-	weak NRM, dispersed
Abagaqi													
25	43°56'N,114°56'E	yellow siltstone	D_3s	242.3/82.3	0/1	-	-	-	-	-	-	-	viscous
26	43°56'N,114°56'E	yellow siltstone	D_3s	77.5/51.5	0/1	-	-	-	-	-	-	-	viscous
27	43°56'N,114°56'E	yellow siltstone	D_3s	76/40	0/1	-	-	-	-	-	-	-	viscous
28	43°56'N,114°56'E	yellow siltstone	D_3s	72.5/53	0/1	-	-	-	-	-	-	-	viscous

29	43°56'N,114°56'E	yellow siltstone	D_3s	82/73.5	0/1	-	-	-	-	-	-	-	viscous
30	43°56'N,114°56'E	yellow siltstone	D_3s	90/62.3	0/1	-	-	-	-	-	-	-	viscous
Keshiketengqi													
N08[a]	43°01'N,117°40'E	coarse sandstone	P_3t	110.7/34	5/6	5/0	350.5	63.4	252.6	73.2	220.0	5.2	
N09[a]	43°01'N,117°40'E	coarse sandstone	P_3t	120/16.5	7/7	7/0	350.0	72.2	288.7	77.0	180.0	4.5	
N10[a]	43°01'N,117°40'E	coarse sandstone	P_3t	136.3/17	7/7	7/0	355	68.4	306.3	73.1	208.0	4.2	
N11[a]	43°01'N,117°40'E	coarse sandstone	P_3t	128/14	4/4	4/0	6.5	70.2	323.1	77.7	1240	3.5	
N12[a]	43°01'N,117°40'E	coarse sandstone	P_3t	128/14	3/5	3/0	1.2	67.2	320.0	74.4	344.0	6.6	
			mean[a]		5S/5S		356.5	68.4			372.0	4.0	λ=81.1° φ=103.5° dp=5.7° dm=6.7°
									297.5	76.5	114.0	7.2	
Linxi													
O01[a]	43°43'N,118°08'E	sandstone	P_3l	332/84	9/9	9/0	6.4	73.2	134.0	18.5	269.0	3.1	
O02	43°42'N,118°25'E	tuff	P_1d	203/46	0/3	-	-	-	-	-	-	-	dispersed
O03	**43°42'N,118°25'E**	**basalt**	**P_1d**	**200/50**	**5/8**	**0/5**	**201.6**	**-55.1**	**148.0**	**-36.1**	**148.0**	**7.6**	
O04	**43°42'N,118°25'E**	**basalt**	**P_1d**	**200/50**	**4/7**	**0/4**	**166.5**	**-63.4**	**129.5**	**-24.8**	**138.0**	**7.8**	
O05	**43°41'N,118°17'E**	**sandstone**	**P_3l**	**210/34**	**4/4**	**4/0**	**7.8**	**57.4**	**334.7**	**38.1**	**37.4**	**17.7**	
O06	**43°41'N,118°17'E**	**sandstone**	**P_3l**	**210/34**	**8/9**	**7/1**	**347.7**	**67.3**	**326.0**	**37.4**	**95.4**	**5.7**	
West Ujimqin													
O07	44°55'N,117°27'E	sandstone	P_2g	20/65	0/4	-	-	-	-	-	-	-	weak NRM, viscous
O08	**44°55'N,117°28'E**	**sandstone**	**P_2g**	**12/68**	**6/8**	**0/6**	**125.9**	**-56.4**	**136.4**	**-30.4**	**35.0**	**10.0**	
O09	44°55'N,117°29'E	sandstone	P_2g	20/60	0/9	-	-	-	-	-	-	-	viscous
O10	**44°55'N,117°28'E**	**sandstone**	**P_2g**	**220/28**	**3/3**	**2/1**	**324.0**	**68.1**	**312.7**	**35.0**	**623.2**	**10.0**	
O11	44°55'N,117°29'E	sandstone	P_2g	225/31	0/5	-	-	-	-	-	-	-	dispersed
		mean Permian (site O02-O11)			**6S/10S**		**167.2**	**-63.9**			**30.4**	**12.3**	
									140.8	**-34.0**	**70.9**	**8.0**	**λ=48.7° φ=3.7° dp=5.2° dm=9.1°**
O12	**45°01'N,117°18'E**	**sandstone**	**C_2a**	**277.5/67.5**	**3/3**	**0/3**	**-**	**-**	**-**	**-**	**-**	**-**	

O13	**45°01'N,117°18'E**	**sandstone**	**C_2a**	**277.5/67.5**	**5/6**	**0/5**	**-**	**-**	**-**	**-**	**-**	**-**	
O14	**45°01'N,117°18'E**	**sandstone**	**C_2a**	**275/65**	**0/1**	**-**	**-**	**-**	**-**	**-**	**-**	**-**	
			mean C_2a		**8s/10s**	**0/8**	**95.2**	**-86.4**	**178.1**	**-19.5**	**41.0**	**9.1**	**λ=55.0° φ=300.6° dp=5.0° dm=9.5°**
O15	44°50'N,116°28'E	sandstone	D_{2-4}	352.5/12	0/5	-	-	-	-	-	-	-	weak NRM, viscous
N13[a]	44°31'N,117°33'E	limestone	P_2z	86/88	3/3	3/0	-	-	-	-	-	-	
N14[a]	44°31'N,117°33'E	limestone	P_2z	91.5/84	3/3	3/0	-	-	-	-	-	-	
N15[a]	44°31'N,117°33'E	limestone	P_2z	93/88	2/2	2/0	-	-	-	-	-	-	
N16[a]	44°31'N,117°33'E	limestone	P_2z	93.5/85.5	2/2	2/0	-	-	-	-	-	-	
N17[a]	44°31'N,117°33'E	limestone	P_2z	93/85	2/2	2/0	-	-	-	-	-	-	
N18[a]	44°31'N,117°33'E	limestone	P_2z	93/85	3/3	3/0	-	-	-	-	-	-	
			mean[a]		11s/11s		23.7	69.5			64.4	5.7	λ=72.8° φ=171.5° dp=8.4° dm=9.8°
									187.9	16.3	39.6	7.3	
N19	44°15'N,117°50'E	limestone	C_2a	80/43	1/3	1/0	-	-	-	-	-	-	
N20	44°15'N,117°50'E	limestone	C_2a	80/43	3/3	3/0	-	-	-	-	-	-	
N21	44°15'N,117°50'E	limestone	C_2a	80/43	0/3	-	-	-	-	-	-	-	
N22	44°15'N,117°50'E	limestone	C_2a	80/43	0/3	-	-	-	-	-	-	-	
N23	44°15'N,117°50'E	limestone	C_2a	80/43	3/3	3/0	-	-	-	-	-	-	
N24	44°15'N,117°50'E	limestone	C_2a	80/43	3/3	3/0	-	-	-	-	-	-	
N25	44°15'N,117°50'E	limestone	C_2a	80/43	1/3	3/0	-	-	-	-	-	-	
N26	44°15'N,117°50'E	limestone	C_2a	80/43	3/3	3/0	-	-	-	-	-	-	
			mean		14s/14s		356.1	61.4	158.4	75.2	24.1	8.3	PEF
					Mongolia Block (MOB)								
Erenhot													
16	44°30'N,111°57'E	red coarse sandstone	$D_{1-2}n$	50/54	5/8	0/5	186.9	-55.9	277.3	-52.8	85.3	8.3	
17[a]	44°30'N,111°57'E	red coarse sandstone	$D_{1-2}n$	50/54	6/8	6/0	52.8	71.3	117.6	33.0	25.5	13.5	
18	44°30'N,111°57'E	pebble	$D_{1-2}n$	50/54	0/5		-	-	-	-	-	-	dispersed

19[a]	44°31'N,111°56'E	red coarse sandstone	$D_{1\text{-}2}n$	164/51	7/7	6/1	5.9	67.2	284.0	43.8	78.0	6.9	
20[a]	44°31'N,111°56'E	red coarse sandstone	$D_{1\text{-}2}n$	164/51	8/8	8/0	2.1	67.8	283.1	42.4	110.0	5.3	
21[a]	44°31'N,111°56'E	red coarse sandstone	$D_{1\text{-}2}n$	190/30	7/8	7/0	2.1	59.7	325.2	46.3	45.0	9.0	
22[a]	44°31'N,111°56'E	red coarse sandstone	$D_{1\text{-}2}n$	177/25	4/4	4/0	345.8	62.7	311.6	50.2	143.0	7.7	
23[a]	44°31'N,111°56'E	red coarse sandstone	$D_{1\text{-}2}n$	276/22	6/8	6/0	7.9	59.3	14.7	38.1	92.0	7.0	
24[a]	44°31'N,111°56'E	red coarse sandstone	$D_{1\text{-}2}n$	206/77	5/5	5/0	3.1	60.7	322.8	0.6	137.0	6.6	
			mean[a]		7S/7S		5.7	65.4			89.7	5.9	λ=85.0° φ=162.6° dp=7.8° dm=9.6°
									315.1	51.1	3.6	34.3	
East Ujimqin													
N27[a]	45°22'N,116°59'E	volcanoclastic rock	C_2-P_1g	277.3/83.7	4/5	4/0	18.7	67.3	11.7	-16.3	24.5	18.9	
N28(LTC)[a]	45°22'N,116°59'E	volcanoclastic rock	C_2-P_1g	285/76.5	7/7	7/0	44.4	62.0	28.6	-11.0	40.7	9.6	
N28(HTC)[b]	45°22'N,116°59'E	volcanoclastic rock	C_2-P_1g		5/7	0/5	213.2	-17.4	225.7	54.2	89.5	10.4	λ=43.7° φ=248.5° dp=5.6° dm=10.8°
N29(LTC)[a]	45°22'N,116°59'E	volcanoclastic rock	C_2-P_1g	107.5/84	4/8	4/0	52.5	46.8	167.0	39.4	54.4	12.6	
N29(HTC)[b]	45°22'N,116°59'E	volcanoclastic rock	C_2-P_1g		4/8	0/4	216.7	-22.4	330.8	-65.3	65.5	8.9	λ=44.1° φ=242.5° dp=5.0° dm=9.4°
N30(LTC)[a]	45°22'N,116°59'E	volcanoclastic rock	C_2-P_1g	104/84	6/6	6/0	46.3	72.5	184.1	20.6	106.0	6.5	
N30(HTC)[b]	45°22'N,116°59'E	volcanoclastic rock	C_2-P_1g		5/6	0/5	205.2	-28.0	349.5	-65.5	100.0	8.8	λ=52.9° φ=254.0° dp=5.3° dm=9.6°
N31[a]	45°22'N,116°59'E	volcanoclastic rock	C_2-P_1g	104/84	9/9	9/0	68.6	60.8	38.2	-4.4	91.3	5.4	
N32[a]	45°22'N,116°59'E	volcanoclastic rock	C_2-P_1g	281.5/75.5	7/7	7/0	33.0	57.0	23.5	-16.3	41.0	9.5	
			mean[a](except three HTC)		6S/6S		45.3	62.4			47.7	9.8	λ=58.1° φ=193.4° dp=11.9° dm=15.3°
									196.7	18.1	15.5	17.6	

Abbreviations. n'/ n: number of samples used to calculation/ measured sample number; N/R: normal/reversed polarity; Dg, Ig, Ds, Is: declination (D) and inclination (I) in in-situ (g) and tilt-corrected (s) coordinates; k: the best estimate of the precision parameter; α_{95}: the radius that mean direction lies within 95% confidence; S, s: number of sites (S) or samples (s) used to determine pole; λ and φ: latitude and longitude of paleomagnetic pole; dp/dm: semi-axes of the confidence ellipse of paleomagnetic pole. S_3x: upper Silurian Xibiehe Formation

(Fm); $D_{1\text{-}2}n$ and D3s: lower-middle Devonian Niqiuhe Fm and upper Devonian Seribayanaobao Fm; C_1g, C_1h and C_2a: lower Carboniferous Gouhuduge Fm, lower Carboniferous Houfangshengou Fm, and upper Carboniferous Amushan Fm; $C_2\text{-}P_1g$: upper Carboniferou-lower Permian Gegenaobao Fm; P_1d, P_2z, P_3l and P_3t: lower Permian Dashizhai Fm, middle Permian Zhesi Fm, upper Permian Linxi and Tieyingzi Fm, respectively.

Sites in bold are considered to be primary remanences. Detailed discussion is in the text.

[a] *Early Cretaceous remagnetized. Detailed discussion is in the text.*

[b] *Early Permian remagnetized. Detailed discussion is in the text.*

When sun measurements were not available, the average value of the locality was used to correct the orientation of the samples. Overall, about 680 cores of 86 sites were sampled from nine localities, covering most areas of central-eastern InnerMongolia (Fig. 6-1b and Table 6-1). It is worth noting that a considerable effort has been made to find all possible outcrops in this area for paleomagnetic sampling.

6.2 Measurement results

6.2.1 Magnetic mineralogy

Three main types of magnetic carriers are identified from both thermomagnetic experiment and IRM measurement. (a) 55 out of 86 sites show magnetite is the main magnetic carrier as revealed by the sharp drop of the magnetic susceptibility at 550°C-585°C during thermomagnetic experiments (Figs. 6-3a and 6-3b) and by the rapid increase of the IRM until to a total magnetic saturation at about 300 mT (Fig. 6-3f-1). (b) For 22 out of 86 sites, both magnetite and hematite may coexist as the main magnetic carriers, as deduced from the successive drops of the magnetic susceptibility from 580°C until to 680°C (Fig. 6-3c), and the relatively rapid increase of IRM at the weak applied field but without a total saturation at about 1.0 T (Fig. 6-3f-2). (3) For 9 out of 86 sites, hematite as the main magnetic carrier was indicated from the linear increase of IRM up to about 1.0 T without a total saturation (Fig. 6-3f-3), and with no drop at ca. 120°C of the magnetic susceptibility. Meanwhile, mineral transformation is often observed during the thermomagnetic experiments. The heating curve of the Curie temperature measurements displays a rapid increase of the magnetic susceptibility at about 150°C followed by a slow increase to reach a peak at about 300°C, which may correspond to the transformation of goethite and/or pyrite into pyrrhotite and/or magnetite. In addition, the abrupt decrease from 300°C to 400°C is potentially due to maghemite destabilization (Figs. 6-3a and 6-3c). For 35 out out of 86 sites, heating and cooling thermomagnetic curves do not coincide, and the rapid increase of magnetic susceptibility during the cooling also indicates mineral oxidation during experiments (Figs. 6-3d and 6-3e). However, it seems that mineral

transformation does not disturb the thermal demagnetization, as in the majority of cases, specimens display a relatively stable remanent direction.

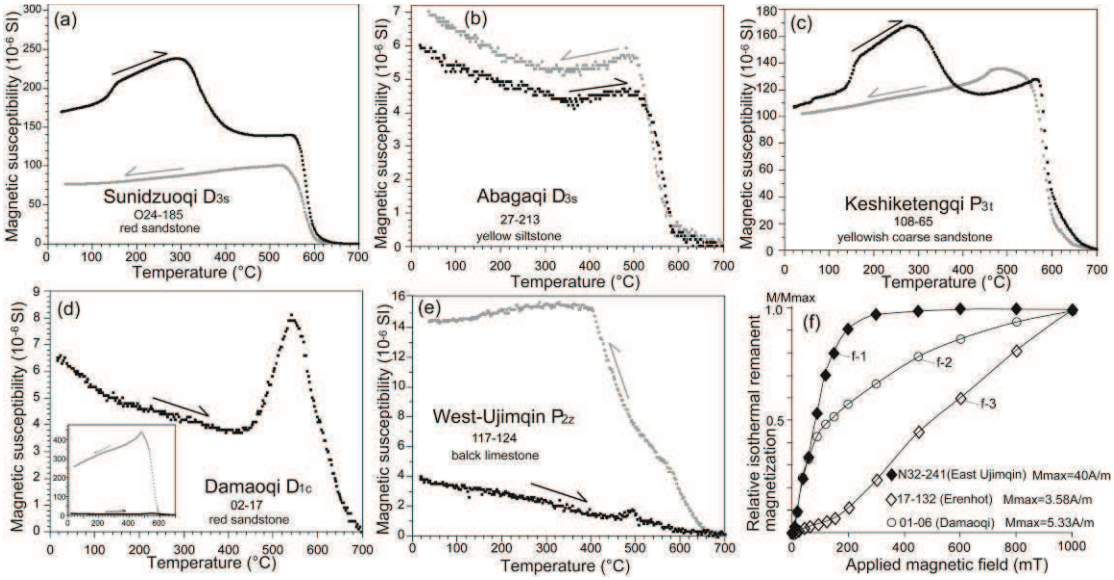

Figure 6-3 Representative results of thermo-magnetic experiments (a-e) and isothermal magnetization measurements (IRM, f) showing different magnetic carries. Sample name, site locality, stratigraphic age and lithology are shown on each figure.

6.2.2 AMS results

The AMS results for each site are presented in Table 6-2. For each locality except East Ujimqin, the equal-area projection of the principal axes of the magnetic susceptibility (Fig. 6-4a) shows nearly horizontal K_1 (D=243.5°, I=8.8°) axes and highly inclined K_3 axes (D=102.5°, I=78.8°) in tilt corrected coordinates, which well define a horizontal fabric consistent with the initial sedimentary bedding. Meanwhile, the K_3 axes are better clustered after unfolding with the maximum/minimum radius at 95% confidence of mean K_3 axes lies at 48.5°/35.2° in in-situ coordinates and 28.7°/25.6° in tilt-corrected coordinates. All samples show a relatively weak anisotropy degree with P_J<1.08 (Fig. 6-4b), suggesting that, at least at the sample scale, these rocks have not experienced intense deformation since their formation. Conversely, the dataset of the volcaniclastic rocks from East Ujimqin show well-clustered and nearly horizontal K_1, but K_3 directions are distributed along a girdle (Fig. 6-4c). Such pattern, combining with the relatively high and heterogeneous

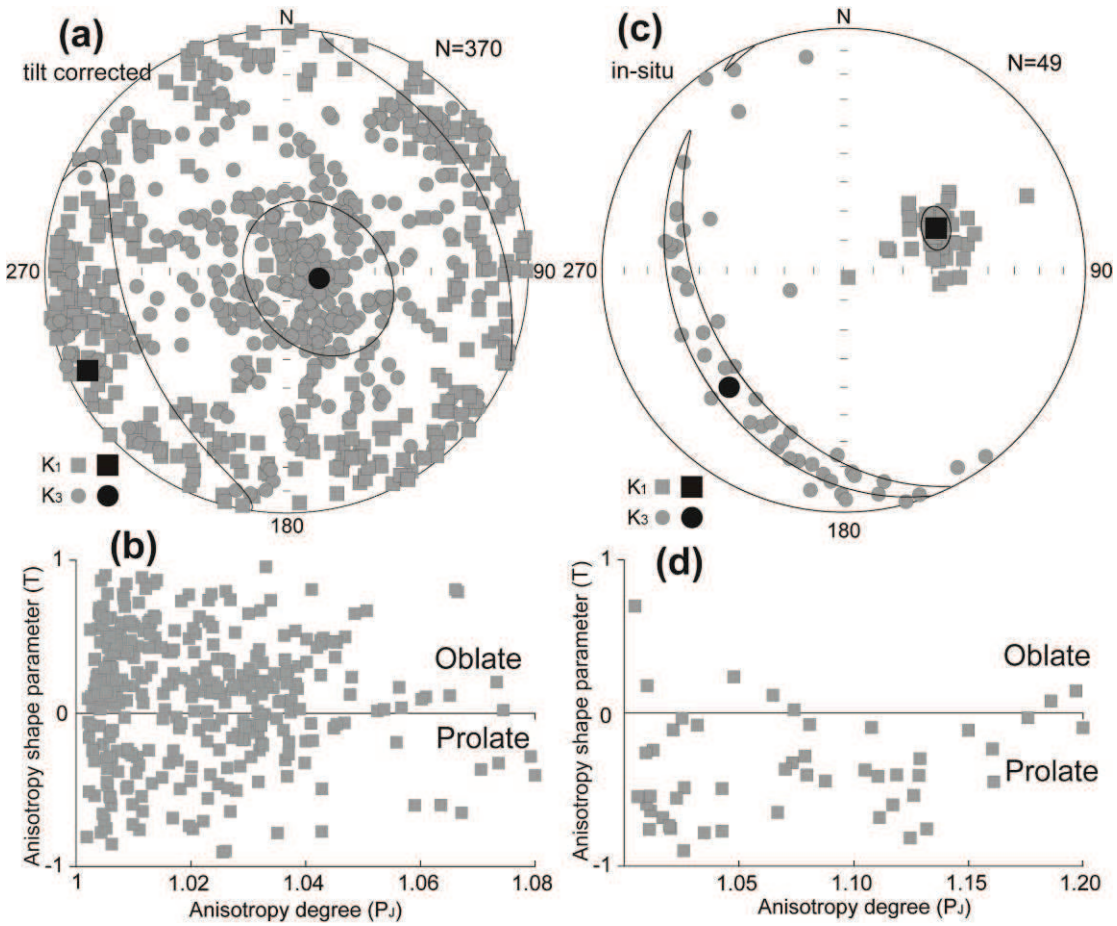

Figure 6-4 Results of Anisotropy of Magnetic Susceptibility (AMS) measurements. P_J is anisotropy degree and T is anisotropy shape parameter; K_1, K_2 and K_3 are the maximum, intermediate and minimum anisotropy axes, respectively. $P_J = \exp\{2[(\ln K_1-\ln K_m)^2+(\ln K_2-\ln K_m)^2+(\ln K_3-\ln K_m)^2]^{1/2}\}$, and $T= 2\ln(K_2/K_3)/\ln(K_1/K_3)-1$. (a) and (b): equal-area projection of K_1 and K_3 directions in tilt corrected coordinates and the corresponding plots of anisotropy degree (P_J) versus anisotropy shape (T) of magnetic susceptibility for all the samples in Appendix table 1 except site N27-N32; (c) and (d): equal-area projection of K_1 and K_3 directions in in-situ coordinates for the volcanoclastic samples from East Ujimqin (site N27-N32) and the corresponding plots of anisotropy degree (P_J) versus anisotropy shape (T) of magnetic susceptibility (Jelínek, 1978)

*Table 6-2: Anisotropy of Magnetic Susceptibility data for the sites that are included in mean direction calculations**

site	n	Km	st-deviation	P_j	T	K_1				K_3			
		(10^{-6}SI)	(10^{-6}SI)			Dec(°)	Inc(°)	α_{95}max	α_{95}min	Dec(°)	Inc(°)	α_{95}max	α_{95}min
01	10	4.02E-04	2.29E-05	1.032	-0.216	284.9	22.2	7.7	4.3	152.4	58.9	9.2	3.6

02	11	1.41E-04	6.52E-06	1.033	0.169	253.6	25.9	7.8	4.4	111.2	58.4	6.2	2.5
03	8	3.67E-04	7.32E-05	1.053	-0.023	263.2	12.5	8.2	3	79.4	77.4	11.2	4.6
04	7	2.89E-04	7.03E-05	1.034	0.129	263.6	1.1	11.4	5.4	358.7	77.5	11.8	6.1
05	7	2.86E-04	6.75E-05	1.031	0.179	264.3	0.4	15.7	10.5	173	74.5	14	10.6
06	7	2.84E-04	5.99E-05	1.039	-0.114	268.6	18.8	6.5	5	116.8	68.9	7.8	6.1
07	8	3.48E-04	6.64E-05	1.04	0.247	259.2	5	19	1.5	114.9	83.8	10.7	2.9
08	8	3.09E-04	4.86E-05	1.045	0.582	310.2	19.7	55.2	15.2	110.7	69.2	31.9	10
09	9	1.01E-04	9.03E-05	1.015	-0.091	66.7	4.2	29.8	12.5	160.7	44	17.5	13
10	11	1.70E-04	1.07E-04	1.009	0.239	54	2.9	16.6	7.7	177.8	84.8	18.9	13.1
12	10	2.83E-04	4.26E-05	1.013	-0.123	255.5	10.7	11.2	5.8	129.2	72.3	18	6.8
13	9	3.63E-04	1.71E-05	1.024	0.235	97.9	16	32.7	3.1	207.5	49.4	13.5	7.5
14	9	1.57E-04	3.90E-05	1.014	0.462	50.5	14	22	4.3	172.5	64.8	13.7	3.8
15	9	3.30E-04	2.37E-05	1.02	0.235	234.1	0.6	35.9	13.1	328	81.1	29.2	18.7
16	8	1.55E-04	2.22E-05	1.012	0.36	139.6	27.4	44.1	9.8	252.9	37.3	28.4	9.7
17	9	2.89E-04	1.54E-04	1.01	0.366	113.2	18.7	18.7	6.2	270.9	70	9.9	6.5
18	8	1.53E-04	4.65E-05	1.048	0.413	110	14.9	33	8.7	18.9	4.3	58.4	8.1
19	9	3.92E-04	8.46E-05	1.008	0.176	317.5	24.2	21.4	17.4	96.6	59.3	23.9	20.3
20	9	3.88E-04	8.35E-05	1.006	0.322	35.7	17.2	27.6	8	203.8	72.4	24	8
21	9	1.56E-04	4.65E-05	1.006	0.308	223.5	81.7	66.4	14.9	53.6	8.2	51	20
22	8	2.17E-04	4.37E-05	1.003	-0.154	259.3	57.7	43	24.2	31.6	22.9	68.4	20.5
23	10	3.39E-04	1.12E-04	1.007	0.289	249.5	4.8	73.7	10.3	148.7	65.7	12.5	7.6
24	7	2.34E-04	3.00E-05	1.005	-0.099	330.2	4.7	13.6	8.7	61.4	14.5	32.1	6.4
N01	8	4.03E-05	1.37E-05	1.021	-0.414	127.8	73.7	21.1	9.2	15.1	6.4	70.7	11.3
N02	11	2.28E-05	8.40E-06	1.032	-0.004	46.4	1.6	13	10.3	315.4	30.7	27.8	12.6
N03	12	1.42E-05	6.93E-06	1.049	0.038	47.9	18	54.4	15.9	302.3	39.7	23.6	17.3
N04	8	3.41E-05	1.62E-05	1.018	0.236	69	31.6	83.2	28.8	291	50.4	38.2	32.2
N05	9	9.45E-06	4.37E-06	1.088	0.335	27.6	1.4	57.2	12.7	296.8	28.9	14.2	9.9
N06	8	1.74E-05	6.60E-06	1.054	0.474	241.2	35.4	82.9	9.3	143.7	10.4	13.7	3.7
N07	8	2.83E-05	5.96E-06	1.032	0.44	247.2	66.3	41.7	7.2	134.9	9.4	8.5	7.1
N08	6	1.20E-02	3.76E-03	1.022	0.275	45.4	13.5	29.9	9	300	48	45.6	12.7
N09	7	1.78E-02	3.94E-03	1.041	0.174	46.5	15.1	8	2.7	203.1	73.6	11.2	5.3
N10	6	7.58E-03	2.37E-03	1.027	-0.233	201.8	17.5	13	3.5	56.9	69	27.1	4.9
N11	7	4.72E-03	2.81E-03	1.022	-0.084	210.2	33.8	9.2	3.6	112.3	11.5	55.6	5
N12	6	6.03E-03	1.14E-03	1.027	-0.414	199.1	22.8	6.2	3.2	74.5	53.5	17.3	3
N13	7	2.15E-05	4.20E-06	1.036	-0.274	203.4	31.6	14.3	8.8	337.4	48.5	32.3	12.9
N14	6	2.76E-05	9.12E-06	1.073	0.165	270.1	10.5	42.6	5.3	172.2	36.6	33.9	3.7
N15	6	3.13E-05	8.28E-06	1.075	-0.256	103.2	5.1	5.7	3.3	206.8	69.2	27	2.9
N16	6	2.25E-05	1.35E-06	1.031	-0.135	99.8	17.2	45.5	3.2	202	34.4	13.1	4.2
N17	6	3.65E-05	8.61E-06	1.051	-0.117	100	4.1	23.5	2.9	195.1	51.1	49.5	3
N18	5	3.21E-05	7.54E-06	1.045	0.026	104.3	3.2	31.7	3	200	60.8	32.7	2.8
N27	7	3.76E-03	3.81E-03	1.126	-0.282	220	11.9	8.5	3.3	24.3	77.7	31.6	8.4
N28	7	2.07E-03	2.88E-03	1.057	-0.446	221.1	11.9	3.9	2.9	316.7	24.9	23	2.1
N29	8	2.25E-04	9.17E-05	1.017	-0.258	171.7	23	10.8	2.7	316	62.5	26.4	2.7
N30	9	2.52E-03	5.81E-03	1.036	-0.408	176.4	10.3	43.8	6.7	323.9	77.9	27.5	7.4

N31	8	9.44E-03	4.62E-03	1.1	-0.409	215.1	9.6	4.3	3.3	10.9	79.5	17.1	3.3
N32	10	2.40E-03	2.00E-03	1.115	-0.325	219.8	9	4	2.2	311.2	8.7	15.2	2.6
O05-06	9	2.20E-04	2.17E-05	1.028	-0.053	283	10.9	29.9	9.1	188.2	23.4	16.8	9.6
O07-14	11	4.64E-03	9.30E-03	1.058	0.514	30	22.4	13.8	12.2	120.3	0.6	23.4	4.9
O16-17	9	1.88E-03	6.55E-04	1.033	0.256	182.7	0.2	21	4.6	91.6	80.2	4.9	2.7
O23-25	9	3.41E-03	2.14E-03	1.036	0.346	359	11.9	10.6	4.7	210.7	76.1	6.2	4.5

** Site numbers are the same as that of Table 1. Samples from Upper Devonian in Abagaqi (site 25-30) and Upper Carboniferous in West Ujimqin (site N19-N26) are excluded as no mean directions or PEF directions are calculated.*

Abbreviations. $P_J = exp\{2[(lnK_1-lnK_m)^2+(lnK_2-lnK_m)^2+(lnK_3-lnK_m)^2]^{1/2}\}$, *and* $T= 2ln(K_2/K_3)/ln(K_1/K_3)-1)$. K_1 *and* K_3 *are principal axes of the magnetic fabrics.* K_1*: magnetic lineation;* K_3*: pole of the magnetic foliation; Dec/Inc: declination/inclination.* $\alpha_{95}max/\alpha_{95}min$*: the maximum/minimum radius that mean direction lies within 95% confidence.*

values of P_J (Fig. 6-4d), indicates a prominent prolate shape for the fabric. This may be due to a post-deposition deformation, which is compatible with our field observation of vertical dextral strike-slip fault in the vicinity of sampling (Fig. 6-2l). Meanwhile, both the K_1 and K_3 axes are better clustered in in-situ coordinates than in tilt corrected coordinates, suggesting that the magnetic fabric may be secondary.

6.2.3 Paleomagnetic directional analysis

6.2.3.1 North margin of NCB

Damaoqi area (S_3x and D_1c)

The natural remanent magnetization (NRM) intensities of yellow sandstone samples of the Upper Silurian Xibiehe Formation (S_3x) are in the range of 0.25 mA/m to 38.7 mA/m. Among them, two sites (Site 12 and 14) display weak NRM (lower than 1 mA/m) and strong viscosity, and no stable paleomagnetic component can be isolated (Table 6-1). For others, two components were isolated from most of the samples after progressive thermal demagnetization. The low temperature component

(LTC) up to 150°C displays random directions (Figs. 6-5a and 6-5b). The high temperature component (HTC), isolated from 200°C to 680°C, shows two types of direction before bedding adjustments (Table 6-1; Figs. 6-5a and 6-5b).

For the red sandstone of the Lower Devonian Chaganhebu Formation (D_1c), NRM intensities range from 1 mA/m to 202 mA/m with most of them >10 mA/m. For most of the samples, only one component was isolated from room temperature to 680°C (Table 6-1 and Fig. 6-5c). In addition, few samples display two components with random low-middle temperature component (LMTC, up to 500 °C) and reversed HTC (Fig. 6-5d) before tilt correction. The Enkin's direction-correction (DC) fold test is negative for this locality. Except two sites with north-northeast declination and steeply downward inclination (Sites 1 and 3) and one dispersed site (Site 5), the 5 remaining sites display shallow upward inclination and variable declinations ranging from 110° to 315° (Table 6-1).

Aohanqi area (C_1h)

The NRM intensities of black limestone samples of the Lower Carboniferous Houfangshengou Formation (C_1h) range from 0.5 mA/m to 22.6 mA/m. Two components were isolated from most measured samples. After removing a dispersed viscous component up to 200°C or 2 mT, a stable component was isolated with both normal and reversed polarities before bedding adjustments (Figs. 6-5e and 6-5f). A mean direction has been calculated (Table 6-1), and it fails to pass the fold test as the directions are much better clustered before unfolding (Fig. 6-6b).

6.2.3.2 Inner Mongolia Block

Sunidzuoqi area (D_3s)

For the red coarse sandstone of the Upper Devonian Seribayanaobao Formation (D_{3s}), two components of magnetic directions have been isolated from 4 out of 5 sites. The LTC is characterized by prominently viscous and dispersed directions (Fig. 6-5g). After cleaning this viscous magnetic remanence up to 250°C, three sites (O17, O24 and O25) display a uniform reversed polarity in tilt-corrected coordinates, except one sample in Site O25 presents normal polarity (Fig. 6-5g and Table 6-1). Site O16

presents normal polarity, which is much different from other sites. Therefore, we have calculated a mean direction for these three sites (Table 6-1). The fold test is inconclusive but the directions are better clustered after unfolding (Fig. 6-6c). All 5 Lower Carboniferous sites (sites O18 to O22) show weak NRM intensity ranging from 0.25 mA/m to 5.94 mA/m or high viscosity, with no reliable direction obtained (Table 6-1).

Abagaqi area (D_3s)

For the yellow siltstone of the Upper Devonian Seribayanaobao Formation, all specimen present weak NRM values with a range of 0.41 mA/m to 3.69 mA/m. Furthermore, most samples present highly viscous features during demagnetization, since we observe a more than 90% drop of the magnetic intensity after heating up to 150°C. Consequently, no reliable direction was isolated from this locality.

Keshiketengqi area (P_3t)

For the coarse sandstone of the Upper Permian Tieyingzi Formation, The NRM intensities are relatively high, ranging from 46.4 mA/m to 227 mA/m. Only one component has been isolated from all analyzed samples (Fig. 6-5h), and a mean direction has been calculated for these five sites (Table 6-1). The site-mean directions are better clustered before bedding corrections, indicating a negative fold test (Fig. 6-6d).

Linxi area (late P_1d and P_3l)

For the upper part of the tuff and basalt of the Lower Permian Dashizhai Formation (P_1d), NRM intensities vary from 1.91 mA/m to 1.89 A/m. By thermal demagnetization, a random LTC has been isolated below 300°C. Thereafter, a HTC up to about 600°C has been observed and displays southeastward declination and upward inclination in tilt-corrected coordinates (Figs. 6-5i).

For the sandstone of the Upper Permian Linxi Formation (P_3l), After removing a low LTC until about 200°C, the remanent magnetization show a stable decrease of magnetic remanence from the origin up to 550°C. All samples except one display a normal polarity (Table 6-1). Site O01 displays northward declination and steeply downward inclination in in-situ coordinates (Table 6-1). The tilt-corrected directions

for the other two sites display consistent northwestward declination and downward inclinations (Fig. 6-5j).

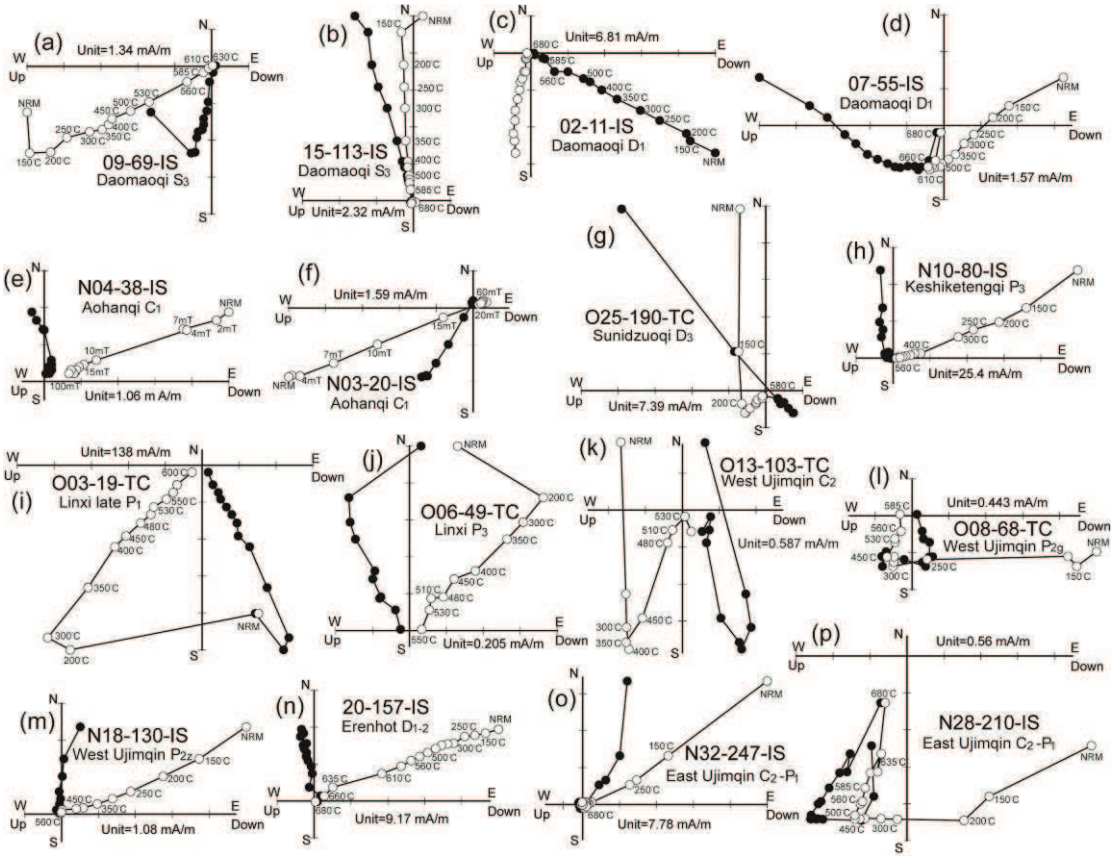

Figure 6-5 Orthogonal vector plots of representative specimens from each sampled age/locality group. Closed (open) symbols present the projection in horizontal (vertical) plane. IS (in-situ) and TC (tilt-corrected) stands for plot in in-situ and tilt-corrected coordinates. Sample name, site locality and stratigraphic age are shown on each figure.

West Ujimqin area (C_2a, P_2g and P_2z)

For the limestone of the Upper Carboniferous Amushan Formation (C_2a), after removing the random LTC until 200°C, all samples show normal polarity before bedding correction and a mean direction has been calculated, which is close to that of the Present Earth Field (PEF; Table 6-1). Only 8 specimens from three sandstone sites of Amushan Formation were successfully demagnetized, and all display reversed polarity (Fig. 6-5k) and a mean direction has been calculated (Table 6-1).

For the Middle Permian yellow sandstone of the Gegenaobao Formation (P_2g), most of samples display weak values of NRM (lower than 1 mA/m) and no reliable direction has been obtained except for Site O08 and O10 (Table 6-1). For specimens

of site O08, after removing the viscous LTC up to about 300 °C, the remanent magnetization linearly decreases to the origin at 585°C, with solo reversed polarity (Figs. 6-5l), while Site O10 displays antipodal normal and reversed polarities (Table 6-1).

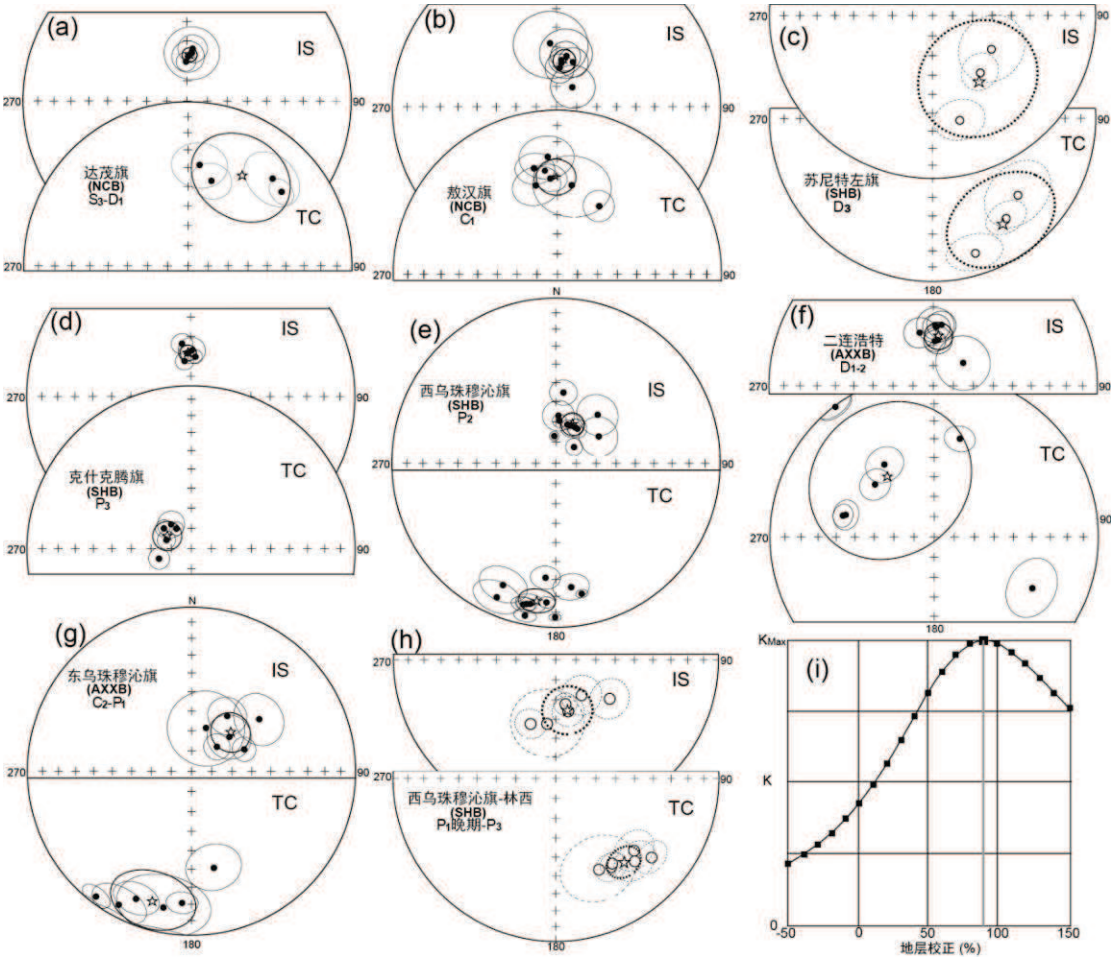

Figure 6. Equal-area projection plots of site-mean directions of studied localities (a-h, data from Table 1). Closed (open) symbols present downward (upward) magnetic directions. Star symbols present the mean directions. IS (TC) stands for in situ/geographic (tilt-corrected/ stratigraphic) coordinates. (i) Enkin (2003) DC fold test: progressive unfolding showing a significant clustering of magnetic directions after bedding corrections at 90% untilting for the 6 Permian sites from West Ujimqin-Linxi area showing in (6h).

For the limestone of the Middle Permian Zhesi Formation (P_2z), after cleaning the low temperature up to 150 °C, all measured samples show consistent directions (Fig. 6-5m) before bedding corrections and a mean direction has been calculated (Table 1). The directions are better clustered before bedding correction (Fig. 6-6e) indicating a

negative fold test.

6.2.3.3 South margin of MOB

Erenhot area ($D_{1\text{-}2}n$)

For the red coarse sandstone of the Lower-Middle Devonian Niqiuhe Formation ($D_{1\text{-}2}n$), only one component is isolated from progressive demagnetization, but samples from these nine sites display variable directions. Site 16 yields magnetic directions of reversed polarity. Site 18, which was selected for conglomerate test, displays scattered directions. All other 7 sites, except one sample from Site 19, display a consistent unique normal polarity (Figs. 6-5n and 6-6f) in-situ coordinates and a mean direction has been calculated (Table 6-1). Although the pebbles give scattered directions, the site-mean directions are better grouped before tilting, suggesting the data fail to pass the fold test (Fig. 6-6f).

East Ujimqin (C_2-P_1g)

For the volcaniclastic rocks of the Upper Carboniferous-Lower Permian Gegenaobao Formation (C_2-P_1g), Only one component has been isolated from three sites (Sites N27, N31 and N32), and two components have been isolated from the other three (Sites N28, N29 and N30). The directions from three single-component sites are consistent with that of the LTC deduced from the three dual-component sites (Figs. 6-5o and 6-5p) and a mean direction has been calculated (Table 6-1). The site-mean directions of these 6 sites are better grouped before tilting, indicating a negative fold test (Fig. 6-6g). The HTC isolated from three dual-component sites displays a solo reversed polarity (Fig. 6-5p). The site-mean directions for these three sites are better grouped before bedding correction, also indicating a negative fold test.

6.3 Calculations of paleomagnetic poles

Magnetic mineralogy studies reveal that titanium-poor magnetite with, sometimes, hematite are the main magnetic remanent carriers with subordinate magnetic minerals, such as goethite, pyrrhotite and maghemite. AMS measurements suggest that all collected rocks, except those from East Ujimqin, have not experienced

intense deformation since their formation and maintain their original sedimentary magnetic fabric. Seventeen out of the 86 analyzed sites present either too weak magnetic remanent intensity or strong viscosity (Table 6-1) to provide reliable paleomagnetic directions. Besides, for 4 sites, specimens display scattered directions that hinder calculation of the site-mean direction. All these 21 sites are rejected for further discussion.

6.3.1 Primary magnetizations

6.3.1.1 Late Devonian

Three Late Devonian sites from Sunidzuoqi show a uniform reversed polarity except one sample in Site O25 displaying an antipodal normal polarity (Table 6-1). Although the fold test is inconclusive due to probably the similarity of bedding attitude, the features that the precision parameter has been well improved after bedding corrections with a ratio of 1.35 for k_s/k_g and the coexistence of antipodal normal and reversed polarities may suggest that the magnetic remanence was at least acquired before the folding. The folding age cannot be, however, estimated by local stratigraphic contacts. At the regional scale, the Upper Devonian-Upper Permian strata are folded or highly tilted, and unconformably covered by the Late Permian conglomerate; therefore, the folding took place during the Late Permian. Meanwhile, the coexistence of antipodal normal and reversed polarities and inexistence of the Early Permian magmatic rocks around sampling places exclude the Early Permian remagnetization, which displays only reversal polarity due to the Permo-Carboniferous Reversed Superchron (PCRS), ranging from 320Ma to 263Ma (Garcia et al., 2006; Cottrell et al., 2008). Thus, the magnetic remanence may be considered as primary and a Late Devonian paleomagnetic pole has consequently been calculated for IMB at λ=46.8°N, φ=349.1°E, dp=14.6°, dm=27.3° with N=3 sites, or λ=43.6°N, φ=356.9°E, dp=5.6°, dm=10.4° with n=17 samples (Table 6-1).

6.3.1.2 Permian

Two sites of Early Permian basalt and two sites of Late Permian sandstone from Linxi, and two site of Middle Permian sandstone from West Ujimqin display similar

or antipodal directions after bedding corrections (Figs. 6-5i, 5l and 6-5j). Zircon U-Pb geochronology yielded ages ranging between 285Ma and 270Ma for the basalt sites (Zhang et al., 2008; Liu, 2009). Our unpublished zircon U-Pb dating provides a Middle Permian age assignment for the sandstone, which overlies the basalt directly. In addition, the solo reversed polarity suggests that the magnetic remanence has been acquired before <263 Ma, which is the upper limit of PCRS. Similarly, the age of the Linxi Formation sandstone is well constrained by abundant plant fossils and detrital zircon geochronology (256 Ma for the youngest grain) (Han et al., 2011). Meanwhile, its chiefly normal polarity may suggest that the magnetic remanence was acquired shortly after ～263 Ma, the upper limit of PCRS. All these rocks were deposited during a period of ca. 30Ma, but they display similar or antipodal magnetic directions (Figs. 6-5i, 6-5j and 6-5l). This indicates a relatively stable paleolatitude for IMB from late Early Permian to Late Permian. Therefore, we have calculated a mean direction for these 6 sites at D_g=167.2°, I_g=-63.9°, k_g=30.4, α_{95g}=12.3°; D_s=140.8°, I_s=-34.0°, k_s=70.9, α_{95s}=8.0° (Fig 6-6h; Table 6-1). Enkin's fold test is positive with maximum value of k parameter at 90% (Figs. 6-6h and 6-6i), and it also pass the reversal test (McFadden and McElhinny, 1990), suggesting that the magnetic remanences were obtained before folding. As discussed above, the folding age is probably of the Late Permian. Therefore, we consider that the remanences were acquired during deposition. Thus, a late Early Permian - Late Permian paleomagnetic pole has been calculated for IMB at λ=48.7°N, φ=3.7°E, dp=5.2°, dm=9.1° with N=6 (Table 6-1).

Table 6-3 Compilation of late Devonian and Permian palaeomagnetic data of North China Block, Inner Mongolia Block, Mongolia Block and Siberia Block

Age	Slat (°N)	Slong (°E)	N	Plat (°N)	Plong (°E)	A95(°) (dp/dm)	test	reference
North China Craton (NCB)								
P_2	39.6	98.0	33s	42.4	350.9	3.9	F	Meng et al., 1990
P_2			11L	50.3	355.2	5.7	F	Yang et al.,1998
P_2	37.8	112.3	12S	44.0	358.0	6.9	F	McElhinny et al., 1981
P_2	37.5	114.4	4S	47.1	356.9	7.7	F	Zhao et al.,1989
P_1	37.6	101.3	5S	23.9	21.2	12.8/21.4	F	Wu et al.,1993

D_3	37.4	105.7	16S	34.2	228.7	8.8	F+R	Zhao et al.,1993
D_{2-3}	37.7	106.0	14S	56.0	336.0	9.2	F+R	Huang et al., 2000
Songliao-Hunshandake Block (SHB)								
Late P_1-P_3	43.7	118.4	6S	48.7	3.7	5.2/9.1	F	This study
D_3	43.5	113.5	3S	46.8	349.1	14.6/27.3	-	This study
Mongolia Block (MOB)								
P_3	48.1	105.9	27s	11.3	35.19	5.4/9.1	F	Pruner, 1987
P_3	51.5	115.4	14S	20.5	200.6	14.5	F	Xu et al., 1997
P_2	50.6	116.9	14S	8.3	183.9	9.5/16.2	F	Kravchinsky et al., 2002b
P_1	51.5	115.4	5S	33.8	207.8	26.3	F	Xu et al., 1997
P_1	47.8	107.1	4S	44.8	335.1	11.6	F	Pruner,1992
P	48.3	106.0	52s	32.8	11.8	5.8/9.9	F	Pruner, 1987
D_3	54.0	123.5	5S	40.5	352.4	9.0/16.7	F+R	Kravchinsky et al., 2002a
D_{2-3}	54.0	123.5	7S	24.6	12.9	8.7/16.9	F+R	Kravchinsky et al., 2002a
Siberian Block (SIB)								
P_3(250)	64.6	114.7	9L	50.8	149.6	9.4	-	Kravchinsky et al., 2002c
P_3(250)			7L	56.2	151.7	3.8	-	Veselovsky et al., 2003
P_3(251)	67.5	104.0	8S	55.1	147.0	5.0	-	Pavlov et al., 2007
P_3(251)	67.0	89.0	8S	57.2	151.1	4.0	-	Pavlov et al., 2007
P_2	50.8	107.2	15S	63.1	151.0	13.5/15.0	F	Kravchinsky et al., 2002b
P_1(275)	51.7	104.1	5S	50.5	121.4	16.9	BC	Pisarevsky et al., 2006
D_3(360Ma)	64.0	116.0	11L	11.1	149.7	8.9	-	Kravchinsky et al., 2002c

Abbreviations. N: the number of sites (S), samples (s) or localities (L) used for calculation; Slat (Plat): the latitude of sampling site (pole); Slong (Plong): the longitude of sampling site (pole); A95: the radius that mean pole lies within 95% confidence, in degree; dp/dm: semi-axes of the confidence ellipse of palaeomagnetic pole; F: fold test; R: reversal test; BC: baked contact test.

6.3.2 Secondary magnetizations

All other 54 remaining sites (including the Late Silurian and Early Devonian of Damaoqi, Early Carboniferous of Aohanqi, Late Permian-Early Triassic of Keshiketengqi, Late Carboniferous and Middle Permian of West-Ujimqin, Early-Middle Devonian of Erenhot and Late Carboniferous-Early Permian of East-Ujimqin) fail to pass Enkin's DC fold test, suggesting post-folding remagnetizations. Two groups of directions have been identified: (a) southward (southeastward and southwestward) declinations and shallow upward inclinations (Figs. 6-5c, 6-5d and 6-5p); (b) northward declinations and steeply downward inclinations or antipodal southward declinations and steeply upward inclinations (Figs.

6-5f, 6-5h, 6-5m and 6-5n).

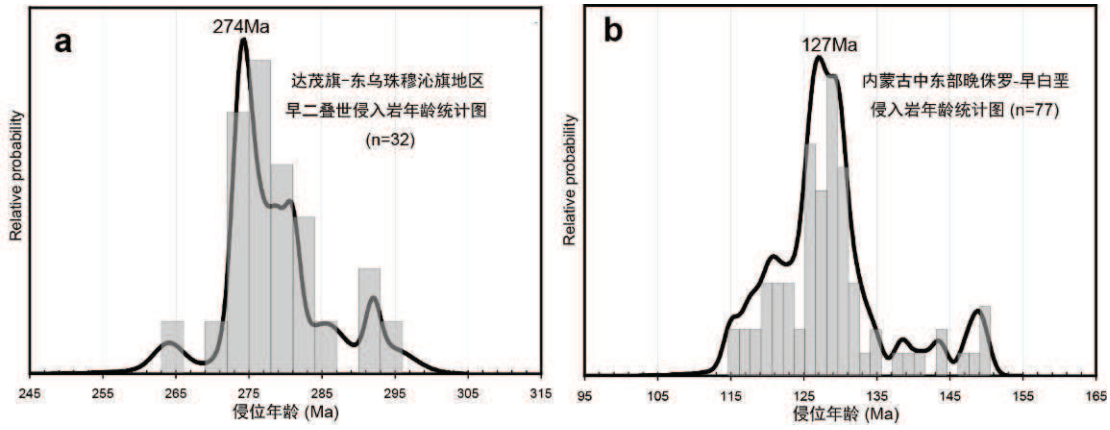

Figure 7. a: Synthesis of geochronological data of the Permian magmatic event around Damaoqi and East Ujimqin (n=32), illustrating the activity peak at 274 Ma, which may be responsible for the Early Permian remagnetization in these two localities. Individual data are from Zhang et al., 2008; Liu, 2009; Luo et al., 2009; Zhao et al., 2011; Chen et al., 2012. b: Synthesis of geochronological data of the Late Jurassic-Early Cretaceous magmatic event in Inner Mongolia and southern Mongolia, showing the activity peak at 127 Ma (n=77), which may be responsible for the Early Cretaceous widespread remagnetization in Inner Mongolia. Individual data are from Liu et al., 2005; Wu et al., 2005; Wei et al., 2012; Daoudene et al., 2012.

The directions of HTC of five sites from the Early Devonian red sandstone in Damaoqi (D_{1c}) and of three sites from vocanochalstic rocks in East Ujimqin (C_2-P_{1g}) show the solo reversed polarity (Table 6-1). Moreover, these sites are located close to Early-Middle Permian granitic plutons and volcanic rocks. In addition, a review of the literature concerning Permian magmatism around these two localities has shown a peak emplacement age at ca. 274 Ma (Fig. 6-7a) (Zhang et al., 2008; Liu et al., 2009; Chen et al., 2012), suggesting a major thermal event that could account for this secondary magnetization. The solo reverse polarity and the estimated age of this remagnetization coincide with timing and features of the PCRS. Among these sites, inclinations vary slightly (-5° to -28°), but the corresponding paleolatitudes remain similar. Conversely, declinations are scattered and vary between 110° and 315° (Table 6-1). The paleomagnetic poles calculated from each site are distributed along a small

circle centered at the sampling zone, which overlap with Permian poles obtained from NCB and MOB (Fig. 6-8b). So, it is reasonable to consider that the remagnetized remanence acquired in Early-Middle Permian. The important difference in declination may be due to posterior late strike-slip faulting, as observed in the field (Fig. 6-2l).

All remaining remagnetized sites display HTC directions close to that of the PEF (Table 6-1), but two major features allow us to distinguish them (except 8 sites of Late Carboniferous limestone in West Ujimqin) from that of PEF: 1) these directions are characterized by magnetic inclinations (65.4° to 69.5°) higher than that of PEF (ca. 62° in central-eastern Inner Mongolia), and 2) the occurrence of reversed polarity for each locality (e.g. Figs. 6-5a, 6-5f and Table 6-1). Therefore, the remagnetization age needs to be estimated. The corresponding poles of these remagnetized sites are compatible with the Early Cretaceous poles of NCB, MOB and SIB (Halim et al., 1998; Hankard et al., 2005; Kravchinsky et al., 2002b; Cogné et al., 2005; Charles et al., 2011). Meanwhile, East Asia, including MOB, IMB and NCB, experienced Mesozoic extensional tectonics, characterized by abundant extensional half-graben basins and emplacement of numerous magmatic massifs (e.g. Webb et al., 1999; Graham et al., 2001; Ren et al., 2002; Liu et al., 2005; Wu et al., 2005; Charles et al., 2011; Wei et al., 2012; Daoudene et al., 2012). The magmatic event, which may induce thermal remgnetization, started in Late Jurassic and reached the peak in the Early Cretaceous (127 Ma, Fig. 6-7b). After the Early Cretaceous, no magmatic event occurred in central-eastern Inner Mongolia until to the Early Pleistocene basalt erupted nearby Xilinhot (IMBGMR, 1991). However, the distribution of the Early Pleistocene basalt is restricted, and the magnetic directions of the Early Pleistocene in this area are different from our remagnetized directions (Zhu et al., 1998). In generally speaking, pervasive remagnetization is caused by regional magmatic event. So, it is reasonable to consider that these secondary magnetizations were acquired in Early Cretaceous.

6.4 Comparisons of the paleomagnetic poles

Up to now, no reliable Paleozoic paleomagnetic data have been documented

from central-eastern Inner Mongolia, except a few remagnetization data obtained from Carboniferous-Permian strata in northeastern Inner Mongolia (Zhao et al., 1990). For MOB, paleomagnetic studies have mostly focused on its northern margin, such as North Amuria (Xu et al., 1997; Kravchinsky et al., 2002a) and North Mongolia (Pruner, 1987), with a few studies on South Mongolia (Pruner, 1987). Most of these data were driven from deformed zones, e.g. the suspected Mongol-Okhotsk suture zone, where the strike-slip movements may have caused significant deflection of the paleomagnetic directions (Kravchinsky et al., 2002a; Webb and Johnson, 2006; Webb et al., 2010; Metelkin et al., 2010).

6.4.1 Late Devonian

Late Devonian poles for these four blocks remain rare. For NCB, two poles were obtained from Hexi Corridor region. Zhao et al. (1993) gave a Late Devonian pole at λ=34.2°N, φ=228.7°E, A_{95}=8.8° with 16 sites of red sandstone and andesite (Table 6-3). Huang et al. (2000) calculated a mean Middle-Late Devonian pole at λ=56°N, φ=336°E, A_{95}=9.2° with 12 sites of Middle-Late Devonian strata (Table 6-3). Despite collecting in close locations less than 40 km, these two poles display huge rotation with declination difference of 72.1°±15.4° (Fig. 6-8a), which is probably caused by the strike-slip fault system in the Hexi Corridor (Huang et al., 2000). In the Upper Amuria region (MOB), Kravchinsky et al. (2002a) obtained two poles for Middle-Late Devonian and Late Devonian ages at λ=24.6°N, φ=12.9°E, dp=8.7°, dm=16.9° with 7 sites of siltstone and tuff, and λ=40.5°N, φ=352.4°E, dp=9°, dm=16.7° with 5 sites of sandstone and siltstone, respectively (Table 6-3). All these four Devonian poles from NCB and MOB are distributed along a small circle, indicating that these two blocks have evolved together without detectable paleolatitude difference (2.3°±5.7°), but with significant relative rotations since the Late Devonian (Fig. 6-8a). Our Late Devonian pole obtained from Sunidzuoqi (IMB) locates on this same small circle (Fig. 6-8a), indicating that these three blocks of compatible paleolatitudes were juxtaposed since at least Late Devonian (Fig. 6-9a). Based on a paleomagnetic study of kimberlite and dyke in the east of Siberia,

Kravchinsky et al. (2002c) gave a Late Devonian pole for SIB at λ=11.1°N, φ=149.7°E, A_{95}=8.9° with 11 localities (Table 6-3). This pole is totally different from the Late Devonian poles of NCB, MOB and IMB (Fig. 6-8a), indicating that SIB was located far away from NCB, MOB and IMB during the Late Devonian (Fig. 6-9a).

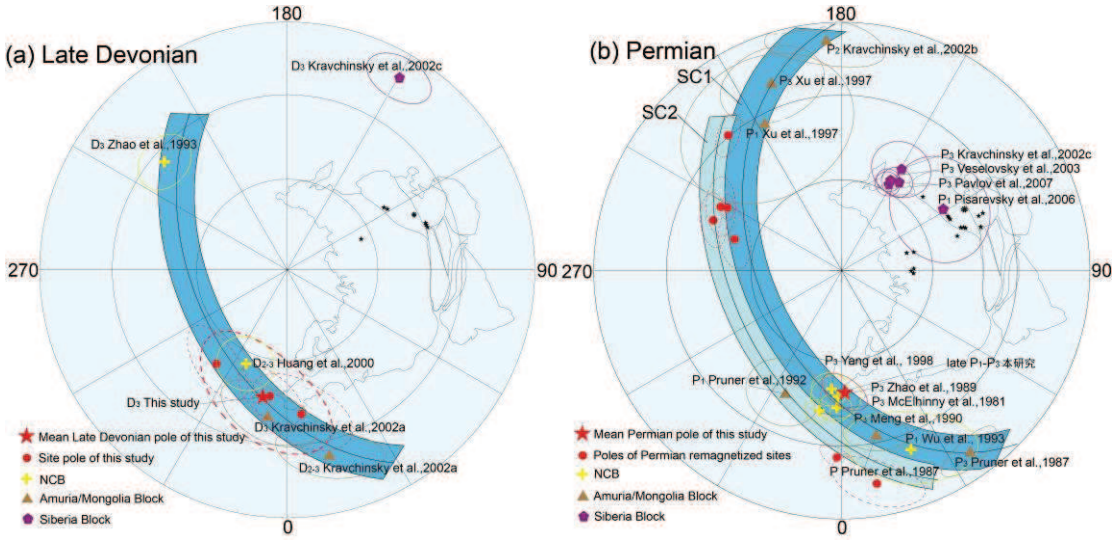

Figure 8. (a) Equal-area projections of Late Devonian poles from Sunidzuoqi (IMB), North China Block (NCB), Mongolia Block (MOB) and Siberia Block (SIB). There is little or no latitudinal difference but huge longitudinal differences between IMB, NCB and MOB, indicating that these three blocks probably aggregated together, but with strong rotation. SIB was far away from other three blocks in Late Devonian as the pole was far away. (b) Equal-area projections of Permian poles from IMB, NCB, MOB and SIB. The pole of our study is consistent with that of NCB, suggesting that these two parts have been welded as a rigid block. There is no latitudinal difference but still huge longitudinal differences between IMB+NCB and MOB, indicating strong postdated rotation, probably due to intra-continental strike-slip movements. SIB was still far away from other three blocks in Permian. The Permian remagnetized sites are also aligned along a small circle (SC2) with a shallower inclination, which probably due to local deformation since samples were collected from zones where strike-slip faults are documented.

6.4.2 Permian

The Permian poles for NCB have been well documented by numerous studies over the last three decades (Table 6-3) (e.g., McElhinny et al., 1981; Zhao et al., 1989; Meng et al., 1990; Wu et al., 1993; Yang et al., 1998). These poles are well consistent

with each other (Fig. 6-8b). Although statistically distinguished from other poles, the pole from Hexi Corridor (Fig. 6-8b) (Wu et al., 1993) presents a compatible paleolatitude, indicating post-Permian rotation of sampling area with respect to the other parts of NCB.

Our primary Permian pole for IMB inferred from West Ujimqin - Linxi is well consistent with the NCB poles (Star in Fig. 6-8b), indicating that no paleomagnetically detectable relative movement has occurred between NCB and IMB during Permian. These two blocks may have been welded as a rigid block (Fig. 6-9b).

The Permian poles of MOB are distributed along a small circle, which intercepts the poles of NCB-IMB (SC1 in Fig. 6-8b) (Xu et al., 1997; Kravchinsky et al., 2002b; Pruner et al., 1987; 1992). This observation indicates that the post Permian relative movements between NCB-IMB and MOB are essentially produced by rotations within these blocks. In fact, as described before, the samples of MOB are come essentially from the marginal zones (e.g. Kravchinsky et al., 2002b). These significant relative rotations may be caused by strike-slip movements along the tectonic boundaries (Cogné et al., 2005; Metelkin et al., 2010).

The Permian remagnetized poles obtained from Damaoqi in the northern margin of NCB and from East Ujimqin in the southern margin of MOB are scattered, but once again, they are distributed along a small circle (SC2 in Fig. 6-8b), revealing importance of strike-slip tectonics. This latter one is slightly different from SC1 that intercepts all other poles from NCB, IMB and MOB. The latitudinal difference of 9.0°±7.6° between SC1 and SC2 may be due to (1) the not well-constrained age determination of remagnetization solely estimated by the regional peak of magmatic activity around the sampling area; (2) local deformation since samples were collected from zones where strike-slip faults are documented (Fig. 6-2l).

The Permian poles from Siberia are statistically grouped (Table 6-3; Kravchinsky et al., 2002c; Veselovsky et al., 2003; Pavlov et al., 2007), except an outlier obtained from mafic dykes (Pisarevski et al., 2006) (Fig. 6-8b). These poles are well far away from all other poles of NCB, IMB and MOB, indicating that significantly latitudinal movements have occurred since Permian between Siberia and other blocks (Fig.

6-9b).

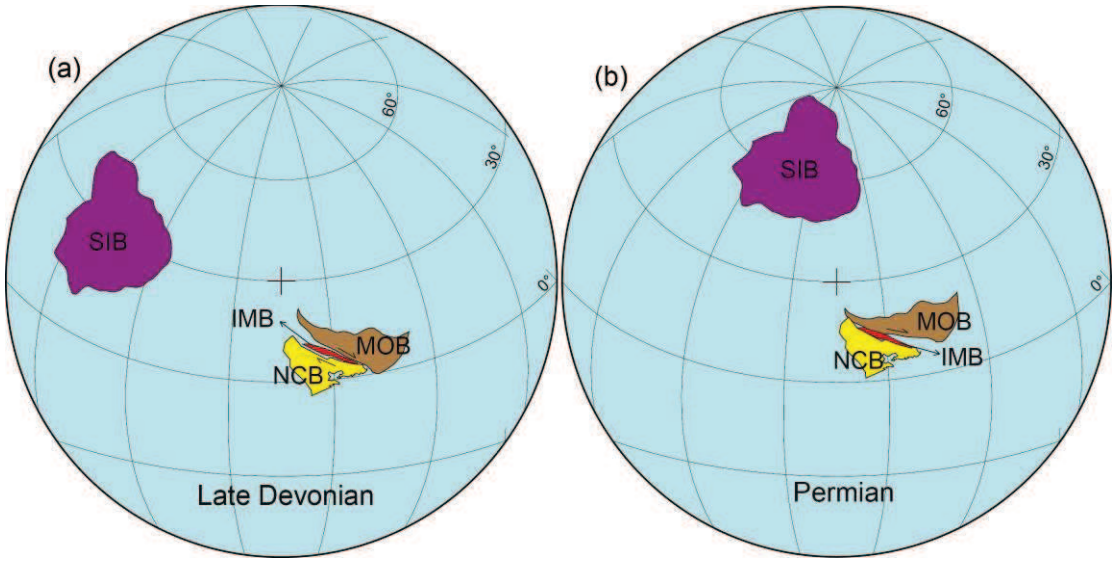

Figure 6-9 The paleogeographic map of the North China Block (NCB), Songliao-Hunshandake Block (SHB), Mongolia Block (MOB) and Siberian Block (SIB) during the Late Devonian (a) and Permian(b)

6.5 Tectonic implications

As a major tectonic implication of this study, no obvious latitudinal differences between IMB, NCB and MOB are observed neither in Late Devonian nor in the Permian (Figs. 6-8 and 6-9), meaning that these three blocks have been amalgamated since the Late Devonian and no wide ocean existed between them during Late Paleozoic. This observation is consistent with the tectonic interpretation showing two Silurian-Devonian orogens between NCB, IMB and IMB (Tang, 1990; Xu et al., 2012). The sedimentological constraints showing the similarity of the Upper Carboniferous to Upper Permian strata between NCB and MOB is also in agreement with our paleomagnetic data (Mueller et al., 1991). Our sedimentological study reveals that, following Late Devonian molassic deposition, IMB was dominated by shallow marine carbonate platform in Carboniferous, followed by volcanic-sedimentary sequences in Early-Middle Permian, and continental environment with thick lacustrine sediments in Late Permian. Consequently, no large ocean existed between NCB and MOB during the Late Paleozoic. Thus, the Paleo-Asian Ocean

between NCB and MOB was closed at least since Late Devonian. NCB, IMB and MOB were welded together as a single block. However, a small remnant sea may still exist in MOB in Late Paleozoic, as Carboniferous arc and Permian marine sedimentary deposits were identified in south Mongolia (Johnson et al., 2007; Heumann et al., 2012). Conversely, the latitudinal differences between the welded NCB-IMB-MOB block and SIB during Devonian and Permian may correspond to the occurrence of the Mongol-Okhotsk Ocean (Fig. 6-9). As shown by the distribution of paleomagnetic poles along small circles centered on the sampling regions, the welded NCB-IMB-MOB block is not totally rigid owing to intracontinental deformation, and significant relative rotations between NCB, IMB and MOB domains (Figs. 6-8a and 6-8b). The rotations are due to transcurrent tectonics that has been already described by the previous studies (Enkin et al., 1992; Kravchinsky et al., 2002a; Metelkin et al., 2010) and documented by numerous Mesozoic shear zones in MOB and IMB (e.g. East Gobi Fault zone) [(Lamb et al., 1999; 2008; Webb et al., 2010).

Chapter 7 Paleozoic tectonic evolution of central-eastern Inner Mongolia

本章将基于本文对晚古生代沉积地层的沉积相划分和对比、碎屑锆石年代学、岩浆岩地球化学和古地磁学结果，对内蒙古中东部晚古生代各个时期沉积-构造演化进行分析。并最终结合区域地质和前人研究成果，对内蒙古中东部沉积特征和岩浆岩活动进行期次划分和对比，对比周围地块二叠纪古地磁数据，探讨内蒙古中部古生代构造演化。

7.1The Paleozoic tectonic evolution of western Erguna-Xing'an Block

According to our sedimentological studies and detrital zircon analyses presented in chapter 3.1, combining with previous studies of the Early Paleozoic strata in this region, a tectonic evolution model of the western Erguna-Xing'an Block was proposed.

The collision between the EKB and AXXB occurred before the Late Cambrian, followed by Late Cambrian granitic and mafic intrusions (Wu et al., 2005; Ge et al., 2005; Wu et al., 2011) on both side of the Xinlin-Xiguitu suture zone (Fig. 7-1a). During this period, the southern margin of this newly formed block was a passive continental margin, and separated from the southern the SHB by the Paleo-Asian Ocean (Fig. 7-1a);

After that, the newly welded Erguna-Xing'an Block (EXB) belonged to an epicontinental setting, with the development of a Ordovician-Silurian sedimentary basin that was adjacent to coeval magmatic intrusions (Fig. 7-1b; IMBGMR, 1991; Ge et al., 2007; Sorokin et al., 2004; 2011; Ren et al., 2012; Guo et al., 2013). The Cambrian (510-485 Ma) orogenic-related granitic and mafic intrusions and subsequent Ordovician-Silurian (485-440 Ma) magmatic intrusions provide provenance for the basin sediments (Fig. 7-1b). Since the Paleo-Asian Ocean subducted beneath the southern margin of the welded EXB, the Baolidao arc formed along this margin from ~ 490 Ma to ~ 420 Ma, with the peak at ~ 460 Ma (Shi et al.,

2005; Jian et al., 2008; Zhang et al., 2009; Xu et al., 2013). The Baolidao arc granitoids intruded into the Xilinhot Precambrian basement, and extensive thermal metamorphism related to the arc magmatism occurred in the Precambian basement (Sun et al., 2013b), which also made contribution for the provenance of the basin deposition (Fig. 7-1).

During the Late Silurian, the magmatic events along the EXB have ceased, with widespread clastic and carbonate deposits buried the EXB and did not include a volcanic component (Fig. 3-2). The striking feature of these Upper Silurian strata is the Tuvaella funa therein, which can be traced from nearly all the Upper Silurian strata in the EXB (Su et al., 1981; IMBGMR, 1991), marking a tectonic stabilization of this newly formed block (Fig. 7-1c; Wang et al., 2009). To the south, the subduction of the Paleo-Asian Ocean was still going on, but the Baolidao arc magmatism ceased at the Late Silurian (Fig. 7-1c), represented by ~ 420 Ma high-K granite (Shi et al., 2005; Jian et al., 2008) and coeval hornblende gabbros (Zhang et al., 2009).

During the Early-Middle Devonian, the marine sedimentary basins on the EXB show significant lateral lithological variations from west to east (Fig. 3-2). In the Chaganaobao area, the distinctive red basal conglomerate (Figs. 3-3f and 7-1) represents a regional unconformity, indicating that the sedimentary basin might have been closed before the Early Devonian in this area. However, to the east, the Early-Middle Devonian strata are mainly composed of shallow marine sandstone with abundant of shallow marine fossils, indicating that marine sedimentary basins still existed. These lithological variations indicate an Early-Middle Devonian eastward regression, revealing an eastward successive closure of the marine basin (Fig. 7-1d). During the Late Devonian, due to the collision between the SHB and the EXB, the Late Devonian molassic deposition uncomformbly overlied the ophiolitic mélange (Xu et al., 2013; Fig. 7-1d). This collision also caused the final closure of the marine sedimentary basins on the EXB, as no Late Devonian sediments were found to the west, and plant-fossils bearing continental Upper Devonian Angeryinwula Formation occurred to the east (West Ujimqin area) (IMBGR, 2007; Fig. 7-1d). After the Late

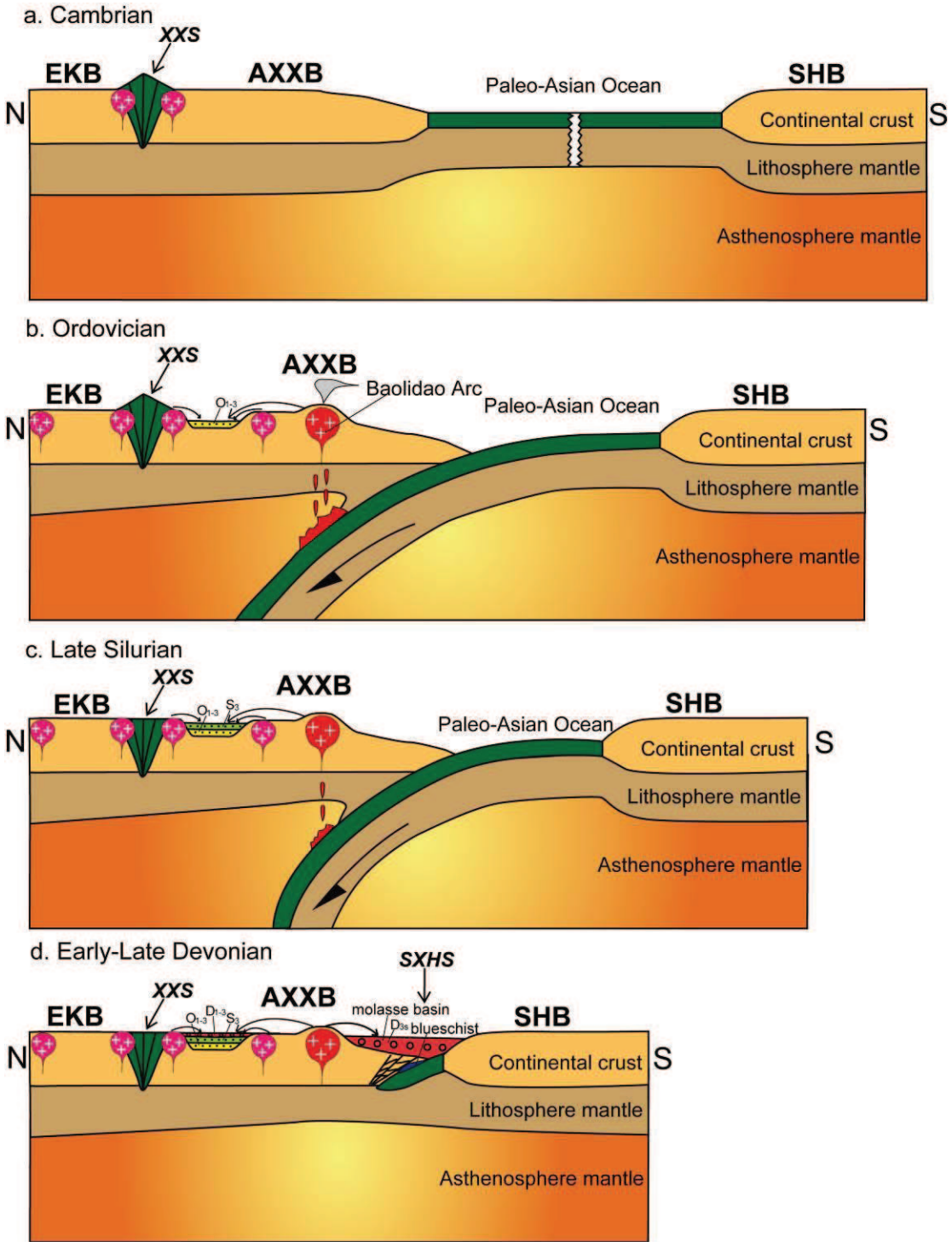

图 7-1 额尔古纳－兴安地块西段寒武纪－泥盆纪构造演化模式：XXS，新林-喜贵图缝合带；SXHS，苏尼特左旗-锡林浩特-黑河缝合带

Figure 7-1 Cambrian-Devonian tectonic evolution of western Erguna-Xing'an Block: XXS, Xinlin-Xiguitu suture; SXHS, Sunidzuoqi-Xilinhot-Heihe suture

Devonian, the EXB came into a subaerial setting without sedimentation until the Late

Carboniferous continental deposition (IMBGMR, 1991).

7.2 The Carboniferous evolution of central-eastern Inner Mongolia

7.2.1 The Late Carboniferous-Early Permian evolution of China-Mongolia border areas

前已述及，泥盆纪之后，中蒙边境地区（额尔古纳-兴安地块西段）进入剥蚀阶段，缺失早石炭世沉积。晚石炭世，沿蒙古南部－中蒙边境一带发生区域伸展作用，形成大量伸展相关双峰式火山岩和富钾花岗岩（Yarmolyuk et al., 2008；辛后田等，2011；许立权等，2012；Zhang et al., 2011；2014）及伸展沉积盆地，并沉积以砾岩、红色砂岩为主的陆相沉积（内蒙古地质矿产局，1991）。其底砾岩不整合于下伏地层之上，代表一个区域不整合接触关系。陆相地层含大量安哥拉植物化石，与额尔古纳－兴安地块和蒙古发现的安哥拉植物群可以对比（Wnuk, 1996; Deng et al., 2009），说明此时这些陆块已经成为一个整体。另外，在东乌旗东部宝力高庙组沉积中发现了华夏植物群与安哥拉植物群的共生，说明此时华夏植物已经跨越内蒙古进入额尔古纳－兴安地块（辛后田等，2011）。李朋武等（2012）对苏尼特左旗西北部白音乌拉地区宝力高庙组进行古地磁研究，其古地磁极及古纬度均与华北相似，而与西伯利亚板块相差较大，说明晚石炭世－早二叠世额尔古纳－兴安地块西段与华北板块关系密切，距离较近，而远离西伯利亚板块。此时内蒙古中部可能是华北板块的组成部分。古地磁结果与植物群的共生关系相一致，均认为华北板块与其北部陆块的碰撞拼贴可能发生于晚石炭世之前。

根据最新的西乌珠穆沁旗 1:25 万填图，鲍庆中等（2005; 2006）认为该区晚石炭世由北向南分布同时异相的宝力高庙组、格根敖包组和阿木山组，分别代表陆相沉积、海陆交互相沉积和浅海相沉积。晚古生代内蒙古中部发育广泛海进，发育以本巴图组和阿木山组为代表的浅海相沉积，而中蒙边界地区的宝力高庙组和格根敖包组则作为该海盆北部边缘陆相沉积（图 7-2）。

7.2.2 The Carboniferous evolution of central-eastern Inner Mongolia

The sedimentological analyses and detrital zircon dating of the Carboniferous

strata in central Inner Mongolia display the same depositional setting and similar provenance, indicating that they deposited in the same geological setting. The sedimentological analyses document that most of the Carboniferous strata overlie the Neoproterozoic basement, Early Paleozoic magmatic arc, accretionary complex, and Devonian strata. This conclusion is supported by our detrital zircon results (Figs. 4-15 and 4-17). This unconformity represents a regional transgression during the Late Carboniferous after the Devonian-Early Carboniferous sedimentary hiatus in most regions of central Inner Mongolia (Fig. 7-2; IMBGMR, 1991; Tang, 1990; Shao et al., 1991).

The subduction of PAO produced two arc magmatic belts along two subduction zones of opposite polarities, named the Bainaimiao Arc at the northern margin of NCC and the Baolidao Arc at the southern margin of AXXB (Fig. 7-2a; Jian et al., 2008; Xu et al., 2013). Both arc activities started from ca. 500 Ma, and ceased at 420-410 Ma (Jian et al., 2008; Shi et al., 2005; Zhang et al., 2013). The magmatism was accompanied by blueschist facies metamorphism (Xu et al., 2001; De Jong et al., 2006). The final continental collision was postdated by Late Silurian-Early Devonian molassic deposition along the Southern Orogen (Fig. 7-2a; Tang, 1990; Zhang et al., 2010; Shi et al., 2013), and Late Devonian molassic deposition along the Northern Orogen (Fig. 7-2a; Xu et al., 2013). After the twice collision, NCC, SHB and AXXB were welded into a unified continent (Xu et al., 2013). This scenario is supported by recent paleomagnetic studies (Zhao et al., 2013). Except for the molassic deposition along the two orogenic belts, most parts of the central Inner Mongolia came into a subaerial environment, without Devonian-Early Carboniferous deposits (Fig. 7-2a; Tang, 1990; Shao et al., 1991).

During the Late Carboniferous, abundant bimodal volcanic rocks and granite emplaced, forming a huge extensional related magmatic belt in the southern Mongolia and northern Inner Mongolia areas (Fig. 7-2b; Shi et al., 2003; Bao et al., 2007; Xue et al., 2010; Yarmolyuk et al., 2008; Cheng et al., 2012; Xu et al., 2012; Liang et al., 2013). Nevertheless, geochemical studies of the Late Carboniferous granitoids from Sunidzuoqi and West-Ujimqin display calc-alkaline affinities (Chen et al., 2000; Liu

et al., 2009; 2013). The Late Carboniferous magmatic intrusions from Chengde area at the northern margin of NCC also display arc-like geochemistry affinities (S.H. Zhang et al., 2007; 2009a). These results were considered as evidences for the existence of magmatic arcs and oceanic subduction in central Inner Mongolia during the Late Carboniferous (Chen et al., 2000; S.H. Zhang et al., 2007; 2009a; Liu et al., 2013). However, the Late Carboniferous granitoids in West-Ujimqin were also interpreted as extension-related (Bao et al., 2007; Xue et al., 2010). The Chagannur bimodal volcanic rocks in Sunidzuoqi-Sunidyouqi were also considered to be formed in post-collisional extensional setting (Tang et al., 2011). X.H. Zhang et al. (2012) reported the Late Carboniferous appinitic intrusions in Hohhot area, which were interpreted to be formed within a post-subduction transtensional regime. Moreover, he also considered that the Late Carboniferous magmatic intrusions S.H. Zhang et al. (2007; 2009a) reported in Chengde area are also belong to appinitic magmatic rocks, which should emplace in the same transtensional setting. Furthermore, these Late Carboniferous magmatic rocks can be found on both sides of the suture zone, which can't be explained by arc model. In addition, the arc interpretation is contradictory with our sedimentary analyses, as the Late Carboniferous deposits on both sides of this assumed Late Carboniferous arc are comparable, indicating the same sedimentary environment (Figs. 4-1b and 7-2b; IMBGMR, 1991; Shao et al., 1991). Meanwhile, the basal conglomerate of the Late Carboniferous strata uncomformably overlies the underlying Precambrian basement, ophiolitic mélange, Early Paleozoic magmatic arc, and Late Carboniferous magmatic intrusions, indicating an extensive transgression on a single continent. Hence, the Late Carboniferous magmatic rocks may be emplaced in a local extensional or transtensional trough (Fig. 7-2b; Bao et al., 2007; Tang et al., 2011).

Furthermore, during the Late Carboniferous, the northern Inner Mongolia (from Erenhot to East-Ujimqin) was dominated by terrestrial facies deposits (Fig. 7-2b), represented by the Baoligaomiao Formation, from which abundant of Angara flora was identified (IMBGMR, 1991). This terrestrial deposit belt indicates the intracontinental environment of AXXB during the Late Carboniferous, which can be

treated as the north margin of the inland sea (Fig. 7-2b; Bao et al., 2006).

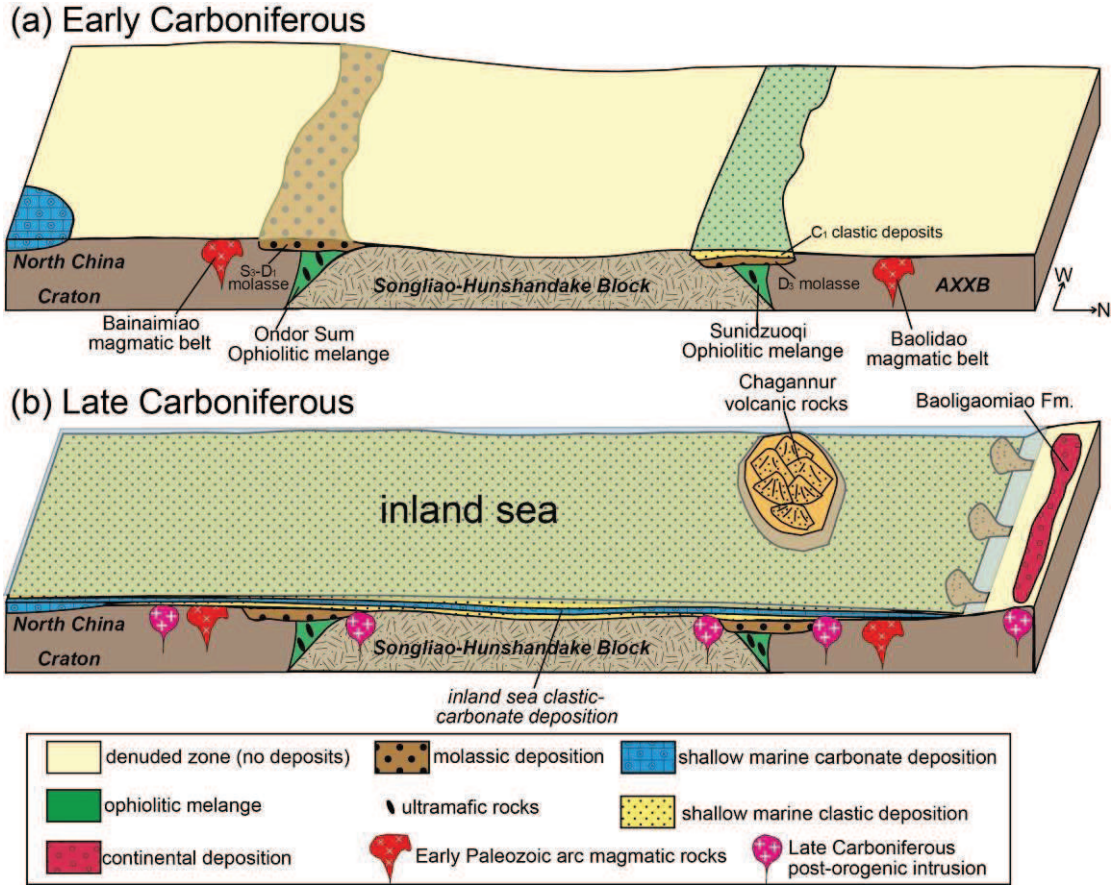

图 7-2 华北板块、松辽—浑善达克地块和艾里格庙-锡林浩特-兴安地块石炭纪演化模式

Figure 7-2. Schematic evolutionary model between the North China Craton, Songliao-Hunshandake Block and Airgin Sum-Xilinhot-Xing'an Block (AXXB) during the Carboniferous. Detailed interpretation is discussed in the text.

Our sedimentological analyses and depositional setting interpretation are consistent with both the paleontological (Zhou et al., 2010; Xin et al., 2011) and the paleomagnetic data in this region (Pruner, 1987; Xu et al., 1997; Chen et al., 1997; Li et al., 2012; Zhao et al., 2013).

In recent paleontological studies, typical Cathaysia flora fossils were identified from the Baoligaomiao Formation in East-Ujimqin, mixed with Angara flora (Xin et al., 2011). Furthermore, Cathaysia flora fossils were also identified from the Late-Middle Permian strata in East-Ujimqin (Zhou et al., 2010). The newly found Late Carboniferous-Middle Permian mixture of Cathaysia and Angara flora in the northern part of Inner Mongolia indicate that PAO has closed at least before the Late

Carboniferous. These new discoveries improved the traditional paleontological division, which considered the mixture of Cathaysia and Angara flora did not happen until the Late Permian along the Solonker (Huang, 1980; Deng et al., 2009; Shi, 2006). This pre-Late Carboniferous closure of PAO was also suggested by Dobretsov et al. (1995; 2003) and then confirmed by Safonova et al. (2009) and Donskaya et al. (2013).

Moreover, although paleomagnetic results indicate a long distance from the NCC and SIB during the Carboniferous, the intervening microblocks were located nearby the NCC since at least the Late Carboniferous (Pruner, 1987; Xu et al., 1997; Chen et al., 1997; Li et al., 2012). Xu et al. (1997) carried out paleomagnetic studies on the Carboniferous-Permian strata from the Chita area (Amur region of Russia), and got a similar paleolatitude of the Amur block with that of NCC. From paleomagnetic studies of the Carboniferous-Permian strata from central Mongolia, Pruner (1987) considered that the central Mongolia was a part of the NCC ever since the Early Permian. For the Chinese part, paleomagnetic studies were performed on the Upper Carboniferous strata in East-Ujimqin and Sunidzuoqi area, northern Inner Mongolia, both of which gave similar paleolatitudes with NCC and placed the northern Inner Mongolia at the northern margin of NCC during the Late Carboniferous (Chen et al., 1997; Li et al., 2012). Recently, paleomagnetic studies were carried out on the Devonian-Permian strata of Hunshandake Block, showing that this block was located at the northern margin of NCC ever since the Late Devonian (Zhao et al., 2013). These blocks were accreted to the northern margin of NCC, and thus formed a large continental block before the Late Devonian (Zhao et al., 2013; Xu et al., 2013).

7.3 The Permian evolution of central-eastern Inner Mongolia

第五章沉积学研究表明，内蒙古中东部地区二叠纪沉积发育于晚石炭世陆表海沉积之上，表现为由早－中二叠世陆内伸展盆地向晚二叠世陆相盆地沉积演变的过程。整个早－中二叠世沉积均以浅海相和海陆交互相为主，不存在广阔大洋沉积。而晚二叠世陆相地层的普遍出现标志着内蒙古中东部已结束海相沉积演化。此阶段，内蒙古中东部已不存在广阔的大洋和洋壳俯冲作用。

早二叠世内蒙古中东部普遍发育双峰式火山岩和花岗岩类侵入体，并呈面状分布（图 5-1）。双峰式火山岩地球化学特征显示其形成于碰撞后伸展环境（Zhang et al., 2008; Chen et al., 2012; 邵济安等，2014）。花岗岩类侵入晚石炭世地层，地球化学特征多表现为高钾钙碱性和 A 型花岗岩特征，显示其侵位于伸展构造环境（施光海等，2004; 鲍庆中等，2007a,b; 罗红玲等，2009；聂凤军等，2009）。中二叠世沿南造山带（达茂旗－镶黄旗－克什克腾旗）发育碱性岩带（鲁颖淮等，2009; 路彦明等，2011；江小均等，2011；蒋孝君等，2013；刘军等，2014），与中蒙边境早二叠世碱性岩带一起，构成内蒙古中东部二叠纪两条重要的伸展构造背景下的碱性侵入岩带。晚二叠世花岗岩在内蒙古中东部分布较少，但多数显示碱性花岗岩的特征，代表区域伸展构造背景（刘翼飞等，2012）。

古生物方面，周志广等（2010）在东乌珠穆沁旗东部满都胡宝拉格地区（位于艾里格庙－锡林浩特－兴安地块之上）新识别出的早－中二叠统陆相地层中发现大量华夏植物群化石。说明早二叠世华夏植物群已经由华北板块向北跨越内蒙古地区进入中蒙边境一带，并与该区安哥拉植物群发生混生。证明华北板块与其北部陆块的碰撞应发生于早二叠世之前（周志广等，2010）。考虑到辛后田等（2011）在东乌珠穆沁旗晚石炭世地层中已发现华夏植物群与安哥拉植物群的混生，华北板块与其北部陆块（松辽－浑善达克地块和艾里格庙－锡林浩特－兴安地块）的碰撞在晚石炭世之前已完成。

我们对内蒙古中部二叠纪的古地磁结果表明，二叠纪松辽－浑善达克地块具有与华北板块重合的古地磁极，证明二叠系松辽－浑善达克地块已经与华北板块称为一个刚性块体。另外，Chen et al.（1997）和李朋武等（2012）在中蒙边境一带（属于艾里格庙－锡林浩特－兴安地块）的晚石炭世地层中得到与华北板块相同的古纬度，进而说明华北板块与其北部陆块的碰撞发生于晚石炭世之前。

According to new field investigation, lithofacies and sedimentary facies comparison, a sedimentary evolutionary model for the Late Paleozoic rift in eastern Inner Mongolia is established as following (Fig. 7-3).

In Carboniferous, inland sea carbonates and subordinate clastic rocks deposited above the former molasse basin and orogenic basement (Fig. 7-3). The continuous carbonate deposition from south to north suggests a huge inland sea covered eastern Inner Mongolia with local alluvial deposition in its north margin (Fig. 7-3).

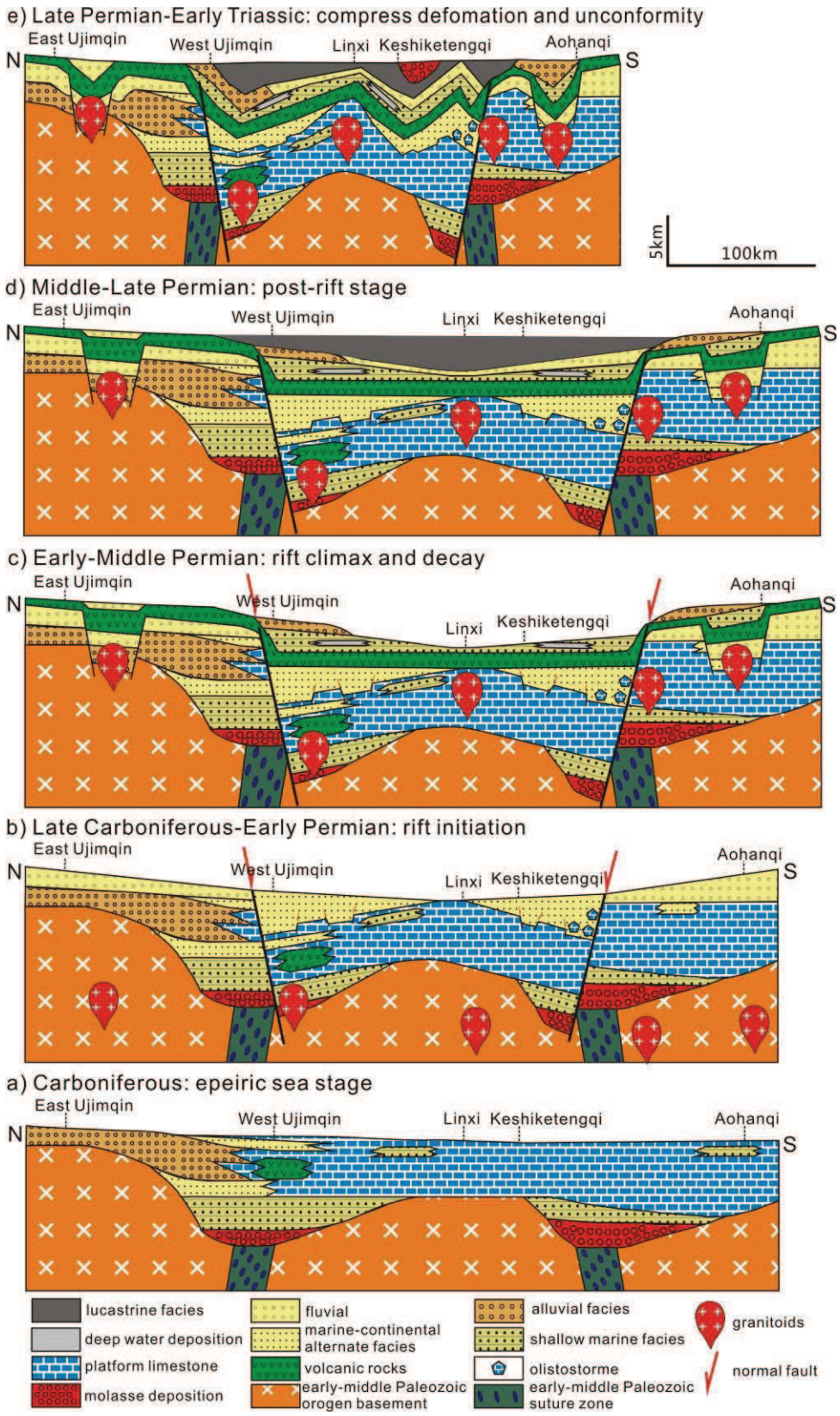

图 7-3 内蒙古东部晚石炭世－晚二叠世沉积过程演化示意图

Figure 7-3. Simplified sedimentary evolutionary model for late Paleozoic strata in eastern Inner Mongolia

During late Carboniferous-middle Permian, an intracontinental rift developed in eastern Inner Mongolia. The initiation of rift started in late Carboniferous to early Permian, with olistrostromes and fluvial deposition covered the carbonate platform (Fig. 7-3b). During early-middle Permian, the rift came into the climax, characterized by intensive magmatic events, both bimodal volcanic rocks, A-type granite and mafic intrusions, thick stable shallow marine strata and restrained deep water deposition (Fig. 7-3c). At the end of Middle Permian, the rift decayed by shallowing upward sequence and top conglomerate (Fig. 7-3c).

At Middle-Late Permian, post-rift sediments displaced the syn-rift deposition gradually, from Middle Permian lacustrine and fluvial deposition in north (East Ujimqin) and south (Aohanqi) margin of the rift basin to the significant Late Permian lacustrine deposition in the middle of the basin (West Ujimqin-Linxi-Keshiketengqi) (Fig. 7-3d).

In latest Permian-early Triassic, a regional compression happened, which strongly folded the former strata and uplift the whole area into the subaerial environment. After this tectonic movement the regional alluvial conglomerate deposited unconformbly on the underneath strata in Keshiketengqi, with other places exposed (Fig. 7-3e).

中二叠世，前人在杏树洼、毛登和哲斯敖包等地分别发现放射虫化石，并认为代表大洋深水沉积（王玉净和樊志永，1997；尚庆华, 2004; 王惠等, 2005）。但关于放射虫所代表沉积环境的解释需谨慎。放射虫是一种正常盐度下的广海浮游微体生物，可以生活在海洋的各个深度，其死后可以埋藏于海洋的不同深度，从远洋深海到浅海区，甚至潮坪等滨浅海环境中也可存在（孔庆玉和龚与觐, 1986; 龚一鸣, 1992; 王博和舒良树, 2001）。例如，新疆卡拉麦里蛇绿岩混杂带和南天山蛇绿混杂岩带中均发现与蛇绿岩共生的深海放射虫硅质岩（舒良树和王玉净, 2003; 舒良树等, 2007）。孔庆玉和龚与觐（1986, 1987）通过对扬子地台二叠纪孤峰组放射虫的研究，认为孤峰组沉积于狭长而闭塞的局部深裂陷槽中，裂陷槽两侧为浅水碳酸盐岩台地和滨岸三角洲沉积，裂陷槽两侧同时发现从深水带至浅水环境的放射虫。而 Kametaka et al.（2005）通过对安徽巢湖附近孤峰组硅质岩

中放射虫的研究，认为其产于广阔的大陆架地区。Caridroit et al.（2000, 2002）分别在希腊 Mount Parnis 的和墨西哥 San Salvador Patlanoaya 浅海相灰岩中发现放射虫化石，相同层位同时发现牙形石、蝬等化石，并认为放射虫的出现仅代表海相地层，并非深海环境。因此，需要其他沉积和古生物证据进行综合分析才能确定放射虫代表的沉积环境。

方俊钦等（2014）在毛登地区发现放射虫的层位鉴别出代表浅海相沉积的螺类化石，表明该区哲斯组砂岩沉积于浅海相环境，而非深海洋盆。另外，发现放射虫的哲斯敖包发育大量中二叠统哲斯组灰岩，并发育著名的浅海相哲斯动物群，代表典型的浅海相沉积（Wang et al., 2004）。因此，中二叠世内蒙古中东部以浅海相沉积和海陆交互相沉积为主。内蒙古南部沿南造山带发育中二叠世碱性岩带，说明中二叠世仍存在局部伸展作用，并导致碱性岩浆作用（鲁颖淮等，2009; 路彦明等，2011；江小均等，2011；蒋孝君等，2013；刘军等，2014），但这种局部伸展作用并未产生伸展盆地沉积。在局部伸展较为强烈的地方可能出现类似现今红海的新生局限洋盆（Chen et al., 2012）。这种局限洋盆可能为放射虫提供了生存环境。但其仅持续很短时间并被中二叠统浅海相沉积所覆盖。

7.4 The Paleozoic tectonic evolutional model of central-eastern Inner Mongolia

7.4.1 Comparison of sedimentological features

7.4.1.1 The Early Paleozoic deposits

早古生代艾里格庙－锡林浩特－兴安地块北部发育奥陶系细碎屑沉积（图 7-1），代表该地块与北部额尔古纳地块碰撞后的陆内盆地碎屑沉积。由于距离北造山带较远，该区奥陶系沉积并未发生严重韧性变形及变质。

松辽－浑善达克地块发育早古生代温都尔庙群，以强烈片理化绢云母片岩、绢云石英片岩、含铁石英岩和变质火山岩组成（图 7-1；Xu and Chen, 1997; 李承东等，2012）。温都尔庙群属于被动大陆边缘沉积（张臣和吴泰然, 1999; 2001），被认为是松辽－浑善达克地块的早古生代沉积盖层，并卷入南北两个造山带中发生强烈变形（Xu et al., 2013）。虽然前人将温都尔庙群归入新元古代（Xu and Chen, 1997），但最新的锆石 U-Pb 年代学研究得到其变质安山岩年龄为 470±2 Ma，碎

屑岩中碎屑锆石多集中于 445-480 Ma，说明温都尔庙群沉积于奥陶纪-早志留世（李承东等，2012）。

华北板块北缘发育奥陶系包尔汉图群和白乃庙群（内蒙古地质矿产局，1991）。包尔汉图群分布于华北板块北缘西段（达茂旗－白云鄂博一带），由下部布龙山组和上部哈拉组构成（唐克东，1992）。布龙山组由喷出岩和凝灰质沉积岩组成，早期喷出拉斑玄武岩，后期喷出钙碱性安山岩、英安岩及火山角砾岩等（唐克东，1992）。其中凝灰质沉积岩占整个序列厚度的 65%以上，为典型岛弧火山岩建造特征（唐克东，1992）。哈拉组则主要为碱性玄武岩，底部含苦橄岩。白乃庙群分布于华北板块北缘中段（白乃庙－温都尔庙一带），由下部乌鲁乌素组和上部榆树沟组组成。乌鲁乌素组由基性火山岩及火山沉积岩组成，下部以沉积岩为主，向上为基性熔岩、安山岩。榆树沟组为另一个火山喷发旋回，下部沉积岩中含大理岩透镜体。白乃庙群和包尔汉图群可以对比，均代表古亚洲洋向南俯冲产生的岛弧火山－沉积建造（图 7-1；Tang，1990）。白乃庙群和包尔汉图群均受到南造山带的影响，发生强烈变质和变形，并被西别河组砾岩不整合覆盖（唐克东，1992；Shi et al., 2013）。

7.4.1.2 Silurian-Devonian deposits

艾里格庙－锡林浩特－兴安地块北部发育上志留统卧都河组和下－中泥盆统泥鳅河组滨浅海相碎屑沉积及上泥盆统安格尔音乌拉组陆相碎屑沉积（图 7-4），卧都河组以著名的图瓦动物群为特征，与蒙古地块和额尔古纳地块上志留统沉积可以对比，代表艾里格庙－锡林浩特－兴安地块与额尔古纳地块及蒙古地块碰撞后统一的沉积盖层。泥鳅河组沿中蒙边境呈带状分布，由二连浩特北部经东乌珠穆沁旗直达大兴安岭地区，虽然沉积相横向变化较大，但整体以滨浅海相碎屑沉积为主，夹少量灰岩，代表陆内盆地碎屑沉积。而随着泥鳅河组沉积的结束，艾里格庙－锡林浩特－兴安地块大部分地区进入剥蚀阶段，仅在少数地区发育上泥盆统陆相沉积。

北造山带，上泥盆统色日巴彦敖包组发育于苏尼特左旗南－阿巴嘎旗一带，下部为陆相磨拉斯砾岩，向上渐变为海陆交互相粗砂岩，并发育少量生物碎屑灰岩，不整合覆盖于蛇绿混杂带上及早古生代温都尔庙群之上，标志着北造山带的结束（Xu et al., 2013）。

南造山带，上志留统－下泥盆统西别河组发育于达茂旗－温都尔庙一带，下

部为陆相磨拉斯砾岩，向上转变为浅海相碎屑岩和灰岩，不整合覆盖于蛇绿混杂带及奥陶系岛弧相关火山－沉积岩系之上，标志着南造山带的结束（张允平等，2010；Shi et al., 2013）。

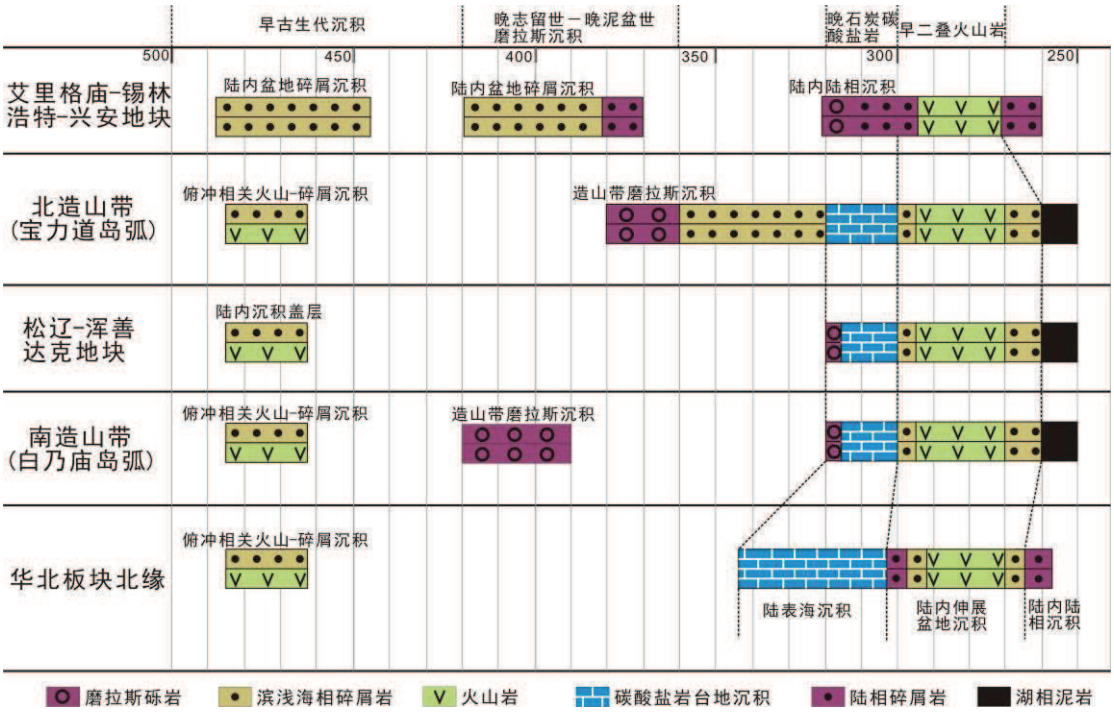

图 7-4 内蒙古中东部地区各地块沉积类型对比图（数据来源于本文及 Tang, 1990；邵济安等，1991；内蒙古地质矿产局，1991）

Figure 7-4 Sedimentological comparison of each block in central-eastern Inner Mongolia (data from this study and Tang, 1990; Shao et al., 1991; IMBGMR, 1991)

7.4.1.3 Carboniferous-Permian deposits

晚泥盆世起，艾里格庙－锡林浩特－兴安地块、松辽－浑善达克地块和华北克拉通已经通过南北两条造山带完成拼贴过程。整个内蒙古中东部开始经历相似的演化过程。

早石炭世内蒙古中东部普遍为剥蚀阶段，沉积分布局限，仅出现于北造山带和华北板块北缘（图 7-4）。北造山带下石炭统沉积整合于上泥盆统磨拉斯沉积之上，代表磨拉斯盆地继续发育的潮坪碎屑沉积（Xu and Chen，1997; Xu et al., 2013）。华北北缘下石炭统沉积发育于敖汉旗北部，为浅海相碳酸盐岩台地沉积，代表华北板块北缘的局部海相盆地沉积。

上石炭统除中蒙边境一带发育陆相碎屑沉积外，整个内蒙古中东部均发育浅

海相碎屑－碳酸盐岩建造（图 7-4），并不整合覆盖于下伏各时代地层及侵入岩之上（鲍庆中等，2006），代表三板块拼合后的板内陆表海沉积。陆表海沉积覆盖内蒙古大部分地区，而中蒙边境一带发育的陆相沉积则代表该陆表海的北部边缘。

早二叠世初期内蒙古东部地区出现不同的沉积类型。北部和南部出现以冲积扇相和河流相为主的陆相沉积，而中部则以滨浅海相和海陆交互相碎屑岩沉积为主（图 7-4）。该期沉积中心位于西乌珠穆沁旗地区，以巨厚的寿山沟组浅海相细碎屑沉积为代表（郑月娟等，2013；公繁浩等，2013）。早二叠世初期继承了晚石炭世沉积的古地理格局，表现出南北高，中间低的盆地特征。

早二叠世中晚期内蒙古中东部地区发生强烈裂谷伸展，产生大量伸展相关双峰式火山岩和侵入岩，锆石 U-Pb 年龄集中于 280-270 Ma（图 7-4；施光海等，2004; 鲍庆中等，2007a,b; 薛怀民等，2010; Zhang et al., 2008; Chen et al., 2012; 邵济安等，2014）。

中二叠世，内蒙古北部率先进入陆相沉积阶段，以含植物化石砂岩为特征（图 7-4）。中二叠世中蒙边境一带大部分地区为陆表剥蚀阶段，仅在东乌珠穆沁旗地区新识别出含华夏植物群的下－中二叠统陆相沉积（周志广等，2010）。中部和南部地区则以浅海相碳酸盐岩和碎屑岩沉积为主（图 7-4），以哲斯组、黄岗梁组和索仓组下段为代表，代表伸展盆地内稳定沉积。含丰富的浅海相动物化石，特别是著名的哲斯动物群（Wang et al., 2004）。局部伸展较为强烈的地区可能出现类似现今红海的新生局限洋盆（Chen et al., 2012），并为放射虫提供生存环境（王玉净和樊志永，1997；尚庆华, 2004; 王惠等, 2005）。南部华北板块北缘于中二叠世晚期进入陆相沉积阶段，以敖汉旗索仓组二段河流相沉积为代表，含丰富华夏植物群化石。

晚二叠世，研究区北部、南部和西部均进入剥蚀阶段，沉积仅出现于东部西乌珠穆沁旗南部－克什克腾旗一带（图 7-4）。晚二叠世盆地结构继承了早－中二叠世伸展盆地南北高中间低的特征。上二叠统沉积以河流相砾岩和湖相黑色泥页岩为主，含大量植物化石，标志着整个内蒙古中东部进入陆相盆地沉积阶段（图 7-4）。

7.4.2 Comparison of magmatic rocks

内蒙古中东部发育两期主要岩浆事件：早古生代岛弧岩浆岩和晚石炭－晚二叠世造山后伸展相关岩浆岩。另外，在华北板块北缘还发育早泥盆世碱性岩。

7.4.2.1 The Early Paleozoic arc magmatism

早古生代古亚洲洋的双向俯冲在艾里格庙－锡林浩特－兴安地块南缘和华北克拉通北缘，分别产生宝力道岛弧和白乃庙岛弧（图（图 7-5；Jian et al., 2008; Xu et al., 2013）。宝力道岛弧沿艾里格庙－苏尼特左旗－锡林浩特一带分布，岩石组成以闪长岩和辉长岩为主，地球化学以低钾拉斑和钙碱性为主，显示岛弧地球化学特征（Chen et al., 2000; Jian et al., 2008; X.H. Zhang et al., 2009）。岛弧岩浆侵位于 500-420 Ma（Chen et al., 2000; Jian et al., 2008; X.H. Zhang et al., 2009），并以高钾花岗岩的出现标志着岛弧岩浆的结束（石玉若等，2005）。白乃庙岛弧沿图古日格－达茂旗－四子王旗－温都尔庙－镶黄旗－敖汉旗一线分布，岩性包含侵入岩（辉长岩、闪长岩和花岗闪长岩为主）和火山岩（玄武岩、安山岩和凝灰岩）（徐备等，2014）。地球化学以低钾拉斑和钙碱性为主，显示岛弧地球化学特征（Jian et al., 2008; Xu et al., 2013; Zhang et al., 2013），岩浆侵位时代为 500-420 Ma（刘敦一等，2003; 张维和简平，2008; Jian et al., 2008; Xu et al., 2013; Zhang et al., 2013; 秦亚等，2013），并以未变形伟晶花岗岩（411±8Ma）的侵入标志着岛弧岩浆的结束（Zhang et al., 2013）。

7.4.2.2 The Early Devonian alkaline intrusions

早泥盆世碱性岩仅出现于华北板块北缘，沿固阳－察哈尔右翼后旗－张家口一带分布，年龄集中于 390-410 Ma（图 7-5；罗镇宽等，2001; Jiang, 2005; 曾俊杰，2009; X.H. Zhang et al., 2010; 张晓晖和翟明国，2010）。承德附近则出现时代为 395 Ma 的铁镁－超铁镁侵入岩和 390 Ma 的闪长岩（S.H. Zhang et al., 2007; 2009b）。早泥盆世碱性岩地球化学呈现后碰撞/后造山型碱性岩类的典型岩石组合特征（张晓晖和翟明国，2010）。结合华北板块与松辽－浑善达克地块于晚志留世完成碰撞拼合形成南造山带，早泥盆世碱性岩可能形成于造山后俯冲板片断离产生的伸展环境（X.H. Zhang et al., 2010）。

7.4.2.3 The Carboniferous-Permian post-orogenic magmatism

晚石炭世岩浆岩分布于艾里格庙－锡林浩特－兴安地块、北造山带、松辽－浑善达克地块和华北板块北缘（图 7-5）。

艾里格庙－锡林浩特－兴安地块上，曾维顺等（2011）获得大石寨地区大石寨组火山岩年龄为 314±1 Ma，据此提出晚石炭世应为裂陷盆地。辛后田等（2011）在东乌珠穆沁旗获得宝力高庙组 320-303Ma 的陆相火山岩，认为侵位于裂谷伸展环境。梁玉伟等在东乌珠穆沁旗东部获得 319±4Ma 的中粗粒花岗岩，并认为其形成于晚石炭世后碰撞伸展环境。许立权等（2012）在二连浩特北部查干敖包地区获得 317-308Ma 的碱性花岗岩，并显示 A 型花岗岩的地球化学特征。该陆块上，沿着中蒙边境分布大量晚石炭世花岗岩，并向西延伸至蒙古南部。Yamolyuk 等（2008）在蒙古南部报道大量 300-330Ma 的双峰式火山岩和碱性花岗岩带，构成两条晚石炭世裂谷岩浆岩带。

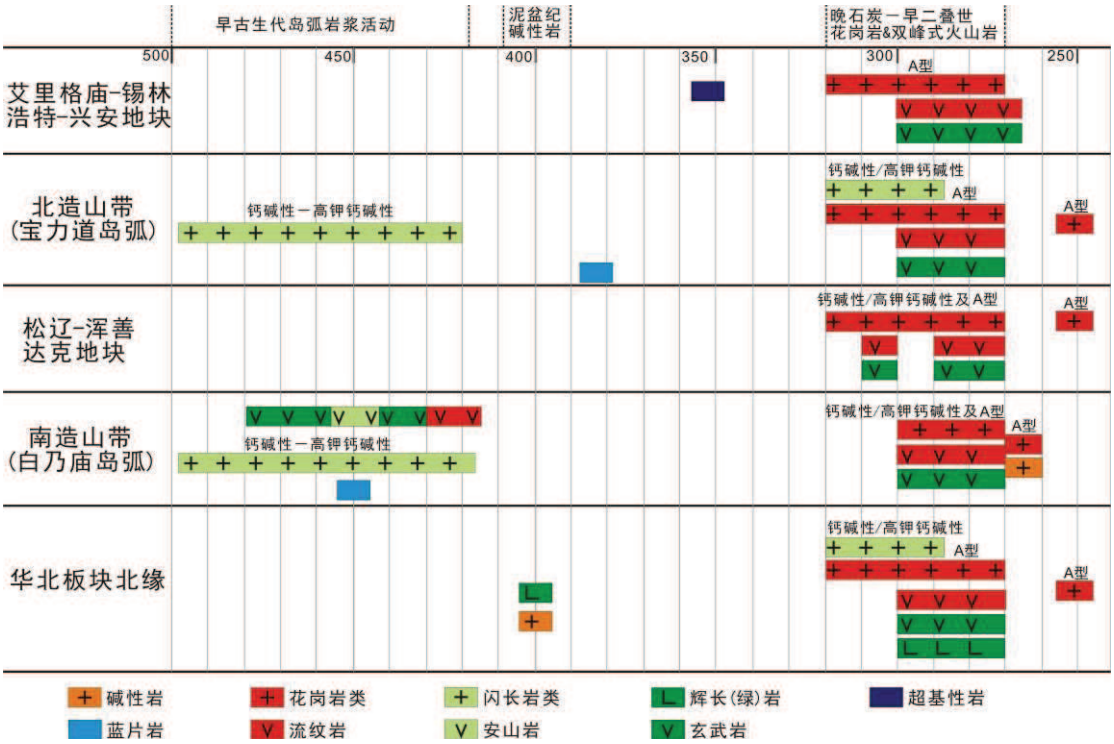

图 7-5 内蒙古中东部地区各地块岩浆活动对比图（数据来源于徐备等，2014）

Figure 7-5 Magmatism comparison of each block in central-eastern Inner Mongolia (data from Xu et al., 2014 and references therein)

北造山带晚石炭世岩浆岩集中于锡林浩特和西乌珠穆沁旗地区。施光海等（2003）报道了侵入锡林郭勒杂岩中的未变形石榴石花岗岩，侵位年龄为 316±3Ma。西乌珠穆沁旗南部发育大量晚石炭世侵入岩，侵位年龄集中于 325-300 Ma（刘建峰等，2009；鲍庆中等，2007a, b；薛怀民等，2010）。虽对其侵入构造背景存在争议，但其与上覆未变形晚石炭世地层的侵入关系表明，该区晚石炭

世花岗岩类侵位于伸展构造背景中。

松辽－浑善达克地块晚石炭世岩浆作用不明显，仅出现于西部苏尼特右旗－苏尼特左旗南部附近，以达里诺尔火山岩为代表。汤文豪等（2011）在苏尼特右旗本巴图组中识别出 313-308Ma 的双峰式火山岩，并认为研究区应处于裂谷构造环境。

华北板块北缘发育大量早石炭晚期－晚石炭岩浆岩。周志广等（2009）在四子王旗得到 331±4 Ma 和 302±2 Ma 的辉长岩，并侵入太古代片麻岩中。承德附近发育大量晚石炭世花岗质侵入岩，年龄集中于 324-302 Ma，地球化学显示钙碱性－高钾钙碱性的特征，并为解释为岛弧岩浆岩（Zhang et al., 2007; 2009a）。Zhang et al.（2012）在呼和浩特北部鉴定出年代为 320-317 Ma 的高 Ba-Sr 富闪深成岩体，并认为承德附近的晚石炭世侵入岩同样属于此类型岩体。高 Ba-Sr 富闪深成岩体一般产出于造山后板片断离或板片拆沉背景（Atherton and Ghani, 2002；Ye et al., 2008），说明华北北缘晚石炭世侵入岩形成于造山后转换伸展背景（Zhang et al., 2012）。

二叠纪岩浆岩在整个内蒙古中东部呈面状分布（图 2-4；图 7-5），以花岗岩和双峰式火山岩为主。

中蒙边境从二连浩特北部至东乌珠穆沁旗一带发育大量早二叠世碱性花岗岩（洪大卫等，1994；Jahn et al., 2009；Zhang et al., 2014）和宝力高庙组双峰式火山岩（Zhang et al., 2011），构成一条早二叠世裂谷岩浆岩带。该带向西延至蒙古国南部，与 Yarmolyuk 等（2008）所划分的裂谷岩浆岩带连通。

裂谷岩浆岩带以南至华北板块北缘发育以大石寨组和清凤山组为代表的早二叠世火山岩及同时期花岗岩类。火山岩由西向东见于西部达茂旗、中部林西到东部大石寨等地，构成 3 条火山-沉积岩带（邵济安等，2014），并显示为双峰式特征（Zhang et al., 2008；Chen et al., 2012），被解释为喷发于伸展构造背景。与早二叠世火山岩相伴的花岗岩类分布于各个地块之上（图 7-2）。例如，鲍庆中等（2006）报道了西乌珠穆沁旗南部大量早二叠－晚二叠世花岗岩类，并认为其侵位于石炭－二叠纪裂谷发育时期。Chen et al.（2012）在达茂旗附近鉴别出 278Ma 的辉长岩，认为其侵位于裂谷伸展环境。

值得注意的是，沿达茂旗－温都尔庙－镶黄旗－克什克腾旗一线，前人报道

了大量中二叠世碱性岩、碱性花岗岩及含基性包体的花岗岩。范宏瑞等（2009）报道了达茂旗北部 270-257 Ma 的花岗岩。镶黄旗南部毕力赫钾长花岗岩时代为 264 Ma（路严明等, 2012）。镶黄旗一带同时发育后造山性质的 S 型花岗岩，年龄为 275-262 Ma（洪大卫等，2007）。克什克腾旗南部碱性岩时代为 264-263Ma（江小均等, 2011）。另外，章永梅等（2009）在四子王旗识别出 265Ma 的黑云母花岗岩，含大量基性岩包体。熊光强等（2013）得到四子王旗黑脑包黑云母花岗岩的锆石年龄为 268 Ma。这些碱性岩、碱性花岗岩和含基性包体花岗岩共同构成兴蒙造山带南部中二叠世岩浆岩带，可能代表中二叠世裂谷带（图 7-5）。

晚二叠世－早三叠世岩浆岩在内蒙古中东部分布较少，但均表现出 A 型花岗岩的地球化学特征（图 7-5）。张晓晖等（2006）在锡林浩特－西乌珠穆沁旗一带识别出 245Ma 的英安岩－流纹岩组合，地球化学表现出 A 型花岗岩的特征。刘建峰等（2013）在巴林右旗得到 249Ma 的花岗闪长岩。郭志军等（2012）在巴林右旗幸福之路苏木识别出大量 245Ma 的中酸性侵入岩。刘伟等（2007）在林西得到 241Ma 的花岗岩。江思宏等（2012）在林西附近识别出 252Ma 的安山玢岩和 243Ma 的黑云母二长花岗岩。王芳等（2009）在华北北缘崇礼－赤城得到 254M 的花岗岩。Zhang et al.（2009a）总结了承德附近 253-245Ma 的二长花岗岩，其地球化学特征显示 A 型花岗岩，并将其解释为于碰撞后发生侵位。结合区域地质特征和地球化学特征，这些晚二叠－早三叠世岩浆岩形成于造山后陆内伸展环境。

7.4.3 Comparison of paleolatitude

7.4.3.1 Late Devonian

晚泥盆世，华北克拉通、松辽－浑善达克地块和蒙古地块古地磁极位于同一个小圆弧上，表明这三个陆块在晚泥盆世距离较近。而西伯利亚克拉通古地磁极距离上述三个板块较远，说明晚泥盆世西伯利亚克拉通远离上述三个板块。

通过计算晚泥盆世古纬度，华北克拉通位于北纬 0-14°，蒙古地块位于北纬 8-14°，说明晚泥盆世两地块之间没有古地磁可以识别的纬度差（图 7-6）。而西伯利亚克拉通晚泥盆世位于北纬 40°左右，与蒙古及华北均具有 25-30°的纬度差（图 7-6）。

7.4.3.2 Carboniferous

李朋武等（2012）分别对苏尼特左旗北部上石炭-下二叠统宝力高庙组和敖汉旗地区上石炭统酒局子进行古地磁研究，得到其古纬度分别为 18°和 16.9°，分别代表艾里格庙-锡林浩特-兴安地块和华北克拉通晚古生代古纬度（图 7-6）。说明晚石炭世艾里格庙-锡林浩特-兴安地块已经位于华北克拉通北缘，距离很近。

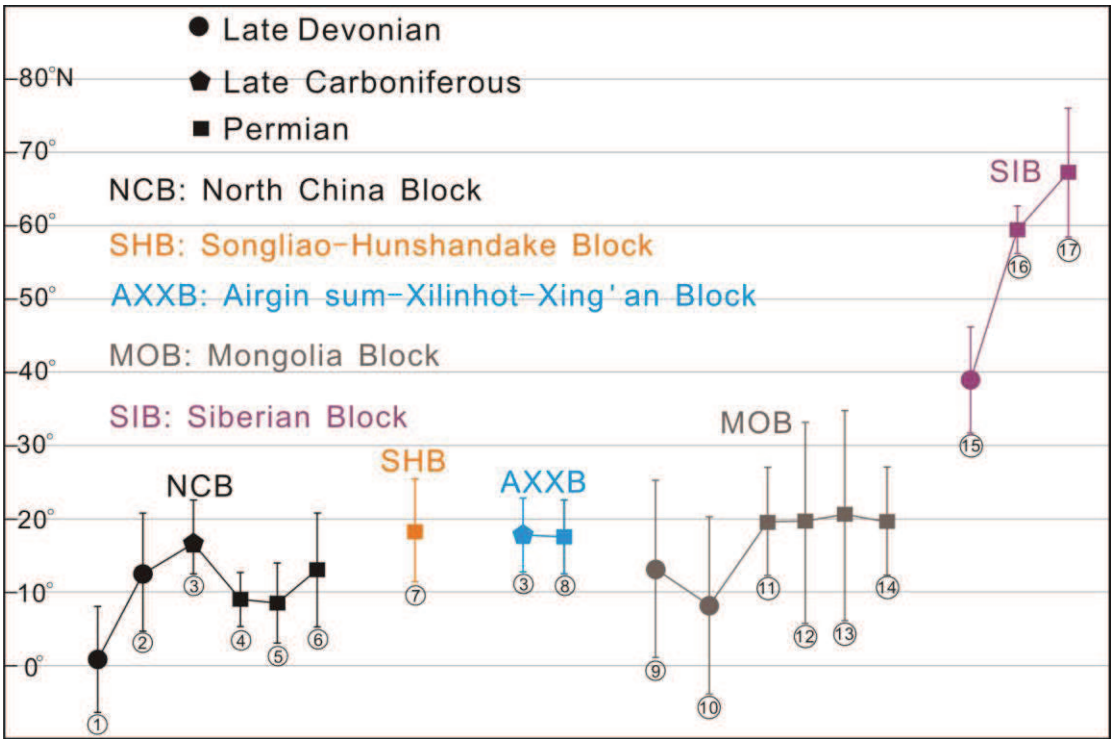

图 7-6 亚洲东部各地块晚泥盆世和二叠纪古纬度对比图(数据来自表 6-1：1, Zhao et al., 1993; 2, Huang et al., 2000; 3, 李朋武等，2012; 4, Meng et al., 1990; 5, Yang et al., 1998; 6, Zhao et al., 1989; 7, 本文第六章; 8, 李朋武等，2012; 9, Kravchinsky et al., 2002a; 10, Kravchinsky et al., 2002a; 11, Pruner, 1987; 12, Xu et al., 1997; 13, Kravchinsky et al., 2002b; 14, Pruner, 1987; 15, Kravchinsky et al., 2002c; 16, Veselovsky et al., 2003; 17, Kravchinsky et al., 2002c）

Figure 7-6 Paleolatitude comparison of each block in eastern Asia (data from Table 6-3: Zhao et al., 1993; 2, Huang et al., 2000; 3, Li et al.,2012; 4, Meng et al., 1990; 5, Yang et al., 1998; 6, Zhao et al., 1989; 7, This study; 8, Li et al., 2012; 9, Kravchinsky et al., 2002a; 10, Kravchinsky et al., 2002a; 11, Pruner, 1987; 12, Xu et al., 1997; 13, Kravchinsky et al., 2002b; 14, Pruner, 1987; 15, Kravchinsky et al., 2002c; 16, Veselovsky et al., 2003; 17, Kravchinsky et al., 2002c)

7.4.3.3 Permian

与晚泥盆世相似，华北克拉通、松辽一浑善达克地块和蒙古地块古地磁极同样位于同一个小圆弧上，表明这三个陆块在二叠纪相距很近。而华北克拉通和松

辽－浑善达克地块古地磁的相互重合则代表此时松辽－浑善达克已经焊接至华北克拉通北缘。而西伯利亚克拉通古地磁极距离上述三个板块较远，说明二叠纪西伯利亚板块仍远离上述三个板块。

通过计算二叠纪古纬度，华北克拉通位于北纬 9-15°，松辽-浑善达克地块位于北纬 19°左右，艾里格庙-锡林浩特-兴安地块位于北纬 18°左右，蒙古地块位于北纬 20°左右，考虑到采点位置纬度差，二叠纪以上四个地块之间没有古地磁可以识别的纬度差（图 7-6）。西伯利亚克拉通二叠纪位于北纬 60-70°左右，与蒙古及华北均具有 40-50°的纬度差（图 7-6）。

7.4.4 The Paleozoic tectonic evolutional model of central-eastern Inner Mongolia

通过对内蒙古中东部晚古生代进行沉积学、地质年代学、地球化学和古地磁学研究，并结合前人对该区古生代构造、古生物学、岩石学和地球化学等方面的研究，本文提出内蒙古中东部晚古生代构造演化模式。

（1）500-420Ma：古亚洲洋双向俯冲。向南俯冲至华北克拉通北缘，产生白乃庙岛弧；向北俯冲至艾里格庙－锡林浩特－兴安地块北缘，并产生宝力道岛弧（图 7-7a）。

（2）420-400Ma：松辽浑善达克地块与南部华北克拉通发生碰撞，古亚洲洋南支闭合，产生温都尔庙蛇绿混杂带，并被上志留－下泥盆统西别河组不整合覆盖（图 7-7b）。同时，华北克拉通北缘发育早泥盆世碱性岩，侵位于碰撞后板片断离相关伸展构造背景。此时，古亚洲洋北支向北俯冲仍在继续。

（3）400-360Ma：松辽－浑善达克地块与北部艾里格庙－锡林浩特－兴安地块发生碰撞，古亚洲洋北支闭合，产生苏尼特左旗蛇绿混杂带，并被上泥盆统色日巴彦敖包组不整合覆盖（图 7-7c）。该阶段，南造山带进入剥蚀阶段。

（4）360-320Ma：早石炭世，造山作用结束，内蒙古中东部大部分地区为陆相剥蚀阶段，仅在少数地区（如苏尼特左旗南部和敖汉旗北部）出现滨浅海相沉积。

（5）320-300Ma：晚石炭世，内蒙古中东部出现造山后第一个稳定的沉积盖层，以遍布全区的碳酸盐岩沉积为特征，并不整合覆盖于下伏地层和岩浆岩之上，代表造山后广泛的海侵作用（图 7-7d）。作为海侵的北部边缘，中蒙边境一带（艾里格庙－锡林浩特－兴安地块）发育宝力高庙组陆相沉积地层。伴随碳酸

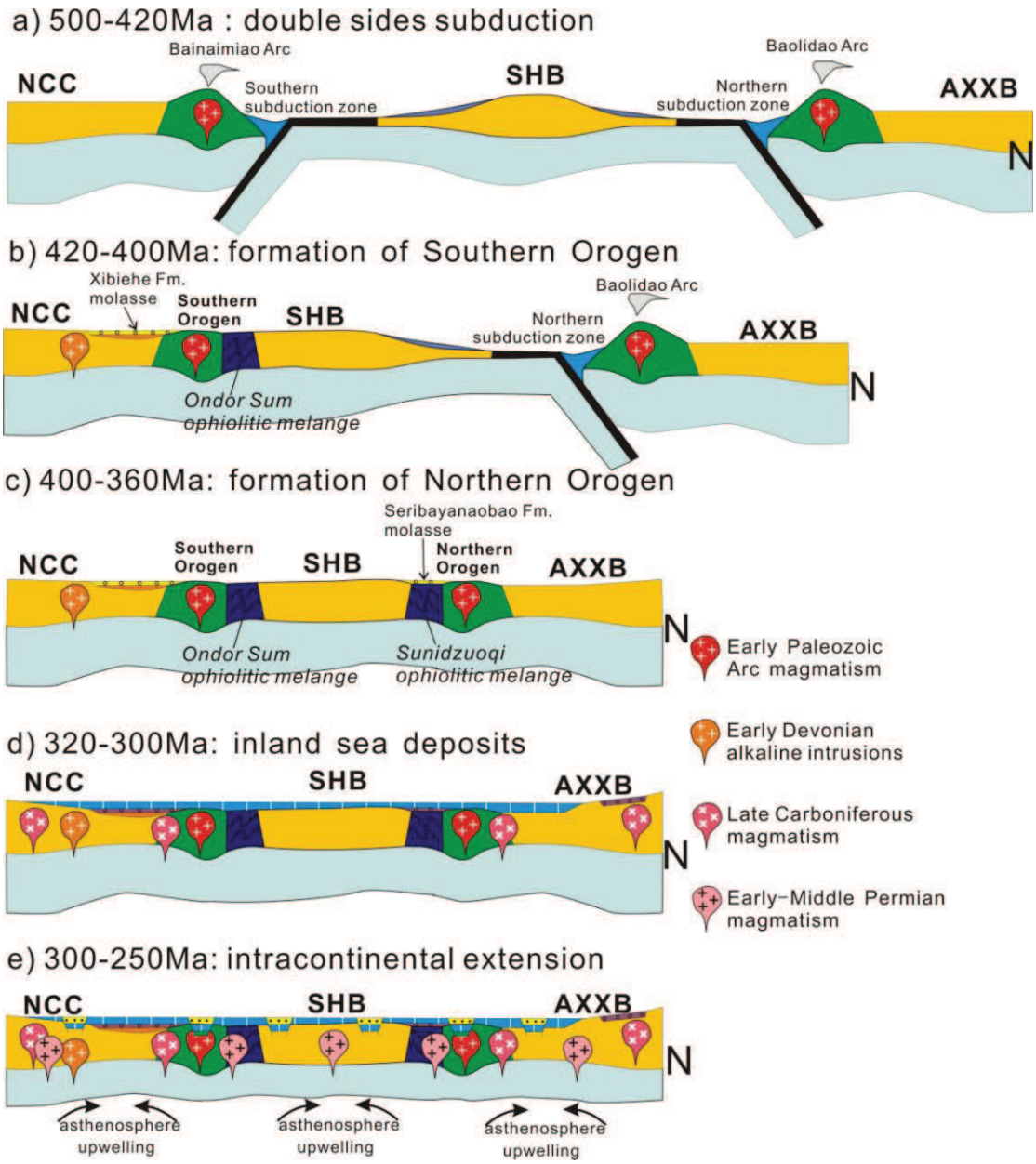

图 7-7 内蒙古中东部地区古生代构造演化模式图（早古生代阶段修改自 Xu et al., 2013）

Figure 7-7 The Paleozoic tectonic evolutional model of central-eastern Inner Mongolia (the Early Paleozoic part was modified from Xu et al., 2013)

盐岩的沉积，内蒙古中东部发育晚石炭世岩浆作用。

（6）300-250Ma：早二叠世，内蒙古中东部地区发育裂谷伸展作用，产生大石寨组双峰式火山岩和大量基性-酸性侵入岩（图 7-7e）。裂谷伸展作用的发生可能与软流圈上涌有关。中二叠世艾里格庙－锡林浩特－兴安地块处于陆相剥蚀阶段。南部大部分地区于伸展盆地内发育浅海相碳酸盐－碎屑沉积，以哲斯组为

代表。晚二叠世，伸展作用停止，伴随着海退过程，内蒙古中东部已基本不存在海相沉积，仅西乌珠穆沁旗－林西－克什克腾旗一带发育湖相黑色泥岩沉积，标志着内蒙古海相演化的结束。

Chapter 8 Conclusion

通过沉积学分析、碎屑锆石年代学限定、地球化学研究和古地磁对比，结合前人岩石学、地球化学和古生物学研究，对内蒙古中东部晚古生代沉积－构造演化历史进行限定，并提出完整的古生代俯冲－碰撞－造山后伸展构造演化模式。本文主要取得以下研究成果：

1. 泥盆纪艾里格庙-锡林浩特-兴安地块西段（中蒙边境一带）发育下-中泥盆统泥鳅河组滨浅海相沉积，含丰富腕足类、三叶虫和珊瑚等浅海相动物化石，局部为陆相沉积，代表艾里格庙-锡林浩特-兴安地块与额尔古纳地块早古生代碰撞拼合后的陆内海相盆地沉积。碎屑锆石测试显示其两个主要年龄峰值为 510 Ma 和 440 Ma，说明来自额尔古纳-兴安地块地块本身及南部宝力道岛弧岩浆岩的双向物源。晚泥盆世沿苏尼特左旗南部-阿巴嘎旗发育磨拉斯沉积，不整合于蛇绿混杂带之上，标志着北造山带造山作用的结束。碎屑锆石年代学结果显示单一年龄峰值 462 Ma，指示来自北部宝力道岛弧的单一物源。

2. 晚石炭世内蒙古中东部地区发育陆表海碎屑－碳酸盐岩沉积，以本巴图组和阿木山组为代表，底部不整合覆盖在前寒武纪基底、早古生代岛弧岩浆岩、蛇绿混杂带、前石炭纪地层及石炭纪侵入岩之上，代表区域超覆不整合。通过地层对比表明晚石炭世相同的沉积类型和沉积环境。碎屑锆石年代学显示 310 Ma 和 440 Ma 两个主要年龄峰值及大量新元古代锆石，说明晚石炭世物源主要为本地岩浆岩和变质基底，表明原地剥蚀和近源沉积的特征。晚石炭世陆表海沉积覆盖于整个内蒙古中东部地区，横跨南北三个板块（艾里格庙－锡林浩特－兴安地块、松辽－浑善达克地块和华北克拉通）和两个造山带（北造山带和南造山带），代表陆块拼合后的第一个稳定盖层沉积。晚石炭世中蒙边境发育宝力高庙组陆相碎屑-火山沉积岩系。碎屑锆石年代学研究显示 310 Ma 和 440 Ma 两个主要年龄峰，显示其物源主要来自于额尔古纳－兴安地块原地岩浆岩及南部宝力道岛弧。该陆相沉积可作为内蒙古中东部陆表海沉积的北部边缘。作为代表早古生代岛弧岩浆事件的 440Ma 年龄峰，其出现于由南北两条缝合带分隔的三个陆块之上，说明石炭纪沉积时，作为物源的早古生代岛弧岩浆岩已经跨越缝合带进行沉积，同样说明三个陆块在石炭纪之前已经碰撞拼合。

3. 二叠纪内蒙古中东部地区发育陆内伸展盆地碎屑-火山沉积岩系，由早二叠世双峰式火山岩、中二叠世富含动物化石浅海相碎屑-碳酸盐岩和晚二叠世含植物化石陆相沉积组成。早二叠世双峰式火山岩地球化学特征显示其喷发于陆内裂谷环境。晚二叠世陆相地层的普遍出现标志着内蒙古中东部已结束海相沉积演化。在内蒙古中东部沿镶黄旗-克什克腾旗识别出一条中二叠世碱性岩带，代表该时期的一条陆内伸展裂谷带。二叠纪地层沉积于晚石炭世陆表海碳酸盐岩之上，代表造山后稳定盖层之上的裂谷伸展作用。

4. 古地磁研究得到松辽-浑善达克地块晚泥盆世和二叠纪两个古地磁极，分别为 λ=46.8°N, φ=349.1°E, dp=14.6°, dm=27.3°, N=3 和 λ=48.7°N, φ=3.7°E, dp=5.2°, dm=9.1°, N=6。通过与周围块体进行古地磁极对比得出：（1）古亚洲洋至少于晚泥盆世已经闭合，华北克拉通、松辽-浑善达克地块和蒙古地块已经碰撞拼合；（2）华北克拉通、浑善达克地块和蒙古地块完成拼合后并非形成一个刚体，板块内部及板块边缘的走滑运动导致板块之间的相对旋转。

5. 详细的沉积学和地球化学研究展示了内蒙古中东部由泥盆纪磨拉斯不整合，到早石炭世造山后剥蚀，以及晚石炭世陆表海向二叠纪伸展盆地的演化过程。在综合分析沉积组合、碎屑锆石年龄、地球化学特征和古地磁数据基础上，提出古生代内蒙古中东部地区完整的俯冲-造山-造山后伸展的构造演化模式：早古生代古亚洲洋双向俯冲，于华北克拉通北缘产生白乃庙岛弧，并于艾里格庙－锡林浩特－兴安地块北缘产生宝力道岛弧。晚志留世-晚泥盆世，通过南北两个造山带完成华北克拉通、松辽-浑善达克地块和艾里格庙-锡林浩特-兴安地块的碰撞拼合。晚石炭世，内蒙古中东部出现造山后第一个稳定的沉积盖层，以遍布全区的碳酸盐岩沉积为特征，并不整合覆盖于下伏地层和岩浆岩之上，代表造山后陆表海沉积。早-中二叠世，内蒙古中东部地区发育裂谷伸展作用，以面状分布的火山岩和基性-酸性侵入岩为特征。晚二叠世内蒙古中东部进入陆相演化阶段。

References

鲍庆中, 张长捷, 吴之理, 王宏, 李伟, 桑加和, 刘永生. 2007a. 内蒙古白音高勒地区石炭纪闪长岩 SHRIMP 锆石 U-Pb 年代学及其意义. 吉林大学学报(地球科学版)，37：15–23.

鲍庆中, 张长捷, 吴之理, 王宏, 李伟, 桑加和, 刘永生. 2007b. 内蒙古东南部晚古生代裂谷区花岗质岩石锆石 SHRIMP U-Pb 定年及其地质意义. 中国地质，34：790-798.

鲍庆中，张长健，吴之理，王宏，李伟，苏养正，桑家和，刘永生. 2005. 内蒙古西乌珠穆沁旗地区石炭二叠纪岩石地层. 地层学杂志，29：512-519.

鲍庆中，张长健，吴之理，王宏，李伟，苏养正，桑家和，刘永生. 2006. 内蒙古东南部西乌珠穆沁旗地区石炭纪-二叠纪岩石地层和层序地层. 地质通报，25：572-579.

程胜东，方俊钦，赵盼，徐备，鲍庆中，周永恒，邓荣敬. 2014. 内蒙古西拉木伦河两岸志留-泥盆系碎屑锆石年龄及其构造意义. 岩石学报，待刊.

程银行，滕学建，辛后田，杨俊泉，冀世平，张永，李艳锋. 2012. 内蒙古东乌旗狠麦温都尔花岗岩 SHRIMP 锆石 U-Pb 年龄及其地质意义. 岩石矿物学杂志，31：323-334.

曾维顺，周建波，张兴洲，邱海峻. 2011. 内蒙古科右前旗大石寨组火山岩锆石 LA-ICP-MSU-Pb 年龄及其形成背景. 地质通报，30：271-277.

陈斌， 马星华，刘安坤，木合塔尔.扎日. 2012. 锡林浩特杂岩和蓝片岩的锆石 U-Pb 年代学及其对索伦缝合带演化的意义. 岩石学报，25：3123-3129.

范宏瑞，胡芳芳，杨奎锋，王凯怡，刘勇胜. 2009. 内蒙古白云鄂博地区晚古生代闪长质-花岗质岩石年代学框架及其地质意义. 岩石学报，25:2933-2938.

方俊钦，赵盼，徐备，邵军，汪岩. 2014. 内蒙古西乌珠穆沁旗哲斯组宏体化石新发现和沉积相分析. 岩石学报，待刊.

葛梦春，周文孝，于洋，孙俊俊，鲍建泉，王世海. 2011. 内蒙古锡林郭勒杂岩接替及表壳岩系年代确定. 地学前缘，18：182-195.

葛文春，吴福元，周长勇，Abdel Rahman AA．2005．大兴安岭北部塔河花岗岩体的时代及对额尔古纳地块构造归属的制约．科学通报，50：1239-1246.

公繁浩，黄欣，陈树旺，郑月娟，张健，苏飞. 2013. 内蒙古西乌珠穆沁旗地区寿山沟组烃源岩有机地球化学特征. 地质通报，32：1322-1328.

龚一鸣. 1992. 新疆北部泥盆纪放射虫及其岩相分布和环境意义. 地层学杂志，16：224-228.

郭志华，张宝林，沈晓丽，贾文臣，黄雪飞. 2013. 蒙古国东南部巨斑状二长花岗岩地球化

学特征与岩石成因机制探讨. 吉林大学学报（地球科学版），43：776-787.

郭志军，周振华，李贵涛，李进文，武新丽，欧阳荷根，王挨顺，向安平，董旭舟. 2012. 内蒙古敖尔盖铜矿中－酸性侵入岩体 SHRIMP 锆石 U-Pb 定年与岩石地球化学特征研究. 中国地质，39：1486-1500.

韩宝福，郭召杰，何国琦. 2010. “钉合岩体”与新疆北部主要缝合带的形成时限. 岩石学报，26：2233-2246.

韩国卿，刘永江，温泉波，李伟，吴琳娜，赵英利，丁凌，赵立敏，梁琛岳. 2011. 西拉沐沦河缝合带北侧二叠纪砂岩碎屑锆石 LA-ICP-MS U-Pb 年代学及其构造意义. 地球科学-中国地质大学学报，36：687-702.

韩杰，周建波，张兴洲，邱海峻. 2011. 内蒙古林西地球上二叠统林西组砂岩碎屑锆石的年龄及其大地构造意义. 地质通报，30：258-269.

郝旭和徐备. 1997. 内蒙古锡林浩特锡林郭勒杂岩的原岩年代和变质年代. 地质论评，43：10-105.

洪大卫，黄怀曾，肖宜君，徐海明，靳满元. 1994. 内蒙古中部二叠纪碱性花岗岩及其地球动力学意义. 地质学报，68：219-230.

洪大卫，王涛，童英. 2007. 中国花岗岩概述. 地质论评，53 增刊：9-16.

胡骁，许传诗，牛树银.1990.华北地台北缘早古生代大陆边缘演化. 北京：北京大学出版社.

蒋干清，高德臻，张维杰，李述靖，徐元恺，罗飞. 1995a. 内蒙古苏尼特左旗下二叠统哲斯组沉积组合类型及沉积序列演化. 现代地质， 9：162-169.

蒋干清，张维杰，肖荣阁，罗照华，李述靖，高德臻. 1995b. 内蒙古苏尼特左旗地区二叠纪地层的划分和对比. 现代地质，9：149-161.

江思宏，梁清玲，刘翼飞，刘妍. 2012. 内蒙古大井矿物及外围岩浆岩锆石 U-Pb 年龄及其对成矿时间的约束. 岩石学报，28：495-513.

江小均，柳永清，彭楠，石玉若，许欢，魏文通，刘增校，赵华平，姚宝钢.2011.内蒙古克什克腾旗广兴源复式岩体定年及地质意义讨论. 地质通报，85：114-125.

蒋干清，高德臻，张维杰，李述靖，徐元凯，罗飞. 1995a. 内蒙古苏尼特左旗下二叠统哲斯组沉积组合类型及沉积序列演化. 现代地质，9：162-169.

蒋干清，张维杰，肖荣阁，罗照华，李述靖，高德臻. 1995b. 内蒙古苏尼特左旗地区二叠纪地层的划分和对比. 现代地质，9：149-161.

蒋孝君，刘正宏，徐仲元，王挽琼，王兴安，张超. 2013. 内蒙古镶黄旗乌兰哈达中二叠世

碱长花岗岩 LA-ICP-MS 锆石 U-Pb 年龄和地球化学特征. 地质通报，32：1760-1768.

孔庆玉和龚与觐. 1986. 安徽巢湖下二叠统茅口阶放射虫硅质岩的发现及其地质意义. 地质论评，32：505-510.

孔庆玉和龚与觐. 1987. 苏皖地区下二叠统放射虫硅质岩形成环境探讨. 石油与天然气地质, 8：86-89.

李承东，冉暟，赵利刚，王惠初，张阔，许雅雯，谷永昌，张永青. 2012. 温都尔庙群锆石的 LA-MC-ICP-MS U-Pb 年龄及构造意义. 岩石学报，28：3705-3714.

李朋武，张世红，高锐，李海燕，赵庆乐，李秋生，管烨. 2012. 内蒙古中部晚石炭世-早二叠世古地磁新数据及其地质意义. 吉林大学学报（地球科学版），42：423-440.

李瑞彪，徐备，赵盼，童勤龙，张晋瑞. 2014. 二连浩特艾力格庙地区蓝片岩相岩石的发现及其构造意义. 科学通报，59：66-71.

李瑞山. 1991. 新林蛇绿岩. 黑龙江地质，2：19-31.

李文国，李庆富，姜万德. 1996. 内蒙古岩石地层. 中国地质大学出版社，1-344.

梁玉伟, 余存林, 沈国珍, 孙庆茹, 李进文, 杨郧城, 佘宏全, 张斌, 谭刚. 2013. 内蒙古东乌旗索纳嘎铅锌银矿物花岗岩地球化学特征及其构造与成矿意义. 中国地质，40：767-779.

刘敦一，简平，张旗，张福勤，石玉若，施光海，张履桥，陶华. 2003. 内蒙古图林凯蛇绿岩中埃达克岩 SHRIMP 测年：早古生代洋壳消减的证据．地质学报，77：317-327.

刘建峰, 迟效国, 张兴洲, 马志红, 赵芝, 王铁夫, 胡兆初, 赵秀羽. 2009. 内蒙古西乌旗南部石炭纪石英闪长岩地球化学特征及其构造意义. 地质学报, 83：365-376.

刘建峰，李锦轶，迟效国，冯乾文，胡兆初，周坤. 2013. 华北克拉通北缘与弧-陆碰撞相关的早泥盆世长英质火山岩—锆石 U-Pb 定年及地球化学证据. 地质通报，32：267-278.

刘建峰. 2009. 内蒙古林西－东乌旗地区晚古生代岩浆作用及其对区域构造演化的制约. 吉林大学博士论文.

刘建峰，迟效国，赵芝，胡兆初，陈军强. 内蒙古巴林右旗建设屯埃达克岩锆石 U-Pb 年龄及成因讨论. 29：827-839.

刘军，武广，李铁刚，王国瑞，吴昊. 2014. 内蒙古镶黄旗哈达庙地区晚古生代中酸性侵入岩的年代学、地球化学、Sr-Nd 同位素组成及其地质意义. 岩石学报，30：95-108.

刘伟，潘小菲，谢烈文，李禾. 2007. 大兴安岭南段林西地球花岗岩类的源岩：地壳生长的时代和方式. 岩石学报，23：441-460.

刘翼飞，聂凤军，江思宏，席忠，张志刚，肖伟，张可，刘永. 2012. 内蒙古查干花钼矿区

成矿花岗岩地球化学、年代学及成岩作用. 岩石学报，28：409-420.

鲁颖淮，李文博，赖勇. 2009. 内蒙古镶黄旗哈达庙金矿斑岩体形成时代和成矿构造背景. 岩石学报，25：2615-2620.

路彦明，潘懋，卿敏，张玉杰，韩先菊，朝银银. 2012. 内蒙古毕力赫含金花岗岩类侵入岩锆石 U-Pb 年龄及地质意义. 岩石学报，28：993-1004.

罗红玲，吴泰然，赵磊. 2009. 华北板块北缘乌梁斯太 A 型花岗岩体锆石 SHRIMP U-Pb 定年及构造意义. 岩石学报，25：515-526.

罗镇宽，苗来成，关康，裘有守. 2001. 河北张家口水泉沟岩体 SHRIMP 年代学研究及其意义. 地球化学，30：116-122.

罗红玲，吴泰然，赵磊. 2009. 华北板块北缘乌梁斯太 A 型花岗岩体锆石 SHRIMP U-Pb 定年及构造意义. 岩石学报，25：515-526.

内蒙古自治区地质矿产局. 1991. 内蒙古自治区区域地质志.北京:地质出版社, 1-725.

内蒙古自治区地质局. 1976. 1:20 万地质图镶黄旗幅.

聂凤军，许东青，江思宏，胡朋. 2009. 内蒙古苏莫查干敖包萤石矿区流纹岩锆石 SHRIMP 定年及地质意义. 地质学报，83：496-504.

裴福萍，许文良，杨德彬，赵全国，柳小明，胡兆初. 2006. 松辽盆地基底变质岩中锆石 U—Pb 年代学及其地质意义. 科学通报，51：2881-2887.

秦亚，梁一鸿，邢济麟，张青伟，刘城先. 2013. 内蒙古正镶白旗地区早古生代 O 型埃达克岩的厘定及其意义. 地学前缘，20：106-114.

权京玉，迟效国，张蕊，孙巍，范乐夫，胡兆初. 2013. 松嫩地块东部新元古代东风山群碎屑锆石 LA-ICP-MS U-Pb 年龄及其地质意义. 地质通报，32: 353-364.

任邦方，孙立新，程银行，李艳锋，郝爽. 2012. 大兴安岭北部永庆林场－十八站花岗岩锆石 U-Pb 年龄、Hf 同位素特征. 地质调查与研究，35：109-117.

尚庆华. 2004. 北方造山带内蒙古中-东部地区二叠纪放射虫的发现及意义. 科学通报, 49: 2574-2579.

邵济安. 1991. 中朝板块北缘中段的地壳演化. 北京: 北京大学出版社, 1-136.

邵济安，唐克东，何国琦. 2014. 内蒙古早二叠世构造古地理的再造. 岩石学报, 待刊.

施光海, 刘敦一, 张福勤, 简平, 苗来成, 石玉若, 陶华. 2003. 中国内蒙古锡林郭勒杂岩 SHRIMP 锆石 U-Pb 年代学及意义. 科学通报，48：2187-2192.

施光海，苗来成，张福勤，简平，范蔚茗，刘敦一. 2004. 内蒙古锡林浩特 A 型花岗岩的时

代及区域构造意义. 科学通报，49：384-389.

石玉若，刘敦一，张旗，简平，张福勤，苗来成，施光海，张履桥，陶华. 2004. 内蒙古苏左旗地区闪长－花岗岩类 SHRIMP 年代学. 地质学报，78：789-799.

石玉若，刘敦一，张旗，简平，张福勤，苗来成，施光海，张履桥，陶华. 2005. 内蒙古中部苏尼特左旗富钾花岗岩锆石 SHRIMP U-Pb 年龄. 地质通报，24：424-428.

舒良树, 王玉净. 2003. 新疆卡拉麦里蛇绿岩带中硅质岩的放射虫化石. 地质论评，49: 408-412.

舒良树, 王博, 朱文斌. 2007. 南天山蛇绿混杂岩中放射虫化石的时代及其构造意义. 地质学报，81：1161-1168.

孙立新，任邦方，赵凤清，谷永昌，李艳峰，刘卉. 2013. 内蒙古锡林浩特地块中元古代花岗片麻岩的锆石 U-Pb 年龄和 Hf 同位素特征. 地质通报，32：327-340.

孙立新，任邦方，赵凤清，彭丽娜. 2012. 额尔古纳地块太平川巨斑状花岗岩的锆石 U-Pb 年龄和 Hf 同位素特征. 地学前缘，19：114-122.

汤文豪, 张志诚, 李建锋, 冯志硕, 晨辰. 2011. 内蒙古苏尼特右旗查干诺尔石炭系本巴图组火山岩地球化学特征及其意义. 北京大学学报(自然科学版), 47：321-330.

唐克东. 1992. 中朝陆台北侧褶皱带构造演化和成矿规律. 北京: 北京大学出版社, 1-277.

童英，洪大卫，王涛，史兴俊，张建军，曾涛. 2010. 中蒙边境中段花岗岩时空分布特征及构造和找矿意义. 地球学报，31：395-412.

王博和舒良树. 2001. 对赣东北晚古生代放射虫的初步认识. 地质论评，47：337-344.

王芳，陈福坤，侯振辉，彭澎，翟明国. 2009. 华北陆块北缘崇礼－赤城地区晚古生代花岗岩类的锆石年龄和 Sr-Nd-Hf 同位素组成. 岩石学报，25：3057-3074.

王惠, 王玉净, 陈志勇, 李玉玺, 苏茂荣, 白立兵. 2005. 内蒙古巴彦敖包二叠纪放射虫化石的发现. 地层学杂志，29：368-371.

王 颖，张福勤，张大伟，苗来成，李铁胜，颉颃强，孟庆任，刘敦一. 2006. 松辽盆地南部变闪长岩 SHRIMP 锆石 U-Pb 年龄及其地质意义. 科学通报，51：1810-1816.

王玉净和樊志永. 1997. 内蒙古西拉木伦河北部蛇绿岩带中二叠纪放射虫的发现及其地质意义. 古生物学报，36：58-69.

王子进，许文良，裴福萍，曹花花.2013.兴蒙造山带南缘东段中二叠世末—早三叠世镁铁质岩浆作用及其构造意义—来自锆石 U-Pb 年龄与地球化学的证据. 地质通报，32：374-387.

魏连喜，孙丰月，薛明轩，于晓飞，孙乃权. 2013. 小兴安岭东南部晨明地区早古生代花岗

岩锆石 U-Pb 年龄及岩石地球化学特征. 世界地质，32：229-235.

辛后田，滕学建，程银行.2011.内蒙古东乌旗宝力高庙组地层划分及其同位素年代学研究. 地质调查与研究，34：1-9.

熊光强，赵洪涛，刘敏，张达，王浩然，王忠. 2013. 内蒙古四子王旗黑脑包岩体年代学与地球化学特征及其构造演化. 地质力学学报，19：162-177.

徐备, Charvet J, 张福勤. 2001. 内蒙古北部苏尼特左旗蓝片岩岩石学和年代学研究. 地质科学，36：424-434.

徐备，陈斌，白志强，张臣. 1994. 内蒙古白音宝力道地区 1:50000 地质图和地质报告. 北京大学出版社.

徐备，陈斌，邵济安. 1996. 内蒙古锡林郭勒杂岩 Sm-Nd, Rb-Sr 同位素年代研究. 科学通报，2：153-155.

徐备，刘树文，王长秋，郑海飞，田峰. 2000. 内蒙古西北部宝音图群 Sm-Nd 和 Rb-Sr 地质年代学研究. 地质论评，46：86-90.

徐备，赵盼，鲍庆中，周永恒，王炎阳、罗志文. 2014. 兴蒙造山带前中生代构造单元划分. 岩石学报，待刊.

徐立权, 鞠文信, 刘翠, 贺宏云, 李满英. 2012. 内蒙古二连浩特北部阿仁绍布地区晚石炭世花岗岩 Sr-Yb 分类及其成因. 地质通报，31：1410-1419.

许文良，王枫，孟恩，高福红，裴福萍，于介江，唐杰. 2012. 黑龙江省东部古生代—早中生代的构造演化：火成岩组合与碎屑锆石 U-Pb 年代学证据. 吉林大学学报（地球科学版），42：1378-1389.

薛怀民, 郭立军, 侯增谦, 童英, 潘晓菲, 周喜文. 2010. 大兴安岭西南坡成矿带晚古生代中期末变质岩浆岩的 SHRIMP 锆石 U-Pb 年代学. 岩石矿物学杂志，29：811-823.

薛怀民，郭利军，侯增谦，周喜文，童英，潘晓菲. 2009. 中亚－蒙古造山带东段的锡林郭勒杂岩：早华力西期造山作用的产物而非古老陆块？－锆石 SHRIMP U-Pb 年代学证据. 岩石学报，25：2001-2010.

曾俊杰. 2009. 内蒙古固阳地区晚古生代埃达克质花岗岩特征及其地质意义。硕士学位论文. 北京: 中国地质大学.

曾维顺，周建波，张兴洲，邱海峻. 2011. 内蒙古科右前旗大石寨组火山岩锆石 LA-ICP-MS U-Pb 年龄及其形成背景. 地质通报，30：270-277.

张臣，吴泰然. 1999. 内蒙古苏左旗南部早古生代蛇绿混杂岩特征及其构造意义. 地质科学，

34：381-389.

张臣，吴泰然. 2001. 内蒙古苏左旗南部华北板块北缘中新元古代古生代裂解－汇聚时间的地质记录. 岩石学报，17：199-205.

张丽，刘永江，李伟民，韩国卿，张金带，郭庆银，李长华. 2013. 关于额尔古纳地块基底性质和东界的讨论. 地质科学，48：227-244.

张维和简平, 2008. 内蒙古达茂旗北部早古生代花岗岩类 SHRIMP U-Pb 年代学. 地质学报，82：778-787.

张晓晖和翟明国, 2010. 华北北部古生代大陆地壳增生过程中的岩浆作用与成矿效应. 岩石学报，26：1329-1341.

张晓辉，张宏幅，汤艳杰，刘建明. 2006. 内蒙古中部锡林浩特－西乌旗早三叠世 A 型酸性火山岩的地球化学特征及其地质意义. 岩石学报，22：2769-2780.

张兴洲，马玉霞，迟效国，张凤旭，孙跃武，郭冶，曾振. 2012. 东北及内蒙古东部地区显生宙构造演化的有关问题. 吉林大学学报（地球科学版），42：1269-1285.

张玉清和苏宏伟. 2002. 内蒙古宝音图岩群变质基性火山岩锆石 U-Pb 年龄及意义. 前寒武纪研究进展，25：199-204.

张允平, 苏养正, 李景春. 2010. 内蒙古中部地区晚志留世西别河组的区域构造学意义. 地质通报，29：1559-1605.

张兆忠，冯锦江，张秉良，马宝林，顾芷娟. 1986. 中国的蓝片岩和板块构造. 岩石学报，2：31-40.

章永梅，张华峰，刘文灿，周志广. 2009. 内蒙古中部四子王旗大庙岩体时代及成因. 岩石学报，25：3165-3181.

赵磊，吴泰然，罗红玲. 2011. 内蒙古乌拉特中旗北七哥陶辉长岩 SHRIMP 锆石 U-Pb 年龄、地球化学特征及其地质意义. 岩石学报，27：3071-3082.

郑月娟，公繁浩，陈树旺，黄欣，张立君，张健. 2013. 内蒙古西乌珠穆沁旗地区下二叠统原寿山沟组碎屑锆石 LA-ICP-MS U-Pb 年龄及地质意义. 地质通报，32：1260-1268.

周志广, 张华峰, 刘还林, 柳长峰, 刘文灿. 2009. 内蒙古中部四子王旗地区基性侵入岩锆石定年及其意义. 岩石学报，25：1519-1528.

周志广，谷永昌，柳长峰，於炀森，张冰，田志君，何付兵，王必任. 2010. 内蒙古东乌珠穆沁旗满都胡宝拉格地区早-中二叠世华夏植物群的发现及地质意义. 地质通报，29：21-25.

Andersen, T. 2002. Correction of common lead in U-Pb analyses that do not report ^{204}Pb. Chemical Geology 192, 59-79.

Atherton, M.P., and Ghani, A.A., 2002. Slab breakoff: a model for Caledonian, Late Granite syn-collisional magmatism in the orthotectonic (metamorphic) zone of Scotland and Donegal, Ireland. Lithos 62, 65-85.

Badarch, G., Cunningham, W.D., Windley, B.F., 2002. A new terranne subdivision for Mongolia: implications for the Phanerozoic crustal grouth of Central Asia. Journal of Asian Earth Sciences 21, 87-100.

Bazhenov, M.L., Levashova, N.M., Degtyarev, K.E., Van der Voo, R., Abrajevitch, A.V., McCausland, P.J.A., 2012. Unraveling the early–middle Paleozoic paleogeography of Kazakhstan on the basis of Ordovician and Devonian paleomagnetic results. Gondwana Research 22, 974-991.

Burchette, T.P., and Wright, V.P., 1992. Carbonate ramp depositional systems. Sedimentary Geology 79, 3-57.

Bussien, D., Gombojav, B., Winkler, W., Von Quadt, A., 2011. The Mongol–Okhotsk Belt in Mongolia - An appraisal of the geodynamic development by the study of sandstone provenance and detrital zircons. Tectonophysics 510, 132-150.

Cao, H.H., Xu, W.L., Pei, F.P., Wang, Z.W., Wang, F., Wang Z.J., Wang, F., Wang, Z.J., 2013. Zircon U–Pb geochronology and petrogenesis of the Late Paleozoic–Early Mesozoic intrusive rocks in the eastern segment of the northern margin of the North China Block. Lithos 170-171, 191-207.

Caridroit, M., Ferrière, J., Dégardin, J.M., Vachard, D., Clément, B., 2000. Première datation des lydiennes paléozoïques dans les Hellénides internes (mont Parnis, Grèce); implications géologiques. Science Paris, Sciences de la Terre et des planètes / Earth and Planetary Sciences 331, 413-418.

Caridroit, M., Lamerandt, A., Dégardin, J.M., De Dios, A.F., Vachard, D., 2002. Discovery of radiolaria and conodonts in the Carboniferous-Permian of San Salvador Patlanoaya (Puebla, Mexico); biostratigraphic implications. Comptes Rendus Palevol 1, 205-211.

Cawood, P.A., Kroner, A., Collins, W.J., Kusky, T.M., Mooney, W.D., Windley, B.F., 2009. Accretionary orogens through Earth history, in Cawood P., and Kroner A. (Eds.), Earth

Accretionary systems in space and time. Geological Society, London, Special Publication 318, 1-36.

Chamyal, L.S., Khadkikar, A.S., Malik, J.N., Maurya, D., 1997. Sedimentology of the Narmada alluvial fan, western India. Sedimentary Geology 107, 263-279.

Charles, N., Chen, Y., Augier, R., Gumiaux, C., Lin, W., Faure, M., Monié, P., Choulet, F., Wu, F.Y., Zhu, R.X., Wang, Q.C., 2011. Palaeomagnetic constraints from granodioritic plutons (Jiaodong Peninsula): New insights on Late Mesozoic continental extension in Eastern Asia. Physics of the Earth and Planetary Interiors 187, 276-291.

Chen, B., Jahn, B.M., Tian, W., 2009. Evolution of the Solonker suture zone: constraints from zircon U–Pb ages, Hf isotopic ratios and whole-rock Nd–Sr isotope compositions of subductionand collision-related magmas and forearc sediments. Journal of Asian Earth Sciences 34, 245-257.

Chen, B., Jahn, B.M., Wilde, S., Xu, B., 2000. Two contrasting Paleozoic magmatic belts in northern Inner Mongolia, China: petrogenesis and tectonic implications. Tectonophysics 328, 157-182.

Chen, C., Zhang, Z.C., Guo, Z.J., Li, J.F., Feng, Z.S., Tang, W.H., 2012. Geochronology, geochemistry, and its geological significance of the Permian Mandula mafic rocks in Damaoqi, Inner Mongolia. Science China Earth Sciences 55, 39-52.

Chen, H., Dobson, J.P., Heller, F., Hao, J., 1997. Preliminary paleomagneticre sultsf rom the Upper Carboniferous of Uliastai Block, Inner Mongolia, China. Geophysical Research Letters 24, 2833-2836.

Choulet, F., Chen, Y., Wang, B., Faure, M., Cluzel, D., Charvet, J., Lin, W., Xu, B., 2011. Late Palaeozoic palegeographic reconstruction of western Central Asia based upon paleomagnetic data and its geodynamic implications. Journal of Asian Earth Sciences 42, 867-884.

Choulet, F., Chen, Y., Cogné, J-P., Rabillard, A., Wang, B., Lin, W., Faure, M., Cluzel, D., 2013. First Triassic palaeomagnetic constraints from Junggar (NW China) and their implications for the Mesozoic tectonics in Central Asia. Journal of Asian Earth Sciences 78, 371-394.

Cogné, J.P., 2003. A Macintosh TM application for treating paleomagnetic data and making plate reconstructions. Geochemistry, Geophysics, Geosystems, 4, http://dx.doi.org/10.1029/2001GC000227.

Cogné, J. P., Kravchinsky, V. A., Halim, N., Hankard, F., 2005. Late Jurassic–Early Cretaceous closure of the Mongol-Okhotsk Ocean demonstrated by new Mesozoic palaeomagnetic results from the Trans-Baikal area (SE Siberia). Geophysical Journal International 163, 813-832.

Coniglio, M., and Dix, G.R., 1992. Carbonate slopes. In: Walker, R.G., James, N.P. (Eds.), Facies Models: Response to Sea Level Change. Geological Association of Canada, Saint John's, pp. 349-373.

Corti, G., Van Wijk, J., Cloetingh, S., Morley, C.K., 2007. Tectonic inheritance and continental rift architecture: Numerical and analogue models of the East African Rift system. Tectonics 26, TC6006, doi:10.1029/2006TC002086.

Cottrell, R.D., Tarduno, J. A., Roberts, J., 2008. The Kiaman Reversed Polarity Superchron at Kiama: Toward a field strength estimate based on single silicate crystals. Physics of the Earth and Planetary Interiors 169, 49-58.

Daoudene, Y., Gapais, D., Ruffet, G., Gloaguen, E., Cocherie, A., Ledru, P., 2012. Syn-thinning pluton emplacement during Mesozoic extension in eastern Mongolia. Tectonics 31, TC3001, doi:10.1029/2011TC002926.

De Jong, K., Xiao, W.J., Windley, B.F., Masago, H., Lo, C.H., 2006. Ordovician $^{40}Ar/^{39}Ar$ phengite ages from the blueschist-facies Ondor Sum subduction–accretion complex (Inner Mongolia) and implications for the Early Paleozoic history of continental blocks in China and adjacent areas. American Journal of Science 306, 799-845.

Demoux, A., Kröner, A., Badarch, G.T., Jian, P., Tomurhuu, D., Wingate, M.T.D., 2009a. Zircon ages from the Baydrag Block and the Bayankhongorophiolite zone: time constraints on late Neoproterozoic to Cambrian subduction- and accretion-related magmatism in Central Mongolia. Journal of Geology 117, 377-397.

Demoux, A., Kröner, A., Liu, D., Badarch, G., 2009b. Precambrian crystalline basement in southern Mongolia as revealed by SHRIMP zircon dating. International Journal of Earth Sciences 98, 1365-1380.

Deng, S.H., Wan, C.B., Yang, J.G., 2009. Discovery of a Late Permian Angara-Cathaysia mixed flora from Acheng of Heilongjiang, China, with discussions on the closure of the Paleoasian Ocean. Science China Series D-Earth Science 52, 1746-1755.

Ebinger, C.J., Deino, A.L., Tesha, A.L., Becker, T., Ring, U., 1993. Tectonic Controls on Rift

Basin Morphology: Evolution of the Northern Malawi (Nyasa) Rift. Journal of Geophysical Research 98, 17821-17836.

Eizenhofer, P.R., Zhao, G., Zhang, J., Sun, M., 2014. Final closure of the Paleo-Asian Ocean along the Solonker Suture Zone: Constraints from Geochronological and Geochemical data of Permian volcanic and sedimentary rocks. Tectonics 33, 1-23.

Enkin, R.J., Yang, Z. Y., Chen, Y., Courtillot, V., 1992. PaleomagneticC onstraintso n the GeodynamicH istory of the Major Blocks of China From the Permian to the Present. Journal of Geophysical Research 97, 13953-13989.

Enkin, R.J., 2003. The direction-correction tilt test: an all-purpose tilt/fold test for paleomagnetic studies. Earth and Planetary Science Letters 212, 151-166.

Festa, A., Pini, G.A., Dilek, Y., Codegone, G., 2010. Mélanges and mélange-forming processes: a historical overview and new concepts. International Geology Review 52, 1040-1105.

Festa, A., Dilek, Y., Pini, G.A., Codegone, G., Ogata, K., 2012. Mechanisms and processes of stratal disruption and mixing in the development of mélanges and broken formations: Redefining and classifying mélanges. Tectonophysics 568-569, 7-24.

Fisher, R., 1953. Dispersion on a sphere. Proceeding the Royal of Society, London, Series A 217, 295-305.

Garcia, A.S., Thomas, D.N., Liss, D., Shaw, J., 2006. Low geomagnetic field intensity during the Kiaman superchron: Thellier and microwave results from the Great Whin Sill intrusive complex, northern United Kingdom. Geophysical Research Letter 33, L16308, doi:10.1029/2006GL026729.

Gawthorpe, R.L., and Hurst, J.M., 1993. Transfer zones in extensional basins: their structural style and influence on drainage development and stratigraphy. Journal of the Geological Society, London 150, 1137-1152.

Gawthorpe, R.L., and Leeder, M.R., 2000. Tectono-sedimentary evolution of active extensional basins. Basin Research 12, 195-218.

Gilder, S.A., Gomez, J., Chen, Y., Cogne J.P., 2008. A new paleogeographic configuration of the Eurasian landmass resolves a paleomagnetic paradox of the Tarim Basin (China). Tectonics 27, TC1012, doi:10.1029/2007TC002155.

Goldfarb, R.J., Taylor, R.D., Collins, G.S., Goryachev, N.A., Orlandini, O.F., 2014. Phanerozoic

continental growth and gold metallogeny of Asia. Gondwana Research 25, 48-102.

Graham, S.A., Hendrix, M.S., Johnson, C.L., Badamgarav, D., Badarch, G., Amory, J., Porter, M., Barsbold, R., Webb, L.E., Hacker, B.R., 2001. Sedimentary record and tectonic implications of Mesozoic rifting in southeast Mongolia. Geological Society of America Bulletin 113, 1560-1579.

Groves, D.I., and Bierlein, F.P., 2007. Geodynamic settings of mineral deposit systems. Journal of the Geological Society, London 164, 19-30.

Guy, A., 2012. Caractérisation géologique et géophysique de système d'accrétion et de collision : application à la ceinture orogénique d'Asie centrale et au Massif de Bohême. Doctoral dissertation of Strasbourg University, France, 1-261.

Halim, N., Kravchinsky, V., Gilder, S., Cogne, J.P., Alexyutin, M., Sorokin, A., Courtillot, V., Chen, Y., 1998. A palaeomagnetic study from the Mongol–Okhotsk region: rotated Early Cretaceous volcanics and remagnetized Mesozoic sediments. Earth and Planetary Science Letters 159, 133-145.

Han, B.F., Wang, S.G., Jahn, B.M., Hong, D.W., Kagami, H., Sun, Y.L., 1997. Depleted-mantle magma source for the Ulungur River A-type granites from north Xinjiang, China: geochemistry and Nd-Sr isotopic evidence, and implication for Phanerozoic crustal growth. Chemical Geology 138, 135-159.

Han, G., Liu, Y., Neubauer, F., Genser, J., Li, W., Zhao, Y., Liang, C., 2011.Origin of terranes in the eastern Central Asian Orogenic Belt, NE China: U–Pb ages ofdetrital zircons from Ordovician–Devonian sandstones, North Da Xing'an Mts.Tectonophysics 511, 109-124.

Hendrix, M.S., Graham, S.A., Amory, J.Y., Badarch, G., 1996. Noyon Uul syncline, southern Mongolia: Lower Mesozoic sedimentary record of the tec1tonic amalgamation of central Asia. Geological Society of America Bulletin 108, 1256-1274.

Heumann, M. J., Johnson, C. L., Webb. L. E., Taylor, J.P., Jalbaa, U., Minjin, C., 2012. Paleogeographic reconstruction of a late Paleozoic arc collision zone, southern Mongolia. Geological Society of America Bulletin 124, 1514-1534.

Hsu, K.J., Wang, Q., Li., J., Hao, J., 1991. Geologic evolution of the Neimonids: A working hypothesis. Eclogae Geological Helv. 84, 1-31.

Huang, B.C., Otofuji, Y., Yang, Z.Y., Zhu, R.X., 2000. New Silurian and Devonian

palaeomagnetic results from the Hexi Corridor terrane, northwest China, and their tectonic implications. Geophysical Journal International 140, 132-146.

Jahn, B.M., 2004. The Central Asian Orogenic Belt and Growth of the Continental Crust in the Phanerozoic. Geological Society, London, Special Publication 226, 73-100.

Jahn, B.M., Wu, F.Y., Chen, B., 2000. Granitoids of the Central Asian Orogenic Belt and continental growth in the Phanerozoic. Trans Royal Society Edinburgh: Earth Science 91, 181-193.

Jahn, B.M., Litvinovsky, B.A., Zanvilevich, A.N., Reichow, M., 2009. Peralkaline granitoid magmatism in the Mongolian–Transbaikalian Belt: Evolution, petrogenesis and tectonic significance. Lithos 113, 521-539.

Jian, P., Liu, D.Y., Kröner, A., Windley, B.F., Shi, Y.R., Zhang, F.Q., Shi, G.H., Miao, L.C., Zhang, W., Zhang, Q., Zhang, L.Q., Ren, J.S., 2008. Time scale of an early to mid-Paleozoic orogenic cycle of the long-lived Central Asian Orogenic Belt, Inner Mongolia of China: implications for continental growth. Lithos 101, 233-259.

Jiang, N., 2005. Petrology and geochemistry of the Shuiquangou syenitic complex, northern margin of the North China Craton. Journal of the Geological Society, London 162, 203-215.

Johnson, C.L., Amory, J. A., Zinniker, D., Lamb, M. A., Graham, S. A., Affolter, M., Badarch, G., 2008. Sedimentary response to arc-continent collision, Permian , southern Mongolia, in Draut, A.E., Clift, P.D., and Scholl, D.W., eds., Formation and Applications of the Sedimentary Record in Arc Collision Zones. Geological Society of America Specical Paper 436, 363-390.

Kametaka, M., Takebe, M., Nagai, H., Zhu, S., Takayanagi, Y., 2005. Sedimentary environments of the Middle Permian phosphorite–chert complex from the northeastern Yangtze platform, China; the Gufeng Formation: a continental shelf radiolarian chert. Sedimentary Geology 174, 197-222.

Kelty, T.K., Yin, A., Dash, B., Gehrels, G.E., Ribeiro, A.E., 2008. Detrital-zircon geochronology of Paleozoic sedimentary rocks in the Hangay–Hentey basin, north-central Mongolia: Implications for the tectonic evolution of the Mongol–Okhotsk Ocean in central Asia. Tectonophysics 451, 290-311.

Khain, E.V., Bibikova, E.V., Kroner, A., Zhuravlev, D.Z., Sklyarov, E.V., Fedotova, A.A., Kravchenko-Berezhnoy, I.R., 2002. The most ancient ophiolite of the Central Asian fold belt:

U-Pb and Pb-Pb zircon ages for the Dunzhugur Complex, Eastern Sayan, Siberia, and geodynamic implications. Earth and Planetary Science Letters 199, 311-325.

Kirschvink, J.L., 1980. The least squares line and the analysis of paleomagnetic data. Geophysical Journal of Royal Astronomy Society 62, 699-718.

Kravchinsky, V.A., Sorokin, A.A., Courtillot, V., 2002a. Paleomagnetism of Paleozoic and Mesozoic sediments from the southern margin of Mongol-Okhotsk ocean, far eastern Russia. Journal of Geophysical Research 107, 2253, doi:10.1029/2001JB000672.

Kravchinsky, V.A., Cogné, J.P., Harbert, W., Kuzmin, M.I., 2002b. Evolution of the Mongol-Okhotsk ocean with paleomagnetic data from the suture zone. Geophysical Journal International 148, 34-57.

Kravchinsky, V.A., Konstantinov, K. M., Courtillot, V., Savrasov, J. I., Valet, J. P., Cherniy, S. D., Mishenin, S. G., Parasotka, B.S., 2002c. Palaeomagnetism of East Siberian traps and kimberlites: two new poles and palaeogeographic reconstructions at about 360 and 250 Ma. Geophysical Journal International 148, 1-33.

Kröner, A., Lehmann, J., Schulmann, K., Demoux, A., Lexa, O., Tomurhuu, D., Štípská, P., Otgonbator, D., Liu, D.Y., Wingate, M.T.D., 2010. Lithostratigraphic and geochronological constraints on the evolution of the Central Asian Orogenic Belt in SW Mongolia: Early Paleozoic rifting followed by late Paleozoic accretion. American Journal of Science 310, 523-574.

Kröner, A., Windley, B.F., Badarch, G., Tomurtogoo, O., Hegner, E., Jahn, B.M., Gruschka, S., Khain, E.V., Demoux, A., Wingate, M.T.D. 2007. Accretionary growth and crust formation in the Central Asian Orogenic Belt and comparison with the Arabian-Nubian shield. Geological Society of America Memoirs 200, 181-209.

Kröner, A., Kovach, V., Belousova, E., Hegner, E., Armstong, R., Dolgopolova, A., Seltmann, R., Alexeiev, D.V., Hoffmann, J.E., Wong, J., Sun, M., Cai, K., Wang, T., Tong, Y., Wilde, S.A., Degtyarev, K.E., Rytsk, E., 2014. Reassessment of continental growth during the accretionary history of the Central Asian Orogenic Belt. Gondwana Research 25, 103-125.

Kuhlemann, J., and Kempf, O., 2002. Post-Eocene evolution of the North Alpine Foreland Basin and its response to Alpine tectonics. Sedimentary Geology 152, 45-78.

Lamb, M.A., Badarch, G., Navratil, T., Poier, R., 2008. Structural and geochronologic data from

the Shin Jinst area, eastern Gobi Altai, Mongolia: implications for Phanerozoic intracontinental deformation in Asia. Tectonophysics 451, 312-330.

Lamb, M.A., Hanson, A. D., Graham, S. A., Badarch, G., Webb, L. E., 1999. Left-lateral sense offset of upper Proterozoic to Paleozoic features across the Gobi Onon, Tost, and Zuunbayan faults in southern Mongolia and implications for other Central Asian faults. Earth and Planetary Science Letters 173, 183-194.

Leeder, M.R., and Gawthorpe, R.L., 1987. Sedimentary models for extensional tilt-block/half-graben basins. Geological Society, London, Special Publications 28, 139-152.

Lehmann, J., Schulmann, K., Lexa, O., Corsini, M., Kröner, A., Štípská, P., Tomurhuu, D., Otgonbator, D., 2010. Structural constraints on the evolution of the Central Asian Orogenic Belt in SW Mongolia. American Journal of Science 310, 575-628.

Leppard, C.W., and Gawthorpe, R.L., 2006. Sedimentology of rift climax deep water systems; Lower Rudeis Formation, Hammam Faraun Fault Block, Suez Rift, Egypt. Sedimentary Geology 191, 67-87.

Levashova, N.M., Degtyarev, K.E., Bazhenov, M.L., Collins, A.Q., Van der Voo, R., 2003. Middle Paleozoic paleomagnetism of east Kazakhstan: post-Middle Devonian rotations in a large-scale orocline in the central Ural–Mongol belt. Tectonophysics 377, 249-268.

Levashova, N.M., Mikolaichuk, A.V., McCausland, P.J.A., Bazhenov, M.L., Van der Voo, R., 2007. Devonian paleomagnetism of the North Tian Shan: implications for the Middle–Late Paleozoic paleogeography of Eurasia. Earth and Planetary Science Letters 257, 104-120.

Levashova, N.M., Abrajevitch, A.V., Van der Voo, R., Bazhenov, M.L., 2009. Paleomagnetism of mid-Paleozoic subduction-related volcanics from the Chingiz Range in NE Kazakhstan: the evolving paleogeography of an amalgamating Eurasian supercontinent. Geological Society of America Bulletin 121, 555-573.

Li, D.P., Chen, Y.L., Wang, Z., Hou, K.J., Liu, C.Z., 2011. Detrital zircon U–Pb ages, Hfisotopesand tectonic implications for Palaeozoic sedimentary rocks from the Xing-Mengorogenic belt, middle-east part of Inner Mongolia, China. Geological Journal 46, 63-81.

Liu, J., Li, J., Chi, X., Qu, J., Hu, Z., Fang, F., Zhang, Z., 2013. A late-Carboniferous to early early-Permian subduction–accretion complex in Daqing pasture, southeastern Inner Mongolia:

Evidence of northward subduction beneath the Siberian paleoplate southern margin. Lithos 177, 285-296.

Li, J.Y., 2006. Permian geodynamic setting of Northeast China and adjacent regions: closure of the Paleo-Asian Ocean and subduction of the Paleo-Pacific Plate. Journal of Asian Earth Sciences 26, 207-224.

Liu, S., Hu, R.Z., Gao, S., Feng, C.X., Feng, G.Y., Coulson, I.M., Li, C.,Wang, T., Qi, Y,Q., 2010. Zircon U–Pb age and Sr–Nd–Hf isotope geochemistry of Permian granodiorite and associated gabbro in the Songliao Block, NE China and implications for growth of juvenile crust. Lithos 114, 423-436.

Liu, W., Siebel, W., Li, X. J., Pan, X. F., 2005. Petrogenesis of the Linxi granitoids, northern Inner Mongolia of China: Constraints on basaltic underplating. Chemical Geology 219, 5-35.

Ludwig, K.R., 2003. User's Manual for Isoplot 3.0: A Geochronological Toolkit for Microsoft Excel Berkeley Geochronology Center. special publication 4, 1-71.

Maruyama, S., and Parkinson, C.D., 2000. Overview of the geology, petrology and tectonic framework of the high-pressure-ultrahigh-pressure metamorphic belt of the Kokchetav Massif, Kazakhstan. Island Arc 9, 439-455.

McElhinny, M.W., Embleton, B. J. J., Ma, X. H., Zhang, Z. K., 1981. Fragmentation of Asia in the Permian. Nature 293, 212-216.

McFadden, P.L., and McElhinny, M.W., 1990. Classification of the reversal test in palaeomagnetism. Geophysical Journal International 103, 725-729.

Meng, E., Xu, W.L., Pei, F.P., Yang, D.B., Yu, Y., Zhang, X.Z., 2010. Detrital-zircon geochronology of Late Paleozoic sedimentary rocks in eastern Heilongjiang Province, NE China: Implications for the tectonic evolution of the eastern segment of the Central Asian Orogenic Belt. Tectonophysics 485, 42-51.

Meng, Z., Huang, H.F., Chen, Y.Z., Coe, R.S., 1990. The Late Permian pole of the western Jiuquan Basin (NW China) and its tectonic implication. Acta Sedmentary Sinica 8, 58-65.

Metelkin, D.V., Vernikovsky, V.A., Kazansky, A.Y., Wingate, M.T.D., 2010. Late Mesozoic tectonics of Central Asia based on paleomagnetic evidence. Gondwana Research 18, 400-419.

Mueller, J. F., Rogers, J. J. W., Jin, Y. G., Wang, H., Li, W., Chronic, J., Mueller J. F., 1991. Late Carboniferous to Permian sedimentation in Inner Mongolia, China, and tectonic relationships

between north China and Siberia. Journal of Geology 99, 251-263.

Pascal, C., Cloetingh, S.A.P.L., Davies, G.R., 2004. Asymmetric lithosphere as the cause of rifting and magmatism in the Permo-Carboniferous Oslo Graben. In: Wilson, M., Neumann, E.R., Davies, G.R., Timmerman, M.J., Heeremans, M., Larsen, B.T. (Eds.), Permo-Carboniferous Magmatism and Rifting in Europe. Geological Society, London, Special Publication 223, 139-156.

Pascal, C., van Wijk, J.W., Cloetingh, S.A.P.L., Davies, G.R., 2002. Effect of lithosphere thickness heterogeneities in controlling rift localization: numerical modeling of the Oslo Graben. Geophysical Research Letters 29, 1355, doi:10.1029/2001GL014354.

Pavlov, V.E., Courtillot, V., Bazhenov, M. L., Veselovsky, R. V., 2007. Paleomagnetism of the Siberian traps: New data and a new overall 250 Ma pole for Siberia. Tectonophysics 443, 72-92.

Pisarevsky, S.A., Gladkochub, D. P., Donskaya, T. A., De Waele, B., Mazukabzov, A. M., 2006. Palaeomagnetism and geochronology of mafic dykes in south Siberia, Russia: the first precisely dated Early Permian palaeomagnetic pole from the Siberian craton. Geophysical Journal International 167, 1-10.

Prosser, S., 1993. Rift-related depositional systems and their seismic expression. In: Williams, G.D., Dobb, A. (Eds.), Tectonics and Seismic Sequence Stratigraphy. Geological Society, London, Special Publication 71, 35-66.

Prothero, D.R. and Schwab, F., 2003. Sedimentary Geology An introduction to sedimentary rocks and stratigraphy. New York: W.H. Freeman and Company, pp.1-557.

Pruner, P., 1987. Palaeomagnetism and palaeogeography of Mongolia in the Cretaceous, Permian and Carboniferous - preliminary data. Tectonophysics 139, 155-167.

Pruner, P., 1992. Palaeomagnetism and palaeogeography of Mongolia from the Carboniferous to the Cretaceous-final report. Physics of the Earth and Planetary Interiors 70, 169-177.

Ramos, A., Sopeña, A., Pérez-Arlucca, M., 1986. Evolution of the Buntsandstcin fluvial sedimentation in the northwest lberian Ranges (Central Spain). Journal of Sediment Petrology 56, 862-875.

Ren, J., Tamaki, K., Li, S., Zhang, J., 2002. Late Mesozoic and Cenozoic rifting an dits dynamic setting in eastern China and adjacent areas. Tectonophysics 344, 175-205.

Ring, U., 1994. The influence of preexisting structure on the evolution of the Cenozoic Malawi rift (East African rift system). Tectonic 13, 313-326.

Rojas-Agranonte, A., Kroner, A., Demoux, A., Xia, X., Wang, W., Donskaya, T., Liu, D., Sun, M., 2011.Detrital and xenocrystic zircon ages from Neoproterozoic to Palaeozoic arc terranesof Mongolia: Significance for the origin of crustal fragments in the Central Asian Orogenic Belt. Gondwana Research 19, 751-763.

Rubatto, D., 2002. Zircon trace element geochemistry: partitioning with garnet and the link between U-Pb ages and metamorphism. Chemical Geology 184, 123-138.

Safonova, I.Y., and Santosh, M., 2014. Accretionary complexes in the Asia-Pacific region: Tracing archives of ocean plate stratigraphy and tracking mantle plumes. Gondwana Research 25, 126-158.

Schulmann, K., and Paterson, S., 2011. Geodynamics: Asian continental growth. Nature Geoscience 4, 827-829.

Seltmann, R., Porter, T.M., Pirajno, F., 2014. Geodynamics and metallogeny of the central Eurasian porphyry and related epithermal mineral systems: A review. Journal of Asian Earth Sciences 79, 810-841.

Sengör, A.M.C., Natal'in, B.A., Burtman, V.S. 1993. Evolution of the Altaid tectonic collage and Paleozoic crustal growth in Eurasia. Nature 364, 299-307.

Sengör, A.M.C., and Natal'in, B.A., 1996. Palaeotectonics of Asia: fragments of a synthesis, in: Rubey Colloquium, C.U.P., Cambridge (Ed.), The Tectonic Evolution of Asia, pp. 486-640.

Shen, S.Z., Zhang, H., Shang, Q.H., Li, W.Z., 2006. Permian stratigraphy and correlation of Northeast China: A review. Journal of Asian Earth Sciences 26, 304-326.

Shi, G., Faure, M., Xu, B., Zhao, P., Chen, Y., 2013. Structural and kinematic analysis of the Early Paleozoic Ondor Sum-Hongqi mélange belt, eastern part of the Altaids (CAOB) in Inner Mongolia, China. Journal of Asian Earth Sciences 66, 123-139.

Sorokin, A.A., Kotov, A.B., Sal'nikova, E.B., Kudryashov, N.M., Velikoslavinskii, S.D., Yakovleva, S.Z., Fedoseenko, A.M., Plotkina, Y.V., 2011. Early Paleozoic Granitoids in the Lesser Khingan Terrane, Central Asian Fold belt: Age, Geochemistry, and Geodynamic Interpretations. Petrology 19, 601-617.

Tang, J., Xu, W.L., Wang, F., Wang, W., Xu, M.J., Zhang, Y.H., 2013. Geochronology and

geochemistry of Neoproterozoic magmatism in the Erguna Massif, NE China: Petrogenesis and implications for the breakup of the Rodinia supercontinent. Precambrian Research 224, 597- 611.

Tang, K.D., 1990. Tectonic development of Paleozoic fold belts at the north margin of the Sino–Korean craton. Tectonics 9, 249-260.

Tang, K.D., and Yan, Z.Y., 1993. Regional metamorphism and tectonic evolution of the Inner Mongolian suture zone. Journal of Metamorphic Geology 11, 511-522.

Turner, S.A., 2010. Sedimentary record of Late Neoproterozoic rifting in the NW Tarim Basin, China. Precambrian Research 181, 85-96.

Van der Voo, R., Levashova, N.M., Skrinnik, L.I., Kara, T.V., Bazhenov, M.L., 2006. Late orogenic, large-scale rotations in the Tien Shan and adjacent mobile belts in Kyrgyzstan and Kazakhstan. Tectonophysics 426, 335-360.

Veselovsky, R.V., Gallet, Y., Pavlov, V. E., 2003. Paleomagnetism of Traps in the Podkamennaya Tunguska and Kotui River Valleys: Implications for the Post-Paleozoic Relative Movements of the Siberian and East European Platforms. Physics Solid Earth 39, 856-871.

Wang, B., Chen, Y., Zhan, S., Shu, L.S., Faure, M., Cluzel D., Charvet, J., Laurent-Charvet, S., 2007. Primary Carboniferous and Permian paleomagnetic results from the Yili Block (NW China) and their implications on the geodynamic evolution of Chinese Tianshan Belt. Earth and Planetary Science Letters 263, 288-308.

Wang, C., Wang, P., Li, W., 2004. Conodonts from the Permian Jisu Honguer (Zhesi) Formation of Inner Mongolia, China. Geobios 37, 471-480.

Wang, F., Xu, W.L., Meng, E., Cao, H.H., Gao, F.H., 2012. Early Paleozoic amalgamation of the Songnen–Zhangguangcai Range and Jiamusi massifs in the eastern segment of the Central Asian Orogenic Belt: Geochronological and geochemical evidence from granitoids and rhyolites. Journal of Asian Earth Sciences 49, 234-248.

Wang, F., Xu, W.L., Gao, F.H., Zhang, H.H., Pei, F.P., Zhao, L., Yang, Y., 2014. Precambrian terrane within the Songnen–Zhangguangcai Range Massif, NE China: Evidence from U–Pb ages of detrital zircons from the Dongfengshan and Tadong groups. Gondwana Research 26, 402-413.

Wang, T., Zheng, Y.D., Gehrels, G.E., Mu, Z.G., 2001.Geochronological evidence for existence of

the south Mongolian microcontinent: a zircon U–Pbage of granitoid gneisses from the Yagan–OnchHayrhan metamorphic core complex on the Sino–Mongolian border. China Science Bulltin 46, 2005-2008.

Webb, L.E., Graham, S. A., Johnson, C. L., Badarch, G., Hendrix, M. S., 1999. Occurrence, age, and implications of the Yagan–Onch Hayrhan metamorphic core complex, southern Mongolia. Geology 27, 143-146.

Webb, L.E. and Johnson, C. L., 2006. Tertiary strike-slip faulting in southeastern Mongolia and implications for Asian tectonics. Earth and Planetary Science Letters 241, 323-335.

Wei, H.H., Meng, Q. R., Wu, G. L., Li, L., 2012. Multiple controls on rift basin sedimentation in volcanic settings: Insights from the anatomy of a small Early Cretaceous basin in the Yanshan belt, northern North China. Geological Society of America Bulletin 124, 380-399.

Wilhem, C., Windley, B.F., Stampfli, G.M., 2012. The Altaids of Central Asia: A tectonic and evolutionary innovative review. Earch-Science Reviews 113, 303-341.

Wilson, J.T., 1966. Did the Atlantic close and then re-open? Nature 211, 676-681.

Windley, B.F., Alexeiev, D., Xiao, W.J., Kröner, A., Badarch, G., 2007. Tectonic models for accretion of the Central Asian Orogenic Belt. Journal of the Geological Society London 164, 31-47.

Wnuk, C., 1996. The development of floristic provinciality during the Middle and Late Paleozoic. Review of Palaeobotany and Palynology 90, 5-40.

Wu, F.Y., De, Y.S., Wen, C.G., Zhang, Y.B., Grant, M.L., Wilde, S.A., Jahn, B.M., 2011. Geochronology of the Phanerozoic granitoids in northeastern China. Journal of Asian Earth Sciences 41, 1-30.

Wu, F.Y., Sun, D.Y., Li, H.M., Jahn, B.M., Wilde, S., 2002. A-type granites in northeastern China: age and geochemical constraints on their petrogenesis. Chemical Geology 187, 143-173.

Wu, F.Y., Lin, J. Q., Wilde, S.A., Sun, D. Y., Yang, J. H., 2005. Nature and significance of the Early Cretaceous giant igneous event in eastern China. Earth and Planetary Science Letters 233, 103-119.

Wu, G., Chen, Y., Chen, Y., Zeng Q., 2012. Zircon U–Pb ages of the metamorphic supracrustal rocks of the Xinghuadukou Group and granitic complexes in the Argun massif of the northern Great Hinggan Range, NE China, and their tectonic implications. Journal of Asian Earth

Sciences 49, 214-233.

Wu, G., Sun, F.Y., Zhao, C.S., Li, Z.T., Zhao, A.L., Pang, Q.B., Li, G.Y., 2005. Discovery ofthe Early Paleozoic post-collisional granites in northern margin of theErguna massif and its geological significance. Chinese Science Bulletin 50, 2733-2743.

Wu, H.N., Zhou, L. F., Zhao, Z. Y., 1993. Paleomagnetic study of Carboniferous and Permian rocks from the Alashan and surrounding regions and its tectonic implications. Science China Series B 23, 527-536.

Xiao, W., Huang, B., Han, C., Sun, S., Li, J., 2010. A review of the western part of the Altaids: a key to understanding the architecture of accretionary orogens. Gondwana Research 18, 253-273.

Xiao, W., and Santosh, M., 2014. The western Central Asian Orogenic Belt: A window to accretionary orogenesis and continental growth. Gondwana Research 25, 1429-1444.

Xiao, W.J., Windley, B., Hao, J., Zhai, M.G., 2003. Accretion leading to collision and the Permian Solonker suture, Inner Mongolia, China: termination of the Central Asian Orogenic Belt. Tectonics 22, 1069-1089.

Xu, B. and Chen, B., 1997. Framework and evolution of the middle Paleozoic oroginic belt between Siberian and North China Plates in northern Inner Mongolia. Science in China series D 40, 463-469.

Xu, B., Charvet, J., Chen, Y., Zhao, P., Shi, G.Z., 2013. Middle Paleozoic convergent orogenic belts in western Inner Mongolia (China): framework, kinematics, geochronology and implications for tectonic evolution of the Central Asian Orogenic Belt. Gondwana Research 23, 1342-1364.

Xu, X., Harbert, W., Dril, S., Kravchinksy, V., 1997. New paleomagnetic data from the Mongol–Okhotsk collision zone, Chita region, south-central Russia: Implications for Paleozoic paleogeography of the Mongol–Okhotsk Ocean. Tectonophysics 269, 113-129.

Yakubchuk, A.S., Shatov, V.V., Kirwin, D., Edwards, A., Tomurtogoo, O., Badarch, G., Buryak, V.A., 2005. Gold and Base Metal Metallogeny of the Central Asian Orogenic Supercollage. Economic Geology 100th Anniversary Volume, 1069-1096.

Yang, Z.Y., Ma, X. H. Huang, B. C., Sun, Z. M., Zhou, Y. X., 1998. Apparent polar wander path and tectonic movement of the North China Block in Phanerozoic. Science China Series D 41

Supplement, 51-65.

Yarmolyuk, V.V., Kovalenko, V.I., Sal'nikova E. B., Kovach, V. P., Kotov, A.B., Kovach, V.P., Vladykin, N.V., Yakovleva, S.Z., 2005. U–Pb Age of Syn- and Postmetamorphic Granitoids of South Mongolia: Evidence for the Presence of Grenvillides in the Central Asian Foldbelt. Doklady Earth Sciences 404, 986-990.

Yarmolyuk V. V., KovalenkoV. I., Sal'nikova E. B., Kovach, V. P., Kozlovsky, A.M., Kotov, A.B., Lebedev, V.I., 2008. Geochronology, Igneous Rocks and Formation of the Late Paleozoic South Mongolian Active Margin of the Siberian Continent. Stratigraphy and Geological Correlation 16, 162-181.

Ye, H.M., Li, X.H., Li, Z.X. Zhang, C.L., 2008. Age and origin of high Ba–Sr appinite granites at the northwestern margin of the Tibet plateau: implications for early Paleozoic tectonic evolution of the Western Kunlun orogenic belt. Gondwana Research 13, 126-138.

Yu, Q., Ge, W.C., Yang, H., Zhao, G.C., Zhang, Y.L., Su, Li., 2014. Petrogenesis of late Paleozoic volcanic rocks from the Daheshen Formation in central Jilin Province, NE China, and its tectonic implications: Constraints from geochronology, geochemistry and Sr–Nd–Hf isotopes. Lithos 192-195, 116-131.

Zhai, M.G., and Santosh, M., 2011. The early Precambrian odyssey of the North China Craton: a synoptic overview. Gondwana Research 20, 6-25.

Zhang, S. H., Zhao, Y., Song, B., Hu, J. M., Liu, S. W., Yang, Y. H., Chen, F. K., Liu, X. M., Liu, J., 2009a. Contrasting late Carboniferous and late Permian-middle Triassic intrusive suites from the northern margin of the north China craton. Geological Society of America Bulletin 121, 181-200.

Zhang, S.H., Zhao, Y., Liu, X.C., Liu, D.Y., Chen, F., Xie, L.W., Chen, H.H., 2009b. Late Paleozoic to Early Mesozoic mafic–ultramafic complexes from the northern North China Block: Constraints on the composition and evolution of the lithospheric mantle. Lithos 110, 229-246.

Zhang, S.H., Zhao, Y., Song, B., Yang, Z.Y., Hu, J.M., Wu, H., 2007. Carboniferous granitic plutons from the northern margin of the North China block: implications for a late Palaeozoic active continental margin. Journal of the Geological Society, London 164, 451-463.

Zhang, W., Jian, P., Kröner, A., Shi, Y.R., 2013. Magmatic and metamorphic development of an

early to mid-Paleozoic continental margin arc in the southernmost Central Asian Orogenic Belt, Inner Mongolia, China. Journal of Asian Earth Sciences 72, 63-74.

Zhang, X.H., Wilde, S.A., Zhang, H.F., Tang, Y.J., Zhai, M.G., 2009. Geochemistry of hornblende gabbros from Sonidzuoqi, Inner Mongolia, North China: implications for magmatism during the final stage of suprasubductionzone ophiolite formation. International Geology Review 51, 345 -373.

Zhang, X.H., Gao, Y., Wang, Z., Liu, H., Ma, Y., 2012. Carboniferous appinitic intrusions from the northern North China Craton geochemistry, petrogenesis and tectonic implications. Journal of the Geological Society, London 169, 337-351.

Zhang, X.H., Wilde, S.A., Zhang, H.F., Zhai, M.G., 2011. Early Permian high-K calc-alkaline volcanic rocks from NW Inner Mongolia, North China: geochemistry, origin and tectonic implications. Journal of the Geological Society, London 168, 525-543.

Zhang, X.H., Zhang, H.F., Jiang, N., Zhai, M.G., Zhang, Y.B., 2010. Early Devonian alkaline intrusive complex from the northern North China craton: a petrological monitor of post-collisional tectonics. Journal of the Geological Society, London 167, 717-730.

Zhang, X.H., Zhang, H.F., Tang, Y.J., Wilde, S.A., Hu, Z.C., 2008. Geochemistry of Permian bimodal volcanic rocks from Central Inner Mongolia, North China: Implication for tectonic setting and Phanerozoic continental growth in Central Asian Orogenic Belt. Chemical Geology 249, 261-281.

Zhang, X., Yuan, L., Xue, F., Yan, X., Mao, Q., 2014. Early Permian A-type granites from central Inner Mongolia, North China: Magmatic tracer of post-collisional tectonics and oceanic crustal recycling. Gondwana Research, doi: 10.1016/j.gr.2014.02.011

Zhao, P., Fang, J., Xu, B., Chen, Y., Faure, M., 2014. Early Paleozoic tectonic evolution of the Xing-Meng Orogenic Belt: Constraints from detrital zircon geochronology of western Erguna-Xing'an Block, North China. Journal of Asian Earth Sciences, http://dx.doi.org/10.1016/j.jseaes.2014.04.011

Zhao, X.X. and Coe, R., 1989. Tectonic implications of Permo-Trassic paleomagnetic results from North and South China. In: J.W. Hillhouse (Editor), Deep Structure and Past Kinematics of Accreted Terranes. IUG-G Geophysical Monograph 5, 267-283.

Zhao, X., Coe, R.S., Zhou, Y., Wu, H., Wang, J., 1990. New paleomagnetic results from northern

China: collision and suturing with Siberia and Kazakhstan. Tectonophysics 181, 43-81.

Zhao, X.X., Coe, R. S., Wu, H. N., Zhao, Z.Y., 1993. Silurian and Devonian palaeomagnetic poles from North China and implications for Gondwana. Earth and Planetary Science Letters 117, 497-506.

Zhou, J.B., Wilde, S.A., Zhang, X.Z., Zhao, G.C., Zheng, C.Q., Wang, Y.J., Zhang, X.H., 2009. The onset of Pacific margin accretion in NE China: evidence from the Heilongjiang high-pressure metamorphic belt. Tectonophysics 478, 230-246.

Zhou, J.B, and Wilde, S.A., 2013. The crustal accretion history and tectonic evolution of the NE China segment of the Central Asian Orogenic Belt. Gondwana Research 23, 1365-1377.

Zhou, J.B., Wilde, S.A., Zhang, X.Z., Ren, S.M., Zheng, C.Q., 2011.Early Paleozoic metamorphic rocks of the Erguna block in the Great Xing'an Range, NE China: Evidence for the timing of magmatic and metamorphic events and their tectonic implications. Tectonophysics 499, 105-117.

Appendix Paper published

Zhao, P., Chen, Y., Xu, B., Faure, M., Shi, G., Choulet, F., 2013. Did the Paleo-Asian Ocean between North China Block and Mongolia Block exist during the late Paleozoic? First paleomagnetic evidence from central-eastern Inner Mongolia, China. Journal of Geophysical Research Solid Earth, 118, 1873–1894, doi:10.1002/jgrb.50198.

Zhao, P., Y. Chen, Zhan, S., Xu, B., Faure, M., 2014. The Apparent Polar Wander Path of the Tarim block (NW China) sincethe Neoproterozoic and its implications for a long-term Tarim–Australia connection. Precambrian Research 242, 39-57.

Zhao, P., Fang, J., Xu, B., Chen, Y., Faure, M., 2014. Early Paleozoic tectonic evolution of the Xing-Meng Orogenic Belt: constraints from detrital zircon geochronology of western Erguna-Xing'an Block, North China. Journal of Asian Earth Sciences, http://dx.doi.org/10.1016/j.jseaes.2014.04.011.

Zhao, P., Xu, B., Tong, Q., Chen, Y., Faure, M., Sedimentological and geochronological constrainst on the Carboniferous evolution of central Inner Mogolia, southeastern Central Asian Orogenic Belt: inland sea deposition in a post-orogenic setting. Gondwana Research, in revision.

Xu, B., Charvet, J., Chen, Y., **Zhao, P.,** Shi, G.Z., 2013. Middle Paleozoic convergent orogenic belts in western Inner Mongolia (China): framework, kinematics, geochronology and implications for tectonic evolution of the Central Asian Orogenic Belt. Gondwana Research 23, 1342-1364.

Shi, G., Faure, M., Xu, B., **Zhao, P.**, Chen, Y., 2013. Structural and kinematic analysis of the Early Paleozoic Ondor Sum-Hongqi mélange belt, eastern part of the Altaids (CAOB) in Inner Mongolia, China. Journal of Asian Earth Sciences 66, 123-139.

徐备，**赵盼**，鲍庆中，周永恒，王炎阳、罗志文. 2014. 兴蒙造山带前中生代构造单元划分. 岩石学报，待刊.

方俊钦，**赵盼**，徐备，邵军，汪岩. 2014. 内蒙古西乌珠穆沁旗哲斯组宏体化石新发现和沉积相分析. 岩石学报，待刊.

李瑞彪，徐备，**赵盼**，童勤龙，张晋瑞. 2014. 二连浩特艾力格庙地区蓝片岩相岩石的发现及其构造意义. 科学通报，59：66-71.

程胜东，方俊钦，**赵盼**，徐备，鲍庆中，周永恒，等荣敬. 2014. 内蒙古西拉木伦河两岸志留-泥盆系碎屑锆石年龄及其构造意义. 岩石学报，待刊.

JOURNAL OF GEOPHYSICAL RESEARCH: SOLID EARTH, VOL. 118, 1873–1894, doi:10.1002/jgrb.50198, 2013

Did the Paleo-Asian Ocean between North China Block and Mongolia Block exist during the late Paleozoic? First paleomagnetic evidence from central-eastern Inner Mongolia, China

Pan Zhao,[1,2] Yan Chen,[2] Bei Xu,[1] Michel Faure,[2] Guanzhong Shi,[1,2] and Flavien Choulet[2]

Received 13 December 2012; revised 18 April 2013; accepted 19 April 2013; published 30 May 2013.

[1] The tectonic evolution of the Paleo-Asian Ocean between the North China Block (NCB) and the Mongolia Block (MOB) is a contentious issue, and geodynamic models remain speculative. In an effort to puzzle out this controversy, a paleomagnetic study was carried out on the Silurian to Permian formations in central-eastern Inner Mongolia (China). More than 680 sedimentary and volcanic samples were collected from 86 sites. We have established titanium-poor magnetite and hematite as the principal magnetic carriers. Anisotropy of the magnetic susceptibility measurements demonstrate negligible deformation of the majority of study rocks with sedimentary fabrics. From primary magnetizations, a Late Devonian and a Permian pole are calculated for Inner Mongolia Block (IMB) at $\lambda = 46.8°$N, $\varphi = 349.1°$E, $dp = 14.6°$, $dm = 27.3°$ with $N = 3$ and $\lambda = 48.7°$N, $\varphi = 3.7°$E, $dp = 5.2°$, $dm = 9.1°$ with $N = 6$, respectively. Two stages of secondary magnetization are also identified probably due to Early Permian and Early Cretaceous magmatic events. As preliminary results, the comparison of our new paleomagnetic poles with available data from NCB, MOB, and Siberia indicates that (1) the paleolatitudes of IMB, NCB, and MOB are consistent between Late Devonian and Permian, suggesting pre-Late Devonian closure of the Paleo-Asian Ocean and further evaluation of these three blocks as a single entity and (2) post-Permian intracontinental deformation was significant and characterized by block rotations, which are due to strike-slip faulting within the welded NCB-IMB-MOB block.

Citation: Zhao, P., Y. Chen, B. Xu, M. Faure, G. Shi, and F. Choulet (2013), Did the Paleo-Asian Ocean between North China Block and Mongolia Block exist during the late Paleozoic? First paleomagnetic evidence from central-eastern Inner Mongolia, China, *J. Geophys. Res. Solid Earth*, *118*, 1873–1894, doi:10.1002/jgrb.50198.

1. Introduction

[2] Central-eastern Asia, located between the North China Block (NCB) and Siberia Block (SIB) (Figure 1a), is formed by long-term amalgamation of the NCB, the Mongolia Block (MOB, South Mongolia, and Amuria block), SIB, and several intermediate microcontinents [*Windley et al*., 2007]. It is considered as the southeastern part of the Altaids [*Sengör et al*., 1993], also known as the Central Asian Orogenic Belt (CAOB) in some papers [*Windley et al*., 2007; *Kröner et al*., 2010; *Xu et al*., 2012]. This area has attracted much attention from geoscientists for decades, as it represents a natural laboratory to understand accretionary processes and continental crust formation. Hence, it has been extensively studied from tectonic evolution [e.g., *Xiao et al*., 2003; *Windley et al*., 2007; *Xu et al*., 2012], geochemical and geochronological constrains [e.g., *Jahn et al*., 2009; *Litvinovsky et al*., 2011; *Wu et al*., 2011], and paleomagnetic reconstructions [e.g., *Zhao et al*., 1990; *Enkin et al*., 1992; *Pruner*, 1992; *Xu et al*., 1997; *Kravchinsky et al*., 2002a; *Cogné et al*., 2005].

[3] However, several issues dealing with the Paleozoic evolution of the Paleo-Asian Ocean between NCB and MOB are still controversial, especially the location of suture zone and the timing of the final oceanic closure. According to the unconformity between the Upper Devonian strata and the underlying rocks, and their different deformation patterns as well, *Tang* [1990] and *Xu et al*. [2012] suggested that two branches of the Paleo-Asian Ocean were closed in the Late Devonian to form two orogens between NCB and MOB, namely the North Orogen and the South Orogen (Figure 1b). These two belts are separated by a microcontinent, namely, the Hunshandake Block by *Xu et al*. [2012], referred as Inner Mongolia Block (IMB) in this paper. After that, this region underwent an extensional setting characterized by Early Permian alkine A-type granitoids and bimodal volcanic rocks [*Zhang et al*., 2008; *Jahn et al*., 2009; *Chen et al*., 2012] and extension-related sedimentation [*Tang*, 1990]. However, based on disputable geochemical interpretations, and occurrence of the Permian marine sediments, some authors

[1]Key Laboratory of Orogenic Belts and Crustal Evolution, Ministry of Education, Peking University, Beijing, China.
[2]Université d'Orléans, ISTO, UMR 7327, 45071, Orléans, France and CNRS/INSU, ISTO, UMR 7327, 45071 Orléans, France and BRGM, ISTO, UMR 7327, BP 36009, 45060 Orléans, France.

Corresponding author: B. Xu, Key Laboratory of Orogenic Belts and Crustal Evolution, Ministry of Education, Peking University, Beijing 100871, China. (bxu@pku.edu.cn)

2169-9313/13/10.1002/jgrb.50198

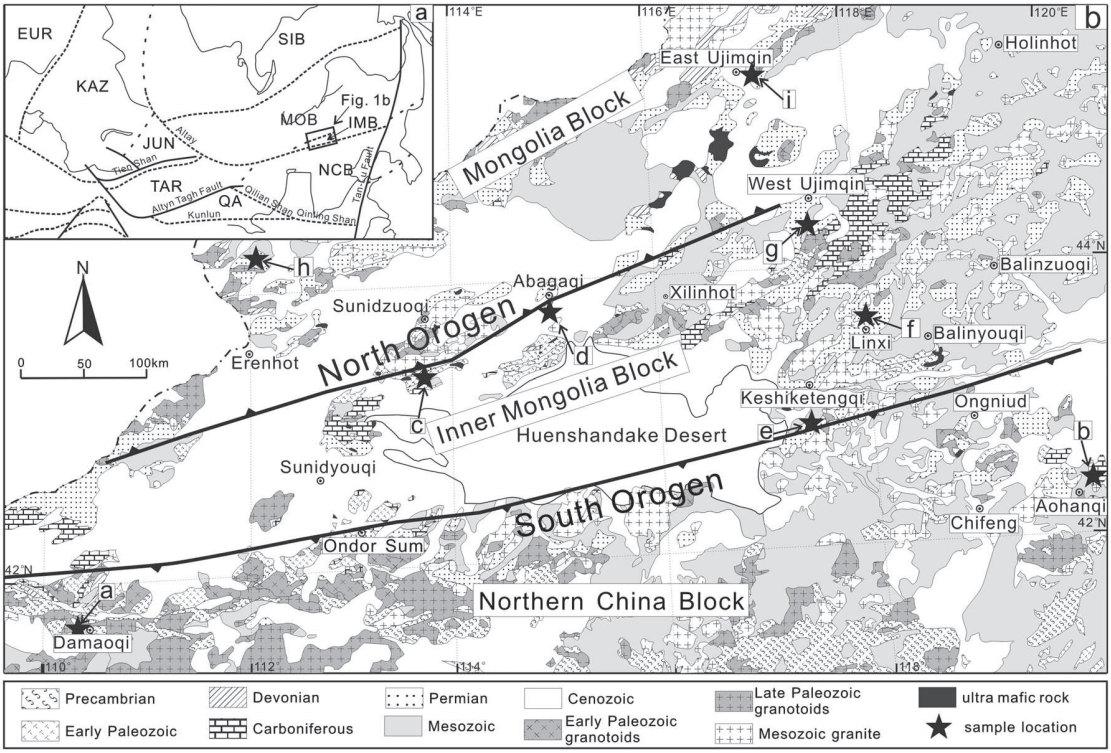

Figure 1. (a) Sketch tectonic map of Northeast Asia showing the main blocks and boundaries (modified after *Enkin et al*. [1992]). Block: EUR = Eurasia main plate; KAZ = Kazakhstan block; JUN = Junggar block; TAR = Tarim block; QA = Qaidam block; SIB = Siberia Block; MOB = Mongolia Block; NCB = North China Block. (b) Geological map of eastern Inner Mongolia emphasizing the two orogenic belts (North Orogen and South Orogen), late Paleozoic strata and intrusions (modified after *IMBGMR* [1991] and *Xu et al*. [2012]). Sampling localities: a, Damaoqi; b, Aohanqi; c, Sunidzuoqi; d, Abagaqi; e, Keshiketengqi; f, Linxi; g, West Ujimqin; h, Erenhot; i, East Ujimqin.

hypothesized that the Paleo-Asian Ocean has existed through the late Paleozoic, until the Late Permian when NCB and MOB collided [*Chen et al*., 2000; *Xiao et al*., 2003; *Johnson et al*., 2008; *Heumann et al*., 2012].

[4] Paleomagnetism is an efficient tool to study plate movements and to propose paleogeographic reconstructions. Thus, it could provide key arguments to solve the aforementioned controversy on Paleo-Asian Ocean. In East Asia, previous paleomagnetic studies have been concentrated on the study of the Mongol-Okhotsk Ocean between MOB and SIB [*Kravchinsky et al*., 2002a, 2002b; *Cogné et al*., 2005]. Conversely, paleomagnetic constraints for the Paleo-Asian Ocean remain rare and they were mostly carried out from the northern part of MOB, such as Trans-Baikal and upper Amur [*Pruner*, 1992; *Xu et al*., 1997; *Kravchinsky et al*., 2002a]. *Zhao et al*. [1990] have reported the first and only paleomagnetic study on Paleozoic rocks from Inner Mongolia; however, their results of the Late Permian (11 samples) and Carboniferous (29 samples) are clearly remagnetized with a negative fold test. Therefore, no reliable or utilizable Paleozoic paleomagnetic data are available up to now for Inner Mongolia area. For these reasons, a paleomagnetic study has been carried out on sedimentary and volcanic rocks from Paleozoic formations in central-eastern Inner Mongolia. The widespread desert and grassland hinder finding suitable outcrops for paleomagnetic sampling. It took us 3 years to investigate the area and to find all the outcrops presented in this paper.

2. Geological Setting and Paleomagnetic Sampling

2.1. Brief Geological Outline

[5] The central-eastern Inner Mongolia, located between the northern margin of the NCB and the southern margin of the MOB (Figure 1b), has recorded a complex subduction-collision history between these two continents [*Xiao et al*., 2003; *Windley et al*., 2007; *Jian et al*., 2008; *Zhang et al*., 2008; *Xu et al*., 2012]. Two well-documented ophiolitic mélange belts exposing blocks of blueschists and chert [*Xu et al*., 2001; *Xiao et al*., 2003; *De Jong et al*., 2006] are juxtaposed with two magmatic arcs, namely, the Baolidao Arc and the Bainaimiao Arc [*Chen et al*., 2000; *Jian et al*., 2008], which are located to the south of Sunidzuoqi and Ondor Sum, respectively (Figure 1b). An unconformable Late Silurian to Late Devonian molasse overlies the mélanges and postdates the early-middle Paleozoic orogenic events, recorded in the North Orogen and the South Orogen (Figure 1b) [*Tang*, 1990; *Xu et al*., 2012]. Between these two orogenic belts, a microcontinent (IMB) exposes a Precambrian basement [*Xu et al*., 2012]. In addition to the two ophiolitic mélanges, the occurrence of numerous ultramafic rocks, mainly serpentinite and metagrabbro, throughout central-eastern Inner Mongolia [*Miao et al*., 2007] led many authors to propose that they represent the ophiolitic remnants of the suture zone and to speculate that oceanic domains have persisted during the late Paleozoic [*Xiao et al*., 2003; *Li*, 2006;

Figure 2. Photographs of sampling outcrops. (a) red sandstone of S_3x in Damaoqi; (b) red sandstone of D_1c in Damaoqi; (c) limestone of C_1h in Aohanqi; (d) coarse sandstone of D_3s in Sunidzuoqi; (e) yellow siltstone of D_3s in Abagaqi; (f)coarse sandstone of P_3t in Keshiketengqi; (g) sandstone of P_3l in Linxi; (h) limestone of C_2a in West Ujimqin; (i) limestone of P_2z in West Ujimqin; (j) red sandstone of $D_{1\text{-}2}n$ in Erenhot; (k) volcaniclastic rocks of C_2-P_1g in East Ujimqin; and (i) dextral strike-slip fault observed 5 m to the right of Figure 2k position.

Miao et al., 2008]. However, the geochemical signature of most of these ultramafic rocks and their geological relationships with the surrounding units do not support an ophiolitic origin, and therefore, they do not represent a ophiolitic suture zone [*Miao et al.*, 2007; *Jian et al.*, 2012].

[6] The Precambrian basement of central-eastern Inner Mongolia is composed of the strongly deformed and metamorphosed Paleoproterozoic Baoyintu Group, and the Mesoproterozoic to Neoproterozoic Xilin Gol complex [*Inner Mongolian Bureau of Geology and Mineral Resources* (*IMBGMR*), 1991; *Xu and Chen*, 1997; *Ge et al.*, 2011]. The widespread undeformed Late Silurian and Late Devonian molassic deposits unconformably overlie the Precambrian rocks [*Xu and Chen*, 1997; *Zhang et al.*, 2010]. During the Carboniferous, IMB was covered by carbonate deposits with subordinate clastic rocks, which grade upward into Early Permian volcanic rocks, Middle Permian shallow marine deposits, and Late Permian lacustrine black mudstone-siltstone deposits [*IMBGMR*, 1991; *Mueller et al.*, 1991]. The widespread Early Permian volcanic and intrusive rocks are mostly alkaline or calc-alkaline, and the volcanic rocks present a bimodal geochemical signature, which suggest emplacement in an extensional tectonic setting [*Zhang et al.*, 2008, 2011; *Chen et al.*, 2012]. These extensional basins were closed at the end of Permian, as the Late Permian conglomerate unconformably overlying the folded Carboniferous-Permian strata. Subsequently, central-eastern Inner Mongolia experienced uplift and erosion until the deposition of Late Jurassic volcanic rocks and the formation of Early Cretaceous rift-related basins [*Meng*, 2003], associated with contemporaneous plutons intruded into the Paleozoic strata (Figure 1b).

[7] Concerning MOB, although there is no agreement for the existence of a single block, several microblocks recognized in southern Mongolia (e.g., Hutag Uul microblock and Baga Bogd massif) [*Wang et al.*, 2001; *Demoux et al.*, 2007], and in Amur area (e.g., central Mongolian, Argun, upper Amur, Khingan-Bureya blocks) [*Zonenshain et al.*, 1990] are thought to be nearby each other [*Zonenshain et al.*, 1990; *Kravchinsky et al.*, 2002a]. Meanwhile, all Paleozoic paleomagnetic results obtained on or at the margin of these microblocks display consistent paleolatitude [*Kravchinsky et al.*, 2002a and references therein], so we use MOB to represent these nearby microblocks. However, in the late Paleozoic, these microblocks may separate from each other with remnant seas, as Carboniferous arcs and marine deposits were identified [*Johnson et al.*, 2008]. The remnant seas were thought to be closed in the Late Permian, with the Permian marine succession overlain unconformably

by the Lower Triassic continental strata [*Johnson et al*., 2008; *Lehmann et al*., 2010; *Blight et al*., 2010; *Heumann et al*., 2012].

2.2. Stratigraphy of Sampled Strata

[8] The sampled strata range from Late Silurian to Late Permian, which are the key stages for studying the evolution of the eastern part of CAOB. In the following part, we describe the sampling localities using the tectonic division presented in the geological outline.

2.2.1. North Margin of NCB

[9] At the northern margin of NCB, two localities were sampled, namely Damaoqi to the west and Aohanqi to the east (localities a and b in Figure 1b, respectively).

[10] Late Silurian rocks are well defined as the Xibiehe Formation (S_3x) near Damaoqi County [*Zhang et al*., 2010]. It is composed of basal conglomerate at the bottom, grading upward into sandstone and limestone, containing corals and brachiopods, such as *Kyphophyllum*, *Progressum, syringopora*, etc. [*IMBGMR*, 1991, 2002]. Six sites of yellow sandstone with variable beddings were collected over a 500 m thick section (Figure 2a and Table 1). The Xibiehe Formation underlies the Lower Devonian Chaganhabu Formation (D_1c) with an unconformable contact. The Early Devonian assignment is based on the abundant corals, brachiopods, and bryozoans, such as *Favosites* sp. *Atrypa* sp. *Leptotrypafragilis* [*IMBGMR*, 2002]. To the north of Damaoqi, eight sites of red sandstone were collected from an about 800 m thick and gently folded section (Figure 2b and Table 1). It is worth noting that a dextral strike-slip fault showing mylonitic deformation has been identified three kilometers to the east of the sampling sites during our field work.

[11] To the north of Aohanqi County, seven sites were selected from the Lower Carboniferous Houfangshengou Formation (C_1h), which consists of thick-bedded (0.2–1 m) black limestone (Figure 2c and Table 1). This formation, more than 1200 m thick, attests for a stable platform carbonate setting. The well-preserved corals and brachiopods (*Gigantoproductus-Dibunophyllum*) constrain its Early Carboniferous age [*IMBGMR*, 1991]. Open fold without cleavage can be observed in this formation.

2.2.2. Inner Mongolia Block (IMB)

[12] Paleomagnetic samples were collected from five localities in IMB. From west to east, they are Sunidzuoqi, Abagaqi, Keshiketengqi, Linxi, and West Ujimqin (localities c, d, e, f and g, respectively, in Figure 1b).

[13] Near Sunidzuoqi and Abagaqi counties (Figure 1b), five sites of red coarse sandstone (Figure 2d) and six sites of yellow siltstone (Figure 2e) of the Upper Devonian Seribayanaobao Formation (D_3s) were collected, respectively (Table 1). The Upper Devonian Seribayanaobao Formation represents continental molasse deposits, which unconformably overlie the ophiolite mélange [*Xu and Chen*, 1997; *Xu et al*., 2012]. This formation mainly consists of red conglomerate, red-yellow sandstone, and yellow siltstone, with a top layer of argillaceous limestone. The plant fossils, such as *Leptophloeum rhombicum* in the sandstone and *Nalivkinella profunda* and *Cyrtospirifer sulcifer* in the limestone, attest to the Late Devonian age [*Xu et al*., 2012]. Near Sunidzuoqi, five sites of red sandstone were also collected from both limbs of a fold within the Lower Carboniferous Gouhuduge Formation (C_1g; Table 1), which conformably overlies the Upper Devonian strata. Open fold has been observed from Lower Carboniferous strata in the Sunidzuoqi, and the Upper Devonian strata in Abagaqi are highly tilted (Table 1).

[14] To the south of Keshiketengqi County, six sites of coarse sandstone of the Upper Permian Tieyingzi Formation (P_3t) were collected from a section with very gentile bedding (Figure 2f and Table 1). The alluvial-fluvial-lacustrine facies Tieyingzi Formation consists of conglomerate at the bottom, coarse-grained to conglomeratic sandstone in the middle, and red and green siltstone on the top. The Tieyingzi Formation unconformably overlies the Early-Middle Permian granite and the Lower-Upper Permian strata, with pebbles of all aforementioned rocks at the bottom. The enriched Late Permian plant fossils, such as *Pecopteris* sp. *Calamites* sp., *Nephropsis* sp, and the occurrence of the unconformity as well, assign the Tieyingzi Formation to the Late Permian.

[15] To the north of Linxi County, three sites of tuff and basalt from the Lower Permian Dashizhai Formation (P_1d) and three sites of sandstone from the Upper Permian Linxi Formation (P_3l) were collected (Figure 2g and Table 1). The Dashizhai Formation is composed of volcanic rocks erupted between 285 and 270 Ma, which belong to the major Late Paleozoic magmatic event widespread in Inner Mongolia [*Zhang et al*., 2008; *Liu*, 2009; *Chen et al*., 2012]. The Linxi Formation is composed of fluvial conglomerate at the bottom with pebbles of volcanic rocks of Dashizhai Formation, covered by approximately 4000 m thick black mudstone and dark yellowish siltstone/sandstone of fluvial-lacustrine facies [*Mueller et al*., 1991]. The plant fossils and fresh water bivalves, such as *Brachythyris* sp. and *Rhombotrypella* sp., and the minimum age of detrital zircons (256 ± 2Ma) [*Han et al*., 2011] well constrain its Late Permian age.

[16] To the south of West Ujimqin County, eight sites of limestone and three sites of grey fine-grained sandstone were sampled from the Upper Carboniferous Amushan Formation (C_2a; Figure 2h). As the most general Late Carboniferous deposits in Inner Mongolia, the Amushan Formation is composed of shallow marine facies carbonate and subordinate terrigeneous deposits with a well-defined age owing to enriched neritic fossils, such as *Pseudoschwagerina* and *Triticites*. To the north of West Ujimqin, five sites of yellow sandstone were sampled from both limbs of an open fold at the top of the Upper Carboniferous-Lower Permian Gegenaobao Formation (C_2-P_1g). The top sandstone of Gegenaobao Formation directly overlies volcanic rocks that have yielded a zircon concordant U-Pb age at 266 ± 2Ma (Zhao, unpublished data). Therefore, the collected sandstone is mid-Permian in age and we further use P_{2g} to represent the age for these five sites. To the south of West Ujimqin, six sites of dark blue thick-bedded limestone were collected from the middle Permian Zhesi Formation (P_2z; Figure 2i). The age determination of Zhesi Formation is based on the well-known Middle Permian Zhesi Fauna [*Wang et al*., 2004a]. The bedding attitude for the Zhesi Formation is nearly vertical, with very slight variations.

2.2.3. Southern Margin of MOB

[17] At the southern margin of MOB, two localities were chosen for paleomagnetic sampling. From west to east, they are Chaganaobao to the north of Erenhot (locality h in Figure 1b) and East-Ujimqin (locality i in Figure 1b).

Table 1. Paleomagnetic Sampling and Analysis Results From Inner Mongolia

Site	Coordinate	Rock	Age	Strike/Dip (°)	n′/n	N/R	Dg (°)	Ig (°)	Ds (°)	Is (°)	k	α_{95} (°)	Comments and Poles
					North China Block (NCB)								
Damaoqi													
1[a]	41°55′N,109°56E	red sandstone	D_1c	343.6/51.5	6/6	6/0	0.7	70.8	53.1	27.4	131.0	6.7	
2[b]	41°55′N,109°56E	red sandstone	D_1c	258.5/14	8/8	5/3	124.7	2.6	123.5	12.7	36.8	9.2	λ = 24.1°, φ = 354.2°, dp = 4.6°, dm = 9.2°
3	41°55′N,109°56E	red sandstone	D_1c	210/29	6/8	6/0	29.5	55.5	354.5	45.9	49.0	9.7	
4[b]	41°55′N,109°56E	red sandstone	D_1c	221/40	8/9	0/8	314.5	−17.2	317.1	−57.1	17.0	15.1	λ = 24.4°, φ = 340.7°, dp = 8.1°, dm = 15.6°
5	41°55′N,109°56E	red sandstone	D_1c	176/35	0/4	0/0	-	-	-	-	-	-	dispersed
6[b]	41°55′N,109°56E	red sandstone	D_1c	220.5/24	4/5	0/4	107.5	−3.6	106.0	18.5	42.0	15.1	λ = 14.2°, φ = 9.4°, dp = 7.6°, dm = 15.1°
7[b]	41°55′N,109°56E	red sandstone	D_1c	179.7/42	4/6 3/4	0/4	211.7	−16.3	195.3	−35.3	594.0	4.0	λ = 46.3°, φ = 241.1°, dp = 2.1°, dm = 4.1°
8[b]	41°55′N,109°56E	red sandstone	D_1c	190/51		0/3	235.3	−12.1	211.7	−42.2	90.0	7.1	λ = 29.5°, φ = 220.0°, dp = 3.7°, dm = 7.2°
9[a]	42°00′N,110°10′E	coarse sandstone	S_3x	289/20	6/6	2/4	6.1	63.8	11.1	44.0	94.0	6.9	
10[a]	42°00′N,110°10′E	coarse sandstone	S_3x	283.5/30	8/8	5/3	4.2	70.9	6.7	38.0	114.0	5.7	
12	42°00′N,110°10′E	coarse sandstone	S_3x	337/48	0/8	0/0	-	-	-	-	-	-	weak NRM, viscous
13[a]	42°00′N,110°10′E	greywacke	S_3x	338/49.5	7/9	4/3	5.8	66.0	44.2	26.7	21.2	13.4	
14	42°00′N,110°10′E	greywacke	S_3x	328/56	0/2	0/0	-	-	-	-	-	-	weak NRM, viscous
15	42°00′N,110°10′E	greywacke	S_3x	304/57	7/9	0/7	337.5	−9.5	314.5	−33.1	53.0	8.4	
			mean[a] (site 1, 9, 10,13)		4S/4S		3.3	67.1			635.0	3.6	λ = 81.9°, φ = 125.4°, dp = 5.0°, dm = 6.0°
									31.1	36.0	23.1	16.8	
Aohanqi													
N01[a]	42°33′N,119°47′E	limestone	C_1h	246/26	8/8	8/0	10.5	64.0	355.1	40.5	59.0	7.3	
N02[a]	42°33′N,119°47′E	limestone	C_1h	248.7/36.3	7/8	7/0	9.0	62.5	354.3	28.8	23.8	12.6	
N03[a]	42°33′N,119°47′E	limestone	C_1h	252/32.3	11/11	10/1	5.4	67.5	352.8	36.2	71.5	5.4	
N04[a]	42°33′N,119°47′E	limestone	C_1h	239/41	8/8	4/4	44.9	76.6	347.3	44.2	32.0	9.9	
N05[a]	42°33′N,119°47′E	limestone	C_1h	238.7/38.3	6/8	6/0	7.2	69.0	346.3	33.4	66.3	8.3	
N06[a]	42°33′N,119°47′E	limestone	C_1h	310/18	5/6	4/1	354.3	57.6	8.2	43.4	19.2	17.9	
N07[a]	42°33′N,119°47′E	limestone	C_1h	312.5/18.5	8/8	7/1	20.0	66.1	29.9	49.2	56.0	7.5	
			mean[a]		7S/7S		9.6	66.6			110.0	5.8	λ = 80.6°, φ = 161.9°, dp = 7.9°, dm = 9.6°
									357.8	40.0	37.8	9.9	
					Inner Mongolia Block (IMB)								
Sunidzuoqi													
O16	43°28′N,113°32′E	red coarse sandstone	D_3s	245/20	4/7	4/0	173.4	14.8	177.4	32.8	40.0	14.6	
O17	**43°28′N,113°32′E**	**red coarse sandstone**	**D_3s**	**245/20**	**6/10**	**0/6**	**164.3**	**−34.6**	**162.8**	**−15.0**	**50.0**	**11.0**	
O23	43°28′N,113°32′E	red coarse sandstone	D_3s	237/38	0/5	0/0	-	-	-	-	-	-	weak NRM, viscous
O24	**43°28′N,113°32′E**	**red coarse sandstone**	**D_3s**	**250/28**	**5/6**	**0/5**	**118.7**	**−55.6**	**131.7**	**−30.8**	**54.0**	**16.7**	
O25	**43°28′N,113°32′E**	**red coarse sandstone**	**D_3s**	**250/28**	**6/6**	**1/5**	**138.6**	**−52.8**	**143.6**	**−25.4**	**54.0**	**9.2**	
			mean		**3S/5S**		**143.6**	**−49.3**			**18.0**	**29.9**	
									144.6	**−24.3**	**24.3**	**25.5**	**λ = 46.8°, φ = 349.1°, dp = 14.6°, dm = 27.2°**
					17s/17s		**134.1**	**−49.9**			**13.0**	**10.3**	
									139.9	**−25.9**	**14.9**	**9.6**	**λ = 43.6°, φ = 356.9°, dp = 5.6°, dm = 10.4°**

Table 1. (continued)

Site	Coordinate	Rock	Age	Strike/Dip (°)	n′/n	N/R	Dg (°)	Ig (°)	Ds (°)	Is (°)	k	α_{95} (°)	Comments and Poles
O18	43°29′N,113°32′E	sandstone	C_1g	58/40	0/6	0/0	-	-	-	-	-	-	weak NRM, dispersed
O19	43°29′N,113°32′E	sandstone	C_1g	58/45	0/2	0/0	-	-	-	-	-	-	weak NRM, dispersed
O20	43°29′N,113°32′E	sandstone	C_1g	80/8	0/3	0/0	-	-	-	-	-	-	weak NRM, dispersed
O21	43°29′N,113°32′E	sandstone	C_1g	220/20	0/7	0/0	-	-	-	-	-	-	weak NRM, dispersed
O22	43°29′N,113°32′E	sandstone	C_1g	195/27	0/6	0/0	-	-	-	-	-	-	weak NRM, dispersed
Abagaqi													
25	43°56′N,114°56′E	yellow siltstone	D_3s	242.3/82.3	0/1	0/0	-	-	-	-	-	-	viscous
26	43°56′N,114°56′E	yellow siltstone	D_3s	77.5/51.5	0/1	0/0	-	-	-	-	-	-	viscous
27	43°56′N,114°56′E	yellow siltstone	D_3s	76/40	0/1	0/0	-	-	-	-	-	-	viscous
28	43°56′N,114°56′E	yellow siltstone	D_3s	72.5/53	0/1	0/0	-	-	-	-	-	-	viscous
29	43°56′N,114°56′E	yellow siltstone	D_3s	82/73.5	0/1	0/0	-	-	-	-	-	-	viscous
30	43°56′N,114°56′E	yellow siltstone	D_3s	90/62.3	0/1	0/0	-	-	-	-	-	-	viscous
Keshiketengqi													
N08 [a]	43°01′N,117°40′E	coarse sandstone	P_3t	110.7/34	5/6	5/0	350.5	63.4	252.6	73.2	220.0	5.2	
N09 [a]	43°01′N,117°40′E	coarse sandstone	P_3t	120/16.5	7/7	7/0	350.0	72.2	288.7	77.0	180.0	4.5	
N10 [a]	43°01′N,117°40′E	coarse sandstone	P_3t	136.3/17	7/7	7/0	355	68.4	306.3	73.1	208.0	4.2	
N11 [a]	43°01′N,117°40′E	coarse sandstone	P_3t	128/14	4/4	4/0	6.5	70.2	323.1	77.7	1240	3.5	
N12 [a]	43°01′N,117°40′E	coarse sandstone	P_3t	128/14	3/5	3/0	1.2	67.2	320.0	74.4	344.0	6.6	
			mean [a]		5S/5S		356.5	68.4			372.0	4.0	λ = 81.1°, φ = 103.5°, dp = 5.7°, dm = 6.7°
									297.5	76.5	114.0	7.2	
Linxi													
O01 [a]	43°43′N,118°08′E	sandstone	P_3l	332/84	9/9	9/0	6.4	73.2	134.0	18.5	269.0	3.1	
O02	43°42′N,118°25′E	tuff	P_1d	203/46	0/3	0/0	-	-	-	-	-	-	dispersed
O03	**43°42′N,118°25′E**	**basalt**	**P_1d**	**200/50**	**5/8**	**0/5**	**201.6**	**−55.1**	**148.0**	**−36.1**	**148.0**	**7.6**	
O04	**43°42′N,118°25′E**	**basalt**	**P_1d**	**200/50**	**4/7**	**0/4**	**166.5**	**−63.4**	**129.5**	**−24.8**	**138.0**	**7.8**	
O05	**43°41′N,118°17′E**	**sandstone**	**P_3l**	**210/34**	**4/4**	**4/0**	**7.8**	**57.4**	**334.7**	**38.1**	**37.4**	**17.7**	
O06	**43°41′N,118°17′E**	**sandstone**	**P_3l**	**210/34**	**8/9**	**7/1**	**347.7**	**67.3**	**326.0**	**37.4**	**95.4**	**5.7**	
West Ujimqin													
O07	44°55′N,117°27′E	sandstone	P_2g	20/65	0/4	0/0	-	-	-	-	-	-	weak NRM, viscous
O08	**44°55′N,117°28′E**	**sandstone**	**P_2g**	**12/68**	**6/8**	**0/6**	**125.9**	**−56.4**	**136.4**	**−30.4**	**35.0**	**10.0**	
O09	44°55′N,117°29′E	sandstone	P_2g	20/60	0/9	0/0	-	-	-	-	-	-	viscous
O10	**44°55′N,117°28′E**	**sandstone**	**P_2g**	**220/28**	**3/3**	**2/1**	**324.0**	**68.1**	**312.7**	**35.0**	**623.2**	**10.0**	
O11	44°55′N,117°29′E	sandstone	P_2g	225/31	0/5	0/0	-	-	-	-	-	-	dispersed
		mean Permian (site O02-O11)			**6S/10S**		**167.2**	**−63.9**			**30.4**	**12.3**	
									140.8	**−34.0**	**70.9**	**80.0**	**λ = 48.7°, φ = 3.7°, dp = 5.2°, dm = 9.1°**
O12	**45°01′N,117°18′E**	**sandstone**	**C_2a**	**277.5/67.5**	**3/3**	**0/3**	-	-	-	-	-	-	
O13	**45°01′N,117°18′E**	**sandstone**	**C_2a**	**277.5/67.5**	**5/6**	**0/5**	-	-	-	-	-	-	
O14	**45°01′N,117°18′E**	**sandstone**	**C_2a**	**275/65**	**0/1**	0/0	-	-	-	-	-	-	
			mean C_2a	**8s/10s**	**0/8**		**95.2**	**−86.4**	**178.1**	**−19.5**	**41.0**	**9.1**	

Table 1. (continued)

Site	Coordinate	Rock	Age	Strike/Dip (°)	n′/n	N/R	Dg (°)	Ig (°)	Ds (°)	Is (°)	k	α_{95} (°)	Comments and Poles
													λ = 55.0°, φ = 300.6°, dp = 5.0°, dm = 9.5°
O15	44°50′N,116°28′E	sandstone	D_{2-4}	352.5/12	0/5	0/0	-	-	-	-	-	-	weak NRM, viscous
N13 [a]	44°31′N,117°33′E	limestone	P_2z	86/88	3/3	3/0	-	-	-	-	-	-	
N14 [a]	44°31′N,117°33′E	limestone	P_2z	91.5/84	3/3	3/0	-	-	-	-	-	-	
N15 [a]	44°31′N,117°33′E	limestone	P_2z	93/88	2/2	2/0	-	-	-	-	-	-	
N16 [a]	44°31′N,117°33′E	limestone	P_2z	93.5/85.5	2/2	2/0	-	-	-	-	-	-	
N17 [a]	44°31′N,117°33′E	limestone	P_2z	93/85	2/2	2/0	-	-	-	-	-	-	
N18 [a]	44°31′N,117°33′E	limestone	P_2z	93/85	3/3	3/0	-	-	-	-	-	-	
			mean [a]		11s/11s		23.7	69.5			64.4	5.7	λ = 72.8°, φ = 171.5°, dp = 8.4°, dm = 9.8°
									187.9	16.3	39.6	7.3	
N19	44°15′N,117°50′E	limestone	C_2a	80/43	1/3	1/0	-	-	-	-	-	-	
N20	44°15′N,117°50′E	limestone	C_2a	80/43	3/3	3/0	-	-	-	-	-	-	
N21	44°15′N,117°50′E	limestone	C_2a	80/43	0/3	0/0	-	-	-	-	-	-	
N22	44°15′N,117°50′E	limestone	C_2a	80/43	0/3	0/0	-	-	-	-	-	-	
N23	44°15′N,117°50′E	limestone	C_2a	80/43	3/3	3/0	-	-	-	-	-	-	
N24	44°15′N,117°50′E	limestone	C_2a	80/43	3/3	3/0	-	-	-	-	-	-	
N25	44°15′N,117°50′E	limestone	C_2a	80/43	1/3	3/0	-	-	-	-	-	-	
N26	44°15′N,117°50′E	limestone	C_2a	80/43	3/3	3/0	-	-	-	-	-	-	
			mean		14s/14s		356.1	61.4	158.4	75.2	24.1	8.3	PEF
					Mongolia Block (MOB)								
Erenhot													
16	44°30′N,111°57′E	red coarse sandstone	$D_{1-2}n$	50/54	5/8	0/5	186.9	−55.9	277.3	−52.8	85.3	8.3	
17 [a]	44°30′N,111°57′E	red coarse sandstone	$D_{1-2}n$	50/54	6/8	6/0	52.8	71.3	117.6	33.0	25.5	13.5	
18	44°30′N,111°57′E	pebble	$D_{1-2}n$	50/54	0/5	0/0	-	-	-	-	-	-	dispersed
19 [a]	44°31′N,111°56′E	red coarse sandstone	$D_{1-2}n$	164/51	7/7	6/1	5.9	67.2	284.0	43.8	78.0	6.9	
20 [a]	44°31′N,111°56′E	red coarse sandstone	$D_{1-2}n$	164/51	8/8	8/0	2.1	67.8	283.1	42.4	110.0	5.3	
21 [a]	44°31′N,111°56′E	red coarse sandstone	$D_{1-2}n$	190/30	7/8	7/0	2.1	59.7	325.2	46.3	45.0	9.0	
22 [a]	44°31′N,111°56′E	red coarse sandstone	$D_{1-2}n$	177/25	4/4	4/0	345.8	62.7	311.6	50.2	143.0	7.7	
23 [a]	44°31′N,111°56′E	red coarse sandstone	$D_{1-2}n$	276/22	6/8	6/0	7.9	59.3	14.7	38.1	92.0	7.0	
24 [a]	44°31′N,111°56′E	red coarse sandstone	$D_{1-2}n$	206/77	5/5	5/0	3.1	60.7	322.8	0.6	137.0	6.6	
			mean [a]		7S/7S		5.7	65.4			89.7	5.9	λ = 85.0°, φ = 162.6°, dp = 7.8°, dm = 9.6°
									315.1	51.1	3.6	34.3	
East Ujimqin													
N27 [a]	45°22′N,116°59′E	volcanoclastic rock	C_2-P_1g	277.3/83.7	4/5	4/0	18.7	67.3	11.7	−16.3	24.5	18.9	
N28(LTC) [a]	45°22′N,116°59′E	volcanoclastic rock	C_2-P_1g	285/76.5	7/7	7/0	44.4	62.0	28.6	−11.0	40.7	9.6	
N28(HTC) [b]	45°22′N,116°59′E	volcanoclastic rock	C_2-P_1g		5/7	0/5	213.2	−17.4	225.7	54.2	89.5	10.4	λ = 43.7°, φ = 248.5°, dp = 5.6°, dm = 10.8°
N29(LTC) [a]	45°22′N,116°59′E	volcanoclastic rock	C_2-P_1g	107.5/84	4/8	4/0	52.5	46.8	167.0	39.4	54.4	12.6	
N29(HTC) [b]	45°22′N,116°59′E	volcanoclastic rock	C_2-P_1g		4/8	0/4	216.7	−22.4	330.8	−65.3	65.5	8.9	λ = 44.1°, φ = 242.5°, dp = 5.0°, dm = 9.4°
N30(LTC) [a]	45°22′N,116°59′E	volcanoclastic rock	C_2-P_1g	104/84	6/6	6/0	46.3	72.5	184.1	20.6	106.0	6.5	
N30(HTC) [b]	45°22′N,116°59′E	volcanoclastic rock	C_2-P_1g		5/6	0/5	205.2	−28.0	349.5	−65.5	100.0	8.8	λ = 52.9°, φ = 254.0°, dp = 5.3°, dm = 9.6°

Table 1. (continued)

Site	Coordinate	Rock	Age	Strike/Dip (°)	n′/n	N/R	Dg (°)	Ig (°)	Ds (°)	Is (°)	k	α_{95} (°)	Comments and Poles
N31 [a]	45°22′N,116°59′E	volcanoclastic rock	C_2-P_1g	104/84	9/9	9/0	68.6	60.8	38.2	−4.4	91.3	5.4	
N32 [a]	45°22′N,116°59′E	volcanoclastic rock	C_2-P_1g	281.5/75.5	7/7	7/0	33.0	57.0	23.5	−16.3	41.0	9.5	
			mean[a]		6S/6S		45.3	62.4			47.7	9.8	λ = 58.1°, φ = 193.4°, dp = 11.9°, dm = 15.3°
			(except three HTC)						196.7	18.1	15.5	17.6	

Sites in bold are considered to be primary remanences. Detailed discussion is in the text.
[a]Early Cretaceous remagnetized. Detailed discussion is in the text.
[b]Early Permian remagnetized. Detailed discussion is in the text.
Abbreviations. n′/ n: number of samples used to calculation/ measured sample number; N/R: normal/reversed polarity; Dg, Ig, Ds, Is: declination (D) and inclination (I) in in-situ (g) and tilt-corrected (s) coordinates; k: the best estimate of the precision parameter; α95: the radius that mean direction lies within 95% confidence; S, s: number of sites (S) or samples (s) used to determine pole; λ and Φ: latitude and longitude of paleomagnetic pole; dp/dm: semi-axes of the confidence ellipse of paleomagnetic pole. S3x: upper Silurian Xibiehe Formation (Fm); D1-2n and D3s: lower-middle Devonian Niqiuhe Fm and upper Devonian Seribayanaobao Fm; C1g, C1h and C2a: lower Carboniferous Houfangshengou Fm, and upper Carboniferous Amushan Fm; C2-P1g: upper Carboniferou-lower Permian Gegenaobao Fm; P1d, P2z, P3l and P3t: lower Permian Dashizhai Fm, middle Permian Zhesi Fm, upper Permian Linxi and Tieyingzi Fm, respectively.

[18] To the north of Chaganaobao village, eight sites of red coarse sandstone (Figure 2j) and one site of conglomerate of the Lower-Middle Devonian Niqiuhe Formation ($D_{1\text{-}2}$n) were sampled on both limbs of the folded 4 km long profile (Table 1). The Niqiuhe Formation is composed of red conglomerate at the bottom, followed by red coarse sandstone and limestone in the middle part, and tuffecous sandstone/siltstone on the top. Corals and brachiopods fossils, such as *Leptaenopyxis bouei*, *Derbina*, and *Coelospira*, define the Early-Middle Devonian age of this formation [*IMBGMR*, 1991]. These strata were further intruded by Late Jurassic-Early Cretaceous granite and covered by contemporary volcanic rocks.

[19] Near East Ujimqin County, six sites of volcaniclastic rocks were collected from the upper part of the Upper Carboniferous-Lower Permian Gegenaobao Formation (C_2-P_1g; Figure 2k and Table 1). The Gegenaobao Formation, overlying the Late Devonian strata and granodiorite unconformably, displays conglomerate and sandstone in the lower part and volcanic breccias-andesite-rhyolite-volcanoclastic rocks in the upper part, both of which display a nearly vertical bedding attitude. The age of this formation is determined by brachiopods fossils in the clastic part, such as *Kochiproductus* sp., *Rhynchopora* sp., *Spirifer* sp. Several meters apart from the sampling sites, a W-E trending dextral strike-slip shear zone was identified (Figure 2l).

[20] For each site, six to eight cores were drilled using a portable gasoline drill. Cores were orientated by both magnetic and, if possible, solar compasses. The average differences between these two azimuths of different localities ranges between $1.5° \pm 0.5°$ and $8.0° \pm 1.4°$. When Sun measurements were not available, the average value of the locality was used to correct the orientation of the samples. Overall, about 680 cores of 86 sites were sampled from nine localities, covering most areas of central-eastern Inner Mongolia (Figure 1b and Table 1). It is worth noting that a considerable effort has been made to find all possible outcrops in this area for paleomagnetic sampling.

3. Laboratory Methods

[21] In the laboratory, cores were prepared into standard specimens with 2.5 cm in diameter and 2.2 cm in length. Before the measurements of magnetic remanence of this paleomagnetic collection, several techniques were performed to magnetic mineralogical investigation: thermal magnetic (Curie point) experiments by KLY-3S kappabridge susceptibility meter coupled with a CS3 furnace and the acquisition of isothermal remanent magnetization (IRM) by IM30 pulse magnetizer at Institut des Sciences de la Terre d'Orléans (ISTO). In order to evaluate the deformation experienced by sampled rocks, measurements of the anisotropy of the magnetic susceptibility (AMS) were also systematically performed on specimens before their demagnetization by KLY3 kappabridge susceptibility meter. The orientation of the principal magnetic fabric axes, namely, K_1, K_2, and K_3, has been measured, and the anisotropy degree (P_J) and shape parameter (T) have been calculated for each specimen as well, following *Jelínek* [1978].

[22] Usually, at least six cores were chosen from each site for demagnetization. Both thermal and alternating magnetic field techniques were carried out to progressively remove

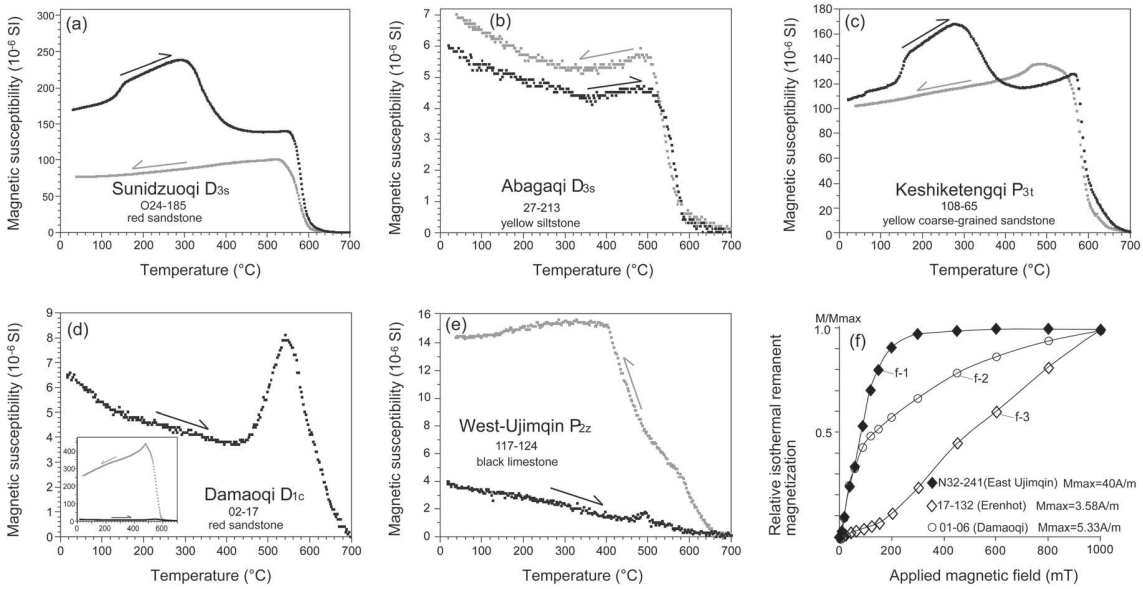

Figure 3. Representative results of (a–e) thermomagnetic experiments and (f) isothermal magnetization measurements (IRM) showing different magnetic carries. Sample name, site locality, stratigraphic age, and lithology are shown on each figure.

the magnetic remanence by about 12–16 steps with temperature intervals from 20°C to 50°C and alternating magnetic field intervals from 2 mT to 20 mT, using a laboratory-built furnace and a LDA-3 demagnetizer, respectively. Magnetic remanence was measured by JR5 magnetometer.

[23] Magnetic directions were isolated by the principal component analysis [*Kirschvink*, 1980] or estimated by great circle technique when end-points were not aligned [*McFadden and McElhinny*, 1988]. The mean magnetic directions were computed by Fisher spherical analysis [*Fisher*, 1953] using paleomagnetic software packages offered by *Cogné* [2003] and R. Enkin (unpublished).

4. Measurement Results

4.1. Magnetic Mineralogy

[24] The detailed mineralogical analyses for each locality are presented in Appendix A and summarized in the following. Three main types of magnetic carriers are identified from both thermomagnetic experiment and IRM measurement. (a) 55 out of 86 sites show magnetite is the main magnetic carrier as revealed by the sharp drop of the magnetic susceptibility at 550–585°C during thermomagnetic experiments (Figures 3a and 3b) and by the rapid increase of the IRM to a total magnetic saturation at about 300 mT (Figure 3f-1). (b) For 22 out of 86 sites, both magnetite and hematite coexist as the main magnetic carriers, deduced from the successive drops of the magnetic susceptibility from 580°C to 680°C (Figure 3c), and the relatively rapid increase of IRM at the weak applied field but without a total saturation at 1.0 T (Figure 3f-2). (c) For 9 out of 86 sites, hematite as the main magnetic carrier was indicated from the linear increase of IRM up to 1.0 T without a total saturation (Figure 3f-3), and with no drop at approximately 120°C of magnetic susceptibility, which excludes the high coercive goethite. Meanwhile, mineral transformations are common during the thermomagnetic experiments. The heating curve of Curie temperature measurements displays a rapid increase of the magnetic susceptibility at about 150°C followed by a slow increase to reach a peak at about 300°C, which may correspond to the transformation of goethite and/or pyrite into pyrrhotite and/or magnetite. In addition, the abrupt decrease from 300°C to 400°C is potentially due to maghemite destabilization (Figures 3a and 3c). For 35 out of 86 sites, heating and cooling thermomagnetic curves do not coincide, and the rapid increase of magnetic susceptibility during the cooling also indicates mineral oxidation during experiments (Figures 3d and 3e). However, it seems that mineral transformation does not disturb the thermal demagnetization, as in the majority of cases, specimens display relatively stable remanent directions.

4.2. AMS Results

[25] The AMS results for each site are presented in Appendix B. For each locality except East Ujimqin, the equal-area projection of the principal axes of the magnetic susceptibility (Figure 4a) shows nearly horizontal K_1 axes (D = 243.5°, I = 8.8°) and highly inclined K_3 axes (D = 102.5°, I = 78.8°) in tilt-corrected coordinates, which well define a horizontal magnetic fabric consistent with the initial sedimentary bedding. Meanwhile, the K_3 axes are better clustered after unfolding with the maximum/minimum radius at 95% confidence of mean K_3 axes lies at 48.5°/35.2° in in situ coordinates and 28.7°/25.6° in tilt-corrected coordinates. All samples show a relatively weak anisotropy degree with $P_J < 1.08$ (Figure 4b), suggesting that at least at the sampling scale, these rocks have not experienced intense deformation since their formation. Conversely, the data set of the volcaniclastic rocks from East Ujimqin shows well-clustered and nearly horizontal K_1, but K_3 directions are distributed along a girdle (Figure 4c). Such pattern, combining with the relatively high and heterogeneous values of P_J (Figure 4d), indicates a

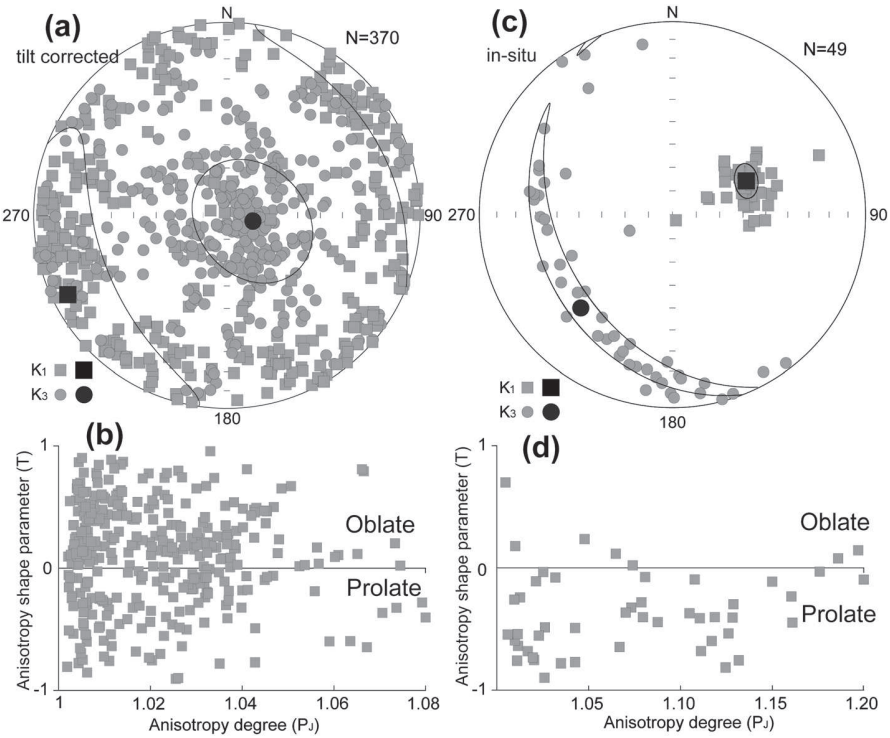

Figure 4. Results of anisotropy of magnetic susceptibility (AMS) measurements. (a and b) Equal-area stereoplot of K_1 and K_3 directions in tilt-corrected coordinates and the corresponding plots of anisotropy degree (P_J) versus anisotropy shape (T) of magnetic susceptibility for all the samples in Table B1 except sites N27–N32; (c and d) equal-area stereoplot of K_1 and K_3 directions in in situ coordinates and the corresponding plots of anisotropy degree (P_J) versus anisotropy shape (T) of magnetic susceptibility for the volcanoclastic samples from East Ujimqin (sites N27–N32) [*Jelínek*, 1978]. $P_J = \exp\{2[(\ln K_1 - \ln K_m)^2 + (\ln K_2 - \ln K_m)^2 + (\ln K_3 - \ln K_m)^2]^{1/2}\}$, and $T = 2\ln(K_2/K_3)/\ln(K_1/K_3) - 1$, where K_1, K_2, and K_3 are the maximum, intermediate, and minimum anisotropy axes, respectively.

prominent prolate shape for the fabric. This may be due to a postdeposition deformation, which is compatible with our field observation of vertical dextral strike-slip fault in the vicinity of sampling (Figure 2l). Meanwhile, both the K_1 and K_3 axes are better clustered in in situ coordinates than in tilt-corrected coordinates, suggesting that the magnetic fabric may be secondary.

4.3. Paleomagnetic Directional Analysis

4.3.1. North Margin of NCB

4.3.1.1. Damaoqi Area (S3x and D1c)

[26] The natural remanent magnetization (NRM) intensities of yellow sandstone samples of the Upper Silurian Xibiehe Formation (S_3x) are in the range of 0.25 mA/m to 38.7 mA/m. Among them, two sites (Site 12 and 14) display weak NRM (lower than 1 mA/m) and strong viscosity, and no stable paleomagnetic component can be isolated (Table 1). For others, two components were isolated from most of the samples after progressive thermal demagnetization. The low temperature component (LTC) up to 150°C displays random directions (Figures 5a and 5b). The high temperature component (HTC), isolated from 200°C to 680°C, shows two types of direction before bedding adjustments (Table 1 and Figures 5a and 5b).

[27] For the red sandstone of the Lower Devonian Chaganhebu Formation (D_1c), NRM intensities range from 1 mA/m to 202 mA/m with most of them >10 mA/m. For most of the samples, only one component was isolated from room temperature to 680°C (Table 1 and Figure 5c). In addition, few samples display two components with random low-middle temperature component (up to 500°C) and reversed HTC (Figure 5d) before tilt correction. The Enkin's direction-correction (DC) fold test [*Enkin*, 2003] is negative for this locality. Except two sites with north-northeast declination and steeply downward inclination (Sites 1 and 3) and one dispersed site (Site 5), the five remaining sites display shallow upward inclination and variable declinations ranging from 110° to 315° (Table 1).

4.3.1.2. Aohanqi Area (C1h)

[28] The NRM intensities of black limestone samples of the Lower Carboniferous Houfangshengou Formation (C_1h) range from 0.5 mA/m to 22.6 mA/m. Two components were isolated from most measured samples. After removing a dispersed viscous component up to 200°C or 2 mT, a stable component was isolated with both normal and reversed polarities before bedding adjustments (Figures 5e and 5f). A mean direction has been calculated (Table 1), which fails to pass the fold test as the directions are much better clustered before unfolding (Figure 6b).

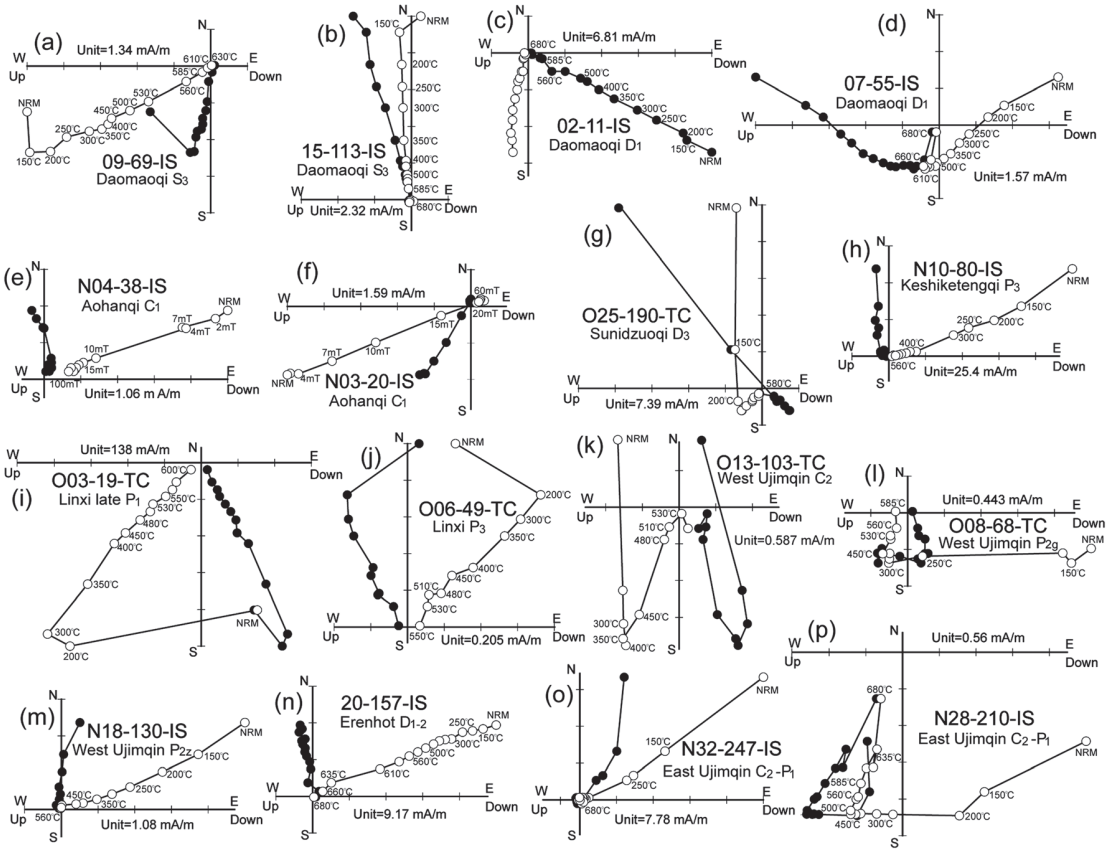

Figure 5. Orthogonal vector plots of representative specimens from each sampled age/locality group. Closed (open) symbols present the projection in horizontal (vertical) plane. IS (in situ) and TC (tilt-corrected) stands for plot in in situ and tilt-corrected coordinates. Sample name, site locality, and stratigraphic age are shown on each figure.

4.3.2. Inner Mongolia Block

4.3.2.1. Sunidzuoqi Area (D3s)

[29] For the red coarse sandstone of the Upper Devonian Seribayanaobao Formation (D_{3s}), two components of magnetic directions have been isolated from four out of five sites. The LTC is characterized by prominently viscous and dispersed directions (Figure 5g). After cleaning this viscous magnetic remanence up to 250°C, three sites (O17, O24, and O25) display a uniform reversed polarity in tilt-corrected coordinates, except one sample in Site O25 presents antipodal normal polarity (Figure 5g and Table 1). Site O16 presents normal polarity, which is much different from other sites. Therefore, we have calculated a mean direction for these three sites (Table 1). The fold test is inconclusive but the directions are better clustered after unfolding (Figure 6c). All five Lower Carboniferous sites (sites O18 to O22) show weak NRM intensity ranging from 0.25 mA/m to 5.94 mA/m or high viscosity, with no reliable direction obtained (Table 1).

4.3.2.2. Abagaqi Area (D3s)

[30] For the yellow siltstone of the Upper Devonian Seribayanaobao Formation, all specimens present weak NRM values with a range of 0.41 mA/m to 3.69 mA/m. Furthermore, most samples present highly viscous features during demagnetization, since we observe a more than 90% drop of the magnetic intensity after heating up to 150°C. Consequently, no reliable direction was isolated from this locality.

4.3.2.3. Keshiketengqi Area (P3t)

[31] For the coarse sandstone of the Upper Permian Tieyingzi Formation, the NRM intensities are relatively high, ranging from 46.4 mA/m to 227 mA/m. Only one component has been isolated from all analyzed samples (Figure 5h), and a mean direction has been calculated for these five sites (Table 1). The site mean directions are better clustered before bedding corrections, indicating a negative fold test (Figure 6d).

4.3.2.4. Linxi Area (Late P1d and P3l)

[32] For the upper part of the tuff and basalt of the Lower Permian Dashizhai Formation (P_1d), NRM intensities vary from 1.91 mA/m to 1.89 A/m. By thermal demagnetization, a random LTC has been isolated below 300°C. Thereafter, a HTC up to about 600°C has been observed and displays southeastward declination and upward inclination in tilt-corrected coordinates (Figure 5i).

[33] Concerning the sandstone of the Upper Permian Linxi Formation (P_3l), after removing the LTC until about 200°C, the remanent magnetization shows a stable decrease of magnetic remanence up to 550°C. All samples except one display unified normal polarity (Table 1). Site O01 displays northward declination and steeply downward inclination in in situ coordinates (Table 1). The tilt-corrected directions

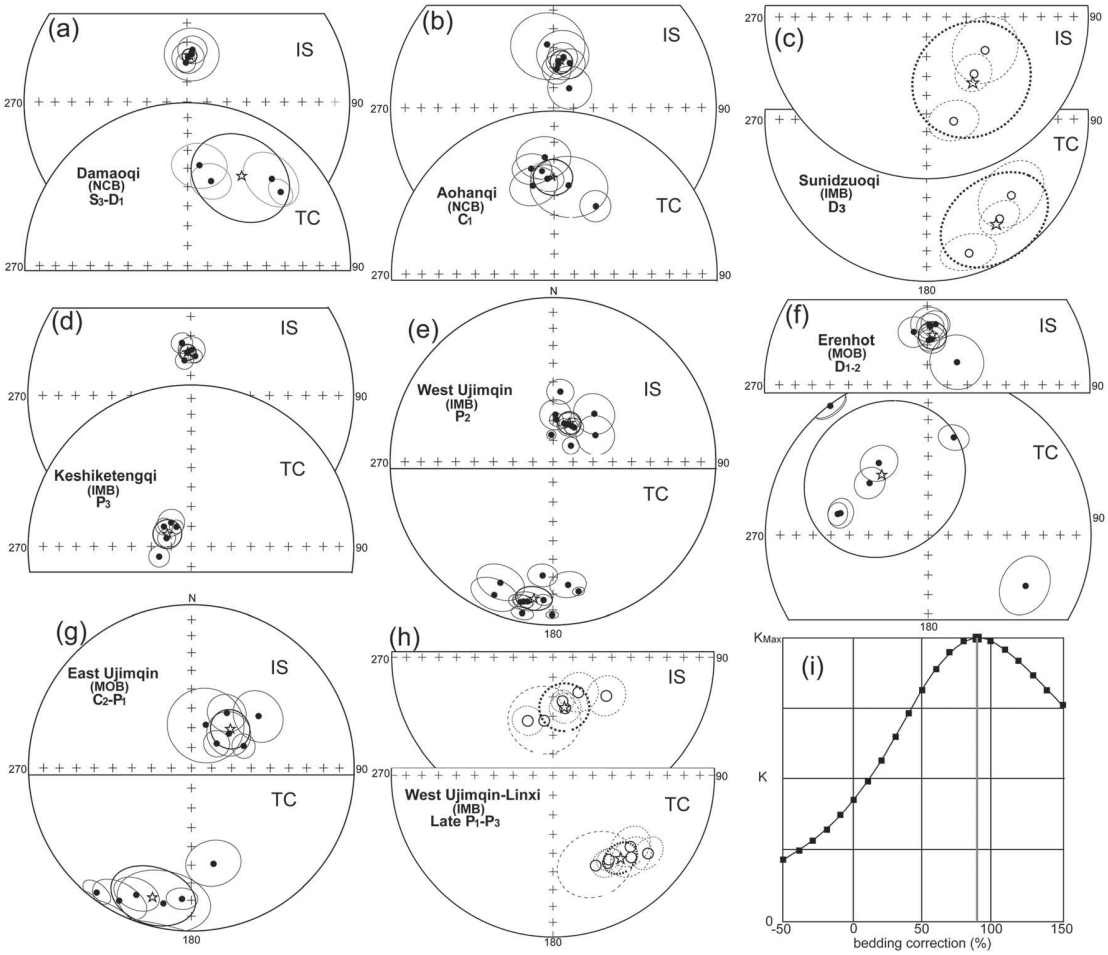

Figure 6. (a–h) Equal-area projection plots of site-mean directions of studied localities (data from Table 1). Closed (open) symbols present downward (upward) magnetic directions. Star symbols present the mean directions. IS (TC) stands for in situ/geographic (tilt-corrected/ stratigraphic) coordinates. (i) *Enkin* [2003] DC fold test: progressive unfolding showing a significant clustering of magnetic directions after bedding corrections at 90% untilting for the six Permian sites from West Ujimqin-Linxi area showing in Figure 6h.

for the other two sites display consistent northwestward declination and downward inclinations (Figure 5j).

4.3.2.5. West Ujimqin Area (C2a, P2g, and P2z)

[34] For the limestone of the Upper Carboniferous Amushan Formation (C_2a), after removing the random LTC until 200°C, all samples show normal polarity before bedding correction and a mean direction has been calculated (Table 1), which is close to that of the Present Earth Field (PEF: D = −4.3°, I = 61.2°) or Geocentric Axial Dipole (GAD: D = 0°, I = 62.2°) for the sampling area. Only eight specimens from three sandstone sites of Amushan Formation were successfully demagnetized and all display reversed polarity (Figure 5k), and a mean direction has been calculated (Table 1).

[35] For the Middle Permian yellow sandstone of the Gegenaobao Formation (P_2g), most of the samples display weak values of NRM (lower than 1 mA/m) and no reliable direction has been obtained except for Sites O08 and O10 (Table 1). For specimens of site O08, after removing the viscous LTC up to about 300°C, the remanent magnetization decreases linearly to the origin at 585°C, with solo reversed polarity (Figure 5l), while Site O10 displays antipodal normal and reversed polarities (Table 1).

[36] For the limestone of the Middle Permian Zhesi Formation (P_2z), after cleaning the LTC up to 150°C, all measured samples show consistent directions (Figure 5m) before bedding corrections and a mean direction has been calculated (Table 1). The directions are better clustered before bedding correction (Figure 6e), indicating a negative fold test.

4.3.3. South Margin of MOB

4.3.3.1. Erenhot Area (D1-2n)

[37] For the red coarse sandstone of the Lower-Middle Devonian Niqiuhe Formation ($D_{1\text{-}2}$n), only one component is isolated after progressive demagnetization, but samples from these nine sites display variable directions. Site 16 yields magnetic directions of reversed polarity. Site 18, which was selected for conglomerate test, displays scattered directions. All other seven sites, except one sample from Site 19, display a consistent normal polarity in in situ coordinates (Figures 5n and 6f) and a mean direction has been calculated (Table 1). Although the pebbles give scattered directions, the site mean directions are better grouped before tilt correction, suggesting a negative fold test (Figure 6f).

4.3.3.2. East Ujimqin (C2-P1g)

[38] For the volcanoclastic rocks of the Upper Carboniferous-Lower Permian Gegenaobao Formation (C_2-P_1g), only one component has been isolated from three sites (Sites N27, N31 and N32), and two components have been isolated from the other three (Sites N28, N29, and N30). The directions from three single-component sites are consistent with that of the LTC deduced from the three dual-component sites (Figures 5o and 5p) and a mean direction has been calculated (Table 1). The site mean directions of these six sites are better grouped before tilt correction, indicating a negative fold test (Figure 6g). The HTC isolated from three dual-component sites displays a solo reversed polarity (Figure 5p). The site mean directions for these three sites are better grouped before bedding correction, also indicating a negative fold test.

5. Discussion

[39] Magnetic mineralogy studies reveal that titanium-poor magnetite and sometimes hematite are the main magnetic remanent carrier with subordinate magnetic minerals, such as goethite, pyrrhotite, and maghemite. AMS measurements suggest that all collected rocks, except those from East Ujimqin, have not experienced intense deformation since their formation and maintain their original sedimentary magnetic fabric. Seventeen out of the 86 analyzed sites present either too weak magnetic remanent intensity or strong viscosity (Table 1) to provide reliable paleomagnetic directions. Besides, for four sites, specimens display scattered directions that hinder calculation of the site mean direction. All these 21 sites are rejected for further discussion.

5.1. Calculations of Paleomagnetic Poles

5.1.1. Primary Magnetizations

[40] Three Late Devonian sites from Sunidzuoqi show a unified reversed polarity, except one sample in Site O25 displaying an antipodal normal polarity (Table 1). Although the fold test is inconclusive due to probably the similarity of bedding attitudes, the features that the precision parameter has been improved after bedding corrections with a ratio of 1.35 for k_s/k_g and the coexistence of antipodal normal and reversed polarities may suggest that the magnetic remanence was at least acquired before the folding. The folding age cannot be, however, estimated by local stratigraphic contacts. At the regional scale, the Upper Devonian-Upper Permian strata are folded or highly tilted, and unconformably covered by the Late Permian conglomerate. Therefore, the folding took place during the Late Permian. Meanwhile, the coexistence of antipodal normal and reversed polarities and inexistence of the Early Permian magmatic rocks around sampling places exclude the Early Permian remagnetization, which displays only reversed polarity due to the Permo-Carboniferous Reversed Superchron (PCRS), ranging from 320 Ma to 263 Ma [*Garcia et al*., 2006; *Cottrell et al*., 2008]. Thus, the magnetic remanence may be considered as primary and a Late Devonian paleomagnetic pole has consequently been calculated for IMB at $\lambda = 46.8°$N, $\varphi = 349.1°$E, dp = 14.6, dm = 27.3 with N = 3 sites, or $\lambda = 43.6°$N, $\varphi = 356.9°$E, dp = 5.6, dm = 10.4 with N = 17 samples (Table 1).

[41] Only eight specimens were successfully demagnetized from three sites of Late Carboniferous sandstone from West Ujimqin, displaying a unified reversed polarity. The corresponding pole was calculated at $\lambda = 55°$N, $\varphi = 300.6°$E, dp = 5°, dm = 9.5° with paleolatitude of ~10° (Table 1). The solo reversed polarity seems to be consistent with the PCRS. The pole and the paleolatitude are comparable with the Late Carboniferous pole from Hexi Corridor in the westernmost part of NCB ($\lambda = 58°$N, $\varphi = 262.5°$E, dp = 7.4°, dm = 14.2°) [*Wu et al*., 1993] and its paleolatitude (9.2°N ± 7.4°N given by *Wu et al*. [1993] and 5.4°N given by *Huang et al*. [2001]). Although no fold test can be applied because of the small amount of samples, it seems reasonable to consider this pole to be representative of IMB for Late Carboniferous. However, for cautious tectonic interpretation, we will not use this pole further.

[42] Two sites of Early Permian basalt and two sites of Late Permian sandstone from Linxi and two sites of Middle Permian sandstone from West Ujimqin display similar or antipodal directions after bedding corrections (Figures 5i, 5l, and 5j). Zircon U-Pb geochronology yielded ages ranging between 285 Ma and 270 Ma for the basalt sites [*Zhang et al*., 2008; *Liu*, 2009]. Our unpublished zircon U-Pb dating provides a Middle Permian age assignment for the sandstone from West Ujimqin, which overlies the basalt directly. In addition, the solo reversed polarity suggests that the magnetic remanence has been acquired before 263 Ma, which is the upper limit of PCRS. Similarly, the age of the Linxi Formation sandstone is well constrained by abundant plant fossils and detrital zircon geochronology (256 Ma for the youngest grain) [*Han et al*., 2011]. Meanwhile, its chiefly normal polarity may suggest that the magnetic remanence was acquired shortly after 263 Ma, the upper limit of PCRS. All these rocks were deposited during a period of ca. 30 Ma, but they display similar or antipodal magnetic directions (Figures 5i, 5j, and 5l). This indicates a relatively stable paleolatitude for IMB from late Early Permian to Late Permian. Therefore, we have calculated a mean direction for these six sites at $D_g = 167.2°$, $I_g = -63.9°$, $k_g = 30.4$, $\alpha_{95g} = 12.3°$ and $D_s = 140.8°$, $I_s = -34.0°$, $k_s = 70.9$, $\alpha_{95s} = 8.0°$ (Figure 6h and Table 1). Enkin's fold test is positive with maximum value of k parameter at 90% (Figures 6h and 6i), and it also passes the reversal test [*McFadden and McElhinny*, 1990], suggesting that the magnetic remanences were obtained before folding. As discussed above, the folding age is considered to be the Late Permian. Therefore, we consider that the remanences were acquired during deposition. Thus, a late Early Permian-Late Permian paleomagnetic pole has been calculated for IMB at $\lambda = 48.7°$N, $\varphi = 3.7°$E, dp = 5.2°, dm = 9.1° with N = 6 (Table 1).

5.1.2. Secondary Magnetizations

[43] All other 54 remaining sites (including the Late Silurian and Early Devonian of Damaoqi, Early Carboniferous of Aohanqi, Late Permian-Early Triassic of Keshiketengqi, Late Carboniferous and Middle Permian of West-Ujimqin, Early-Middle Devonian of Erenhot, and Late Carboniferous-Early Permian of East-Ujimqin) fail to pass the fold test, suggesting post-folding remagnetizations. Two groups of directions have been identified: (a) southward (southeastward and southwestward) declinations and shallow upward inclinations (Figures 5c, 5d, and 5p) and (b) northward declinations and steeply downward inclinations or antipodal southward declinations and steeply upward inclinations (Figures 5f, 5h, 5m, and 5n). In the following, we will discuss the possible reasons and age for these remagnetizations.

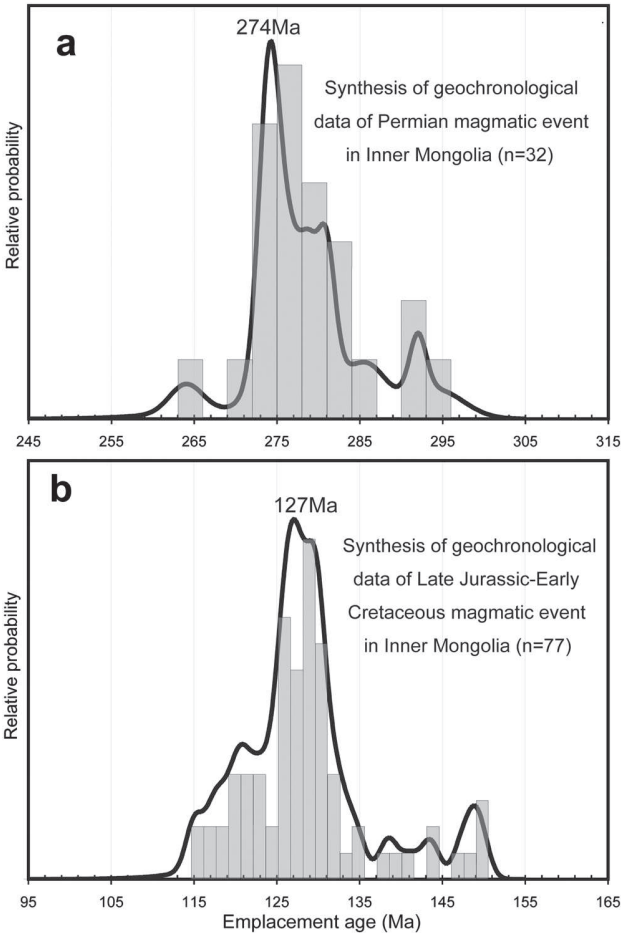

Figure 7. (a) Synthesis of geochronological data of the Permian magmatic event around Damaoqi and East Ujimqin (n = 32), illustrating the activity peak at 274 Ma, which may be responsible for the Early Permian remagnetization in these two localities. Individual data are from *Zhang et al*. [2008], *Liu* [2009], *Luo et al*. [2009], *Zhao et al*. [2011], and *Chen et al*. [2012]. (b) Synthesis of geochronological data of the Late Jurassic-Early Cretaceous magmatic event in Inner Mongolia and southern Mongolia, showing the activity peak at 127 Ma (n = 77), which may be responsible for the Early Cretaceous widespread remagnetization in Inner Mongolia. Individual data are from *Liu et al*. [2005], *Wu et al*. [2005], *Wei et al*. [2012], and *Daoudene et al*. [2012].

[44] The directions of HTC of five sites from the Early Devonian red sandstone in Damaoqi (D_{1c}) and of three sites from volcanoclastic rocks in East Ujimqin (C_2-P_1g) show the solo reversed polarity (Table 1). Moreover, these sites are close to Early Permian granitic plutons and volcanic rocks, which could be the cause of this secondary thermal magnetization. In addition, a review of the literatures concerning Permian magmatism around these two localities has shown a peak emplacement age at ca. 274 Ma (Figure 7a) [*Zhang et al*., 2008; *Liu et al*., 2009; *Chen et al*., 2012]. The solo reversed polarity and the estimated age of this remagnetization coincide with timing and features of the PCRS. Among these sites, inclinations vary slightly (−5° to −28°), but the corresponding paleolatitudes remain similar. Conversely, declinations are scattered and vary between 110° and 315° (Table 1). The paleomagnetic poles calculated from each site are distributed along a small circle centered at the sampling zone, which overlaps with Permian poles obtained from NCB and MOB (Figure 8b). So it is reasonable to consider that the remagnetized remanence acquired during the Early Permian. The important difference in declination may be due to posterior late strike-slip faulting, as observed in the field (Figure 2l).

[45] All remaining remagnetized sites display HTC directions close to that of the PEF (Table 1), but two major features allow us to distinguish them (except eight sites of Late Carboniferous limestone in West Ujimqin) from that of PEF: (1) the magnetic inclinations (62.4° to 69.5°) are higher than that of PEF (61.2° for PDF and 62.2° for GAD) and (2) the occurrence of reversed polarity for each locality (e.g., Figures 5a and 5f and Table 1). Therefore, the remagnetization age needs to be estimated. The corresponding poles of these remagnetized sites are compatible with the Early Cretaceous poles of NCB, MOB, and SIB [*Halim et al*., 1998; *Kravchinsky et al*., 2002b; *Cogné et al*., 2005; *Charles et al*., 2011]. Meanwhile, East Asia, including MOB, IMB, and NCB, experienced Mesozoic extensional tectonics, characterized by abundant extensional half-graben basins and emplacement of numerous magmatic massifs [e.g., *Webb et al*., 1999; *Graham et al*., 2001; *Ren et al*., 2002; *Liu et al*., 2005; *Wu et al*., 2005; *Charles et al*., 2011; *Wei et al*., 2012; *Daoudene et al*., 2012]. The magmatic event, which may induce thermal remagnetization, started in Late Jurassic and reached the peak in the Early Cretaceous (127 Ma, Figure 7b). After the Early Cretaceous, no magmatic event occurred in central-eastern Inner Mongolia until the early Pleistocene basalt erupted nearby Xilinhot [*IMBGMR*, 1991]. However, the distribution of the Early Pleistocene basalt is restricted, and the magnetic directions of the Early Pleistocene in this area are different from our remagnetized directions [*Zhu et al*., 1998]. Generally speaking, pervasive remagnetization is caused by regional magmatic event. So it is reasonable to consider that these secondary thermal magnetizations were acquired in Early Cretaceous.

5.2. Comparisons of the Paleomagnetic Poles

[46] Up to now, no reliable Paleozoic paleomagnetic data have been documented from central-eastern Inner Mongolia, except a few remagnetization data obtained from Carboniferous-Permian strata in northeastern Inner Mongolia [*Zhao et al*., 1990]. For MOB, paleomagnetic studies have mostly focused on its northern margin, such as North Amuria [*Xu et al*., 1997; *Kravchinsky et al*., 2002a] and North Mongolia [*Pruner*, 1987], with a few studies on South Mongolia [*Pruner*, 1987]. Most of these data were driven from deformed zones, e.g., the suspected Mongol-Okhotsk suture zone, where the strike-slip movements may have caused significant deflection of the paleomagnetic directions [*Kravchinsky et al*., 2002a; *Webb and Johnson*, 2006; *Webb et al*., 2010; *Metelkin et al*., 2010].

5.2.1. Late Devonian

[47] Late Devonian poles for these four blocks remain rare. For NCB, two poles were obtained from the Hexi Corridor region. *Zhao et al*. [1993] gave a Late Devonian pole at λ = 34.2°N, φ = 228.7°E, A_{95} = 8.8° with 16 sites of red sandstone and andesite (Table 2). *Huang et al*. [2000] calculated a mean Middle-Late Devonian pole at λ = 56°N, φ = 336°E, A_{95} = 9.2° with 12 sites of Middle-Late

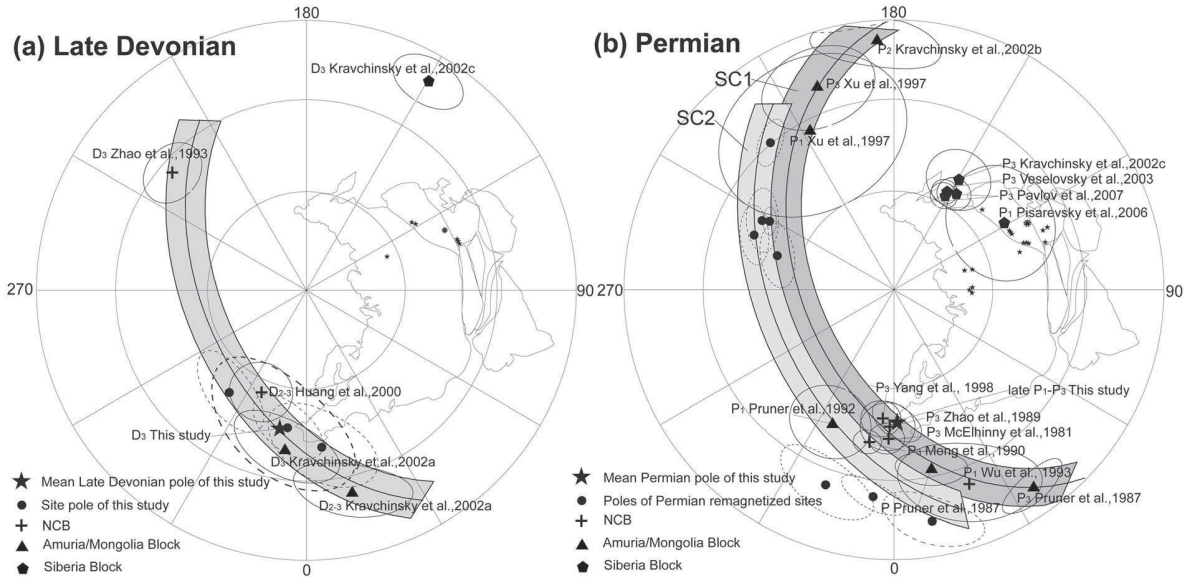

Figure 8. (a) Equal-area projections of Late Devonian poles from Sunidzuoqi (IMB), North China Block (NCB), Mongolia Block (MOB), and Siberia Block (SIB). There is little or no latitudinal difference but huge longitudinal differences between IMB, NCB, and MOB, indicating that these three blocks probably aggregated together, but with strong rotation. SIB was far away from other three blocks in Late Devonian as the pole was far away. (b) Equal-area projections of Permian poles from IMB, NCB, MOB, and SIB. The pole of our study is consistent with that of NCB, suggesting that these two parts have been welded as a rigid block. There is no latitudinal difference but still huge longitudinal differences between IMB + NCB and MOB, indicating strong postdated rotation, probably due to intracontinental strike-slip movements. SIB was still far away from other three blocks in Permian. The Permian remagnetized sites are also aligned along a small circle (SC2) with a shallower inclination, which probably due to local deformation since samples were collected from zones where strike-slip faults are documented.

Devonian strata (Table 2). Despite collecting in close locations less than 40 km, these two poles display huge rotation with declination difference of $72.1° \pm 15.4°$ (Figure 8a), which is probably caused by the strike-slip fault system in the Hexi Corridor [*Huang et al*., 2000]. In the upper Amuria region (MOB), *Kravchinsky et al*. [2002a] obtained two poles for Middle-Late Devonian and Late Devonian ages at $\lambda = 24.6°$N, $\varphi = 12.9°$E, $dp = 8.7°$, $dm = 16.9°$ with seven sites of siltstone and tuff and $\lambda = 40.5°$N, $\varphi = 352.4°$E, $dp = 9°$, $dm = 16.7°$ with five sites of sandstone and siltstone, respectively (Table 2). All these four Devonian poles from NCB and MOB are distributed along a small circle, indicating that these two blocks have evolved together without detectable paleolatitude difference ($2.3° \pm 5.7°$), but with significant relative rotations since the Late Devonian (Figure 8a). Our Late Devonian pole obtained from Sunidzuoqi (IMB) also locates on this small circle (Figure 8a), indicating that these three blocks of compatible paleolatitudes were juxtaposed since at least Late Devonian. Based on a paleomagnetic study of kimberlite and dyke in the east of Siberia, *Kravchinsky et al*. [2002c] gave a Late Devonian pole for SIB at $\lambda = 11.1°$N, $\varphi = 149.7°$E, $A_{95} = 8.9°$ with 11 localities (Table 2). This pole is totally different from the Late Devonian poles of NCB, MOB, and IMB (Figure 8a), indicating that SIB was located far away from NCB, MOB, and IMB during the Late Devonian.

5.2.2. Permian

[48] The Permian poles for NCB have been well documented by numerous studies over the last three decades (Table 2) [e.g., *McElhinny et al*., 1981; *Zhao and Coe*, 1989; *Meng et al*., 1990; *Wu et al*., 1993; *Yang et al*., 1998]. These poles are well consistent with each other (Figure 8b). Although statistically distinguished from other poles, the pole from Hexi Corridor (Figure 8b) [*Wu et al*., 1993] presents a compatible paleolatitude, indicating post-Permian rotation of sampling area with respect to the other parts of NCB.

[49] Our primary Permian pole for IMB inferred from West Ujimqin-Linxi (star in Figure 8b) is well consistent with the poles of NCB, with an indistinguishable angular difference of $2.6° \pm 10.9°$ and a weakly paleolatitudinal difference of $5.8° \pm 8.5°$ comparing with the mean Permian pole of NCB (calculated at $\lambda = 46.0°$N, $\varphi = 355.2°$E, $A_{95} = 4.7°$), indicating that no paleomagnetically detectable relative movement has occurred between NCB and IMB during Permian. These two blocks may have been welded as a rigid block.

[50] The Permian poles of MOB are distributed along a small circle, which intercepts the poles of NCB-IMB (SC1 in Figure 8b) [*Xu et al*., 1997; *Kravchinsky et al*., 2002b; *Pruner*, 1987, 1992]. This observation indicates that the post-Permian relative movements between NCB-IMB and MOB are essentially produced by rotations within these blocks. In fact, as described before, the samples of MOB come essentially from the marginal zones [e.g., *Kravchinsky et al*., 2002b]. These significant relative rotations may be caused by strike-slip movements along the tectonic boundaries [*Cogné et al*., 2005; *Metelkin et al*., 2010].

Table 2. Compilation of Late Devonian and Permian Palaeomagnetic Data of North China Block, Inner Mongolia Block, Mongolia Block and Siberia Block[a]

Age	Slat (°N)	Slong (°E)	N	Plat (°N)	Plong (°E)	A_{95}(°) (dp/dm)	Test	References
				North China Block (NCB)				
P_2	39.6	98.0	33S	42.4	350.9	3.9	F	*Meng et al.* [1990]
P_2			11L	50.3	355.2	5.7	F	*Yang et al.* [1998]
P_2	37.8	112.3	12S	44.0	358.0	6.9	F	*McElhinny et al.* [1981]
P_2	37.5	114.4	4S	47.1	356.9	7.7	F	*Zhao and Coe* [1989]
P_1	37.6	101.3	5S	23.9	21.2	12.8/21.4	F	*Wu et al.* [1993]
D_3	37.4	105.7	16S	34.2	228.7	8.8	F, R	*Zhao et al.* [1993]
D_{2-3}	37.7	106.0	14S	56.0	336.0	9.2	F, R	*Huang et al.* [2000]
				Inner Mongolia Block (IMB)				
Late P_1-P_3	43.7	118.4	6S	48.7	3.7	5.2/9.1	F	This study
D_3	43.5	113.5	3S	46.8	349.1	14.6/27.3	-	This study
				Mongolia Block (MOB)				
P_3	48.1	105.9	27s	11.3	35.2	5.4/9.1	F	*Pruner* [1987]
P_3	51.5	115.4	14S	20.5	200.6	14.5	F	*Xu et al.* [1997]
P_2	50.6	116.9	14S	8.3	183.9	9.5/16.2	F	*Kravchinsky et al.* [2002b]
P_1	51.5	115.4	5S	33.8	207.8	26.3	F	*Xu et al.* [1997]
P_1	47.8	107.1	4S	44.8	335.1	11.6	F	*Pruner* [1992]
P	48.3	106.0	52s	32.8	11.8	5.8/9.9	F	*Pruner* [1987]
D_3	54.0	123.5	5S	40.5	352.4	9.0/16.7	F, R	*Kravchinsky et al.* [2002a]
D_{2-3}	54.0	123.5	7S	24.6	12.9	8.7/16.9	F, R	*Kravchinsky et al.* [2002a]
				Siberia Block (SIB)				
P_3	64.6	114.7	9L	50.8	149.6	9.4	-	*Kravchinsky et al.* [2002c]
P_3			7L	56.2	151.7	3.8	-	*Veselovsky et al.* [2003]
P_3	67.5	104.0	8S	55.1	147.0	5.0	-	*Pavlov et al.* [2007]
P_3	67.0	89.0	8S	57.2	151.1	4.0	-	*Pavlov et al.* [2007]
P_2	50.8	107.2	15S	63.1	151.0	13.5/15.0	F	*Kravchinsky et al.* [2002b]
P_1	51.7	104.1	5S	50.5	121.4	16.9	BC	*Pisarevsky et al.* [2006]
D_3	64.0	116.0	11L	11.1	149.7	8.9	-	*Kravchinsky et al.* [2002c]

[a]Abbreviations. N: the number of sites (S), samples (s) or localities (L) used for calculation. The "S" means several sites in a relatively constrained locality; while the "L" represents a mean pole calculated from several localities, with several sites in each locality; Slat (Plat): the latitude of sampling site (pole); Slong (Plong): the longitude of sampling site (pole); A95: the radius that mean pole lies within 95% confidence, in degree; dp/dm: semi-axes of the confidence ellipse of palaeomagnetic pole; F: fold test; R: reversal test; BC: baked contact test.

[51] The Early Permian remagnetized poles obtained from Damaoqi in the northern margin of NCB and from East Ujimqin in the southern margin of MOB are scattered, but once again, they are distributed along a small circle (SC2 in Figure 8b), revealing importance of strike-slip tectonics. Though both of these two small circles are overlapped (Figure 8b), the SC2 seems slightly shallower than SC1 that intercepts all other poles from NCB, IMB, and MOB. This slight latitudinal difference between SC1 and SC2 may be due to (1) the uncertainty in age estimation for the remagnetization made by the correlation with the regional peak of magmatic activity around the sampling area and (2) the uncertainty in bedding corrections of Permian remagnetized data. As multiphase tectonic events took place after the Early Permian remagnetization, the in situ Permian remagnetized data may also consequently introduce errors in the paleolatitudes.

[52] The Permian poles from Siberia are statistically grouped [*Kravchinsky et al.*, 2002c; *Veselovsky et al.*, 2003; *Pavlov et al.*, 2007], except an outlier obtained from mafic dykes (Figure 8b) [*Pisarevsky et al.*, 2006]. These poles are far away from all other poles of NCB, IMB, and MOB, indicating that significantly latitudinal movements have occurred since Permian between Siberia and other blocks.

5.3. Tectonic Implications

[53] As a major tectonic implication of this study, no obvious latitudinal differences between IMB, NCB, and MOB are observed neither in Late Devonian nor in the Permian (Figures 8a and 8b), indicating that these three blocks have been amalgamated since the Late Devonian and no wide ocean existed between them during the Late Paleozoic. This observation is compatible with the tectonic interpretation showing two Silurian-Devonian orogens between NCB, IMB, and MOB [*Tang*, 1990; *Xu et al.*, 2012]. The sedimentological constraints showing the similarity of the Upper Carboniferous to Upper Permian strata between northern NCB and southern MOB is also in agreement with our paleomagnetic data [*Mueller et al.*, 1991]. Our sedimentological study reveals that following Late Devonian molassic deposition, IMB was dominated by shallow marine carbonate platform in the Carboniferous, followed by volcanic-sedimentary sequences in the Early-Middle Permian, and continental environment with thick lacustrine sediments in the Late Permian. Consequently, no large ocean existed between NCB and MOB during the Late Paleozoic. Thus, the Paleo-Asian Ocean between NCB and MOB was closed at least since Late Devonian. NCB, IMB, and MOB were welded together as a single block. However, a small remnant sea may still exist in MOB in the Late Paleozoic, as Carboniferous arc and Permian marine sedimentary deposits were identified in south Mongolia [*Johnson*, 2004; *Heumann et al.*, 2012]. Conversely, the latitudinal differences between the welded NCB-IMB-MOB block and SIB during Devonian and Permian may correspond to the occurrence of the Mongol-Okhotsk Ocean (Figure 8). As shown by the

distribution of paleomagnetic poles along small circles centered on the sampling regions, the welded NCB-IMB-MOB block is not totally rigid owing to intracontinental deformation and significant relative rotations between NCB, IMB, and MOB domains (Figures 8a and 8b). The rotations are due to transcurrent tectonics that has been already described by the previous studies [*Enkin et al*., 1992; *Kravchinsky et al*., 2002a; *Metelkin et al*., 2010] and documented by numerous Mesozoic shear zones in MOB and IMB (e.g., East Gobi Fault zone) [*Lamb et al*., 1999, 2008; *Webb et al*., 2010].

6. Conclusions

[54] Despite the difficult outcrop conditions, we collected samples over a 3 year period and now present the first paleomagnetic data from central-eastern Inner Mongolia. Magnetic mineralogical analyses show titanium-poor magnetite and hematite as the principal magnetic carriers. From sites showing magnetization of primary origin, we have calculated a Late Devonian pole and a Permian one for IMB. Two stages of remagnetization have been also identified, probably due to Early Permian and Early Cretaceous thermal events. Although the results are still preliminary and remain qualitative, the comparison of our paleomagnetic with available poles from NCB, MOB, and SIB infers that (1) the Paleo-Asian Ocean has been closed to form a single welded block (NCB-IMB-MOB) since at least Late Devonian and (2) intracontinental deformation within NCB-IMB-MOB block has continued throughout the late Paleozoic and the Mesozoic, due to strike-slip movements along unit boundaries or within units. To improve the results from this study and better understand the Paleozoic evolution of CAOB, the study area needs to be widened. Investigating the western extension and especially the connection with the western part of CAOB (e.g., Tianshan, Altay) may be a key challenge for the late Paleozoic tectonics of Asia.

Appendix A: Analyses of Magnetic Mineralogy

[55] The analyses of magnetic mineralogy of 9 localities in this study are detailed described in the following.

A.1. North Margin of NCB

A.1.1. Damaoqi Area (S3x and D1c)

[56] For the yellow sandstone of the Upper Silurian Xibiehe Formation (S_3x), the heating curve of the magnetic susceptibility displays a quick decrease from ambient temperature to about 150°C, a progressive decrease until to 450°C, an abrupt drop from 540°C to 580°C, and a final slow decrease from 580°C to 700°C (Figure A1a), indicating the coexistence of several magnetic minerals with different Curie temperatures. In addition, an important change of the magnetic mineralogy is recorded during thermomagnetic experiments, since the magnetic susceptibility significantly increases after heating up to about 700°C (inset figure of Figure A1a) due to probable oxidation of pyrite into magnetite and pyrrhotite. IRM measurements reveal that after a rapid increase up to 200 mT, the magnetic remanence increases progressively with applied magnetic field without any saturation at 1 T (Figure A2a-1), suggesting the existence of both low and high coercive magnetic minerals in the rock.

[57] For the red sandstone of the Lower Devonian Chaganhebu Formation (D_1c), the heating curve of the magnetic susceptibility successively displays a quick decrease from ambient temperature to about 150°C, a slow decrease until 450°C, an abrupt rise from 450°C to 540°C, and an abrupt drop from 540°C to 700°C (Figure A1b), indicating the presence of several magnetic minerals with different Curie temperatures. Curie temperature measurements also reveal important change of magnetic mineralogy during experiments, as the heating and cooling curves do not overlap and the magnetic susceptibility significantly increases with cooling (inset figure of Figure A1b). This may be due to the oxidation of pyrite into magnetite and pyrrhotite. IRM measurements display a rapid increase up to 200 mT, followed by a progressive increase of the magnetic remanence with applied magnetic field without reaching saturation at 1 T (Figure A2a-2); this indicates that both low and high coercive magnetic minerals occur in the rock.

A.1.2. Aohanqi Area (C1h)

[58] For the black limestone of the Lower Carboniferous Houfangshengou Formation (C_1h), thermomagnetic curves present a slow decrease of magnetic susceptibility followed by a rapid increase from 400°C to 500°C, a sudden and severe drop from 500°C to 580°C, and finally a slow decrease from 580°C to 700°C (Figure A1c), indicating the presence of several magnetic minerals with different Curie temperatures. The diagram deduced from IRM measurements shows an abrupt increase from 0 mT to 300 mT, reaching a 90% magnetic saturation at about 300 mT (Figure A2a-3), suggesting predominantly low coercive magnetic minerals, like magnetite in the rocks.

A.2. Inner Mongolia Block (IMB)

A.2.1. Sunidzuoqi Area (D3s)

[59] For the red coarse sandstone of the Upper Devonian Seribayanaobao Formation (D_3s), the heating curve of the Curie temperature measurements displays an obvious increase of the magnetic susceptibility at about 150°C followed by a progressive increase until to a peak at about 300°C, which may correspond to the transformation of goethite and/or pyrite into pyrrhotite and/or magnetite (Figure A1d). Then an abrupt decrease from 300°C to 400°C is potentially due to maghemite destabilization (Figure A1d). The severe drop from 560°C to 600°C indicates the occurrence of titanium-poor magnetite (Figure A2d). Besides, thermomagnetic plots show an important change of the magnetic mineralogy during experiments, as the magnetic susceptibility displays a rapid increase of magnetic susceptibility at about 150°C followed by a slow increase until to a peak at about 300°C (Figure A1d).

A.2.2. Abagaqi Area (D3s)

[60] For the yellow siltstone of the Upper Devonian Seribayanaobao Formation, thermomagnetic measurements display a progressive decrease of the magnetic susceptibility to reach a plateau at 350°C and an abrupt drop from 540°C to 580°C, with a slow decrease until 700°C (Figure A1e), revealing titanium-poor magnetite. IRM measurements show a rapid increase of the magnetic remanence with applied magnetic field from 0 mT to 100 mT, followed by secondary increase from 400 without saturation at 1 T (Figure A2b-1); this suggests that both low and high coercive magnetic minerals in the rocks.

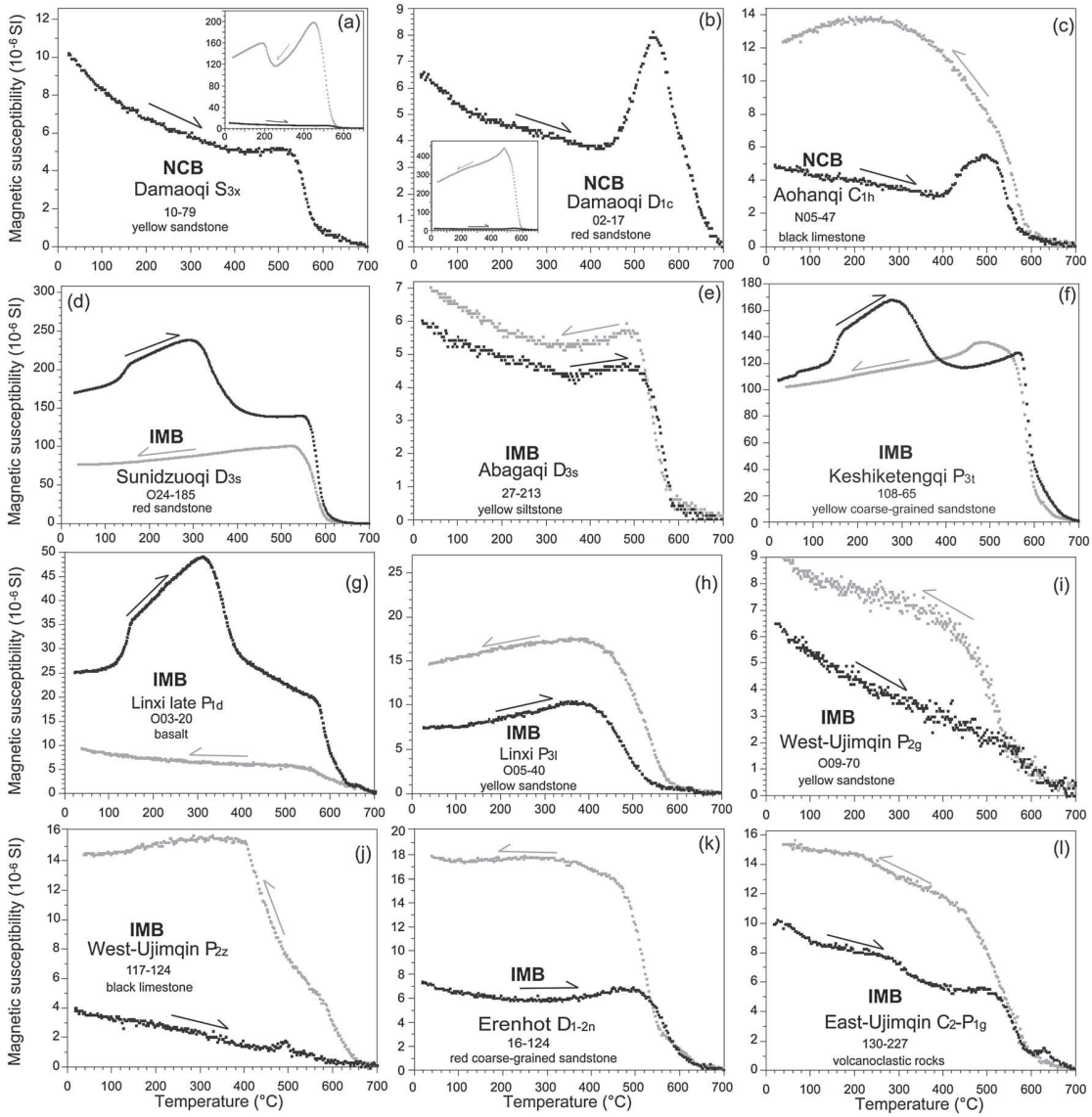

Figure A1. Representative results of thermomagnetic experiments from each sampled locality. Black (grey) curve represents heating (cooling) curve.

A.2.3. Keshiketengqi Area (P3t)

[61] For the coarse sandstone of the Upper Permian Tieyingzi Formation, thermomagnetic curves display an obvious increase of the magnetic susceptibility at about 150°C, a slow increase until to a peak at about 300°C, an abrupt decrease from 300°C to 400°C to reach a plateau, an abrupt drop from 580°C to 600°C, and a final slow decrease until 700°C (Figure A1f), indicating that both low (goethite and maghemite) and high (magnetite and hematite) Curie temperature magnetic minerals occur in the rocks. IRM measurements show an abrupt increase up to a 90% magnetic saturation from 0 mT to 300 mT, suggesting the predominance of low-coercive magnetic minerals in the rocks (Figure A2b-2).

A.2.4. Linxi Area (Late P1d and P3l)

[62] For the tuff and basalt of the upper part of the Lower Permian Dashizhai Formation (P_1d), the heating curve of the Curie temperature measurements displays a rapid increase of the magnetic susceptibility at 120–150°C, followed by a slow increase until to a peak at about 300°C, which may correspond to the transformation of goethite and/or pyrite into pyrrhotite and/or magnetite (Figure A1g). The abrupt decrease from 300°C to 400°C is potentially due to maghemite destabilization (Figure A1g). After a slow decrease between 400°C and 580°C, the susceptibility dramatically drops from 580°C to 640°C indicating the occurrence of titanium-poor magnetite and minor hematite (Figure A1g).

[63] For the sandstone of the Upper Permian Linxi Formation (P_3l), thermal magnetic measurement shows a quick decrease from 400°C to 560°C (Figure A1h), indicating titanium magnetite is probably the main remanent carrier.

A.2.5. West Ujimqin Area (C2a, P2g, and P2z)

[64] For the limestone of the Upper Carboniferous Amushan Formation (C_2a), IRM measurements show an abrupt increase up to approximately 90% saturation at about 300 mT (Figure A2b-3), indicating a predominance of low-coercivity minerals like magnetite in the rocks.

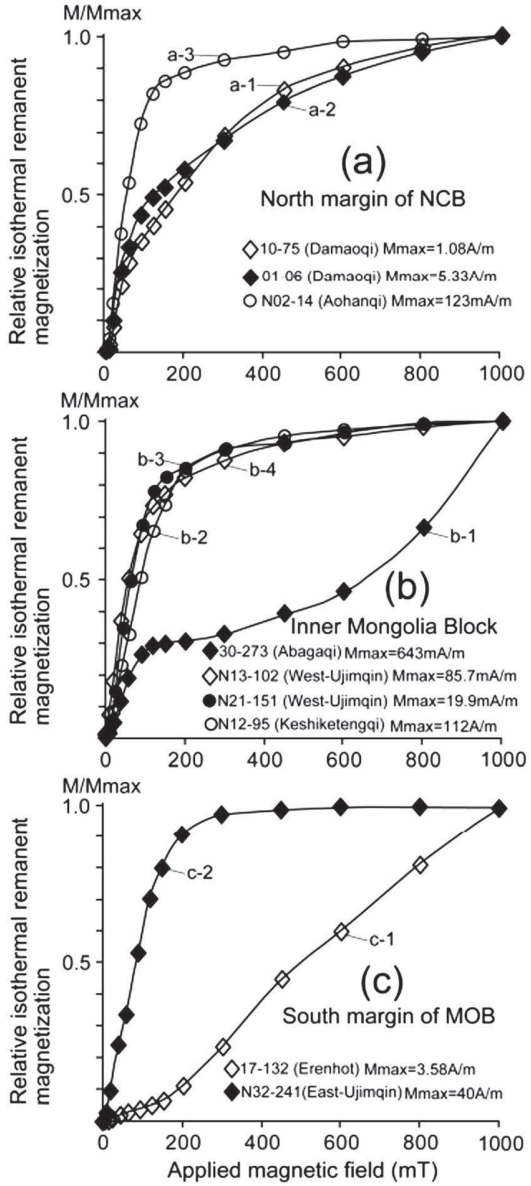

Figure A2. Representative results of isothermal magnetization measurements from each sampled locality.

[65] For the Middle Permian yellow sandstone of Gegenaobao Formation (P_2g), thermal magnetic measurements present a progressive decrease of the magnetic susceptibility from 0°C to 700°C, indicating both magnetite and hematite as the magnetic carriers (Figure A1i).

[66] For the limestone of the Middle Permian Zhesi Formation (P_2z), the heating curve of the thermomagnetic measurements presents a progressive decrease of magnetic susceptibility from 0°C to 700°C, whereas the cooling curve displays a quick increase from 700°C to 400°C (Figure A1j). Since heating and cooling curves do not overlap, changes of the magnetic mineralogy due to oxidation may occur during experiments. IRM measurements show an abrupt increase with approximately 90% saturation at about 300 mT (Figure A2b-4), indicating low-coercive magnetite may be the main magnetic carrier in the rocks.

A.3. South Margin of MOB

A.3.1. Erenhot Area (D1-2n)

[67] For the red coarse sandstone of Lower-Middle Devonian Niqiuhe Formation ($D_{1\text{-}2}n$), thermal magnetic measurements display a gradual drop from 500°C to 660°C (Figure A1h), indicating the coexistence of both magnetite and hematite as the magnetic carriers in the rock. IRM measurements show a first increase below 200 mT and a secondary sharp increase without reaching a total saturation up to 1 T (Figure A2c-1); this suggests that hematite is probably the main magnetic minerals.

A.3.2. East Ujimqin (C2-P1g)

[68] For the volcaniclastic rocks of the Upper Carboniferous-Lower Permian Gegenaobao Formation (C_2-P_1g), thermal magnetic measurements show a progressive decrease of the magnetic susceptibility with three successive drops at about 300°C, 540–580°C, and 620–680°C (Figure A1l), indicating the coexistence of maghemite, magnetite, and hematite, respectively. IRM measurements show a rapid increase to reach a total saturation at about 300 mT (Figure A2c-2), suggesting that a low-coercivity mineral like magnetite is the main magnetic carrier.

Appendix B: Anisotropy of Magnetic Susceptibility Data

Table B1. Anisotropy of Magnetic Susceptibility Data for the Sites That are Included in Mean Direction Calculations[a]

		Km	Standard Deviation			K_1				K_3			
Site	n	(10^{-6}SI)	(10^{-6}SI)	P_j	T	Dec (deg)	Inc (deg)	α_{95}max	α_{95}min	Dec (deg)	Inc (deg)	α_{95}max	α_{95}min
01	10	4.02E-04	2.29E-05	1.032	-0.216	284.9	22.2	7.7	4.3	152.4	58.9	9.2	3.6
02	11	1.41E-04	6.52E-06	1.033	0.169	253.6	25.9	7.8	4.4	111.2	58.4	6.2	2.5
03	8	3.67E-04	7.32E-05	1.053	-0.023	263.2	12.5	8.2	3	79.4	77.4	11.2	4.6
04	7	2.89E-04	7.03E-05	1.034	0.129	263.6	1.1	11.4	5.4	358.7	77.5	11.8	6.1
05	7	2.86E-04	6.75E-05	1.031	0.179	264.3	0.4	15.7	10.5	173	74.5	14	10.6
06	7	2.84E-04	5.99E-05	1.039	-0.114	268.6	18.8	6.5	5	116.8	68.9	7.8	6.1
07	8	3.48E-04	6.64E-05	1.04	0.247	259.2	5	19	1.5	114.9	83.8	10.7	2.9
08	8	3.09E-04	4.86E-05	1.045	0.582	310.2	19.7	55.2	15.2	110.7	69.2	31.9	10
09	9	1.01E-04	9.03E-05	1.015	-0.091	66.7	4.2	29.8	12.5	160.7	44	17.5	13
10	11	1.70E-04	1.07E-04	1.009	0.239	54	2.9	16.6	7.7	177.8	84.8	18.9	13.1
12	10	2.83E-04	4.26E-05	1.013	-0.123	255.5	10.7	11.2	5.8	129.2	72.3	18	6.8

Table B1. (continued)

		Km	Standard Deviation			K_1				K_3			
Site	n	(10^{-6}SI)	(10^{-6}SI)	P_j	T	Dec (deg)	Inc (deg)	α_{95}max	α_{95}min	Dec (deg)	Inc (deg)	α_{95}max	α_{95}min
13	9	3.63E-04	1.71E-05	1.024	0.235	97.9	16	32.7	3.1	207.5	49.4	13.5	7.5
14	9	1.57E-04	3.90E-05	1.014	0.462	50.5	14	22	4.3	172.5	64.8	13.7	3.8
15	9	3.30E-04	2.37E-05	1.02	0.235	234.1	0.6	35.9	13.1	328	81.1	29.2	18.7
16	8	1.55E-04	2.22E-05	1.012	0.36	139.6	27.4	44.1	9.8	252.9	37.3	28.4	9.7
17	9	2.89E-04	1.54E-04	1.01	0.366	113.2	18.7	18.7	6.2	270.9	70	9.9	6.5
18	8	1.53E-04	4.65E-05	1.048	0.413	110	14.9	33	8.7	18.9	4.3	58.4	8.1
19	9	3.92E-04	8.46E-05	1.008	0.176	317.5	24.2	21.4	17.4	96.6	59.3	23.9	20.3
20	9	3.88E-04	8.35E-05	1.006	0.322	35.7	17.2	27.6	8	203.8	72.4	24	8
21	9	1.56E-04	4.65E-05	1.006	0.308	223.5	81.7	66.4	14.9	53.6	8.2	51	20
22	8	2.17E-04	4.37E-05	1.003	-0.154	259.3	57.7	43	24.2	31.6	22.9	68.4	20.5
23	10	3.39E-04	1.12E-04	1.007	0.289	249.5	4.8	73.7	10.3	148.7	65.7	12.5	7.6
24	7	2.34E-04	3.00E-05	1.005	-0.099	330.2	4.7	13.6	8.7	61.4	14.5	32.1	6.4
N01	8	4.03E-05	1.37E-05	1.021	-0.414	127.8	73.7	21.1	9.2	15.1	6.4	70.7	11.3
N02	11	2.28E-05	8.40E-06	1.032	-0.004	46.4	1.6	13	10.3	315.4	30.7	27.8	12.6
N03	12	1.42E-05	6.93E-06	1.049	0.038	47.9	18	54.4	15.9	302.3	39.7	23.6	17.3
N04	8	3.41E-05	1.62E-05	1.018	0.236	69	31.6	83.2	28.8	291	50.4	38.2	32.2
N05	9	9.45E-06	4.37E-06	1.088	0.335	27.6	1.4	57.2	12.7	296.8	28.9	14.2	9.9
N06	8	1.74E-05	6.60E-06	1.054	0.474	241.2	35.4	82.9	9.3	143.7	10.4	13.7	3.7
N07	8	2.83E-05	5.96E-06	1.032	0.44	247.2	66.3	41.7	7.2	134.9	9.4	8.5	7.1
N08	6	1.20E-02	3.76E-03	1.022	0.275	45.4	13.5	29.9	9	300	48	45.6	12.7
N09	7	1.78E-02	3.94E-03	1.041	0.174	46.5	15.1	8	2.7	203.1	73.6	11.2	5.3
N10	6	7.58E-03	2.37E-03	1.027	-0.233	201.8	17.5	13	3.5	56.9	69	27.1	4.9
N11	7	4.72E-03	2.81E-03	1.022	-0.084	210.2	33.8	9.2	3.6	112.3	11.5	55.6	5
N12	6	6.03E-03	1.14E-03	1.027	-0.414	199.1	22.8	6.2	3.2	74.5	53.5	17.3	3
N13	7	2.15E-05	4.20E-06	1.036	-0.274	203.4	31.6	14.3	8.8	337.4	48.5	32.3	12.9
N14	6	2.76E-05	9.12E-06	1.073	0.165	270.1	10.5	42.6	5.3	172.2	36.6	33.9	3.7
N15	6	3.13E-05	8.28E-06	1.075	-0.256	103.2	5.1	5.7	3.3	206.8	69.2	27	2.9
N16	6	2.25E-05	1.35E-06	1.031	-0.135	99.8	17.2	45.5	3.2	202	34.4	13.1	4.2
N17	6	3.65E-05	8.61E-06	1.051	-0.117	100	4.1	23.5	2.9	195.1	51.1	49.5	3
N18	5	3.21E-05	7.54E-06	1.045	0.026	104.3	3.2	31.7	3	200	60.8	32.7	2.8
N27	7	3.76E-03	3.81E-03	1.126	-0.282	220	11.9	8.5	3.3	24.3	77.7	31.6	8.4
N28	7	2.07E-03	2.88E-03	1.057	-0.446	221.1	11.9	3.9	2.9	316.7	24.9	23	2.1
N29	8	2.25E-04	9.17E-05	1.017	-0.258	171.7	23	10.8	2.7	316	62.5	26.4	2.7
N30	9	2.52E-03	5.81E-03	1.036	-0.408	176.4	10.3	43.8	6.7	323.9	77.9	27.5	7.4
N31	8	9.44E-03	4.62E-03	1.1	-0.409	215.1	9.6	4.3	3.3	10.9	79.5	17.1	3.3
N32	10	2.40E-03	2.00E-03	1.115	-0.325	219.8	9	4	2.2	311.2	8.7	15.2	2.6
O05-06	9	2.20E-04	2.17E-05	1.028	-0.053	283	10.9	29.9	9.1	188.2	23.4	16.8	9.6
O07-14	11	4.64E-03	9.30E-03	1.058	0.514	30	22.4	13.8	12.2	120.3	0.6	23.4	4.9
O16-17	9	1.88E-03	6.55E-04	1.033	0.256	182.7	0.2	21	4.6	91.6	80.2	4.9	2.7
O23-25	9	3.41E-03	2.14E-03	1.036	0.346	359	11.9	10.6	4.7	210.7	76.1	6.2	4.5

[a]Site numbers are the same as that of Table 1. Samples from Upper Devonian in Abagaqi (sites 25–30) and Upper Carboniferous in West Ujimqin (sites N19–N26) are excluded as no mean directions or PEF directions are calculated. $P_J = \exp\{2[(\ln K_1 - \ln K_m)^2+(\ln K_2 - \ln K_m)^2+(\ln K_3 - \ln K_m)^2]^{1/2}\}$, and $T = 2\ln(K_2/K_3)/\ln(K_1/K_3) - 1$). K_1 and K_3 are principal axes of the magnetic fabrics. K_1: magnetic lineation; K_3: pole of the magnetic foliation; Dec/Inc: declination/inclination. α_{95}max/α_{95}min: the maximum/minimum radius that mean direction lies within 95% confidence.

[69] **Acknowledgments.** We thank Wei Wei for the technical help in the laboratory and AMS analyses. We thank Tong Qinlong, Li Ruibiao, Fang Junqin, and Cheng Shengdong for their support in the field. We gratefully acknowledge the Associate Editor Stuart Gilder, Cari Johnson, and another anonymous reviewer for their constructive comments that considerably improved this manuscript. This study was supported by grants from the National Natural Science Foundation of China (40872145, 40821002). This is a contribution to IGCP 592 supported by UNESCO-IUGS.

References

Blight, J. H. S., Q. G. Crowley, M. G. Petterson, and D. Cunningham (2010), Granites of the Southern Mongolia Carboniferous Arc: New geochronological and geochemical constraints, *Lithos*, *116*, 35–52, doi:10.1016/j.lithos.2010.01.001.

Charles, N., Y. Chen, R. Augier, C. Gumiaux, W. Lin, M. Faure, P. Monié, F. Choulet, F. Y. Wu, R. X. Zhu, and Q. C. Wang (2011), Palaeomagnetic constraints from granodioritic plutons (Jiaodong Peninsula): New insights on Late Mesozoic continental extension in Eastern Asia, *Phys. Earth. Planet. In.*, *187*, 276–291, doi:10.1016/j.pepi.2011.05.006.

Chen, B., B. M. Jahn, S. Wilde, and B. Xu (2000), Two contrasting Paleozoic magmatic belts in northern Inner Mongolia, China: Petrogenesis and tectonic implications, *Tectonophysics*, *328*, 157–182, doi:10.1016/S0040-1951(00)00182-7.

Chen, C., Z. C. Zhang, Z. J. Guo, J. F. Li, Z. S. Feng, and W. H. Tang (2012), Geochronology, geochemistry, and its geological significance of the Permian Mandula mafic rocks in Damaoqi, Inner Mongolia, *Sci. China Earth Sci.*, *55*, 39–52, doi:10.1007/s11430-011-4277-z.

Cogné, J. P. (2003), A Macintosh^{TM} application for treating paleomagnetic data and making plate reconstructions, *Geochem. Geophys. Geosyst.*, *4*(1), 1007, doi:10.1029/2001GC000227.

Cogné, J. P., V. A. Kravchinsky, N. Halim, and F. Hankard (2005), Late Jurassic–Early Cretaceous closure of the Mongol-Okhotsk Ocean demonstrated by new Mesozoic palaeomagnetic results from the Trans-Baikal area (SE Siberia), *Geophys. J. Int.*, *163*, 813–832, doi:10.1111/j.1365-246X.2005.02782.X.

Cottrell, R. D., J. A. Tarduno, and J. Roberts (2008), The Kiaman Reversed Polarity Superchron at Kiama: Toward a field strength estimate based on single silicate crystals, *Phys. Earth. Planet. Inter.*, *169*, 49–58, doi:10.1016/j.pepi.2008.07.041.

Daoudene, Y., D. Gapais, G. Ruffet, E. Gloaguen, A. Cocherie, and P. Ledru (2012), Syn-thinning pluton emplacement during Mesozoic extension in eastern Mongolia, *Tectonics*, *31*, TC3001, doi:10.1029/2011TC002926

De Jong, K., W. J. Xiao, B. F. Windley, H. Masago, and C. H. Lo (2006), Ordovician $^{40}Ar/^{39}Ar$ phengite ages from the blueschist-facies Ondor

Sum subduction-accretion complex (Inner Mongolia) and implications for the early Paleozoic history of continental blocks in China and adjacent areas, *Am. J. Sci.*, *306*, 799–845, doi:10.2475/10.2006.02.

Demoux, A., A. Kroner, D. Y. Liu, and G. Badarch (2007), Precambrian crystalline basement in southern Mongolia as revealed by SHRIMP zircon dating, *Int. J. Earth Sci.*, *98*, 1365–1380, doi:10.1007/s00531-008-0321-4.

Enkin, R. J. (2003), The direction-correction tilt test: An all-purpose tilt/fold test for paleomagnetic studies, *Earth Planet. Sci. Lett.*, *212*, 151–166, doi:10.1016/S0012-821X(03)00238-3.

Enkin, R. J., Z. Y. Yang, Y. Chen, and V. Courtillot (1992), Paleomagnetic constraints on the geodynamic history of the major blocks of China from the Permian to the present, *J. Geophys. Res.*, *97*, 13953–13989, doi:10.1029/92JB00648.

Fisher, R. (1953), Dispersion on a sphere, *Proc. R. Soc. London, Ser. A*, *217*, 295–305.

Garcia, A. S., D. N. Thomas, D. Liss, and J. Shaw (2006), Low geomagnetic field intensity during the Kiaman superchron: Thellier and microwave results from the Great Whin Sill intrusive complex, northern United Kingdom, *Geophys. Res. Lett.*, *33*, L16308, doi:10.1029/2006GL026729

Ge, M., W. Zhou, Y. Yu, J. Sun, J. Bao, and S. Wang (2011), Dissolution and supracrustal rocks dating of Xilin Gol Complex, Inner Mongolia, China (in Chinese with English abstract), *Earth Sci. Frontiers*, 2011, *18*(5), 182–195.

Graham, S. A., M. S. Hendrix, C. L. Johnson, D. Badamgarav, G. Badarch, J. Amory, M. Porter, R. Barsbold, L. E. Webb, and B. R. Hacker (2001), Sedimentary record and tectonic implications of Mesozoic rifting in southeast Mongolia, *Geol. Soc. Am. Bull.*, *113*, 1560–1579, doi:10.1130/0016-7606(2001)113<1580:PTMATC>2.0.CO;2.

Halim, N., V. Kravchinsky, S. Gilder, J. P. Cogne, M. Alexyutin, A. Sorokin, V. Courtillot, and Y. Chen (1998), A palaeomagnetic study from the Mongol–Okhotsk region: Rotated Early Cretaceous volcanics and remagnetized Mesozoic sediments, *Earth Planet. Sci. Lett.*, *159*, 133–145, doi:10.1016/S0012-821X(98)00072-7.

Han, J., J. B. Zhou, X. Z. Zhang, and H. J. Qiu (2011), Detrital zircon U-Pb dating from sandstone of the Upper Permian Linxi Formation, Linxi area, Inner Mongolia, China and its tectonic implications (in Chinese with English abstract), *Geol. Bull. China*, *30*, 258–269.

Heumann, M. J., C. L. Johnson, L. E. Webb, J. P. Taylor, U. Jalbaa, and C. Minjin (2012), Paleogeographic reconstruction of a late Paleozoic arc collision zone, southern Mongolia, *Geol. Soc. Am. Bull.*, *124*, 1514–1534, doi:10.1130/B30510.1.

Huang, B. C., Y. Otofuji, Z. Y. Yang, and R. X. Zhu (2000), New Silurian and Devonian palaeomagnetic results from the Hexi Corridor terrane, northwest China, and their tectonic implications, *Geophys. J. Int.*, *140*, 132–146, doi:10.1046/j.1365-246x.2000.00983.x.

Huang, B. C., Y. Otofuji, R. X. Zhu, R. P. Shi, and Y. C. Wang (2001), Paleomagnetism of Carboniferous sediments in the Hexi Corridor: Its origin and tectonic implications, *Earth Planet. Sci. Lett.*, *194*, 135–149, doi:10.1016/S0012-821X(01)00557-X.

IMBGMR (Inner Mongolian Bureau of Geology and Mineral Resources) (1991), *Regional Geology of Inner Mongolian Autonomous Region (in Chinese with English abstract)*, pp. 1–725, Geological Publishing House, Beijing.

IMBGMR (Inner Mongolian Bureau of Geology and Mineral Resources) (2002), Regional Geological Investigation Report of 1:250000 scale BaiyunObo Quadrangle (in Chinese), Inner Mongolian Bureau of Geology and Mineral Resources.

Jahn, B. M., B. A. Litvinovsky, A. N. Zanvilevich, and M. Reichow (2009), Peralkaline granitoid magmatism in the Mongolian–Transbaikalian Belt: Evolution, petrogenesis and tectonic significance, *Lithos*, *113*, 521–539, doi:10.1016/j.lithos.2009.06.015.

Jelínek, V. (1978), Statistical processing of anisotropy of magnetic susceptibility measured on groups of specimen, *Stud. Geofyz. Geodet.*, *22*, 50–62.

Jian, P. et al. (2008), Time scale of an early to mid-Paleozoic orogenic cycle of the long-lived Central Asian Orogenic Belt, Inner Mongolia of China: Implications for continental growth, *Lithos*, *101*, 233–259, doi:10.1016/j.lithos.2007.07.005.

Jian, P., A. Kröner, B. F. Windley, Y. Shi, W. Zhang, L. Zhang, and W. Yang (2012), Carboniferous and Cretaceous mafic-ultramafic massifs in Inner Mongolia (China): A SHRIMP zircon and geochemical study of the previously presumed integral "Hegenshan ophiolite", *Lithos*, *142-143*, 48–66, doi:10.1016/j.lithos.2012.03.007.

Johnson, C. L. (2004), Polyphase evolution of the East Gobi basin: Sedimentary and structural records of Mesozoic-Cenozoic intraplate deformation in Mongolia, *Basin Res.*, *16*, 79–99, doi:10.1046/j.1365-2117.2003.00221.X.

Johnson, C. L., J. A. Amory, D. Zinniker, M. A. Lamb, S. A. Graham, M. Affolter, and G. Badarch (2008), Sedimentary response to arc-continent collision, Permian, southern Mongolia, in *Formation and Applications of the Sedimentary Record in Arc Collision Zones*, edited by A. E. Draut, P. D. Clift, and D. W. Scholl, Geol. Soc. Am. Spec. Paper, *436*, pp. 363–390, Geological Society of America, Boulder, Colo.

Kirschvink, J. L. (1980), The least-squares line and plane and the analysis of paleomagnetic data, *Geophys. J. R. Astron. Soc.*, *62*, 699–718, doi:10.1111/j.1365-246X.1980.tb02601.X.

Kravchinsky, V. A., A. A. Sorokin, and V. Courtillot (2002a), Paleomagnetism of Paleozoic and Mesozoic sediments from the southern margin of Mongol-Okhotsk ocean, far eastern Russia, *J. Geophys. Res.*, *107*(B10), 2253, 2253, doi:10.1029/2001JB000672

Kravchinsky, V. A., J. P. Cogné, W. Harbert, and M. I. Kuzmin (2002b), Evolution of the Mongol-Okhotsk Ocean with paleomagnetic data from the suture zone, *Geophys. J. Int.*, *148*, 34–57, doi:10.1046/j.1365-246x.2002.01557.X.

Kravchinsky, V. A., K. M. Konstantinov, V. Courtillot, J. I. Savrasov, J. P. Valet, S. D. Cherniy, S. G. Mishenin, and B. S. Parasotka (2002c), Palaeomagnetism of East Siberian traps and kimberlites: Two new poles and palaeogeographic reconstructions at about 360 and 250 Ma, *Geophys. J. Int.*, *148*, 1–33, doi:10.1046/j.0956-540x.2001.01548.X.

Kröner, A., J. Lehmann, K. Schulmann, A. Demoux, O. Lexa, D. Tomurhuu, P. Štípská, D. Liu, and M. T. D. Wingate (2010), Lithostratigraphic and geochronological constraints on the evolution of the Central Asian Orogenic Belt in SW Mongolia: Early Paleozoic rifting followed by late Paleozoic accretion, *Am. J. Sci.*, *310*, 523–574, doi:10.2475/07.2010.01.

Lamb, M. A., A. D. Hanson, S. A. Graham, G. Badarch, and L. E. Webb (1999), Left-lateral sense offset of upper Proterozoic to Paleozoic features across the Gobi Onon, Tost, and Zuunbayan faults in southern Mongolia and implications for other Central Asian faults, *Earth Planet. Sci. Lett.*, *173*, 183–194, doi:10.1016/S0012-821X(99)00227-7.

Lamb, M. A., G. Badarch, T. Navratil, and R. Poier (2008), Structural and geochronologic data from the Shin Jinst area, eastern Gobi Altai, Mongolia: Implications for Phanerozoic intracontinental deformation in Asia, *Tectonophysics*, *451*, 312–330, doi:10.1016/j.tecto.2007.11.061.

Lehmann, J., K. Schulmann, O. Lexa, M. Corsini, A. Kröner, P. Štípská, D. Tomurhuu, and D. Otgonbator (2010), Structural constraints on the evolution of the central Asian Orogenic Belt In SW Mongolia, *Am. J. Sci.*, *310*, 575–628, doi:10.2475/07.2010.02.

Li, J. Y. (2006), Permian geodynamic setting of Northeast China and adjacent regions: Closure of the Paleo-Asian Ocean and subduction of the Paleo-Pacific Plate, *J. Asian Earth Sci.*, *26*, 207–224, doi:10.1016/j.jseaes.2005.09.001.

Litvinovsky, B. A., A. A. Tsygankov, B. M. Jahn, Y. Katzir, and Y. Be'eri-Shlevin (2011), Origin and evolution of overlapping calc-alkaline and alkaline magmas: The late Palaeozoic post-collisional igneous province of Transbaikalia (Russia), *Lithos*, *125*, 845–874, doi:10.1016/j.lithos.2011.04.007.

Liu, J. F. (2009), Late Paleozoic magmatism and its constraints on regional tectonic evolution in Linxi-Dongwuqi area, Inner Mongolia (in Chinese with English abstract), Doc. thesis, Univ. of Jilin, Changchun, Jilin, China

Liu, W., W. Siebel, X. J. Li, and X. F. Pan (2005), Petrogenesis of the Linxi granitoids, northern Inner Mongolia of China: Constraints on basaltic underplating, *Chem. Geol.*, *219*, 5–35, doi:10.1016/j.chemgeo.2005.01.013.

Luo, H. L., T. R. Wu, and L. Zhao (2009), Zircon SHRIMP U-Pb dating of Wuliangsitai A-type granite on the northern margin of the North China Plate and tectonic significance (in Chinese with English abstract), *Acta Petrol. Sin.*, *25*(3), 515–526.

McElhinny, M. W., B. J. J. Embleton, X. H. Ma, and Z. K. Zhang (1981), Fragmentation of Asia in the Permian, *Nature*, *293*, 212–216.

McFadden, P. L., and M. W. McElhinny (1988), The combined analysis of remagnetization circles and direct observations in paleomagnetism, *Earth Plant. Sci. Lett.*, *87*, 161–172, doi:10.1016/0012-821X(88)90072-6.

McFadden, P. L., and M. W. McElhinny (1990), Classification of the reversal test in palaeomagnetism, *Geophys. J. Int.*, *103*, 725–729, doi:10.1111/j.1365-246X.1990.tb05683.X.

Meng, Q. R. (2003), What drove late Mesozoic extension of the northern China-Mongolia tract?, *Tectonophysics*, *369*, 155–174, doi:10.1016/S0040-1951(03)00195-1.

Meng, Z., H. F. Huang, Y. Z. Chen, and R. S. Coe (1990), The Late Permian pole of the western Jiuquan Basin (NW China) and its tectonic implication, *Acta Sedment. Sin.*, *8*, 58–65.

Metelkin, D. V., V. A. Vernikovsky, A. Y. Kazansky, and M. T. D. Wingate (2010), Late Mesozoic tectonics of Central Asia based on paleomagnetic evidence, *Gond. Res.*, *18*, 400–419, doi:10.1016/j.gr.2009.12.008.

Miao, L., F. Zhang, W. M. Fan, and D. Liu (2007), Phanerozoic evolution of the Inner Mongolia-Daxinganling orogenic belt in North China: Constraints from geochronology of ophiolites and associated formations, *Geol. Soc. London, Spec. Pub.*, *280*, 223–237, doi:10.1144/SP280.11.

Miao, L., W. Fan, D. Liu, F. Zhang, Y. Shi, and F. Guo (2008), Geochronology and geochemistry of the Hegenshan ophiolitic complex: Implications

for late-stage tectonic evolution of the Inner Mongolia-Daxinganling Orogenic Belt, China, *J. Asian Earth Sci.*, *32*, 348–370, doi:10.1016/j.jseaes.2007.11.005.

Mueller, J. F., J. J. W. Rogers, Y. G. Jin, H. Wang, W. Li, J. Chronic, and J. F. Mueller (1991), Late Carboniferous to Permian sedimentation in Inner Mongolia, China, and tectonic relationships between north China and Siberia, *J. Geol.*, *99*, 251–263.

Pavlov, V. E., V. Courtillot, M. L. Bazhenov, and R. V. Veselovsky (2007), Paleomagnetism of the Siberian traps: New data and a new overall 250 Ma pole for Siberia, *Tectonophysics*, *443*, 72–92, doi:10.1016/j.tecto.2007.07.005.

Pisarevsky, S. A., D. P. Gladkochub, T. A. Donskaya, B. De Waele, and A. M. Mazukabzov (2006), Palaeomagnetism and geochronology of mafic dykes in south Siberia, Russia: The first precisely dated Early Permian palaeomagnetic pole from the Siberian craton, *Geophys. J. Int.*, doi:10.1111/j.1365-246X.2006.03160.X.

Pruner, P. (1987), Palaeomagnetism and palaeogeography of Mongolia in the Cretaceous, Permian and Carboniferous-preliminary data, *Tectonophysics*, *139*, 155–167, doi:10.1016/0040-1951(87)90204-6.

Pruner, P. (1992), Palaeomagnetism and palaeogeography of Mongolia from the Carboniferous to the Cretaceous-final report, *Phys. Earth Planet. Inter.*, *70*, 169–177, doi:10.1016/0031-9201(92)90179-Y.

Ren, J., K. Tamaki, S. Li, and J. Zhang (2002), Late Mesozoic and Cenozoic rifting and its dynamic setting in eastern China and adjacent areas, *Tectonophysics*, *344*, 175–205, doi:10.1016/S0040-1951(01)00271-2.

Sengör, A. M. C., B. A. Natal'in, and V. S. Burtman (1993), Evolution of the Altaid tectonic collage and Palaeozoic crustal growth in Eurasia, *Nature*, *364*, 299–307.

Tang, K. D. (1990), Tectonic development of Paleozoic fold belts at the north margin of the Sino–Korean craton, *Tectonics*, *9*, 249–260, doi:10.1029/TC009i002p00231.

Veselovsky, R. V., Y. Gallet, and V. E. Pavlov (2003), Paleomagnetism of traps in the Podkamennaya Tunguska and Kotui River Valleys: Implications for the post-Paleozoic relative movements of the Siberian and East European platforms, *Phys. Solid Earth*, *39*, 856–871.

Wang, T., Y. Zheng, G. H. Gehrels, and Z. Mu (2001), Geochronological evidence for the existence of South Mongolian microcontinent—A zircon U-Pb age of granitoid gneisses from the Yagan-Onch Hayrhan metamorphic core complex, *Chi. Sci. Bull.*, *46*, 2005–2008, doi:10.1007/BF02901917.

Wang, C. Y., P. Wang, and W. G. Li (2004a), Gonodonts from the Permian Jisu Honguer (Zhesi) Formation of Inner Mongolia, *Geobios*, *37*, 471–480, doi:10.1016/j.geobios.2003.06.003.

Wang, T., Y. Zheng, T. Li, and Y. Gao (2004b), Mesozoic granitic magmatism in extensional tectonics near the Mongolian border in China and its implications for crustal growth, *J. Asian Earth Sci.*, *23*, 715–729, doi:10.1016/S1367-9120(03)00133-0.

Webb, L. E., and C. L. Johnson (2006), Tertiary strike-slip faulting in southeastern Mongolia and implications for Asian tectonics, *Earth Planet. Sci. Lett.*, *241*, 323–335, doi:10.1016/j.epsl.2005.10.033.

Webb, L. E., S. A. Graham, C. L. Johnson, G. Badarch, and M. S. Hendrix (1999), Occurrence, age, and implications of the Yagan–Onch Hayrhan metamorphic core complex, southern Mongolia, *Geology*, *27*, 143–146, doi:10.1130/0091-7613(1999)027<0147:RSPAIT>2.3.CO;2.

Webb, L. E., C. L. Johnson, and C. Minjin (2010), Late Triassic sinistral shear in the East Gobi Fault Zone, Mongolia, *Tectonophysics*, *495*, 246–255, doi:10.1016/j.tecto.2010.09.033.

Wei, H. H., Q. R. Meng, G. L. Wu, and L. Li (2012), Multiple controls on rift basin sedimentation in volcanic settings: Insights from the anatomy of a small Early Cretaceous basin in the Yanshan belt, northern North China, *Geol. Soc. Am. Bull.*, *124*, 380–399, doi:10.1130/B30495.1.

Windley, B. F., D. Alexeiev, W. J. Xiao, A. Kröner, and G. Badarch (2007), Tectonic models for accretion of the Central Asian Orogenic Belt, *J. Geol. Soc. London*, *164*, 31–47, doi:10.1144/0016-764920006-022.

Wu, H. N., L. F. Zhou, and Z. Y. Zhao (1993), Paleomagnetic study of Carboniferous and Permian rocks from the Alashan and surrounding regions and its tectonic implications (in Chinese), *Sci. China Ser. B*, *23*, 527–536.

Wu, F. Y., J. Q. Lin, S. A. Wilde, D. Y. Sun, and J. H. Yang (2005), Nature and significance of the Early Cretaceous giant igneous event in eastern China, *Earth Planet. Sci. Lett.*, *233*, 103–119, doi:10.1016/j.epsl.2005.02.019.

Wu, F. Y., D. Y. Sun, W. C. Ge, Y. B. Zhang, M. L. Grant, S. A. Wilde, and B. M. Jahn (2011), Geochronology of the Phanerozoic granitoids in northeastern China, *J. Asian Earth Sci.*, *41*, 1–30, doi:10.1016/j.jseaes.2010.11.014.

Xiao, W. J., B. Windley, J. Hao, and M. G. Zhai (2003), Accretion leading to collision and the Permian Solonker suture, Inner Mongolia, China: Termination of the Central Asian Orogenic Belt, *Tectonics*, *22*(6), 1069, doi:10.1029/2002TC001484

Xu, B., and B. Chen (1997), Framework and evolution of the middle Paleozoic orogenic belt between Siberian and North China Plates in northern Inner Mongolia, *Sci. China Ser. D*, *40*(5), 463–469, doi:10.1007/BF02877610.

Xu, X., W. Harbert, S. Dril, and V. Kravchinksy (1997), New paleomagnetic data from the Mongol–Okhotsk collision zone, Chita region, south-central Russia: Implications for Paleozoic paleogeography of the Mongol–Okhotsk Ocean, *Tectonophysics*, *269*, 113–129, doi:10.1016/S0040-1951(96)00140-0.

Xu, B., J. Charvet, and F. Q. Zhang (2001), Primary study on petrology and geochronology of the blueschist in Sonid Zuoqi, northern Inner Mongolia (in Chinese with English abstract), *Chin. J. Geol.*, *36*, 424–434.

Xu, B., J. Charvet, Y. Chen, P. Zhao, and G. Z. Shi (2012), Middle Paleozoic convergent orogenic belts in western Inner Mongolia (China): Framework, kinematics, geochronology and implications for tectonic evolution of the Central Asian Orogenic Belt, *Gond. Res.*, doi:10.1016/j.gr.2012.05.015.

Yang, Z. Y., X. H. Ma, B. C. Huang, Z. M. Sun, and Y. X. Zhou (1998), Apparent polar wander path and tectonic movement of the North China Block in Phanerozoic, *Sci. China Ser. D*, *41* Supp., 51–65, doi:10.1007/BF02984513.

Zhang, X. H., H. F. Zhang, Y. J. Tang, S. A. Wilde, and Z. C. Hu (2008), Geochemistry of Permian bimodal volcanic rocks from Central Inner Mongolia, North China: Implication for tectonic setting and Phanerozoic continental growth in Central Asian Orogenic Belt, *Chem. Geol.*, *249*, 261–281, doi:10.1016/j.chemgeo.2008.01.005.

Zhang, Y. P., Y. Z. Su, and J. C. Li (2010), Regional tectonics significance of the Late Silurian Xibiehe Formation in central Inner Mongolia, China, *Geol. Bull. China*, *29*(11), 1599–1605.

Zhang, X. H., S. A. Wilde, H. F. Zhang, and M. G. Zhai (2011), Early Permian high-K calc-alkaline volcanic rocks from NW Inner Mongolia, North China: Geochemistry, origin and tectonic implications, *J. Geol. Soc. London*, *168*, 525–543, doi:10.1144/0016-76492010-094.

Zhao, X. X., and R. Coe (1989), Tectonic implications of Permo-Triassic paleomagnetic results from North and South China. In: J.W. Hillhouse (Editor), Deep Structure and Past Kinematics of Accreted Terranes, *IUG-G Geophys. Monogr.*, *5*, 267–283.

Zhao, X., R. S. Coe, Y. Zhou, H. Wu, and J. Wang (1990), New paleomagnetic results from northern China: Collision and suturing with Siberia and Kazakhstan, *Tectonophysics*, *181*, 43–81, doi:10.1016/0040-1951(90)90008-V.

Zhao, X. X., R. S. Coe, H. N. Wu, and Z. Y. Zhao (1993), Silurian and Devonian palaeomagnetic poles from North China and implications for Gondwana, *Earth Planet. Sci. Lett.*, *117*, 497–506, doi:10.1016/0012-821X(93)90099-U.

Zhao, L., T. R. Wu, and H. L. Luo (2011), SHRIMP U-Pb dating, geochemistry and tectonic implications of the Beiqigetao gabbros in Urad Zhongqi area, Inner Mongolia (in Chinese with English abstract), *Acta Petrol. Sin.*, *27*(10), 3071–3082.

Zhu, R., Z. Yang, H. Wu, X. Ma, B. Huang, Z. Meng, and D. Fang (1998), Paleomagnetic constraints on the tectonic history of the major blocks of China during the Phanerozoic, *Sci. China Ser. D*, *41*, 1–19, doi:10.1007/BF02984508.

Zonenshain, L. P., M. I. Kuzmin, and L. M. Natapov (1990), *Tectonics of Lithosphere Plates of the Territory of the USSR (in Russian)*, Nedra, Moscow, vol. *1*, pp. 328.

Precambrian Research 242 (2014) 39–57

Contents lists available at ScienceDirect

Precambrian Research

journal homepage: www.elsevier.com/locate/precamres

The Apparent Polar Wander Path of the Tarim block (NW China) since the Neoproterozoic and its implications for a long-term Tarim–Australia connection

P. Zhao[a,b], Y. Chen[b], S. Zhan[c], B. Xu[a,*], M. Faure[b]

[a] Key Laboratory of Orogenic Belts and Crustal Evolution, Ministry of Education, Peking University, Beijing 100871, China
[b] Institut des Sciences de la Terre d'Orléans, UMR 7327-Université d'Orléans-INSU/CNRS-BRGM, 1A rue de la Férollerie, 45071 Orléans Cedex 2, France
[c] Blackstone Mining Associates Limited, 100 Queens Road, Central, Hong Kong, China

ARTICLE INFO

Article history:
Received 27 February 2013
Received in revised form 9 December 2013
Accepted 12 December 2013
Available online 25 December 2013

Keywords:
Neoproterozoic
Paleomagnetism
Tarim block
Australia
APWP

ABSTRACT

In order to better understand the kinematic history of the Tarim block after the breakup of the Rodinia supercontinent, paleomagnetic studies have been carried out on Neoproterozoic strata from the Quruqtagh and Yecheng areas in the northeastern and southwestern Tarim block (NW China), respectively. Totally, 547 sedimentary and volcanic samples were collected from 64 sites. Magnetic mineralogical studies show that titanium-poor magnetite and hematite are the principal magnetic remanent carriers. For the Quruqtagh area, the directional analyses reveal that the stable and primary magnetic remanences have been isolated from the ca. 635 Ma Tereeken Formation cap carbonate and the 615 Ma Zhamoketi basaltic andesite, providing two Neoproterozoic paleomagnetic poles at: $\lambda = 27.6^{\circ}$N, $\varphi = 140.4^{\circ}$E, dp = 8.8°, dm = 11.1° for the Tereeken Formation and $\lambda = -4.9^{\circ}$N, $\varphi = 146.7^{\circ}$E, dp = 3.0°, dm = 5.2° for the Zhamoketi formation. Nevertheless, all other Neoproterozoic formations from this area show magnetic directions close to either the Present Earth Field (PEF) or the Late Carboniferous–Early Permian ones. Samples from the Yecheng area yield high anisotropy degree values and near vertical magnetic fabrics indicating the absence of reliable Neoproterozoic magnetic remanence. Combined these two newly obtained paleomagnetic poles with the previously published ones, an Apparent Polar Wander Path (APWP) from the Neoproterozoic to the Present has been built for the Tarim block. The comparison between the APWPs of Tarim and Australia implies a long-term Australia–Tarim connection and/or same kinematic evolution from at least the Neoproterozoic until the Middle Silurian. The Tarim block probably began to break away from northwestern Australia since the Late Ordovician and the final separation occurred at the Late Silurian–Early Devonian.

1. Introduction

The western part of the Rodinia supercontinent, composed of Australia, East Antarctica, India, South China and Tarim (Li et al., 1996; Li and Powell, 2001; Powell and Pisarevsky, 2002), was considered to break up from the Rodinia supercontinent during 800–700 Ma rifting events (Meert and Torsvik, 2003; Li et al., 2008). After the breakup, each block displayed a different kinematic history. For East Antarctica, it situated against the southern margin of Australia and evolved together with Australia (Li et al., 2008). Concerning the India block, it separated from the western part of Australia and drifted northwestwards at the beginning of the Rodinia breakup event (Torsvik et al., 2001; Li et al., 2008; Gregory et al., 2009). While for the drift history of the Tarim block after the Rodinia breakup, different ideas have been proposed. Chen et al. (2004) and Zhan et al. (2007) suggested that the Tarim block was situated against northwestern Australia at ~800 Ma and ~600 Ma. In a recent reconstruction model (Li et al., 2008), the Tarim block was placed at northwestern Australia and moved together with Australia during the entire Late Neoproterozoic. However, Huang et al. (2005) proposed that the Tarim block was situated against Southwest Australia at ca. 740 Ma after a southward drift and a counterclockwise rotation. It is obvious that further paleomagnetic studies from geochronologically well constrained strata can provide critical answers for these controversies and the kinematic history of the Tarim block. For this reason, in this paper, we present new Late Neoproterozoic paleomagnetic data from the Quruqtagh and Yecheng areas in the northeastern and southwestern parts of the Tarim block, respectively. With these new results and the previous paleomagnetic data, we try to build up the Apparent Polar Wander Path (APWP) of the Tarim block and discuss its kinematic history after the breakup of the Rodinia supercontinent.

* Corresponding author. Tel.: +86 01062767288.
E-mail address: bxu@pku.edu.cn (B. Xu).

0301-9268/$ – see front matter © 2014 Published by Elsevier B.V.
http://dx.doi.org/10.1016/j.precamres.2013.12.009

2. Geological setting and paleomagnetic sampling

2.1. Geological setting

The Tarim block, situated in northwestern China (Fig. 1a), is bounded by the Tianshan Mountain to the north, the Western Kunlun Mountain to the southwest, and the Altyn Tagh Fault to the southeast (Fig. 1b). Archean gneisses and Paleo- to Mesoproterozoic metasedimentary and metavolcanic rocks constitute the basement of the Tarim block (Lu et al., 2008). The cratonization of the Tarim block occurred between 1.05 Ga to 0.9 Ga by the Tarimian Orogeny with the Aksu blueschist dated at 962 ± 12 Ma and 944 ± 12 Ma (Gao et al., 1993; Lu et al., 2008). The basement was intruded by middle Neoproterozoic mafic dykes and granitoid plutons with a peak age at 800 Ma, which attributed to the breakup of the Rodinia supercontinent (Lu et al., 2008; Zhang et al., 2007, 2009; Shu et al., 2011). The middle Neoproterozoic to Phanerozoic sedimentary rocks unconformably covered the metamorphic basement and intrusions (Gao et al., 1993; Lu et al., 2008). Late Neoproterozoic diamictite bearing deposits have been identified from three areas in the Tarim block, namely Quruqtagh on the northeastern margin, Aksu on the northwestern margin and Yecheng on the southwestern margin (Fig. 1b; Lu et al., 2008). Three glaciations have been described from the Quruqtagh area (Xu et al., 2009), while two glaciations have been identified from the Aksu and Yecheng areas (Zhu and Wang, 2012; Tong et al., 2013). As paleomagnetic studies have been already performed on the Neoproterozoic dykes and strata in the Aksu area (Li et al., 1991; Chen et al., 2004; Zhan et al., 2007; Wen et al., 2013), this study focuses on the Quruqtagh and Yecheng areas.

2.1.1. Quruqtagh area

The Quruqtagh area is located on the northeastern margin of the Tarim block, NW China (Fig. 1). The oldest Archean Tuoge Complex is composed of granitic gneisses with minor amphibolites (Lu et al., 2008; Long et al., 2010; Zhang et al., 2012a). The Paleoproterozoic gneisses and marbles underwent amphibolite- to granulite-facies metamorphism and are unconformably overlain by the Mesoproterozoic low-grade metamorphosed clastic and volcanic rocks (XJBGMR, 1993; Lu et al., 2008). The Neoproterozoic strata are characterized by several layers of diamictites and volcanic rocks, separated by shale, sandstone and limestone (Xiao et al., 2004; Xu et al., 2009). The Neoproterozoic Quruqtagh succession includes, stratigraphically from the bottom to the top, the Baiyisi, Zhaobishan, Altungol, Tereeken, Yukengol, Zhamoketi, Shuiquan and Hankalchough formations (Fig. 2a and b). Three glaciations, i.e. Baiyisi, Tereeken and Hancalchough, have been recognized from the Baiyisi, Altungol, Tereeken and Hankalchough formations (Wang et al., 1981; Gao and Qian, 1985; Brookfield, 1994; Knoll, 2000; Xiao et al., 2004; Xu et al., 2009). Volcanic rocks from the bottom and top of the Baiyisi formation yield zircon U–Pb ages of 740 ± 7 Ma and 725 ± 10 Ma, respectively. And volcanic rocks from the top of the Zhamoketi formation gives a zircon U–Pb age of 615 ± 6 Ma (Xu et al., 2009). Meanwhile, Chemo-stratigraphic and sedimentary features of the Tereeken diamictite suggest a Marinoan age (ca. 635 Ma) for the Tereeken glaciation (Xiao et al., 2004). Except for these four diamictite-bearing formations, interglacial deposits contain interbedded sandstone-shale of the Zhaobishan and Zhamoketi formations, carbonate of the Shuiquan formation and shale of the Yukengou formation (Fig. 1d). The lower Cambrian siliceous rocks unconformably overlie the Quruqtagh succession (Xu et al., 2005).

2.1.2. Yecheng area

The Yecheng area is located in the southwest of the Tarim block, which is separated from the Tibetan plateau to the south along the West Kunlun Mountain (Fig. 1b). The Proterozoic strata crop out at ca. 100 km south of Yecheng city. The strata include, in ascending order, the Silu Group of the Qingbaikou series, the Yalaguz formation and the Qakmaklik Group of the Nanhua (Cryogenian) series, the Kurcak and Kzisuhum formations of the Sinian (Ediacaran) series (Fig. 2c). These Neoproterozoic formations are unconformably overlain by the Devonian clastic-carbonate rocks. The Silu Group of the Qingbaikou series is mainly composed of

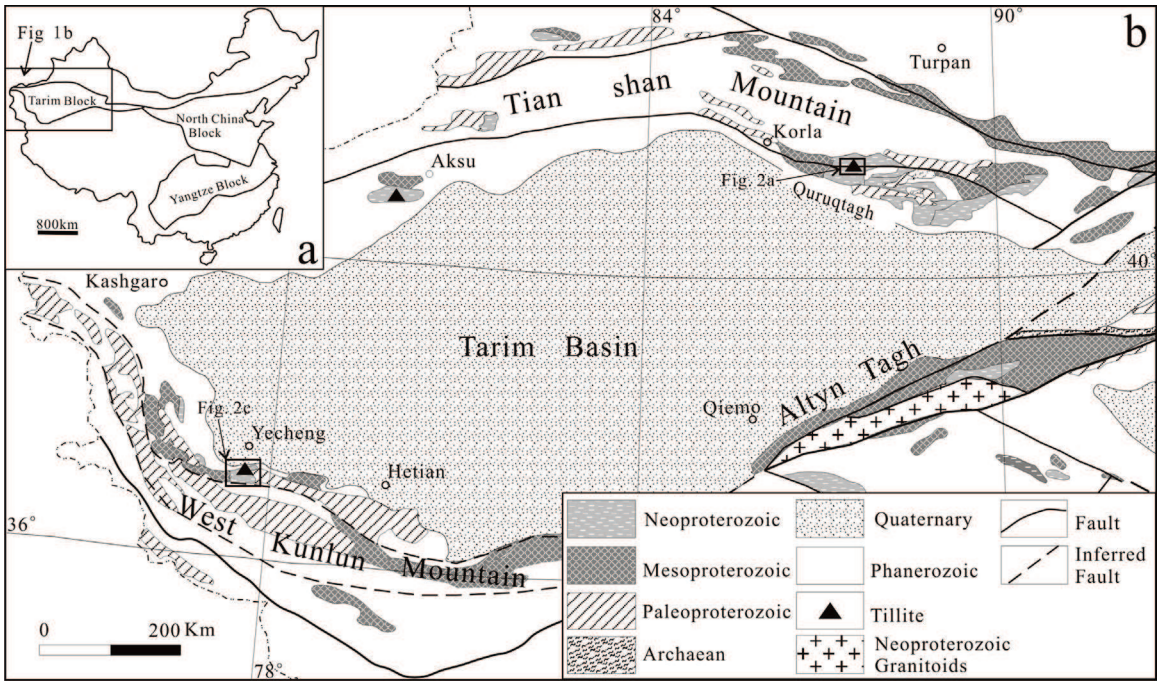

Fig. 1. (a) Schematic tectonic map of China showing the three major Precambrian blocks. (b) Sketch map of the Tarim block and adjacent areas showing the Precambrian geology and surrounding orogens (after Lu et al., 2008).

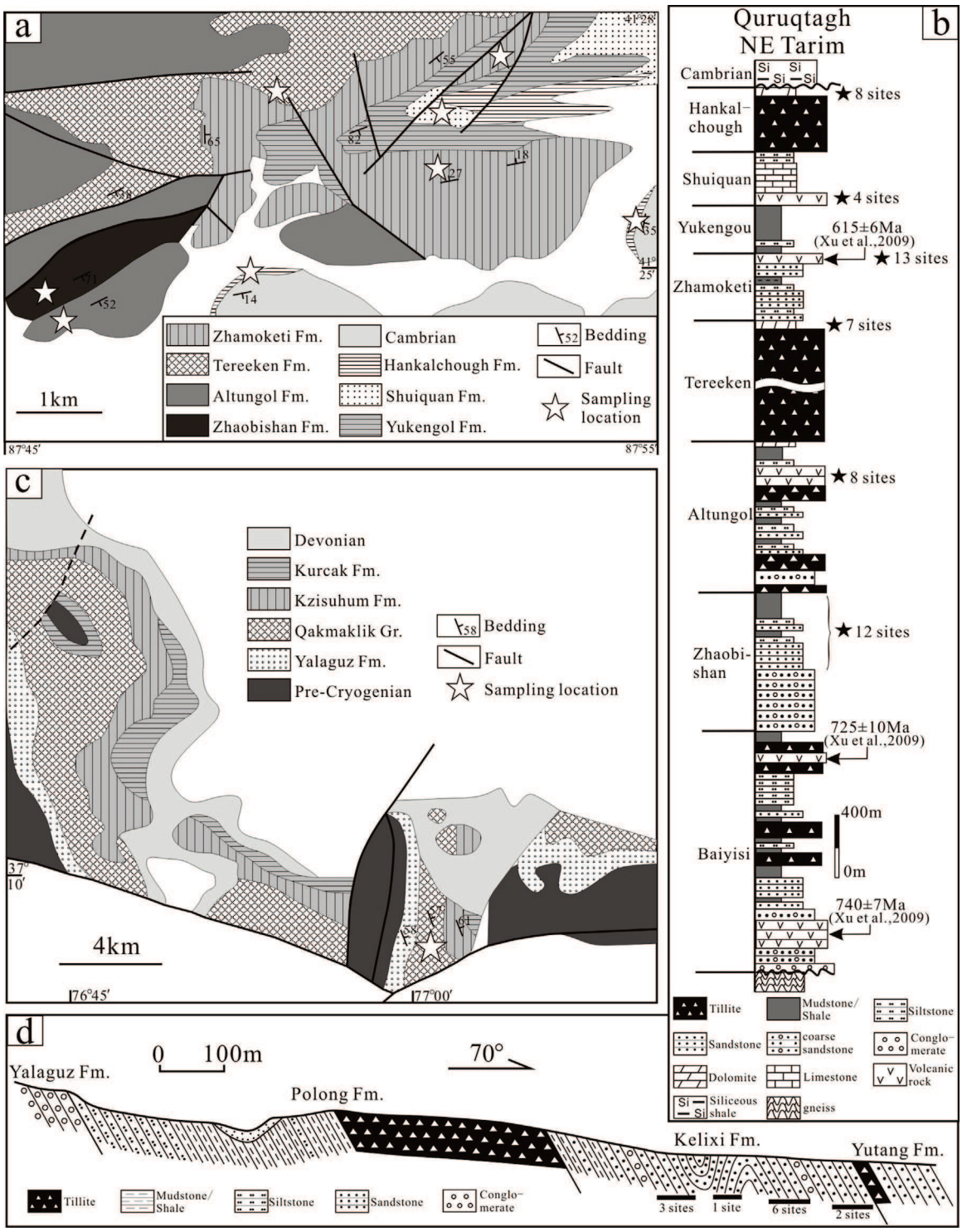

Fig. 2. (a) Simplified geologic map of the Heishan-Zhaobishan area showing the paleomagnetic sampling details. The black lines show major faults. (b) Simplified geologic map of the Qiakelikemake valley area showing the paleomagnetic sampling location (modified after Zhu and Wang, 2012). (c) Stratigrsphic column of the Quruqtagh area (modified after Xu et al., 2005, 2009), showing the sampling layers. (d) Succession of the section in the Qiakelikemake valley area showing the paleomagnetic sampling details as well as the bedding attitudes of the Kelixi Formation.

weakly deformed sandstone and dolomite with abundant of stromatolite and algae fossils, e.g. *Gymonsolen*, *Inzeria*, *Oscillatorites* sp., *Polyedryxium* sp., which well constrain its age (Wang et al., 2004; Zhang et al., 2003, 2004). It unconformably overlies Paleo- and Mesoproterozoic gneisses (Ma et al., 1991; Zhang et al., 2003). Both the gneisses and the Silu Group were intruded by granites and mafic dykes dated at 815–800 Ma (Zhang et al., 2003, 2004). In turn, the Silu Group and mafic dykes are unconformably overlain by the Yalaguz formation conglomerate (Fig. 2c; Zhang et al., 2004; Wang et al., 2004). The Yalaguz Formation mainly consists of versicolor conglomerate with interbedded siltstone (Zhang et al., 2003). The Qakmaklik Group is upwardly composed of the Polong, Kelixi and Yutang formations (Fig. 1c). The Polong formation consists of purple-green siltstone and mudstone at the lower part

and thick dark purple tillite at the upper part, which is considered as marine glacier deposits (Zhang et al., 2003; Tong et al., 2013). The Kelixi formation consists of red sandstone and conglomerate with large trough-planar cross beddings, considered as delta or peritidal deposits (Zhang et al., 2003; Tong et al., 2013). The Yutang formation contains dark purple tillite at the lower part and red sandstone-siltstone on the upper part. No direct biostratigraphic age has been obtained from the Qakmaklik Group because of rare fossils therein. The Sinian strata, composed of the Kzisuhum and Kurcak formations, are mainly made up of dolomite, red-black sandstone and mudstone with characteristic gypsum layers (Tong et al., 2013). The wealth of stromatolite and algae fossils, e.g. *Trematosphaeridium* sp., *Polyedryxium* sp., *Pseudozonosphaera rugosa*, well constrain their age and make this series comparable with the Hankalchough formation in the Quruktagh area (Gao et al., 1985).

2.2. Paleomagntic sampling

In the field, 6–12 cores were drilled from each site using a portable gasoline drill. Cores were oriented by both magnetic and solar compasses, when it was possible. The average difference between these two azimuth measurements is about $2.2 \pm 1.6^\circ$ for the Quruqtagh area and $4.0 \pm 1.8^\circ$ for the Yecheng area. This mean value is used for the orientation corrections for the samples measured only by magnetic compass as well as for the sedimentary bedding measurement.

In the Quruktagh area, paleomagnetic samples were collected from 6 out of 8 Late Neoproterozoic formations except the Baiyisi and Yukengou formations (Fig. 2c). Totally, 392 cores of 52 sites were paleomagnetically sampled (Fig. 2a; Table 1). Most samples were collected from the Heishan-Zhaobishan area in the central part of the Quruqtagh area (ca. 200 km southeast of Korla, Fig. 2a), with 4 sites of the Zhaobishan formation collected from the same section in the Xishankou area where the paleomagnetic results of the Baiyisi volcanic rocks were published (Huang et al., 2005). A notable fact of the strata from the Xishankou area is that the green-colored volcanic rocks contain metamorphic chlorite. Detailed sampling information can be found in Table 1.

In the Yecheng area, paleomagnetic samples were collected from the red sandstone of the Kelixi formation between two tillite layers (Fig. 2d) at the West Kunlun Mountain front (Fig. 1b). The strata are intensively tilted with high angle bedding (Fig. 2d; Table 1). Several faults have been observed in the sampling zone (Fig. 2c). Two folds were identified within the Kelixi Formation (Fig. 1d), providing a good opportunity for future fold test. Totally, 155 samples of 12 sites were collected from both limbs of folds (Table 1).

3. Laboratory methods

In the laboratory, cores were prepared into standard specimens with 2.5 cm in diameter and 2.2 cm in length. Before the measurements of magnetic remanence of this paleomagnetic collection, several methods were performed to investigate the magnetic mineralogy: thermal magnetic experiment (Curie point) by KLY-3S kappabridge susceptibility-meter coupled with a CS3 furnace and acquisition of isothermal remanent magnetization (IRM) by IM30 pulse magnetizer and JR5A magnetometer in the Laboratoire de Magnétisme des Roches d'Orléans (LMRO), and magnetic hysteretic curves in the Laboratoire de Paleomagnétisme of Institut de Physique du Globe de Paris (IPGP) at Saint Maur.

In order to evaluate the deformation experienced by sampled rocks, measurements of the anisotropy of the magnetic susceptibility (AMS) were also systematically performed on specimens before their demagnetization by KLY3 kappabridge susceptibility-meter. The orientation of the principal magnetic fabric axes, namely K_1, K_2 and K_3, has been measured, and the anisotropy degree (P_J) and shape parameter (T) have been calculated for each specimen following Jelínek (1978).

Usually, at least 6 cores were chosen from each site for demagnetization. Both thermal and alternative magnetic field (AF) techniques were applied to progressively remove the magnetic remanence by about 12–16 steps with temperature intervals from 20 to 50 °C and alternative magnetic field intervals from 2 to 20 mT. The majority of the sandstone specimens were measured in LMRO with JR5-A spinner magnetometer; the remaining samples were measured in IPGP with a 2G cryogenic magnetometer for comparison reason. Almost all limestone specimens were measured in IPGP with a 2G cryogenic magnetometer because of their low magnetic remanent intensity. No significant difference was found between the results of these two laboratories.

Magnetic directions were isolated by the principal component analysis method (Zijderveld, 1967; Kirschvink, 1980) or estimated by great circle technique when end-points were not aligned (McFadden and McElhinny, 1988). The mean magnetic directions were computed by Fisher spherical analysis (Fisher, 1953) using paleomagnetic software packages offered by Cogné (2003) and R. Enkin (unpublished).

4. Measurement results

4.1. Quruqtagh area

4.1.1. Zhamoketi Formation

For the sandstone of the Zhaobishan formation, isothermal magnetization measurements show a rapid increase until to 30 mT, then a slow increase of IRM without a total magnetic saturation at about 1.5 T (Fig. 3a), indicating the existence of both low and high magnetic coercive minerals in the rock. Thermal magnetic experiments reveal a gradually decrease of magnetic susceptibility and an obvious drop from 580 °C to 700 °C (Fig. 3b), indicating the existence of magnetite and hematite. The paramagnetic feature of hysteresis loop (Fig. 3c) may be caused by the weak amount of ferromagnetic minerals. Four sites of sandstone collected from the Xishankou area present two magnetic components (Fig. 4a). The low temperature component (LTC) displays northeastward declinations and downward inclinations (Fig. 4a). The high temperature component (HTC) gives unified southwestward declinations and upward inclinations (Fig. 4a), and a site-mean direction has been calculated at: $D_g = 222.7^\circ$, $I_g = -38.6^\circ$, $k_g = 27.5$, $\alpha_{95g} = 24.0^\circ$; $D_s = 227.2^\circ$, $I_s = -6.9^\circ$, $k_s = 10.6$, $\alpha_{95s} = 40.0^\circ$ with $n = 3$ (Table 1). Tilt-corrected directions are less clustered than the in situ directions with a k_s/k_g ratio of 0.39. Meanwhile, the optimal concentration of direction correction (DC) of tilt test is achieved at −30% unfolding, with DC slope at -0.317 ± 0.600 (Enkin, 2003). Both of them indicate a negative fold test at the 95% confidence level (McElhinny, 1964; Enkin, 2003; Fig. 5a and b; Table 1). The 8 sites from Heishan-Zhaobishan area show northward declinations and downward inclinations (Fig. 4b) with a site-mean direction at: $D_g = 0.6^\circ$, $I_g = 56.5^\circ$, $k_g = 210.5$, $\alpha_{95g} = 3.8^\circ$; $D_s = 99.3^\circ$, $I_s = 34.4^\circ$, $k_s = 25.6$, $\alpha_{95s} = 11.2^\circ$ with $n = 8$ (Fig. 5c and d; Table 1). The mean direction in in situ coordinates is close to the Present Earth Field (PEF; Fig. 5c and d) and a negative fold test is concluded (McElhinny, 1964; Enkin, 2003).

4.1.2. Altungol Formation

Eight sites of trachybasalt from the Altungol Formation were sampled in a monoclinal section. The abrupt increase of IRM up to 90% saturation at about 200 mT, and the magnetic hysteresis

Table 1
Summarized paleomagnetic sampling and measurement results of this study.

Site	Lithology	Slong (E)	Slat (N)	n/N	Polarity	D_g (°)	I_g (°)	D_s (°)	I_s (°)	K (°)	α_{95} (°)	Strike (°)	Dip (°)	Comment
Zhaobishan Formation – Quruqtagh area														
Xishankou area														
632	Sandstone	86°33′08″	41°36′09″	4/7	R	200.0	−38.0	208.5	−19.0	72.8	10.8	333.5	24.3	
633	Sandstone	86°33′08″	41°36′09″	0/7	–	–	–	–	–	–	–	333.5	24.3	Dispersed
634	Sandstone	86°33′08″	41°36′09″	5/6	R	232.3	−39.1	235.3	−16.7	14.0	21.2	337.7	23.0	
635	Sandstone	86°33′08″	41°36′09″	4/7	N	235.2	−35.5	237.2	16.0	30.0	17.1	338.0	52.5	
	Average			3/4		222.7	−38.6			27.5	24.0			
								227.2	−6.9	10.6	40.0			
Heishan-Zhaobishan area														
601	Sandstone	87°46′24″	41°24′29″	4/7	N	6.5	59.3	97.3	20.3	46.0	13.7	35.7	83.3	PEF
602	Sandstone	87°46′24″	41°24′29″	3/7	N	1.9	60.5	95.8	46.9	37.2	20.5	40.2	57.0	PEF
603	Sandstone	87°46′24″	41°24′29″	6/7	N	358.7	60.5	68.8	52.6	56.5	9.0	25.2	42.0	PEF
604	Sandstone	87°46′24″	41°24′29″	6/7	N	5.1	49.5	89.2	26.6	51.5	9.4	37.2	82.0	PEF
605	Sandstone	87°46′24″	41°24′29″	7/7	N	7.3	61.1	103.7	24.2	21.5	13.3	40.2	80.0	PEF
606	Sandstone	87°46′24″	41°24′29″	7/7	N	359.4	54.4	98.9	31.9	41.4	9.5	40.2	79.0	PEF
607	Sandstone	87°46′24″	41°24′29″	5/7	N	348.7	52.5	117.6	35.7	79.5	8.6	49.2	86.0	PEF
608	Sandstone	87°46′24″	41°24′29″	5/7	N	359.1	53.5	114.2	31.7	29.5	14.3	50.2	85.5	PEF
	Average			8/8		0.6	56.5			210.5	3.8			
								99.3	34.4	25.6	11.2			
Altungol Formation – Quruqtagh area														
609	Trachybasalt	87°46′24″	41°24′29″	0/6	–	–	–	–	–	–	–	–	–	Dispersed
610	Trachybasalt	87°46′24″	41°24′29″	4/6	N	13.7	62.4	111.1	45.6	82.9	10.2	52.5	58.0	PEF
611	Trachybasalt	87°46′24″	41°24′29″	4/6	N	12.7	64.6	114.1	45.3	139.4	7.8	52.5	58.0	PEF
612	Trachybasalt	87°46′24″	41°24′29″	0/6	–	–	–	–	–	–	–	–	–	Dispersed
613	Trachybasalt	87°46′24″	41°24′29″	3/6	N	19.1	56.4	101.9	44.2	34.6	21.3	52.5	58.0	PEF
614	Trachybasalt	87°46′24″	41°24′29″	6/6	N	3.2	60.3	111.0	51.0	298.4	3.9	52.5	58.0	PEF
615	Trachybasalt	87°46′28″	41°24′18″	5/6	N	346.3	59.0	118.4	58.6	157.0	6.3	52.5	58.0	PEF
616	Trachybasalt	87°46′28″	41°24′18″	6/6	N	355.8	45.5	89.6	60.8	82.1	7.4	52.5	58.0	PEF
	Average			6/8		4.4	58.6			74.3	7.8			
								108.1	51.2	74.6	7.8			
Tereeken Formation – Quruqtagh area														
617	Carbonate	87°48′50″	41°27′08″	4/7	N	97.1	45.5	101.2	62.3	27.1	19	179.2	17.0	
618	Carbonate	87°48′50″	41°27′08″	4/7	N	114.1	36.4	94.0	63.1	25.4	25.0	224.2	29.0	
619	Carbonate	87°48′50″	41°27′08″	7/7	N	79.2	61.3	115.7	64.4	55.2	8.3	106.7	18.5	
620	Carbonate	87°48′50″	41°27′08″	7/8	N	82.2	61.6	76.7	61.8	54.8	8.3	255.7	3.0	
621	Carbonate	87°48′50″	41°27′08″	4/6	N	112.2	54.3	92.8	59.1	62.2	11.7	261.7	13.5	
622	Carbonate	87°48′42″	41°27′03″	4/6	N	96.4	52.9	62.4	65.7	160.5	8.4	227.7	23.0	
623	Carbonate	87°48′42″	41°27′03″	0/6	N	–	–	–	–	–	–	228.7	35.0	Dispersed
	Average			6/7		98.8	52.7			39.4	10.8			
								90.8	63.7	91.4	7.0	$\lambda = 27.6°$, $\varphi = 140.4°$, dp = 8.8°, dm = 11.1°		
Zhamoketi Formation – Quruqtagh area														
S05	Basaltic andesite	87°52′57″	41°27′41″	4/8	N	45.3	65.9	112	40.1	83.6	10.1	53.8	49.0	
S06	Basaltic andesite	87°52′57″	41°27′41″	8/8	N	73.6	63.2	115.1	28.1	108.7	5.3	53.8	49.0	
S07	Basaltic andesite	87°52′57″	41°27′41″	4/8	N	63.4	65.8	114.9	33.2	115.4	8.6	53.8	49.0	
S08	Basaltic andesite	87°52′57″	41°27′41″	3/8	N	50.1	65.1	111.6	38	220.7	8.3	53.8	49.0	
S09	Basaltic andesite	87°52′57″	41°27′41″	0/7	–	–	–	–	–	–	–	53.8	49.0	Dispersed
S10	Basaltic andesite	87°52′57″	41°27′41″	5/8	N	52.1	69.8	117.7	38.6	524.6	3.3	53.8	49.0	
S11	Basaltic andesite	87°52′57″	41°27′41″	7/8	N	72.4	69.2	120.5	31.9	115.5	5.6	53.8	49.0	
S12	Basaltic andesite	87°52′57″	41°27′41″	0/8	–	–	–	–	–	–	–	53.8	49.0	Dispersed
S13	Basaltic andesite	87°52′57″	41°27′41″	0/8	–	–	–	–	–	–	–	53.8	49.0	Dispersed
628	Basaltic andesite	87°52′14″	41°26′19″	0/6	–	–	–	–	–	–	–	93.5	43.5	Viscous

Table 1 (*Continued*)

Site	Lithology	Slong (E)	Slat (N)	*n*/*N*	Polarity	D_g (°)	I_g (°)	D_s (°)	I_s (°)	*K* (°)	α_{95} (°)	Strike (°)	Dip (°)	Comment
629	Basaltic andesite	87°52′14″	41°26′19″	0/6	–	–	–	–	–	–	–	86.0	44.0	Viscous
630	Basaltic andesite	87°52′05″	41°26′24″	0/6	–	–	–	–	–	–	–	88.5	42.5	Viscous
631	Basaltic andesite	87°52′05″	41°26′24″	0/6	–	–	–	–	–	–	–	67.0	62.0	Viscous
	Average			6/13		59.6	66.9			222.6	4.5			
								115.4	35.0	223.9	4.5	λ = −4.9°, φ = 146.7°, dp = 3.0°, dm = 5.2°		
Shuiquan Formation – Quruqtagh area														
S01	Basalt	87°52′52″	41°25′51″	0/7	–	–	–	–	–	–	–	244.3	23.1	Dispersed
S02	Basalt	87°52′52″	41°25′51″	6/7	N	359.1	30.1	356.7	15.6	13.1	19.2	244.3	23.1	
S03	Basalt	87°52′29″	41°26′48″	6/7	N	344.3	24.6	343.5	−8.8	14.0	18.5	243.9	33.9	
S04	Basalt	87°52′29″	41°26′48″	4/7	N	352.9	13.3	353.3	−5.0	10.7	19.4	243.9	33.9	
	Average			3/4		352.0	22.8			55.4	16.7			
								351.1	0.6	30.2	22.8			
Hancalchough Formation – Quruqtagh area														
501	Carbonate	87°48′55″	41°24′59″	5/7	N	22.3	57.6	108.1	70.0	280.1	4.6	78.5	38.0	PEF
502	Carbonate	87°48′55″	41°24′59″	7/7	N	12.8	65.1	134.5	72.0	35.6	10.4	78.5	38.0	PEF
503	Carbonate	87°48′55″	41°24′59″	7/7	N	17.1	57.0	106.6	72.8	56.3	8.1	78.5	38.0	PEF
504	Carbonate	87°48′55″	41°24′59″	6/7	N	24.2	57.9	109.0	68.9	84.0	7.4	78.5	38.0	PEF
624	Carbonate	87°55′51″	41°26′50″	5/6	N	22.5	57.3	48.3	23.7	210.4	5.3	347.2	43.0	PEF
625	Carbonate	87°55′51″	41°26′50″	5/6	N	16.4	64.0	50.7	31.1	83.9	8.7	340.2	43.0	PEF
626	Carbonate	87°55′51″	41°26′50″	5/6	N	26.5	55.1	47.8	16.3	41.6	12.0	340.2	48.0	PEF
627	Carbonate	87°55′51″	41°26′50″	6/6	N	12.4	59.6	46.9	28.7	82.3	7.4	349.2	47.0	PEF
	Average			8/8		19.6	59.3			331.1	3.0			
								64.2	51.8	6.6	23.2			
Kelixi Formation – Yecheng area														
X01	Sandstone	77°01′34″	37°07′44″	12/12	M	31.8	−3.0	15.9	−30.2	9.3	15.0	356.5	55.0	
X02	Sandstone	77°01′34″	37°07′44″	0/8	–	–	–	–	–	–	–	349.0	57.0	Dispersed
X03	Sandstone	77°01′17″	37°07′46″	0/7	–	–	–	–	–	–	–	0.7	54.3	Dispersed
X04	Sandstone	77°01′23″	37°07′49″	8/9	R	1.2	37.4	8.5	−16.4	14.8	14.9	309.0	63.0	
X05	Sandstone	77°01′22″	37°07′49″	0/10	–	–	–	–	–	–	–	301.7	58.7	Dispersed
X06	Sandstone	77°01′22″	37°07′49″	8/12	M	6.6	42.1	14.7	−13.4	23.0	11.8	308.3	61.3	
X07	Sandstone	77°01′22″	37°07′49″	7/11	M	345.7	25.2	347.2	−20.1	18.5	14.4	304.0	61.3	
901	Sandstone	77°01′34″	37°07′44″	6/12	R	7.0	38.2	9.5	−22.1	20.3	17.4	292.6	59.4	
902	Sandstone	77°01′17″	37°07′46″	7/11	M	357.3	−29.8	1.5	−19.0	29.8	11.2	88.3	43.4	
903	Sandstone	77°01′24″	37°07′52″	9/12	R	357.7	44.1	8.2	−11.9	27.9	11.6	298.0	60.0	
904	Sandstone	77°01′23″	37°07′49″	6/11	R	13.5	55.0	21.4	−11.9	19.2	17.9	304.0	66.5	
905	Sandstone	77°01′21″	37°08′01″	0/12	–	–	–	–	–	–	–	310.5	66.5	Dispersed
	Average			8/12		5.2	27.9			7.2	22.2			
								8.4	−18.4	48.5	8.0	λ = 42.8°, φ = 245.7°, dp = 4.3°, dm = 8.3°		

Abbreviations: Lith, lithology; Slong/Slat, longitude and latitude of sampling site; *n*/*N*, number of samples used to calculate mean direction/number of demagnetized samples; N, R and M, magnetic normal, reversal and mixed polarities, respectively; D_g, I_g D_s, I_s, declination and inclination in geographic and stratigraphic coordinates, respectively; *k*, the best estimate of the precision parameter; α_{95}, radius that mean direction lies within 95% confidence; λ/φ, latitude and longitude of paleomagnetic pole; dp/dm, oval of 95% confidence for the paleomagnetic pole. PEF, Present Earth Field.

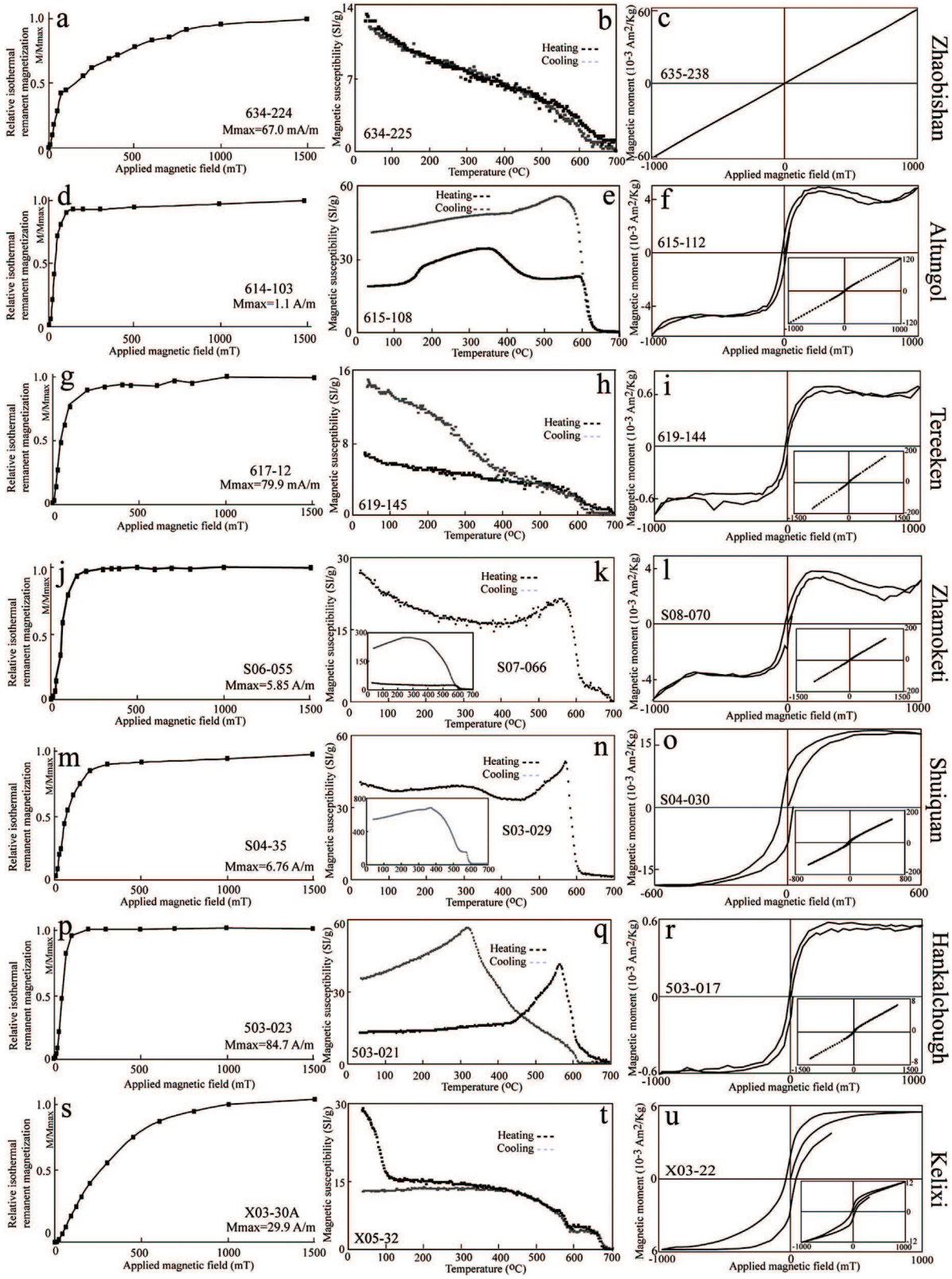

Fig. 3. Magnetic mineralogical analyses. Isothermal magnetization measurements (IRM), thermal magnetic experiments (Curie temperature) and the magnetic hysteretic curve of each formation are presented.

measurements (Fig. 3d and f) suggest mainly low coercive magnetic minerals in the rocks. Thermal magnetic experiment shows an evident drop of magnetic susceptibility at 580–620 °C during the heating process (Fig. 3e), implying titanium-poor magnetite as the main magnetic mineral, which is confirmed by hysteresis curve (Fig. 3f). Two out of eight sites display too weak NRM to give reliable direction (Table 1). Only one component was isolated with northward declinations and downward inclinations from other 6 sites (Fig. 4c; Table 1). A site-mean direction has been calculated for this formation: $D_g = 4.4°$, $I_g = 58.6°$, $k_g = 74.3$, $\alpha_{95g} = 7.8°$; $D_s = 108.1°$,

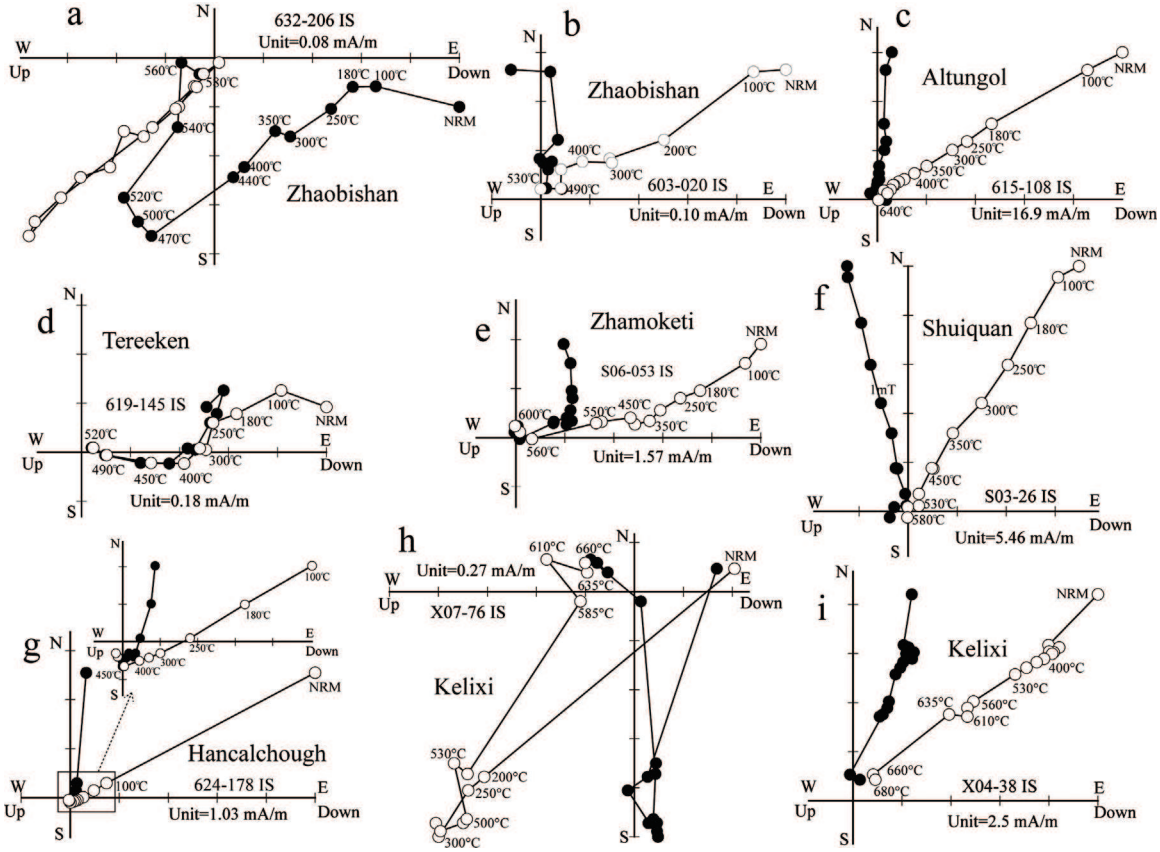

Fig. 4. Typical orthogonal vector plots (Zijderveld, 1967). Directions are plotted in in situ coordinates. Black/white circles represent vector endpoints projected onto the horizontal/vertical plane. Numbers on the plots indicate particular temperature steps. NRM: natural remanent magnetization.

$I_s = 51.2°$, $k_s = 74.6$, $\alpha_{95s} = 7.8°$ with $n = 6$ (Table 1). The mean direction in in situ coordinates shows a close to the PEF direction (Fig. 5e and f) and no fold test could be applied because of the monoclinal bedding.

4.1.3. Tereeken Formation

Seven sites of carbonate were collected from the cap carbonate above the Tereeken tillite (Fig. 2c). The abrupt increase of IRM up to 90% saturation at about 200 mT and narrow wasp-waisted hysteresis loops (Fig. 3g and i) suggest the predominant low coercive magnetic minerals in the rock. Thermal magnetic experiment shows an obvious drop of magnetic susceptibility from 540 °C to 700 °C during the heating process (Fig. 3h), implying the occurrence of both magnetite and hematite. The hysteresis curve reveals both lower and higher coercive magnetic minerals in the rock (Fig. 3i), Two components were isolated from most of the demagnetized samples distinguished at about 350 °C (Fig. 4d) except for Site 623, which displays scattered directions due to its weak NRM (Table 1). The magnetic directions of the LTC (up to about 350 °C) display a close to the PEF direction in in situ coordinates, and become dispersed in tilt corrected ones (Fig. 5g and h). After removing the LTC, the HTC shows a stable direction and a site-mean direction has been calculated at: $D_g = 98.8°$, $I_g = 52.7°$, $k_g = 39.4$, $\alpha_{95g} = 10.8°$; $D_s = 90.8°$, $I_s = 63.7°$, $k_s = 91.4$, $\alpha_{95s} = 7.0°$ with $n = 6$ (Table 1). Tilt corrected directions are much more clustered than in situ directions (Fig. 5i and j). Both McElhinny's and Enkin's fold tests give a positive answer for this formation (McElhinny, 1964; Enkin, 2003).

4.1.4. Zhamoketi Formation

Thirteen sites of basaltic andesite were sampled from the top of the Zhamoketi formation (Fig. 2c). IRM measurement shows an abrupt increase with the total saturation at about 200 mT (Fig. 3j), indicating predominant low coercive magnetic minerals in the rock. Thermal magnetic experiment shows an obvious drop of magnetic susceptibility from 580 °C to 600 °C with subordinate decrease to 700 °C (Fig. 3k), implying the presence of titanium-poor magnetite and some hematite. Although the low coercive minerals have been observed by hysteresis curves, the weak induced magnetization indicates a lower concentration of ferromagnetic mineral in the rock (Fig. 3l). Among 13 sites, 4 sites display a viscous component without stable HTC and 3 sites present dispersed directions (Table 1). For the remaining 6 sites, two components were isolated from most of the demagnetized samples (Fig. 4e). The LTC (up to 250–350 °C) shows a close to the PEF direction in in situ coordinates (Fig. 5k and l). After removing the LTC, six sites show a unified HTC direction, and a site-mean direction has been calculated at: $D_g = 56.9°$, $I_g = 66.9°$, $k_g = 222.6$, $\alpha_{95g} = 4.5°$; $D_s = 115.4°$, $I_s = 35.0°$, $k_s = 223.9$, $\alpha_{95s} = 3.5°$ with $n = 6$ (Fig. 5m and n; Table 1). No fold test could be applied as the bedding is monoclinal.

4.1.5. Shuiquan Formation

Four sites of basalt were sampled from the top of the Shuiquan formation (Fig. 2c). Both the abrupt IRM increase with a 90% saturation at about 300 mT (Fig. 3m) and the wide wasp-waisted hysteresis loops (Fig. 3o) suggest low coercive magnetic minerals as the principal remanent carrier. Thermal magnetic experiment shows a sharp drop of magnetic susceptibility at around 580 °C with the obvious Hopkinson effect before 580 °C (Fig. 3n; Radhakrishnamurty and Likhite, 1970), confirming the titanium-poor magnetite as the principal remanent carrier. Only one magnetic component was isolated from this formation. Three sites display northwestward declinations and shallow downward

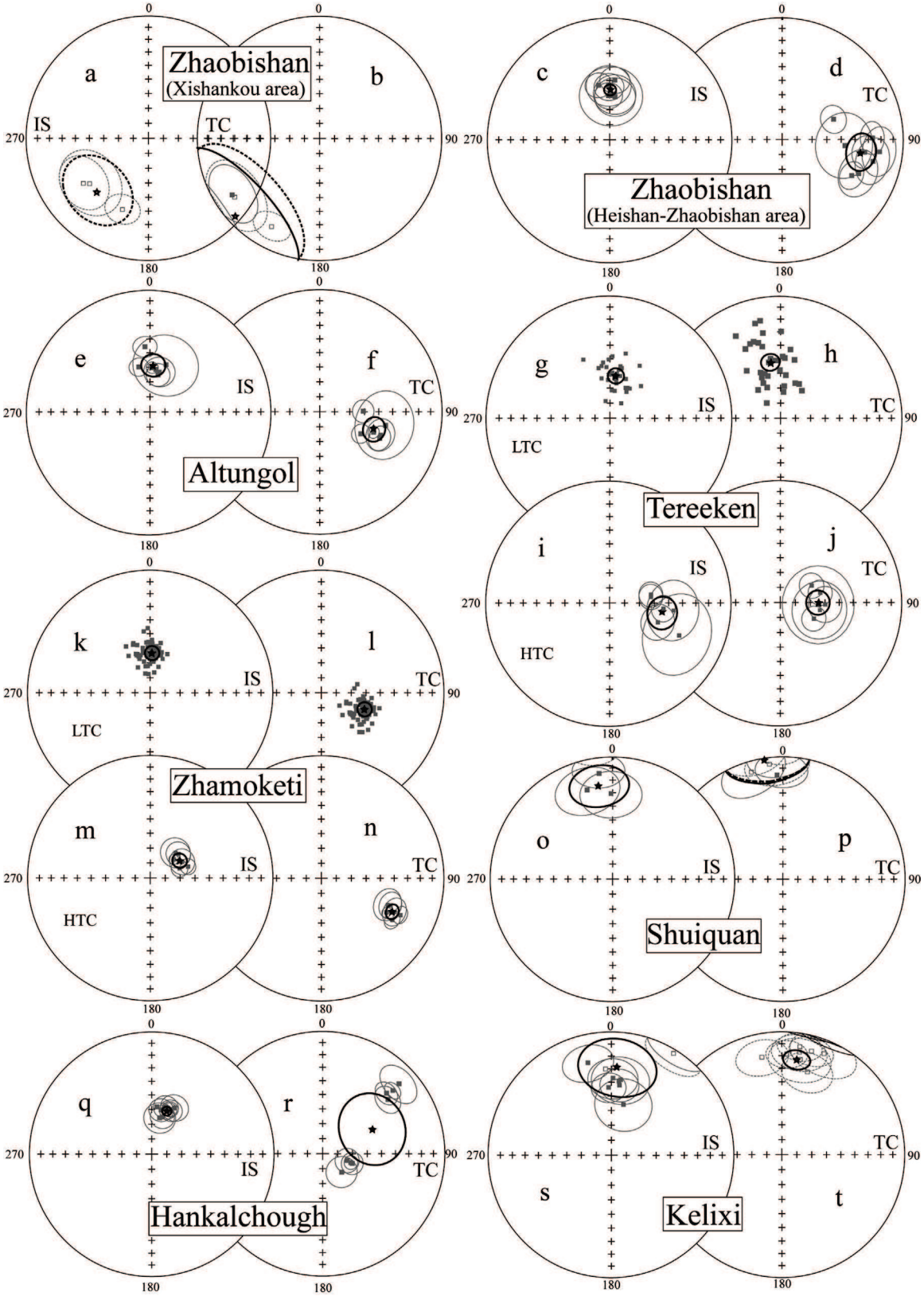

Fig. 5. Equal-area projection of mean-site directions in in situ (IS) and tilt-corrected (TC) coordinates for each formation. Projections are shown in pairs, the left projection is IS coordinates and the right one is in TC coordinates. For the Tereeken and Zhamoketi formations, low temperature components (LTC) are also plotted to distinguish the high temperature components (HTC). Stars show the average of sites, solid squares represent normal polarity while hollow squares represent reversal polarity.

inclinations (Fig. 4f) with one site showing eastward declinations and downward inclinations in in situ coordinates (Table 1). A site-mean direction has been calculated at: $D_g = 352.0^\circ$, $I_g = 22.8^\circ$, $k_g = 55.4$, $\alpha_{95g} = 16.7^\circ$; $D_s = 351.1^\circ$, $I_s = 0.6^\circ$, $k_s = 30.2$, $\alpha_{95s} = 22.8^\circ$ with $n = 3$ (Table 1). Tilt corrected directions are less clustered than in situ directions (Fig. 5o and p), indicating a negative fold test.

4.1.6. Hankalchough Formation

Eight sites of carbonate rocks were collected from the top of the Hankalchough formation (Fig. 2c). IRM measurement shows an abrupt increase with the total saturation at about 200 mT (Fig. 3p), indicating predominant low coercive magnetic minerals in the rock. Thermal magnetic experiment shows a sharp drop of magnetic susceptibility from 560 °C to 600 °C with the obvious Hopkinson effect at about 560 °C and subordinate decrease to 700 °C (Fig. 3q), implying the existence of predominant titanium-poor magnetite and some hematite. The narrow wasp-waisted hysteresis loops (Fig. 3r) also suggest low coercive magnetic minerals as the magnetic remanent carrier. Only one component was isolated after removing the viscous component (Fig. 4g). All samples show a close to the PEF direction in in situ coordinates and a site-mean direction has been calculated at: $D_g = 19.6^\circ$, $I_g = 59.3^\circ$, $k_g = 331.1$, $\alpha_{95g} = 3.0^\circ$; $D_s = 64.2^\circ$, $I_s = 51.8^\circ$, $k_s = 6.6$, $\alpha_{95s} = 23.2^\circ$ with $n = 8$ (Table 1). Tilt corrected directions are much less clustered than in situ directions with a ratio of 0.02 for ks/kg, indicating a negative fold test (Fig. 5q and r).

4.2. Yecheng area

For the red sandstone of the Kelixi formation, both low and high coercive magnetic minerals were identified on the basis of gradually increase of IRM without a total magnetic saturation at 1.5 T (Fig. 3s) and wasp-waisted hysteresis without saturation (Fig. 3u). Thermal magnetic experiment shows three drops of magnetic susceptibility at around 100 °C, 560–580 °C and 680 °C (Fig. 3t), indicating the coexistence of goethite, magnetite and hematite. Single or dual components were isolated after removing the random LTC (Fig. 4h and i). The HTC shows both normal and reversal polarities with antipodal magnetic directions (Fig. 4h and i). A site-mean direction has been calculated at: $D_g = 5.2^\circ$, $I_g = 27.9^\circ$, $k_g = 7.2$, $\alpha_{95g} = 22.2^\circ$; $D_s = 8.4^\circ$, $I_s = -18.4^\circ$, $k_s = 48.5$, $\alpha_{95s} = 8.0^\circ$ with $n = 8$ (Table 1). Tilt corrected directions are more clustered than in situ directions (Fig. 5s and t). Both McElhinny's and Enkin's fold test give positive answers for this formation (McElhinny, 1964; Enkin, 2003) and it also passes the reversal test (McFadden and McElhinny, 1990).

5. Discussion

As the Tarim block experienced several important tectonic events since the Paleozoic, for instance, the continental collision between the Tarim block and the Kunlun block in the Early Paleozoic (Matte et al., 1996), the continental collision/welding of the Tarim block with Yili and Junggar blocks (Wang et al., 2007) in the Late Paleozoic, and the strike-slip related deformation along the margins of the Tarim block due to the India–Asia collision (Chen et al., 1993; J. Chen et al., 2002), before putting these paleomagnetic data for further tectonic interpretations, their reliability and remanence ages should be discussed.

5.1. Reliability of paleomagnetic data

5.1.1. Rock deformation

Although no direct evidence of a penetrative deformation (except tilting and folding of the strata) has been observed in the field in both studied areas, these sampled rocks have experienced polyphased tectonics since the Neoproterozoic. As mentioned above, the AMS measurements have been therefore carried out in order to further assess the effect of deformation. For the samples from the Quruqtagh area, a weak anisotropy has been observed with the anisotropy degree $P_J < 1.08$ (Fig. 6a), indicating that these rocks have probably not experienced pervasive deformation since their deposition. However, it is not the case for the samples from the Yecheng area. The anisotropy degree is much bigger with about 30% samples showing P_J value higher than 1.15 (Fig. 6b), which suggests that these rocks have probably experienced a pervasive deformation since their diagenesis. For further evaluation, the statistical results of the three principal magnetic anisotropic axes have also been calculated for these formations. For the Tereeken and Zhamoketi formations in the Quruqtagh area, well-grouped vertical K_3 (poles of magnetic foliation: $D = 348.9^\circ$, $I = 77.8^\circ$ with $\alpha_{95max/min} = 28.1^\circ/14.9^\circ$ and $D = 283.1^\circ$, $I = 81.3^\circ$ with $\alpha_{95max/min} = 29.2^\circ/16.2^\circ$, respectively) have been obtained (Fig. 6c and d), indicating that the magnetic fabrics were developed during their deposition and the original deposition surface was close to horizontal. While for the Kelixi formation in the Yecheng area, a nearly horizontal K_3 ($D = 290.8^\circ$, $I = 9.5^\circ$ $\alpha_{95max/min} = 32.1^\circ/21.1^\circ$) has been calculated (Fig. 6e), suggesting that the magnetic fabrics should be developed after the sedimentation, and the rocks have been affected by later tectonics as shown by their high anisotropy degree values. Therefore, the paleomagnetic directions from this formation will be excluded from the following discussion.

5.1.2. Origins of magnetic remanence

Among remained 6 formations in the Quruqtagh area, the magnetic direction analysis shows that only one, the Tereeken formation, passes the fold test, indicating that the remanence was acquired before the folding. During the Ordovician to the Middle Silurian, Central Tianshan Ocean subducted beneath the northeastern margin of Tarim (Wang et al., 2008; Charvet et al., 2011), causing the transition from Cambrian–Ordovician intra-craton extensional basin to Silurian–Devonian compressive uplift (Tang, 1997; Cheng et al., 2006), which may therefore be responsible for the absent of Silurian–Devonian sediments in most parts (Fang et al., 2006) and the folding of pre-Silurian strata of the Quruqtagh area. Since magnetite and hematite are the stable magnetic remanence carriers, and the sedimentary magnetic fabric is weak in the analyzed samples, the magnetic direction measured from this formation is likely primary. Moreover, this mean direction is significantly distinct from all those measured for Phanerozoic rocks (Zhu et al., 1998; Fang et al., 2006; Gilder et al., 2008; Huang et al., 2008). The corresponding paleomagnetic pole was therefore calculated at $\lambda = 27.6^\circ$N, $\varphi = 140.4^\circ$E, dp = 8.8°, dm = 11.1° with $N = 6$. No fold test can be applied to the paleomagnetic directions from the Zhamoketi formation because of its monoclinal bedding attitude. Nevertheless, the HTC magnetic directions in tilt corrected coordinates are close to those of the Tereeken formation and Sugetbrak formation in the Aksu area (Zhan et al., 2007), and different from those of all other younger periods (Table 2). These observations argue for a primary origin of the magnetic remanence. Meanwhile, the volcanic rocks at the top of Zhamoketi Formation consist of 80–330 m thick basaltic and andesitic lavas and pyroclastic rocks in numerous layers of decimeter to several decimeters in thickness (Xu et al., 2009). Volcanic rocks and pyroclastic rocks are interbedded. This interbedded relationship indicates that the eruption of these volcanic rocks might last a long period with even several long intervals of eruption, implying that the Geomagnetic Secular Variation (GSV) has been averaged out. Consequently, a paleomagnetic pole for the Zhamoketi Formation was also calculated at: $\lambda = -4.9^\circ$N, $\varphi = 146.7^\circ$E, dp = 3.0°, dm = 5.2° with $N = 6$. All other formations display negative fold tests, indicating that they are of secondary magnetic remanences. The Zhaobishan formation from the Xishankou area displays the same direction of a sole reversal

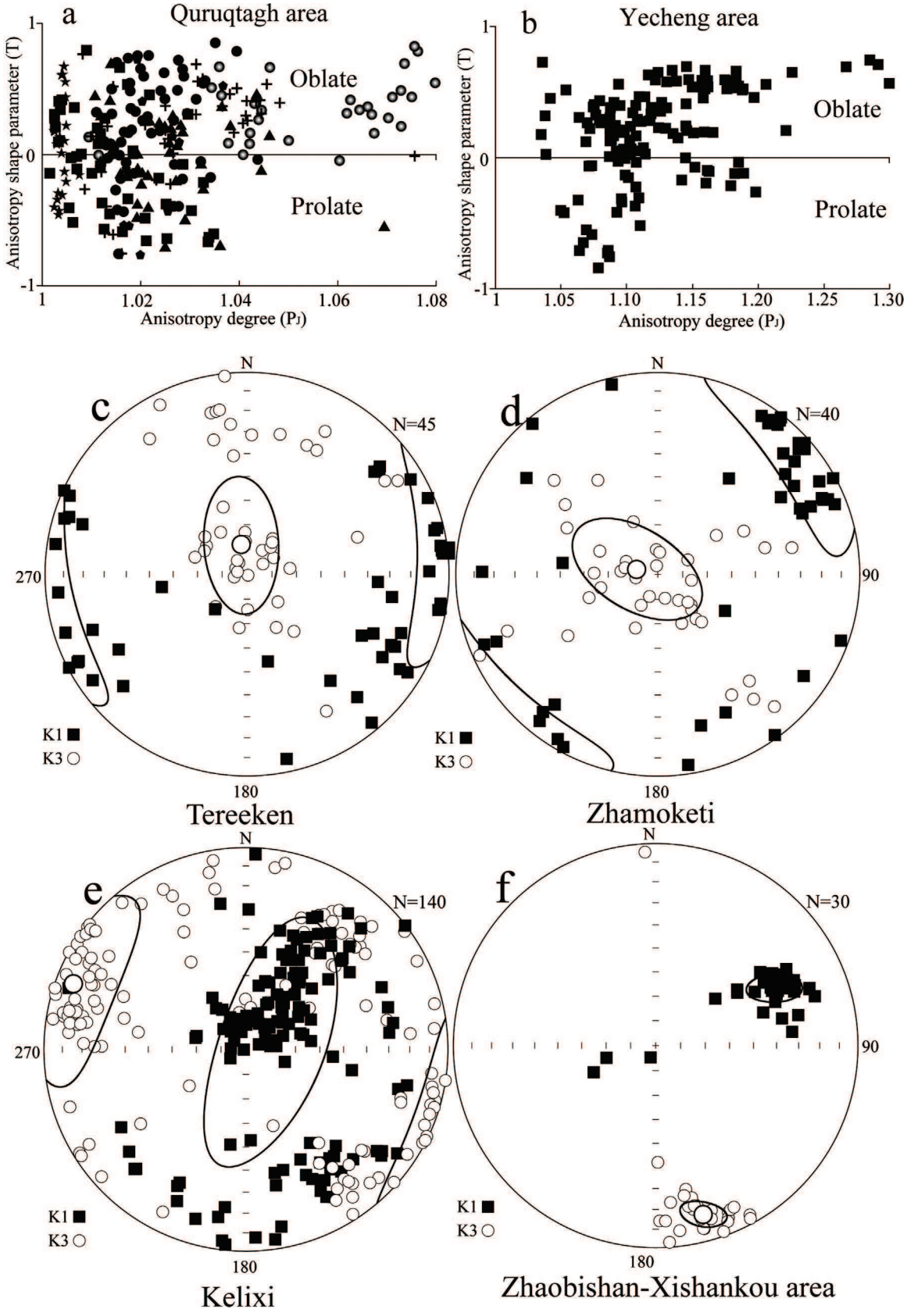

Fig. 6. Results of Anisotropy of Magnetic Susceptibility (AMS) measurements. (a) and (b) Plots of anisotropy degree (P_J) vs shape parameter (T) of magnetic susceptibility for the samples of the Quruqtagh and Yecheng areas, respectively. Legend for Quruqtagh area (a): solid circle, Zhamoketi Fm. from Heishan-Zhamoketi area; hollow circle, Zhamoketi Fm. from Xishankou area; cross, Altungol Fm.; solid square, Tereeken Fm.; solid triangle, Zhamoketi Fm.; solid pentagon, Shuiquan Fm.; solid star, Hancalchough Fm. (c)–(f) Stereoplot of K_1 and K_3 directions of the samples from the Tereeken, Zhamoketi, Kelixi formations, and Zhaobishan formation in Xishankou area. K_1 and K_3 are the magnetic lineation and pole of magnetic foliation; $P_J = \exp\{2[(\ln K_1 - \ln K_m)^2 + (\ln K_2 - \ln K_m)^2 + (\ln K_3 - \ln K_m)^2]^{1/2}\}$, and $T = 2\ln(K_2/K_3)/\ln(K_1/K_3) - 1$).

Table 2
Paleomagnetic poles for the Tarim bock from the Neoproterozoic to the Present.

Age	*N*	Slat (°N)	Slon (°E)	Plat (°N)	Plon (°E)	dp/A95 (°)	dm (°)	Reference	Comment
Neoproterozoic									
*NP2, 775	9S	41.1	80.1	19.0	128.0	6.0	7.0	Chen et al. (2004)	RT
NP2, 740	6S	41.6	86.5	−17.7	14.2	3.0	6.0	Huang et al. (2005)	Remag.
NP2, 730	14S	40.9	79.5	−6.3	17.5	9.1		Wen et al. (2013)	
*NP3, 635	6S	41.5	87.8	27.6	140.4	8.8	11.1	This study	FT
*NP3, 625	24S	41.0	80.0	19.1	149.7	9.3		Zhan et al. (2007)	FT, N + R
NP3, 625	29S	41.0	80.0	55.0	233.0	7.9		Li et al. (1991)	Remag.
*NP3, 615	6S	41.5	87.8	−4.9	146.7	3.0	5.2	This study	
Early Ordovician									
*480	5S	41.3	83.4	−20.4	180.6	8.5	15.0	Fang et al. (1996)	
Late Ordovician									
*450	5S	40.6	78.9	−40.7	183.3	4.8	6.9	Sun and Huang (2009)	FT
Middle Silurian									
S_2	6S	40.5	79.7	12.1	158.4	4.1	7.2	Fang et al. (1996)	
S_2	40S	40.6	79.0	16.5	165.2	2.9	5.3	Li et al. (1990)	
S_2	18S	40.6	79.4	9.9	160.2	4.5	8.4	Fang et al. (1998)	
*Ave., 425	3/3			12.8	159.8	7.3			
Early-middle Devonian									
*400	3S	40.5	79.6	13.5	160.8	4.9		Fang et al. (1996)	
Late Devonian									
*370	47S	40.5	78.6	16.5	165.0	4.3		Li et al. (1990)	FT, RT
Late Carboniferous									
* 310	3L			48.7	175.7	3.0	4.8	Fang et al. (1998)	
Early Permian									
C_3–P_2	15S	37.0	79.0	64.6	166.5	2.5		Gilder et al. (1996)	FT
P_1	5S	40.6	79.5	56.1	179.4	2.5		Fang et al. (1998)	FT
P_1	26S	40.8	79.8	56.5	190.1	4.6		Bai et al. (1987)	
P_1	21S	40.5	78.8	54.5	172.3	4.0		Sharps et al. (1989)	FT
P_1	11S	40.5	78.8	65.1	162.5	4.1		Sharps et al. (1989)	FT
*Ave., 280	5/5			59.7	175.1	7.1			
Late Permian									
P_2	7S	44.0	88.1	75.8	195.0	13.6	18.5	Nie (1991)	FT, RT
P_2	24S	40.8	79.8	62.9	190.7	6.3		Cheng et al. (1983)	
P_2	10S	42.1	83.4	73.2	191.0	7.2	10.3	McFadden et al. (1988)	RT
P_3	21S	40.0	79.0	65.6	181.2	3.9		Li et al. (1988b)	RT
P_3–T_1	16S	42.1	83.3	71.8	187.6	5.5	7.8	McFadden et al. (1988)	FT
*Ave., 255	5/5			69.9	188.5	5.4			
Triassic									
T_1	5S	41.0	74.9	52.8	175.5	6.3	10.1	Fang et al. (1992)	RT
T_2	26S	40.9	81.5	52.5	168.2	4.2	6.1	Fang et al. (1992)	RT
T_3	8S	41.7	80.5	52.1	166.8	5.6	8.1	Fang et al. (1992)	RT
T	6S	41.6	83.5	59.0	160.0	13.0		Li et al. (1990)	FT, RT
T_3	6S	42.1	83.2	69.3	182.9	10.8	15.2	McFadden et al. (1988)	FT
*Ave., 230	5/5			57.3	169.9	8.1			
Middle Jurassic									
J_2	10S	36.0	79.2	52.4	187.9	3.7	6.5	Fang et al. (1992)	RT
J_2	7S	41.8	83.0	49.9	173.0	2.8	4.1	Fang et al. (1992)	FT
J_2	9S	40.2	75.3	54.0	188.3	6.8		Meng et al. (1998)	FT, RT
J_2	6S	42.1	83.2	75.7	198.0	8.1		Gilder et al. (2008)	FT
*170	3/3			52.3	182.8	8.8			
Late Jurassic									
J_3	7S	40.4	75.2	81.0	247.0	5.0	7.6	Li et al. (2003)	FT
J_3	6S	38.6	75.3	4.9	120.6	9.1	12.6	Li et al. (2003)	
J_3	3S	41.8	82.0	63.0	197.0	14.0		Zhang et al. (1989)	
Early Cretaceous									
J_3–K_1	13S	44.2	86.0	72.3	227.3	4.8	7.2	Chen et al. (1991)	FT, RT
J_3–K_1	6S	41.8	82.0	65.0	209.0	9.0		Li et al. (1988b)	RT
K_1	13S	40.2	75.3	64.1	172.1	12.0		Gilder et al. (2003)	FT
K_1	5S	40.2	75.3	53.2	183.4	6.1		Gilder et al. (2003)	FT

Table 2 (*Continued*)

Age	*N*	Slat (°N)	Slon (°E)	Plat (°N)	Plon (°E)	dp/A95 (°)	dm (°)	Reference	Comment
K_1	7S	39.5	75.0	66.3	226.6	9.0	15.9	Chen et al. (1992)	RT
K_1	3S	38.5	76.4	70.4	212.1	6.6	10.8	Chen et al. (1992)	RT
K_1	8S	36.3	78.8	72.3	206.6	9.8	15.9	Zhu et al. (1998)	FT, RT
K_1	21S	39.5	75.0	70.1	225.8	7.0		Tan et al. (2003)	FT, RT
*Ave., 120	8/8			68.0	205.1	7.2			
Late Cretaceous									
K_2	7S	41.6	83.5	66.3	222.9	8.7	8.7	Li et al. (1988a)	FT
K_2	10S	42.0	82.9	64.0	229.0	7.3	12.7	Zhu et al. (1998)	RT
K_2	11S	39.5	75.0	70.8	222.6	5.4	8.9	Chen et al. (1992)	FT
K_2	6S	38.5	76.4	71.0	234.0	6.8	11.6	Chen et al. (1992)	RT
K_2–E	9S	44.2	86.0	74.3	223.1	6.4	9.4	Chen et al. (1991)	FT, RT
*Ave., 80	5/5			69.3	226.4	4.2			
Paleogene									
E_1	4S	41.6	83.5	73.0	245.4	6.0	9.7	Fang et al. (1998)	
E_1	5S	37.0	79.0	58.1	202.0	12.7		Gilder et al. (1996)	FT
E-N	7S	38.1	86.6	75.8	229.5	9.6		Y. Chen et al. (2002)	FT
E_3	6S	39.2	94.3	63.9	219.7	9.8		Y. Chen et al. (2002)	FT
E_3–N_1	9S	38.5	76.4	71.2	226.7	6.7		Chen et al. (1991)	FT
*Ave., 50	5/5			69.1	221.2	8.9			
Neogene									
16.5–5.7	44S	42.0	83.3	75.5	285.1	2.2		Huang et al. (2006)	RT
*10, (12.6–5.2)	406s	41.9	83.3	72.5	284.5	1.4	2.2	Charreau et al. (2006)	RT
Quaternary									
*2, (3.3–1.1)	258s	39.8	76.2	73.9	297.5	1.9		J. Chen et al. (2002)	RT

Abbreviations: S, the number of the sites; N, number of localities (L), sites (S) or samples (s) used to determine pole; Slong/Slat, longitude and latitude of sampling site; Plat/Plong, latitude and longitude of paleomagnetic pole; dp/dm, oval of 95% confidence for the paleomagnetic pole; A95, radius that mean direction lies within 95% confidence; N + R, normal and reversal polarities; FT, fold test; RT, reversal test.
Poles with * were used to build the Apparent Polar Wonder Path of Tarim. No mean pole was calculated for Late Jurassic because the three published Late Jurassic poles are not consistent.

polarity with that of the Late Carboniferous–Early Permian formations indicating a remagnetization corresponding to the Late Carboniferous–Early Permian magmatic event developed in the northern margin of the Tarim block and southern Tianshan (Gao et al., 2009; Chen et al., 2011). The basalt samples from the Shuiquan formation display a direction different from any of the younger periods (Table 2), which may be ascribed to local fault movements (see Fig. 2a). Another reason for this abnormal direction may the short cooling time of basalt so that the secular variation has not been averaged out from the magnetic remanence from these rocks. All other formations display the recent geomagnetic directions (Fig. 5).

5.2. The age of primary magnetic remanences

The age constraints of glacier deposits in the Tarim block are obtained from zircon U–Pb dating of interlayered volcanic rocks (Xu et al., 2005, 2009) and chemostratigraphic correlations (Xiao et al., 2004; He et al., 2007). In the Quruqtagh area, two zircon SHRIMP U–Pb ages of 740 ± 7 Ma and 725 ± 10 Ma have been obtained in volcanic beds from the bottom and top of the Baiyisi Formation (Xu et al., 2009; Fig. 7), which constrain the Sturtian age for the Baiyisi glaciation, although the glacial origin of diamictites in the Baiyisi formation is still ambiguous (Xiao et al., 2004). The zircon U–Pb dating obtained from the top of the Zhamoketi formation (the same layer where we collected the paleomagnetic samples) yields a post-Marinoan age at 615 ± 6 Ma (Xu et al., 2009; Fig. 7), which constrains the age of our paleomagnetic pole of the Zhamoketi formation. The chemostratigraphic investigation of the Tereeken cap dolostone shows the same $\delta^{13}C$ pattern as that of Marinoan cap carbonates (Xiao et al., 2004). Meanwhile, the characteristic macropeloids of Tereeken cap dolostone are similar to those found in the Marinoan-age Raventhroat cap carbonate (Xiao et al., 2004). Both of these two similarities constrain the Marinoan age of the Tereeken glaciation. Based on the dating of the Marinoan glaciation in the South China block from the Doushantuo cap carbonate (Condon et al., 2005), the termination age of this glaciation should be at 635.2 ± 0.6 Ma. Therefore the age of our paleomagnetic pole obtained from the Tereeken formation should be at ca. 635 Ma.

5.3. Apparent Polar Wander Path (APWP) of the Tarim block

The paleomagnetic studies of the Tarim block began in 1980s (e.g. Bai et al., 1987; Li et al., 1990) and several syntheses have been tentatively established for the Phanerozoic with small paleomagnetic dataset (Nie, 1991;Enkin et al., 1991; Fang et al., 1998; Zhu et al., 1998). Since this century, new paleomagnetic poles have been reported (Gilder et al., 2003, 2008; Chen et al., 2004; Huang et al., 2005; Charreau et al., 2006; Zhan et al., 2007; Wen et al., 2013), two APWPs of Tarim have been built up, however, both of them concentrate on the only Paleozoic period (Fang et al., 2006; Huang et al., 2008). Newly obtained Neoproterozoic results provide a good opportunity to extend the APWP for the Tarim block from the Neoproterozoic to Present by integrating the paleomagnetic poles published after 2008 and to discuss its kinematic history, especially in connection with Australia since the break-up of the Rodinia supercontinent. Before using the available Neoproterozoic poles into the APWP establishment, some assessments should be made on the age and reliability of the published data.

In the Aksu area, four Neoproterozoic poles have been reported (Fig. 7): one from Aksu dykes (Chen et al., 2004), one from the Qiaoenbrak Formation (Wen et al., 2013) and other two from the Sugetbrak Formation (Li et al., 1991; Zhan et al., 2007). The first zircon SHRIMP U–Pb age of Aksu dykes has been obtained at

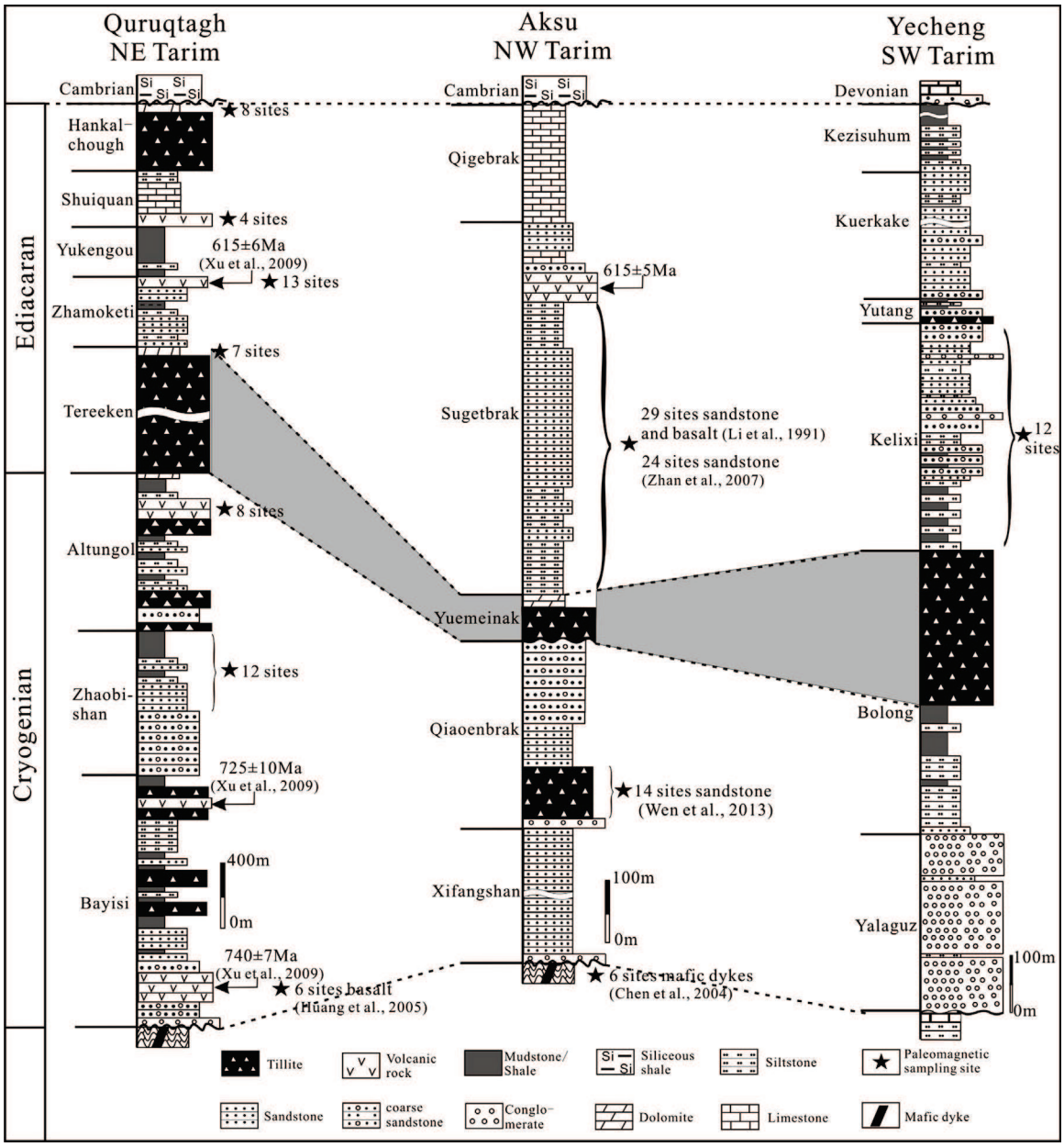

Fig. 7. Stratigraphic correlation of the Cryogenian and Ediacaran successions of the Quruqtagh, Aksu and Yecheng areas in the Tarim block according to the zircon U–Pb dating of volcanic layers and chemostratigraphic comparisons (Xu et al., 2009, 2013a; Xiao et al., 2004; He et al., 2007; Tong et al., 2013; Zhu and Wang, 2011). The age assignment is based on the geological time scale of Gradstein et al. (2004). The stars show paleomagnetical sampling position in the Neoproterozoic strata by this and previous studies.

807 ± 12 Ma (Chen et al., 2004). By newly obtained geochronological dating, Zhan et al. (2007) reassessed this age and considered that the age of this pole from the Aksu dykes should be at ca. 785 Ma. Zhang et al. (2009) gave a new zircon SHRIMP U–Pb age of 759 ± 7 Ma for Aksu dykes. Consequently, the intrusion of the Aksu dykes might last for a long period from ca. 807 Ma to ca. 760 Ma. Recently, new $^{40}Ar/^{39}Ar$ ages on phengite from the metapelites of the Aksu blueschist were obtained at 748–757 Ma (Yong et al., 2012). As the Aksu dykes crosscut the blueschists, they should be younger than 748 Ma. However, the reported mafic dykes, gneissic granite and granodiorite along the margin of the Tarim block are from 824 Ma to 752 Ma (Zhang et al., 2012b), and are unconformably overlain by ca. 740 Ma Baiyisi Formation in the Quruqtagh area (Shu et al., 2011). Besides, the $^{40}Ar–^{39}Ar$ isotopic system is easily to be disturbed by later thermal event with the relatively low closure temperature at ~350–400 °C (Lee, 1991; Maluski et al., 1993). The $^{40}Ar/^{39}Ar$ ages of blueschists may be related to the later thermal input due to intrusions and slow cooling. So, the SHRIMP zircon U–Pb ages may be the most reliable ones. In the following, we use an average U–Pb age of 785 Ma for the pole of Aksu dykes. For the ~730 Ma pole from the Qiaoenbrak Formation (Wen et al., 2013), the AMS study of this collection displays uncommon sedimentary fabrics: nearly vertical fabrics for both lineation and foliation before bedding corrections, and nearly vertical magnetic foliations with relatively well grouped and ~30° southwestward inclined magnetic lineation after bedding corrections. Meanwhile, the directions of magnetic lineation is highly consistent with the magnetic remanent directions, suggesting that the magnetic remanent orientation may be principally controlled by the tectonic deformation process or/and glacier deposition one, as the authors proposed, instead of the geomagnetic field. Accordingly, we deduce that this pole cannot be used to present the true

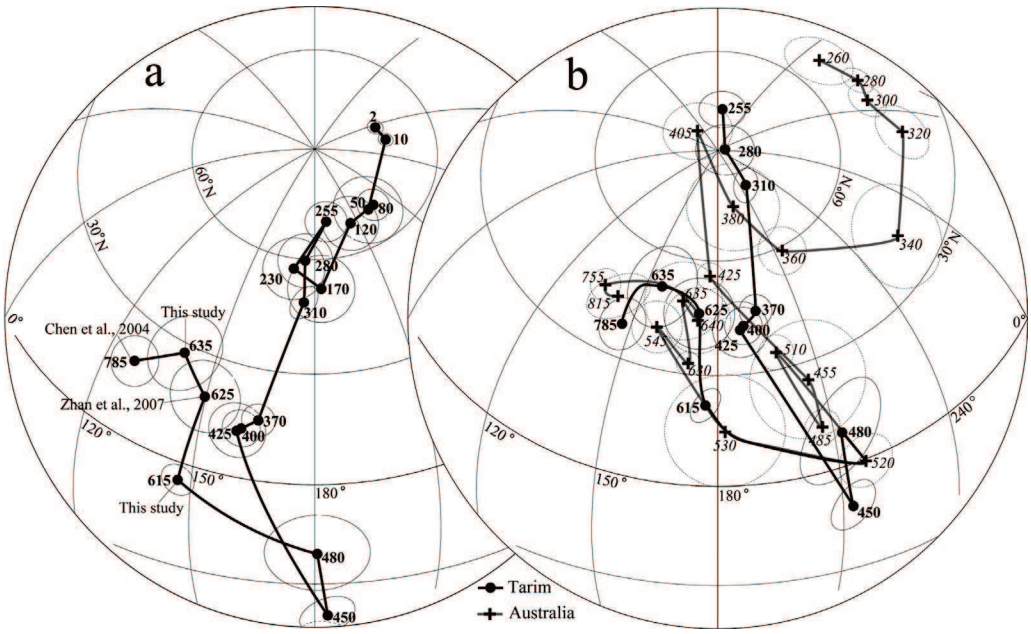

Fig. 8. (a) Apparent Polar Wander Path (APWP) of the Tarim block from the Neoproterozoic to Present. The poles used to build this APWP are listed in Table 2. (b) Comparison of APWPs of Tarim and Australia (East Gondwana). Australian APWP (cross and dotted circle) is plotted in Australian coordinates with Neoproterozoic poles from Sohl et al. (1999), Wingate and Giddings (2000a,b), Schmidt et al. (2009) and Li and Evans (2011) and Paleozoic poles from McElhinny et al. (2003). The APWP of Tarim was rotated to the Australian coordinates around an Euler pole at 45.9°S, 277.6°E with an angle of −43.4°.

paleomagnetic field for the period of ~730 Ma and is excluded from our APWP establishment. Two remained paleomagnetic poles obtained from the same stratigraphic part of the Sugetbrak Formation are significantly different (Li et al., 1991; Zhan et al., 2007;Table 2). In fact, the one from Li et al. (1990) is statistically indistinguishable from the Cretaceous poles of Tarim and could represent a Cretaceous overprint. Therefore, we use the pole from Zhan et al. (2007) for this formation. A new zircon U–Pb age at 615 ± 6 Ma (Xu et al., 2013a) has been recently obtained from the basaltic flow interlayered in the upper Sugetbrak formation, which may constrain the age estimation for this pole. Another approach to estimate this age concerns the correlation of the $\delta^{13}C$ chemostratigtaphic variation between the Sugetbrak formation and the Doushantuo formation in the South China block. These two formations show a similar variation pattern (He et al., 2007; Zhan et al., 2007). The Doushantuo cap carbonate has been dated by numerous studies and gives a zircon U–Pb age of 635.2 ± 0.6 Ma (e.g. Condon et al., 2005). This age constrains the lower limit of the Sugetbrak formation. Therefore, the age of the pole (Zhan et al., 2007) may extend from 635 Ma to 615 Ma. In the following discussion, we use 625 Ma, the average age of the sampling strata, as the age of the pole of Zhan et al. (2007).

Concerning the paleomagnetic pole from the green colored basalts of the Baiyisi formation in the Xishankou area of Quruqtagh (Huang et al., 2005), neither fold test due to its uniform bedding nor reversal polarity has been obtained. These basalts are, in fact, metamorphosed as the chlorite can be widely observed in these rocks. Moreover, the magnetic directions isolated from these basalts are similar to those of the overlying Zhaobishan formation by this study (Table 1), which failed the fold test and are thought to be secondary (see Section 4.1.1 above). Furthermore, the AMS measurements have been made on the paleomagnetic samples from the overlying Zhaobishan Formation. The AMS results display a nearly horizontal K_3 (D = 164.3°, I = 14.2°, $\alpha_{95max/min}$ = 9.1°/5.2°; Fig. 6f), suggesting that the magnetic fabrics must be developed after the sedimentation and the rocks have been affected by later deformation. So, it is reasonable to consider that both the Baiyisi Formation (Huang et al., 2005) and its overlaying Zhaobishan formation (Table 1) in the Xishankou area have been remagnetized and cannot be used for the Neoproterozoic period.

Concerning the Phanerozoic poles used to establish the APWP of the Tarim block, we refer to the recent synthetic publications by Fang et al. (2006), Huang et al. (2008) and Gilder et al. (2008), with also poles published after 2008. An age-mean pole has been calculated when several poles are available for one geological period (Table 2). Combining our two paleomagnetic poles with the previously published ones, the APWP of the Tarim block was buildup using the paleomagnetic poles listed in Table 2. Most of these poles satisfy at least one of the following two characters: positive fold test, both normal and reverse polarities. The paleomagnetic poles and their uncertainties are shown by black dots and their confidence ellipse, respectively, and the probable APWP is shown by the dark line in Fig. 8a.

5.4. Kinematic history of the Tarim block: a long term Australia–Tarim connection

According to this new APWP, we may characterize the kinematic history of the Tarim block as following. At ~800 Ma, Tarim was located at about 45°N with a perpendicular orientation with respect to its present shape. From the Late Neoproterozoic (Ediacarian) to Ordovician, the Tarim block moved southwards with variable velocities until ca. 18°S. Since Ordovician, the Tarim block changed its motion direction to the north, reaching the latitude of ca. 15°N in Early Silurian (Sun and Huang, 2009). From this time to the Late Devonian, the paleomagnetic poles show a good consistency, implying that the Tarim block was stationary during this period. From the Late Devonian to the Late Carboniferous, a significant northward drift of Tarim is identified with also a clockwise rotation of the block. Since the Late Carboniferous, the poles of Tarim become stationary indicating that this block did not experience a significant movement since then (Fang et al., 2006; Gilder et al., 2008; Huang et al., 2008). Of course, cautions should be taken for this simplified kinematic story as the paleomagnetic poles are not determined for equal time intervals.

The Paleozoic paleomagnetic data from Australia have been summarized by McEhlinny et al. (2003). After a thorough assessment of Paleozoic paleomagnetic results from different localities of Australia, a coherent path with respect to that of the Gondwana supercontinent has been documented, and the corresponding Paleozoic APWP has also been established in the Northwest Africa coordinates (McEhlinny et al., 2003). For the convenience of comparison, the Australian APWP in the Northwest Africa coordinates is restored to its own ones around an Euler pole at 28.1°S, 293.2°E with angle of −52.1° (McEhlinny et al., 2003). The Neoproterozoic and Paleozoic APWP for Australia may join the key Neoproterozoic poles of 755 ± 3 Ma derived from the Mundine Well dyke swarm (MDS) of the Pilbara Craton, Western Australia (Wingate and Giddings, 2000a,b), the Yaltipena Formation (ca. 640 Ma) of the central Flinders Range of South Australia (Sohl et al., 1999; Li and Evans, 2011), the mean Elatina formations (ca. 635 Ma) of the central Flinders Range of South Australia (Li and Evans, 2011) and the Nuccaleena Formation (ca. 630 Ma) of the Adelaide Geosyncline of South Australia (Schmidt et al., 2009; Li and Evans, 2011).

For a better comparison, Tarim was rotated into the Australian coordinates using an Euler pole at 45.9°S, 277.6°E with an angle of −43.4°. After this rotation, these two APWPs fit well with each other from ~750 Ma to ~480 Ma (Fig. 8b), which indicates the connection between Tarim and Australia during this time interval. However, the ~640 Ma to ~615 Ma poles of the two APWPs do not perfectly overlap. This discrepancy may be due to the poorly constrained ages of these poles, as no direct isotopic age has been obtained for the three Australian poles, and their ages were estimated by tillite comparison and stratigraphic contact (Sohl et al., 1999; Schmidt et al., 2009; Li and Evans, 2011). Nevertheless, considering the large A_{95} of these poles, they are statistically indistinguishable (Fig. 8b). The Early Ordovician (480 Ma) pole of Tarim overlaps well with that of Australia (Fig. 8), while both the Late Ordovician (450 Ma) and the Middle Silurian (425 Ma) poles are distinguished, which may indicate that these two blocks began to separate with each other during the Late Ordovician to Silurian (Fig. 8). However, the rapid break away of Tarim from Australia may occur after the Middle Silurian, as the poles begin to significantly separate and lay far away from each other since the Middle Silurian (Fig. 8).

Several reconstructions of Tarim and Australia during the Neoproterozoic have been attempted (Powell and Pisarevsky, 2002; Chen et al., 2004; Zhan et al., 2007; Li et al., 2008). Although the debate still exists about whether these two continents connected directly (Chen et al., 2004; Zhan et al., 2007) or Tarim was located at the margin of an Australia-centered continent (Powell and Pisarevsky, 2002; Li et al., 2008), both of these reconstructions placed Tarim to the northwest of Australia, and considered that Tarim and Australia displayed the same evolutional pattern from the breakup of the Rodinia supercontinent to the amalgamation of the Gondwana supercontinent (Fig. 9). The penetrative 800–750 Ma mafic dykes, identified from both northern Tarim (Chen et al., 2004; Zhang et al., 2007) and northwestern Australia (Wingate and Giddings, 2000a,b), suggest the connection between Tarim and Australia at least since ca. 800 Ma. The tectonostratigraphic analysis from both blocks also suggests that the Tarim block was adjacent to the Kimberley region, northwestern Australia in the Neoproterozoic (Li et al., 1996). New sedimentary analysis carried out from the Sugetbrak and Qigebrak formations in the Aksu area, northwestern Tarim, suggests that the nonmarine, fluvial and lacustrine facies of the Sugetbrak formation can correlate with the upper part of the Louisa Downs and Albert Edward groups in northwestern Australia, indicating the connection between these two blocks in the Late Neoproterozoic (Turner, 2010). New researches about the basement of Tarim reveal that the unified Tarim block in the Neoproterozoic should be much larger than the present Tarim basin, as hundreds of kilometers of continental margin has subducted due

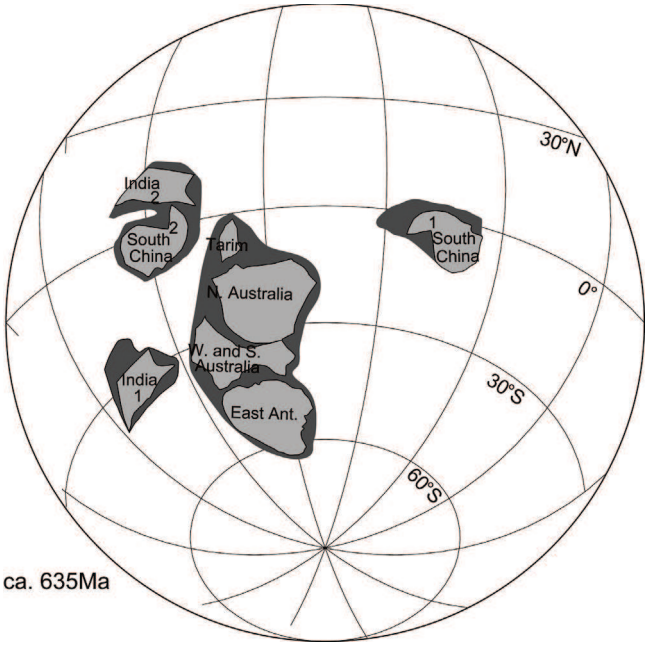

Fig. 9. Paleogeographic reconstruction of the major part of Rodinia at ca. 635 Ma in Australian coordinate, showing the relative position of Australia, East Antarctica, Tarim, South China and India (modified from Li and Evans, 2011; Zhang et al., 2013). This reconstruction is made by rotating the Neoproterozoic to Early Paleozoic poles (crosses with 95% confidence levels) of Tarim, which coincide with those of Australia, 43.4° CCW around an Euler pole at 277.6°E and 45.9°S. Australia is at its present location. Positions 1 and 2 of South China and India represent the possible locations of these two blocks in Australian coordinate during the breakup of Rodiania.

to posterior continental convergence (Xu et al., 2013b). In our paleogeographic reconstruction map, the same rotation transfers the Tarim to the northwest of Australia, in broad agreement with previous reconstruction (Fig. 9; Chen et al., 2004; Zhan et al., 2007; Li and Evans, 2011; Zhang et al., 2013), and during the break-up of Rodinia supercontinent, Tarim still stay close to Australia.

The timing of the separation between Tarim and Australia is still in debate, with different ages from the latest Neoproterozoic (Li et al., 1996) to the Middle Paleozoic (e.g. Metcalfe, 2006, 2009, 2011). The upper Neoproterozoic succession in the Kimberley region, northwestern Australia, is unconformably overlain by the Cambrian Antrim Plateau mafic volcanics (Hanley and Wingate, 2000; Glass and Phillips, 2006), which were thought to represent the extensional event corresponding to the separation of Tarim from Australia (Li et al., 1996). For the Tarim part, Early Cambrian volcanic rocks were also found in the Quruqtagh area, northeast of the Tarim block (Jia et al., 2004). Meanwhile, trace element study of the phosphorite shale at the base of the Lower Cambrian in the northwestern Tarim block indicates the mafic material sources (Yu et al., 2003). Furthermore, the Cambrian strata of the Tarim block consist of phosphates and evaporites at similar stratigraphic levels to those of Australia (Metcalfe, 2006, 2009); and the same microfossil assemblages have been found from the Ordovician and Silurian successions of both the Tarim and Australia blocks (Burrett et al., 1990; Metcalfe, 2011). The deposition facies and fossil similarities from the Cambrian to Silurian indicate the connection of these two blocks in this period (Metcalfe, 2006, 2011). The separation was proposed to take place in the Early Devonian as the splitting of the Silurian Sino-Australian brachiopod province into two sub-provinces and the apparent loss of links between Tarim and Australia (Metcalfe, 2006). These paleontological observations coincide with our APWP comparison: the proximity of the Ordovician and Silurian poles, while far away from each other of the Devonian poles from two blocks (Fig. 8b). After the Silurian,

Australia moved southwards to the southern hemisphere (Schmidt et al., 1987; Thrupp et al., 1991), whereas the Tarim block stayed at the low latitude position in the northern hemisphere and drifted northwards from the Devonian to Carboniferous (Li et al., 1990; Zhao et al., 1993). Taking the paleomagnetic, sedimentary and paleontology evidences into account, the hypothesis of an initial break-up at the Late Ordovician and a fast separation at the Late Silurian–Early Devonian between Tarim and Australia seems the most documented.

Although no consensus about the relative position between the South China block (SCB) and Australia so far (Li et al., 2008; Li and Evans, 2011; Zhang et al., 2013), the similarity in APWPs between Australia and the SCB has been described by Yang et al. (2004) based only on three poles, showing that the South China block was connected to the northwestern Australia during the Neoproterozoic until the Late Silurian–Early Devonian. The biostratigraphic study revealed that the upper *T. anozos–T. conoideum* assemblage of the Ediacaran Doushantuo formation in the Yangtze Gorge area can be correlated with the Ediacaran complex acritarch palynoflora (ECAP) of South and Central Australia (Liu et al., 2013). Besides, the lower Paleozoic strata of the South China block display the same depositional pattern (Metcalfe, 2006) and fossil assemblages (Burrett et al., 1990; Yao et al., 2005; Moczydlowska and Zang, 2006; Dong et al., 2009; Metcalfe, 2013) as those of Tarim and Australia. Instead of putting SCB to the northwestern Australia, Li et al. (2008) and Li and Evans (2011) putted the SCB to the northeastern Australia to fit the "missing link model" at 750 Ma and considered that the SCB had moved northeast away from Australia at ca. 635 Ma (Position 1 of SCB in Fig. 9; see also Fig. 2c in Li and Evans, 2011). Moreover, Zhang et al. (2013) had recently published their new paleomagnetic results from the Nantuo formation of SCB (636.3 ± 4.9 Ma) and show a relatively high paleolatitude of SCB. Combining geologic and paleomagnetic data, they concluded that nevertheless the SCB was closely situated to the north of Australia, and the direct SCB-northwestern Australia connection at the Early Cambrian–Early Devonian, had not formed at the time of ca. 635 Ma (Position 2 of SCB in Fig. 9; see also Fig. 10 in Zhang et al., 2013). Consequently, the kinematic history between SCB and Australia is still controversial; more results are needed to improve the understanding.

6. Conclusions

New paleomagnetic study is performed on the Neoproterozoic strata from the Quruqtagh and Yecheng areas in the northeastern and southwestern Tarim block, respectively. Magnetic mineralogical analyses show that titanium-poor magnetite and hematite are the principal magnetic carriers. The directional analyses reveal both primary and secondary magnetizations. Among the 64 studied sites, except the viscous and dispersed sites due to the too weak NRM (10 sites), 16 sites near the active tectonic zone present a high anisotropic degree, vertical magnetic foliation with no tectonically interpretable magnetic directions; 26 sites show the effect of remagnetization. However, 6 sites from the ca. 635 Ma Tereeken Formation cap carbonate, and 6 sites from the 615 Ma Zhamoketi basaltic andesite from the Quruqtagh area present stable and probably primary magnetic remanences with a weak anisotropic degree, and either a positive fold test for the former or a consistent direction with previous results for the latter. Therefore, two Neoproterozoic paleomagnetic poles were calculated at: $\lambda = 27.6^\circ$N, $\varphi = 140.4^\circ$E, dp = 8.8°, dm = 11.1°, and $\lambda = -4.9^\circ$N, $\varphi = 146.7^\circ$E, dp = 3.0°, dm = 5.2° for the Tereeken and Zhamoketi formations, respectively. Combining these two poles with the paleomagnetic poles previously reported from Tarim, a new APWP from the Neoproterozoic to the Present has been built for the Tarim block. The comparison between the APWPs from Tarim and Australia implicates that there is a long-term, from at least the Neoproterozoic to the Middle Silurian, Australia–Tarim connection and/or they share the same kinematic evolution. The Tarim block probably began to break away from northwestern Australia since the Late Ordovician and the final separation occurred at the Late Silurian–Early Devonian.

Acknowledgements

This study was supported by grants from the National Natural Science Foundation of China (Nos. 40972126 and 41121062). We appreciate the detailed and constructive comments on the first version of manuscript by two anonymous reviewers. We also present our thanks to Jinyou He, Wei Wei and Qinlong Tong for their field assistance.

References

Bai, Y.H., Chen, G.L., Sun, Q.G., Sun, Y.H., Li, Y.A., Dong, Y.J., Sun, D.J., 1987. Late Paleozoic polar wander path for the Tarim platform and its tectonic significance. Tectonophysics 139, 145–153.

Brookfield, M.E., 1994. Problems in applying preservation facies and sequence models to the Sinian (Neoproterozoic) glacial sequences in Australia and Asia. Precam. Res. 70, 143–147.

Burrett, C., Long, J., Stait, B., 1990. Early–middle Palaeozoic biogeography of Asian terranes derived from Gondwana. Geol. Soc. Lond. Memoirs 12, 163–174.

Charreau, J., Gilder, S., Chen, Y., Dominguez, S., Avouac, J.P., Sen, S., Jolivet, M., Li, Y.A., Wang, W.M., 2006. Magnetostratigraphy of the Yaha section, Tarim Basin (China): 11 Ma acceleration in erosion and uplift of the Tianshan Mountains. Geology 34, 181–184.

Charvet, J., Shu, L.S., Laurent-Charvet, S., Wang, B., Faure, M., Cluzel, D., Chen, Y., De Jong, K., 2011. Palaeozoic tectonic evolution of the Tianshan belt, NW China. Sci. China Earth Sci. 56 (2), 166–184.

Chen, J., Burbank, D.W., Scharer, K.M., Sobel, E., Yin, J.H., Rubin, C., Zhao, R.B., 2002. Magnetochronology of the Upper Cenozoic strata in the Southwestern Chinese Tian Shan: rates of Pleistocene folding and thrusting. Earth Planet. Sci. Lett. 195, 113–130.

Chen, X., Shu, L., Santosh, M., 2011. Late Paleozoic post-collisional magmatism in the Eastern Tianshan Belt, Northwest China: new insights from geochemistry, geochronology and petrology of bimodal volcanic rocks. Lithos 127, 581–598.

Chen, Y., Cogné, J.P., Courtillot, V., 1992. New paleomagnetic poles from the Tarim Basin, Northwestern China. Earth Planet. Sci. Lett. 114, 17–38.

Chen, Y., Cogné, J.P., Courtillot, V., Avouac, J.Ph., Tapponnier, P., Buffetaut, E., Wang, G., Bai, M., You, H., Li, M., Wei, C., 1991. Paleomagneitc study of Mesozoic continental sediments along the northern Tien Shan (China) and heterogeneous strain in central Asia. J. Geophys. Res. 96, 4065–4082.

Chen, Y., Courtillot, V., Cogné, J.P., Besse, J., Yang, Z., Enkin, R., 1993. The configuration of Asia prior to the collision of India Cretaceous paleomagnetic constraints. J. Geophys. Res. 98, 21937–21941.

Chen, Y., Xu, B., Zhan, S., Li, Y.A., 2004. First mid-Neoproterozoic paleomagnetic results from the Tarim Basin (NW China) and their geodynamic implications. Precam. Res. 133, 271–281.

Chen, Y., Gilder, S., Halim, N.M., Cogné, J.P., Courtillot, V., 2002. New paleomagnetic constraints on central Asian kinematics: displacement along the Altyn Tagh fault and rotation of the Qaidam Basin. Tectonics 21 (5), 1042, http://dx.doi.org/10.1029/2001TC901030.

Cheng, G.L., Bai, Y.H., Li, Y.A., 1983. Paleomagnetism of the Lower Permian in the Wushi-Aksu area of Xinjiang. Seimol. Geol. 4, 12.

Cheng, R., Wang, P., Sun, X., Bai, Y., 2006. Sequence stratigraphy and sea level changes of Ordovician in Kuruktag, Xinjiang. Geotectonica et Metallogenia 30 (3), 283–293 (in Chinese with English abstract).

Cogné, J.P., 2003. A MacintoshTM application for treating paleomagnetic data and making plate reconstructions. Geochem. Geophys. Geosyst. 4 (1.), http://dx.doi.org/10.1029/2001GC000227.

Condon, D., Zhu, M.Y., Bowring, S., Wang, W., Yang, A.H., Jin, Y.G., 2005. U–Pb ages from the Neoproterozoic Doushantuo formation, China. Science 308, 95–98.

Dong, L., Xiao, S., Shen, B., Zhou, C., Li, G., Yao, J., 2009. Basal Cambrian microfossils from the Yangtze Gorges area (South China) and the Aksu area (Tarim Block, northwestern China). J. Paleont. 83 (1), 30–44.

Enkin, R.J., 2003. The direction–correction tilt test: an all-purpose tilt/fold test for paleomagnetic studies. Earth Planet. Sci. Lett. 212, 151–166.

Enkin, R.J., Chen, Y., Courtillot, V., Besse, J., Xing, L., Zhang, Z., Zhuang, Z., Zhang, J., 1991. A Cretaceous pole from South China, and the Mesozoic hairpin turn of the Eurasian APWP. J. Geophys. Res. 96, 4007–4027.

Fang, D.J., Jin, G.H., Jiang, L.P., Wang, P.Y., Wang, Z.L., 1996. Paleozoic paleomagnetic results and the tectonic significance of Tarim palte. Acta Geophys. Sin. 39 (4), 522–532 (in Chinese with English abstract).

Fang, D.J., Wang, P.Y., Shen, Z.Y., Tan, X.D., 1998. Paleomagnetic results and Phanerozoic apparent polar wandering path of Tarim block. Sci. China Ser. D 41 (Suppl.), 105–112.

Fang, D.J., Shen, Z.Y., Tan, X.D., Chen, H.L., 2006. Paleomagnetism of Tarim Basin and the Plate Motion. Zhejiang University Press, Hangzhou, pp. 1–364 (in Chinese with English abstract).
Fisher, R., 1953. Dispersion on a sphere. Proc. R. Soc. London Ser. A 217, 295–305.
Gao, J., Long, L., Klemd, R., Qian, Q., Liu, D., Xiong, X., Su, W., Liu, W., Wang, Y., Yang, F., 2009. Tectonic evolution of the South Tianshan orogen and adjacent regions, NW China: geochemical and age constraints of granitoid rocks. Int. J. Earth Sci. 98, 1221–1238.
Gao, J.Z., Chen, J.B., Lu, S.N., Peng, C.W., Qin, Z.Y., 1993. The Precambrian Geology in Northern Xinjiang. Precambrian Geology No. 6. Geological Publishing House, Beijing, pp. 1–171 (in Chinese).
Gao, Z., Qian, J., 1985. Sinian glacial deposits in Xinjiang, Northwest China. Precam. Res. 29, 143–147.
Gao, Z.J., Wang, W.Y., Peng, C.W., Li, Y.A., Xiao, B., 1985. The Sinian System of Xinjiang. Xinjiang People's Publishing House, Urumqi, pp. 35–93 (in Chinese with English abstract).
Gilder, S.A., Zhao, X., Coe, R.S., Meng, Z.F., Courtillot, V., Besse, J., 1996. Paleomagnetism and tectonics of the southern Tarim Basin, northwestern China. J. Geophys. Res. 126, 303–313.
Gilder, S., Chen, Y., Cogné, J.P., Tan, X.D., Courtillot, V., Sun, D.J., Li, Y.A., 2003. Paleomagnetism of Upper Jurassic to Lower Cretaceous volcanic and sedimentary rocks from the western Tarim Basin and implications for inclination shallowing and absolute dating of the M-0 (ISEA?) chron. Earth Planet. Sci. Lett. 206, 587–600.
Gilder, S.A., Gomez, J., Chen, Y., Cogné, J.P., 2008. A new paleogeographic configuration of the Eurasian landmass resolves a paleomagnetic paradox of the Tarim Basin (China). Tectonics 27, TC1012, http://dx.doi.org/10.1029/2007TC002155.
Glass, L.M., Phillips, D., 2006. The Kalkarindji continental flood basalt province: a new Cambrian large igneous province in Australia with possible links to faunal extinctions. Geology 34, 461–646.
Gradstein, F.M., Ogg, J.G., Smith, A.G., Bleeker, W., Lourens, L.J., 2004. A new geological time scale, with special reference to Precambrian and Neogene. Episodes 27 (2), 83–100.
Gregory, L.C., Meert, J.G., Bingen, B., Pandit, M.K., Torsvik, T.H., 2009. Paleomagnetism and geochronology of the Malani Igneous Suite, Northwest India: implications for the configuration of Rodinia and the assembly of Gondwana. Precam. Res. 170, 13–26.
Hanley, L.M., Wingate, M.T.D., 2000. SHRIMP zircon age for an Early Cambrian dolerite dyke: an intrusive phase of the Antrim Plateau Volcanics of northern Australia. Aust. J. Earth Sci. 47, 1029–1040.
He, X.B., Xu, B., Yuan, Z.Y., 2007. C-isotope composition and correlation of the Upper Neoproterozoic in Keping area, Xinjiang. Chin. Sci. Bull. 52 (4), 504–511.
Huang, B.C., Xu, B., Zhang, C.X., Li, Y.A., Zhu, R.X., 2005. Paleomagnetism of the Baiyisi volcanic rocks (ca. 740 Ma) of Tarim, Northwest China: a continental fragment of Neoproterozoic Western Australia? Precam. Res. 142, 83–92.
Huang, B.C., Piper, J.D.A., Peng, S.T., Liu, T., Li, Z., Wang, Q.C., Zhu, R.X., 2006. Magnetostratigraphic study of the Kuche Depression, Tarim Basin, and Cenozoic uplift of the Tian Shan Range, Western China. Earth Planet. Sci. Lett. 251, 346–364, http://dx.doi.org/10.1016/j.epsl.2006.09.020.
Huang, B.C., Zhou, Y.X., Zhu, R.X., 2008. Discussions on Phanerozoic evolution and formation of continental China, based on paleomagnetic studies. Earth Sci. Front. 15 (3), 348–358.
Jelínek, V., 1978. Statistical processing of anisotropy of magnetic susceptibility measured on groups of specimen. Stud. Geofyz. Geodet. 22, 50–62.
Jia, C.Z., Zhang, S.B., Wu, S.Z., 2004. Stratigraphy of the Tarim Basin and Adjacent Areas. China Science Publishing House, Beijing, pp. 1–1063 (in Chinese with English abstract).
Kirschvink, J.L., 1980. The least squares line and the analysis of paleomagnetic data. Geophys. J. R. Astro. Soc. 62, 699–718.
Knoll, A.H., 2000. Learning to tell Neoproterozoic time. Precam. Res. 100, 3–20.
Lee, J., 1991. Incremental $^{40}Ar/^{39}Ar$ thermochronology of mylonitic rocks from the northern Snake Range, Nevada. Tectonics 10, 77–100.
Li, Y.A., Chen, Y., Cogne, J.P., Gilder, S., Sun, D.J., 2003. Paleomagnetic study of the Late Jurassic at the southwestern margin of Tarim. Acta Geol. Sin. 77 (2), 151–157 (in Chinese with English abstract).
Li, Y.P., McWilliams, M., Cox, A., Shrarps, R., Li, Y., Gao, Z., Zhang, Z., Zhai, Y., 1988a. Late Permian Paleomagnetic pole from dikes of the Tarim craton, China. Geology 16, 275–278.
Li, Y.P., Zhang, Z., McWilliams, M., Sharps, R., Zhai, Y., Li, Y.A., Li, Q., Cox, A., 1988b. Mesozoic paleomagnetic results of the Tarim Craton: tertiary relative motion between China and Siberia? Geophys. Res. Lett. 15, 217–220.
Li, Y.P., McWilliams, M., Sharps, R., Li, Y.A., Gao, Z.J., 1990. A Devonian paleomagnetic pole from red beds of the Tarim Block, China. J. Geophys. Res. 98, 185–198.
Li, Y.P., Li, Y., Sharps, R., McWilliams, M., Gao, J., 1991. Sinian paleomagnetic results from the Tarim block, western China. Precam. Res. 49, 61–71.
Li, Z.X., Evans, D.A.D., 2011. Late Neoproterozoic 40° intraplate rotation within Australia allows for a tighter-fitting and longer-lasting Rodinia. Geology 39, 39–42.
Li, Z.X., Powell, C.M., 2001. An outline of the palaeogeographic evolution of the Australasian region since the beginning of the Neoproterozoic. Earth-Sci. Rev. 53, 237–277.
Li, Z.X., Zhang, L., Powell, C.McA., 1996. Positions of the East Asian cratons in the Neoproterozoic supercontinent Rodinia. Aust. J. Earth Sci. 43, 593–604.
Li, Z.X., Bogdanova, S.V., Collins, A.S., Davidson, A., DeWaele, B., Ernst, R.E., Fitzsimons, I.C.W., Fuck, R.A., Gladkochub, D.P., Jacobs, J., Karlstrom, K.E., Lu, S., Natapov, L.M., Pease, V., Pisarevsky, S.A., Thrane, K., Vernikovsky, V., 2008. Assembly, configuration, and break-up history of Rodinia: a synthesis. Precam. Res. 160, 179–210.
Liu, P., Yin, C., Chen, S., Tang, F., Gao, L., 2013. The biostratigraphic succession of acanthomorphic acritarchs of the Ediacaran Doushantuo Formation in the Yangtze Gorges area, South China and its biostratigraphic correlation with Australia. Precam. Res. 225, 29–43.
Long, X.P., Yuan, C., Sun, M., Zhao, G.C., Xiao, W.J., Wang, Y.J., Yang, Y.H., Hu, A.Q., 2010. Archean crustal evolution of the northern Tarim craton, NW China: Zircon U–Pb and Hf isotopic constraints. Precam. Res. 180, 272–284.
Lu, S., Li, H., Zhang, C., Niu, G., 2008. Geological and geochronological evidence for the Precambrian evolution of the Tarim Craton and surrounding continental fragments. Precam. Res. 160, 94–107.
Ma, S., Wang, Y., Fang, X., 1991. Basic characteristics of Proterozoic Eonothem as a table cover on Northern slope of Western Kunlun Mountain. Xinjiang Geol. 9, 59–71 (in Chinese with English abstract).
Maluski, H., Rajlich, P., Matte, P., 1993. $^{40}Ar/^{39}Ar$ dating of the inner Carpathians Variscan basement and Alpine mylonitic overprinting. Tectonophysics 223, 313–337.
Matte, P., Tapponnier, P., Arnaud, N., Bourjot, L., Avouac, J.P., Vidal, P., Liu, Q., Pan, Y., Wang, Y., 1996. Tectonics of Western Tibet, between the Tarim and the Indus. Earth Planet. Sci. Lett. 142, 311–330.
McElhinny, M.W., 1964. Statistical significance of the fold test in paleomagnetism. Geophys. J. R. Astro. Soc. 8, 33–40.
McElhinny, M.W., Powell, C.M., Pisarevsky, S.A., 2003. Paleozoic terranes of eastern Australia and the drift history of Gondwana. Tectonophysics 362, 41–65.
McFadden, P.L., Ma, X.H., McElhinny, M.W., Zhang, Z.K., 1988. Permo-Triassic magnetostratigraphy in China: northern Tarim. Earth Planet. Sci. Lett. 87, 152–160.
McFadden, P.L., McElhinny, M.W., 1988. The combined analysis of remagnetization circles and direct observations in palaeomagnetism. Earth Planet. Sci. Lett. 87, 161–172.
McFadden, P.L., McElhinny, M.W., 1990. Classification of the reversal test in palaeomagnetism. Geophys. J. Int. 103, 725–729.
Meert, J.G., Torsvik, T.H., 2003. The making and unmaking of a supercontinent: Rodinia revisited. Tectonophysics 375, 261–288.
Meng, Z.F., Deng, Y.S., Ding, Z.H., Zheng, Y.P., Li, Y.A., Sun, D.J., 1998. New paleomagnetic results from Ceno-Mesozoic volcanic rocks along southern rim of the Tarim Basin, China. Sci. China Ser. D 41 (Suppl.), 91–104.
Metcalfe, I., 2006. Palaeozoic and Mesozoic tectonic evolution and palaeogeography of East Asian crustal fragments: the Korean Peninsula in context. Gondwana Res. 9, 24–46.
Metcalfe, I., 2009. Late Palaeozoic and Mesozoic tectonic and palaeogeographical evolution of SE Asia. In: Buffetaut, E., Cuny, G., Le Loeuff, J., Suteethorn, V. (Eds.), Late Palaeozoic and Mesozoic Ecosystems in SE Asia, vol. 315. Geol. Soc. London, Spec. Publ., London, Great Britain, pp. 7–23.
Metcalfe, I., 2011. Palaeozoic–Mesozoic history of South Asia. In: Hall, R., Cottam, M., Wilson, M.E.J. (Eds.), The SE Asian Gateway: History and Tectonics of the Australia–Asia Collision, vol. 355. Geol. Soc. London, Spec. Publ., London, Great Britain, pp. 7–35.
Metcalfe, I., 2013. Gondwana dispersion and Asian accretion: tectonic and palaeogeographic evolution of eastern Tethys. J. Asian Earth Sci., http://dx.doi.org/10.1016/j.jseaes.
Moczydlowska, M., Zang, W.L., 2006. The Early Cambrian acritarch Skiagia and its significance for global correlation. Palaeoworld 15, 328–347.
Nie, S.Y., 1991. Paleoclimatic and paleomagnetic constraints on the Paleozoic reconstruction of south China, north China and Tarim. Tectonophysics 196, 279–308.
Powell, C.M., Pisarevsky, S.A., 2002. Late Neoproterozoic assembly of East Gondwana. Geology 30, 3–6.
Radhakrishnamurty, C., Likhite, S.D., 1970. Hopkinson effect, blocking temperature and Curie point in basalts. Earth Planet. Sci. Lett. 7, 389–396.
Schmidt, P.W., Embleton, B.J.J., Palmer, H.C., 1987. Pre- and post-folding magnetizations from the early Devonian Snowy River Volcanics and Buchan Caves Limestone, Victoria. Geophys. J. R. Astro. Soc. 91, 155–170.
Schmidt, P.W., Williams, G.E., McWilliams, M.O., 2009. Palaeomagnetism and magnetic anisotropy of late Neoproterozoic strata, South Australia: implications for the palaeolatitude of late Cryogenian glaciation, cap carbonate and the Ediacaran System. Precam. Res. 174, 35–52.
Sharps, R., McWilliams, M., Li, Y.P., Cox, A., Zhang, Z.K., Zhai, Y.J., Gao, Z.J., Li, Y.A., Li, Q., 1989. Lower Permian paleomagnetism of the Tarim block, northwestern China. Earth Planet. Sci. Lett. 92, 275–291.
Shu, L.S., Deng, X.L., Zhu, W.B., Ma, D.S., Xiao, W.J., 2011. Precambrian tectonic evolution of the Tarim Block, NW China: new geochronological insights from the Quruqtagh domain. J. Asian Earth Sci. 42, 774–790.
Sohl, L.E., Christie-Blick, N., Kent, D.V., 1999. Paleomagnetic polarity reversals in Marinoan (ca. 600 Ma) glacial deposits of Australia: implications for the duration of low-latitude glaciation in Neoproterozoic time. Geolo. Soc. Am. Bull. 111, 1120–1139.
Sun, L.S., Huang, B.C., 2009. New paleomagnetic result for Ordovician rocks from the Tarim Block, Northwest China and its tectonic implications. Chinese Journal of Geophysics 52 (7), 1836–1848 (in Chinese with English abstract).
Tan, X.D., Kodama, K.P., Chen, H.L., Fang, D.J., Sun, D.J., Li, Y.A., 2003. Paleomagnetism and magnetic anisotropy of Cretaceous red beds from the Tarim Basin, northwest China: evidence for a rock magnetic cause of anomalously shallow paleomagnetic inclinations from central Asia. J. Geophys. Res. 108 (B2), 2107, http://dx.doi.org/10.1029/2001JB001608.
Tang, L., 1997. An approach to major tectogenesis of Tarim Basin. Experimental Petroleum Geology 19 (2), 108–114 (in Chinese with English abstract).

Thrupp, G.A., Kent, D.V., Schmidt, P.W., Powell, C.M., 1991. Palaeomagnetism of red beds of the Late Devonian Worange Point Formation, SE Australia. Geophys. J. Int. 104, 179–201.
Tong, Q.L., Wei, W., Xu, B., 2013. Neoproterozoic sedimentary facies and glacial periods in the southwest of Tarim Block. Sci. China: Earth Sci. 56, 901–912, http://dx.doi.org/10.1007/s11430-013-4595-4.
Torsvik, T.H., Carter, L.M., Ashwal, L.D., Bhushan, S.K., Pandit, M.K., Jamtveit, B., 2001. Rodinia refined or obscured: palaeomagnetism of the Malani igneous suite (NW India). Precam. Res. 108, 319–333.
Turner, S.A., 2010. Sedimentary record of Late Neoproterozoic rifting in the NW Tarim Basin, China. Precam. Res. 181, 85–96.
Wang, A., Zhang, C., Zhao, Y., Guo, K., Dong, Y., 2004. Depositional types of lower part of Nanhuan system on the northern margin of southwest Tarim and their tectonic significance. J. Stratigr. 28 (3), 248–256 (in Chinese with English abstract).
Wang, B., Chen, Y., Zhan, S., Shu, L.S., Faure, M., Cluzel, D., Charvet, J., Laurent-Charvet, S., 2007. Primary Carboniferous and Permian paleomagnetic results from the Yili Block (NW China) and their implications on the geodynamic evolution of Chinese Tianshan Belt. Earth Planet. Sci. Lett. 263, 288–308.
Wang, B., Faure, M., Shu, L.S., Cluzel, D., Charvet, J., De Jong, K., Chen, Y., 2008. Paleozoic tectonic evolution of the Yili Block, western Chinese Tianshan. Bull. Soc. Geol. France 179, 483–490.
Wang, Y., Lu, S., Gao, Z., Lin, W., Ma, G., 1981. Sinian tillites of China. In: Hambrey, M.J., Harland, W.B. (Eds.), Earth's Pre-Pleistocene Glacial Record. Cambridge University Press, Cambridge, Great Britain, pp. 386–401.
Wen, B., Li, Y.X., Zhu, W., 2013. Paleomagnetism of the Neoproterozoic diamictites of the Qiaoenbrak formation in the Aksu area, NW China: constraints on the paleogeographic position of the Tarim Block. Precam. Res. 226, 75–90.
Wingate, M.T.D., Giddings, J.W., 2000a. Age and palaeomagnetism of the Mundine Well dyke swarm, Western Australia: implications for an Australia–Laurentia connection at 755 Ma. Precam. Res. 100, 335–357, http://dx.doi.org/10.1016/S0301-9268(99)00080-7.
Wingate, M.T.D., Giddings, J.W., 2000b. Age and palaeomagnetism of the Mundine Well dyke swarm, Western Australia: implications for an Australia–Laurentia connection at 755 Ma. Precam. Res. 100, 335–357.
Xiao, S., Bao, H., Wang, H., Kaufman, A.J., Zhou, C., Li, G., Yuan, X., Ling, H., 2004. The Neoproterozoic Quruqtagh Group in eastern Chinese Tianshan: evidence for a post-Marinoan glaciation. Precam. Res. 130, 1–26.
XJBGMR (Xinjiang Bureau of Geology and Mineral Resources), 1993. Regional Geology of Xinjiang Uygur Autonomous Region. Geological Publishing House, Beijing, pp. 8–33 (in Chinese).
Xu, B., Jian, P., Zheng, H.F., Zou, H.B., Zhang, L.F., Liu, D.Y., 2005. U–Pb zircon geochronology and geochemistry of Neoproterozoic volcanic rocks in the Tarim Block of northwest China: implications for the breakup of Rodinia supercontinent and Neoproterozoic glaciations. Precam. Res. 136, 107–123.
Xu, B., Xiao, S.H., Zou, H.B., Chen, Y., Li, Z.X., Song, B., Liu, D.Y., Zhou, C.M., Yuan, X.L., 2009. SHRIMP zircon U–Pb age constraints on Neoproterozoic Quruqtagh diamictites in NW China. Precam. Res. 168, 247–258.
Xu, B., Zou, H., Chen, Y., He, J., Wang, Y., 2013a. Basalts from Sugetbrak, the northwestern Tarim Block, northwest China: geochronology, geochemistry and implications for Rodinia breakup and ice age during the Late Neoproterozoic. Precam. Res. 236, 214–226.
Xu, Z.-Q., He, B.-Z., Zhang, C.-L., Zhang, J.-X., Wang, Z.-M., Cai, Z.-H., 2013b. Tectonic framework and crustal evolution of the Precambrian basement of the Tarim Block in NW China: new geochronological evidence from deep drilling samples. Precam. Res. 235, 150–162.
Yang, Z.Y., Sun, Z.M., Yang, T.S., Pei, Y.L., 2004. A long connection (750–380 Ma) between South China and Australia: paleomagnetic constraints. Earth Planet. Sci. Lett. 220, 423–434.
Yao, J., Xiao, S., Yin, L., Li, G., Yuan, X., 2005. Basal Cambrian microfossils from the Yurtus and Xishanblaq formations (Tarim, north-west China): systematic revision and biostratigraphic correlation of Micrhystridium-like acritarchs from China. Palaeontology 48, 687–708.
Yong, W., Zhang, L., Hall, C.M., Mukasa, S.B., Essene, E.J., 2012. The 40Ar/39Ar and Rb–Sr chronology of the Precambrian Aksu blueschists in western China. J. Asian Earth Sci., http://dx.doi.org/10.1016/j.jseaes.2012.05.024.
Yu, B., Chen, J., Li, X., Lin, C., 2003. Geochemistry of black shale at the bottom of the Lower Cambrian in Tarim Basin and its significance for lithosphere evolution. Sci. Chi. (Ser. D) 46 (5), 498–507.
Zhan, S., Chen, Y., Xu, B., Wang, B., Faure, M., 2007. Late Neoproterozoic paleomagnetic results from the Sugetbrak Formation of the Aksu area, Tarim basin (NW China) and their implications to paleogeographic reconstructions and the snowball Earth hypothesis. Precam. Res. 154, 143–158.
Zhang, C., Yang, C., Shen, J., Zhao, Y., Wang, A., Dong, Y., Guo, K., 2003. Zircon SHRIMP age of Neoproterozoic Gneissoid Granites in the west Kunlun and its significance. Geol. Rev. 49 (3), 239–244 (in Chinese with English abstract).
Zhang, C.L., Li, H.K., Santosh, M., Li, Z.X., Zou, H.B., Wang, H., Ye, H., 2012a. Precambrian evolution and cratonization of the Tarim Block, NW China: petrology, geochemistry, Nd-isotopes and U–Pb zircon geochronology from Archaean gabbro-TTG–potassic granite suite and Paleoproterozoic metamorphic belt. J. Asian Earth Sci. 47, 5–20.
Zhang, C.L., Zou, H.B., Li, H., Wang, H.Y., 2012b. Tectonic framework and evolution of the Tarim Block in NW China. Gondwana Res., http://dx.doi.org/10.1016/j.gr.2012.05.009.
Zhang, C.L., Li, Z.X., Li, X.H., Ye, H.M., 2009. Neoproterozoic mafic dyke swarms at the northern margin of the Tarim Block, NW China: age, geochemistry, petrogenesis and tectonic implications. J. Asian Earth Sci. 35, 167–179.
Zhang, C.L., Li, X.H., Li, Z.X., Lu, S.N., Ye, H.M., Li, H.M., 2007. Neoproterozoic mafic–ultramafic–carbonatite complex and granitoids in Quruqtagh of northeasternTarim Block, western China: geochronology, geochemistry and tectonic implications. Precam. Res. 152, 149–169.
Zhang, C.L., Ye, H.M., Wang, A.G., Guo, K.Y., Dong, Y.G., 2004. Geochemistry of the Neoproterozoic diabase and basalt in South of Tarim plate: evidence for the Neoproterozoic breakup of the Rodinia super-continent in south of Tarim. Acta Petrol. Sin. 20 (3), 473–482 (in Chinese with English abstract).
Zhang, S., Evans, D.A.D., Li, H., Wu, H., Jiang, G., Dong, J., Zhao, Q., Raub, T., Yang, T., 2013. Paleomagnetism of the late Cryogenian Nantuo formation and paleogeographic implication for the South China Block. Journal of Asian Earth Science 72, 164–177.
Zhang, Z.K., Li, Y.A., Li, Q., Zhai, Y.J., Li, Y.P., McWilliams, M., Cox, A., Sharps, R., 1989. Paleomagnetic results of Jurassic-Cretaceous in the Tarim. Seismology and Geology 34 (3), 343–354 (in Chinese with English abstract).
Zhao, X., Coe, R., Wu, H., Zhao, Z., 1993. Silurian and Devonian paleomagnetic poles from North China and implications for Gondwana. Earth Planet. Sci. Lett. 117, 497–506.
Zhu, M.Y., Wang, H.F., 2012. Neoproterozoic glaciogenic diamictites of the Tarim Block, NW China. In: Arnaud, E., Halverson, G.P., Shields-Zhou, G. (Eds.), The Geological Record of Neoproterozoic Glaciations, vol. 36. Geol. Soc. London, Mem., London, Great Britain, pp. 367–378.
Zhu, R.X., Yang, Z.Y., Wu, H.N., Ma, X.H., Huang, B.C., Meng, Z.F., Fang, D.J., 1998. Paleomagnetic apparent polar wander paths and movement for China main continental blocks during Phanerozoic. Sci. China Ser. D 28 (Suppl.), 1–16.
Zijderveld, J.D.A., 1967. Demagnetization of rocks: analysis of results. In: Collision, D.W., Creer, K.M., Runcorn, S.K. (Eds.), Methods in Paleomagnetism. Elsevier, pp. 254–286.

Journal of Asian Earth Sciences xxx (2014) xxx–xxx

Contents lists available at ScienceDirect

Journal of Asian Earth Sciences

journal homepage: www.elsevier.com/locate/jseaes

Early Paleozoic tectonic evolution of the Xing-Meng Orogenic Belt: Constraints from detrital zircon geochronology of western Erguna–Xing'an Block, North China

Pan Zhao [a,b], Junqin Fang [a], Bei Xu [a,*], Yan Chen [b,c,d], Michel Faure [b,c,d]

[a] Key Laboratory of Orogenic Belts and Crustal Evolution, Ministry of Education, Peking University, Beijing 100871, China
[b] Universitéd'Orléans, ISTO, UMR 7327, 45071 Orléans, France
[c] CNRS/INSU, ISTO, UMR 7327, 45071 Orléans, France
[d] BRGM, ISTO, UMR 7327, BP 36009, 45060 Orléans, France

ARTICLE INFO

Article history:
Received 26 January 2014
Received in revised form 6 April 2014
Accepted 11 April 2014
Available online xxxx

Keywords:
Xing-Meng Orogenic Belt
Early Paleozoic
Detrital zircon
Erguna–Xing'an Block
Inner Mongolia

ABSTRACT

To better constrain the Early Paleozoic tectonic evolution of the western part of the Erguna–Xing'an Block, detrital zircon U–Pb dating was applied on the Ordovician to Devonian sedimentary strata along the southeast part of the China–Mongolia border. Most of the zircons from five sedimentary samples display fine-scale oscillatory growth zoning and Th/U ratios higher than 0.1, indicating a magmatic origin. All five Ordovician–Devonian samples display the similar age distribution patterns with age groups at ~440 Ma, ~510 Ma, ~800 Ma, ~950 Ma, and few Meso- to Paleo-Proterozoic and Neoarchean grains. This age distribution pattern is similar to those from adjacent blocks in the southeastern Central Asian Orogenic Belt. Considering previous tectonic studies, we propose bidirectional provenances from the Erguna–Xing'an Block and Baolidao Arc.

Consequently, a new model was proposed to highlight the Early Paleozoic tectonic evolution of the western Erguna–Xing'an Block, which constrains two main Early Paleozoic tectonic events of the Xing-Meng Orogenic Belt: (a) pre-Late Cambrian collision between Erguna–Kerulen Block and Arigin Sum-Xilinhot-Xing'an Block; (b) the Early Paleozoic subduction of Paleo-Asian Ocean and pre-Late Devonian collision between Erguna–Xing'an Block and Songliao-Hunshandake Block.

1. Introduction

The Xing-Meng Orogenic Belt (XMOB), as the southeastern part of the Central Asian Orogenic Belt (CAOB; Fig. 1a), recorded the accretionary history among several main blocks, such as North China Craton (NCC), Songliao-Hunshandake Block (SHB), Airgin Sum-Xilinhot-Xing'an Block (AXXB) and Erguna Block (EB) (Fig. 1a; Wu et al., 2007; Zhou et al., 2011a). These blocks experienced multi-stage amalgamation during the Paleozoic. Numerous studies have been carried out in the past two decades; however, no consensus about the tectonic evolution of XMOB has been reached (e.g., Xiao et al., 2003; Wu et al., 2011; Zhou et al., 2011a; Zhang et al., 2012; Xu et al., 2013). The collision between EB and AXXB is considered to have occurred before the Late Cambrian, as orogenic related Late Cambrian alkaline granites, granitoids and gabbros were identified from both sides of the Xinlin-Xiguitu suture zone, representing a post-collisional setting (Fig. 1a; Sorokin et al., 2004; 2011; Ge et al., 2005; Wu et al., 2005, 2007; Wu et al., 2011). After that, the newly formed Erguna–Xing'an Block (EXB) involved into the following Paleozoic accretionary process. From the Late Cambrian, the Paleo-Asian Ocean subducted beneath the EXB to the north and the NCC to the south, with two arc magmatic belts developed (Liu et al., 2003; Jian et al., 2008; Zhang et al., 2009b; Xu et al., 2013; Zhang et al., 2013). High-pressure metamorphic blueschists were identified from both northern and southern belts, with ^{40}Ar–^{39}Ar ages of 383 ± 13 Ma and 453–446 Ma, respectively (Xu et al., 2001; Tang and Yan, 1993; De Jong et al., 2006). Based on structural and sedimentary investigations, two unconformities have been described. The ductilely deformed Ondor Sum Group and ophiolitic mélange were unconformably overlain by the Late Devonian molasse along the northern suture and by the Late Silurian molasse along the southern one, respectively (Tang, 1990; Xu et al., 2013). After the orogenesis, Devonian alkaline intrusive complex followed, indicating a post-collisional setting (Zhang et al., 2010). It means that the amalgamation of EXB, SHB and NCC occurred

* Corresponding author. Tel.: +86 01062767288.
E-mail address: bxu@pku.edu.cn (B. Xu).

http://dx.doi.org/10.1016/j.jseaes.2014.04.011
1367-9120/

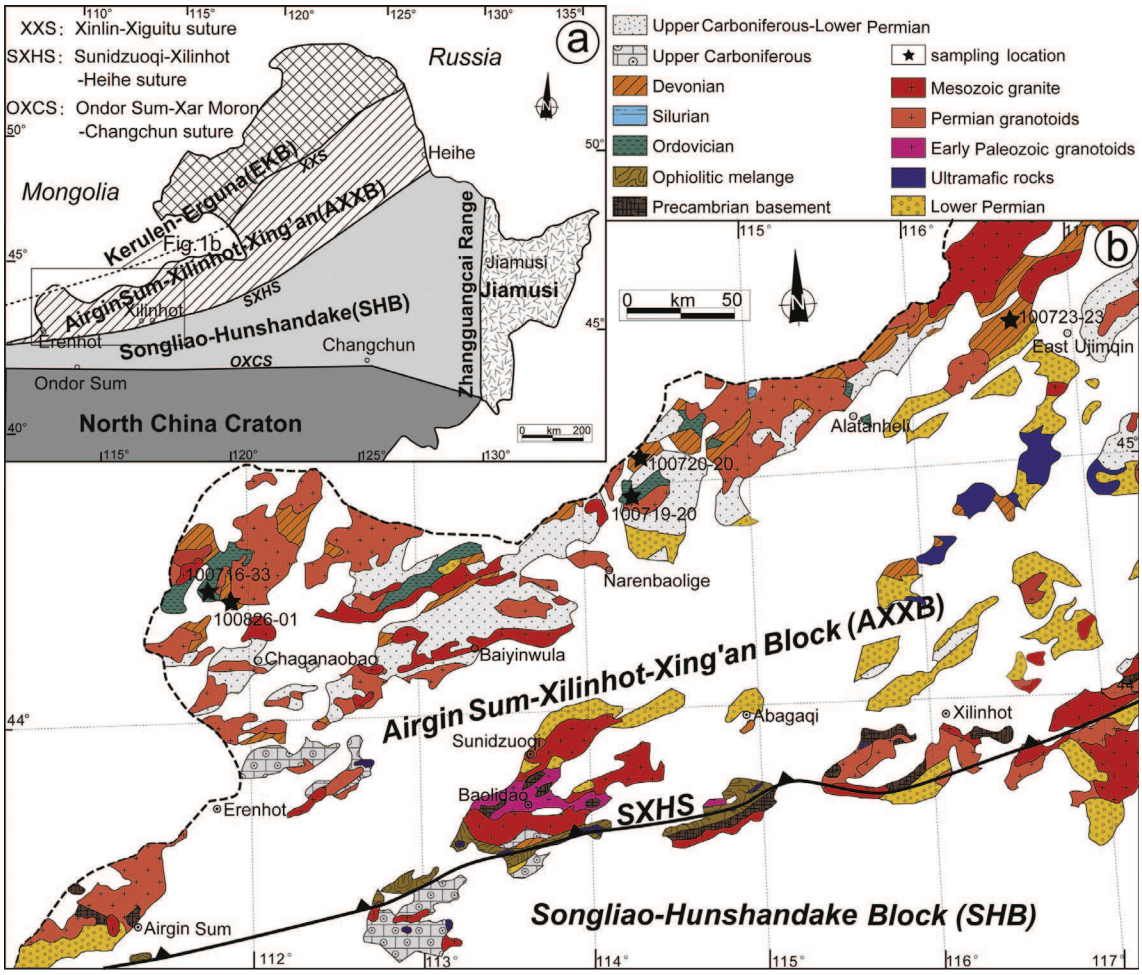

Fig. 1. (a) Tectonic sketch map of Northeastern China, modified after Wu et al. (2007) and Xu et al. (2013). (b) Geological map of the southwestern margin of the Airgin Sum-Xilinhot-Xing'an Block from the Erenhot to Dongwuqi, after IMBGMR (1991).

before the end of Devonian, without wide ocean existing in between, which is confirmed by recent paleomagnetic (Zhao et al., 2013) and palaeontological studies (Zhou et al., 2010; Xin et al., 2011). However, different arguments have been put forward to consider that the final collision occurred in the Late Permian based on the geochemistry studies on the Carboniferous-Permian magmatic rocks (Chen et al., 2000; Zhang et al., 2009a). Therefore, the tectonic evolution between EXB and SHB is still controversal, especially on the south margin of the EXB.

In this study, a detrital zircon geochronological investigation was performed on the Ordovician–Devonian strata in the western part of the AXXB (Fig. 1), where investigations remain rare. From these new data, we try to decipher the sedimentary record and the Early Paleozoic tectonic evolution of western EXB.

2. Geological setting

The northeastern China is divided into several blocks, namely Erguna Block, Airgin Sum-Xilinhot-Xing'an Block, Songliao-Hunshandake Block and Jiamusi Block from north to south (Fig. 1a; Wu et al., 2007; Xu et al., 2013). These blocks share the similar Paleo- to Neo-Proterozoic basement, which was revealed by both geochronological studies of magmatic massifs and metasedimentary rocks (Wang et al., 2001; Wu et al., 2011; Li et al., 2011; Han et al., 2011; Zhang et al., 2012 and references therein; Wu et al., 2012; Sun et al., 2013a,b; Tang et al., 2013). To the west, according to the new tectonic subdivision of Mongolia (personal communication with Tomurtogoo), the Erguna Block might connect with the Kerulen Block (Erguna–Kerulen Block, EKB), and the Airgin Sum-Xilinhot-Xing'an Block connected with the Totoshan Block in the southernmost Mongolia (Fig. 1a; Wang et al., 2001; Xu et al., 2013; Zhou et al., 2013). However, some researchers suspect the existence of AXXB due to the lack of Precambrian basement and some Paleozoic zircons identified from geochronological studies of the Xilinhot complex (Wu et al., 2007; Xue et al., 2009; Chen et al., 2012). This uncertainty was solved by recent studies, as Ge et al. (2011) isolated the late Meso-Proterozoic supracrustal rocks from the Xilinhot complex, which was intruded by ~740 Ma metagabbro, indicating the existence of Precambrian basement. Meanwhile, Meso-proterozoic granitic gneisses were recently reported from the east of Sunidzuoqi with zircon U–Pb age of 1516–1390 Ma, considered as the basement of AXXB (Sun et al., 2013b).

The study area is located along the southeastern part of China–Mongolia border, belonging to the western part of the AXXB, which was separated from the northern EKB by the Xinlin-Xiguitu suture zone (XXS) (Fig. 1a). To the south, it was separated from the Songliao-Hunshandake Block by the Suzuoqi-Xilinhot-Heihe suture zone (SXHS), which formed during the Late Devonian-Early Carboniferous based on the Late Devonian unconformity and Carboniferous post-collisional intrusions (Fig. 1; Zhang et al., 2012; Xu et al., 2013).

The oldest strata of the study area are of the Ordovician period, consisting of Lower-Middle Ordovician Wubinaobao and Tongshan formations, Middle Ordovician Duobaoshan Formation,

Please cite this article in press as: Zhao, P., et al. Early Paleozoic tectonic evolution of the Xing-Meng Orogenic Belt: Constraints from detrital zircon geochronology of western Erguna–Xing'an Block, North China. Journal of Asian Earth Sciences (2014), http://dx.doi.org/10.1016/j.jseaes.2014.04.011

and Middle-Upper Ordovician Luohe Formation (Fig. 2). Except for the Duobaoshan Formation, which is mainly composed of basaltic andesite, the other formations are mainly composed of fine-grained clastic sediments. The Silurian strata are rare in the study area, only Upper Silurian Woduhe Formation was identified from the Narenbaolige and West Ujimqin areas (Fig. 2). These sediments were characterized by Late Silurian *Tuvaella* fauna-bearing clastic rocks and carbonates (Su, 1981; IMBGMR, 1991; Wang et al., 2009). The widely distributed Lower-Middle Devonian Niqiuhe Formation (Fig. 1b) mainly consists of clastic rocks from conglomerate to siltstone with several limestone interlayers, and displays differences of sedimentary facies from western to eastern parts (Fig. 2). It is characterized by its abundant shallow marine fossils, such as brachiopoda, bivalve, coral and trilobita (IMBGMR, 1991). The Middle-Upper Devonian strata were mainly distributed in the west of West Ujimqin, namely Middle-Upper Devonian Tarbaget Formation and Upper Devonian Angeryinwula Formation (Fig. 2). Both of these formations mainly consist of fine-grained clastic rocks (Fig. 2). However, corals and brachiopoda were also found in the Tarbaget Formation, while plant fossils were identified in the Angeryinwula Formation, indicating a regression related depositional facies transition from shallow marine to continental facies (IMBGR, 2007). The Upper Carboniferous-Lower Permian Baoligaomiao/Gegenaobao Formation, a ca. 5000-m-thick sequence, unconformbly cover the underlying strata. It is composed of conglomerate, coarse-grained sandstone and red siltstone in the lower part and volcanic and volcano-clastic rocks in the upper part. The abundant flora found therein and the geochemical signatures of volcanic rocks reveal the continental deposition (IMBGMR, 1991; Li et al., 1996; Zhang et al., 2011). The volcanic rocks are coeval or slightly older than the Early Permian alkaline granite, and together they constitute an Early Permian rift-related alkaline magmatic belt (Hong et al., 1994, 1996; Jahn et al., 2009).

3. Sampling

Five sandstone–siltstone samples were collected from three localities for detrital zircon U–Pb dating. The detailed sampling information is described below.

Two samples were collected from the northwest of Chaganaobao County (Fig. 1b). Sample 100716-33 (GPS: 44°32′33″N, 111°47′52″E) is siltstone from ca. 4500-m-thick Lower-Middle Ordovician Wubinabo Formation (Fig. 2). It is mainly composed of dark green siltstone with schistosity (Fig. 3a), with grey sandstone interlayers (Fig. 2). Sample 100826-01 (GPS: 44°30′88″N, 111°57′39″E) is red coarse-grained sandstone from the Lower-Middle Devonian Niqiuhe Formation (Fig. 2). Overlying the conglomerate (Fig. 3f), the red coarse-grained sandstone is considered as near-shore deposition with plenty of lithic grains (Fig. 3b).

Two samples were collected from the northwest of Narenbaolige County (Fig. 1b). Sample 100719-20 (GPS: 44°56′50″N, 114°20′14″E) was collected from a sandstone layer at the bottom of the Middle-Upper Ordovician Luohe Formation (Fig. 2). It was grayish-green in color with high proportion of basaltic lithic fragments (Fig. 3c), which might come from the underlying Duobaoshan basaltic andesite (Fig. 2). Sample 100720-20 (GPS: 45°11′15″N, 114°39′18″E) was collected from the lower part of the Lower-Middle Devonian Niqiuhe Formation (Fig. 2). This sandstone is gray in color with wavy and parallel bedding. Lithic grains, polycrystal and monocrystal quartz constitute the main clastic part of this sandstone (Fig. 3d).

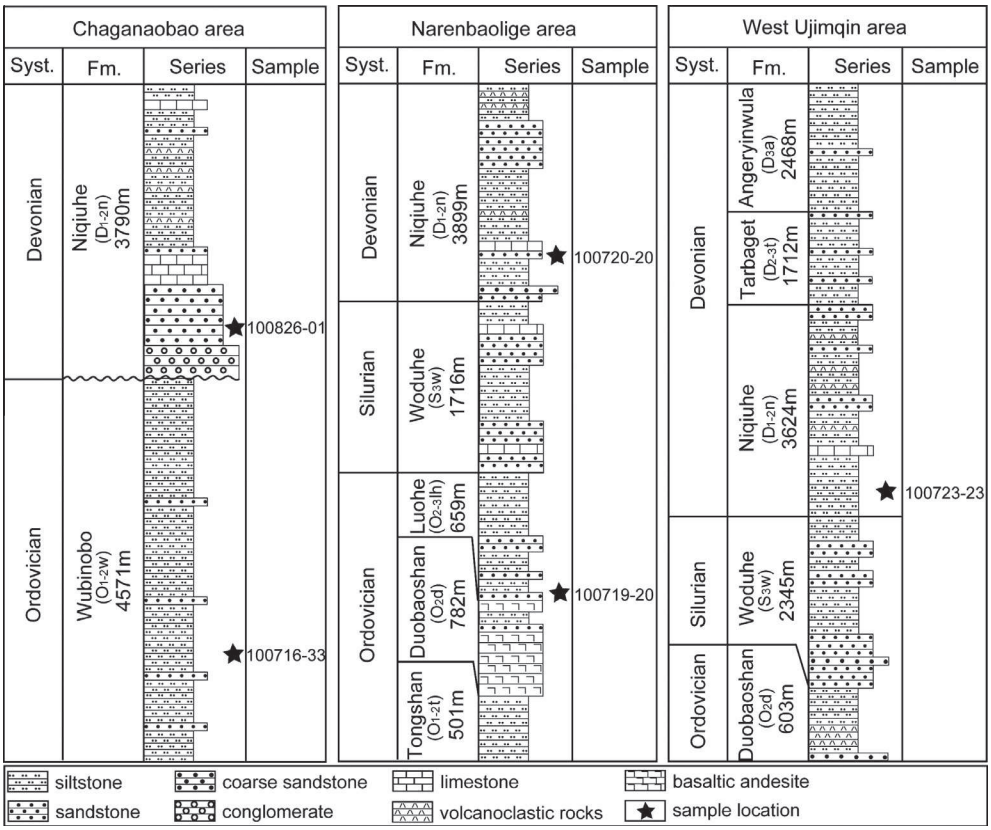

Fig. 2. Stratigraphic column of Ordovician to Devonian strata from Chaganaobao, Narenbaolige and West Ujimqin areas, showing lithology and sample sites.

Please cite this article in press as: Zhao, P., et al. Early Paleozoic tectonic evolution of the Xing-Meng Orogenic Belt: Constraints from detrital zircon geochronology of western Erguna–Xing'an Block, North China. Journal of Asian Earth Sciences (2014), http://dx.doi.org/10.1016/j.jseaes.2014.04.011

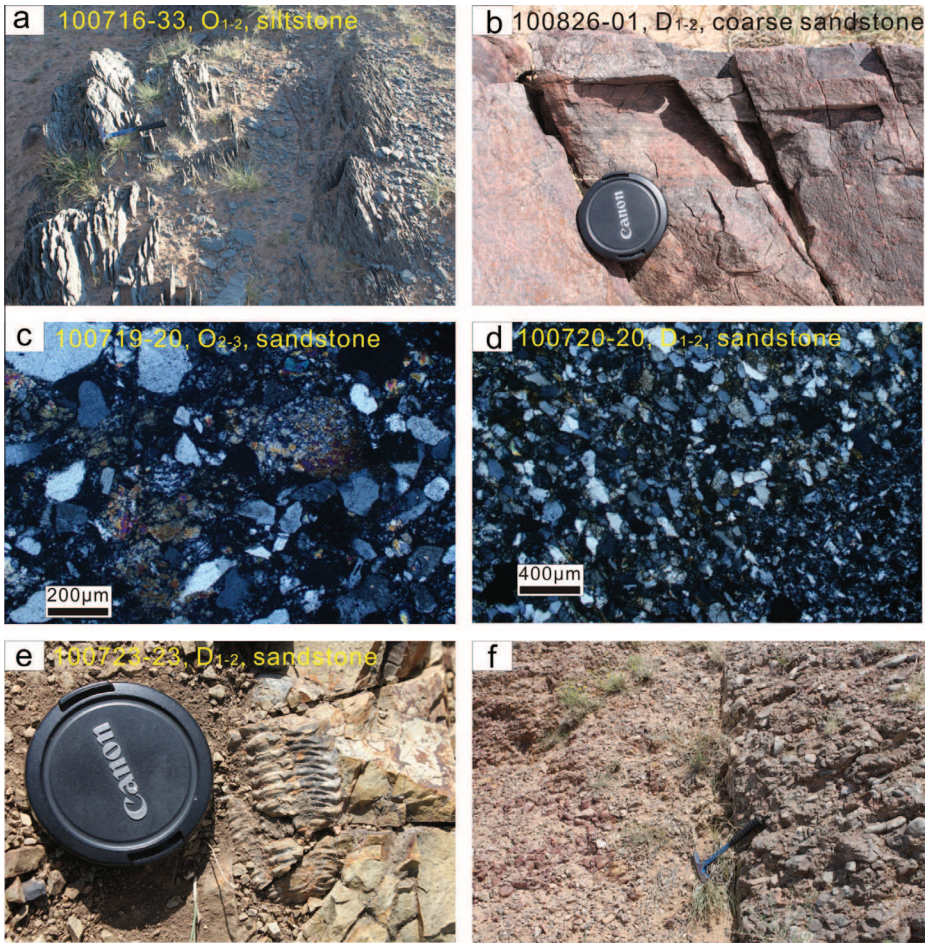

Fig. 3. (a–e) Field photographs and photomicrographs of dated strata, with number, age and lithology at the top; (f) the basal conglomerate of the Lower-Middle Devonian Niqiuhe Formation at the Chagenaobao area.

Sample 100723-23 (GPS: 45°36′38″N, 116°44′06″E) was collected from the Lower-Middle Devonian Niqiuhe Formation in the northwest of West Ujimqin County (Fig. 1b). It is yellowish fine-grained sandstone with trilobita and brachiopoda fossils found nearby, indicating stable sedimentation and long-distance transport of provenance (Fig. 3e).

4. Analytical procedures

Zircons were separated using conventional heavy liquid and magnetic techniques before handpicking under a binocular microscope at the Langfang Regional Geological Survey, Hebei Province, China. Handpicked zircons were photographed under transmitted and reflected light under optical microscope before cathodoluminescence (CL) imaging using a Quanta 200 FEG Scanning Electron Microscope in Peking University. The CL revealed the internal textures and potential target sites for U–Pb analyses. Zircon U–Pb dating was carried out using an Agilient 7500c ICP-MS instrument coupled with a 193-nm ArFExcimer laser with the automatic positioning system at the Key Laboratory of Orogen and Crust Evolution, Peking University. Calibrations for zircon analyses were carried out using NIST 610 glass as an external standard and Si as internal standard. U–Pb isotope fractionation effects were corrected using zircon Plesovice (337 Ma) as external standard. Zircon standard 91,500 is used as a secondary standard to supervise the deviation of age measurement/calculation. Isotopic ratios and element concentrations of zircons were calculated using GLITTER (ver. 4.4.2, Macquarie University). Concordia ages and diagrams were obtained using Isoplot/Ex (3.0) (Ludwig, 2003). The common lead was corrected using LA-ICP-MS Common Lead Correction (ver. 3.15), followed the method of Andersen (2002). The analytical data are presented on U–Pb Concordia diagrams with 2σ errors. The mean ages are weighted means at 95% confidence levels (Ludwig, 2003).

5. U–Pb zircon dating results

5.1. Chaganaobao area

5.1.1. Lower-Middle Ordovician siltstone (sample 100716-33)

The zircon grains are euhedral to subhedral, ranging from 30 to 50 μm in width and 50–100 μm in length with fine-scale oscillatory growth zoning (Fig. 4a). The Th/U ratios range from 0.12 to 1.44, indicating magmatic origin (e.g., Rubatto, 2002; Corfu et al., 2003). A total of 75 zircons were analyzed and 12 of them were discarded because of high discordance (Supplementary Table). The 63 concordant analyses yielded apparent ages ranging from 440 ± 6 Ma to 2534 ± 12 Ma and fall into three main age populations: 440–577 Ma (n = 30) with a peak at 491 Ma, 766–956 Ma (n = 25) with peaks at 827 and 950 Ma, 1019–1598 Ma (n = 5) without peak age, respectively (Fig. 5a and b). In addition, one grain yielded an age of 697 ± 8 Ma and two grains yielded Archean ages of 2530 ± 12 and 2534 ± 12 Ma (Supplementary Table).

5.1.2. Lower-Middle Devonian coarse-grained sandstone (sample 100826-01)

The zircon grains are euhedral to subhedral, ranging from 50 to 150 μm in width and 100–250 μm in length with well-developed

Please cite this article in press as: Zhao, P., et al. Early Paleozoic tectonic evolution of the Xing-Meng Orogenic Belt: Constraints from detrital zircon geochronology of western Erguna–Xing'an Block, North China. Journal of Asian Earth Sciences (2014), http://dx.doi.org/10.1016/j.jseaes.2014.04.011

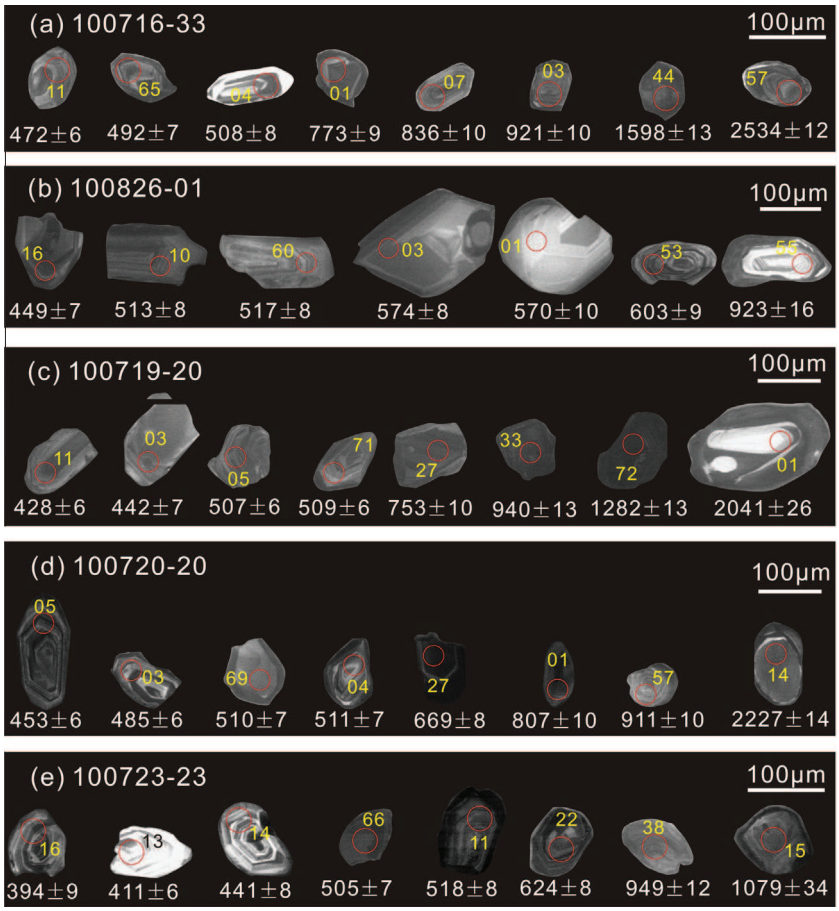

Fig. 4. Cathodoluminescence (CL) images of selected detrital zircons from each sample. The circles represent U–Pb analytical sites with ages presented below.

oscillatory growth zoning (Fig. 4b). The majority of zircons display high Th/U ratios ranging from 0.24 to 1.06, indicative of magmatic origin. However, seven grains show Th/U ratios less than 0.1 (0.08–0.09), which may indicate their metamorphic origin (Rubatto, 2002). All of 75 analyses are concordant, ranging from 449 ± 7 to 923 ± 16 Ma. Two main age populations are defined at 487–527 Ma (n = 40) with a peak at 508 Ma, and 536–608 Ma (n = 30) with a peak at 576 Ma (Fig. 5c and d). Meanwhile, five zircons yielded ungrouped ages of 449, 678, 794, 892 and 923 Ma (Supplementary Table; Fig. 5c and d).

5.2. Narenbaolige area

5.2.1. Middle-Upper Ordovician siltstone (sample 100719-20)

The majority of zircon grains are subhedral to subrounded, ranging from 30 to 100 μm in width and 60–200 μm in length (Fig. 4c). Most zircon grains display oscillatory growth zoning, with a few showing inherited cores and rims (Fig. 4c). All zircons except one (0.03 for #1920-01 with an age of 2081 ± 19 Ma) give high Th/U ratios from 0.24 to 1.47, indicating magmatic origin. Among a total of 75 analyses, 69 concordant analyses yielded ages ranging from 428 ± 6 Ma to 2092 ± 17 Ma (Supplementary Table; Fig. 5e and f), and fell into one main age population at 428–547 Ma (n = 63), with two peaks at 442 Ma and 511 Ma (Fig. 5e and f). Meanwhile, six zircons yielded ungrouped ages of 753, 940, 1282, 1461, 2081 and 2092 Ma.

5.2.2. Lower-Middle Devonian sandstone (sample 100720-20)

Most of zircon grains are subhedral to subrounded, ranging from 40 to 80 μm in width and 50–200 μm in length (Fig. 4d). Most zircon grains display oscillatory growth zoning, while a small proportion shows inherited cores and rims (Fig. 4d). Except two grains with Th/U ratio less than 0.1, all other zircons show high Th/U ratios from 0.11 to 1.09, indicating magmatic origin. Among a total of 75 U–Pb analyses, 67 of them are concordant and yielded ages ranging from 453 ± 6 Ma to 2227 ± 14 Ma (Supplementary Table; Fig. 5g and h). These grains fall into two main age populations at 453–581 Ma (n = 49) with two peaks at 459 Ma and 512 Ma, and 669–917 Ma (n = 17) with peak at 794 Ma (Fig. 5g and h). In addition, one grain yielded ages of 2227 ± 14 Ma.

5.3. West Ujimqin Lower-Middle Devonian sandstone (sample 100723-23)

The zircon grains are euhedral to subhedral, ranging from 50 to 100 μm in width and 80–150 μm in length with oscillatory growth zoning (Fig. 4e). Except one grain showing Th/U ratio of 0.04, all other zircons show high Th/U ratios from 0.13 to 0.91, indicating magmatic origin. Among a total of 74 analyses, eight analyses were discarded because of high discordance, and one grain (#2325-20 with age of 214 ± 3) was also discarded (Supplementary Table). The 65 concordant analyses yielded ages ranging from 394 ± 6 Ma to 2018 ± 45 Ma (Supplementary Table; Fig. 5i and j). Broadly, the grains fall into three age populations at 394–495 Ma (n = 37) with a peak at 435 Ma, 505–546 Ma (n = 15) with peak at 511 Ma, and 778–1078 Ma (n = 11) with a small peak at 959 Ma, respectively (Fig. 5j). Meanwhile, two zircons yielded ages of 624 and 2018 Ma (Supplementary Table; Fig. 7i and j).

Please cite this article in press as: Zhao, P., et al. Early Paleozoic tectonic evolution of the Xing-Meng Orogenic Belt: Constraints from detrital zircon geochronology of western Erguna–Xing'an Block, North China. Journal of Asian Earth Sciences (2014), http://dx.doi.org/10.1016/j.jseaes.2014.04.011

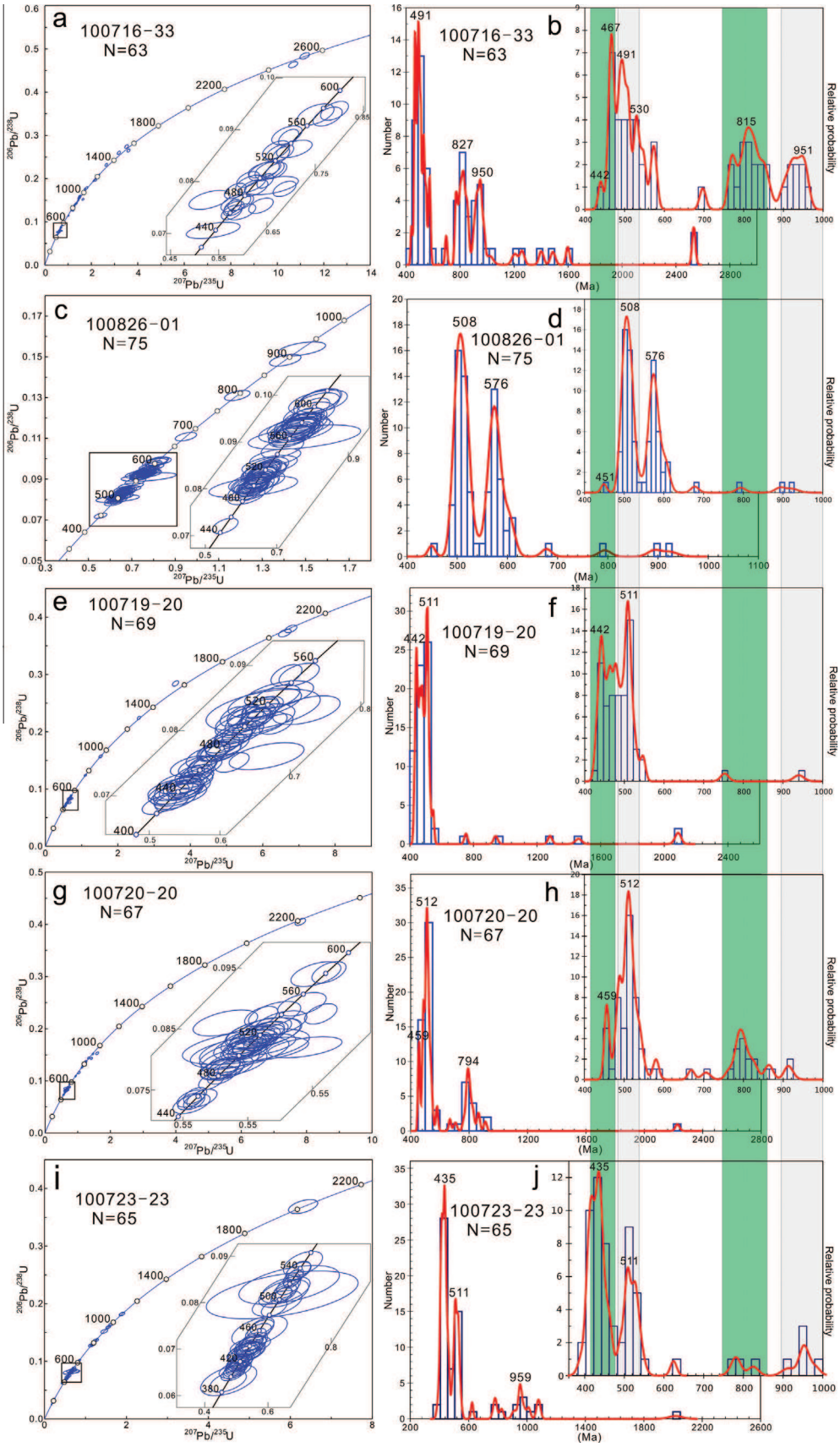

Fig. 5. U–Pb concordia and probability diagrams of zircon ages from Ordovician to Devonian sandstone and siltstone of this study. The inset figures within each U–Pb Concordia diagram show zircon grains with ages of 400–600 Ma.

Please cite this article in press as: Zhao, P., et al. Early Paleozoic tectonic evolution of the Xing-Meng Orogenic Belt: Constraints from detrital zircon geochronology of western Erguna–Xing'an Block, North China. Journal of Asian Earth Sciences (2014), http://dx.doi.org/10.1016/j.jseaes.2014.04.011

6. Discussion

6.1. Constraint on the depositional age of the studied Ordovician–Devonian strata

The depositional ages of the investigated Ordovician to Devonian formations were determined using association of fossils and regional lithological correlation. Due to the poorly preserved fossils (especially for Ordovician strata) and lithological variations from region to region, the stratigraphic division of the Ordovician–Devonian strata in this area is not precise. Our detrital-zircon data provide new constraint for their age assignment.

The youngest zircon age of the Lower-Middle Ordovician Wubinaobao Formation siltstone is 440 ± 6 Ma, but defined by just one grain. Consequently, the youngest grouped zircon age of 461 ± 6 Ma, as defined by 14 grains (Supplementary Table), was used to constrain the depositional age of the Wubinaobao Formation. This age falls into the Middle Ordovician, and is therefore consistent with the former fossil constraint (IMBGMR, 1991). For the Middle-Upper Ordovician Luohe Formation, the youngest grouped zircon age is 428 ± 6 Ma, constraining the depositional age to be younger than the Early Silurian, which is slightly younger than the previous assignment (IMBGMR, 1991). The abundant fossils found within the Niqiuhe Formation have well constrained its Early-Middle Devonian age, and our detrital-zircon data from Chaganaobao (449 ± 7 Ma for the youngest zircon age), Baiyintuga (453 ± 6 Ma for the youngest zircon age) and West Ujimqin (394 ± 6 Ma for the youngest zircon age) are consistent with this age assignment. Hence, the depositional age of the Niqiuhe Formation should be the Early-Middle Devonian.

6.2. Provenance of Ordovician and Devonian strata

The detrital-zircon dating results presented above give us new clues to trace the provenance of these sediments and decipher the tectonic evolution. All these five Ordovician-Devonian samples display similar distributions in zircon-age probability diagrams, characterized by predominant Early Paleozoic groups at ~440 Ma and ~510 Ma, and subordinate Neoproterozoic groups at ~570 Ma, ~800 Ma and ~950 Ma, respectively, with only few pre-1.0 Ga grains (Figs. 5 and 6a). It indicates relatively stable provenance for this belt from the Ordovician to the Devonian.

The most striking feature of zircon-age distribution for this study is the predominant peak age at ~510 Ma (Fig. 6a). This significant age group was well documented from the EKB (Wu et al., 2005, 2012) and AXXB (Fig. 6b and c; Li et al., 2011; Han et al., 2011) by geochronological studies of granitoids and clastic rocks, which was considered as the orogenic related magmatic event due to the collision between the EKB and AXXB (Wu et al., 2005). Furthermore, this age group has also been revealed by zircon studies of igneous rocks from northwestern-central Mongolia (Fig. 6d; Rojas-Agranonte et al., 2011), central Mongolia (Demoux et al., 2009a), and southern Mongolia (Demoux et al., 2009b), and by detrital-zircon studies from northwestern Mongolia (Kelty et al., 2008) and central Mongolia (Bussien et al., 2011). Most of the ~510 Ma zircons display Th/U ratios higher than 0.1 (Supplementary Table), implying that these zircon grains probably came from the Cambrian magmatic rocks exposed on the EKB, AXXB or/and the Mongolian blocks. Moreover, it was noticed that four zircons from Sample 100826-01 and one zircon from Sample 100723-23 present Th/U ratios less than 0.1 and U–Pb age of 497–517 Ma (Supplementary Table), showing the same feature with zircons from Pan-African events in the northeastern margin of the EKB and AXXB (Zhou et al., 2011a,b; Zhou and Wilde, 2013).

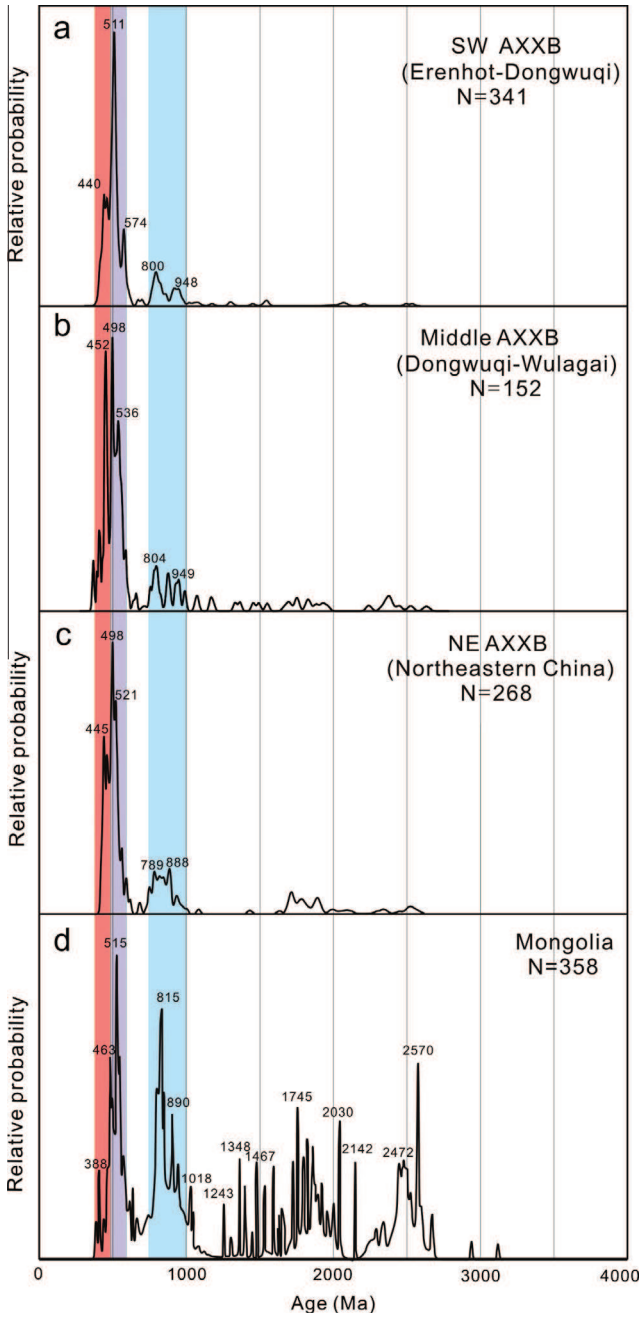

Fig. 6. Comparison of probability plots for the data from the western Airgin Sum-Xilinhot-Xing'an Block ((a) this study), middle Airgin Sum-Xilinhot-Xing'an Block ((b); Li et al., 2011), northeastern Airgin Sum-Xilinhot-Xing'an Block ((c); Han et al., 2011) and Mongolia ((d); Rojas-Agranonte et al., 2011).

The age peak of ~440 Ma may represent the regional Early Paleozoic magmatic event. Two Early Paleozoic magmatic events have been documented from nearby blocks. After the amalgamation of the EKB and AXXB at the Cambrian, the Early Paleozoic post-collisional magmatic intrusions from ~490 to ~440 Ma were taken place on the newly formed EXB (Wu et al., 2005; Ge et al., 2005; Sorokin et al., 2011; Ren et al., 2012; Guo et al., 2013). To the south, the Early Paleozoic Baolidao arc magmatism at the southern margin of the AXXB was dated at 498–415 Ma (Jian et al., 2008; Xu et al., 2013). These two kinds of magmatic rocks can both be considered as provenance regions for this zircon group. Notably, only one zircon from the western Chaganaobao Devonian sample (100826-01) presents an age around this age peak, with the

Please cite this article in press as: Zhao, P., et al. Early Paleozoic tectonic evolution of the Xing-Meng Orogenic Belt: Constraints from detrital zircon geochronology of western Erguna–Xing'an Block, North China. Journal of Asian Earth Sciences (2014), http://dx.doi.org/10.1016/j.jseaes.2014.04.011

main age group at 508 Ma (Fig. 6b), indicating that the main provenance for the Devonian strata therein could be the EXB. However, the percentage of the Early Paleozoic zircon grains increases eastwards (Fig. 6b, d and e). The easternmost Devonian sample from West Ujimqin (100723-23) presents the main age peak at 435 Ma, which is most likely from the southern Baolidao magmatic arc. This eastward tendency indicates that the contribution of the Baolidao arc to the provenance of Devonian strata increases from west to east.

The Neoproterozoic peaks (800–1000 Ma) are subordinate in our results (Fig. 5), and they cannot be used as an effective provenance indicator because this peak age represents the universal basement of nearly all blocks between NCC and Siberia Block (SIB). Neoproterozoic alkaline plutons have been identified from the EKB with the age of 950–737 Ma (Wu et al., 2011; Tang et al., 2013), which represent an extensive environment (Tang et al., 2013). For the eastern Jiamusi Block, gneisses and granitoids with the age of 913–777 Ma were reported at its western margin (Xie et al., 2008). This Neoproterozoic basement was also identified from the SHB by detrital-zircon dating of Late Neoproterozoic-Cambrian metasedimentary rocks (Xu et al., 2013; Wang et al., 2013). For the AXXB, ca. 900 Ma gneisses were reported along the China-Mongolia border (Wang et al., 2001; Zhou et al., 2013). The ca. 950 Ma magmatic events were also recorded in the central

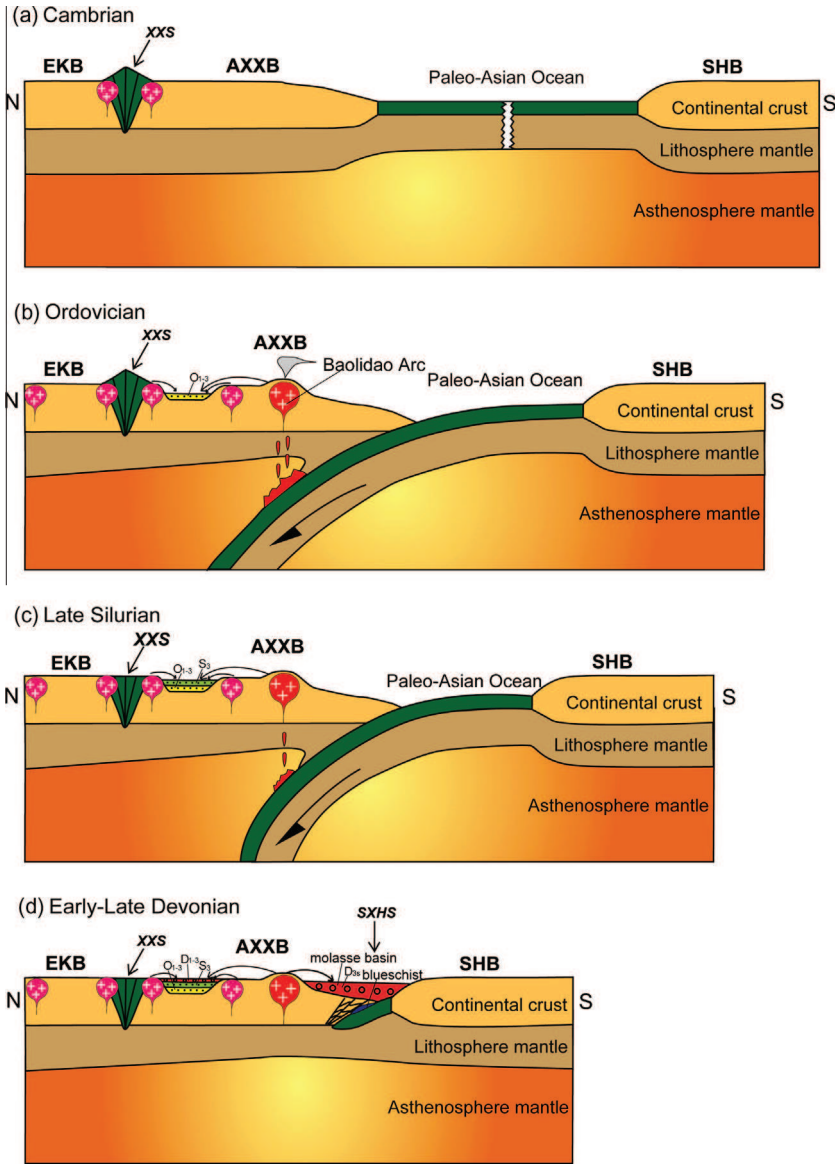

Fig. 7. Schematic geodynamic evolutionary model between the Erguna–Kerulen Block (EKB), Airgin Sum-Xilinhot-Xing'an Block (AXXB) and Songliao-Hunshandaka Block (SHB). (a) The collision between EKB and AXXB occurred before the Middle Cambrian, followed by ~510–485 Ma post-collisional granite. This newly formed Erguna–Xing'an Block (EXB) separated from the SHB by the Paleo-Asian Ocean. (b) Started from the Late Cambrian, The Paleo-Asian Ocean subducted beneath the AXXB from the Late Cambrian to the Middle Silurian, producing the Baolidao arc at its southern margin. Meanwhile, on EXB, Ordovician–Silurian magmatic rocks intruded and extensional sedimentary basins developed. The contemporary Baolidao arc magmatic rocks and post-orogenic rocks provided provenance for the sedimentary basins. (c) Late Silurian Tuvaella fauna-bearing sediments were widespread on EKB, representing the stabilization of this welded block. The Baolidao arc magmatism ceased during this period. (d) During the Early-Middle Devonian, this belt underwent different evolution from west to east. To the west, the basal conglomerate represents the closure of this basin and the cease of the northward subduction. While to the east, shallow marine sediments still exists until to the Late Devonian, indicating an eastward successive closure of the sedimentary basin. As the pre-Late Devonian collision between SHB and AXXB occurred, the Upper Devonian molassic sediments were unconformably deposited over the ophiolitic mélange (Xu et al., 2013). Meanwhile, the marine basins on EXB were closed. No Late Devonian sediments were deposited in the west and Late Devonian continental facies sediments were deposited to the east.

Please cite this article in press as: Zhao, P., et al. Early Paleozoic tectonic evolution of the Xing-Meng Orogenic Belt: Constraints from detrital zircon geochronology of western Erguna–Xing'an Block, North China. Journal of Asian Earth Sciences (2014), http://dx.doi.org/10.1016/j.jseaes.2014.04.011

and southern Mongolia (Kröner et al., 2007; Demoux et al., 2009b). To the northern Tuva-Mongolia Block, a magmatism of the same age was also reported along the southern margin of SIB (Kuzmichev et al., 2001; Gladkochub et al., 2007). These universal Neoproterozoic magmatic rocks in these blocks correspond to an important global magmatic event, which may be related to the assemblage and break-up of Rodinia supercontinent (Li et al., 2008).

In summary, the results presented above indicate bidirectional provenances from the EXB to the north and the Early Paleozoic Baolidao arc to the south for the Ordovician–Devonian deposition. It provides new evidence to decipher the tectonic evolution of this region.

6.3. Tectonic implications

A new model was proposed based on our geochological data to illustrate the Early Paleozoic tectonic evolution of the AXXB with its neighboring blocks.

The collision between the EKB and AXXB occurred before the Late Cambrian, followed by Late Cambrian granitic and mafic intrusions (Wu et al., 2005; Ge et al., 2005; Wu et al., 2011) on both side of the Xinlin-Xiguitu suture zone (Fig. 7a). During this period, the southern margin of this newly formed block was a passive continental margin, and separated from the southern the SHB by the Paleo-Asian Ocean (Fig. 7a);

After that, the newly welded Erguna–Xing'an Block (EXB) belonged to an epicontinental setting, with the development of a Ordovician–Silurian sedimentary basin that was adjacent to coeval magmatic intrusions (Fig. 7b; IMBGMR, 1991;Ge et al., 2007; Sorokin et al., 2004; 2011; Ren et al., 2012; Guo et al., 2013). The Cambrian (510–485 Ma) orogenic-related granitic and mafic intrusions and subsequent Ordovician–Silurian (485–440 Ma) magmatic intrusions provide provenance for the basin sediments (Fig. 7b). Since the Paleo-Asian Ocean subducted beneath the southern margin of the welded EXB, the Baolidao arc formed along this margin from ~490 Ma to ~420 Ma, with the peak at ~460 Ma (Shi et al., 2005; Jian et al., 2008; Zhang et al., 2009b; Xu et al., 2013). The Baolidao arc granitoids intruded into the Xilinhot Precambrian basement, and extensive thermal metamorphism related to the arc magmatism occurred in the Precambian basement (Sun et al., 2013b), which also made contribution for the provenance of the basin deposition (Fig. 7).

During the Late Silurian, the magmatic events along the EXB have ceased, with widespread clastic and carbonate deposits buried the EXB and did not include a volcanic component (Fig. 2). The striking feature of these Upper Silurian strata is the *Tuvaella* funa therein, which can be traced from nearly all the Upper Silurian strata in the EXB (Su, 1981; IMBGMR, 1991), marking a tectonic stabilization of this newly formed block (Fig. 7c; Wang et al., 2009). To the south, the subduction of the Paleo-Asian Ocean was still going on, but the Baolidao arc magmatism ceased at the Late Silurian (Fig. 7c), represented by ~420 Ma high-K granite (Shi et al., 2005; Jian et al., 2008) and coeval hornblende gabbros (Zhang et al., 2009b).

During the Early-Middle Devonian, the marine sedimentary basins on the EXB show significant lateral lithological variations from west to east (Fig. 2). In the Chaganaobao area, the distinctive red basal conglomerate (Fig. 3f and Fig. 7) represents a regional unconformity, indicating that the sedimentary basin might have been closed before the Early Devonian in this area. However, to the east, the Early-Middle Devonian strata are mainly composed of shallow marine sandstone with abundant of shallow marine fossils, indicating that marine sedimentary basins still existed. These lithological variations indicate an Early-Middle Devonian eastward regression, revealing an eastward successive closure of the marine basin (Fig. 7d). During the Late Devonian, due to the collision between the SHB and the EXB, the Late Devonian molassic deposition uncomformbly overlied the ophiolitic mélange (Xu et al., 2013; Fig. 7d). This collision also caused the final closure of the marine sedimentary basins on the EXB, as no Late Devonian sediments were found to the west, and plant-fossils bearing continental Upper Devonian Angeryinwula Formation occurred to the east (West Ujimqin area) (IMBGR, 2007; Fig. 7d). After the Late Devonian, the EXB came into a subaerial setting without sedimentation until the Late Carboniferous continental deposition (IMBGMR, 1991).

7. Conclusions

Combining new detrital-zircon dating results with previous tectonic, sedimentological, geochemical and geochronological studies, lead to the following conclusions.

(1) The detrital-zircon geochronological study of the five Ordovician–Devonian samples from Erenhot-West Ujimqin (the southeastern part of the China–Mongolia border) display the similar age distribution patterns with age groups at ~440 Ma, ~510 Ma, ~800 Ma, ~950 Ma, with few Meso- to Paleo-Proterozoic and Neoarchean grains.
(2) This age distribution displays the same patterns with the magmatic periods of the Erguna–Xing'an Block. Meanwhile, the youngest age group is consistent with the Bolidao arc magmatism at the southern margin of the Erguna–Xing'an Block. Hence, a bidirectional provenance from the Erguna–Xing'an Block in the north and Baolidao arc in the south was proposed.
(3) A new model was proposed to highlight the Early Paleozoic tectonic evolution of the western part of the Arigin Sum-Xilinhot-Xing'an Block, which constrains two main Early Paleozoic tectonic events of the Xing-Meng Orogenic Belt: pre-Late Cambrian collision between Erguna–Kerulen Block and Arigin Sum-Xilinhot-Xing'an Block; and the Early Paleozoic subduction of Paleo-Asian Ocean and pre-Late Devonian collision between Erguna–Xing'an Block and Songliao–Hunshandake Block.

Acknowledgments

We thank Shi Guanzhong and Li Ruibiao for their support in the field. This work has been funded by the National Key Basic Research Program of China (2013CB429806), the National Science Foundation of China (40872145 and 41121062), and the China Geological Survey Grant (No. 1212011220906).

Appendix A. Supplementary material

Supplementary data associated with this article can be found, in the online version, at http://dx.doi.org/10.1016/j.jseaes.2014.04.011.

References

Andersen, T., 2002. Correction of common lead in U–Pb analyses that do not report ^{204}Pb. Chem. Geol. 192, 59–79.
Bussien, D., Gombojav, B., Winkler, W., Von Quadt, A., 2011. The Mongol-Okhotsk Belt in Mongolia – an appraisal of the geodynamic development by the study of sandstone provenance and detrital zircons. Tectonophysics 510, 132–150.
Chen, B., Jahn, B.M., Wilde, S., Xu, B., 2000. Two contrasting Paleozoic magmatic belts in northern Inner Mongolia, China: petrogenesis and tectonic implications. Tectonophysics 328, 157–182.
Chen, B., Ma, X.H., Liu, A.K., Muhetaer, Z., 2012. Zircon U–Pb ages of the Xilinhot Metamorphic complex and blueschist, and implications for tectonic evolution

of the Solonker suture. Acta Petrol. Sin. 25 (12), 3123–3129 (in Chinese with English abstract).
Corfu, F., Hanchar, J.M., Hoskin, P.W.O., Kinny, P.D., 2003. Atlas of zircon textures. Rev. Mineral. Geochem. 53, 469–500.
De Jong, K., Xiao, W.J., Windley, B.F., Masago, H., Lo, C.H., 2006. Ordovician $^{40}Ar/^{39}Ar$ phengite ages from the blueschist-faciesOndor Sum subduction–accretion complex (Inner Mongolia) and implications for the Early Paleozoic history of continental blocks in China and adjacent areas. Am. J. Sci. 306, 799–845.
Demoux, A., Kröner, A., Badarch, G.T., Jian, P., Tomurhuu, D., Wingate, M.T.D., 2009a. Zircon ages from the Baydrag Block and the Bayankhongorophiolite zone: time constraints on late Neoproterozoic to Cambrian subduction- and accretion-related magmatism in Central Mongolia. J. Geol. 117, 377–397.
Demoux, A., Kröner, A., Liu, D., Badarch, G., 2009b. Precambrian crystalline basement in southern Mongolia as revealed by SHRIMP zircon dating. Int. J. Earth Sci. 98, 1365–1380.
Ge, M., Zhou, W., Yu, Y., Sun, J., Bao, J., Wang, S., 2011. Dissolution and supracrustal rocks dating of XilinGol Complex, Inner Mongolia, China. Earth Sci. Front. 18 (5), 182–195 (in Chinese with English abstract).
Ge, W.C., Sui, Z.M., Wu, F.Y., Zhang, J.H., Xu, X.C., Cheng, R.Y., 2007. Zircon U–Pb ages, Hf isotopic characteristics and their implications of the Early Paleozoic granites in the northeastern Da Hinggan Mts., northeastern China. Acta Petrol. Sin. 23 (2), 423–440 (in Chinese with English abstract).
Ge, W.C., Wu, F.Y., Zhou, C.Y., Rahman, A.A.A., 2005. Emplacement age of the Tahegranite and its constraints on the tectonic nature of the Ergun block in thenorthern part of the Da Hinggan Range. Chin. Sci. Bull. 50, 2097–2105.
Gladkochub, D.P., Donskaya, T.V., Mazukabzov, A.M., Stanevich, A.M., Sklyarov, E.V., Ponomarchuk, V.A., 2007. Signature of Precambrian extension events in the southern Siberian craton. Russ. Geol. Geophys. 48, 17–31.
Guo, Z., Zhang, B., Shen, X., Jia, W., Huang, X., 2013. Discussion on the Geological characteristics and Mechanism of rock formation of the Giant Phenocrystadamellite in Southeast Mongolia. J. Jilin Univ. (Earth Sci. Ed.) 43 (3), 776–787 (in Chinese with English abstract).
Han, G., Liu, Y., Neubauer, F., Genser, J., Li, W., Zhao, Y., Liang, C., 2011. Origin of terranes in the eastern Central Asian Orogenic Belt, NE China: U–Pb ages of detrital zircons from Ordovician–Devonian sandstones, North Da Xing'an Mts. Tectonophysics 511, 109–124.
Hong, D., Huang, H., Xiao, Y., Xu, H., Jin, M., 1994. The Permian alkaline granites in central Inner Mongolia and their geodynamic significance. Acta Geol. Sin. 69 (3), 219–230 (in Chinese with English abstract).
Hong, D.W., Wang, S.G., Han, B.F., Jin, M.Y., 1996. Post-orogenic alkaline granites from China and comparisons with an orogenic alkaline granites elsewere. J. SE Asian Sci. 13, 13–27.
IMBGMR (Inner Mongolian Bureau of Geology and Mineral Resources), 1991.Regional geology of Inner Mongolian Autonomous Region. Geological Publishing House, Beijing (in Chinese with English abstract).
IMBGR, 2007. Geological map of China, Dongwuzhumuqinqi sheet (L50C003002), scale 1:250000.
Jahn, B.M., Litvinovsky, B.A., Zanvilevich, A.N., Reichow, M., 2009. Peralkaline granitoid magmatism in the Mongolian-Transbaikalian Belt: evolution, petrogenesis and tectonic significance. Lithos 113, 521–539.
Jian, P., Liu, D., Kröner, A., Windley, B.F., Shi, Y., Zhanf, F., Shi, G., Miao, L., Zhang, W., Zhang, Q., Zhang, L., Ren, J., 2008. Time scale of an early to mid-Paleozoicorogenic cycle of the long-lived Central Asian Orogenic Belt, Inner Mongolia of China: implications for continental growth. Lithos 101, 233–259.
Kelty, T.K., Yin, A., Dash, B., Gehrels, G.E., Ribeiro, A.E., 2008. Detrital-zircon geochronology of Paleozoic sedimentary rocks in the Hangay-Hentey basin, north-central Mongolia: implications for the tectonic evolution of the Mongol-Okhotsk Ocean in central Asia. Tectonophysics 451, 290–311.
Kröner, A., Windley, B.F., Badarch, G., Tomurtogoo, O., Hegner, E., Jahn, B.M., Gruschka, S., Khain, E.V., Demoux, A., Wingate, M.T.D., 2007. Accretionary growth and crust-formation in the Central Asian Orogenic Belt and comparison with the Arabian–Nubian shield.Geological Society of America. Memoirs 200, 181–209.
Kuzmichev, A.B., Bibikova, E.V., Zhuravlev, D.Z., 2001. Neoproterozoic (~800 Ma) orogeny in the Tuva-Mongolia Massif (Siberia): island arc–continent collision at the northeast Rodinia margin. Precambr. Res. 110, 109–126.
Li, D.P., Chen, Y.L., Wang, Z., Hou, K.J., Liu, C.Z., 2011. Detrital zircon U–Pb ages, Hfisotopesand tectonic implications for Palaeozoic sedimentary rocks from the Xing-Mengorogenic belt, middle-east part of inner Mongolia, China. Geol. J. 46, 63–81.
Li, W.G., Li, Q.F., Jiang, W.D., 1996. Lithostratigraphy of Inner Mongolia Autonomous Region. Chinese University of Geoscience Press, Beijing, p. 1–344.
Li, Z.X., Bogdanova, S.V., Collins, A.S., Davidson, A., DeWaele, B., Ernst, R.E., Fitzsimons, I.C.W., Fuck, R.A., Gladkochub, D.P., Jacobs, J., Karlstrom, K.E., Lu, S., Natapov, L.M., Pease, V., Pisarevsky, S.A., Thrane, K., Vernikovsky, V., 2008. Assembly, configuration, and break-up history of Rodinia: a synthesis. Precambr. Res. 160, 179–210.
Liu, D., Jian, P., Zhang, Q., Zhanf, F., Shi, Y., Shi, G., Zhang, L., Tao, H., 2003. SHRIMP dating of adakites in the Tulingkaiophiolite, Inner Mongolia: evidence for the Early Paleozoic subduction. Acta Geol. Sin. 77 (3), 317–326.
Ludwig, K.R., 2003. User's Manual for Isoplot 3.0: A Geochronological Toolkit for Microsoft Excel Berkeley Geochronology Center. Special publication, 4, pp. 1–71.
Ren, B., Sun, L., Cheng, Y., Teng, X., Li, Y., Hao, S., 2012. Zircon U–Pb ages, Hf isotopic characteristics of the Yongqinglinchang-Shibazhan granites in the Northern Da Hinggan Mountains, Northeastern China. Geol. Surv. Res. 35 (2), 109–117 (in Chinese with English abstract).
Rojas-Agranonte, A., Kroner, A., Demoux, A., Xia, X., Wang, W., Donskaya, T., Liu, D., Sun, M., 2011. Detrital and xenocrystic zircon ages from Neoproterozoic to Palaeozoic arc terranesof Mongolia: significance for the origin of crustal fragments in the Central Asian Orogenic Belt. Gondwana Res. 19, 751–763.
Rubatto, D., 2002. Zircon trace element geochemistry: partitioning with garnet and the link between U–Pb ages and metamorphism. Chem. Geol. 184, 123–138.
Shi, Y.R., Liu, D.Y., Jian, P., Zhang, Q., Zhang, F.Q., Miao, L.C., Shi, G.H., Zhang, L.Q., Tao, H., 2005. Zircon SHRIMP dating of K-rich granites in Sonidzuoqi, central Inner Mongolia. Geol. Bull. China 24 (5), 424–428 (in Chinese with English abstract).
Sorokin, A.A., Kudryashov, N.M., Li, J.Y., 2004. Early Paleozoicgranitoids in the Eastern Margin of the Argun' Terrane, Amur area: first geochemical and geochronologic data. Petrology 12 (4), 367–376.
Sorokin, A.A., Kotov, A.B., Sal'nikova, E.B., Kudryashov, N.M., Velikoslavinskii, S.D., Yakovleva, S.Z., Fedoseenko, A.M., Plotkina, Y.V., 2011. Early Paleozoic Granitoids in the Lesser Khingan Terrane, Central Asian Fold belt: age, geochemistry, and geodynamic interpretations. Petrology 19 (6), 601–617.
Su, Y.Z., 1981. The distribution and entironment of Tuvaella fauna. Acta Palaeontol. Sin. 20 (6), 567–574 (in Chinese).
Sun, L.X., Ren, B.F., Zhao, F.Q., Ji, S.P., Geng, J.Z., 2013a. Late Paleoproterozoic magmatic records in the Eerguna massif: evidences from the zircon U–Pb dating of granitic gneisses. Geol. Bull. China 32 (2/3), 341–352 (in Chinese with English abstract).
Sun, L.X., Ren, B.F., Zhao, F.Q., Gu, Y.C., Li, Y.F., Liu, H., 2013b. Zircon U–Pb dating and Hf isotopic compositions of the Mesoporterozoic granitic gneiss in Xilinhot Block, Inner Mongolia. Geol. Bull. China 32 (2/3), 327–340 (in Chinese with English abstract).
Tang, J., Xu, W.L., Wang, F., Wang, W., Xu, M.J., Zhang, Y.H., 2013. Geochronology and geochemistry of Neoproterozoic magmatism in the Erguna Massif, NE China: petrogenesis and implications for the breakup of the Rodinia supercontinent. Precambr. Res. 224, 597–611.
Tang, K.D., 1990. Tectonic development of Paleozoic fold belts at the north margin of the Sino-Korean craton. Tectonics 9, 249–260.
Tang, K., Yan, Z., 1993. Regional metamorphism and tectonic evolution of the Inner Mongolia suture zone. J. Metamor. Geol. 11, 511–522.
Wang, C.W., Sun, Y.W., Li, N., Zhao, G.W., Ma, X.Q., 2009. Tectonic implication of the late Paleozoic stratigraphic distribution in Northeast China and adjacent region. Sci. China Series D: Earth Sci. 52 (5), 619–626.
Wang, F., Xu, W.L., Gao, F.H., Zhang, H.H., Pei, F.P., Zhao, L., Yang, Y., 2013. Precambrian terrane within the Songnen–Zhangguangcai Range Massif, NE China: Evidence from U–Pb ages of detrital zircons from the Dongfengshan and Tadong groups. Gondwana Research. <http://dx.doi.org/10.1016/j.gr.2013.06.017>.
Wang, T., Zheng, Y.D., Gehrels, G.E., Mu, Z.G., 2001. Geochronological evidence for existence of the south Mongolian microcontinent: a zircon U–Pb age of granitoid gneisses from the Yagan–Onch Hayrhan metamorphic core complex on the Sino-Mongolian border. China Sci. Bull. 46, 2005–2008.
Wu, F.Y., Sun, D.Y., Ge, W.C., Zhang, Y.B., Grant, M.L., Wilde, S.A., Jahn, B.M., 2011. Geochronology of the Phanerozoic granitoids in northeastern China. J. Asian Earth Sci. 41, 1–30.
Wu, F.Y., Zhao, G.C., Sun, D.Y., Wilde, S.A., Yang, J.H., 2007. The Hulan group: its role in the evolution of the Central Asian Orogenic Belt of NE China. J. Asian Earth Sci. 30, 542–556.
Wu, G., Chen, Y., Chen, Y., Zeng, Q., 2012. Zircon U–Pb ages of the metamorphic supracrustal rocks of the Xinghuadukou Group and granitic complexes in the Argun massif of the northern Great Hinggan Range, NE China, and their tectonic implications. J. Asian Earth Sci. 49, 214–233.
Wu, G., Sun, F.Y., Zhao, C.S., Li, Z.T., Zhao, A.L., Pang, Q.B., Li, G.Y., 2005. Discovery of the Early Paleozoic post-collisional granites in northern margin of the Erguna massif and its geological significance. Chin. Sci. Bull. 50, 2733–2743.
Xiao, W.J., Windley, B.F., Hao, J., Zhai, M.G., 2003. Accretion leading to collision and the Permian Solonker suture, Inner Mongolia, China: termination of the Central Asian Orogenic Belt. Tectonics 22, 1069–1089.
Xie, H.Q., Zhang, F.Q., Miao, L.C., Chen, F.K., Liu, D.Y., 2008. Zircon SHRIMP U–Pb dating of the amphibolite from "Heilongjiang Group" and the granite in Mudanjiang area, NE China, and its geological significance. Acta Pertrol. Sin. 24 (6), 1237–1250 (in Chinese with English abstract).
Xin, H., Teng, X., Cheng, Y., 2011. Stratigraphic Subdivision and Isotope Geochronology Study on the Baoligaomiao Formation in the East Ujimqin County, Inner Mongolia. Geol. Surv. Res. 34 (1), 1–9.
Xu, B., Charvet, J., Zhang, F.Q., 2001. Primary study on petrology and geochronology of the blueschist in Sonid Zuoqi, northern Inner Mongolia. Chin. J. Geol. 36, 424–434 (in Chinese with English abstract).
Xu, B., Charvet, J., Chen, Y., Zhao, P., Shi, G.Z., 2013. Middle Paleozoic convergent orogenic belts in western Inner Mongolia (China): framework, kinematics, geochronology and implications for tectonic evolution of the Central Asian Orogenic Belt. Gondwana Res. 23, 1324–1364.
Xue, H.M., Gou, L.J., Hou, Z.Q., Zhou, X.W., Tong, Y., Pan, X.F., 2009. The Xilingele complex from the eastern part of the Central Asian-Mongolia Orogenic Belt, China: products of Early Variscan orogeny other than ancient block: evidence from zircon SHRIMP U–Pb ages. Acta Pertol. Sin. 25 (8), 2001–2010 (in Chinese with English abstract).
Zhang, S.H., Zhao, Y., Song, B., Hu, J.M., Liu, S.W., Yang, Y.H., Chen, F.K., Liu, X.M., Liu, J., 2009a. Contrasting late Carboniferous and late Permian-middle Triassic

Please cite this article in press as: Zhao, P., et al. Early Paleozoic tectonic evolution of the Xing-Meng Orogenic Belt: Constraints from detrital zircon geochronology of western Erguna–Xing'an Block, North China. Journal of Asian Earth Sciences (2014), http://dx.doi.org/10.1016/j.jseaes.2014.04.011

intrusive suites from the northern margin of the north China craton. Geol. Soc. Am. Bull. 121, 181–200.

Zhang, W., Jian, P., Kroner, A., Shi, Y., 2013. Magmatic and metamorphic development of an early to mid-Paleozoic continental margin arc in the southernmost Central Asian Orogenic Belt, Inner Mongolia, China. J. Asian Earth Sci. 72, 63–74.

Zhang, X.H., Wilde, S.A., Zhang, H.F., Tang, Y.J., Zhai, M.G., 2009b. Geochemistry of hornblende gabbros from Sonidzuoqi, Inner Mongolia, North China: implication for magmatism during the final stage of suprasubduction zone ophiolite formation. Int. Geol. Rev. 51, 345–373.

Zhang, X.H., Zhang, H.F., Jiang, N., Zhai, M.G., et al., 2010. Early Devonian alkaline intrusive complex from the northern North China Craton: a petrologic monitor of post- collisional tectonics. J. Geol. Soc., Lond. 167, 717–730.

Zhang, X., Ma, Y., Chi, X., Zhang, F., Sun, Y., Guo, Y., Zeng, Z., 2012. Discussion on Phanerozoic tectonic evolution in Northeastern China. J. Jilin Univ. (Earth Sci. Ed.) 42 (5), 1269–1285 (in Chinese with English abstract).

Zhang, X., Wilde, S.A., Zhang, H., Zhai, M., 2011. Early Permian high-K calc-alkaline volcanic rocks from NW Inner Mongolia, North China: geochemistry, origin and tectonic implications. J. Geol. Soc., Lond. 168, 525–543.

Zhao, P., Chen, Y., Xu, B., Faure, M., Shi, G., Choulet, F., 2013. Did the Paleo-Asian Ocean between North China Block and Mongolia Block exist during the late Paleozoic? First paleomagnetic evidence from central-eastern Inner Mongolia, China. J. Geophys. Res.: Solid Earth 118, 1873–1894.

Zhou, J.B., Wilde, S.A., 2013. The crustal accretion history and tectonic evolution of the NE China segment of the Central Asian Orogenic Belt. Gondwana Res. 23, 1365–1377.

Zhou, J.B., Wilde, S.A., Zhang, X.Z., Ren, S.M., Zheng, C.Q., 2011a. Early Paleozoic metamorphic rocks of the Erguna block in the Great Xing'an Range, NE China: evidence for the timing of magmatic and metamorphic events and their tectonic implications. Tectonophysics 499, 105–117.

Zhou, J.B., Wilde, S.A., Zhang, X.Z., Zhao, G.C., Liu, F.L., 2011b. A >1300 km late Pan-African metamorphic belt in NE China: new evidence from the Xing'an Block and its tectonic implications. Tectonophysics 509, 280–292.

Zhou, Y.Z., Han, B.F., Xu, Z., Ren, R., Su, L., 2013. The age of the Proterozoic rocks in Yingba area in western Inner Mongolia: constraints on the distribution of the South Gobi micro-continent in the Central Asian Orogenic belt. Geol. Bull. China 32 (2/3), 318–326 (in Chinese with English abstract).

Zhou, Z.G., Gu, Y.C., Liu, C.F., Yu, Y.S., Zhang, B., Tian, Z.J., He, F.B., Wang, B.R., 2010. Discovery of Early-Middle Permian cathaysian flora in Manduhubaolage area, Dong Ujimqin Qi, Inner Mongolia, China and its geological significance. Geol. Bull. China 28 (12), 21–25 (in Chinese with English abstract).

Please cite this article in press as: Zhao, P., et al. Early Paleozoic tectonic evolution of the Xing-Meng Orogenic Belt: Constraints from detrital zircon geochronology of western Erguna–Xing'an Block, North China. Journal of Asian Earth Sciences (2014), http://dx.doi.org/10.1016/j.jseaes.2014.04.011

THÈSE EN COTUTELLE INTERNATIONALE
PRESENTÉE A L'UNIVERSITÉ DE PÉKIN

POUR OBTENIR LE GRADE DE DOCTEUR
DE L'UNIVERSITÉ D'ORLÉANS ET DE L'UNIVERSITE DE PÉKIN

Par
Pan ZHAO

ÉCOLE DOCTORALE [SCIENCES ET TECHNOLOGIE]
Discipline : Sciences de la Terre et de l'Univers

L'évolution tectonique du Paléozoïque supérieur de la Ceinture Orogénique de l'Asie Centrale du Centre-Oriental de la Mongolie intérieure

Soutenue Publiquement
le 17 Octobre 2014 à 10 heures
Pékin, Chine

MEMBRES DU JURY :

CHEN Yan	Professeur, Université d'Orléans, Directeur de thèse
FAURE Michel	Professeur, Université d'Orléans, examinateur
LIN Wei	Professeur, Institute of Geology and Geophysics, CAS, examinateur
LIU Junlai	Professeur, China University of Geosciences (Beijing), examinateur
SCAILLET Bruno	Professeur, Université d'Orléans, examinateur
WANG Tao	Professeur, Chinese Academy of Geological Sciences, examinateur
XU Bei	Professeur, Peking University, co-directeur de thèse
ZHANG Shihong	Professeur, China University of Geosciences (Beijing), examinateur

RÉSUMÉ

Le Centre-Est de la Mongolie intérieure, faisant la partie sud-est de la Ceinture Orogénique de l'Asie Centrale (CAOB), est une zone de clé pour étudier l'histoire de l'accrétion-collision entre la Chine du Nord (NCC) et les blocs continentaux du Nord. Les contraintes du cadre tectonique et de la connaissance de l'évolution tectonique sont importantes pour comprendre l'accrétion de la CAOB car il n'y a pas de consensus sur le mode et la période de l'accrétion entre NCC et les blocs du Nord. Par conséquent, des études pluridisciplinaires ont été effectuées sur les roches sédimentaires et magmatiques du Paléozoïque supérieur dans le centre-oriental de la Mongolie Intérieure. Sur la base de nos études sédimentologiques, géochronologiques, géochimiques et paléomagnétiques, et compte tenu des résultats précédents en pétrographie, géochimie et paléontologie, l'évolution sédimentaire et tectonique du Paléozoïque supérieur du Centre-Oriental de la Mongolie Intérieure a été bien établie. Les études détaillées en sédimentologie et géochimie montrent une transition entre les dépôts molassiques du Dévonien à la dénudation du Carbonifère inférieur et les sédiments marins du Carbonifère supérieure vers les dépôts de bassin d'extension au Permien. D'après nos analyses détaillées des faciès sédimentaires, des caractéristiques géochimiques des roches magmatiques et nos données paléomagnétiques, nous proposons un modèle géodynamique de subduction-collision-extension post-orogénique pour le Paléozoïque au Centre-Oriental de la Mongolie Intérieure.
Mots-clés: Ceinture Orogénique de l'Asie Centrale (CAOB), Centre-Oriental de la Mongolie intérieure, Paléozoïque supérieure, sédimentologie, paléomagnétisme

Institut des Sciences de la Terre d'Orléans, 45067 Orléans, France

Institut des Sciences de laTerre et Espace de l'Universite de Pékin, 100871, Pékin, Chine